INVESTIGATING THE ROLE OF MR AND PLVAP IN HEPATIC LEUKOCYTE RECRUITMENT DURING CHRONIC LIVER INFLAMMATION

by

ALEX LOUISE WILKINSON

A thesis submitted to

The University of Birmingham

For the degree of

DOCTOR OF PHILOSOPHY

Centre for Liver and Gastrointestinal Research
Institute of Immunology and Immunotherapy
College of Medical and Dental Sciences
University of Birmingham
22nd July 2022

Abstract

Chronic liver diseases (CLDs) are characterised by inflammation and fibrosis which are driven by aberrant leukocyte recruitment. This process is mediated by specialised discontinuous endothelia, known as hepatic sinusoidal endothelial cells (HSEC), which act as the liver gatekeepers. During chronic inflammation, HSEC undergo substantial phenotypic changes, including upregulation of adhesion molecules, further driving leukocyte recruitment and exacerbating inflammation. The composition of the hepatic immune microenvironment determines the outcome of liver injury and understanding the mechanisms which regulate this process is critical to identify novel therapeutic targets. Mannose receptor (MR) and plasmalemma vesicle-associated protein (PLVAP) have previously been implicated in immune cell trafficking but their contribution to hepatic leukocyte recruitment remains undefined. This study aimed to characterise the expression of MR and PLVAP in normal and diseased human liver, understand their regulation in the hepatic sinusoids, and investigate their potential role in hepatic leukocyte recruitment. Immunohistochemistry and gene expression studies demonstrated that MR and PLVAP are differentially expressed in liver endothelium, with MR being downregulated and PLVAP being upregulated, in CLD and hepatocellular carcinoma. MR was resistant to regulation in primary human HSEC and did not seem to be involved in lymphocyte recruitment. In contrast, PLVAP was upregulated by several soluble factors, most notably by the senescence-associated secretory phenotype (SASP). The SASP, comprised of several cytokines and chemokines, is known to facilitate senescence surveillance by stimulating leukocyte recruitment. Additional experiments using patient tissue samples uncovered a previously unreported link between hepatic senescence, immune cell infiltration, and PLVAP expression in CLD. Furthermore, *in vitro* flow adhesion assays showed that PLVAP plays a selective functional role in monocyte paracellular transmigration, whilst having no impact on lymphocyte recruitment. These findings suggest that senescent cell-endothelial crosstalk drives PLVAP expression and shapes the immune landscape in chronic liver inflammation.

Acknowledgements

The work presented in this thesis was funded by the Wellcome Trust to whom I am extremely grateful for the opportunity to complete a PhD. I also pay thanks to the patients of the Queen Elizabeth Hospital Birmingham and all the healthy volunteers who have donated tissue and blood, without whom this work would not have been possible. I thank my supervisory team, David Hodson, David Wraith, Eva-Maria Frickel and Robin May, for their support and scientific advice. Many thanks are also given to our collaborators, Marko Salmi, Pia Rantakari, Matt Hoare, Kelvin Yin, Tom Bird, Christos Kiourtis, Paul Horn, Wei-Yu Lu and Gareth Hardisty, who have generously provided reagents and samples, and whose insight into the project has been invaluable. Thank you to everyone in the Centre for Liver and Gastrointestinal Research, particularly Janine Fear, Subin Modit and Norma Gregory for their technical assistance, and the rest of Team Shetty who I have been privileged to work with. I also need to thank Laura Harford and Pantelitsa Papakyriacou for being there throughout this whole experience – we have dragged each other through the toughest lab days. Thank you to Emma Shepherd and Daniel Patten, for your mentorship and friendship, and for believing in me when I didn't believe in myself. I also give huge thanks to my supervisor, Shishir Shetty, to whom I am grateful for the opportunity to complete this impactful work and who has supported me throughout. Finally, I thank my loving family and friends, especially my parents, Donna and Antony – your support has never wavered. I must also thank my Granny, Lesley, who is no longer with us – you continue to inspire me and I hope I have made you proud. And last but most certainly not least, I pay the biggest thanks to my partner and best friend, Jordan Bachelor. You have been my rock and I could not have done this without you.

Table of Contents

List of Figures

List of Tables

List of Abbreviations

15dPGJ2, 15-Deoxy-Delta-12,14-prostaglandin J2
4-OHT, 4-hydroxytamoxifen
AcLDL, acetylated low-density lipoprotein
αGalCer, alpha galactosylceramide
ALD, alcoholic liver disease
ALK, activin receptor-like kinase
ALK5i, activin receptor-like kinase 5 inhibitor
aLMF, activated liver myofibroblast
ALT, alanine transaminase
APC, antigen presenting cell
αSMA, alpha smooth muscle actin
AST, aspartate transaminase
AT1, angiotensin II type 1 receptor
ATRA, all trans retinoic acid
AWERB, Animal Welfare and Ethical Review Body
BBB, blood-brain-barrier
BEC, biliary epithelial cell
BMDDC, bone marrow-derived dendritic cell
BMDMφ, bone marrow-derived macrophage
BMP9, bone morphogenic protein 9
BRB, blood-retina-barrier
BSA, bovine serum albumin
CD32b, Fcγ receptor IIb
CDK, cyclin-dependent kinase
CLCA1, chloride channel accessory 1
CLD, chronic liver disease
CM, conditioned medium
CME, clathrin-mediated endocytosis
CNS, central nervous system
CR, cysteine-rich region
CRIg, complement receptor of the immunoglobulin superfamily
CTG, CellTracker Green
CTL, cytotoxic T lymphocyte
CTLD, C-type lectin domain
CX_3CL1, fractalkine
CYP, cytrochrome P450
DAB, 3,3'-diaminobenzidine
DAMP, danger-associated molecular pattern
DAPI, 4′,6-diamidino-2-phenylindole
DC, dendritic cell
DCR2, decoy receptor 2
DMEM, Dulbecco's modified Eagle's medium
DMSO, dimethyl sulphoxide
dNTP, deoxyribonucleotide triphosphate
DPX, distyrene plasticiser xylene
DTT, dithiothreitol
ECM, extracellular matrix
EDTA, ethylenediaminetetraacetic acid
EEA-1, early endosomal antigen 1
EGF, epidermal growth factor
EndMT, endothelial-to-mesenchymal transition
eNOS, endothelial nitric oxide synthase
EpCAM, epithelial cell adhesion molecule
ESAM, endothelial cell-selective adhesion molecule
ET-1, endothelin 1
FBS, foetal bovine serum
FELS, fenestrated endothelial-linked structure protein
FFPE, formalin-fixed paraffin-embedded
FGF2, fibroblast growth factor 2
FITC, fluorescein isothiocyanate
FNII, fibronectin type 2
FoxP3, Forkhead-Box-Protein P3
FZD4, frizzled class receptor 4
γH2A.X, gamma-H2A histone family member X
GOF, gain-of-function
GPCR, G protein-coupled receptor
GSK3, glycogen synthase kinase 3
HBV, hepatitis B virus
HCC, hepatocellular carcinoma
HCI, high-content imaging
HCV, hepatitis C virus
HDL, high-density lipoprotein
HDMVEC, human dermal microvascular endothelial cells
HEV, high endothelial venules
HGF, hepatocyte growth factor
HMVEC, human microvascular endothelial cells
hMφ, human macrophage
HRP, horseradish peroxidase
HSC, hepatic stellate cell
HSEC, hepatic sinusoidal endothelial cell
HUVEC, human umbilical vein endothelial cell
ICAM, intercellular adhesion molecule 1
ICC, immunocytochemistry
IDO, indoleamine 2,3-dioxygenase
IFNγ, interferon gamma
IHC-Fr, immunohistochemistry-frozen
IHC-P, immunohistochemistry-paraffin
IL, interleukin
ILC, innate lymphoid cell
IMC, isotype-matched control
IDA, industrial denatured alcohol
iNKT, invariant natural killer T cells
IQR, interquartile range
JAM, junctional adhesion molecule
KC, Kupffer cell
KLF2, Krüppel-like factor 2
KO, knockout
L-SIGN, liver/lymph node-specific intercellular adhesion molecule 3-grabbing non-integrin
LBRC, lateral border recycling complex
LDL, low-density lipoprotein
LiCl, lithium chloride
LPA, lysophosphatidic acid
LPS, lipopolysaccharide
LRP5, LDL receptor-related protein 5

LSECtin, liver sinusoidal endothelial cell lectin
LYVE-1, lymphatic vessel endothelial hyaluronan receptor 1
MACS, magnetic-activated cell sorting
MAdCAM, mucosal addressin cell adhesion molecule 1
MAIT, mucosal-associated invariant T
MAPK, mitogen-activated protein kinases
MCP-1, monocyte chemoattractant protein 1
MDA-5, melanoma differentiation-associated protein 5
MDDC, monocyte-derived dendritic cell
Mdm2, Murine double minute 2
MDSC, myeloid-derived suppressor cell
MECA-32, mouse endothelial cell antigen 32
MHC, major histocompatibility complex
MMP, matrix metalloproteinases
mMφ, murine macrophage
MR, mannose receptor
MRP14, migration inhibitory factor-related protein 14
mTOR, mammalian target of rapamycin
NAFLD, non-alcoholic fatty liver disease
NASH, non-alcoholic steatohepatitis
NE, neutrophil elastase
NET, neutrophil extracellular trap
NFκB, nuclear factor kappa-light-chain-enhancer of activated B cells
NK, natural killer
NKT, natural killer T
NO, nitric oxide
NOD, nucleotide-binding and oligomerization domain
NRP1, neuropilin 1
NT, non-tumour
OIS, oncogene-induced senescence
oxLDL, oxidised low-density lipoprotein
pA2, phospholipase A2
PAL-E, Pathologische Anatomie Leiden-endothelium
PAMP, pathogen-associated molecular pattern
PBC, primary biliary cholangitis
PBMC, peripheral blood mononuclear cell
PBS, phosphate buffered saline
PD-1, programmed cell death protein 1
PD-L1, programmed death ligand 1
PDGFβ, platelet-derived growth factor beta
PECAM, platelet/endothelial cell adhesion molecule 1
PFA, paraformaldehyde
PGE1, prostaglandin E1
PI3K, phosphoinositide 3-kinases
PLVAP, plasmalemma vesicle-associated protein
PMA, phorbol 12-myristate 13- acetate
PPAR, peroxisome proliferator-activated receptor
PRR, pattern recognition receptor
PSC, primary sclerosing cholangitis
PSG, penicillin-streptomycin-glutamine
pSTAT6, phospho-signal transducer and activator of transcription 6
qRT-PCR, quantitative real-time polymerase chain reaction
RIG-I, retinoic acid-inducible gene-I-like receptor
RME, receptor-mediated endocytosis
ROS, reactive oxygen species
Rpm, rotations per minute
S1P, sphinosine-1-phosphate
SA-β-Gal, senescence-associated β-galactosidase
SAEndo, scar-associated endothelial cells
SAHF, senescence-associated heterochromatin foci
SASP, senescence-associated secretory phenotype
SBB, Sudan black B
SCARF1, scavenger receptor class F member 1
SCID, severe combined immunodeficient
scRNAseq, single-cell RNA sequencing
SDF1α, stromal-derived factor 1α
SEM, standard error of the mean
SFM, serum-free medium
siRNA, short-interfering RNA
sMR, soluble mannose receptor
SR, scavenger receptor
SR-A1, scavenger receptor type A1
T, tumour
TAM, tumour-associated macrophage
TCGA, The Cancer Genome Atlas
TCR, T cell receptor
TEC, transendothelial channel
TEM, transendothelial migration
TGFβ, transforming growth factor beta
TLR, toll-like receptor
TNFα, tumour necrosis factor alpha
T_{reg}, regulatory T cell
UUO, unilateral ureteral obstruction
VAMP7, vesicle-associated membrane protein 7
VAP1, vascular adhesion protein 1
VCAM, vascular cell adhesion molecule 1
VE-cadherin, vascular endothelial cadherin
VEGF, vascular endothelial growth factor
VEGFR2, vascular endothelial growth factor receptor 2
VLDL, very-low density lipoprotein
Zeb1, zinc-finger E-box binding homeobox 1

1 INTRODUCTION

1.1 Liver Disease Burden

Liver disease is a growing epidemic that accounts for approximately two million deaths worldwide[1], with one million occurring due to hepatocellular carcinoma (HCC) and viral hepatitis, and the remainder as a result of cirrhosis complications. In the UK, liver cirrhosis was the second most common cause of premature death amongst those aged 30-60 years in 2019 (**Figure 1.1)**[2]. Furthermore, liver disease mortality rates have seen a 400% increase since 1970, whilst deaths due to other major diseases are gradually declining[3]. Besides rising mortality rates, liver disease substantially contributes to global morbidity, which represents a massive public health and economic burden[1]. The increased adoption of the Westernised diet, particularly in developing countries, has seen a concerning 6-fold increase in global obesity incidence over the last four decades[4]. As such, global prevalence of metabolic liver disease has reached an all-time high, with an estimated 25.2% of adults now suffering from some form of non-alcoholic fatty liver disease (NAFLD)[5].

Since many patients present with symptoms only at advanced stages, liver disease is now the leading cause of death in 35–49-year olds, often being referred to as a "silent killer"[3]. Once patients have progressed to end-stage disease, current treatment options are limited, with the only curative therapy being liver transplant. Whilst transplantation has shown relative success with a five-year survival rate of 73.6–80%[1], relapse rates are high (~20% alcoholic liver disease patients) and there are also significant caveats associated with organ shortage, disease recurrence and graft rejection[6-9]. Furthermore, the requirement for, often life-long, treatment with immunosuppressive drugs following transplant is associated with its own pitfalls further contributing to the overall global health burden[10]. Thus, research to identify novel therapeutic targets is a valuable pursuit, and will be required to overcome these issues and improve diagnosis, prognosis and treatment of liver disease patients.

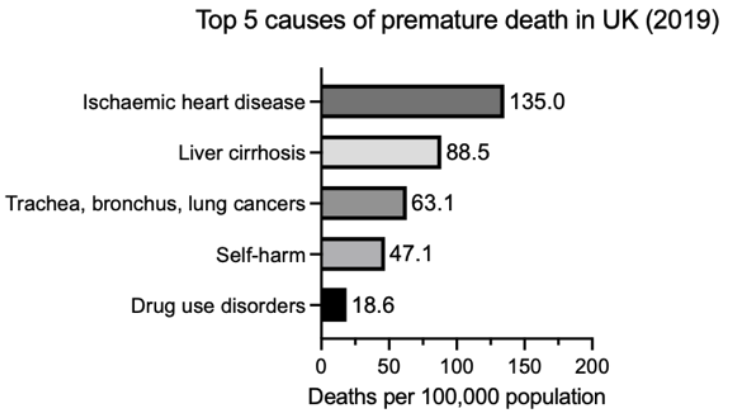

Figure 1.1: The top five causes of premature death in the UK amongst 30-60-year olds in 2019.

Data accessible from https://www.who.int/data/gho/data/themes/mortality-and-global-health-estimates/ghe-leading-causes-of-death.

1.2 Liver Structure

The liver is the largest solid organ in the body weighing approximately 1.5 kg, and can be grossly divided into two lobes (left and right), separated by the falciform ligament (**Figure 1.2**)[11]. The right lobe is subdivided into caudate and quadrate lobes, which can be identified from the posterior surface of the liver, and lie adjacent to the inferior vena cava and gallbladder, respectively[12]. These lobes can be further divided into eight distinct anatomical segments based on their independent vascularisation and biliary drainage[13]. It is this anatomical feature which allows the liver to be resected without damage to the remaining segments[14, 15].

The liver consists of approximately 100,000 structural units (~1 mm in diameter) referred to as hepatic lobules, in which hepatocytes are arranged in hexagonal plates, with the central vein residing in the middle and portal triads located at the vertices of each lobule (**Figure 1.2)**[12, 16, 17]. Portal triads comprise terminal branches of the portal vein and hepatic artery in close proximity to a bile duct[17, 18]. The smallest functional unit of the liver is known as the acinus, which encompasses hepatocytes and sinusoids from two adjacent lobules supplied by one portal triad[19, 20].

Hepatocytes are the principle parenchymal cell type comprising approximately 77.8% of the total liver volume[16, 21]. These polarised epithelial cells are strategically arranged into one- or two-cell thick cords;

tight junctions between hepatocytes form bile canaliculi at the apical surface, whilst their basolateral surfaces are flanked by fenestrated endothelia[16, 17]. These specialised discontinuous endothelial cells, known as hepatic sinusoidal endothelial cells (HSEC), line the liver capillary network referred to as the hepatic sinusoids. Fenestrations are pore-like structures arranged in "sieve plates", which perforate the HSEC cytoplasm and regulate vascular permeability[22-24]. The presence of these fenestrae, paired with the lack of basement membrane, allows the relatively free exchange of fluid and solutes between the bloodstream and the interstitium surrounding hepatocytes[16, 24]. This not only facilitates their metabolic and detoxifying function but also allows movement of macromolecules, such as plasma proteins, secreted by hepatocytes[12]. Furthermore, fenestrations allow direct contact between hepatocytes and cells residing within the sinusoids[25, 26], and can permit regulated passage of immune cells from the bloodstream to the parenchyma[27]. Thus, the structural organisation of the hepatic sinusoids facilitates exocrine, endocrine, metabolic and immune functions of the liver.

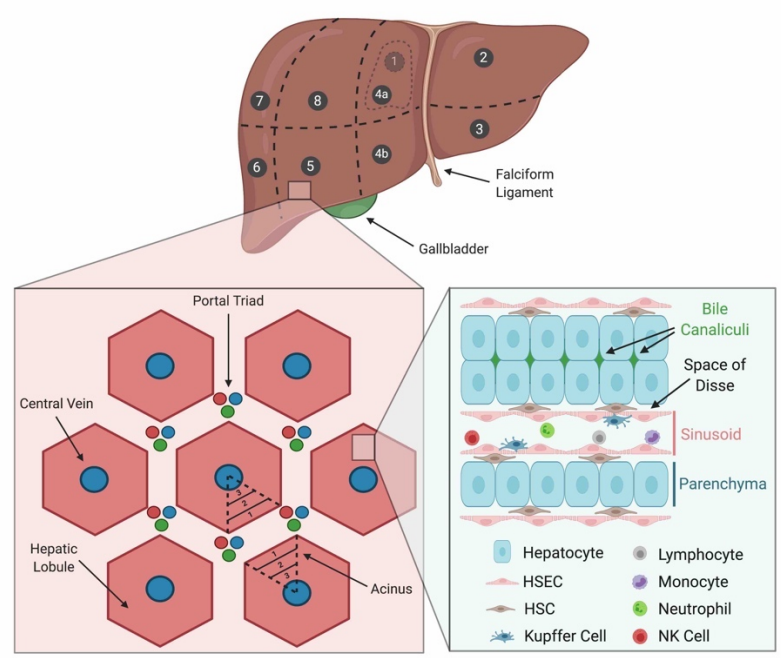

Figure 1.2: The structural anatomy of the liver.

The liver is grossly made up of two lobes, separated by the falciform ligament, and can be further sub-divided into eight distinct anatomical segments. Hepatic lobules are supplied by the portal triads and comprise hepatocytes arranged in one- or two-cell thick cords which span three metabolic zones. These polarised epithelia form bile canaliculi at their apical surface and are flanked by fenestrated endothelia which line the hepatic capillary beds known as the sinusoids. The hepatic sinusoids are resident to several non-parenchymal cell types, including hepatic stellate cells (HSC) and Kupffer cells, and are the sites of leukocyte extravasation during inflammation, including lymphocytes, monocytes, neutrophils and natural killer (NK) cells.

1.3 Liver Function

The liver is estimated to perform around 500 physiological functions, including biotransformation and detoxification of xenobiotic and pharmacological substances, metabolism of dietary carbohydrates, proteins and lipids, glycogen synthesis and storage, production of plasma proteins, hormones and bile, and removal of waste products such as spent erythrocytes and bilirubin (**Figure 1.3**). These most notable functions will be discussed in more detail below.

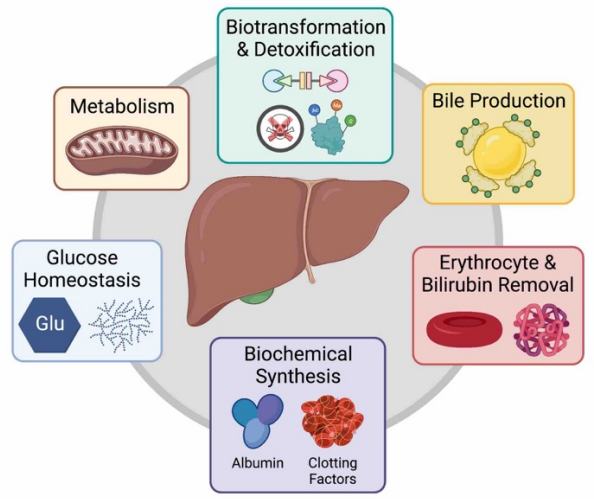

Figure 1.3: The primary functions of the liver are carried out predominantly by hepatocytes.

These include: biotransformation and detoxification of xenobiotic products; protein and lipid metabolism; glucose homeostasis and glycogen storage; removal of spent erythrocytes and haemoglobin in the form of bilirubin; bile production to aid lipid emulsification and absorption; and synthesis of biochemical molecules including albumin, clotting factors and arachidonic acid.

1.3.1 Biotransformation and Detoxification

The liver plays a pivotal role in drug metabolism and detoxification of xenobiotic products[28]. Orally administered drugs, including alcohol, access the liver via the portal vein and undergo first pass metabolism. This has important implications for pharmacology, since hepatic drug metabolism can produce more or less pharmacologically active metabolites than the parent drug, as well as toxic metabolites.

Phase I metabolic reactions involve microsomal enzymes, such as cytochrome P450 (CYP) enzymes, which mediate oxidation, reduction and hydrolysis reactions[20, 29]. Occasionally, the liver can metabolise

"pro-drugs" into more pharmacologically active compounds, as is the case for opioids such as codeine and tramadol, which are converted to morphine via *O*-demethylation by CYP2D6 enzymes[29, 30]. Some drugs can also induce expression of CYPs, such as alcohol, which upregulates CYP2E1 activity to facilitate breakdown[31, 32]. Alcohol dehydrogenase and aldehyde dehydrogenase within the hepatocyte cytoplasm are also important for alcohol metabolism[33]. Alcohol is known to elicit hepatotoxic effects, owing to its metabolism to acetaldehyde which is both toxic and carcinogenic[34], and due to CYP2E1-induced oxidative stress via generation of reactive oxygen species (ROS)[35, 36].

Several other xenobiotic substances can display profoundly hepatotoxic effects which are typically absorbed via ingestion of contaminated food products. Some examples include aflatoxin B1, which is a fungal mycoprotein that can be found on contaminated grains and nuts[28, 37], and polycyclic aromatic hydrocarbons, which can be generated during food processing[38]. The liver is tasked with detoxification of these harmful products; failure to do so poses the risk that the liver will succumb to acute chemical-induced toxicity or chronic hepatitis and/or HCC[28, 37-39].

Phase II metabolic reactions generally involve conjugation of phase I metabolites, namely, glucuronidation, acetylation and methylation, amongst others[20]. This usually results in pharmacological inactivation and increased solubility, enhancing their secretion in urine and/or bile[20]. In contrast to phase I reactions, phase II conjugation reactions remain relatively stable in chronic viral hepatitis and established cirrhosis[40, 41]. Although biotransformation performs an indispensable role, potential for generation of metabolites and metabolic conjugates with higher toxicity than the parent provides a mechanism for metabolic injury to occur. This is the case for acetaminophen (paracetamol) which can cause lethal hepatoxicity and liver failure following overdose[42, 43].

1.3.2 Metabolism

Protein and lipid metabolism are mediated by hepatocytes within the liver[12, 19]. Amino acids from the gastrointestinal tract undergo transamination and deamination, producing toxic ammonia as a by-product, which is subsequently removed via the urea cycle[20]. These reactions are mediated by specific

transaminase enzymes, including aspartate transaminase (AST) and alanine transaminase (ALT)[20]. The levels of these enzymes are elevated in almost all liver diseases, and the ratio between them is often used as a diagnostic indicator of parenchymal liver damage, with a ratio of more than 2 indicating alcoholic steatosis and cirrhosis[44, 45].

Fat provides up to 90% of an individual's dietary needs during prolonged starvation, which is fuelled by β-oxidation of free fatty acids within hepatocyte mitochondria[20, 46]. Fatty acids derived from insoluble dietary lipids in the gut are used to synthesise triglycerides and lipoproteins in the liver, including triacylglycerol, very-low-density lipoproteins (VLDLs), high-density lipoproteins (HDLs) and cholesterol[20]. Hepatic lipase hydrolyses triglycerides in lipoproteins, converting VLDLs into low-density lipoproteins (LDLs)[20, 47]. HDLs circulate in the plasma acting as cholesterol scavengers, and thus, are considered protective against atherosclerosis[48]. The liver also plays a key role in cholesterol removal via excretion as bile salts or sterols[19].

1.3.3 Glucose Homeostasis and Glycogen Storage

The liver is a key player in regulation of glucose homeostasis, with blood glucose levels being maintained at around 90 mg/dL[12, 19]. Following consumption of dietary carbohydrates, glucose is absorbed by perivenous hepatocytes and glycogen is produced. This glycogen is stored in the liver, and can be broken down into glucose by glucose-6-phosphatase during glycogenolysis[20]. Thus, the liver acts as a glucose reservoir. Synthesis of glucose from non-carbohydrate sources, such as amino acids, lactate and glycerol, can also occur during a process called gluconeogenesis[20]. This is essential for maintaining glucose levels during starvation when glycogen levels are depleted.

1.3.4 Biochemical Synthesis

The liver acts as the predominant source of plasma proteins, namely albumin, which regulate oncotic pressure of the blood[49]. The liver is also the primary producer of coagulation factors prothrombin, fibrinogen, and factors V, VII, IX, and XIII[19]. The importance of these factors is exemplified by their defective production, resulting in coagulation disorders characterised by spontaneous bruising,

prolonged bleeding and risk of haemorrhage[50]. Since the liver is the main producer of clotting factors and is also responsible for clearance of activated clotting factors and synthesis of fibrinolytic products, severe liver dysfunction is associated with both coagulopathy and disseminated intravascular coagulation[50].

Several other bioactive molecules are synthesised in the liver, including enzymes, steroids, hormones, growth factors and bioactive lipids. For instance, the liver is the principal site of thrombopoietin synthesis, which regulates platelet production within the bone marrow[51]. The liver also produces angiotensinogen, a precursor for angiotensin, which is important for regulating blood pressure[52]. Further, CYP enzymes are important in the production of arachidonic acid, which is a precursor of eicosanoids, such as prostaglandins and thromboxane[53, 54]. The liver can also be involved in hormone activation and inactivation; it converts inactive cholecalciferol to 25-hydroxycalciferol, which is essential for vitamin D metabolism, whilst inactivating insulin, glucagon, glucocorticoids, thyroxine and growth/sex hormones[19, 20].

1.3.5 Erythrocyte and Bilirubin Removal

Erythrocytes, or red blood cells, have a circulating lifespan of approximately 115 days, after which time they become senescent and are decomposed by the reticuloendothelial system[55]. The liver is a major site for this process. Erythrocytes possess a cholesterol-rich lipid bilayer for a cell membrane and contain haemoglobin which facilitates oxygen transport. Kupffer cells (KCs) remove the globin and iron groups from haemoglobin, where they are re-used and recycled via transferrin, respectively[19]. Haem is then catabolised by KCs into bilirubin which is subsequently biotransformed and excreted into the bile by hepatocytes[20]. Liver failure is often characterised by jaundice[56], which arises as a result of elevated bilirubin concentrations, causing yellow discolouration of the eyes and skin.

1.3.6 Bile Production

Numerous endogenous and exogenous substances are primarily excreted via the biliary tract[20]. Hepatocytes are separated by tight junctions which form a relatively small apical lumen known as the

bile canaliculus, into which hepatocytes secrete bile[57]. Bile canaliculi form a network between hepatocytes, where bile flows through the intra-hepatic small bile ductules and ultimately, is stored and concentrated in the gallbladder before draining to the duodenum[11]. Bile is a fluid composed of water, electrolytes, bile salts, cholesterol, phospholipids and bilirubin, synthesis of which occurs at a rate of roughly 0.6–1.2 L/day[12, 19]. Bile salts are amphipathic which aids the emulsification of lipids in the gastrointestinal tract[20]. Bile salts are then reabsorbed in the distal ilium and returned to the liver in a circuit known as the enterohepatic recycling system[20, 57]. Thus, bile facilitates both absorption and digestion of dietary lipids and excretion of metabolites and cholesterol. Cholestasis, in which there is an obstruction in bile flow, is a hallmark of cholestatic liver diseases including primary biliary cholangitis (PBC) and primary sclerosing cholangitis (PSC).

1.4 Liver Vasculature

The liver is a highly vascularised organ which receives 25% of the cardiac output (1–2 L/min)[11, 18]. It has a dual blood supply, with around 75% blood coming from the gastrointestinal tract, pancreas and spleen via the hepatic portal vein, whilst the remaining 25% is supplied by the hepatic artery[16, 18]. The region where the hepatic artery and hepatic portal vein, together with the common bile duct, enter the liver's ventral surface is known as the hilum[19]. Blood flow within the sinusoids is low (400-450 mm/s) compared with most other tissue capillary beds (500-1000 mm/s) which maximises the time for fluid and solute exchange to occur[11, 12]. Thus, the liver is uniquely positioned to carry out its metabolic and detoxifying function.

Partially oxygenated and nutrient-rich blood enters the liver lobules via portal venules where it mixes with arterial blood in the periportal zone[11, 17]. Blood then travels through the sinusoids, collecting within the central veins which merge to form hepatic veins that drain into the inferior vena cava[17, 18]. Due to the architecture of the liver lobule and the spatial arrangement of hepatocytes relative to the vasculature[20], hepatocytes span three designated zones (**Figure 1.2**), in which they are exposed to distinct metabolic conditions[58-61]. Zone 1 (periportal) hepatocytes are located near the portal triads where

oxygen and nutrients are plentiful, whilst zone 3 (pericentral) hepatocytes lie closest to the central vein and are thus subject to hypoxic conditions. Zone 2 (midlobular) hepatocytes are equidistant from the portal triad and draining central vein (**Figure 1.4**).

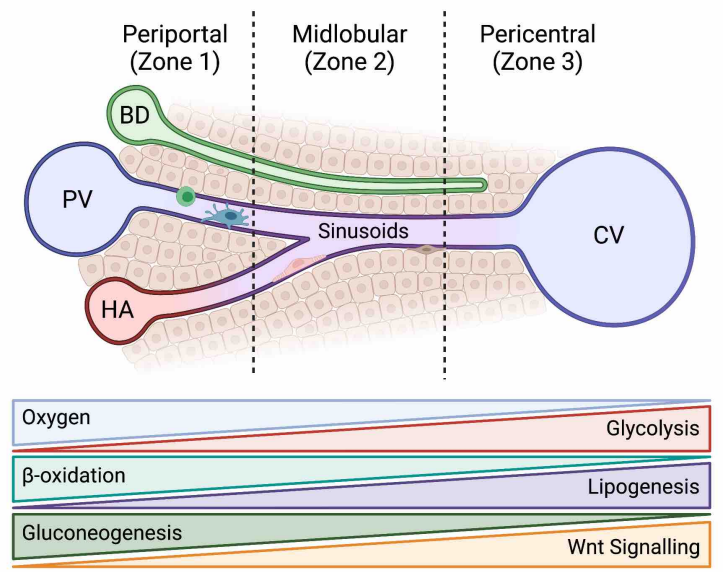

Figure 1.4: The liver structure and vasculature create biochemical gradients that span the liver lobule which can be separated into three distinct metabolic zones.

The periportal zone (zone 1) is rich in oxygen and nutrients, where oxidative metabolic functions dominate, including β-oxidation and gluconeogenesis. The pericentral zone (zone 3) favours glycolysis and lipogenesis. Liver zonation is controlled by Wnt signalling. Zonation has been reported not just for hepatocytes but for multiple hepatic cell types, including hepatic stellate cells, hepatic sinusoidal endothelial cells and resident immune cell populations.

Metabolic zonation is controlled by Wnt signalling[62, 63], and has been reported for carbohydrate, lipid, amino acid, ammonia and xenobiotic metabolism[58, 60, 61]. For instance, oxidative metabolic functions, such as β-oxidation, gluconeogenesis, and amino acid metabolism, are concentrated in the periportal hepatocytes[20]. In contrast, pericentral hepatocytes carry out biotransformation, lipid synthesis and glycolysis[20, 28]. This allows the capacity of key metabolic pathways to preferentially lie in one zone or another, which is advantageous since it allows spatial separation of opposing pathways, and thus prevents competition for common substrates and futile cycles[58]. Zonation for other liver cell types has also been described, including hepatic stellate cells (HSC) and HSEC[64-67]. Moreover, "immune zonation" is created by the periportal positioning of myeloid and lymphoid resident immune cells to promote host defence, and is thought to be driven by constitutive exposure of HSEC to the commensal

microbiome[68]. Disruption of metabolic zonation occurs during parenchymal injury and cirrhosis, whereby fibrosis and septum formation lead to portal hypertension and a "metabolism-perfusion mismatch", which contributes to hepatic dysfunction[20].

1.5 Liver Cells

The most abundant cells within the liver are parenchymal cells, namely hepatocytes, which perform the dominant roles of the liver[69]. There are also several types of non-parenchymal cells, which collectively represent around 40% of all liver cells but only 6.3% of the total liver mass, including HSEC, KCs, HSCs, biliary epithelial cells (BEC) and liver-resident lymphocyte populations[16, 21]. These cell types regulate liver function and control the microenvironment[69]. There is considerable crosstalk between parenchymal and non-parenchymal cell types, including exchange of materials, ligand-receptor interactions and signal transduction, which is critical for maintaining liver function and homeostasis[69, 70].

1.5.1 Parenchymal Cells

Hepatocytes are the principle parenchymal cell type, comprising approximately 60% of the total liver cells and roughly 78% of the total liver volume[21]. Hepatocytes are polarised cuboidal-shaped epithelia with large basolateral surfaces and a small apical surfaces, linked by tight junctions, which form bile canaliculi[57] (**Figure 1.2**). They are biochemical powerhouses, possessing abundant mitochondria, endoplasmic reticulum and microsomal enzymes which are crucial for liver function[71]. Hepatocytes have nuclei with round dispersed chromatin and prominent nucleoli[71]; they are often multinucleate with as many as 30-40% displaying polyploidy in adult human liver[72]. Generally quiescent under steady state conditions, hepatocytes have a lifespan of around five months and can proliferate following injury, facilitating self-renewal and repair[57, 73, 74].

1.5.2 Non-parenchymal Cells

Non-parenchymal cell types reside in close proximity to hepatocytes (**Figure 1.2**) and have key roles in both physiology and pathogenesis. The most abundant non-parenchymal cell type (~ 45%) are HSEC,

which represent approximately 5-20% of all liver cells but only around 3% of the total liver volume[16, 21]. Hepatocyte chords are flanked by HSEC which line the hepatic sinusoids (**Figure 1.2**); these are highly specialised discontinuous endothelia that form a unique barrier between the bloodstream and the parenchyma. There are several structural features of HSEC which facilitate their function, including their lack of basement membrane, presence of fenestrations arranged in sieve plates, and expression of numerous endocytic and scavenger receptors[24, 75, 76]. Collectively, these features render HSEC the most permeable endothelial cells, with the most powerful scavenging capacity, in the mammalian body. Thus, HSEC facilitate fluid and nutrient exchange which is crucial for maintaining metabolic homeostasis and sustaining hepatic function. HSEC also play an essential role in hepatic immune responses, acting as gatekeepers and regulating the immune microenvironment during homeostasis and inflammation by orchestrating leukocyte recruitment[75, 77]. The physiological and pathophysiological roles of HSEC in maintaining homeostasis and influencing the inflammation-cancer axis have been extensively reviewed[76].

Hepatic stellate cells (HSCs), also known as pericytes or Ito cells, represent 5-8% of liver cells[21] and reside within the space of Disse between the sinusoidal endothelium and the hepatocytes (**Figure 1.2**). These astral-like cells envelop the sinusoids via extension of long dendritic processes. HSCs are a major source of retinoids, storing 50-80% of the body's vitamin A in the form of retinyl palmitate within cytoplasmic lipid droplets[78, 79]. They are also contractile cells expressing alpha smooth muscle actin (αSMA), and their positioning around the sinusoid exterior allows them to regulate hepatic blood flow in response to paracrine signals from neighbouring cells[80, 81]. Whilst HSCs maintain normal tissue architecture by controlling extracellular matrix (ECM) turnover, they are a major contributor to fibrosis, undergoing transformation into aberrant fibrogenic myofibroblasts in response to chronic inflammation and injury[82].

BEC, or cholangiocytes, line the bile ducts and represent 3-10% of liver cells[71]. They are less metabolically active than hepatocytes, yet still have some metabolic functions including bicarbonate synthesis[57]. Cholangiocytes are responsible for modification of primary bile, produced by hepatocytes,

by secreting water, bicarbonate and cations that represent around 30% of the total bile volume[71]. These cells are also the target of immune-mediated cholestatic diseases PBC and PSC.

1.5.3 Immune Cells

KCs are the self-renewing tissue-resident macrophages which permanently reside within the hepatic sinusoids (**Figure 1.2**) and represent around 2.1% of the total liver mass[21]. They act as immune sentinels, sensing and responding to danger signals following parenchymal injury[83]. KCs express an array of pattern recognition (PRR) and scavenger receptors (SR) meaning they can recognise a variety of food- and microbial-derived antigens. KCs are also part of the reticuloendothelial system which is responsible for removal of spent erythrocytes, playing a key role in haemoglobin metabolism and excretion in the form of bilirubin[19, 20].

There are also several liver-resident lymphocyte populations, which are phenotypically and functionally distinct from circulating lymphocytes, and have roles in both health and disease[84, 85]. Many of these liver-resident cells express adhesion molecules such as CD44, CD103 and CD49a, which aid tissue retention, and lack lymphoid homing markers (e.g. CCR7 and CD62L) and tissue egress receptors (e.g. sphingosine-1-phosphate receptor and CD69)[86, 87]. Natural killer (NK) cells are enriched in the liver representing 1% of the total liver mass[71]. These are innate cells important for immune surveillance and they mediate immune responses towards virally-infected or cancerous cells. Similarly, NKT cells, which share properties of NK cells and T lymphocytes, localise within the hepatic sinusoids and elicit a patrolling phenotype[88]. Together, NK and NKT cells constitute approximately 50% of total intrahepatic lymphocytes[89]. Type I NKT cells, also known as invariant NKT (iNKT) cells, possess a semi-invariant T cell receptor (TCR), whilst type II NKT cells express a variable TCR[90]. Liver-resident B cells are thought to account for up to 8% of the total lymphocyte population, whilst there are also populations of conventional and non-conventional T lymphocytes that serve as frontline defenders but have also been implicated in CLD. These include memory $CD8^+$ T cells, γδ T cells (3-5% of total liver lymphocytes), innate lymphoid cells (ILCs) and mucosal-associated invariant T (MAIT) cells[84].

1.5.4 Cell-cell Crosstalk in Homeostasis

The parenchymal structure and its spatial organisation with respect to non-parenchymal liver cells facilitates the co-operative interactions between cell types (**Figure 1.2**). Material exchange between the portal circulation and the parenchyma is mediated by HSEC, due to their fenestrated and endocytic phenotype, allowing hepatocyte oxygenation and uptake of macromolecules. Liver cells remain in close proximity via receptor-ligand interactions. For example, stromal-derived factor 1α (SDF1α) released by HSC interacts with chemokine receptor CXCR4 on HSEC, whilst HSEC secrete platelet-derived growth factor β (PDGFβ) which binds to HSC PDGFRβ[76, 91].

Juxtacrine and paracrine signalling also plays a key role in facilitating cell-cell crosstalk. The well-organised ECM provides a structural and biochemical environment for this communication to occur and contributes to cellular programming. For instance, release of vasoactive mediators from neighbouring hepatocytes and HSEC impact HSC contractility, which is key for regulating vascular blood flow within the sinusoids[76, 92]. Specifically, HSEC respond to shear stress by producing nitric oxide (NO), via activation of transcription factor Krüppel-like factor 2 (KLF2) and subsequent stimulation of endothelial nitric oxide synthase (eNOS) activity[93-95]. Simultaneously, KLF2 activation downregulates expression of vasoconstrictive mediators, such as endothelin 1 (ET-1)[96], and collectively, these effects act on HSC to maintain their quiescence and promote vasodilatory responses[97]. Concomitantly, the HSEC phenotype is maintained by vascular endothelial growth factor (VEGF), released by hepatocytes and HSC, in a paracrine manner[98].

Following liver injury, hepatocytes release factors which influence surrounding cells, including transition of quiescent HSCs into myofibroblast-like cells and activation of KCs, which recognise danger-associated molecular patterns (DAMPs)[83]. Equally, hepatocytes are regulated by mediators released from non-parenchymal cells during both homeostasis and pathophysiology. For instance, HSEC and HSCs release growth factors (e.g. hepatocyte growth factor (HGF)) that can mediate hepatocyte proliferation and regeneration, whilst KCs produce enzymes and cytokines that may damage hepatocytes during liver injury and inflammation[83, 92].

1.6 Liver Immunology

Although the primary functions of the liver are not traditionally considered to be immunological, it has been proposed as an immune organ, since the liver performs many essential immune tasks including induction of tolerance, immune surveillance, and the ability to mount effective immune responses[16, 99, 100]. The liver is home to a significant proportion of all tissue-resident immune cells, whilst hepatocytes are responsible for production of 80-90% of innate immunity proteins (e.g. acute-phase proteins and complement) in the circulation[99, 101]. Furthermore, due to its anatomical location and dual blood supply, the liver is ideally positioned to screen the blood for toxic agents and gut-derived pathogens. Moreover, the liver is uniquely equipped with the immune machinery to induce both tolerogenic and immunogenic responses, which result from the complex interactions between liver-resident immune sentinels and recruited leukocyte populations. The balance between tolerance and immunity is not only essential for liver function but also impacts the fate of liver injury – resolution and maintenance of homeostasis or persistence and chronic inflammation.

1.6.1 Immune Tolerance

Although the liver forms a barrier against harmful gut-derived toxins and pathogens, the portal blood supply is also a source of harmless foreign molecules, such as food and commensal microbial antigens. Thus, the liver remains immunotolerant and anti-inflammatory by default, so as not to initiate constant inappropriate immune responses. The maintenance of liver-mediated immune tolerance requires complex interactions between hepatocytes, non-parenchymal cells and immune cells.

Both professional and non-professional antigen presenting cells (APCs) contribute to the maintenance of immune tolerance[102]. KCs and HSEC are poor activators of the adaptive immune response under basal conditions, which is attributed to insufficient co-stimulation, low level expression of major histocompatibility complex (MHC) and constitutive production of anti-inflammatory cytokines such as IL-10[103-109]. HSEC express both MHC class I and MHC class II, meaning they are capable of antigen cross-presentation to $CD8^+$ T cells as well as priming of naïve $CD4^+$ T cells[110-113] (**Figure 1.5**). T cell

tolerance is actively induced by HSEC expression of programmed death ligand 1 (PD-L1), which engages inhibitory receptor programmed cell death protein 1 (PD-1) on T cells to elicit alternative activation[109, 111, 113, 114]. Strikingly, HSEC cross-present soluble antigen more proficiently than dendritic cells (DCs), although this is limited to a short time frame due to their superior transcytotic transport[102, 115]. HSEC presentation of a cognate antigen fails to stimulate cytotoxic effector responses and cytokine production despite inducing rapid T cell proliferation[109-111, 114]. Thus, antigen presentation by HSEC can activate $CD8^+$ T cells, however these assume an anergic-like phenotype and lack their conventional cell killing function. Despite their refractory phenotype, HSEC-primed $CD8^+$ T cells assume capacity for memory, and are able to migrate to the lymph nodes where they can elicit immunogenic responses upon re-stimulation in the presence of co-stimulatory molecules[116]. This provides a mechanism whereby quiescent $CD8^+$ T cells are not lost from the T cell repertoire but instead can offer protection in response to future infectious injury.

Similar to HSEC induction of $CD8^+$ T cell tolerance, HSEC antigen presentation to $CD4^+$ T cells via MHCII under steady state conditions results in transforming growth factor β (TGFβ)-mediated induction of regulatory T cells (T_{reg}), which act to suppress immune responses[117]. Indeed, it has been shown that, in contrast to T_{reg} induced by professional APCs, HSEC-induced T_{reg} which lack transcription factor Forkhead-Box-Protein P3 (FoxP3) are particularly immunosuppressive[118]. In addition to their antigen presentation capabilities, HSEC can also inhibit bystander T cell activity directly, via liver sinusoidal endothelial cell lectin (LSECtin)[119], and indirectly, via intercellular adhesion molecule 1 (ICAM1) which impedes DC-mediated antigen presentation[120].

Liver dendritic cells (DCs) are also tolerogenic by default. Both $CD11c^{hi}$ myeloid DCs (mDCs) and $CD123^+$ plasmacytoid DCs (pDCs) are poor T cell activators when compared with DCs originating from other tissues[121-123]. This is thought to be due to anti-inflammatory cytokine secretion (e.g. IL-10), co-inhibitory molecule expression (PD-L1), and lack of co-stimulatory molecules[121, 123]. T_H2-type responses are also favoured over T_H1-type responses due to DC-derived IL-10, suppressing cellular immunity and driving T_{reg} differentiation[124]. In mice, two additional DC populations have been identified, which

display seemingly opposing responses. $CD11c^+CD8^+$ lymphoid DCs permit robust T cell activation characterised by production of IL-12 and TNFα, and $CD11c^+NK1.1^+$ cytotoxic DCs drive efficient T cell activation and elicit direct cytotoxic effects against cellular targets[121, 125, 126]. This diversity in the liver DC population is thought to maintain the balance between tolerance and immunity.

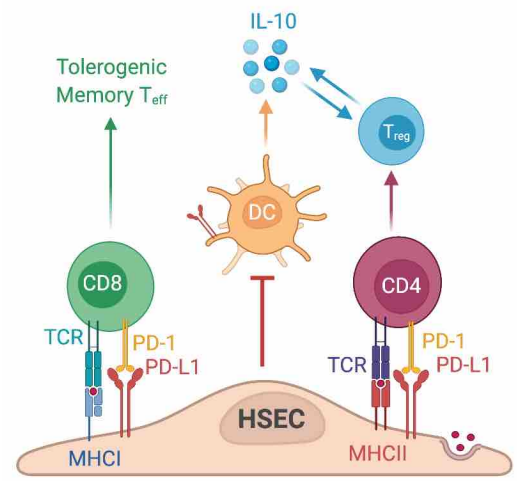

Figure 1.5: Antigen presentation by hepatic sinusoidal endothelial cells (HSEC) via major histocompatibility complex (MHC) I and II is an important mechanism for induction of immune tolerance within the liver.

Expression of programmed cell death ligand 1 (PD-L1) on HSEC induces tolerogenic memory $CD8^+$ T cells which lack their cytotoxic properties, and regulatory $CD4^+$ T cells which produce immunosuppressive cytokine interleukin 10 (IL-10). HSEC can also directly inhibit dendritic cell (DC)-mediated antigen presentation.

Hepatocytes are also capable of antigen cross-presentation, priming naïve $CD8^+$ T cells but failing to provide survival factors[127, 128]; this results in T cell deletion rather than expansion[129]. In addition, hepatocytes can acquire MHCII during inflammatory states[130], although the contribution of hepatocyte-mediated $CD4^+$ T cell activation to local and systemic immune responses remains to be fully elucidated.

HSCs also have immunoregulatory capacity. Whilst the antigen presentation abilities of HSC remain controversial, they are known to drive generation of tolerogenic indoleamine 2,3-dioxygenase $(IDO)^+$ DCs[131] and differentiation of myeloid-derived suppressor cells from circulating monocytes[132]. Inducible expression of PD-L1 by HSCs can inhibit T cell responses via B7-H1-mediated apoptosis[133]. HSC also orchestrate induction of T_{reg}, in the presence of DCs, which is likely mediated by retinoid metabolites[134]. Furthermore, inhibition of DC-mediated $CD8^+$ T cell priming is induced by HSCs via a CD54-dependent mechanism[135].

The tolerogenic environment of the liver is exemplified by the relative success of liver transplantation and the persistence of hepatotropic viruses which exploit the liver's nature for immunosuppression.

1.6.2 Immune Surveillance

An increasing body of evidence suggests that the liver is a primary surveillance mechanism for intravascular infections, contrary to the prevailing view that it is the spleen, which represents the predominant first line of defence against blood-borne pathogens. In fact, there is considerable functional redundancy of the spleen following splenectomy, aside from a handful of encapsulated bacteria[100]. The same cannot be said for the liver's immune surveillance system, highlighting its pivotal role in host defence and survival[136-138]. The capacity of the liver to identify and neutralise infectious agents is a product of both liver anatomy (i.e. anatomical location and dual blood supply) and cellular composition (**Figure 1.2, Figure 1.6**). Aside from housing the largest proportion of tissue-resident macrophages (KCs)[99], which contribute to the most expansive reticuloendothelial network in the body, the liver is also enriched for NK and NKT cells. Collectively, the liver and immune sentinel cell populations residing within it, are designed to maximise immune surveillance.

Natural killer cells, which represent around half of all liver-resident lymphocytes[89, 100], play a crucial role in screening for infection and tissue pathology[139]. In contrast to other immune sentinels, which identify potential threats by searching for foreign antigens (i.e. PAMPs), NK cells recognise targets by probing for absence of self[99]. Both infected and cancerous cells downregulate antigen-presenting machinery as a mechanism of immune evasion[99]. This absence of self is utilised by NK cells to target pathological cells for destruction. Specifically, NK cells express activating and inhibitory receptors; failure of self-molecules to interact with inhibitory receptors leads to NK cell activation and target killing mediated by cytotoxic perforin and granzyme release[100]. Despite the notion that NK cells are innate lymphocytes, increasing evidence suggests they are capable of generating memory, resulting in rapid and stronger responses following secondary viral infection[140, 141].

The role of iNKT cells in immune surveillance has been well-established. The liver is home to the largest proportion of iNKT cells which continuously patrol the sinusoids, even under basal conditions, and play a key role in orchestrating immune responses[99, 142]. These cells form in the thymus as $CD4^-CD8^-$ precursors, but develop into $CD4^+CD8^+$ cells, randomly rearranging their TCRs which generally recognise a selection of glycolipid antigens presented by CD1d[143]. There are also iNKT cells of double-negative origin which bypass the $CD4^+CD8^+$ stage and elicit strong cytotoxicity towards tumour cells[144].

The first identified and most potent glycolipid antigen recognised by iNKT cells is α-galactosylceramide (αGalCer), an event which is conserved in mice and humans and leads to specific iNKT activation[145]. Liver iNKT cells express high levels of chemokine receptors CCR5 and CXCR3 which are key for directing iNKT cells in particular inflammatory states. Following TCR stimulation, iNKT cells have rapid effector potential, owing to their activation in the absence of co-stimulation[146]. Their effector functions resemble those of conventional cytotoxic T cells, yet their rapid responses suggest iNKT cells are an important component of innate immunity[147, 148]. Indeed, iNKT cells can rapidly release a combination of pro-inflammatory and anti-inflammatory cytokines depending on the stimulus, type of antigen presenting cell (APC), and cytokine milieu, demonstrating their role in shaping the immune microenvironment[99, 148, 149]. Specifically, KC presentation of bacterial glycolipids to iNKT cells initiates release of pro-inflammatory interferon γ (IFNγ)[137], whilst recognition of endogenous glycolipid self-antigens from dead cells drives an anti-inflammatory regenerative response characterised by interleukin 4 (IL-4) production and hepatocyte proliferation[150].

Similar results have also been shown for HSCs pulsed with αGalCer[151]. HSCs can release IL-15 which drives proliferation of activated NKT cells[151]. NKT cells can also be activated by hepatocytes[152], which release IL-4, in contrast to DC-activated NKTs which predominantly display an IFNγ-mediated response[153]. Interestingly, IFNγ release was only possible in the presence of exogenous IL-12 following hepatocyte presentation, in contrast to HBV-infected hepatocytes which were able to initiate an IFNγ response in isolation[153, 154].

In addition to NK and NKT cell populations, $CD8^+$ T cells actively patrol the sinusoids by crawling along the endothelium and extending cell processes through endothelial fenestrations in search for infected hepatocytes[25, 26]. Following recognition of a cognate antigen, these cells firmly adhere to the hepatocyte and directly kill the infected cell in a diapedesis-independent manner[26]. Furthermore, HSEC can cross-present antigens from virally-infected hepatocytes, stimulating TNFα release from cross-primed effector cytotoxic T lymphocytes (CTL) and subsequent caspase-mediated killing of infected hepatocytes[155].

1.6.3 Immunogenic Responses

The liver appears to be the most dominant organ at responding to infections with the exception of a few encapsulated bacteria. Consequently, most liver failure patients die primarily of infection due to defective liver-mediated immune responses. The liver can mount an innate immune response within seconds of exposure to blood-borne pathogens; this occurs via several mechanisms which are outlined below (**Figure 1.7**).

Due to its positioning directly downstream of the gut, the liver is constantly exposed to pathogen-derived molecules, such as lipopolysaccharide (LPS)[156]. Additionally, in the case of intestinal epithelial damage, whole intact pathogens can translocate and gain access to portal blood[157]. Whilst some translocated pathogens drain to the mesenteric lymph nodes via the lymphatic system[158], the majority bypass classic immune sentinel tissues and are delivered to the liver via the portal system. The low blood flow within the hepatic sinusoids (roughly half that of other capillary beds) not only allows sufficient time for nutrient and solute exchange to occur, but also maximises the contact between the blood and KC/HSEC to facilitate immunological filtration[99, 100].

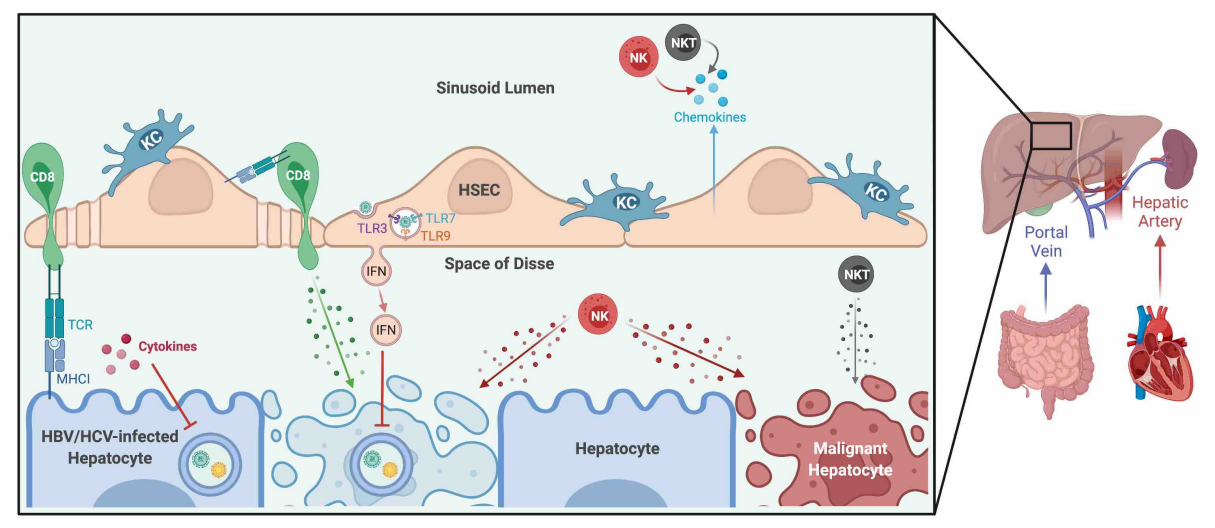

Figure 1.6: Immune surveillance in the liver is facilitated by its anatomy and dual blood supply, along with its enriched populations of innate and adaptive immune cells.

Along with housing the largest population of tissue-resident macrophages (Kupffer cells, KCs) which screen the blood for foreign antigens, the liver is also home to many NK and NKT cells which actively patrol the sinusoids in search of the absence of self. This is a characteristic of both virally-infected and malignant hepatocytes, which downregulate antigen presentation machinery in attempt to evade the host immune system. $CD8^+$ T cells also play an active role in hepatic immune surveillance, crawling along the endothelium and probing for virally-infected cells by extending cell processes through endothelial fenestrations. Hepatic sinusoidal endothelial cells (HSEC) also contribute to anti-viral responses, releasing interferons (IFN) which inhibit viral replication following recognition of viral particles by intracellular toll-like receptors (TLRs).

KCs represent around 35% of non-parenchymal liver cells and 90% of all tissue-resident macrophages[99]. They are tasked with the discrimination of a few pathogens, amongst the millions of blood cells, and subsequent capture of these pathogens under flow conditions. Whilst complement receptors (e.g. CR1-4) recognise opsonins such as C3b on the pathogen surface, only complement receptor of the immunoglobulin superfamily (CRIg) is able to bind C3b and inactivated C3b under conditions of shear stress[138, 159, 160]. CRIg also acts as a PRR, meaning KCs can capture circulating gram-positive bacteria via direct binding to lipoteichoic acid in the absence of complement[161].

Both KCs and HSEC also express a plethora of scavenger receptors and PRRs which allow them to bind, detect and internalise pathogens and pathogen-associated molecules[162, 163]. For instance, dietary LPS is cleared by the liver via recognition by TLR4 on KC and HSEC[162]. Indeed, LPS concentration drops 100-fold between portal blood and peripheral venous blood[156]. Despite induction of tolerogenic responses following exposure to low level LPS, KCs and HSEC are able to drive T cell activation in the presence

of high antigen concentrations[164, 165] via enhanced TCR signalling, or in the presence of other pathogen-associated molecular patterns (PAMPs) which are recognised by PRRs (e.g. TLR3/9)[103, 166]. These receptor-ligand interactions drive activation of KCs and HSEC, leading to phagocytosis (or receptor-mediated endocytosis in the case of HSEC) and/or release of cytokines and chemokines, which facilitate leukocyte recruitment and allow neutralisation of microbial threats.

Another mechanism by which the liver rapidly targets invading pathogens for destruction is the formation of neutrophil extracellular traps (NETs)[167]. In response to pathogen invasion, neutrophils and platelets are rapidly recruited to the infection site within minutes of exposure, as has been demonstrated in elegant intravital microscopy studies[168-170]. Platelet aggregation on the neutrophil surface drives the formation of NETs within the sinusoids[168, 169]. NETosis is the process whereby neutrophils release webs of decondensed nuclear DNA containing several cytotoxic and antimicrobial molecules, including histones, neutrophil elastase, defensins and lysozymes[167]. These NETs ensnare bacteria and viruses in the bloodstream and act to limit pathogen dissemination[167-169].

Cellular debris and immune complexes also undergo clearance in the liver. Hepatocytes, KCs, HSCs, and BEC have all been shown to clear apoptotic cells[171-175], whilst KCs are known to remove activated neutrophils and platelets from the circulation[176, 177]. Small circulating immune complexes are cleared predominantly by HSEC via Fcγ receptor IIb (CD32b)[178, 179] whilst larger complexes are removed by KCs[180, 181]. Nevertheless, HSEC have previously been shown to internalise macromolecules up to 1 μm in diameter, via their array of scavenger receptors[163, 182]. These processes are essential for initiating resolution of inflammation and maintaining homeostasis.

Although not traditionally classed as a secondary lymphoid organ, the liver represents an environment which fosters development and function of adaptive immune responses (**Figure 1.7**). Numerous liver cells are capable of antigen presentation, including KCs, HSEC, hepatocytes and BEC, as well as DCs and macrophages[102, 183]. This, paired with the capacity for rapid recruitment of immune cells, makes the liver a key organ in which adaptive immune responses are initiated. Under steady state conditions, the

liver's default response is immunotolerance, which allows expansion of cognate T lymphocytes but prohibits cytotoxic effector functions. Liver-resident cells sustain immune hyporesponsiveness by functionally suppressing the adaptive immune response[107, 121, 123, 128]. However, following phagocytic engulfment of pathogens in the presence of several PAMPs (e.g. TLR3/9 ligands) and/or inflammatory cytokines, KC antigen presentation is a key step in driving an immunogenic response and robust T cell activation[103, 166]. As mentioned previously, KCs are also potent activators of iNKT cells following bacterial capture by antigen presentation via CD1d[137]. Furthermore, HSEC are capable of mounting effective CTL responses in the presence of high antigen concentrations[164], mediated by strengthened T cell receptor (TCR)-MHC signalling and IL-2 release which overcomes the PD1-PD-L1 signalling axis[165].

B cells also comprise an important arm of the hepatic adaptive immune system. These antibody- and cytokine-producing cells are usually found within the spleen and secondary lymphoid tissues, yet liver-resident B cells comprise up to 8% of the hepatic lymphocyte population. Futhermore, the expansion of B lymphocytes during immune-mediated liver disease is thought to contribute to pathogenesis[184]. Specifically, B lymphocytes have been shown to form tertiary lymphoid structures, in which cell aggregates mimic B cell follicles commonly observed in secondary lymphoid tissues. These structures have been associated with chronic inflammatory liver diseases, particularly PBC and PSC, but also during viral hepatitis[185-187].

Hepatocytes are also known to play important roles in both innate and adaptive immune responses. They express PRRs, as well as MHC and costimulatory/adhesion molecules, many of which are polarised to the basolateral surface to enhance their potential for lymphocyte interaction and activation[25, 128, 188, 189]. Futhermore, hepatocytes express cytoplasmic viral RNA receptors, melanoma differentiation-associated protein 5 (MDA-5) and retinoic acid-inducible gene-I-like receptor (RIG-I)[190, 191], with the latter necessary for initiating immune responses towards HCV infection[192]. Both hepatocytes and HSEC express nucleotide-binding and oligomerization domain (NOD)-like receptors which also reside in the cytoplasm and detect bacterial cell wall components[193, 194]. Ligation of these receptors results in pro-

inflammatory cytokine production, thus, these PRRs play a key role in detection and neutralisation of intracellular viral and bacterial infections. Hepatocytes are also capable of direct antigen presentation to naïve T cells via physical interactions mediated by ICAM1 and MHC[25, 195-198]. Although there is strong evidence in support of hepatocyte-mediated T cell activation, its role in the wider context of host immunity remains to be defined given the presence of more dominant APCs within the liver. Nevertheless, hepatocytes produce the majority of soluble innate immunity proteins, including acute-phase proteins and complement, which represent an evolutionarily conserved first line of defence against pathogens[101, 199, 200]. For instance, C-reactive protein and complement proteins, C3 and mannose-binding lectin, bind to microbial surfaces, alerting the immune system to potential pathogens and accelerating phagocytosis[200, 201]. Release of these soluble innate immune proteins into the systemic circulation means the hepatocyte not only plays a role in local immune responses in the liver, but also immune defence at distal sites within the body.

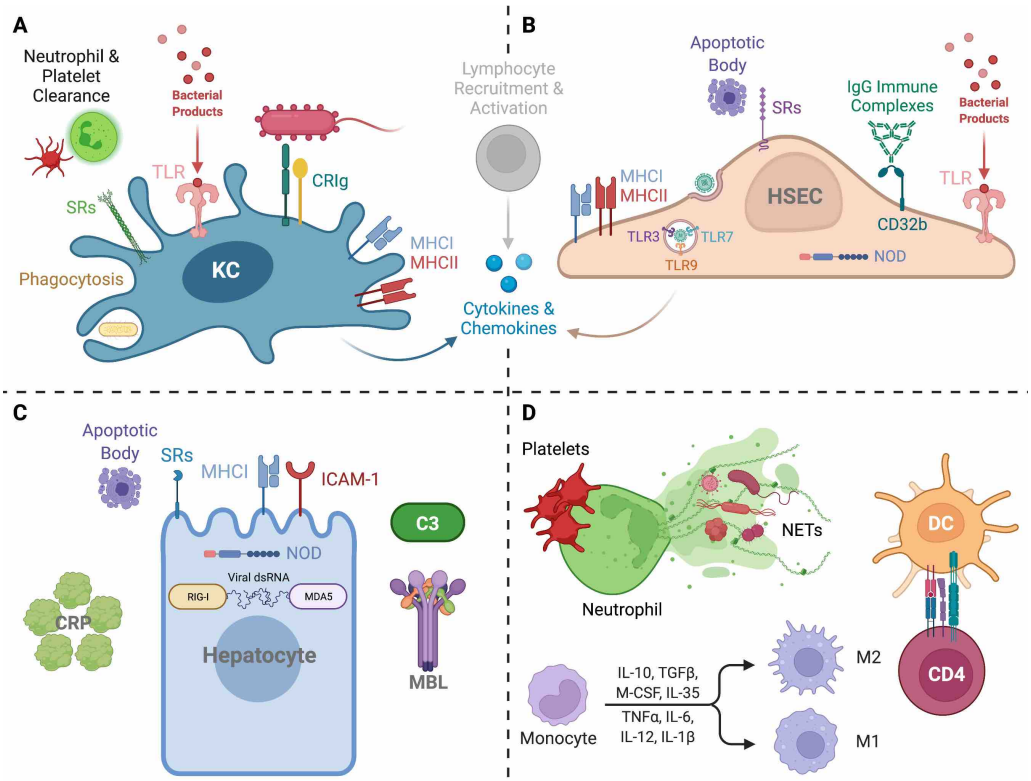

Figure 1.7: The liver is a critical immunological organ capable of mounting both innate and adaptive immune responses.

These are mediated by the **(A)** Kupffer cells (KC) and **(B)** hepatic sinusoidal endothelial cells (HSEC) which comprise the reticuloendothelial system, **(C)** hepatocytes themselves, and **(D)** recruited immune cell populations.

1.7 Liver Repair and Regeneration

1.7.1 Mechanisms of Repair

Following insult or injury, the liver coordinates a rapid response to restore tissue integrity and homeostasis. This wound repair response involves a complex interplay of several cellular and extracellular components, including liver-resident cells, immune cells, the coagulation cascade and inflammatory signalling pathways. Several of these reparative mechanisms are discussed briefly below.

The initiation of a repair response first requires detection of the injurious stimuli, such as an invading pathogen or metabolic insult. These are sensed by immune sentinels of the liver, including KCs and HSEC, via detection of PAMPs or DAMPs[83, 162, 163]. Subsequent KC and HSEC activation results in release of inflammatory cytokines and chemokines which recruit immune cells, shaping the liver microenvironment and acting to neutralise the threat[83]. Following removal of the insult, activated immune cells undergo cell death and, together with damaged or dead cells resulting from the initial injury, are removed by professional and non-professional phagocytes in a process called efferocytosis. This is important for limiting collateral host cell damage and initiating tissue repair[175, 202]. Damaged tissue is replaced either by cell proliferation and migration or expansion of liver progenitor cells.

Several factors are released by liver cells which contribute to the reparative process. KCs promote hepatocyte regeneration through production of TNFα and IL-6[203-205]. Angiogenesis, or formation of new blood vessels, is driven primarily by VEGF and fibroblast growth factor 2 (FGF2), but also from recruitment of bone marrow-derived endothelial progenitor cells. Indeed, $CXCR7^+$ bone marrow-derived progenitor cells of the sinusoidal endothelium are recruited following liver injury or partial hepatectomy and drive liver regeneration, a response which is thought to be mediated by VEGF-SDF1α signalling[206]. HSEC are also known to regulate hepatocyte regeneration via the CXCR7-Id1 pathway and release of HGF and Wnt2[207]. Further, HSC activation results in their differentiation into contractile myofibroblasts, which secrete ECM components such as collagen, and contribute to tissue repair. NK

cells also play a role in tissue resolution, directly killing senescence-activated HSCs and prohibiting excess fibrogenic HSC activity[83].

Macrophages are known to play an important role in tissue repair since their depletion results in delayed regenerative responses and decreased hepatocyte proliferation[208]. However, their phenotype and functions are temporally distinct depending on the stage of tissue inflammation and repair, as has been shown by ablation of macrophages at various time points following liver injury[209]. Specifically, macrophages are thought to contribute to excess scarring and myofibroblast activation during the fibrogenic phase, whilst co-ordinating resolution mediated by matrix degradation during the tissue remodelling phase. Recent work in mice has characterised a pro-resolution macrophage phenotype ($Ly6C^{lo}CCR2^{lo}CX_3CR1^{hi}$) whose role in fibrosis resolution is imperative. These cells have been shown to drive downregulation of CCL3 secretion, removal of lipid peroxidation products such as oxidised LDLs via stabilin-1, and degradation of scar tissue via matrix metalloproteinase 13[210-213]. Aberrant wound healing responses result in excess ECM deposition, scar formation and distortion of tissue architecture known as fibrosis, which is a common feature of most chronic liver diseases.

1.7.2 Mechanisms of Regeneration

Generally, tissue regeneration following injury encompasses three main mechanisms: (i) replication of existing cells; (ii) proliferation and differentiation of stem/progenitor cells; (iii) transdifferentiation or dedifferentiation from one cell type to another[57]. During homeostasis, cellular turnover in the liver is low with most hepatocytes (98-99%) residing in a quiescent state[73, 74]. Following injury, however, the liver is an organ with remarkable regenerative capability, owing to its resident stem cell and progenitor populations and the proliferative capacity of hepatocytes in response to insult[73].

In response to partial hepatectomy (up to 70%), the liver can rapidly regenerate to its original volume through cellular hypertrophy and proliferation[57, 214]. Recently, genetic labelling was used to show that most hepatocytes descend from pre-existing hepatocytes during regenerative responses, following various types of injury[215]. Alternatively, the facultative stem cell hypothesis proposes that stem cell

populations are utilised for regeneration following non-surgical injury[57]. These facultative stem cells, also known as oval cells, are thought to originate from the canal of Hering, which is found at the interface between the hepatocyte-lined canaliculi and the BEC-lined bile ducts. Oval cells emerge, in a process known as ductular reaction, following experimental hepatocarcinogenesis or toxin-induced injury[216-218]. Their positioning in close proximity to the bile ducts, along with the fact they have a combination of BEC and hepatocyte characteristics, has led researchers to assume oval cells arise from BEC[219-222]. However, their ability to differentiate into hepatocytes and overall contribution to liver regeneration remains controversial[57].

Conversely, there is also evidence to support transdifferentiation or reprogramming of hepatocytes into BEC, which is frequently associated with toxin-induced biliary injury[223-226]. This process is thought to be mediated by the Notch pathway, with constitutive Notch signalling conferring an identity switch from hepatocyte to BEC[223, 224]. Notably, ductal expansion is also polarised, with reprogramming being concentrated in periportal hepatocytes[223]; this suggests centrilobular hepatocytes do not receive transdifferentiation cues, either due to lack of initiating signal or presence of endogenous inhibitors of this plasticity. Specifically, HGF and epidermal growth factor (EGF) have been implicated in biliary reprogramming[227], as has the Hippo (YAP/TAZ) pathway whose dysregulation is considered a key contributor to liver tumourigenesis[228-230].

The generally accepted consensus for hepatocyte regeneration is that under homeostatic conditions repopulation of the hepatic niche is achieved through self-replication of hepatocytes[214, 215]. However, in the case of CLD, where proliferative capacity of hepatocytes is often impaired, ductular reaction prevails[231].

1.8 Liver Pathophysiology

1.8.1 Liver Injury

Due to its anatomical location at the interface between the systemic and portal venous circulation, the liver is exposed to a vast array of noxious substances, and is thus susceptible to substantial insult and

injury. In particular, the liver is the first port of call for gut-derived microbial and xenobiotic substances, acting as a sentinel which often renders the liver vulnerable to extensive damage. There are several types of liver injury which can be categorised by their temporal nature (acute vs. chronic) and principal site of injury (hepatitis vs. cholestasis)[57].

Acute hepatitis (liver inflammation) is generally characterised by jaundice, loss of appetite, vomiting, diarrhoea, fatigue and abdominal pain, and can often be self-resolving following removal or neutralisation of the inflammatory insult. When hepatic homeostatic processes are overwhelmed, usually due to persistent infection or drug-induced toxicity, acute hepatitis can progress to acute liver failure. In contrast, chronic hepatitis arises following persistent hepatic injury over many years, often leading to liver failure following progressive damage which disrupts ~70-80% of hepatocyte function[57]. Acute-on-chronic liver failure can also occur in some cases, and is defined by acute hepatic decompensation, along with persistent inflammation and immune dysfunction, which drives a systemic inflammatory response that can predispose patients to developing sepsis[232].

Cholestasis is the accumulation of bile within the liver, which occurs due to a reduction or blockage of bile flow, and shares several clinical features with hepatitis. However, whereas hepatitis and subsequent hepatocyte death is diagnosed clinically by elevated transaminases ALT and AST, cholestasis is diagnosed by the presence of bilirubin in the bloodstream. Cholestasis occurs due to bile duct damage or obstruction, which in the acute setting is most commonly caused by gallstones. However, chronic cholestasis usually arises due to diseases which target the BEC, including PBC, PSC or biliary atresia. Since bile acids can have a toxic effect at high concentrations, hepatocyte damage and hepatitis are often secondary consequences of chronic biliary obstruction.

The initial trigger of liver injury can take a variety of forms, originating from genetic mutations, chronic viral infection, immune-mediated tissue damage or metabolic insult. For instance, congenital liver conditions such as Wilson's disease and alpha-1 anti-trypsin deficiency are caused by mutations in the *ATP7B* and *SERPINA1* genes, respectively. Whilst Wilson's disease is caused by inefficient removal of copper by the liver, alpha-1 anti-trypsin deficiency predisposes sufferers to both liver and lung disease

along with vasculitis and skin problems. Virus-specific immunity during chronic infection with hepatotropic viruses HBV and HCV is simultaneously responsible for viral clearance and non-cytopathic immune-mediated hepatocyte destruction[16]. In non-alcoholic steatohepatitis (NASH) and alcoholic liver disease (ALD), hepatocyte death occurs following metabolic insult due to lipotoxicity and toxic alcohol metabolites, respectively. Although there are a number of key clinical features and initiating triggers which relate to specific aetiologies, CLD follows a common progressive pathway (**Figure 1.8**) comprised of several pathophysiological processes, including sinusoidal capillarisation and endothelial dysfunction, inflammation, fibrosis, cirrhosis, and hepatocellular carcinoma. These processes are outlined in more detail below.

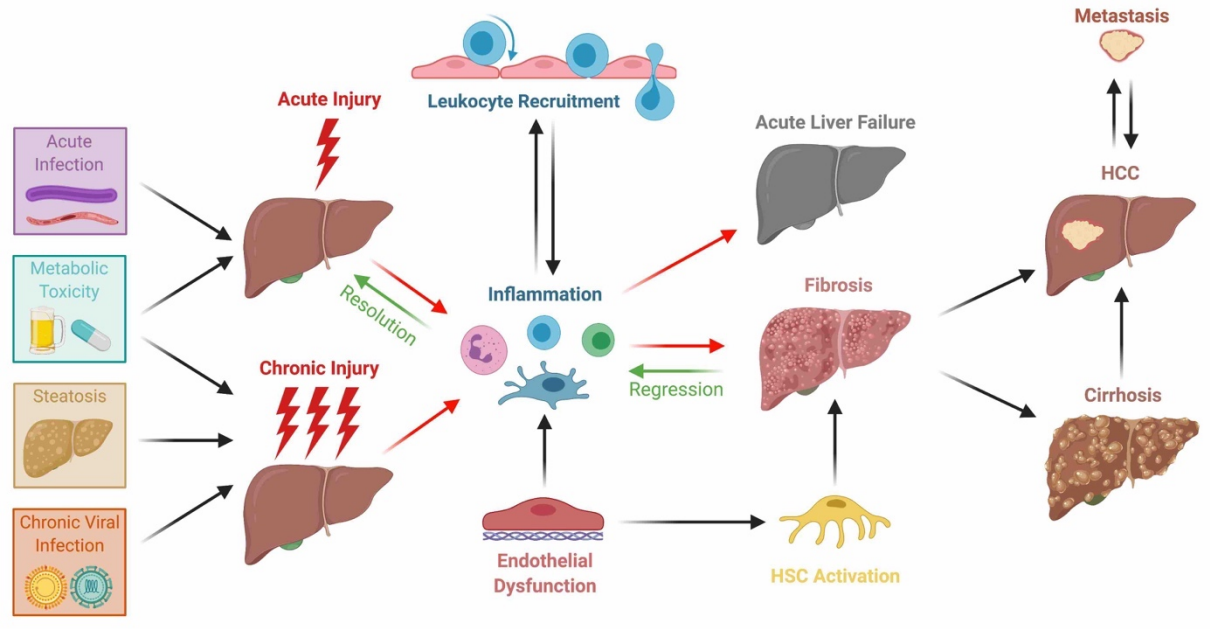

Figure 1.8: The pathophysiological progression of liver disease.

Acute or chronic liver injury, induced by various noxious stimuli, elicits liver inflammation which if unresolved can progress to fibrosis and/or liver failure. Liver inflammation is underpinned by both endothelial dysfunction and sinusoidal capillarisation, which drives leukocyte recruitment to further exacerbate inflammation, and also hepatic stellate cell (HSC) activation which pre-disposes fibrogenesis. Cirrhosis is the most common risk factor for development of hepatocellular carcinoma (HCC) which may then metastasise to distal sites within the body. The liver is also a frequent site of secondary tumour development, particularly colorectal cancer, due to its anatomical positioning and dual blood supply.

1.8.2 Sinusoidal Capillarisation and Endothelial Dysfunction

It is generally well-accepted that endothelial dysfunction precedes both inflammation and fibrosis, a process which persists throughout advanced cirrhosis, since HSEC often represent the first liver cell population exposed to toxic stimuli[233, 234]. As discussed above, HSEC play an important role in hepatic homeostasis via their interactions with both circulating and liver-resident immune cells and their ability to maintain HSC quiescence in response to shear stress[93-97]. For HSEC to carry out their homeostatic physiological function they must maintain their differentiated phenotype. Sinusoidal capillarisation is triggered by hepatic injury and refers to the process in which HSEC lose their fenestrated morphology and adopt a more "capillary-like" phenotype. This process is associated with basement membrane synthesis, loss of GATA4-dependent signals and sinusoidal markers liver/lymph node-specific intercellular adhesion molecule 3-grabbing non-integrin (L-SIGN) and lymphatic vessel endothelial hyaluronan receptor 1 (LYVE-1), and upregulation of CD31 and vascular cell adhesion molecule 1 (VCAM-1)[77, 235].

Endothelial dysfunction is analogous with capillarisation, leading to HSC activation which is considered an initiating fibrogenic event[97, 236]. Defective HSEC NO pathways lead to induction of vasoconstriction and increased intrahepatic resistance, and despite an increased expression of KLF2 in cirrhotic livers in attempt to overcome this dysfunction, this compensatory mechanism is insufficient in preventing portal hypertension[93, 237, 238]. This is supported by the therapeutic benefit of restoring the NO pathway in rodent models of cirrhosis, via the administration of statins, sildenafil, and soluble guanylate cyclase activator BAY-60-2770[236, 239-242]. Indeed, perturbed mechano-sensing by HSEC is a hallmark of CLD, driving alterations in hepatic blood pressure and liver stiffness soon after hepatic injury[243-245]. Not only does increased matrix stiffness drive HSC activation[246], but HSEC mechano-transduction, via PIEZO channels and Notch-dependent HES1/HEY1 nuclear translocation, results in CXCL1-mediated neutrophil recruitment and subsequent microthrombus formation through the production of NETs[247]. This was thought to further exacerbate portal hypertension and microvascular dysfunction in murine models.

Capillarisation of HSEC is a key feature of chronic liver disease and is one of the several underlying mechanisms of liver pathophysiology. HSEC acquire a distinct fenestrated morphology by 20 weeks of gestation which is dependent on the transcription factor GATA4[248, 249]. These fenestrations allow the passage of metabolites, plasma proteins and lipoproteins whilst retaining erythrocytes, leukocytes and platelets within the sinusoids[233]. Several factors produced locally are responsible for the maintenance of the HSEC differentiated phenotype, the most well-studied of which is VEGF, released from hepatocytes, cholangiocytes, HSC and HSEC themselves[76, 98]. Other paracrine factors have also been suggested to regulate the HSEC phenotype, including bone morphogenic protein 9 (BMP-9), produced primarily by HSC. In murine models, BMP-9 was shown to maintain both fenestrations and vascular quiescence, and genetic deletion of BMP-9 drove HSEC capillarisation and perisinusoidal fibrosis. Following fenestration loss, nutrient exchange and metabolic homeostasis is impaired which can further exacerbate inflammation and hepatotoxicity. Furthermore, T-cell-mediated immune surveillance is also impaired following HSEC capillarisation, limiting the neutralisation of virally-infected hepatocytes and/or promoting HCC development by allowing persistence of malignantly-transformed hepatocytes[25, 26].

1.8.3 Fibrosis

Following cellular stress due to lipotoxicity, accumulation of toxic alcohol metabolites, or the presence of hepatotropic viruses, DAMPs released into the microenvironment by damaged hepatocytes are sensed by the innate immune system, predominantly by KCs which lie in close proximity within the sinusoids. Activated KCs then release a concoction of cytokines and chemokines, leading to HSEC activation and recruitment of immune cells from the circulation. Amongst these immune cells are $CCR2^{+}$ pro-inflammatory monocytes which migrate to the parenchyma, differentiate into macrophages, and regulate inflammation resolution and tissue repair.

Fibrosis is an aberrant wound healing response characterised by excessive deposition of ECM and increased tissue stiffness, which distorts the liver architecture and impairs its function (cirrhosis). The major producer of ECM proteins and therefore the main driver of liver fibrosis is the HSC, which when activated assumes a proliferative myofibroblast phenotype. Fibrogenesis enhances VEGF production by

hepatocytes, cholangiocytes and HSC themselves, activating HSC directly, but also stimulating angiogenesis which is a known driver of liver fibrosis. HSEC which have undergone capillarisation begin to produce pro-fibrotic TGFβ, further perpetuating the cycle of HSC activation and fibrosis.

The recruitment of various immune cells subsets during chronic liver inflammation can have both protective and detrimental effects in the context of fibrosis. For instance, NKT cells have been shown to promote inflammation and fibrosis in liver injury models, in part due to their production of pro-fibrogenic factors including osteopontin and hedgehog ligands[250]. In contrast, $CCR6^+$ γδ T cells accumulate during liver injury and are considered protective, due to their induction of HSC apoptosis and their production of IL-17 which has been shown to downregulate NKT cell function[251]. It is possible for fibrosis to regress provided that the fibrogenic stimulus is removed and the liver switches to a pro-resolution microenvironment. This process is mediated by tissue-resident and monocyte-derived macrophages which stimulate hepatocyte regeneration, via IL-6 and TNFα production, and secrete matrix metalloproteinases (e.g. MMP13) that degrade ECM proteins. In many cases of CLD, however, fibrosis progresses to an irreversible stage, with an extremely high risk of developing HCC and only very limited treatment options.

1.8.4 Senescence

Senescence has also been identified as a key contributor to CLD and HCC pathogenesis. Cellular senescence is defined as an irreversible state of cell cycle arrest in which cells cease to proliferate but remain metabolically active[252]. Senescence is a physiological process which occurs during development, where megakaryocytes, placental NK cells and the syncytiotrophoblast undergo senescence as part of their normal maturation[253-255]. Senescence is also an important mechanism for maintaining homeostasis in response to cellular injury, but can become pathological and contribute to tissue damage or tumourigenesis if dysregulated.

Senescence is considered a double-edged sword in that it can elicit both beneficial and deleterious effects in a context-dependent manner. It is a process thought to occur in response to cellular stress, such as

DNA damage or mutation, acting as a protective mechanism which prevents proliferation of altered cells that could give rise to further injury or cancer. This is supported by the notion that tumourigenesis arises from cells that have escaped senescence, and alterations in senescence effectors, such as p53, are frequently observed in tumours of numerous tissue types. Moreover, mice deficient in p53, p21 or p16 develop spontaneous tumours and also display enhanced susceptibility to carcinogen-induced tumourigenesis[256-258].

On the other hand, the persistence of senescent cells contributes to chronic low-level inflammation associated with ageing ("inflammageing") and is pro-angiogenic and pro-metastatic, thereby driving tumour progression and invasion. Indeed, cellular senescence is increased in both ageing and chronic inflammatory disease, which is thought to be attributed to the combined effect of accumulation of deleterious mutations and impaired senescent cell clearance mechanisms. Generally, acute self-resolving senescence is considered beneficial, promoting tissue regeneration and acting as a fail-safe mechanism against tumourigenesis. However, the effects of chronic senescence on the tissue microenvironment are insidious, promoting local and systemic inflammation and carcinogenesis.

In the case of the liver, several pivotal studies have implicated a key role for senescence in disease pathogenesis. Despite acquisition of some senescent markers with ageing, hepatocyte senescence is strongly induced during both acute and chronic liver injury. Following paracetamol-induced liver damage, hepatocytes display positivity for senescence-associated β-galactosidase (SA-β-Gal), p21 and gamma-H2A histone family member X (γH2A.X) and induce paracrine senescence via a macrophage-derived TGFβ1-dependent mechanism[259]. Furthermore, hepatocyte senescence induction in telomerase knockout mice exacerbates fibrosis, whilst p21-deficient mice which have defective senescent responses display improved CCl_4-induced fibrosis[260, 261]. Yet, the implications of hepatic senescence appear to be cell-type- and context-dependent, since HSC senescence has also been shown to limit fibrosis in several mouse models[262-264]. More recently, Omori *et al.* (2020) generated a p16-Cre^{ERT2}-tdTomato mouse model to enable *in vivo* analysis of $p16^{high}$ populations at the single-cell level[265]. They used this model to demonstrate that $p16^{high}$ cells exhibit a heterogenous senescence-associated phenotype, predominantly

found within the hepatic endothelium, and that depletion of these cells ameliorates inflammation and steatosis in a murine model of NASH. In the case of cholestatic liver disease, cholangiocyte senescence is a key pathological feature, indicated by increased SA-β-Gal, p21, p16, γH2A.X and p27 staining in liver samples from PBC and PSC patients[266, 267]. Notably, senescence is also present in paediatric patient specimens, such as those suffering from biliary atresia, suggesting pathological senescence is not simply a consequence of ageing[268].

1.8.5 Hepatocellular Carcinoma

Hepatocellular carcinoma (HCC) is the sixth most common cancer worldwide, accounting for 90% of primary liver cancer cases, and estimated to affect more than one million individuals annually by 2025[269]. The most prominent risk factors for HCC development include HBV/HCV infection, NASH, and chronic alcohol consumption, with more than 90% of cases arising on the background of liver cirrhosis[270]. The exception to this is in the case of chronic HBV infection, where HCC often precedes cirrhosis, following integration of the DNA virus into the host genome and subsequent insertional mutagenesis and oncogene activation[271]. The molecular pathogenesis of HCC is variable, and is dependent on distinct aetiologies and genotoxic insults. Hepatocyte malignant transformation originates from the complex interplay between several factors, including genetic predisposition, reciprocal interactions between viral and non-viral risk factors, the immune microenvironment and the contribution of the underlying chronic liver disease.

There are several mutational drivers in HCC which have been identified. The most frequent genetic predisposition, occurring in 80% of HCC cases, arises following telomerase activation, occurring due to mutations in the promoter region of *TERT*, viral insertions, chromosome translocation or gene amplification[272]. In addition, 30-50% of cases display activation of the Wnt-β-catenin signalling pathway, occurring due to mutations in *CTNNB1* (β-catenin), *AXIN1* or *APC* (Wnt inhibitors)[272]. Several other common genetic alterations have been identified, most of which alter cell cycle control (e.g. *TP53*, *RB1*, *CCNA2*, *CCNE1*, *PTEN*, *AIRD1A*, *ARID2*, *RSP6KA3* or *NFE2L2*) or lead to overexpression of

oncogenic signalling pathways (e.g. *CCND1*, *FGF19*, *VEGFA*, *MYC*, or *MET*). Furthermore, the co-operativity between genetic polymorphisms and non-genetic risk factors have been well-described in the pathogenesis of HCC. For instance, HBV patients with null *GSTT1* polymorphisms have potentiated toxicity in response to aflatoxin B1 exposure[273]. In addition, NASH severity and HCC incidence is associated with *PNPLA3*, *TM6SF2* and *HSD17B13* polymorphisms, particularly in patients with a high chronic alcohol consumption[274].

Given that HCC is the prototypic inflammation-associated cancer, the immune and inflammatory microenvironment is a key contributor to HCC pathogenesis[76, 275]. The immune cell status of HCC can be stratified into four distinct sub-categories: immune-active; immune-exhausted; immune-intermediate; and immune-excluded[276]. Around 20% of HCC cases are considered immune-active, characterised by infiltration of $CD4^+$ and $CD8^+$ T cells, and responsive to immune checkpoint inhibitor therapy. In contrast, immune-excluded HCC tumours display a lack of immunogenic T cells (often referred to as cold tumours) and increased T_{reg} infiltrate, and are thus resistant to immune checkpoint blockade. Immune-exhausted tumours are mostly populated by hypo-responsive $CD8^+$ T cells, driven by excessive TCR antigenic stimulation and increased TGFβ within the tumour microenvironment[276].

Generally, the presence of an immune infiltrate is associated with favourable outcomes, likely due to more efficient anti-tumour immune responses. However, the presence of immunosuppressive subsets, including tumour-associated macrophages, T_{reg} and myeloid-derived suppressor cells (MDSCs), and the upregulation of inhibitory receptors and their ligands, can promote immune evasion and drive tumour growth and progression[277-280]. The recruitment of leukocytes is mediated by the tumour endothelium, whose role in regulating the tumour microenvironment has been recently reviewed[76]. Specifically, expression of scavenger receptors, stabilin-1 and scavenger receptor class F member 1 (SCARF1), have been shown to play opposing roles in $CD4^+$ T cell recruitment. Whereas stabilin-1 mediates T_{reg} transmigration and has been highlighted as a promising therapeutic target[281-283], SCARF1 favours the adhesion of $CD4^+$ T effector cells over their T_{reg} counterparts and could represent a valuable prognostic marker for HCC[284].

1.8.6 Liver Metastasis

Owing to its anatomical location and tolerogenic nature, the liver is a frequent site of metastasis for many solid tumours, including colon, pancreatic and lung cancer[285, 286]. One of the best studied examples is colorectal cancer, from which metastatic tumours display remarkable tropism for the liver. This is likely due to a number of contributing factors: (1) The anatomical location of the liver places it directly downstream of the colon via the portal circulation; (2) The reduced hepatic blood pressure and specialised liver vasculature likely facilitates physical trapping of cancer cells, allowing them to bind to endothelial adhesion molecules and invade the surrounding tissue; (3) The liver is primed by the primary cancer to drive the formation of a pre-metastatic niche, creating an ideal setting in which metastases can seed and thrive[76].

Unlike HCC, which usually occurs on the background of chronic inflammation, liver metastasis can occur in an otherwise healthy liver. Despite this, several cell types lend themselves to exploitation by numerous cancer types. For metastatic cells to colonise the liver, they must first adhere to and cross the endothelial barrier, which is guarded by the HSEC. It is thought that this process is predominantly mediated by ICAM-1, although several other HSEC-expressed adhesion molecules have also been implicated in cancer cell adhesion to the vasculature, including stabilin-1 and mannose receptor[287, 288]. Furthermore, ICAM-1 is also involved in tumour cell extravasation, via its role in actin cytoskeletal remodelling[289, 290]. Another adhesion molecule implicated in the endothelial attachment of cancer cells is E-selectin, which is increased in areas surrounding liver metastases from colorectal primary tumours[291-293]. HSEC also secrete fibronectin, which has been shown to interact with $\alpha 9\beta 1$ integrins on the cancer cell surface and promote epithelial-to-mesenchymal transition, thus enhancing their metastatic potential[294].

Once cancer cells gain access to the space of Disse and underlying parenchymal tissues, they are relatively protected from the patrolling NK cells and KCs residing within the hepatic sinusoids. A state of immune hyporesponsiveness is also maintained by recruitment of MDSCs via HSEC production of CXCL1 and CXCL2[295]. MDSCs elicit their pro-metastatic effects by a number of mechanisms, including

suppression of T cell activation, inhibition of NK cell activity, and induction of T_{reg}[296, 297]. Ultimately, these factors foster a pro-metastatic and pro-tumourigenic microenvironment which drives the seeding and persistence of cancer cells within the liver tissue.

1.9 Leukocyte Trafficking

1.9.1 Lymphocyte Homing and Migration

Leukocyte migration from the bloodstream into the tissues is one of the central paradigms of inflammation and immunity. The recirculation and homing of lymphocytes is a complex trafficking system designed for constant immune surveillance and recognition of foreign antigen wherever it may arise. Briefly, naïve T cells migrate to secondary lymphoid tissues, where they interact with peripheral antigens presented by DCs. Upon recognition of their cognate antigen, T cells undergo activation and rapid proliferation into effector T cells, which migrate to inflammation sites and other secondary lymphoid tissues where they can interact with B cells[298]. This process requires the ability to cross vascular and lymphatic barriers, involving a series of receptor-ligand interactions between the circulating immune cell and the endothelium[299], in what is known as the leukocyte adhesion cascade[300].

1.9.2 Leukocyte Adhesion Cascade

Following infection or injury, circulating leukocytes access inflamed tissues via the vascular endothelium, aiming to neutralise the injurious trigger and initiate tissue repair. Under conditions of blood flow, leukocytes undergo a series of steps in order to adhere and transmigrate through activated endothelium (**Figure 1.9**), mediated by chemokines and adhesion molecules that regulate populations of recruited immune cells[75, 300]. This process generally takes place in the post-capillary venules, except in the spleen, lung and liver[298].

Endothelial activation can be stratified based on the initial triggering stimulus. Type I activation occurs independently of protein synthesis and is, for the most part, regulated by G-protein coupled receptor (GPCR) ligands, including histamine and thrombin[75]. This process involves rapid membrane trafficking of pre-formed P-selectin and subsequent neutrophil recruitment[301, 302], which is a transient response

mediated by GPCR desensitisation to limit the extent of extravasation. In contrast, effects of endothelial type II activation are longer-lived, triggered by numerous inflammatory stimuli including TNFα, IFNγ, IL-1β[303], microbial antigens[304, 305] and oxLDL[306, 307]. These responses involve actin reorganisation and *de novo* expression of chemokines and adhesion molecules, including ICAM-1 and VCAM-1[308-311]. It is common for type II activation to persist until the injurious trigger is removed, since this process is not regulated by receptor desensitisation, but rather regulation of the NFκB pathway which counteracts pro-inflammatory signalling[312].

Initial tethering and rolling of leukocytes are mediated by $Ca2^{+}$-dependent selectins (E-, P- and L-selectin)[313] and integrins, which are dictated by the "catch-bond phenomenon", whereby receptor-ligand interactions are strengthened under conditions of increased shear stress[314, 315]. This also facilitates formation of new bonds before old ones are broken, in the "tether and sling" phenomenon, allowing the rolling motion across the endothelial surface[316-318].

Slow rolling and cell arrest initiate further leukocyte activation and are mediated by leukocyte integrins and members of the immunoglobulin superfamily, such as ICAM-1/2 and VCAM-1, along with more atypical adhesion molecules such as scavenger receptors[75, 319-321]. Tetraspanins also play a role in leukocyte recruitment; ICAM-1 and VCAM-1 form endothelial adhesive platforms by establishing microdomains with CD151, facilitating adhesion under physiological flow rates[233, 322]. The stabilisation of immune cells on the endothelium allows the interaction of GPCRs on their surface with chemokines embedded within the endothelial glycocalyx, facilitating high-affinity integrin binding and firm adhesion[323-328]. Leukocytes can then patrol the surface of the vessel wall in search of an exit site for transmigration, in a process known as intraluminal crawling, which is mediated by integrins and ICAM-1[329-331]. Transendothelial migration is then initiated by chemoattractants and formation of ICAM-1- and VCAM-1-rich trans-migratory cups[332, 333]. There is also evidence to suggest that leukocytes can undergo sub-endothelial crawling after crossing the endothelial barrier but before migrating into the tissue proper[334-336].

1.9.3 Transendothelial Migration

Transendothelial migration of leukocytes across the endothelium is a highly regulated process, mediated by distinct mechanisms depending on the route taken[300, 337]. To facilitate this process, endothelial cells must undergo profound morphological changes, including cytoskeletal remodelling and alteration of cell-cell junctions, to allow passage of leukocytes whilst maintaining vascular integrity[338]. Around 80-95% of cells transmigrate paracellularly whilst the remainder transmigrate via the transcellular route.

Paracellular transmigration, that is, extravasation of leukocytes between endothelial cells, is a complex process mediated by endothelial junctional proteins. Adhesion molecule ligation weakens inter-endothelial junctions, a process thought to be mediated by mobilisation of intracellular calcium and p38 MAPK/RHO GTPase (p38 mitogen activated protein kinase/Ras homologue) activation[339, 340]. Junctional molecules, such as platelet/endothelial cell adhesion molecule 1 (PECAM-1/CD31) and junctional adhesion molecule A (JAM-A), become mobilised within endothelial cell-cell junctions, creating a haptotactic gradient and a path of least resistance[341-343]. Other molecules implicated in paracellular transmigration include ICAM-1, ICAM-2, JAM-B, JAM-C, CD99, and vascular adhesion protein 1 (VAP1), whilst endothelial adherens junctions are maintained by vascular endothelial cadherin (VE-cadherin)[300, 341, 344]. Notably, VE-cadherin has been shown to play an inhibitory role in leukocyte extravasation and must be re-localised away from the migration site to permit leukocytes across the endothelium[345, 346].

Transcellular migration involves diapedesis of leukocytes directly through the endothelial cell body and accounts for around 5-20% of cells bound to activated human umbilical vein endothelial cell (HUVEC). Extensive reorganisation of the actin cytoskeleton is required to form an adequately-sized pore which will allow leukocyte passage through the endothelial cytoplasm[347]. This highly regulated process involves the formation of an F-actin-rich channel through which the immune cell can extravasate following translocation of apical ICAM-1 to caveolae and caveolin-1 to the basal membrane[309, 338, 348-350]. Although this process is less well-studied than paracellular transmigration, other molecules have also been implicated, including PECAM-1, JAM-A and CD99[351, 352].

Regardless of the route taken, transmigration not only offers additional selectivity regarding which leukocyte subsets are permitted access to the tissues, but also acts to prime infiltrating immune cells to ensure rapid and effective immunological responses[353].

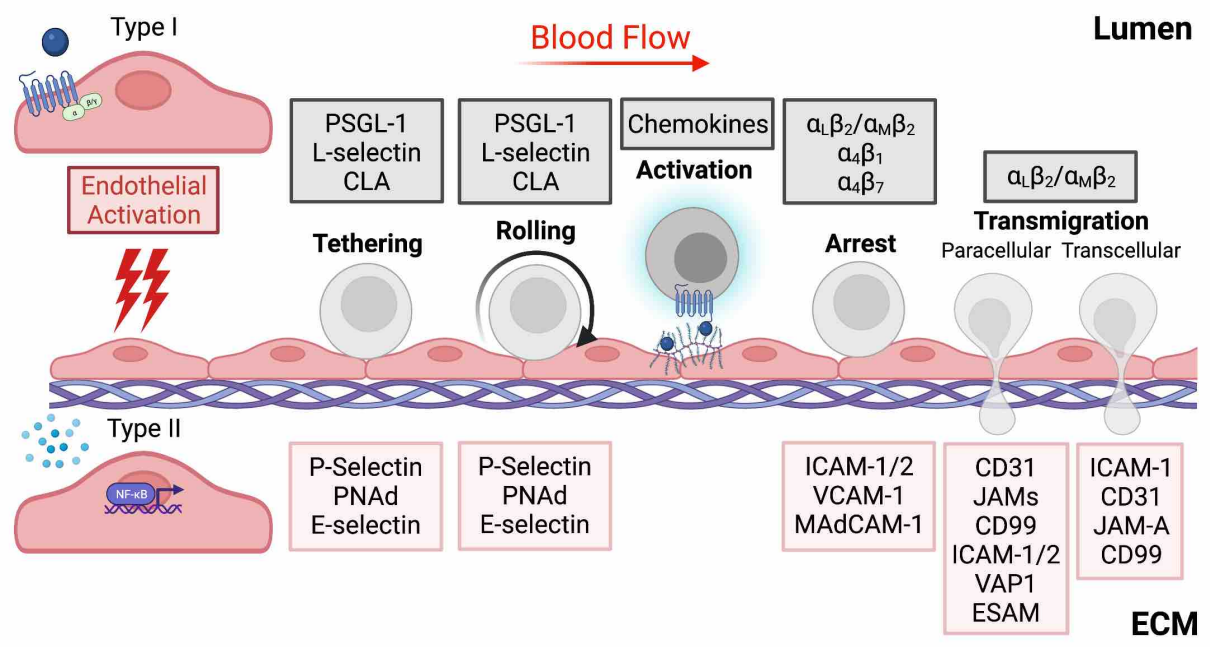

Figure 1.9: The leukocyte adhesion cascade involves a complex interplay of receptor-ligand interactions.

These interactions mediate the initial tethering, rolling, activation, firm adhesion and transmigration of leukocytes. Classical endothelial adhesion molecules and their corresponding leukocyte-derived ligands involved in each stage of the process are detailed in the pink and grey boxes, respectively.

1.9.4 Lymphocyte Trafficking in Lymph Nodes

Lymphocyte trafficking between vascular and lymphatic systems and the tissues is a requirement for mounting antigen-driven adaptive immune responses and memory[354]. T cells access the lymph nodes either by the afferent lymphatic vessels or high endothelial venules (HEVs)[355], where they interact with antigen presenting cells and become activated in the presence of relevant co-stimulatory signals[356]. Whilst the classic leukocyte adhesion cascade is relatively well-characterised, the endothelial molecules involved in lymphatic trafficking are less well-understood, with atypical adhesion molecules and scavenger receptors being implicated in this process.

Scavenger receptors often contain several structural domains also found in selectins, including C-type lectin domains and epidermal growth factor (EGF)-like domains, meaning they are also capable of binding leukocytes. Amongst their ability to bind numerous endogenous products[75], many of these scavenger receptors have been found in lymphatic endothelial cells where they mediate immune cell trafficking, including scavenger receptor type A1 (SR-A1)[357, 358], stabilin-1[359-362] and mannose receptor (MR)[288, 363-365]. Despite compelling evidence that scavenger receptors are involved in leukocyte trafficking, many knockout studies do not show differences in lymphocyte populations[210, 357], suggesting that scavenger receptors may have redundant roles in lymphocyte binding which can be compensated for by other receptors. Another molecule which has been implicated in lymphocyte entry into the lymph nodes is plasmalemma vesicle-associated protein (PLVAP), an endothelial-specific type II membrane glycoprotein which forms a size-selective sieve, associated with endothelial fenestrae and caveolae[366, 367].

1.9.5 Leukocyte Recruitment to the Liver

Chronic liver diseases are characterised by leukocyte infiltration which drives inflammation, fibrosis and cirrhosis. Intravital microscopy studies have shown that although leukocytes can bind and transmigrate across various regions of the liver vasculature, in fact, most migration takes place within the hepatic sinusoids[368]. This is in contrast to most other tissues, in which leukocyte extravasation predominantly occurs in the post-capillary venules. HSEC are activated by cytokines released during liver inflammation, resulting in upregulation of adhesion molecules[369] and synthesis of chemokines, which are presented on their luminal surface via binding to glycosaminoglycans within the endothelial glycocalyx[370]. Chemokines are also secreted by HSC, BEC and hepatocytes within the space of Disse which are subsequently transcytosed by HSEC and presented on their surface[371-373]. These processes facilitate leukocyte recruitment and regulate the immune microenvironment; the balance of immunosuppressive and inflammatory leukocyte subsets dictates the outcome of liver injury.

The low shear environment of the hepatic sinusoids, much like that of the lymph nodes, allows redundancy of the initial tethering and rolling stages of the leukocyte adhesion cascade. As such, selectin

expression within the hepatic sinusoids is negligible[374], whereas more atypical adhesion molecules such as scavenger receptors are enriched in HSEC[75]. Classical adhesion molecules such as ICAM-1 and VCAM-1 are upregulated following endothelial activation by pro-inflammatory stimuli and play a crucial role in leukocyte recruitment to the liver[298, 375]. Whereas ICAM-1 interacts with its ligand αLβ2 on leukocytes to mediate their binding and transmigration, VCAM-1 mediates lymphocyte capture and firm adhesion via α4β1 integrins. As such, ICAM-1-deficient mice display reduced leukocyte adhesion to the hepatic sinusoids[368], and lymphocyte adhesion is impaired in human HSEC *in vitro* following antibody-mediated blockade of ICAM-1 and VCAM-1[27, 376].

It is interesting to also consider the role of atypical adhesion molecules in the context of ICAM-1- and VCAM-1-mediated recruitment, particularly since several have been implicated in the recruitment of specific leukocyte subsets (**Figure 1.10**). For instance, scavenger receptor class F, member 1 (SCARF1) is upregulated in CLD, associating with fibrotic regions and preferentially mediating adhesion of $CD4^+CD25^-$ T effector cells over $CD4^+CD25^+$ Treg and $CD8^+$ T lymphocytes[284, 377]. Vascular adhesion protein 1 (VAP-1) is also elevated in CLD and influences recruitment of leukocytes directly, and indirectly, via its monoamine oxidase activity[376, 378, 379]. It has been shown that VAP-1 promotes recruitment of T_H2 lymphocytes over T_H1 cells in a concanavalin A-induced liver injury model[380].

Stabilin-1 is another scavenger receptor (Class H) involved in lymphocyte recruitment, promoting preferential transmigration of $CD4^+$ $FoxP3^+$ T_{reg}, with the support of ICAM-1 and VAP-1[381]. Consistent with this finding, a reduction in the number of immunosuppressive leukocyte subsets within tumours, and thus positive outcomes, were observed following antibody blockade or genetic deficiency of stabilin-1 in mice[362]. Stabilin-2 is the second member of the Class H family of scavenger receptors, whose fasciclin 1 (FAS1) domains play a role in lymphocyte adhesion to the hepatic endothelium via $\alpha_M\beta_2$ integrins[382]. Notably, stabilin-2 expression does not seem to be regulated by pro-inflammatory stimuli, in contrast to several other atypical adhesion molecules which are upregulated during inflammation.

Another protein which plays a pivotal role in recruitment to the liver is CD44, specifically the selectin-independent adhesion of neutrophils during sepsis, which is enhanced following deposition of CD44 ligand hyaluronan on the sinusoidal endothelium[383, 384]. Mucosal addressin cell adhesion molecule 1 (MAdCAM) is normally restricted to the gut mucosal endothelium, yet its expression is induced in the hepatic endothelium in some inflammatory states, where it mediates trafficking of gut-specific mucosal lymphocytes[385]. This may explain the hepatic complications which often arise in inflammatory bowel disease patients, since MAdCAM mediates recruitment of activated mucosal T cells which drive immune-mediated liver damage[379].

Alongside their role in the classic adhesion cascade discussed above, chemokines are also involved in recruitment of distinct leukocyte subsets to the liver[324]. Importantly, chemokines contribute to lymphocyte compartmentalisation, with CXCR3 ligands CXCL9-11 promoting parenchymal recruitment during lobular hepatitis and CCR5 ligands CCL3-5 driving portal infiltration in the case of interface hepatitis[386-388]. Moreover, *in vivo* experiments have shown that CXCR3 and its ligands promote recruitment of virus-specific $CD8^+$ T cells in mice[389]. Fractalkine (CX_3CL1) produced by HSEC facilitates integrin- and VAP-1-dependent adhesion and transmigration of $CD16^+$ monocytes by interacting with CX_3CR1[390]. Under homeostatic conditions, HSEC also secrete CXCL16 which facilitates immune surveillance via recruitment of $CXCR6^+$ NK and NKT cells[88, 391, 392]. During inflammation, hepatocyte- and cholangiocyte-derived CXCL16 drives the recruitment of $CXCR6^+$ liver-infiltrating lymphocytes, including $CD4^+$ and $CD8^+$ T cells[393, 394]. Furthermore, activated KCs produce CCL2, promoting $CCR2^+$ inflammatory monocyte recruitment from the circulation which form aggregates associated with portal tracts in CLD[213, 395, 396]. Thus, chemokines may represent novel targets for selectively modulating recruitment of immune cell populations during chronic inflammation.

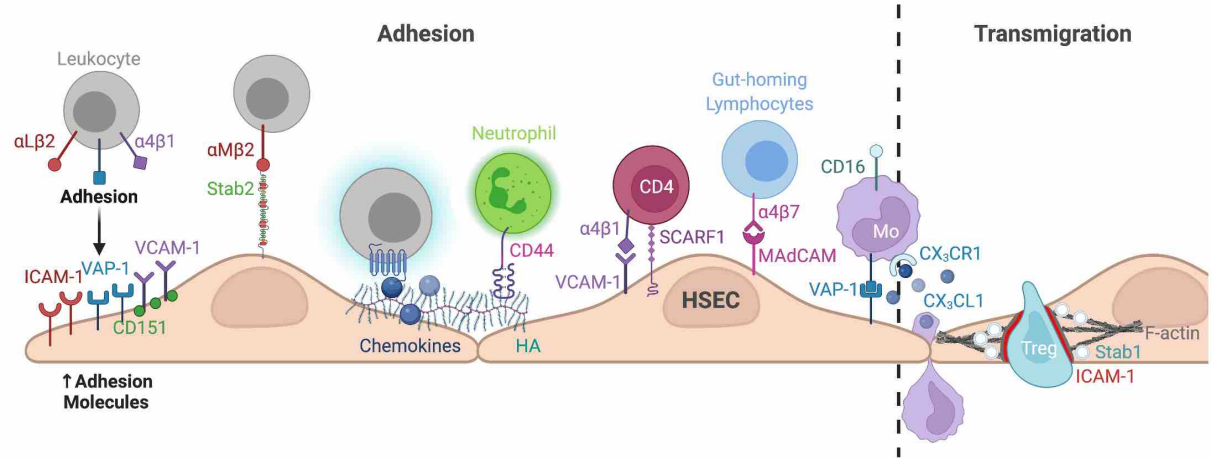

Figure 1.10: Mechanisms of hepatic leukocyte recruitment.

This process involves several atypical adhesion molecules alongside classical adhesion molecules, vascular cell adhesion molecule 1 (VCAM-1) and intercellular adhesion molecule 1 (ICAM-1), which mediate adhesion and/or transmigration of specific immune cell subsets.

1.9.6 Novel Targets in the Hepatic Sinusoids

As discussed above, the distinctive HSEC phenotype and low level of shear stress experienced within the hepatic sinusoids offers a unique environment in which leukocyte recruitment can occur. Many of the molecules identified to play a role in hepatic leukocyte recruitment are in fact enriched in HSEC compared to their low levels of expression within other vascular beds. As such, many of these atypical adhesion molecules could make valid therapeutic targets to manipulate hepatic leukocyte recruitment specifically whilst preserving trafficking at distal tissue sites. In recent years, several single-cell RNA sequencing studies, in both humans and mice, have set out to characterise the heterogeneous nature of endothelial cells during liver homeostasis, inflammation and cancer[66, 67, 397, 398]. These datasets have identified a sinusoidal signature which is disrupted in liver cirrhosis and HCC. Instead, endothelial cells adopt a scar-associated or tumour-associated phenotype, which have the potential to contribute to disease pathogenesis. Two of the endothelial-expressed genes highlighted in these studies, *MRC1* (**Figure 1.11**) and *PLVAP* (**Figure 1.12**), encode proteins which have been implicated in leukocyte trafficking within specialised vascular beds, and will remain the focus subject for the remainder of this thesis.

1.10 Mannose Receptor

The mannose receptor (MR), also known as macrophage mannose receptor (MMR), CD206, and mannose receptor C, type 1 (MRC1), is a carbohydrate-binding C-type lectin encoded by the *MRC1* gene. Mannose receptor is the prototypic member of the MR family of endocytic receptors, which also comprises urokinase-type plasminogen activator receptor-associated protein (uPARAP)/Endo180 (CD280), the M-type phosopholipase A2 receptor (PLA2R), and DEC-205 (CD205)[399]. Structurally, MR possesses several binding domains, meaning it can recognise and bind numerous endogenous and exogenous ligands, and therefore plays a widespread role in various physiological processes[400]. Furthermore, the ability of MR to recycle between the plasma membrane and the endosomal system, paired with the existence of a soluble form of MR (sMR)[401-403], means that MR is subject to various forms of regulation from *de novo* expression to intracellular trafficking and proteolytic cleavage. The structure and function of MR along with its expression pattern and role in leukocyte recruitment is discussed below.

1.10.1 Structure

Mannose receptor is a type I membrane glycoprotein with a large extracellular binding domain and a short C-terminal cytoplasmic tail. Members of the MR family share a similar structure consisting of an N-terminal cysteine-rich (CR) domain, a highly conserved single fibronectin type II (FNII) domain, and multiple C-type lectin-like domains (CTLDs) which define the C-type lectin superfamily[399]. Mannose receptor is unique in that it contains a functional CR domain[404], unlike the other MR family members which lack the sugar binding region within this domain[405]. Specifically, MR binds sulphated carbohydrates including galactose and GalNAc via the CR domain, whilst the FNII domain and eight CTLDs facilitate recognition of collagens I-IV (and collagen V at much lower affinity)[406, 407] and mannose-, fucose- and GlcNAc-terminated glycoproteins, respectively[408-410]. Furthermore, MR family members contain FENTLY (Phe-Glu-Asn-Thr-Leu-Tyr) sequence motifs within their cytoplasmic tails which confer interactions with the cellular endocytic machinery, permitting delivery of extracellular

ligands via clathrin-mediated endocytosis (CME) and rapid recycling between membranous and endosomal compartments. As such, 10-30% of MR is found at the cell surface whilst 70-90% resides intracellularly under steady state conditions[399].

MR is susceptible to conformational alterations and post-translational modifications which can drastically affect its structural and functional properties. For instance, the bent conformation of MR, in which the CR domain and CTLD4 reside within close proximity, can influence ligand selectivity and binding avidity[411]. This interaction is pH-dependent, and could therefore represent a mechanism by which ligands are selectively released in response to pH changes within the endo-lysosomal system. Furthermore, MR is a heavily glycosylated molecule, containing N-glycosylation sites which are evolutionarily conserved in humans and mice. Many N-glycans contain sialic acids, and terminal sialylation of MR is important for its recognition of mannosylated glycoproteins[412]. MR can also undergo proteolytic cleavage to produce a soluble form of the receptor (sMR) which consists of the whole extracellular domain, thereby retaining its binding properties[401]. Recognition of sulphated carbohydrates by sMR depends upon receptor multimerisation, which in turn is influenced by lack of sialylation[412]. Whilst macrophage MR shedding was initially considered to be a constitutive process, some studies have suggested that it can be stimulated during fungal infection by engagement of β-glucan receptor dectin-1, potentially shaping anti-fungal immune responses[403].

1.10.2 Expression

Despite being originally named macrophage mannose receptor when it was initially identified in 1986[413], MR expression is not restricted to macrophages alone. In fact, MR is also highly expressed in DCs, kidney mesangial cells, tracheal smooth muscle cells, retinal pigment epithelia and nonvascular endothelium within the lymphatics, spleen, dermis and liver[400]. Despite a previous demonstration of MR expression in monocytes[414], these cells are generally considered to lack MR prior to their differentiation into macrophages, after which MR is rapidly upregulated. Furthermore, MR has long been used as a marker for alternative “M2-like” macrophage activation, characterising a more immunosuppressive

phenotype observed in tumour-associated macrophages[415] and following the onset of inflammation resolution.

Regarding the tissue distribution of MR, although the expression pattern in murine tissue has been well-characterised, similar expression profiling in humans remains incomplete. However, there are important species differences in MR expression between mice and humans which must be considered; for example, MR is absent from human splenic macrophages in contrast to their murine counterparts[416, 417]. Unfortunately, human tissue expression studies have been hindered by the limited MR-specific antibodies that work on formalin-fixed paraffin-embedded (FFPE) sections. However, a recent single-cell RNA-sequencing study has reported *MRC1* expression in endothelial and mononuclear phagocyte cell fractions of the human liver, highlighting an enrichment of MR gene expression in uninjured endothelia which were annotated to have a liver sinusoidal endothelial cell phenotype (**Figure 1.11**)[397].

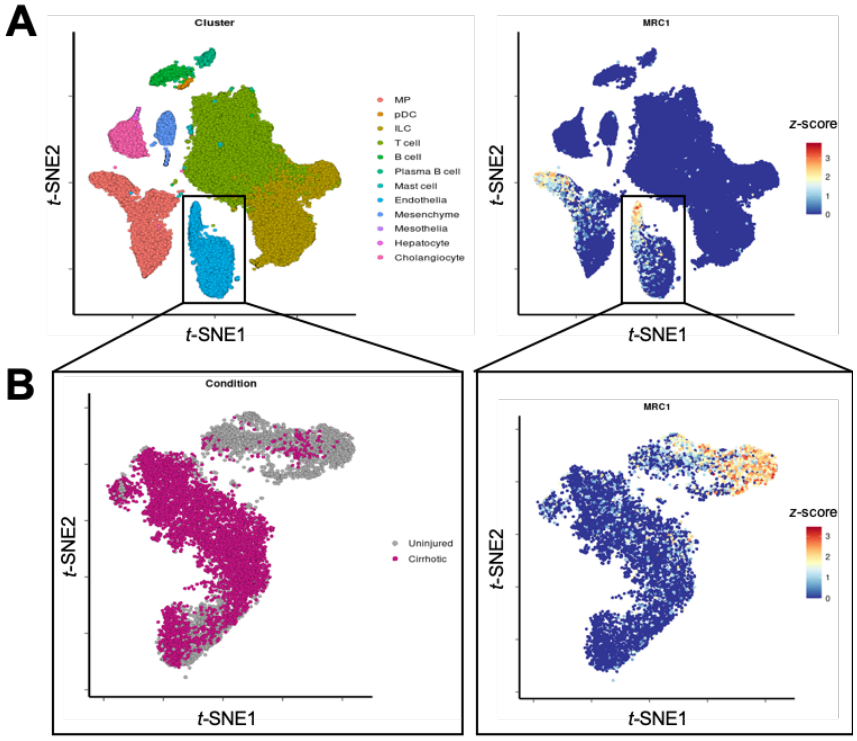

Figure 1.11: The expression of *MRC1* in human liver cirrhosis.

(A) Publicly-available RNA-sequencing data from healthy (n=5) and cirrhotic (n=5) human livers showed that mannose receptor (*MRC1*) is expressed in endothelial cells and mononuclear phagocytes. **(B)** *MRC1* expression was prevalent in uninjured endothelia which were annotated as having a liver sinusoidal endothelial cell signature. Data shown are taken from single-cell RNA-sequencing study Ramachandran *et al.* 2019 and *t*-SNE plots were generated using livercellatlas.mvm.ed.ac.uk.

1.10.3 Function

The structural properties of MR described above allow it to carry out its endocytic function, and the recognition of numerous ligands facilitates the role of MR in several physiological processes. The binding of endogenous ligands and subsequent endocytosis is important for scavenging of waste material, including FNII-mediated collagen uptake and internalisation of myeloperoxidase and lysosomal enzymes. The non-redundant role of MR in collagen clearance has been demonstrated in human and mouse macrophages[406, 407], as well as in rat and murine HSEC[418, 419], and was shown to occur independently of collagen glycosylation and lectin activity[420]. Moreover, MR-mediated uptake of lysosomal enzymes cathepsin-D, α-mannosidase, β-hexosaminidase and arylsulphatase by HSEC permits effective catabolism and is required to maintain their degradative capacity[421]. A key role for MR in glycoprotein homeostasis has also been defined in studies utilising MR-deficient mice. Lack of mannose receptor confers disruption of serum glycoprotein levels, including candidate MR ligands mannose-bovine serum albumin (Man-BSA) and GlcNAc-BSA, which was attributed to defective clearance in the liver and spleen[422]. The same study also showed an accumulation of most lysosomal hydrolases in knockout mice compared with wild-type controls under steady state conditions, further supporting a role for MR in uptake of lysosomal enzymes.

Mannose receptor has also been implicated in both innate and adaptive immune pathways owing to its role in pattern recognition of foreign particles and contribution to antigen uptake prior to presentation[423]. Specifically, MR has been shown to recognise mannose and *N*-acetylglucosamine residues frequently found on the surface of various pathogenic microorganisms, via its CTLDs, including *Candida albicans*[424], *Pneumocystis carinii*[425], *Mycobacterium tuberculosis*[426], *Klebsiella pneumoniae*[427] and *Streptococcus pneumoniae.* Moreover, in addition to CME, MR has been suggested to support phagocytosis (internalisation of large particles >0.5 μm), although the mechanisms of this process are incompletely understood. Exogenous expression of MR in COS-1 cells was shown to mediate both endocytosis of Man-BSA and phagocytosis of non-opsonised *C. albicans* and *P. carinii*[423, 424], yet MR is absent from the phagocytic cup during the early stages of *C. albicans* engulfment[428]. Instead, MR was

transiently recruited during phagosome maturation, suggesting a potential role in phagosome sampling and processing of internalised cargo. Furthermore, MR was required for production of TNFα and monocyte chemoattractant protein 1 (MCP-1) following fungal recognition[428]. Since MR-deficient mice do not show increased susceptibility to *C. albicans* or *P. carinii* infection[429, 430], this suggests that MR is not essential for phagocytosis and there may be some redundancy with other phagocytic and pattern recognition receptors. One possibility is that MR may not mediate phagocytosis in isolation, but rather bind particles and engage classic phagocytic receptors which could indirectly drive phagocytic processes. Since MR lacks an intracellular signalling motif within its cytoplasmic tail, this could also provide a mechanism by which MR can indirectly mediate intracellular signalling and subsequent innate immune activation, given that MR is essential for cytokine production[423, 428]. Nevertheless, the ability of MR to recognise foreign antigens and elicit cellular responses is important for mediating innate immunity.

Mannose receptor plays a key role in antigen uptake and presentation due to its endocytic capacity and expression in professional and non-professional antigen presenting cells (APCs). Antigen internalisation and presentation was shown to be mediated by MR in cultured human DCs in the context of MHCII and CD1b[431-433]. The importance of MR in this process is illustrated in MR-deficient mice challenged with *Cryptococcus neoformans*, who have reduced survival and increased pulmonary fungal burden compared to wild-type controls, due to defective induction of T cell responses[434]. Mannose receptor-mediated endocytosis has also been shown to promote selective antigen presentation to $CD8^+$ T cells[435, 436], and indeed this has been shown as a mechanism for antigen cross-presentation in HSEC[110]. Importantly, MR-mediated antigen uptake and presentation in HSEC induces T cell tolerance via upregulation of programmed cell death ligand 1 (PD-L1)[109-111]. Similarly, recognition of tumour antigens by MR activates an immunosuppressive phenotype in tumour-associated macrophages[415].

1.10.4 Role in Leukocyte Recruitment

More than 20 years ago, Irjala *et al.* (2001) discovered a novel role for MR in leukocyte trafficking within the efferent lymphatic system[363]. By performing *in vitro* static adhesion assays, which were

thought to most accurately represent physiological conditions within the lymph nodes *in vivo*, authors demonstrated that pre-incubation of lymph node sections with an anti-MR antibody significantly impaired lymphocyte binding. Furthermore, this interaction was shown to involve L-selectin as the lymphocyte-derived ligand, since adhesion of L-selectin^{+}, but not L-selectin^{-}, lymphocytes was significantly inhibited. Later work by the same group further supported the adhesive properties MR, showing that the binding of multiple cancer cell lines to lymphatic endothelium was inhibited following antibody-mediated MR blockade[288]. MR has also been implicated in lymphocyte migration via the afferent lymphatics, where MR and CD44 act as a receptor-ligand pair to facilitate trafficking of L-selectin^{-} cells[365]. These characteristics were confirmed *in vivo* by utilising MR knockout mice to demonstrate that adhesion of both normal lymphocytes and tumour cells is significantly lower in MR-deficient mice[364]. This observation was accompanied by a faster primary tumour growth rate, but smaller metastatic tumours, in knockout mice compared to wild-type controls. Authors concluded that MR on lymphatic endothelium therefore contributes to the metastatic behaviour of cancer cells and could be a novel therapeutic target in inflammation and cancer metastasis. Despite the role of MR in leukocyte recruitment within the lymphatic system being generally well-studied, its role within other specialised vascular beds, such as the liver sinusoids, has not been reported previously.

1.11 Plasmalemma Vesicle-associated Protein

Plasmalemma vesicle-associated protein (PLVAP), also known as plasmalemmal vesicle 1 (PV-1) and fenestrated endothelial-linked structure protein (FELS), has long been recognised as an endothelial-enriched protein, even before its molecular identity was confirmed. It is the antigen recognised by PAL-E (Pathologische Anatomie Leiden-endothelium) and MECA-32 (mouse endothelial cell antigen-32) antibodies frequently used to identify endothelial cells in humans and mice, respectively[437, 438]. Although PLVAP is present in most types of vascular endothelium, hence its widespread use as a pan-endothelial marker, its expression pattern is species-, organ- and context-dependent. Furthermore, single-cell sequencing studies have highlighted the emergence of PLVAP^{+} endothelial sub-populations in the liver during foetal development and diseased states, further adding to the complexity of its expression and

function[397, 398, 439]. Several lines of research have identified PLVAP as a potential target in cancer and neurological diseases, such as spinal cord injury, brain ischaemia and diabetic retinopathy, due to its known roles in mediating vascular permeability and angiogenesis. However, its contribution to CLD and its potential as a therapeutic target remains poorly understood. The physiological and pathophysiological properties of PLVAP are discussed in more detail below.

1.11.1 Structure

The cDNA and protein sequence of rat, human and murine PLVAP was reported over 20 years ago, highlighting that its molecular structure is highly conserved across all three species[440, 441]. PLVAP is a type II integral membrane glycoprotein of 55-65 kDa, comprising a short (27 aa) intracellular tail at its N-terminus, a transmembrane domain, and a long (380 aa) extracellular C-terminal domain. The extracellular domain consists of two coiled-coiled domains, flanked by four N-glycosylation sites and a proline-rich region proximal to the C-terminus, and the intracellular portion contains a putative caveolin-1 binding domain. *In situ*, PLVAP forms homodimers and is capable of binding heparin at physiological pH.

1.11.2 Function

Initial immunoelectron microscopy studies with the PAL-E antibody showed that PLVAP localised to the exterior surface of endothelial vesicles, and was therefore suggested to play a role in transendothelial transport[438]. Since this original study in 1985, PLVAP has been identified as the only known molecular component of fenestral and stomatal diaphragms[442]. These diaphragms are comprised of PLVAP homodimers assembled in a radial fibril-like orientation, which span the openings of sub-endothelial structures including fenestrations, caveolae and transendothelial channels (TECs)[443, 444]. Whereas fenestrae and TECs resemble pore-like structures which facilitate molecule exchange between the circulation and the underlying tissues, caveolae are flask-shaped invaginations of the cell membrane, which are characterised by caveolin-1 expression and are involved in transcytosis. Functionally, these diaphragms are responsible for maintaining basal permeability and vascular integrity. Studies with

plvap-deficient mice have reported that PLVAP is essential for the formation of fenestral and stomatal diaphragms, with knockout mice displaying disrupted barrier function of fenestrated capillaries and succumbing to lethal protein-losing enteropathy[445-447]. A similar phenotype is recapitulated in humans who possess homozygous non-sense mutations in the PLVAP gene[448-450].

PLVAP has also been implicated in vascular development and angiogenesis. Genetic *Plvap* deletion in mice with a C57BL/6N or C57BL/6J background is embryo-lethal, causing subcutaneous oedema, haemorrhages and vascular defects before birth[445, 446]. This has been overcome by the use of mice from mixed (BALB/c-C57BL/6J-129Sv/J) backgrounds and conditional knockouts[445]. In barrier endothelium during the late embryonic stage, the presence of Wnt and Norrin ligands inhibits the β-catenin destruction complex, allowing accumulation of β-catenin and subsequent downregulation of PLVAP expression[451]. This is critical in allowing maturation of the blood-brain- and blood-retina-barrier (BBB and BRB). Within non-barrier endothelium, or in early embryonic stages within barrier endothelium, the absence of Wnt and Norrin ligands for the Lpr5/Frzd receptor complex favours inactive canonical β-catenin signalling[452]. Cytosolic β-catenin is targeted for proteolytic degradation via the β-catenin destruction complex, inducing PLVAP upregulation, which facilitates angiogenesis. *In vitro*, siRNA-silencing of PLVAP inhibited endothelial sprout formation and cell migration, and was associated with reduced VEGFR2 and sphingosine kinase 1 activity[453, 454]. In the murine foetal liver, PLVAP has been shown to form angiogenic signalling complexes also comprised of VEGFR2, neuropilin-1 and LYVE-1, yet these complexes were absent in adult liver[444]. Whether PLVAP directly promotes angiogenesis or merely provides mechanical support to capillaries during vascular remodelling remains unclear.

1.11.3 Expression

The expression of PLVAP has been unknowingly studied for decades due to the availability of PAL-E and MECA-32 antibodies. The PAL-E antibody has been widely used due to its endothelial specificity and ability to distinguish vascular endothelium from lymphatic endothelium. PAL-E stains endothelial cells of capillaries, medium-sized veins, venules and splenic sinusoids, but is mostly absent from

arteries, arterioles, large veins and lymphatic vessels[452]. MECA-32 displays a similar staining pattern, although arterioles and large veins also appear positive when murine tissues are stained with this antibody[452]. PLVAP is localised to the cell membrane of an endothelial subset in the normal microvasculature, displaying an enriched expression in the lungs, kidneys, spleen, endocrine glands and digestive tract[442]. In the brain and eye, where the endothelium is integral in maintaining the BBB and BRB, PLVAP is present in the fenestrated capillaries of the choroid plexus and choriocapillaris but absent from the continuous endothelium of the cerebral cortex, cerebellum, optic nerve, retina, iris and ciliary muscle[452].

In mice, PLVAP is highly expressed in the foetal liver sinusoids, coinciding with the presence of fenestral diaphragms. Importantly, these diaphragms are absent in adult sinusoids, yet PLVAP is still expressed throughout, albeit to a lesser extent than the portal and central veins[444]. Authors proposed that the contribution of stomatal diaphragms to the observed PLVAP levels was likely minimal given that caveolin-1-deficient mice displayed comparable PLVAP expression. This study therefore challenged the existing dogma that PLVAP is only thought to be present within diaphragms, suggesting that perhaps PLVAP has alternative roles, at least within the context of the liver. In contrast to mice, human PLVAP is restricted to the periportal sinusoids[438]. However, several studies, including those which apply single-cell RNA-sequencing technologies, have indicated a re-emergence of PLVAP in diseased states suggesting it may have a role in pathogenesis[397, 398].

1.11.4 Role in Disease

As discussed above, the re-emergence of PLVAP has been reported in several diseases. Breakdown of the BBB and BRB is characterised by PLVAP expression and is associated with conditions such as cerebral oedema and diabetic macular oedema[452]. Similarly, PLVAP expression following ischaemic stroke or traumatic spinal cord injury is concomitant with disrupted neurovascular integrity[455]. PLVAP upregulation has also been observed in several cancers, including tumours of the brain, lung, breast, stomach, liver, pancreas, colon, small intestine, kidneys, ovaries, prostate, uterus, skin and lymph nodes. PLVAP expression is thought to be linked to tumour angiogenesis which has been demonstrated using

human samples from glioblastoma and cholangiocarcinoma patients[456, 457]. Furthermore, the potential of PLVAP as a therapeutic target for HCC has been investigated previously; this study documented anti-tumour effects and minimal systemic toxicity following PLVAP antibody blockade in a Hep3B murine xenograft model[458].

Recent single-cell RNA sequencing studies of human liver tissue have highlighted the upregulation of *PLVAP* gene expression in cirrhosis and HCC[397, 398]. Ramachandran *et al.* (2019) identified two scar-associated endothelial (SAEndo) sub-populations which displayed increased *PLVAP* expression and were enriched within the fibrotic niche of cirrhotic patients (**Figure 1.12**) – *CD34*$^{+}$*PLVAP*$^{+}$*VWA1*$^{+}$ and *CD34*$^{+}$*PLVAP*$^{+}$*ACKR1*$^{+}$ cells. SAEndo cells expressed pro-fibrogenic genes including *PDGFD*, *PDGFB*, *LOX*, and *LOXL2*, with gene ontology terms associated with extracellular matrix organisation. These populations were distinct from the sinusoidal endothelial cell population, which was negative for *CD34* and *PLVAP* and displayed high expression of sinusoidal markers including *CLEC4M*, *LYVE1* and *STAB2*[397]. Sharma *et al.* (2020) performed single-cell RNA sequencing on foetal and cancerous liver tissues, demonstrating onco-foetal reprogramming of endothelial cells in HCC patients, in which three subsets of PLVAP^{+} populations were documented – *PLVAP*$^{+}$*VEGFR2*$^{+}$, *PLVAP*$^{+}$*HLA-DRA*$^{+}$, and *PLVAP*$^{+}$*HLA-DRA*$^{+}$*ACKR1*$^{+}$ cells[398]. These populations were suggested to drive an immunosuppressive microenvironment in HCC tumours. The re-emergence of similar PLVAP^{+} endothelial cells observed in the above studies suggests there could be common phenotypic changes in fibrosis-associated and cancer-associated endothelial cells.

1.11.5 Role in Leukocyte Recruitment

Alongside its well-established role in regulating vascular permeability, PLVAP has also been implicated more specifically as a leukocyte trafficking molecule. Pivotal studies by Jalkanen and Salmi's research groups highlighted that PLVAP (PAL-E) redistributes to the cell periphery within TNFα-treated HUVEC, enwrapping transmigrating lymphocytes in association with caveolin-1[459]. Furthermore, they demonstrated that lymphocyte transmigration was inhibited in response to an anti-PLVAP antibody, whilst lymphocyte rolling and adhesion were unaffected. This finding was further supported by *in vivo*

studies of acute peritonitis, in which administration of the anti-PLVAP antibody significantly decreased lymphocyte migration.

More recent studies have documented a convincing role for PLVAP in leukocyte positioning *in vivo* by utilising *Plvap*-deficient mice. Specifically, PLVAP has been shown to control lymphocyte and antigen entry to the lymph nodes, where it forms a size-selective sieve that was dependent on PLVAP-containing diaphragms within transendothelial channels[366]. Interestingly, lymphocyte transmigration through the lymph node sinus floor was increased in *Plvap*-deficient mice compared to wild-type controls, an outcome that was seemingly independent of stomatal diaphragms since caveolin-1 knockout had no effect on lymphocyte transmigration. Yet, in a seemingly contradictory manner, PLVAP antibody ligation inhibited lymphocyte transmigration; these data suggested that PLVAP-containing diaphragms could form the path of least resistance for lymphocyte migration, and that antibody-mediated PLVAP blockade hampers lymphocyte entry to the lymph nodes. *Plvap* knockout mice have also offered insight into its developmental role, in particular the positioning of foetal tissue-resident macrophages[460]. Rantakari *et al*. (2016) published elegant *in vivo* studies showing that PLVAP, selectively expressed in liver sinusoidal endothelial cells, is integral for the egress of foetal liver monocytes to the systemic vasculature and the subsequent seeding of macrophage populations within the tissues. In contrast, yolk-sac-dependent macrophage seeding was independent of PLVAP, highlighting a selective and important hepatic role for PLVAP during foetal development. However, the role of PLVAP in leukocyte trafficking and recruitment within the adult human liver has not been studied previously.

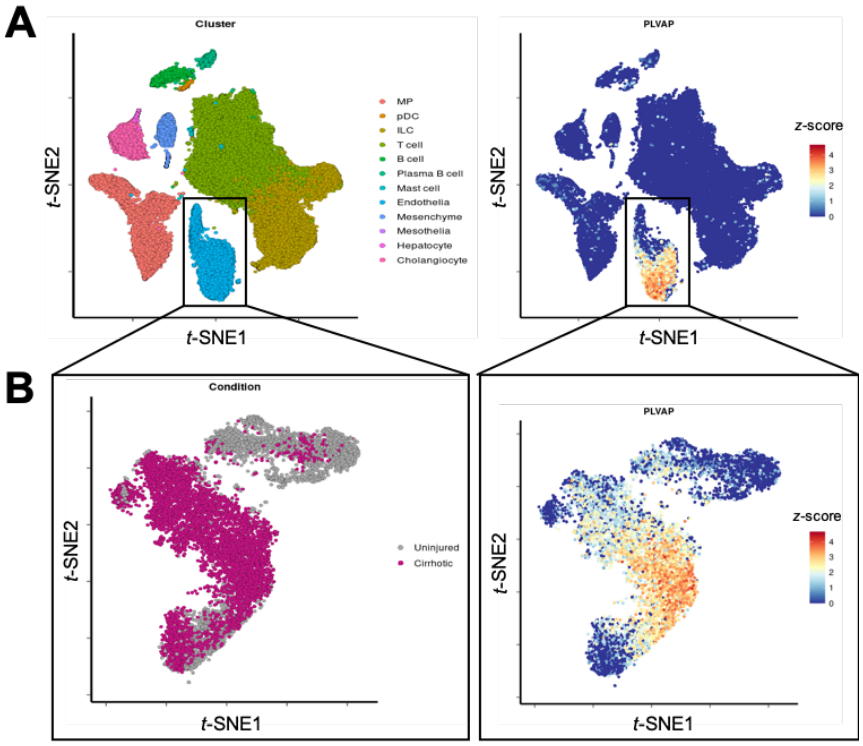

Figure 1.12: The expression of PLVAP in human liver cirrhosis.

(A) Publicly-available RNA-sequencing data from healthy (n=5) and cirrhotic (n=5) human livers showed that *PLVAP* displayed marked enrichment in the endothelial cell fraction. **(B)** PLVAP expression defined a scar-associated endothelial cell population that was expanded in cirrhotic liver patients. Data shown are taken from single-cell RNA-sequencing study Ramachandran *et al.* 2019 and t-SNE plots were generated using livercellatlas.mvm.ed.ac.uk.

1.12 Aims and Hypotheses

Previous studies have implicated MR and PLVAP in the recruitment of leukocytes across specialised endothelium such as that found in the lymphatic system[363, 366]. This thesis will test the hypothesis that MR and PLVAP mediate leukocyte recruitment across human hepatic sinusoidal endothelium, and therefore play a role in shaping the tissue microenvironment during CLD and HCC. This study will address the following core aims:

(i) Characterise MR and PLVAP expression in normal and diseased human liver tissue

(ii) Understand how MR and PLVAP expression is regulated in primary human HSEC

(iii) Investigate a potential role for MR and PLVAP in leukocyte recruitment across human HSEC

2 MATERIALS AND METHODS

2.1 Human Samples

2.1.1 Human Liver Tissue

Non-cirrhotic ("normal") human liver tissue was obtained from rejected donor livers or those surplus to clinical requirement under ethical study numbers 06/Q2702/61 and 18/WA/0214. Non-neoplastic liver tissue was also acquired from margins of resected tumours from hepatocellular carcinoma patients, alongside matched tumour tissue, under ethical study numbers 06/Q2702/61 and 18/LO/0102. Diseased liver tissue was obtained from liver explants from patients undergoing transplantation at the Queen Elizabeth Hospital Birmingham, under ethical study numbers 06/Q2702/61 and 18/WA/0214. All tissue was obtained with prior consent and ethically approved for use in research.

2.1.2 Human Blood

Peripheral human blood was collected from healthy volunteers. Prior consent was obtained and blood was used for research under ethical study number 18/WA/0214.

2.2 Murine Samples

All murine formalin-fixed paraffin-embedded tissue sections were a kind gift from Dr Thomas Bird (Beatson Institute, UK). All mouse experiments were carried out under procedural guidelines, severity protocols and within UK with ethical permission from the Animal Welfare and Ethical Review Body (AWERB) and the Home Office. Male and female mice were housed in a specific pathogen-free environment and kept under standard conditions with a twelve-hour day/night cycle and access to food and water *ad libitum*.

2.2.1 Mdm2 Model

Male 8-12 week old mice on a mixed background (129P2/OlaHsdWtsi;C57Bl/6J) were homozygous for the $Mdm2^{tm2.1Glo}$ allele (MGI: 2385439) and the $Gt(ROSA)26Sort^{m14(CAG-tdTomato)Hze}$ allele (MGI: 3809524). The $Mdm2^{tm2.1Glo}$ allele encodes the p53-binding domain of Mdm2 (exons 5 and 6 flanked by

loxP sequences). Mice were injected via tail vein with 2 x 10^{11} genomic copies of AAV8-TBG-Cre vector, resulting in hepatocyte-specific expression of the Cre recombinase and subsequent excision of Mdm2 exons 5 and 6, referred to hereafter as $\Delta Mdm2^{Hep}$ mice. Control mice were injected with the AAV8-TBG-Null vector causing hepatocyte-specific expression of a scrambled sequence. Mice were euthanised by CO_2 inhalation 4 days post-AAV injection.

2.3 Immunohistochemistry

Equipment and reagents used in immunohistochemistry studies are detailed in **Table 2.1**.

2.3.1 Preparation of Frozen Sections

Mannose receptor and PLVAP expression in non-cirrhotic and diseased human liver tissue was investigated via chromogenic and fluorescent immunohistochemistry. One-centimetre-thick cubes of fresh human liver tissue were snap frozen in liquid nitrogen and stored at -80°C until processing. Five-seven micron-thick sections were cut using a cryostat from liver tissue embedded in O.C.T.™ TissueTek® mount. Sections were then mounted on glass microscope slides, fixed in acetone, and stored wrapped in foil at -20°C. Sections were obtained from at least five different donors, for non-cirrhotic liver tissue, and from patients with ALD, NASH, PBC and PSC. Sections from HCC tumour and matched non-tumour tissue were obtained from four patients. Isotype-matched controls were performed on matched serial tissue sections where possible.

2.3.2 Preparation of Formalin-fixed Paraffin-embedded Sections

Five-millimetre-thick slices of fresh human or mouse liver tissue were fixed in 10% neutral buffered formalin for 24 hours and processed as follows: wash with water; dehydration with 99% denatured alcohol; clearing with xylene; infiltration with Histowax. Paraffin-embedded blocks were cut using a Microtome to a thickness of 3 μm, and sections were collected on microscope slides before being dried at 37°C for at least one hour before immunostaining.

2.3.3 Chromogenic and Fluorescent Immunohistochemistry

All incubations were carried out in a humidified chamber at 20-22°C with gentle agitation (20 rpm on laboratory rocker) unless otherwise stated. Frozen sections were thawed at 20-22°C for 10 minutes and then washed in PBS containing 0.1% (v/v) Tween® 20 (PBS-T) for five minutes with gentle agitation (20 rpm). Formalin-fixed paraffin-embedded (FFPE) sections were de-waxed and rehydrated by static incubation for three minutes with increasing concentrations of xylene, followed by increasing concentrations of industrial denatured alcohol (IDA), and finally distilled water. Antigen retrieval of FFPE sections was performed by microwaving for 20-30 minutes with 1% Tris-based (pH 9) or Citrate-based (pH 6) Antigen Retrieval Buffer followed by washing with PBS-T for five minutes.

Sections were then incubated with either methanol containing 0.3% (v/v) hydrogen peroxide for 30 minutes, or Bloxall® Endogenous Blocking Solution for 15 minutes, followed by two five-minute washing steps with PBS-T. To block non-specific antibody binding, sections were incubated with blocking buffer (PBS containing 2X casein) for 20 minutes. For immunofluorescent staining of frozen sections, blocking of non-specific binding was performed immediately after thawing and washing, by incubating with PBS containing 2X casein and 10% goat serum for 20 minutes.

Primary antibodies were diluted in sterile PBS to the concentration specified in **Table 2.2** and incubated with sections for one hour, followed by two washing steps as indicated above. Pre-diluted secondary antibodies (detailed in **Table 2.3**) were added to sections for 30 minutes before an additional two washing steps as performed previously. Chromogenic substrate ImmPACT® DAB Peroxidase (HRP) Substrate Kit) was added for approximately five minutes as per the manufacturer's instructions before rinsing with tap water. Sections were then counterstained with Mayer's haematoxylin for 20 seconds, before rinsing with cold tap water, and then washing in warm water for two minutes. Sections were de-hydrated by static incubation with increasing concentrations of IDA and xylene, before mounting on glass coverslips using non-aqueous mounting medium (DPX) and leaving to dry overnight. Chromogenic IHC samples were imaged using an Axio Scan.Z1 slide scanner and visual fields were selected using Zen (blue) software. For quantification of immunohistochemical staining, percentage

staining area was calculated for a minimum of five visual fields per case using the "Threshold" and "Measure" functions in ImageJ.

For immunofluorescent staining, fluorescently-conjugated secondary antibodies were diluted in sterile PBS to concentrations indicated in **Table 2.3** and incubated with thawed cryopreserved sections in the dark for 30 minutes. Nuclear staining was performed by incubating for five minutes with 300 nM 4′,6-diamidino-2-phenylindole (DAPI), followed by washing with PBS-T and mounting of slides on glass coverslips using ProLong™ Gold Antifade Mountant. Slides were then stored in the dark at 4ºC until imaging using an Axio Scan.Z1 slide scanner (Zeiss). Visual fields were selected and co-localisation was analysed by generating intensity profiles using Zen (blue) software (Zen 2012, Zeiss). Alternatively, slides were imaged using either a Zeiss LSM780 or LSM880 confocal microscope.

2.3.4 Sirius Red Staining

Sirius red staining was performed in matched serial liver sections, where possible, to visualise collagen deposition. Sirius red solution (0.1% w/v) was made in advance (1.3% picric acid containing 1 g/L Direct Red 80). All incubations were carried out in a humidified chamber at 20-22°C with gentle agitation (20 rpm on laboratory rocker) unless otherwise stated. Cryopreserved sections were thawed at 20-22°C for 10 minutes before being rinsed with distilled water and incubated with 5% (v/v) phorbol 12-myristate 13- acetate (PMA) in distilled water for five minutes. After removal of PMA, Sirius red solution was added to sections followed by a 30-minute incubation. Sirius red was then removed from slides and replaced briefly with 0.1 M hydrochloric acid before rinsing with distilled water. Slides were then dehydrated by incubating with increasing concentrations of IDA and xylene under static conditions, before mounting onto glass coverslips with non-aqueous mounting medium (DPX). Slides were then imaged as detailed in **2.3.3 Chromogenic and Fluorescent Immunohistochemistry**.

2.4 HSEC Isolation and Cell Culture

All cell culture work was carried out in a class II microflow safety cabinet and aseptic technique was followed at all times to prevent contamination. Cells were maintained at 37°C in a humidified incubator

with 5% CO_2 unless otherwise stated. Equipment, plastics and reagents used in cell isolation and culture are detailed in **Table 2.4**.

2.4.1 HSEC Isolation

Human HSEC were isolated according to a previously established protocol[376]. Slices of liver (10-50 g) from normal and diseased donors were mechanically digested using two sterile scalpels. Enzymatic digestion was achieved by incubating minced liver tissue with 20% (v/v) collagenase type 1A solution in sterile PBS for 25-45 minutes at 37°C with agitation. Digested liver was then filtered and washed through a fine mesh with PBS into a sterile beaker and the filtrate was centrifuged at 2000 rpm for five minutes (all centrifugation steps unless otherwise specified). Supernatant was removed and pellet was concentrated through serial centrifugation steps, before separation of non-parenchymal cells by centrifugation using a 33:77% Percoll™ density gradient. Biliary epithelial cells were depleted using a mouse anti-EpCAM (epithelial cell adhesion molecule) antibody (4.55 μg/mL, 30 minutes at 37°C) followed by positive magnetic selection using ice-cold goat anti-mouse IgG Dynabeads™ (8 x 10^6 beads/mL, 30 minutes at 4°C with agitation). $CD45^+$ immune cells were depleted using CD45-coated Dynabeads™ (8 x 10^6 beads/mL, 30 minutes at 4°C with agitation). Human HSEC were then purified by positive magnetic selection using CD31-coated Dynabeads™ (8 x 10^6 beads/mL, 30 minutes at 4°C with agitation).

2.4.2 HSEC Culture and Passage

Isolated primary human HSEC (designated passage 0 (p0)) were maintained in endothelial cell serum-free medium (SFM) supplemented with 10 ng/mL VEGF, 10 ng/mL HGF, 10% (v/v) human serum and 1% Pencillin-Streptomycin-Glutamine (PSG). Cells were cultured in collagen-coated 25 cm^2 flasks immediately following isolation and then passaged at approximately 80% confluence and seeded into 75 cm^2 flasks thereafter. Cells were passaged by washing with sterile PBS and then incubating with warm TrypLE™ enzyme for 2-3 minutes followed by gentle agitation to dislodge cells from plastic. Enzyme was then diluted with PBS and cells were centrifuged at 2000 rpm for five minutes. The cell

pellet was resuspended in HSEC culture medium and split accordingly up to a maximum of passage 6 (p6).

2.4.3 HSEC Storage

Reagents used in HSEC freezing are highlighted in **Table 2.4.** Isolated HSEC were expanded to p2 before freezing for long-term storage in liquid nitrogen. Confluent cells were harvested with TrypLE™ as described in **2.4.2 HSEC Culture and Passage** and counted using a haemocytometer. Cells were then centrifuged at 2000 rpm for five minutes and pellet was resuspended in foetal bovine serum (FBS) containing 10% (v/v) dimethyl sulphoxide (DMSO) at a density of 1-1.5 x 10^6 cells/mL. One millilitre of cell suspension was then added to cryovials which were frozen slowly overnight at -80°C in MrFrosty™ freezing containers to allow optimum cell preservation. Once frozen, cryovials were transferred to liquid nitrogen for long-term storage. Cells were thawed quickly at 37°C as required, washed with PBS and centrifuged at 2000 rpm for five minutes. Pelleted cells were then resuspended in HSEC culture medium (detailed in **2.4.2 HSEC Culture and Passage**) and allowed to recover for at least 24 hours before use.

2.5 Polymerase Chain Reaction (PCR)

Equipment, plastics and reagents used in PCR are detailed in **Table 2.5** and **Table 2.6**.

2.5.1 Tissue Lysis

Approximately 20-30 mg of liver tissue was homogenised in gentleMACS™ M-tubes containing RLT Buffer (in RNeasy® Mini Kit) and 1% (v/v) β-mercaptoethanol, using a gentleMACS™ Dissociator, as per the manufacturer's instructions. RNA was then extracted immediately, or alternatively, lysates were the stored in single-use aliquots at -20°C until RNA extraction.

2.5.2 Cell Lysis

Unstimulated or treated HSEC were washed twice with sterile PBS and then cells were lysed within 6 multi-well plates in 350 µL of RLT Buffer (in RNeasy® Micro Kit) containing 1% β-mercaptoethanol. Lysates were stored at -20°C until RNA extraction.

2.5.3 RNA Extraction

RNA was extracted from tissue and cell lysates using the RNeasy® Mini Kit and RNeasy® Micro Kit, respectively, as per the manufacturer's instructions. All centrifugation steps were for 15 seconds at >8000 *g* unless otherwise stated. Briefly, 350 µL 70% ethanol was added to each sample and mixed thoroughly by pipetting, before being transferred to RNeasy MinElute spin columns each fitted with a 2 mL collection tube. Samples were centrifuged and flow-through was discarded. Columns were washed by adding 350 µL RW1 Buffer before centrifugation, followed by addition of 10 µL DNase I stock solution in 70 µL RDD Buffer directly to the membrane and incubation at 20-30°C for 15 minutes. Wash buffer (RW1) was then added (350 µL) followed by centrifugation and collection tubes were discarded and replaced with new collection tubes. RPE Buffer (500 µL) was then added, tubes were centrifuged and flow-through was discarded, followed by addition of 500 µL 80% ethanol and centrifugation for two minutes at >8000 *g*. Collection tubes were discarded and replaced with new collection tubes, and membranes were dried by centrifugation at maximum speed for five minutes. Collection tubes were then replaced with 1.5 mL collection tubes and RNA was eluted by adding 14 µL RNase-free water directly to the membrane and centrifugation at maximum speed for one minute. Purity and integrity of total RNA were assessed using a NanoPhotometer™ and samples with an A260/A280 ratio of 2 ± 0.2 were used for cDNA synthesis.

2.5.4 cDNA Synthesis

Random primers (0.5 µL/sample) were added to 10 mM dNTP Mix (1 µL/sample) in a nuclease-free microcentrifuge tube and heated to 65°C for five minutes using a SensoQuest Labcycler 48. Random primers and dNTP Mix were then added to a reaction mixture containing RNA (1 µg/sample), 5X First

Strand Buffer (4 µL/sample), SuperScript® III Reverse Transcriptase (1 µL/sample), RNaseOUT™ (1 µL/sample) and 0.1 M dithiothreitol (DTT) (1 µL/sample), which was diluted in nuclease-free water to a total reaction volume of 20 µL. Using a SensoQuest Labcycler 48, the following incubation steps were performed: ten minutes at 25°C; 50 minutes at 50°C; 5 minutes at 85°C. cDNA was then stored at -20°C until use in qRT-PCR.

2.5.5 Quantitative Real-time PCR

Quantitative real-time PCR (qRT-PCR) was performed on each sample in triplicate using TaqMan® Gene Expression Assays and reactions were prepared in white 96 or 384 multi-well plates. All reagents were thawed and prepared on ice. Each reaction contained 5% (v/v) cDNA sample, 50% 2X TaqMan® Universal PCR Master Mix and 5% TaqMan® Gene Expression Assay primer probes in nuclease-free water (final volume of 20 µL for 96-well and 10 µL for 384-well). *GAPDH* was used as a housekeeping gene for cell-derived cDNA, whereas *18S* and *GUSB* were used as housekeeping genes for CLD tissue- and HCC tissue-derived cDNA, respectively. Reactions were performed in a LightCycler® 480 Instrument II (Roche) by completing 40 cycles of the following steps: 95°C for 10 seconds; 60°C for 50 seconds; 72°C for one second. Data were normalised to appropriate housekeeping gene expression using "E-analysis" software (Roche). For analysis of whole liver tissue, tumour tissue, and HSEC, data were normalised expression relative to *18S*, *GUSB* and *GAPDH*, respectively.

2.6 Immunocytochemistry

Equipment, antibodies and reagents used in immunocytochemistry studies are detailed in **Table 2.7**. Primary HSEC isolated from liver tissue (as described in **2.4 HSEC Isolation and Cell Culture**) were cultured *in vitro*, and were stained via immunofluorescence to visualise MR and PLVAP, amongst several other markers. Prior to staining, HSEC were seeded into collagen-coated ibidi® 6-channel µ slides (75,000 cells/channel) and allowed to adhere for at least two hours. Cells were then washed twice with PBS (whilst avoiding aspirating all liquid within channels) and fixed with 4% (w/v) paraformaldehyde (PFA) for 10 minutes at 37°C. Once fixed, cells were permeabilised by incubating

with PBS containing 0.3% (v/v) Triton™ X-100 for five minutes at 20-22°C with gentle agitation (20 rpm) (all incubation steps were carried out under these conditions unless otherwise stated). Permeabilisation buffer was then replaced with blocking buffer (PBS containing 10% (v/v) goat serum and 2X casein) and incubated for 30 minutes. Blocking buffer was next removed and primary antibodies were added at optimum concentrations and incubated for one hour. Following three five-minute washing steps with PBS-T, corresponding secondary antibodies were added and cells were incubated in the dark for 30 minutes. Cells were then washed as above, incubated with 300 nM DAPI for two minutes, and then washed again. Slides were stored in either PBS (short-term) or aqueous mounting medium (longer-term) in the dark at 4°C until imaging. Single-plane and z-stack images were acquired on either a Zeiss LSM780 or LSM880 confocal microscope (Zeiss) and analysed in Zen (blue) software (Zen 2012, Zeiss). For quantification of immunofluorescent staining, percentage staining area was calculated for a minimum of five visual fields per case using the "Threshold" and "Measure" functions in ImageJ.

2.7 Intracellular Trafficking Studies

Intracellular trafficking studies were performed in ibidi® six-channel μ-slide VI 0.4 and imaged using an LSM780 or LSM880 confocal microscope unless otherwise stated.

2.7.1 Cellular Localisation

Immunocytochemistry was performed to investigate the cellular localisation of MR and PLVAP. Primary HSEC were dual-stained for MR or PLVAP and markers of either the cell membrane or intracellular organelles, including the Golgi apparatus, early endosomes, recycling endosomes, lysosomes and caveolae. Antibodies used in these studies are detailed in **Table 2.2**.

2.7.2 Intracellular Trafficking

Trafficking of MR and PLVAP was investigated using vacuolar-type ATPase inhibitor bafilomycin A1, which has been shown previously to inhibit endocytic transport and lysosomal degradation[461, 462]. Primary HSEC were treated with 10 nM bafilomycin A1 for 24 hours, followed by fixation, permeabilisation and immunocytochemistry as described in section **2.6 Immunocytochemistry**.

2.7.3 Uptake and Internalisation Assays

To study endocytic and scavenging capacity, cells were incubated with either 1 mg/mL 40 kDa fluorescein isothiocyanate (FITC)-conjugated Dextran or Dil Acetylated low-density lipoproteins (AcLDLs) for various time periods (indicated in results). Cells were then fixed and imaged via confocal microscopy, and number of vesicles per cell was quantified using the "Analyse Particles" function in ImageJ.

To understand if MR or PLVAP undergo internalisation or trafficking following receptor ligation, HSEC were incubated with 2 μg/mL anti-MR or 10 μg/mL anti-PLVAP antibody diluted in growth medium for various time periods (indicated in results). Cells were then fixed in 4% PFA, permeabilised with 0.3% Triton™ X-100, and stained with appropriate secondary antibodies to identify the ligated pool of MR/PLVAP. In some cases, cells were also dual stained with antibodies detailed in **Table 2.2**.

2.8 High-content Imaging Assay

High-content imaging was performed in Falcon® 96-well Black TC-treated Imaging Microplates using a CellInsight™ CX5 High-content Screening Platform (ThermoFisher Scientific).

2.8.1 High-content Screening

High-content screening was performed to identify modulators of MR and PLVAP expression. A list of putative regulators was generated from previous reports and is shown in **Table 2.8**. Primary HSEC were seeded into collagen-coated Falcon® 96-well plates at a density of 25,000 cells per well and left to adhere overnight. Cells were serum- and growth factor-starved for two hours before being treated for 24 hours with various cytokines, chemokines, growth factors and compounds, which were diluted in Endothelial Cell SFM to concentrations stated in **Table 2.8**. Relevant unstimulated and vehicle-treated controls were incorporated and each condition was performed in triplicate. Cells were then fixed in 4% PFA for 10 minutes at 37°C and subsequently stained for either MR or PLVAP as described previously in section **2.6 Immunocytochemistry**. Stained cells were imaged using a CellInsight™ CX5 High-content

Screening Platform, and fluorescence area and intensity was quantified by utilising a Spot Detection algorithm optimised within HCS Studio Software version 2.0 (ThermoFisher Scientific).

2.9 Additional Regulation Studies

2.9.1 Hypoxia

HSEC were seeded in collagen-coated 6-well plates at a cell density of 300,000/well in 2 mL complete culture medium and left to adhere overnight. Cells were then placed either in a standard cell culture incubator (95% air: 5% CO_2) or a hypoxic chamber (2% O_2: 5% CO_2) for 24 hours before being lysed in RLT buffer containing 1% β-mercaptoethanol and stored at -20°C until RNA extraction. *MRC1* and *PLVAP* gene expression were then determined as described in **2.5 Polymerase Chain Reaction (PCR)**.

2.9.2 Shear Stress

HSEC were seeded in collagen-coated 6-well plates at a cell density of 150,000/well in 2 mL complete culture medium and left to adhere overnight. Culture medium was then replaced before cells were placed in either a static or rotating incubator for 72 hours. The orbital shaker was used to subject HSEC to arterial levels of shear stress estimated to be around 10 dynes/cm^2[463]. After 72 hours, HSEC were lysed in RLT buffer containing 1% β-mercaptoethanol and stored at -20°C until RNA extraction. *MRC1* and *PLVAP* gene expression were then determined as described in **2.5 Polymerase Chain Reaction (PCR)**

2.9.3 Conditioned Medium

The effects of conditioned medium from HCC cell lines on PLVAP expression was determined by high-content imaging. Huh-7 and HepG2 cells. were maintained in Dulbecco's modified Eagle's medium (DMEM) containing 10% FBS and 1% PSG and passaged using TrypLE™ enzyme as described in **2.4.2 HSEC Culture and Passage**. One day post-passaging, when the cells were around 80% confluent, conditioned medium was harvested, centrifuged at 300 *g* for five minutes to remove cell debris, and stored at -20°C until use.

HSEC were seeded in collagen-coated 96-well black imaging plates at a cell density of 25,000/well in complete culture medium and left to adhere overnight. The following day, HSEC were treated with either conditioned medium from cell lines or respective media control (DMEM + 10% FBS) and incubated for 24 hours. Cells were then fixed and stained for PLVAP as described in **2.6 Immunocytochemistry**. PLVAP immunofluorescence was quantified as detailed in **2.8 High-content Imaging Assay**.

2.10 RNA Interference

2.10.1 Short-interfering (si)RNA Transfection of HSEC

Reagents used in RNA interference studies are detailed in **Table 2.9**. Cells were seeded at an appropriate density to form a confluent monolayer overnight. For analysis of gene expression knockdowns were performed in collagen-coated 6-well plates. For immunocytochemistry and imaging, knockdowns were performed in 96-well black plates. For flow assays, knockdowns were performed in 6-channel ibidi® μ-slides. Working volumes were scaled up or down according to the application. siRNA duplexes were diluted in OptiMEM such that the final concentration was 3.125 nM and then incubated at 20-22°C for 10 minutes. Lipofectamine was mixed with OptiMEM to enable a final concentration of 0.3% and incubated at 20-22°C for 10 minutes. Lipofectamine and siRNA duplexes were then mixed and incubated at 20-22°C for a further 10 minutes. Cells were washed twice with sterile PBS and then siRNA/lipofectamine mix was diluted in OptiMEM (1:4) and added to the cells before being incubated at 37°C for four hours. Media was then replaced with antibiotic- and growth factor-free culture medium and incubated for 48 hours, prior to cell lysis or fixation, or use in subsequent functional assays.

2.10.2 Cell Lysis

Cells were washed twice with sterile PBS and then lysed for RNA as described above (**2.5.2 Cell Lysis**). Cell lysates were stored at -20°C until RNA extraction and qRT-PCR.

2.10.3 Assessment of Knockdown

Genetic knockdown of MR and PLVAP was carried out in collagen-coated 6-well plates during optimisation stages so that cells could be lysed and knockdown efficiency could be assessed at the RNA level. This was done via qRT-PCR as described above in **2.5 Polymerase Chain Reaction (PCR)**. Knockdown was also performed in 96-well plates and efficiency was confirmed by immunofluorescent staining via high-content imaging (**2.6 Immunocytochemistry, 2.8 High-content Imaging Assay**). After confirming successful genetic knockdown, via these methods, siRNA-treated cells were used in functional studies such as flow adhesion assays.

2.11 SASP Stimulation

2.11.1 Generation of SASP from IMR90 Fibroblasts

The senescence-associated secretory phenotype (SASP) was a kind gift from Dr. Matt Hoare (CRUK Cambridge Centre). The SASP was generated by obtaining conditioned medium from IMR90 cells expressing a 4-hydroxytamofixen (4-OHT)-inducible form of oncogenic $HRAS^{G12V}$ (ER:$HRAS^{G12V}$). These cells undergo oncogene-induced senescence in the presence of 4-OHT as a result of RAS overexpression[464]. ER:$HRAS^{G12V}$ IMR90 cells were generated using the pLNCX2 ER:$HRAS^{G12V}$ (RRID:Addgene_67844) retroviral vector and were maintained in DMEM containing 10% FBS and 1% PSG. Cells were passaged using TrypLE™ enzyme as described in **2.4.2 HSEC Culture and Passage**. Frozen IMR90 cells were thawed and cultured until fully confluent before being split into three T75 cm^2 culture flasks, one of which contained culture medium supplemented with 100 nM 4-OHT (Sigma). Cells were then cultured for six days and passaged as necessary, before supernatant was harvested, centrifuged at 300 *g* for five minutes and stored at -80°C until use. Conditioned medium from senescent IMR90 cells was designated “Ras-CM” and was compared to conditioned medium from the growing IMR90 controls (“Grow-CM”).

2.11.2 SASP Stimulation of HSEC

HSEC were treated for 24 hours with Grow-CM or Ras-CM at a dilution of 1 in 4 or 1 in 2 in either complete culture media or antibiotic- and growth factor-free media (following siRNA treatment). The HSEC phenotype was then characterised in a number of ways, including analysis of gene expression by qRT-PCR, morphological analysis by brightfield and confocal microscopy, and analysis of protein expression by immunocytochemistry followed by high-content imaging or confocal microscopy. These methodologies are described above. The effects of SASP treatment on cytokine production (in the presence or absence of PLVAP) and leukocyte recruitment were determined by performing cytokine arrays on cell supernatants or flow adhesion assays, respectively.

2.12 Cytokine Arrays

2.12.1 Generation of HSEC Supernatants

The role of PLVAP in regulating the HSEC secretome in response to SASP stimulation was investigated. HSEC were seeded in collagen-coated 6-well plates at a cell density of 300,000/well in complete culture medium and left to adhere overnight. Cells were then transfected with siRNAs targeted against *PLVAP* as described in **2.10 RNA Interference**. After 24 hours, HSEC were stimulated with either the Grow-CM or Ras-CM (1 in 2 dilution in Endothelial SFM containing 10% human serum) for 24 hours, before washing with warm PBS, addition of fresh Endothelial SFM containing 10% human serum, and incubation for a further 24 hours. Cell supernatants were then harvested, centrifuged at 300 *g* for three minutes to remove cell debris, and stored at -80°C until use. Successful knockdown was confirmed at the RNA level by qRT-PCR before cell supernatants were used in cytokine arrays.

2.12.2 Cytokine Array Method

HSEC supernatants were analysed using a Proteome Profiler Human Cytokine Array Kit (R&D #ARY005B) as per the manufacturer's instructions. All incubation steps were performed with gentle agitation (20 rpm on laboratory rocker). Briefly, nitrocellulose membranes containing capture antibodies were blocked by incubating for one hour with Array Buffer. Supernatants were thawed on ice before

adding 1 mL of sample to 0.5 mL Array Buffer. To each sample, 15 μL Detection Antibody Cocktail was added and incubated for one hour at 20-22°C. Blocking buffer was then replaced with sample/antibody mixture and incubated overnight at 4°C. Membranes were then washed three times for ten minutes each with 1X Wash Buffer, before addition of Streptavidin-HRP and incubation for 30 minutes at 20-22°C. Membranes were washed as described previously before being incubated for one minute with Chemi Reagent Mix. After blotting on paper towel to remove excess Chemi Reagent, membranes were auto-exposed and imaged in the chemiluminescence channel using a ChemiDoc™ Imaging System (Bio-Rad).

2.12.3 Cytokine Array Analysis

Each spot on each membrane was selected using the oval selection tool in ImageJ and the integrated density was measured and recorded. The density of each spot was normalised to the reference spots on the same membrane; i.e. the fold change in density relative to the average density of the reference spots was calculated. Data shown are from duplicate spots for each cytokine, with each experimental condition performed in singlicate from one HSEC isolate.

2.13 Flow Adhesion Assay

Equipment, plastics and reagents used in flow adhesion assays are detailed in **Table 2.10** and **Table 2.11**.

2.13.1 Lymphocyte Isolation from Peripheral Blood

Peripheral whole blood (~30 mL per 6-channel Ibidi® μ-slide) was gently layered on top of Lympholyte® cell separation media and centrifuged at 800 *g* for 20 minutes with the brake switched off. Peripheral blood mononuclear cells (PBMCs) at the plasma-separation media interface were then removed, diluted in PBS, and centrifuged at 2000 rpm for five minutes. Cells were then washed by resuspending pellet in 35 mL PBS, before centrifugation at 800 rpm for 10 minutes to remove platelets. Supernatant was discarded and PBMCs were resuspended in flow assay medium (Endothelial SFM containing 0.1% (v/v)

BSA). To isolate lymphocytes, PBMCs were added to a 75 cm^2 culture flask and monocytes were allowed to adhere to the plastic for one hour, and then cell suspension was removed and lymphocytes were counted using a haemocytometer. Lymphocytes were then centrifuged at 2000 rpm for five minutes and the cell pellet was resuspended in flow assay medium to a density of 1 x 10^6 cells/mL. All cells were kept at 37°C in a humidified incubator until use in flow adhesion assay.

2.13.2 Monocyte Isolation from Peripheral Blood

PBMCs were isolated from 60 mL peripheral whole blood as described in **2.13.1 Lymphocyte Isolation from Peripheral Blood**. Monocytes were then isolated using a Pan Monocyte Isolation Kit as per the manufacturer's instructions. Briefly, PBMCs were resuspended in 40 μL/10 million cells of magnetic-activated cell sorting (MACS) buffer (PBS containing 1 mM ethylenediaminetetraacetic acid (EDTA) and 2% FBS) and incubated for 5 min on ice with 10 μL/10 million cells of Fc Receptor Blocking Reagent and 10 μL/10 million cells of Biotin-Antibody Cocktail. Then, 30 μL/10 million cells of MACS buffer and 20 μL/10 million cells of Anti-Biotin Microbeads were added before further incubation on ice for 10 min. Labelled cell suspension was then applied to a pre-wetted LS column, washed three times with 3 mL MACS buffer, and the flow-through was collected. Unlabelled cells (monocytes) were then centrifuged at 2000 rpm for 5 min before being resuspended in flow assay medium at a density of 1 x 10^6/mL prior to use in flow adhesion assay.

2.13.3 Fluorescent Labelling of Live HSEC

In some cases, HSEC were fluorescently labelled prior to flow assays by incubating for 1 h at 37°C with CellTracker™ Green (CTG) CMFDA (10 μM) and SiR-actin Live Actin Probe (1 μM) diluted in flow assay medium (Endothelial SFM containing 0.1% (v/v) BSA). Cells were then washed with PBS and then this was replaced with complete culture medium until use in flow adhesion assay. Following flow assays, pre-labelled cells were fixed with 4% PFA and subject to immunocytochemistry for additional markers. The route of transmigration was determined via confocal microscopy based on the following criteria: (1) Presence of a leukocyte (determined via DAPI) within the HSEC cytoplasm (disrupted CTG

staining); (2) Formation of an F-actin-rich pore (lymphocytes only); (3) Location of transmigratory event (proximal or distal to the cellular junctions); (4) Integrity of the VE-cadherin^{+} cell junction. Paracellular events were defined as occurring close to the cell junction and were associated with disrupted VE-cadherin immunofluorescence.

2.13.4 Flow Assay Method

Flow adhesion assays were performed as previously described[465], using blocking antibody-treated or siRNA-transfected HSEC to investigate a functional role for MR and PLVAP in leukocyte recruitment (adhesion, shape-change or transmigration). Primary HSEC seeded in collagen-coated ibidi® slides and grown to confluence were stimulated with 10 ng/mL TNFα or SASP (1 in 2 or 1 in 4 dilution for lymphocytes and monocytes, respectively) for eight (TNFα) or 24 hours (SASP). For antibody blockade experiments, HSEC were treated with blocking antibody for 40-50 minutes at 37°C prior to the flow assay (

Table 2.12). Each treatment condition was performed in at least duplicate. For genetic knockdown experiments, HSEC were transfected with siRNAs as described in **2.10 RNA Interference**, and treatments were performed in Endothelial SFM containing 10% human serum.

Flow assay apparatus was set-up as detailed previously[465]. Briefly, ibidi® slides were mounted on an inverted microscope, within a thermostatically-controlled chamber pre-warmed to 37°C, to allow phase-contrast microscopy. A 50 mL glass syringe with luer lock was then attached to ~25 cm of silicone tubing and inserted into a syringe pump set at a withdrawal rate of 0.28 mL/min to maintain a shear stress of 0.5 dyne/cm^2. Two 5 mL syringe barrels were attached to separate in-flow ports of an electronic solenoid valve with silicone tubing. The electronic solenoid valve was then connected to a single outflow port using silicone tubing, to enable switching between leukocytes and flow assay medium (Endothelial SFM containing 0.1% (v/v) BSA) with virtually no dead volume. The valve was then flushed with flow assay media to ensure removal of all air bubbles from the system. One syringe barrel was depleted almost fully of flow assay media and replaced with leukocyte suspension. Inlet (from solenoid valve)

and outlet (connected to syringe pump) tubes were then simultaneously connected to the ibidi® slide via microslide adaptors, ensuring there were no bubbles in the flow system.

The endothelial monolayer was then perfused with flow assay buffer for one minute, to remove the stimulant (TNFα, SASP) and/or antibody along with any cell debris, by enabling withdrawal of the syringe pump. Then, the inlet valve was switched to the leukocyte suspension to allow a five-minute bolus of leukocytes at a constant wall shear stress of 0.5 dyne/cm^2. The HSEC monolayer was then perfused with flow assay buffer for three minutes before recording ten fields of view at random along the length of the channel, ensuring movement against the direction of flow to avoid recording of the same leukocyte more than once. Following recording, HSEC were then fixed in 4% PFA for a minimum of 10 minutes and stored at 4°C in PBS until further analysis by immunocytochemistry. Fixed HSEC were then stained via immunofluorescence for markers of interest (MR/PLVAP and adhesion molecules), and in some cases phalloidin to visualise the actin cytoskeleton, using confocal microscopy.

2.13.5 Analysis of Leukocyte Rolling, Adhesion and Transmigration

Recorded fields of view were analysed offline and the number of adhered, shape-changed and transmigrated cells were scored manually by eye using the "Cell Counting" plugin on ImageJ. Stable, round, phase-bright leukocytes were counted as "adhered", whilst leukocytes that were phase-dark were considered "transmigrated". Shape-changed cells were no longer round and could be partially phase-bright/phase-dark (**Figure 2.1)**.

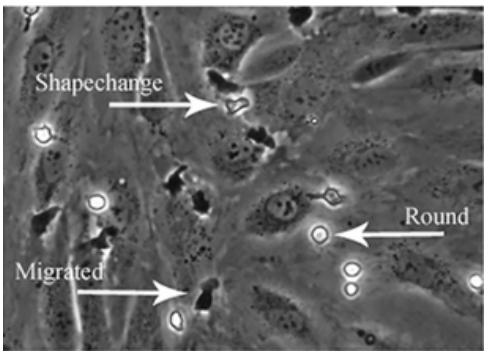

Figure 2.1: Phase-contrast image displaying various stages of the leukocyte adhesion cascade.
Image demonstrates leukocyte adhesion (phase-bright), shape-change and transmigration (phase-dark)[465].

2.14 The Cancer Genome Atlas Data Analysis

To study the gene expression of *MRC1* and *PLVAP*, as well as senescent markers *CDKN1A* (p21) and *CDKN2A* (p16), in a large cohort of HCC patients, The Cancer Genome Atlas (TCGA) dataset was analysed using a variety of widely-available online tools. Gene expression in HCC tumours was compared to matched non-tumour control tissue using https://xenabrowser.net/. Expression levels were then correlated with clinical outcomes including immune infiltrate (ESTIMATE: https://bioinformatics.mdanderson.org/estimate/ TIMER: https://cistrome.shinyapps.io/timer/), tumour aggressiveness (Buffa hypoxia and aneuploidy scores), tumour grade and cancer stage using http://www.cbioportal.org/, and overall and disease-free patient survival accessible via https://kmplot.com/analysis/.

2.15 Data Analysis and Statistics

All data were statistically analysed and presented graphically using GraphPad Prism 9.1.0 software unless otherwise indicated in results. All data shown are mean ± standard error of the mean (SEM) of at least three independent experiments unless otherwise stated in the results section. Data sets were analysed for a normal (Guassian) distribution using a Shapiro-Wilk normality test. Normally distributed data sets were then compared using parametric statistical tests, whereas non-normally distributed data sets were compared using equivalent non-parametric tests. Two independent data sets were statistically compared with an unpaired student's *t*-test (or Mann-Whitney), whilst three or more independent data sets were compared with a one-way analysis of variance (ANOVA) (or Kruskal-Wallis test) followed by an appropriate post-hoc multiple comparisons test. Treatment conditions were compared to their relevant unstimulated or vehicle-treated control with Dunnett's/Dunn's multiple comparison test, unless stated in the results section. Where appropriate, correlation analysis was performed for normally or non-normally distributed data using a Pearson's or Spearman's correlation test, respectively.

2.16 Equipment and Reagents

Table 2.1: Equipment and reagents used in immunohistochemistry studies.

Reagent	Source	Catalogue No.
Acetone	FisherScientific	A/0606/17
Bloxall® Endogenous Blocking Solution	Vector	SP-6000
Casein (10X)	Vector	SP-5020
CellStor (10% neutral buffered formalin)	CellPath	BAF-0010-01A
Citrate-based Antigen Retrieval Buffer	Vector	H-3300-250
Cryostat	Bright	OTF5000
DAPI	Invitrogen	D1306
Direct red 80	Sigma	365548
DPX	CellPath	SEA-1300-00A
Glass coverslips	Marienfeld	102192
Goat serum	Abcam	ab138478
Histowax	pfm Medical	9000R2010
Hydrochloric acid (37% v/v)	Sigma	H1758
Hydrogen peroxide (30% w/w)	Sigma	H1009
ImmPACT® DAB Peroxidase (HRP) Substrate	Vector	SK-4105
Industrial Denatured Alcohol	pfm Medical	PRC/R/101
Mayer's Haematoxylin	pfm Medical	PRC/R/42
Methanol	VWR	20847.307
Microscope Slides	Klinipath	PR-P-001
O.C.T.™	Tissue-Tek®	16-004004
PBS	Sigma	P4417
Picric acid (1.3% v/v)	Sigma	P6744-1GA
Platform Shaker STR6	Stuart Scientific	-
PMA	Sigma	HT153
ProLong™ Gold Antifade Mountant	ThermoFisher Scientific	P10144
Tris-based Antigen Retrieval Buffer	Vector	H-3301-250
Tween® 20	Sigma	P1379
Xylene	pfm Medical	PRC/R/201

DAPI, 4′,6-diamidino-2-phenylindole; **DPX**, distyrene plasticiser xylene; **DAB**, 3,3'-diaminobenzidine; **HRP**, horseradish peroxidase; **PBS**, phosphate buffered saline; **PMA**, phorbol 12-myristate 13- acetate

Table 2.2: Details of primary antibodies.

Antibody	Source	Catalogue No.	Use	Concentration
αSMA	Sigma	A5288	IHC-Fr	20 µg/mL
Caveolin-1	Abcam	ab192869	IHC-Fr, ICC	1.96 µg/mL
CCL2	Novus Bio	NBP1-07035	ICC	2 µg/mL

CD20	Invitrogen	MA5-13141	IHC-P	0.2 µg/mL
CD31	Dako	M0823	IHC-Fr	5 µg/mL
CD31	Abcam	ab9498	ICC, Blocking	5 µg/mL
CD32b	Abcam	ab151497	ICC	2 µg/mL
CD34	Abcam	ab8536	IHC-Fr	10 µg/mL
CD36	Abcam	ab137320	ICC	10 µg/mL
CD45	Abcam	ab10558	IHC-P	2.5 µg/mL
CD68	Biolegend	333802	IHC-Fr	5 µg/mL
CD8	Abcam	ab199016	IHC-P	1.6 µg/mL
Collagen III	Abcam	ab7778	IHC-Fr	1 µg/mL
EEA1	Abcam	ab50313	ICC	5 µg/mL
EEA1	BD Biosciences	610456	ICC	2.5 µg/mL
GM130	BD Biosciences	610823	ICC	2.5 µg/mL
GM130	Merck	MABT-1363	ICC	5 µg/mL
ICAM1	R&D	BBA3	ICC, Blocking	5 µg/mL
L-SIGN	R&D	MAB162	IHC-Fr	5 µg/mL
LYVE-1	Abcam	ab33682	ICC	5 µg/mL
LYVE-1	R&D	MAB20891	IHC-Fr	5 µg/mL
MAC387	Invitrogen	MA5-11213	IHC-P	2 µg/mL
MECA-32	Novus Bio	NB100-77668	IHC-P	2 µg/mL
mIgG1 IMC	Dako	X0931	IHC, ICC	-
mIgG2a IMC	Dako	X0943	IHC, ICC	-
mIgG2b IMC	Dako	X0944	IHC, ICC	-
MR	Abcam	ab64693	IHC-Fr, ICC	2.5 µg/mL
MR	Abcam	ab8918	IHC-Fr, ICC, Blocking	2 µg/mL
NE	Abcam	ab219585	IHC-P	0.515 µg/mL
PLVAP	Abcam	ab8086	IHC-Fr	1 µg/mL
PLVAP	Abcam	ab81719	ICC, Blocking	2 µg/mL
PLVAP	Sigma	HPA002279	IHC-P	1 µg/mL
Rab11a	Abcam	ab65200	ICC	1 µg/mL
Rb IMC	Dako	X0903	IHC, ICC	-
rIgG2a IMC	Invitrogen	14-4321-81	IHC-P	-
Stabilin-1	Gift*	3-372	ICC	10 µg/mL
Stabilin-2	ThermoFisher	PA5-55447	ICC	2 µg/mL
VAMP7	Invitrogen	OSS00047G	ICC	10 µg/mL
VE-cadherin	R&D	MAB9381	ICC	1 µg/mL
Vimentin	Sigma	V6389	IHC-Fr	25 µg/mL

IHC-Fr, immunohistochemistry-frozen; **ICC**, immunocytochemistry; **IHC-P**, immunohistochemistry-paraffin.
*Stabilin-1 antibody was a kind gift from Sirpa Jalkenen (University of Turku, Finland).

Table 2.3: Details of secondary antibodies.

Antibody	Source	Catalogue No.	Use	Concentration
Anti-Mouse Immpress® Kit	Vector	MP-7402	IHC-Fr, IHC-P	Pre-diluted
Anti-Rabbit Immpress® Kit	Vector	MP-7401	IHC-Fr, IHC-P	Pre-diluted
Ant-Rat Immpress® Kit	Vector	MP-7444	IHC-P	Pre-diluted
mIgG1 AF488	Invitrogen™	A21121	IHC-Fr, ICC	4 µg/mL
mIgG1 AF546	Invitrogen™	A21123	IHC-Fr, ICC	4 µg/mL
mIgG2a AF546	Invitrogen™	A21133	IHC-Fr, ICC	4 µg/mL
mIgG2b AF488	Invitrogen™	A21141	IHC-Fr, ICC	4 µg/mL
mIgG2b AF546	Invitrogen™	A21143	IHC-Fr, ICC	4 µg/mL
Rb AF488	Invitrogen™	A11008	IHC-Fr, ICC	4 µg/mL
Rb AF546	Invitrogen™	A110035	IHC-Fr, ICC	4 µg/mL

IHC-Fr, immunohistochemistry-frozen; **ICC**, immunocytochemistry; **IHC-P**, immunohistochemistry-paraffin

Table 2.4: Equipment, plastics and reagents used for cell culture.

Reagent	Source	Catalogue No.
15 ml centrifuge tubes	Corning	352095
25 cm^2 culture flasks	Corning	430639
50 ml centrifuge tubes	Corning	430829
6-well culture plates	Corning	3516
75 cm^2 culture flasks	Corning	430641U
Anti-EpCAM antibody (clone HEA125)	Progen	61004
Class II Microflow Safety Cabinet	-	Holten LaminAir 1.8
Collagen type I from rat tail	Sigma	C3867
Collagenase type 1A from Clistridium histolytcum	Sigma	C9891
CoolCell® LX freezing container	Corning	432003
Cryovials	Corning	431386
DMEM	Gibco	41965-039
DMSO	Sigma	D650
Dynabeads™ CD31 Endothelial Cell	ThermoFisher Scientific	11155D
Dynabeads™ Goat Anti-Mouse IgG	ThermoFisher Scientific	11033
Dynabeads™ CD45	ThermoFisher Scientific	11153D
DynaMag™-15 Separation Magnet	Invitrogen	12301D
Endothlelial Cell Serum-Free Medium	Gibco	11111044
FBS	Gibco	10500064
Haemocytometer	Neubauer	-
Human Serum	TCS Biosciences	CS100-500
Humidified Incubator	phc	IncuSafe
Ibidi® ibiTreat µ-Slide VI 0.4	Ibidi	80606
PBS	Sigma	P4417

Penicillin-Streptomycin-Glutamine (100X)	Gibco	10378016
Percoll™	Sigma	GE17-0891-01
Recombinant human HGF	Peprotech	100-39H
Recombinant human VEGF	Peprotech	100-20
Sterile pasteur pipettes	Fisher	13469108
Sterile Scalpels	Swann-Morton	05XX
TrypLE™ Express Enzyme (1X)	Gibco	12605010

EpCAM, epithelial cell adhesion molecule; **DMEM**, Dulbecco's modified eagle medium; **DMSO**, dimethyl sulphoxide; **FBS**, foetal bovine serum; **PBS**, phosphate buffered saline; **HGF**, hepatocyte growth factor; **VEGF**, vascular endothelial growth factor.

Table 2.5: Equipment and regents used for PCR.

Reagent	Source	Catalogue No.
10 mM dNTP Mix	Invitrogen	18427-013
384 Multi-well Plates	Roche	04729749001
96 Multi-well Plates	Roche	04729692001
β-mercaptoethanol	Sigma	M6250
Ethanol	VWR	20821.330
gentleMACS™ Dissociator	Miltenyi Biotec	-
gentleMACS™ M-tubes	Miltenyi Biotec	130-093-236
LightCycler® 480 Intrument II	Roche	-
NanoPhotometer™	Geneflow	Implen
Nuclease-free Microcentrifuge Tubes	Star Lab	I1402-8100
Nuclease-free Water	Promega	P119C
PBS	Sigma	P4417
Random Primers	Promega	C1181
RNase-free DNase Set	Qiagen	1023460
RNaseOUT™ Ribonuclease Inhibitor	Invitrogen	10777-019
RNeasy® Micro Kit	Qiagen	74004
RNeasy® Mini Kit	Qiagen	74104
SensoQuest Labcycler 48	Geneflow	-
SuperScript® III Reverse Transcriptase	Invitrogen	18080-044
TaqMan® Universal PCR Master Mix	Applied Biosystems	4326708

dNTP, deoxyribonucleotide triphosphate; **PBS**, phosphate buffered saline.

Table 2.6: TaqMan® Gene Expression Assays used for PCR.

Reagent	Source	Catalogue No.
18S TaqMan® Assay	ThermoFisher Scientific	Hs99999901
ACTB TaqMan® Assay	ThermoFisher Scientific	Hs01060665
CCL2 TaqMan® Assay	ThermoFisher Scientific	Hs00234140

CDKN1A TaqMan® Assay	ThermoFisher Scientific	Hs00355782
CDKN2A TaqMan® Assay	ThermoFisher Scientific	Hs00923894
CXCL8 TaqMan® Assay	ThermoFisher Scientific	Hs00174103
GAPDH TaqMan® Assay	ThermoFisher Scientific	Hs99999905
GUSB TaqMan® Assay	ThermoFisher Scientific	Hs00939627
ICAM1 TaqMan® Assay	ThermoFisher Scientific	Hs00164932
IL1B TaqMan® Assay	ThermoFisher Scientific	Hs00174097
IL6 TaqMan® Assay	ThermoFisher Scientific	Hs00985639
MRC1 TaqMan® Assay	ThermoFisher Scientific	Hs00267207
PLVAP TaqMan® Assay	ThermoFisher Scientific	Hs00229941

Table 2.7: Reagents used in immunocytochemistry studies.

Reagent	Source	Catalogue No.
Bafilomycin A1 from Streptomyces griseus	Sigma	196000
Casein (10X)	Vector	SP-5020
DAPI	Invitrogen	D1306
Dil-AcLDL	Sigma	L3484
FITC-dextran	Sigma	FD40
Goat serum	Abcam	ab138478
PBS	Sigma	P4417
PFA	Alfa Aesar	J61899
Phalloidin AF633	Invitrogen	A22284
Triton™ X-100	Sigma	X100
Tween® 20	Sigma	P1379

DAPI, 4′,6-diamidino-2-phenylindole; **AcLDL**, acetylated low-density lipoprotein; **FITC**, fluorescein isothiocyanate; **PBS**, phosphate buffered saline; **PFA**, paraformaldehyde.

Table 2.8: Reagents used in high-content screening.

Reagent	Source	Catalogue No.	Concentration
15d-PGJ2	Cambridge Biosciences	CAY-18570.1	5 mM
Angiopoietin I	Sigma	SRP3007	250 ng/mL
Angiopoietin II	Sigma	SRP6403	250 ng/mL
Angiotensin II	Sigma	A9525	100 nM
ATRA	Sigma	R2625	100 nM
BMP-9	Peprotech	120-07	10 ng/mL
Ciglitazone	Cambridge Biosciences	CAY-71730	5 mM
CX_3CL1	Peprotech	300-31	0.85 mg/mL
Cytochalasin D	Sigma	C2618	1 mg/mL
Dexamethasone	Sigma	D4902	10 mM
Dimethyl Fumarate	Sigma	242926	20 mM

DMSO	Sigma	D650	-
Ethanol	VWR	20821.33	-
Falcon® 96-well Imaging Microplates	Corning	353219	-
Fibrinogen	Sigma	341578	4 mg/mL
HGF	Peprotech	100-39H	48 ng/mL
IFNγ	Peprotech	300-02	11.86 ng/mL
IL-10	Peprotech	200-10	20 ng/mL
IL-13	Peprotech	200-13	10 ng/mL
IL-4	Peprotech	200-04	10 ng/mL
IL-6	Miltenyi Biotec	130-095-3650	10 ng/mL
IL1β	Peprotech	200-01B	10 ng/mL
Latrunculin A	Sigma	428026	1 mM
LiCl	Sigma	L7026	10 mM
LPA	Sigma	L7260	1 mM
LPS from *E. coli* (O111:B4)	Sigma	L2630	1 µg/mL
Methanol	VWR	20847.307	-
PGE1	Sigma	P5515	100 nM
PMA	Sigma	P8139	50 nM
Rosiglitazone	Cambridge Biosciences	CAY-71740	5 mM
S1P	Sigma	73914	100 nM
SB431542 (ALK5i)	Sigma	616461	10 mM
TGFβ	Peprotech	100-21	5 ng/mL
TNFα	Peprotech	300-01A	10 ng/mL
VEGF	Peprotech	100-21	100 ng/mL
Wnt3a	R&D Systems	5036-WN-010	200 ng/mL

$15dPGJ_2$, 15-Deoxy-Delta-12,14-prostaglandin J2; **ATRA**, all-trans retinoic acid; **BMP-9**, bone morphogenic protein 9; **CX_3CL1**, fractalkine; **DMSO**, dimethyl sulphoxide; **HGF**, hepatocyte growth factor; **IFNγ**, interferon γ; **IL**, interleukin; **LiCl**, lithium chloride; **LPA**, lysophosphatidic acid; **LPS**, lipopolysaccharide; **PGE1**, prostaglandin E1; **PMA**, phorbol 12-myristate 13-acetate; **S1P**, sphinosine-1-phosphate; **ALK5i**, activin receptor-like kinase 5 inhibitor; **TGFβ**, transforming growth factor β; **TNFα**, tumour necrosis factor α; **VEGF**, vascular endothelial growth factor.

Table 2.9: Reagents used in RNA interference studies.

Reagent	Source	Catalogue No.
MRC1 siRNA	Ambion	s8957
Negative Control siRNA	Ambion	4390843
Opti-MEM™ Reduced Serum Medium	Gibco	31985-047
PLVAP siRNA	Ambion	s37972
RNAi Max Lipofectamine	Invitrogen	13778-075

Table 2.10: Equipment used in leukocyte isolation.

Reagent	Source	Catalogue No.

EDTA	Sigma	E0270
FBS	Gibco	10500064
LS Separation Column	Miltenyi Biotec	130-042-401
Lympholyte® Cell Separation Media	Cedarlane	CL5020
Magnet Midi MACS	Miltenyi Biotec	130-042-302
Pan Monocyte Isolation Kit (Human)	Miltenyi Biotec	130-096-537
PBS	Sigma	P4417

EDTA, ethylenediaminetetraacetic acid; **FBS**, foetal bovine serum; **MACS**, magnetic-associated cell sorting; **PBS**, phosphate buffered saline.

Table 2.11: Equipment and reagents used in flow adhesion assays.

Reagent	Source	Catalogue No.
5 mL Syringes	BD Emerald	307731
BSA Fraction V	Gibco	15260037
CellTracker™ Green (CMFDA)	Invitrogen	C2925
DAPI	Invitrogen	D1306
Electronic Solenoid Valve	Lee Products	-
Glass syringe	Popper & Sons inc.	-
Harvard Syringe Pump	Harvard Apparatus	PHD2000
PFA	Alfa Aesar	J61899
Phalloidin	Invitrogen	A22284
SiR-actin Live Cell Actin Probe	Spirochrome	SC001
TNFα	Peprotech	300-01A

BSA, bovine serum albumin; **DAPI**, 4′,6-diamidino-2-phenylindole; **PFA**, paraformaldehyde; **TNFα**, tumour necrosis factor α.

Table 2.12: Blocking antibodies used prior to flow adhesion assays.

Antibody	Source	Catalogue No.	Concentration
CD31	Abcam	ab9498	10 µg/mL
ICAM-1	R&D	BBA3	10 µg/mL
MR	Abcam	ab8918	2 µg/mL
PLVAP	Abcam	ab81719	10 µg/mL

ICAM-1, intercellular adhesion molecule 1; **MR**, mannose receptor; **PLVAP**, plasmalemma vesicle-associated protein

3 CHARACTERISATION OF MR AND PLVAP EXPRESSION IN HUMAN LIVER

3.1 Characterisation Studies

Recent single-cell RNA-sequencing studies have highlighted that *MRC1* is highly expressed in healthy sinusoidal endothelial cells, whilst *PLVAP* is upregulated in scar-associated and tumour-associated endothelial cells from cirrhotic and HCC patients, respectively[397, 398]. To investigate MR and PLVAP gene expression in human liver, *MRC1* and *PLVAP* mRNA was measured within whole tissue lysates from normal and chronically diseased liver via qRT-PCR analysis. Primary liver tumour specimens are not as readily accessible as CLD samples, and so publicly-available RNA-sequencing databases were utilised to complement gene expression data from a handful of HCC cases. *MRC1* and *PLVAP* gene expression was analysed, within The Cancer Genome Atlas (TCGA) dataset, in matched tumour and non-tumour HCC samples. Gene expression was then studied in relation to clinical parameters including cancer stage, tumour grade, tumour aggressiveness and patient survival.

To study the protein expression pattern of MR and PLVAP in normal and pathological human liver tissue, chromogenic immunohistochemistry was performed in donor and chronically diseased liver tissue, as well as in tumour and adjacent non-tumour tissue from HCC patients. To confirm the cellular location of these proteins, dual colour immunofluorescence was undertaken to simultaneously visualise MR^+ and $PLVAP^+$ cell populations in liver sections with cell-specific markers to further characterise these populations.

3.1.1 MR was abundantly expressed in normal liver tissue and downregulated in CLD

At the mRNA level, the median *MRC1* gene expression showed a 1.59-fold reduction in CLD patients compared to donor controls, although this difference was not statistically significant (**Figure 3.1A**). In fact, there were no significant differences in *MRC1* gene expression between any of the disease groups studied, despite three out of four aetiologies displaying lower (~1.52–3.76-fold) levels of gene expression (**Figure 3.1B**).

In donor liver tissue sections, MR showed a homogenous sinusoidal expression pattern, with some areas of intense staining within the sinusoidal regions which are characteristic of Kupffer cells (**Figure 3.2**). Staining appeared to be uniform across the hepatic lobule, with little evidence of any zonation in relation to its expression. MR was observed to be absent from other hepatic structures including hepatocytes and bile ducts. Isotype-matched controls were performed in matched sample cases where possible and were shown to be negative. In chronically diseased liver tissue, including metabolic conditions such as ALD and NASH and cholestatic diseases PBC and PSC, MR homogeneity was observed to be disrupted compared with that seen in donor liver tissue (**Figure 3.3**). Sirius red staining was performed on serial liver sections, to highlight collagen deposition, which was used to measure the extent of fibrosis within each case. In particular, MR expression seemed to be much lower, or in some cases absent, in areas proximal to fibrotic septa indicated by Sirius red staining (**Figure 3.3**). Notably, despite the disruption in MR expression close to fibrotic areas, MR was still observed within fibrotic septa.

Chronic liver diseases are characterised by fibrosis independently of aetiology, which was highlighted by the significantly (~4.8-fold) higher levels of collagen deposition (Sirius red staining) (**Figure 3.4A**). In contrast, MR staining area was significantly lower in CLD livers (9.85 ± 1.05%) compared with donor liver controls (17.09 ± 1.63%) (**Figure 3.4B**), although when stratified based on aetiology, only ALD samples were statistically different **(Figure 3.4C**). Although there was no significant correlation between the levels of MR and Sirius red staining in matched patient samples, donor livers did seem to cluster together and displayed higher MR expression and lower collagen deposition (**Figure 3.4D**), which is consistent with MR being highly expressed in normal, non-fibrotic liver.

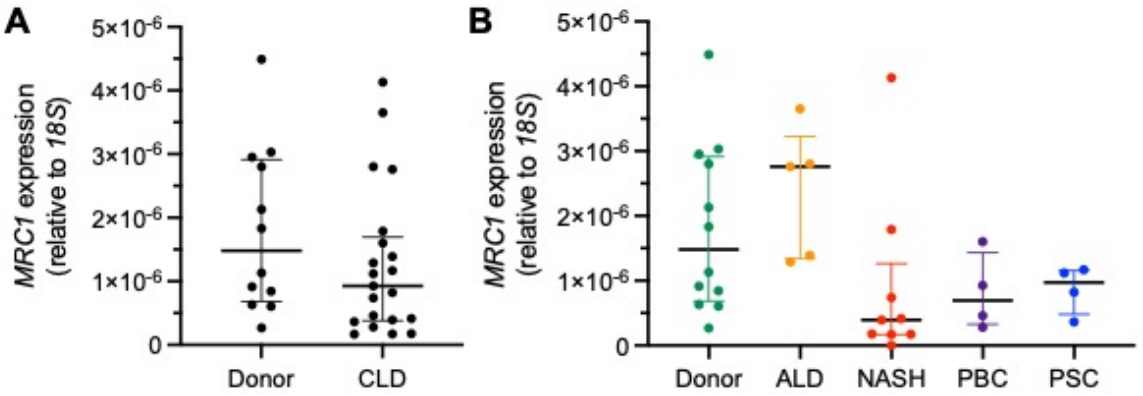

Figure 3.1: Mannose receptor (*MRC1*) gene expression was comparable in normal and cirrhotic human liver.

(A) Gene expression was determined by qRT-PCR of whole liver tissue lysates from donor (n=12) and chronic liver disease (CLD) patients (n=21). **(B)** Data were then stratified based on aetiology (ALD, alcoholic liver disease; NASH, non-alcoholic steatohepatitis; PBC, primary biliary cholangitis; PSC, primary sclerosing cholangitis). There were no significant differences between *MRC1* expression in donor livers compared with either combined CLD samples ($p>0.05$, Mann-Whitney test) **(A)** or each individual aetiology ($p>0.05$, Kruskal-Wallis test followed by Dunn's multiple comparison test) **(B)**. *MRC1* expression is shown relative to *18S* which was used as a housekeeping gene. Data shown are median ± interquartile range where each data point represents an independent patient sample.

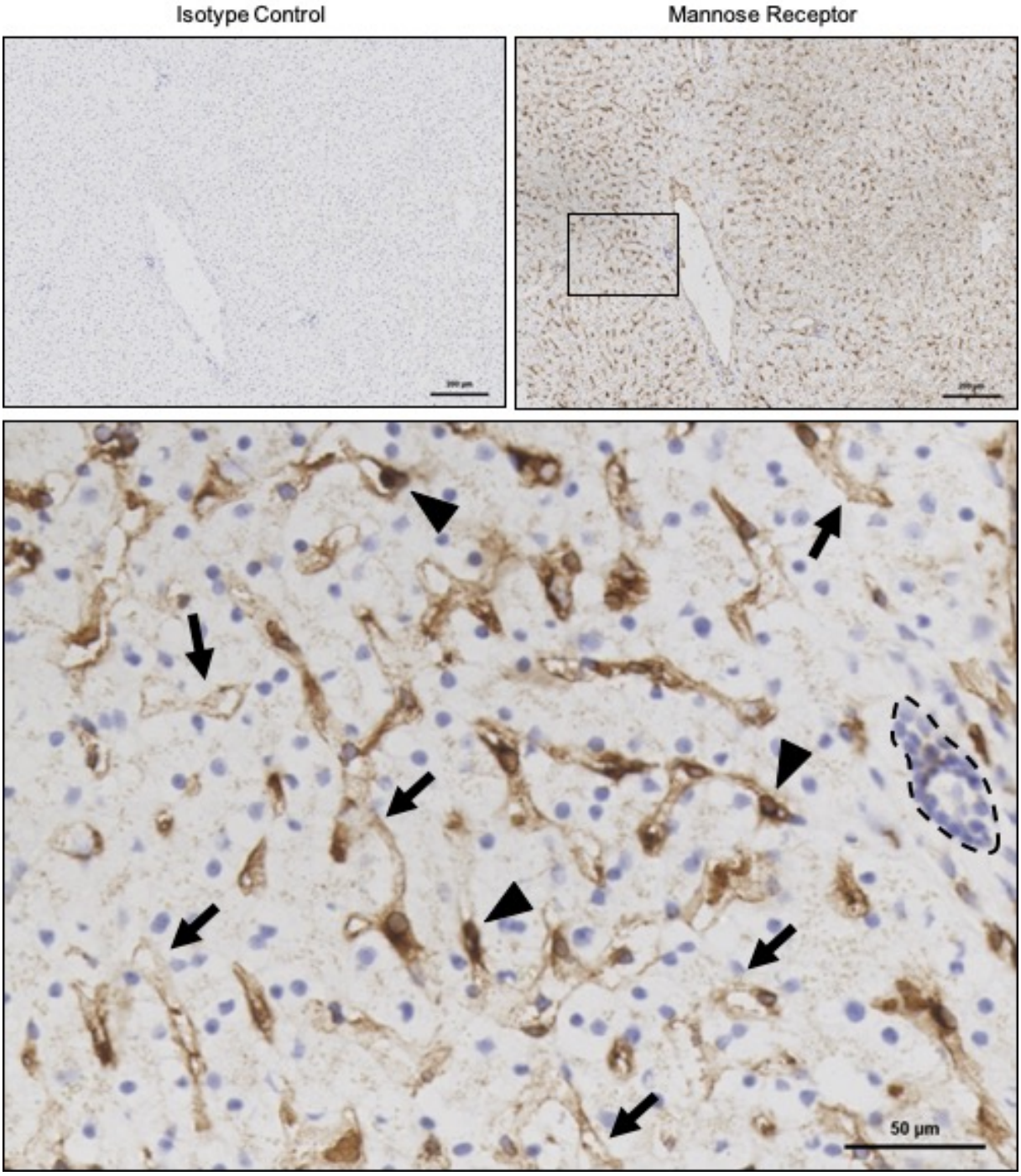

Figure 3.2: Mannose receptor (MR) was abundantly expressed in normal human liver tissue.

MR (*brown*) displayed a sinusoidal expression pattern (*arrows*) with some intense positive staining within sinusoids that resembled Kupffer cells (*arrowheads*) (*inset*, high magnification). Bile ducts (*dashed lines*) and hepatocytes were negative, as were isotype control samples. Fields of view were selected in Zen Blue software (Zeiss) post-acquisition of entire tissue sections using a Zeiss Axio Scan.Z1 and a 20x objective. Images shown are representative of 7-11 patient samples. Scale bars represent 200 µm (*upper*) and 50 µm (*lower*).

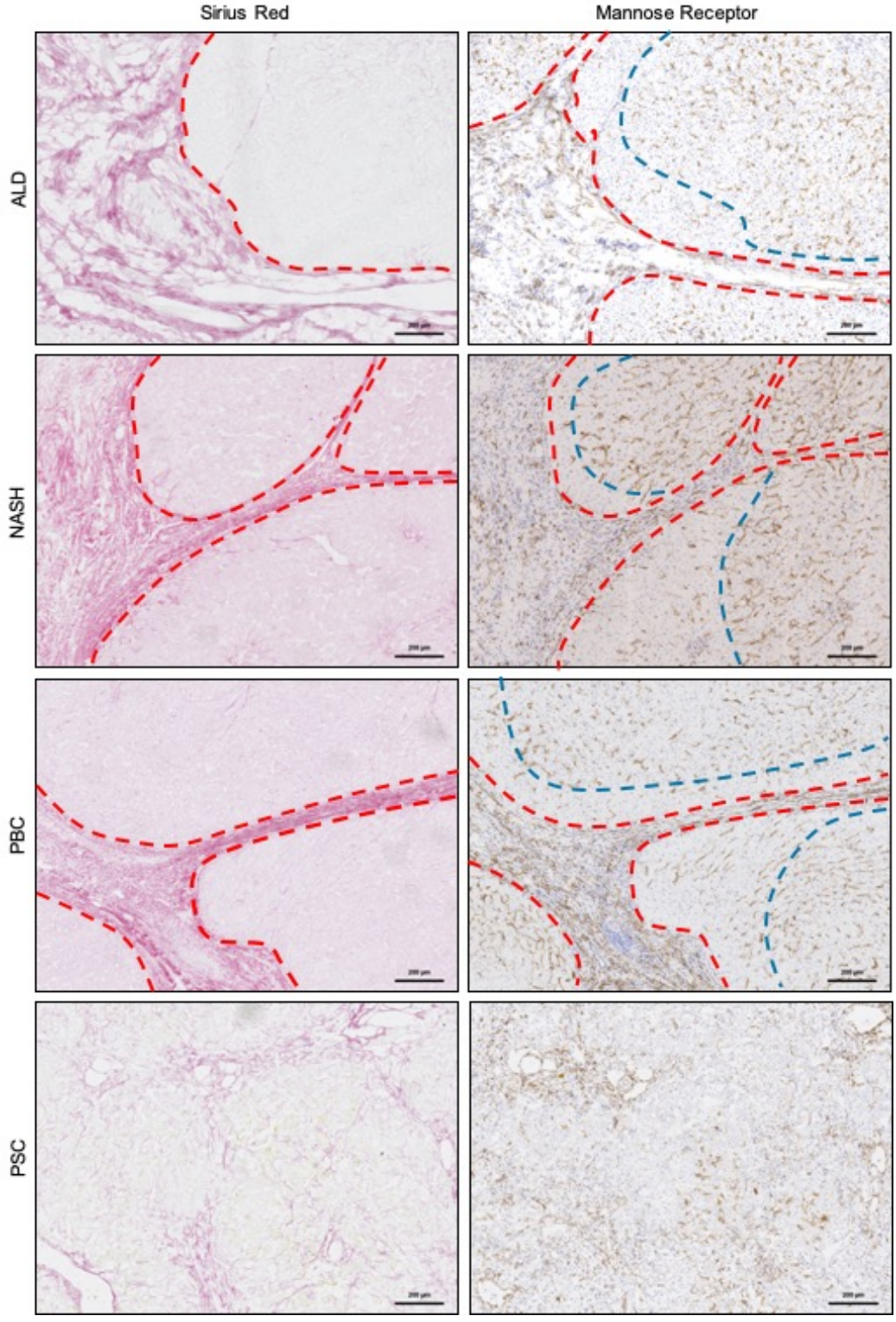

Figure 3.3: Mannose receptor (MR) homogeneity was disrupted in chronic liver disease (CLD).

MR (*brown*) expression was assessed in alcoholic liver disease (ALD), non-alcoholic steatohepatitis (NASH), primary biliary cholangitis (PBC) and primary sclerosing cholangitis (PSC) (*right panels*). Fibrosis was evident within patient samples by visualisation of collagen deposition (*red*) via Sirius red staining (*left panels*). Fibrotic septa are depicted by red dashed lines. MR expression was often particularly low in areas proximal to fibrotic septa, indicated by blue dashed lines, although MR was still present within fibrotic septa. Images shown are representative of 5-6 patient samples per aetiology. Scale bars represent 200 μm. See **Appendix 7.1** for isotype controls.

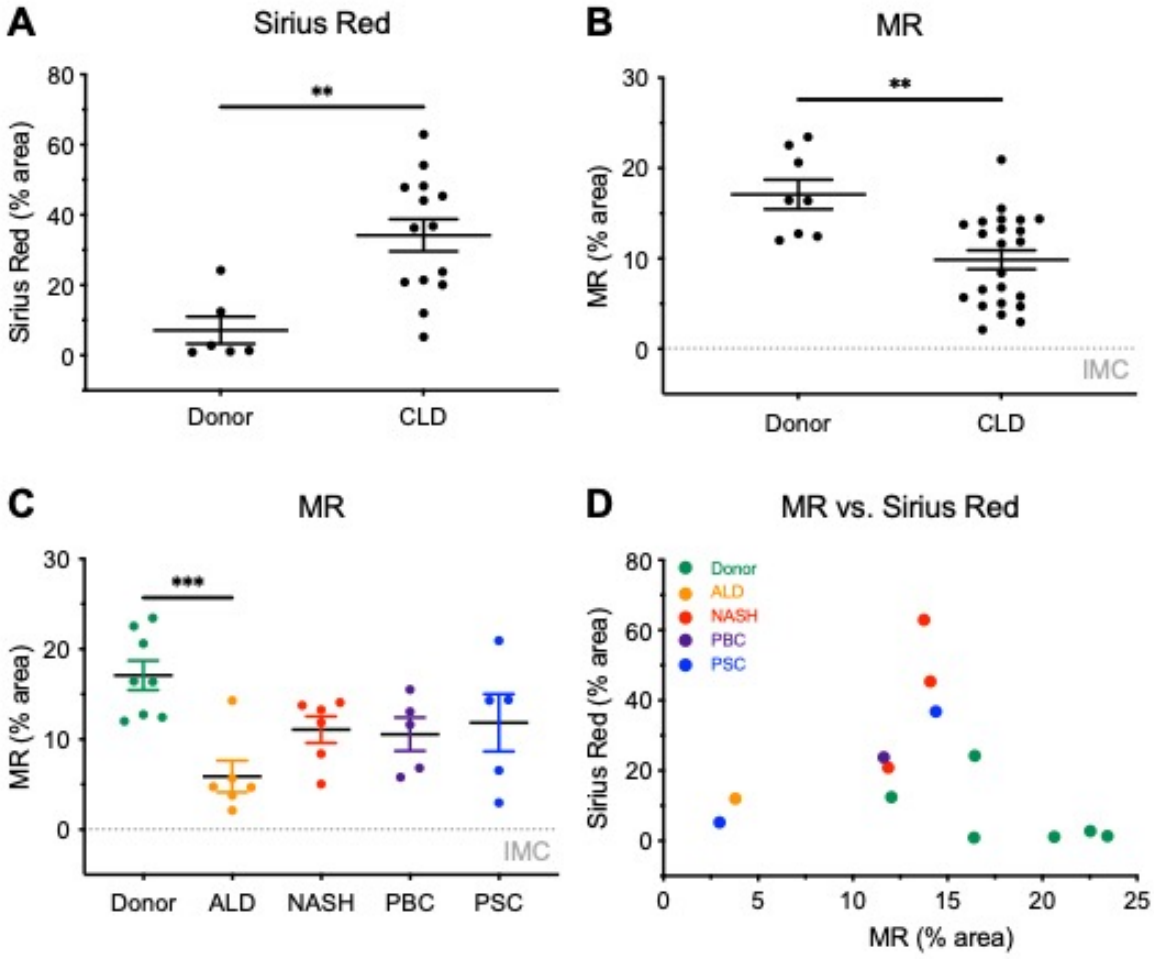

Figure 3.4: Mannose receptor (MR) was downregulated in chronic liver disease (CLD).

(A) Collagen deposition was measured via Sirius red staining of donor (n=6) and CLD (n=14) livers (**p<0.01, Mann-Whitney test). **(B)** MR expression was determined by quantification of immunohistochemical staining of donor (n=8) and CLD patient (n=23) samples (**p<0.01, student's unpaired t-test). **(C)** Data were stratified based on aetiology (ALD, alcoholic liver disease; NASH, non-alcoholic steatohepatitis; PBC, primary biliary cholangitis; PSC, primary sclerosing cholangitis) (***p<0.001, one-way ANOVA and Dunnett's multiple comparison test). Isotype-matched control (IMC) levels are indicated by the grey gridline. Data shown are mean % area ± SEM, where each data point represents an independent patient sample. **(D)** MR expression was plotted against Sirius red staining area measured in serial sections from matched patient samples (n=13).

3.1.2 MR was downregulated in HCC tumour tissue but did not correlate with clinical parameters

In tumour tissue from HCC patients, MR was downregulated at the mRNA level compared with adjacent non-tumour tissue (**Figure 3.5A**). Sequencing data from TCGA databases showed a significant ~3.63-fold reduction in *MRC1* gene expression within HCC tumours compared to matched non-tumour controls (**Figure 3.5A**). When HCC samples were analysed by qRT-PCR, there was no significant difference in *MRC1* gene expression, and some variation was seen between tumour levels relative to the

non-tumour tissue (**Figure 3.5B**). At the protein level, there was no significant difference in MR staining area within tumour tissue sections compared to non-tumour, as determined by immunohistochemistry (**Figure 3.5C, D**). However, despite intense MR staining within the tumour stroma, there appeared to be reduced sinusoidal MR, observed in 5/9 cases (**Figure 3.5D**). Regarding patient prognosis and survival, there was no significant association between *MRC1* expression and cancer stage or tumour grade (**Figure 3.6A, B**). Further, despite showing a negative correlation with aneuploidy score (**Figure 3.6C**), which is a surrogate marker of tumour aggressiveness, *MRC1* gene expression did not seem to be predictive of overall or disease-free patient survival (**Figure 3.6E**).

3.1.3 PLVAP was upregulated in CLD and showed a scar-associated expression pattern

At the gene level, PLVAP mRNA was shown to be increased (~6.85-fold) in CLD, as determined by qRT-PCR analysis (**Figure 3.7A**). When expression data were stratified according to aetiology, only ALD and NASH samples showed a significantly higher *PLVAP* gene expression compared to donor controls (**Figure 3.7B**). These data support the upregulation of PLVAP during chronic liver inflammation.

Expression of PLVAP in donor liver tissue was low (**Figure 3.8, Figure 3.10)**, tending to associate with periportal sinusoidal areas, as well as being expressed on larger vessels (**Figure 3.8)**. In CLD, PLVAP expression was considerably more evident, localising to neovessels within fibrotic septa and the surrounding sinusoids (**Figure 3.9**). When staining area was quantified, PLVAP was significantly upregulated in CLD patient samples overall (14.96 ± 1.44%), and when stratified as individual aetiologies, compared to donor levels (4.23 ± 0.88%) (**Figure 3.10A-B**). Moreover, PLVAP significantly correlated with the extent of collagen deposition and fibrosis in matched patient samples, with its expression being directly proportional to the amount of Sirius red staining (**Figure 3.10C**).

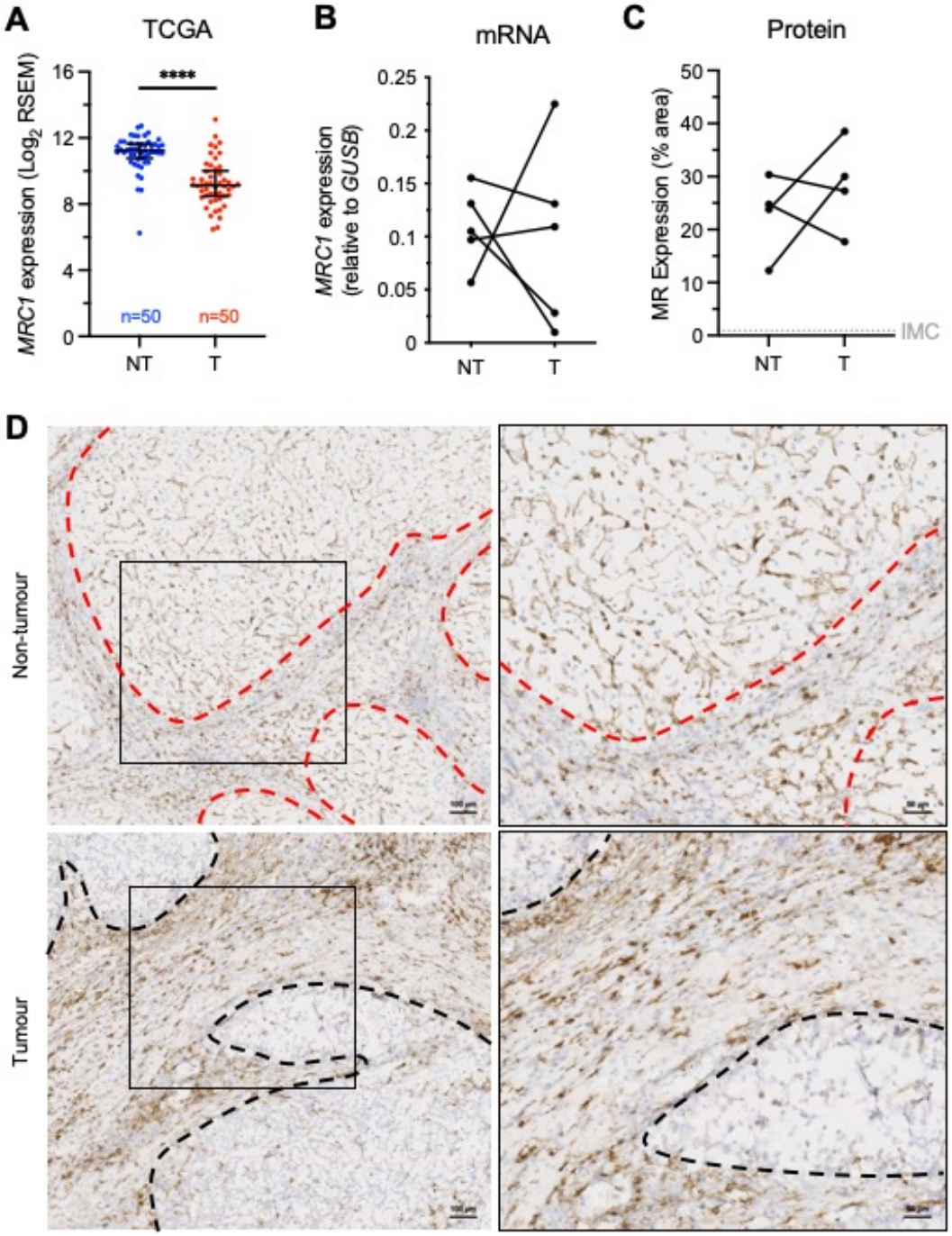

Figure 3.5: Mannose receptor (MR) was downregulated in hepatocellular carcinoma (HCC) tumours.

(A) Publicly-available TCGA (The Cancer Genome Atlas) databases were analysed for *MRC1* expression in matched non-tumour (NT) (n=50) and tumour (T) (n=50) tissues from HCC patients (****p<0.0001, Wilcoxon test). Data shown are median $\log_2$(RNAseq by Expectation-Maximum) ± interquartile range and are accessible via https://xenabrowser.net/. **(B)** *MRC1* expression was determined by qRT-PCR of matched NT and T whole tissue lysates from HCC patients (p>0.05, student's paired t-test). Expression is shown relative to *GUSB* which was used as a housekeeping gene. **(C)** MR protein expression was variable in HCC tumours compared to matched non-tumour controls, determined by immunohistochemistry and quantification of staining area. Each data point in **(A-C)** represents an independent patient sample. **(D)** Representative images of MR immunohistochemical staining (*brown*) in NT and T tissue from HCC patients. Fibrotic septa and tumour stroma are indicated by red and black dashed lines, respectively. Fields of view were selected in Zen Blue software (Zeiss) post-acquisition of entire tissue sections using a Zeiss Axio Scan.Z1 and a 20x objective. Scale bars represent 100 µm (*left*) and 50 µm (*right*).

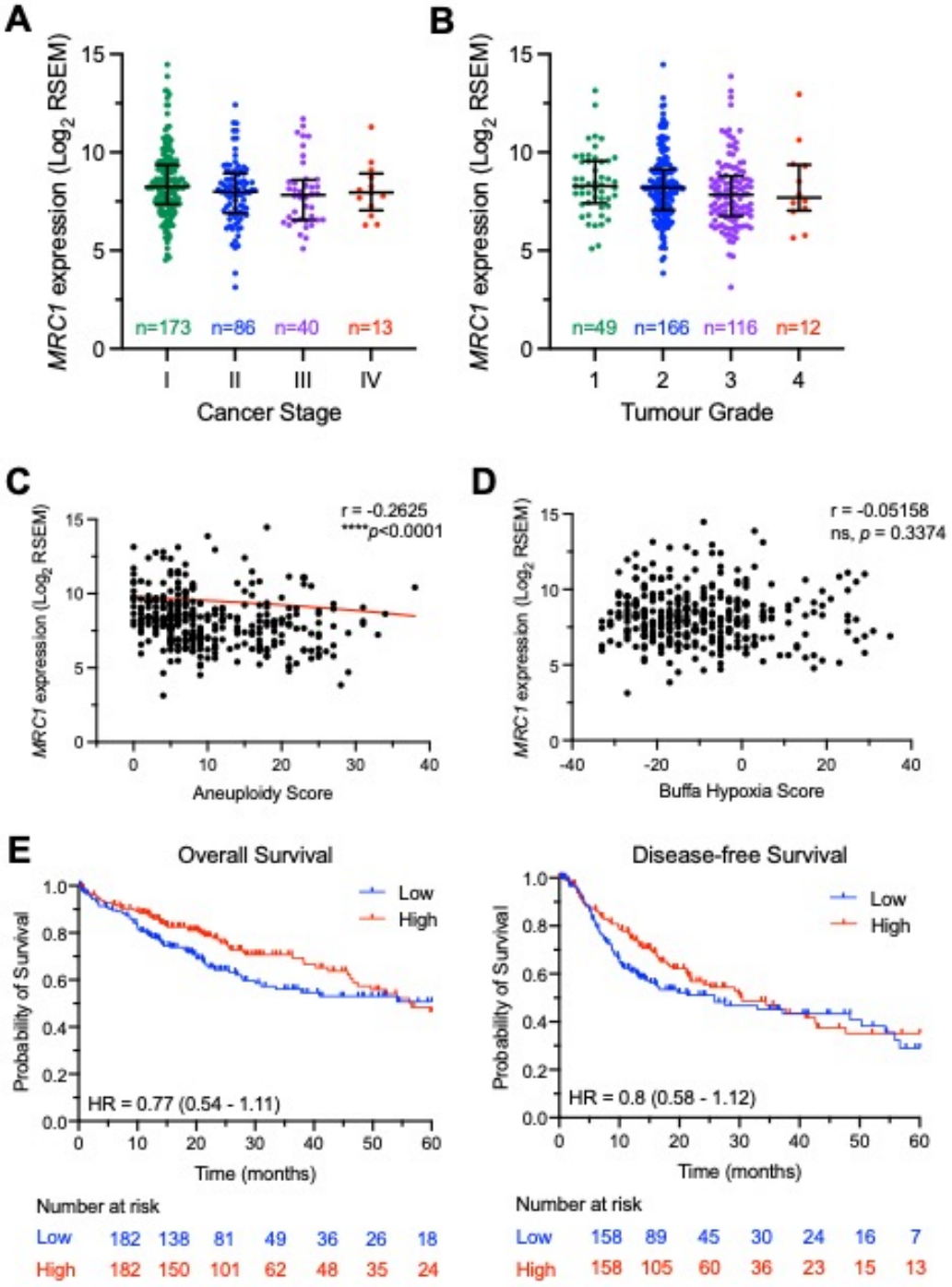

Figure 3.6: *MRC1* expression did not correlate with survival or other hepatocellular carcinoma (HCC) clinical parameters.

Publicly-available TCGA (The Cancer Genome Atlas) databases were analysed for *MRC1* expression relative to **(A)** cancer stage and **(B)** tumour grade (p>0.05, Kruskal-Wallis test followed by Dunn's multiple comparison test). Data shown are median log_2(RNAseq by Expectation-Maximum) ± interquartile range and are available at http://www.cbioportal.org/. **(C, D)** *MRC1* expression showed a significant negative correlation with aneuploidy score (n=344) (****p<0.0001, Spearman's correlation test) but no significant correlation with Buffa hypoxia score (n=348) (p>0.05, Spearman's correlation test), both of which are surrogate markers of tumour aggressiveness. **(E)** Kaplan-Meier plots depicting overall and disease-free survival data for $MRC1^{high}$ and $MRC1^{low}$ HCC patients (p>0.05, Log-rank test) (HR, hazard ratio). High and low expressing groups were stratified based on the median *MRC1* expression. Survival data is accessible via https://kmplot.com/analysis/.

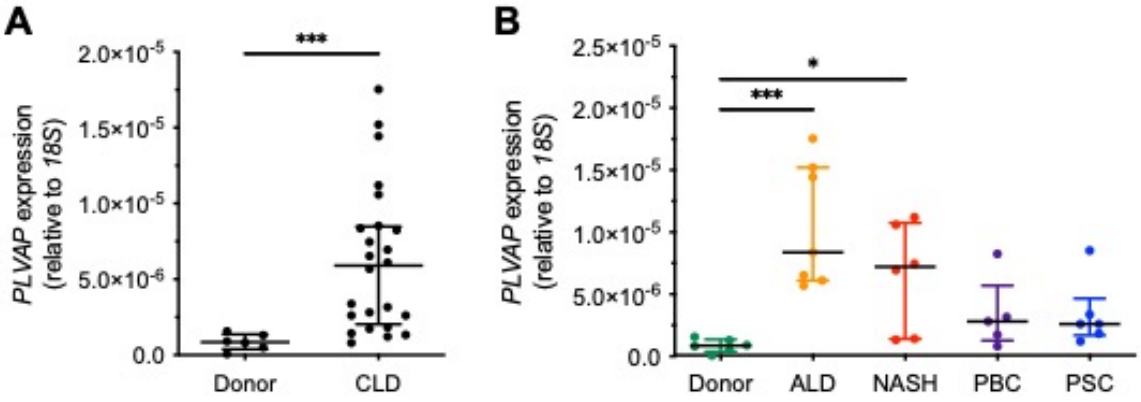

Figure 3.7: Plasmalemma vesicle-associated protein (*PLVAP*) gene expression was upregulated in chronic liver disease (CLD).

(A) Gene expression was determined by qRT-PCR of whole liver tissue lysates from donor (n=5) and CLD patients (n=24) (***p<0.001, Mann-Whitney test). **(B)** Data were then stratified based on aetiology (ALD, alcoholic liver disease; NASH, non-alcoholic steatohepatitis; PBC, primary biliary cholangitis; PSC, primary sclerosing cholangitis) (*p<0.05, ***p<0.001, Kruskal-Wallis test followed by Dunn's multiple comparison test). *PLVAP* expression is shown relative to *18S* which was used as a housekeeping gene. Data shown are median ± interquartile range, where each data point represents an independent patient sample.

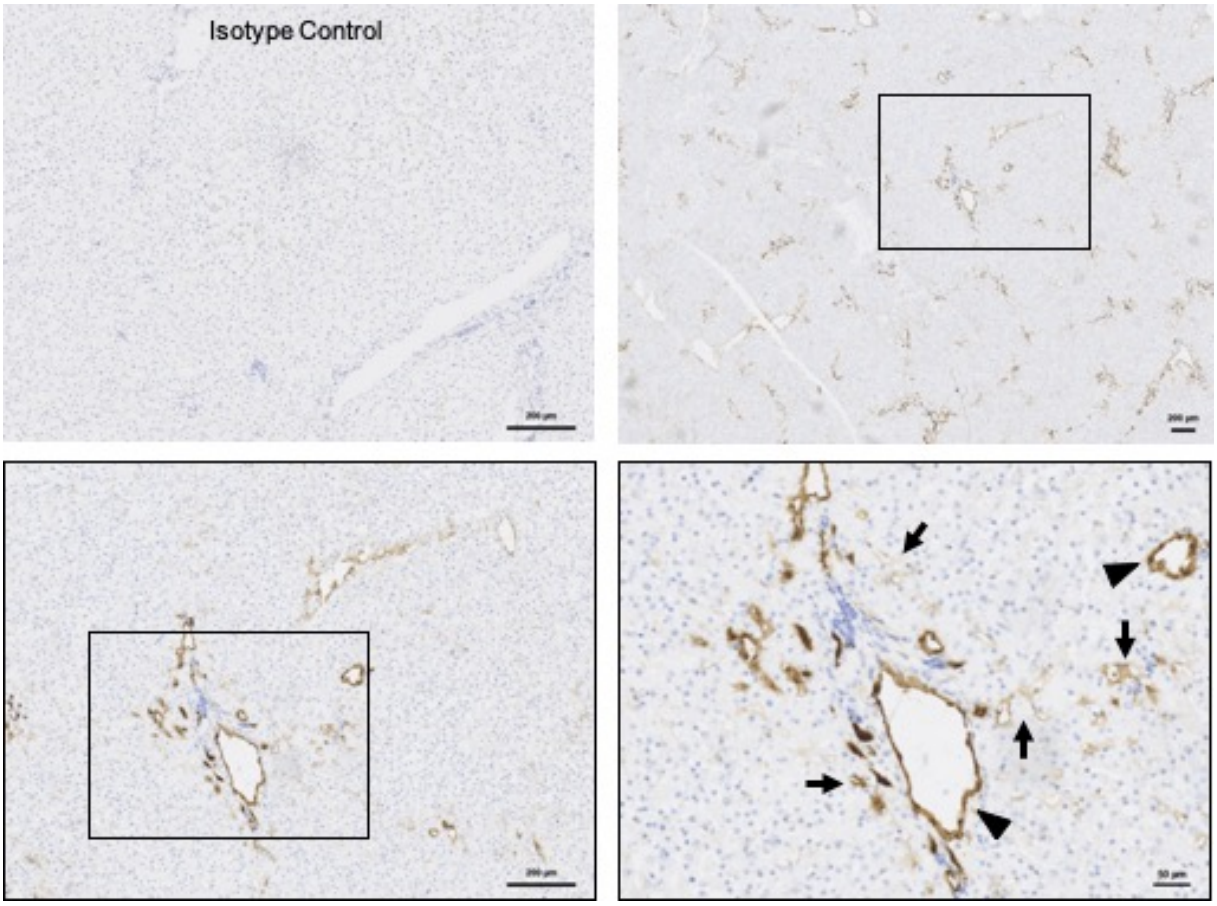

Figure 3.8: Plasmalemma vesicle-associated protein (PLVAP) was expressed at low levels in normal human liver tissue.

PLVAP often localised to periportal sinusoidal areas (*arrows*) and larger vessels (*arrowheads*) (*inset*, high magnification). Isotype control samples were negative. Fields of view were selected in Zen Blue software (Zeiss) post-acquisition of entire tissue sections using a Zeiss Axio Scan.Z1 and a 20x objective. Images shown are representative of 6-8 patient samples. Scale bars represent 200 µm and 50 µm (*inset*).

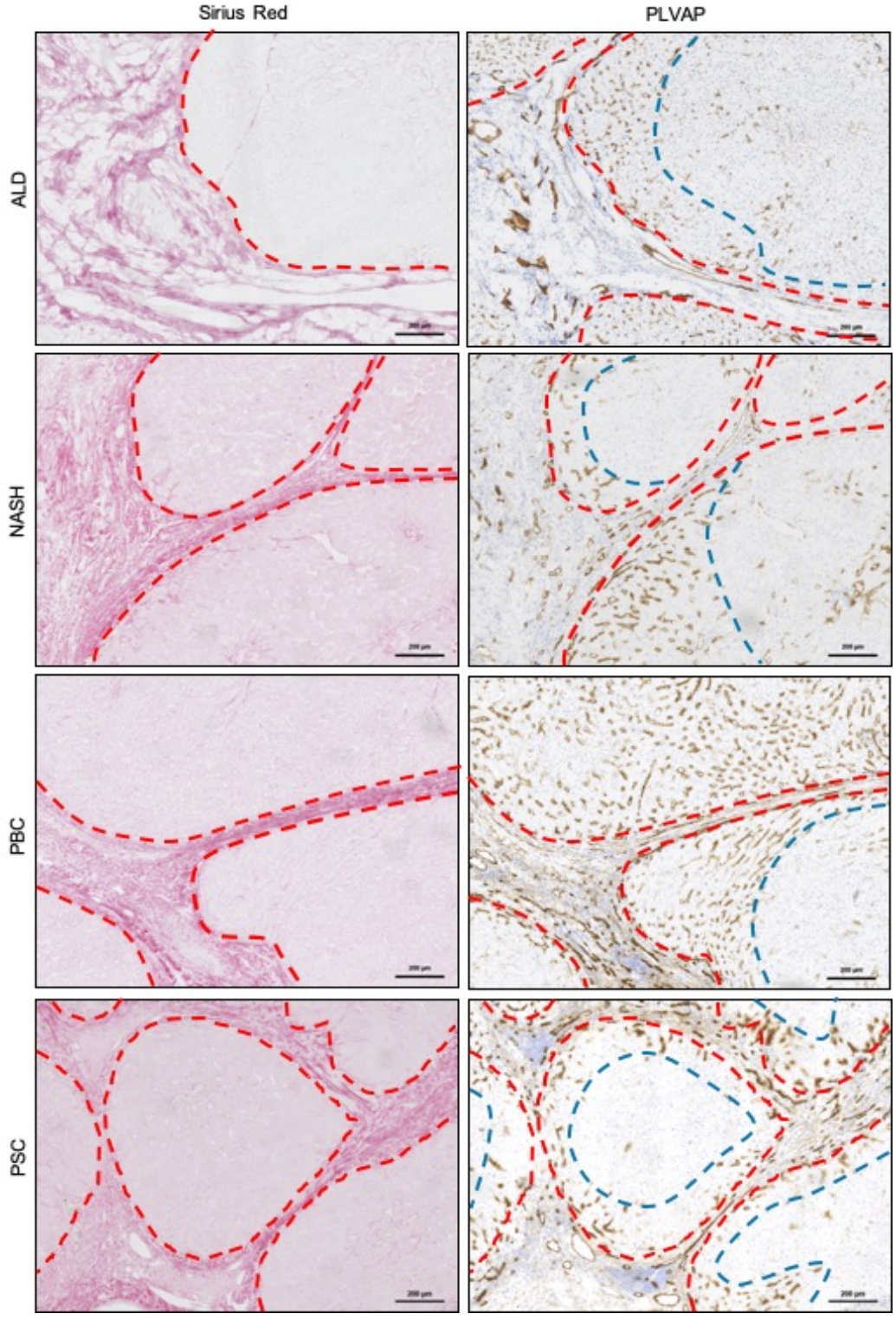

Figure 3.9: Plasmalemma vesicle-associated protein (PLVAP) expression was increased in cirrhotic human liver.

PLVAP (*brown*) expression was assessed in alcoholic liver disease (ALD), non-alcoholic steatohepatitis (NASH), primary biliary cholangitis (PBC) and primary sclerosing cholangitis (PSC) (*right panels*). Sirius red images (*left panels*) are those shown in **Figure 3.3** (except PSC), where the red dashed lines indicate fibrotic septa. PLVAP staining was localised within, and proximal to, fibrotic regions (*blue dashed lines*). Images shown are representative of 3-4 patient samples per aetiology. Scale bars represent 200 μm. See **Appendix 7.2** for isotype controls.

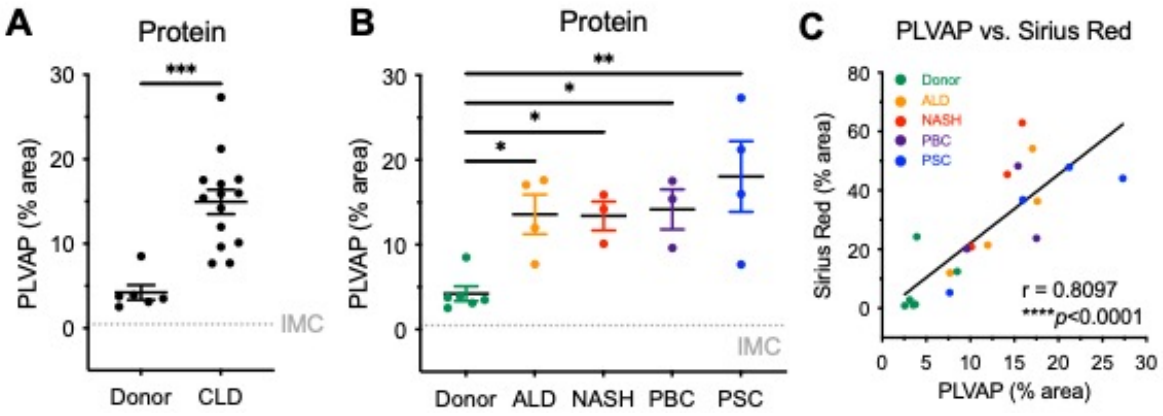

Figure 3.10: Plasmalemma vesicle-associated protein (PLVAP) was upregulated and displayed a scar-associated expression pattern in chronic liver disease (CLD).

(A) PLVAP expression was determined by quantification of immunohistochemical staining of donor (n=6) and CLD patient (n=14) samples (***p<0.001, student's unpaired t-test). **(B)** Data were stratified based on aetiology (ALD, alcoholic liver disease; NASH, non-alcoholic steatohepatitis; PBC, primary biliary cholangitis; PSC, primary sclerosing cholangitis) (*p<0.05, **p<0.01, one-way ANOVA and Dunnett's multiple comparison test). Isotype-matched control (IMC) levels are indicated by the grey gridline. Data shown are mean % area ± SEM, where each data point represents an independent patient sample. **(C)** PLVAP expression was plotted against Sirius red staining area measured in serial sections from matched patient samples (n=20) (****p<0.0001, Pearson's correlation test).

3.1.4 PLVAP was upregulated in HCC tumours and correlated with improved prognosis and survival

Expression of PLVAP is known to be upregulated in several human cancers and has recently been proposed as a therapeutic target for HCC and cholangiocarcinoma[457, 458]. Analysis of TCGA RNA-sequencing data demonstrated that *PLVAP* gene expression was upregulated (~9.49-fold) in HCC tumour tissue compared to non-tumour tissue (**Figure** 3.11**A**). This was validated in-house with qRT-PCR analysis of matched non-tumour and tumour HCC patient samples, which confirmed a significant upregulation (~5.12-fold) of *PLVAP* gene expression in tumour tissue (**Figure** 3.11**B**). At the protein level, PLVAP showed a significant upregulation in tumour sections as measured by immunohistochemistry, with an increase in positive staining area from 3.82 ± 1.29% to 34.4 ± 8.63% (**Figure** 3.11**C, D**).

PLVAP gene expression also seemed to be inversely associated with cancer stage and tumour grade (**Figure 3.12A, B**), and immunohistochemistry studies suggested a downregulation of PLVAP in poorly-differentiated tumours, which are often associated with unfavourable outcomes (**Figure 3.12C**). Consistent with this, *PLVAP* gene expression negatively correlated with clinical parameters associated

with more aggressive tumours, including aneuploidy score and Buffa hypoxia score (**Figure 3.13A, B**). Furthermore, higher *PLVAP* expression was predictive of improved overall and disease-free survival in HCC patients, with the high group surviving on average 18.6 months longer than the low group (**Figure 3.13C**).

3.1.5 MR and PLVAP displayed a strong endothelial signature in HCC

The expression of *MRC1* and *PLVAP* in HCC TCGA patient samples was studied in relation to expression of other genes. Of the genes significantly co-expressed with *MRC1* or *PLVAP*, 2931 genes were shared between the two groups (**Figure 3.14A**). *MRC1*-expressing cells showed a larger repertoire of co-expressed genes (2754) compared with *PLVAP*-expressing cells, which only co-expressed an additional 1107 genes. When the top 20 co-expressed genes were analysed, many of the genes co-expressed with *MRC1* were myeloid-associated genes with a few markers associated with both myeloid and endothelial cells (**Figure 3.14B**). In contrast, genes co-expressed with *PLVAP* were endothelial-specific (or -enriched) markers (determined using livercellatlas.mvm.ed.ac.uk) including *CD34*, *CLEC14A*, and *MMRN2* (**Figure 3.14B**). A selection of genes was studied on the basis of their expression in tumour-specific cell types[67, 466-468]. *MRC1* expression correlated with genes associated with both tumour-associated macrophages and HCC endothelial cells. In contrast, *PLVAP* showed strong association with tumour endothelial cells and a positive correlation with some tumour-associated fibroblast genes (*ACTA2, PDGFRB*) (**Figure 3.14C**). Collectively, these data are consistent with the expression of *MRC1* in tumour-associated macrophages and endothelial cells, whereas *PLVAP* co-expression data suggest an endothelial signature.

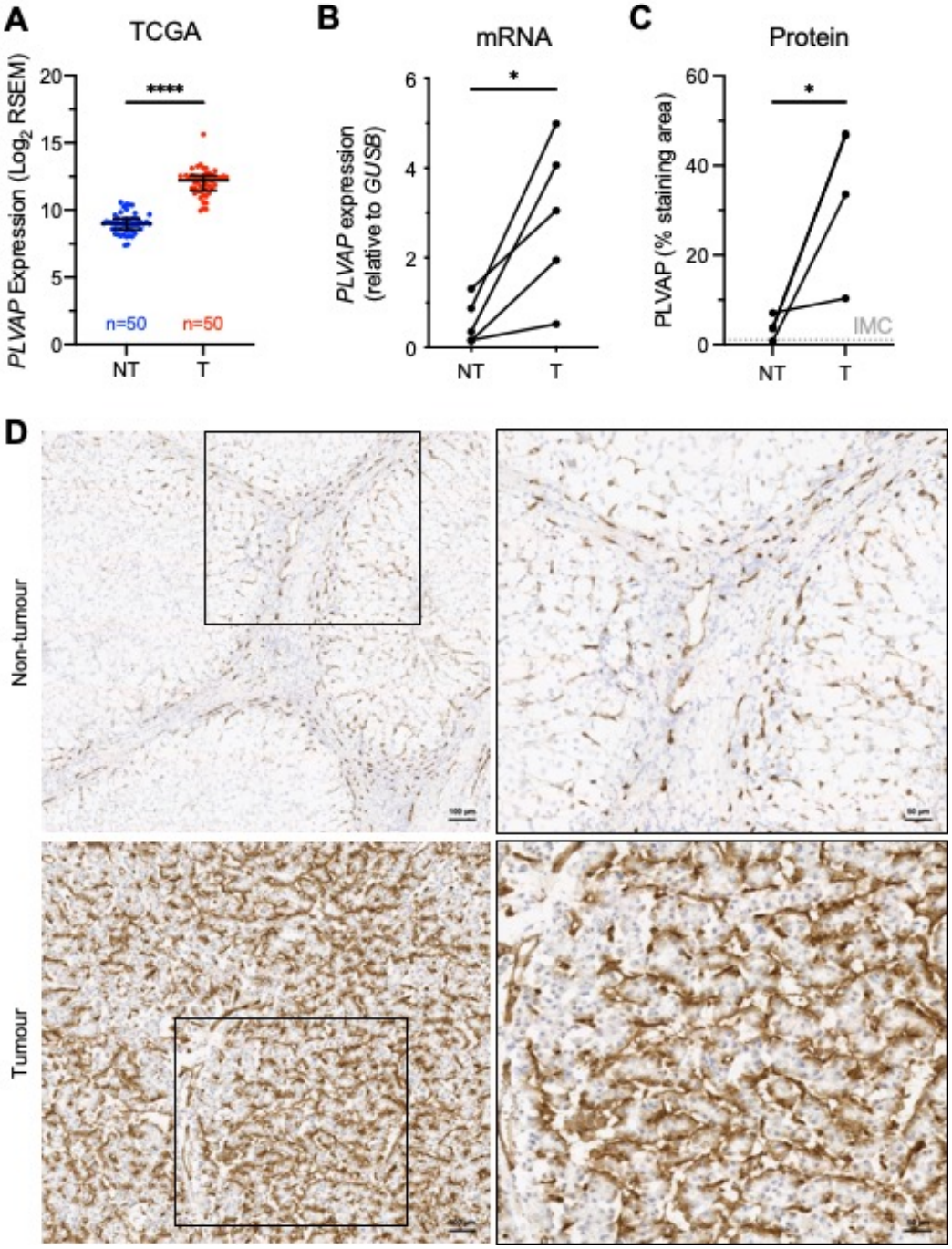

Figure 3.11: Plasmalemma vesicle-associated protein (PLVAP) was upregulated in hepatocellular carcinoma (HCC) tumours.

(A) Publicly-available TCGA (The Cancer Genome Atlas) databases were analysed for *PLVAP* expression in matched non-tumour (NT) and tumour (T) tissues from HCC patients (****p<0.0001, Wilcoxon test). Data shown are median $\log_2$(RNAseq by Expectation-Maximum) ± interquartile range and are accessible via https://xenabrowser.net/. **(B)** *PLVAP* expression was determined by qRT-PCR of matched NT and T tissue lysates from HCC patients (n=5) (*p<0.05, student's paired t-test). Expression is shown relative to *GUSB* which was used as a housekeeping gene. **(C)** PLVAP protein expression was determined by immunohistochemistry and quantification of staining area in matched NT and T tissue sections. Isotype-matched control (IMC) levels are indicated by the grey gridline. **(D)** Images shown are representative of four patient samples. Fields of view were selected in Zen Blue software (Zeiss) post-acquisition of entire tissue sections using a Zeiss Axio Scan.Z1 and a 20x objective. Scale bars represent 100 µm and 50 µm (*inset*).

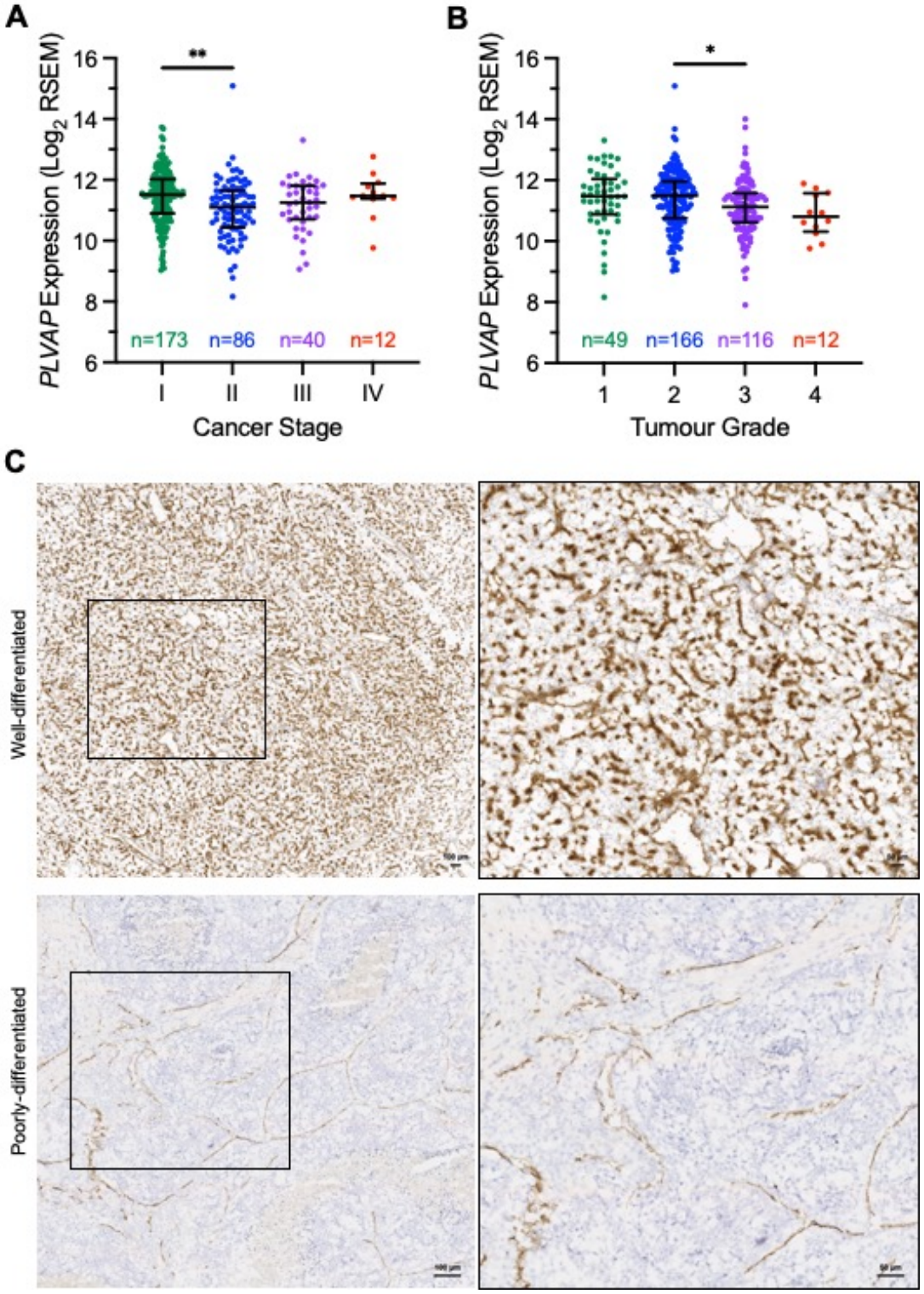

Figure 3.12: *PLVAP* expression inversely correlated with cancer stage and tumour grade.

(A, B) Publicly-available TCGA (The Cancer Genome Atlas) datasets were analysed for *PLVAP* gene expression relative to cancer stage and tumour grade (**p<0.01, *p<0.05, Kruskal-Wallis test followed by Dunn's multiple comparison test). Data shown are median $\log_2$(RNAseq by Expectation-Maximum) ± interquartile range and are available at http://www.cbioportal.org/. **(C)** Immunohistochemistry of cryopreserved hepatocellular carcinoma tumour tissues was performed to stain for PLVAP (*brown*). Representative images of well- and poorly-differentiated tumours are shown. Scale bars represent 100 µm and 50 µm (*inset*).

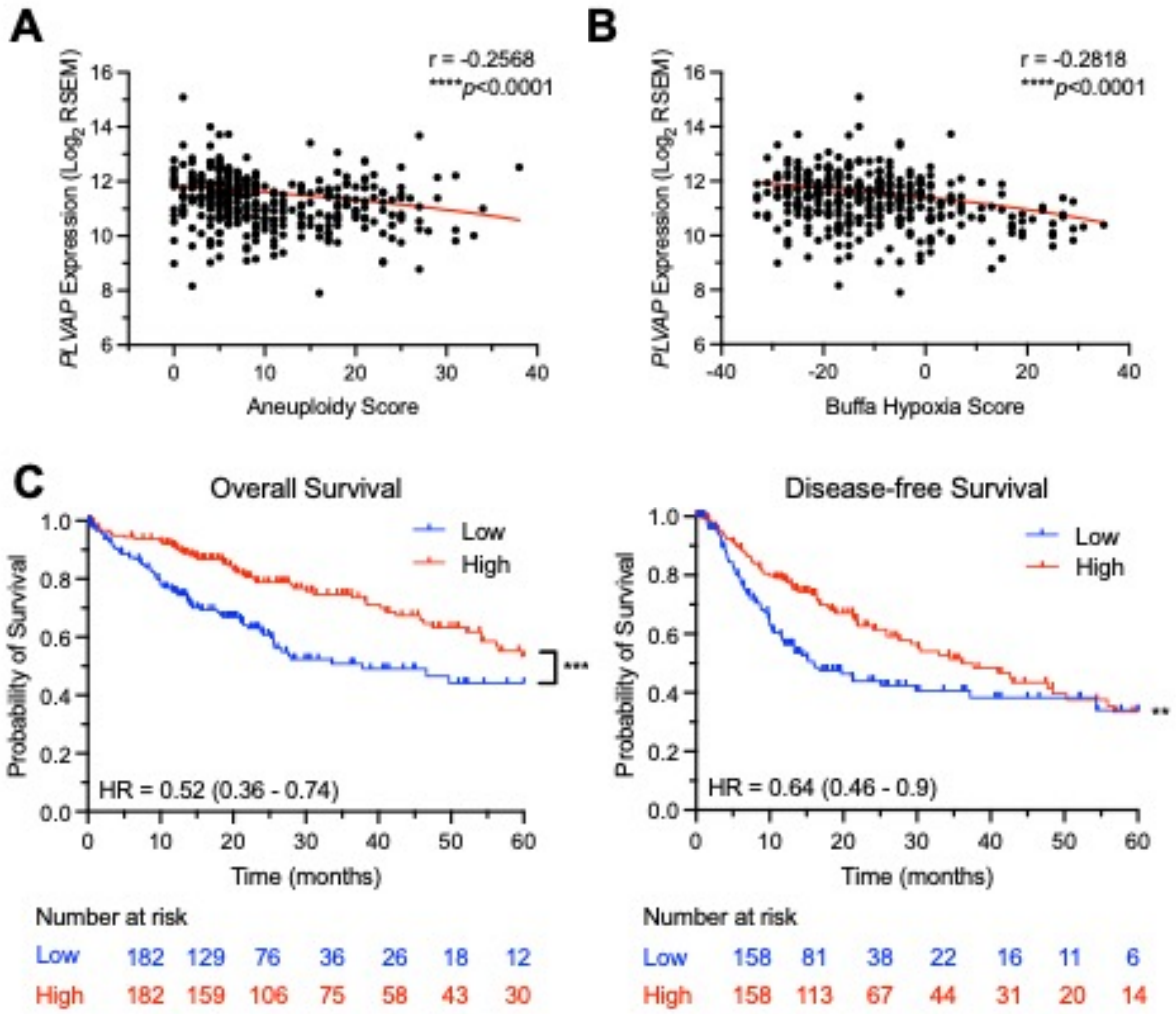

Figure 3.13: *PLVAP* expression inversely correlated with indicators of tumour aggressiveness and hepatocellular carcinoma (HCC) patient survival.

(A, B) PLVAP expression showed a significant negative correlation with aneuploidy score (n=344) and Buffa hypoxia score (n=348) (****p<0.0001, Spearman's correlation test), both of which are surrogate markers of tumour aggressiveness. **(C)** Kaplan-Meier plots depicting overall and disease-free survival data for *PLVAP*^{high} and *PLVAP*^{low} HCC patients (*p<0.05, ***p<0.001, Log-rank test) (HR, hazard ratio). High and low expressing groups were stratified based on the median *PLVAP* expression. Survival data is accessible via https://kmplot.com/analysis/.

3.1.6 MR and PLVAP were differentially expressed in human liver

Dual immunofluorescent staining was performed to visualise MR and PLVAP in the same tissue sections. A distinct and mutually exclusive expression pattern was observed, not only confirming the disruption of MR in CLD and the scar-associated nature of PLVAP, but also highlighting that the PLVAP^{+} populations seemed to reside within areas which were MR low/negative (**Figure 3.15**). Intensity profiles of MR and PLVAP were compared, demonstrating a non-overlapping staining pattern

and confirming their mutually exclusive expression (**Figure 3.15B**). Additional markers were investigated in conjunction with MR/PLVAP to further characterise these cell populations. Chronically diseased liver sections were the focus for these studies since these samples displayed the unique expression patterns of both MR and PLVAP relative to the fibrotic areas.

Liver-specific intercellular adhesion molecule 3-grabbing non-integrin (L-SIGN) is a C-type lectin highly expressed by the sinusoidal endothelium which is known to be downregulated in liver cirrhosis[397, 469]. Lymphatic vessel endothelial hyaluronan receptor 1 (LYVE-1) can be used as a lymphatic endothelial cell marker, but is also enriched in the hepatic sinusoidal endothelium[397]. Mannose receptor was observed to co-localise with sinusoidal marker, L-SIGN, within regenerative hepatic nodules (**Figure 3.16**), whilst there was little overlap between MR and L-SIGN within fibrotic septa (**Figure 3.17**). There was also co-localisation between MR and LYVE-1 within sinusoidal regions (**Figure 3.18)**. One notable observation was that expression of both L-SIGN and LYVE-1 appeared to be disrupted proximal to fibrotic septa, a similar staining pattern to that observed for MR. These data confirm a perturbed sinusoidal phenotype in areas proximal to fibrosis and also suggest the presence of a distinct population of scar-associated MR^+ cells, in addition to the MR^+ sinusoidal endothelium.

In contrast to MR, $PLVAP^+$ cells displayed a distinct phenotype which did not correspond with expression of sinusoidal markers, L-SIGN and LYVE-1 (**Figure 3.19, Figure 3.20)**. In fact, there was virtually no overlap between these markers and PLVAP, which instead co-localised with classic vascular marker CD31 and partially co-localised with CD34 (**Figure 3.21, Figure 3.22**). CD34 is a transmembrane sialomucin protein that defines an inflammatory endothelial cell population which was shown to be expanded in cirrhotic patients[397]. Contrastingly, there was little if any co-localisation between MR and CD31 or CD34 (**Figure 3.23, Figure 3.24**). These data confirm that MR^+ and $PLVAP^+$ endothelial cells represent two distinct populations which could have differential roles in homeostasis and inflammation.

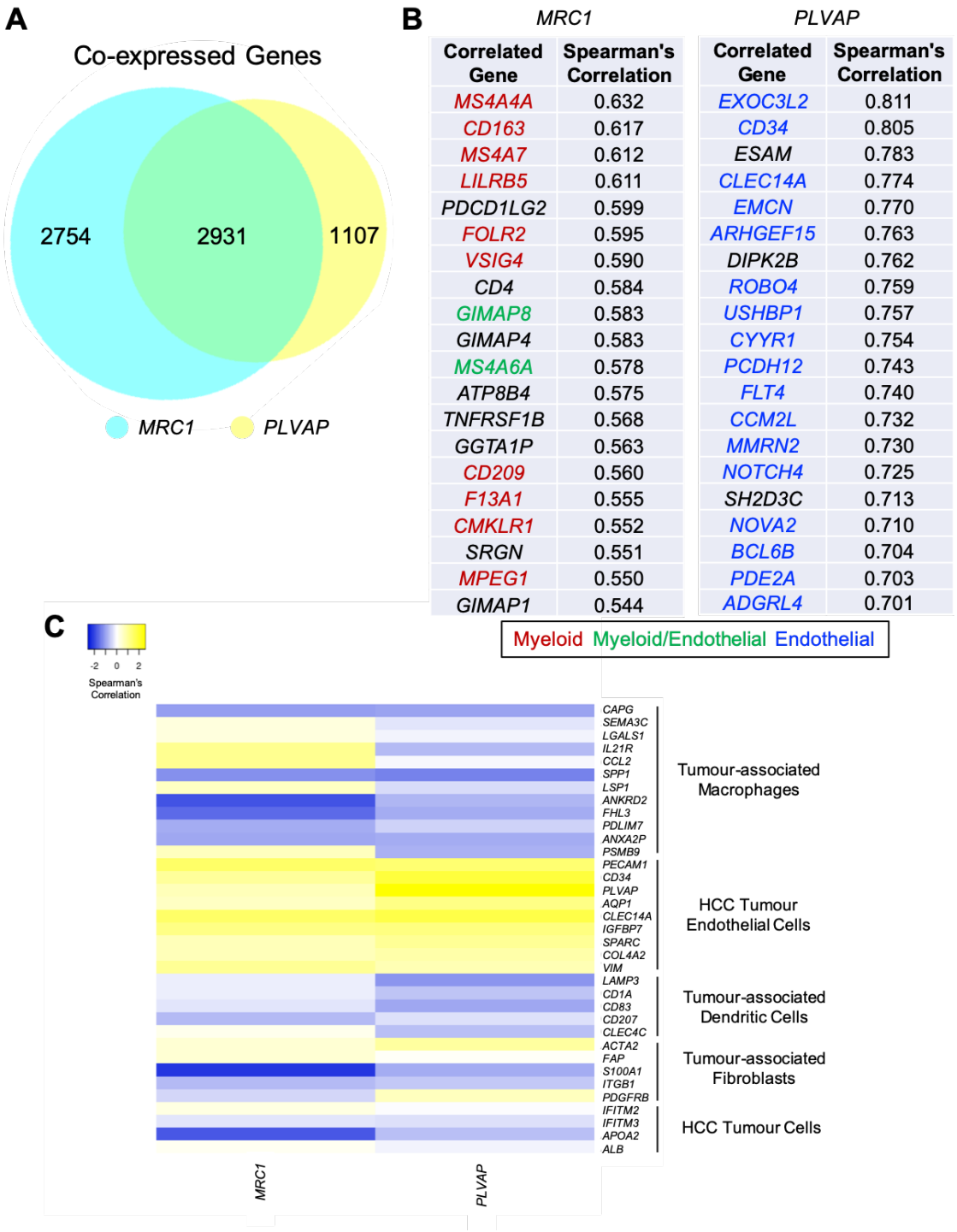

Correlated Gene	Spearman's Correlation
MS4A4A	0.632
CD163	0.617
MS4A7	0.612
LILRB5	0.611
PDCD1LG2	0.599
FOLR2	0.595
VSIG4	0.590
CD4	0.584
GIMAP8	0.583
GIMAP4	0.583
MS4A6A	0.578
ATP8B4	0.575
TNFRSF1B	0.568
GGTA1P	0.563
CD209	0.560
F13A1	0.555
CMKLR1	0.552
SRGN	0.551
MPEG1	0.550
GIMAP1	0.544

Correlated Gene	Spearman's Correlation
EXOC3L2	0.811
CD34	0.805
ESAM	0.783
CLEC14A	0.774
EMCN	0.770
ARHGEF15	0.763
DIPK2B	0.762
ROBO4	0.759
USHBP1	0.757
CYYR1	0.754
PCDH12	0.743
FLT4	0.740
CCM2L	0.732
MMRN2	0.730
NOTCH4	0.725
SH2D3C	0.713
NOVA2	0.710
BCL6B	0.704
PDE2A	0.703
ADGRL4	0.701

Figure 3.14: *MRC1*- and *PLVAP*-expressing cell populations displayed strong endothelial signatures in hepatocellular carcinoma (HCC) patients.

(A) Of all the genes displaying significant co-expression with *MRC1* and *PLVAP*, 2931 genes were shared between both populations. *MRC1*-expressing cell populations showed a larger repertoire of co-expressed genes (2754) compared with *PLVAP*-expressing cells which only expressed an additional 1107 genes. **(B)** The top 20 co-expressed genes with *MRC1* were predominantly myeloid markers (*red*), with some genes expressed in both myeloid and endothelial hepatic populations (*green*) (determined using http://www.livercellatlas.mvm.ed.ac.uk). *PLVAP* co-expressed genes were predominantly endothelial (*blue*). **(C)** Correlation of *MRC1* and *PLVAP* with tumour-associated cell-specific genes. Co-expression data is available at http://www.cbioportal.org/ and heat map was generated using http://www.heatmapper.ca/.

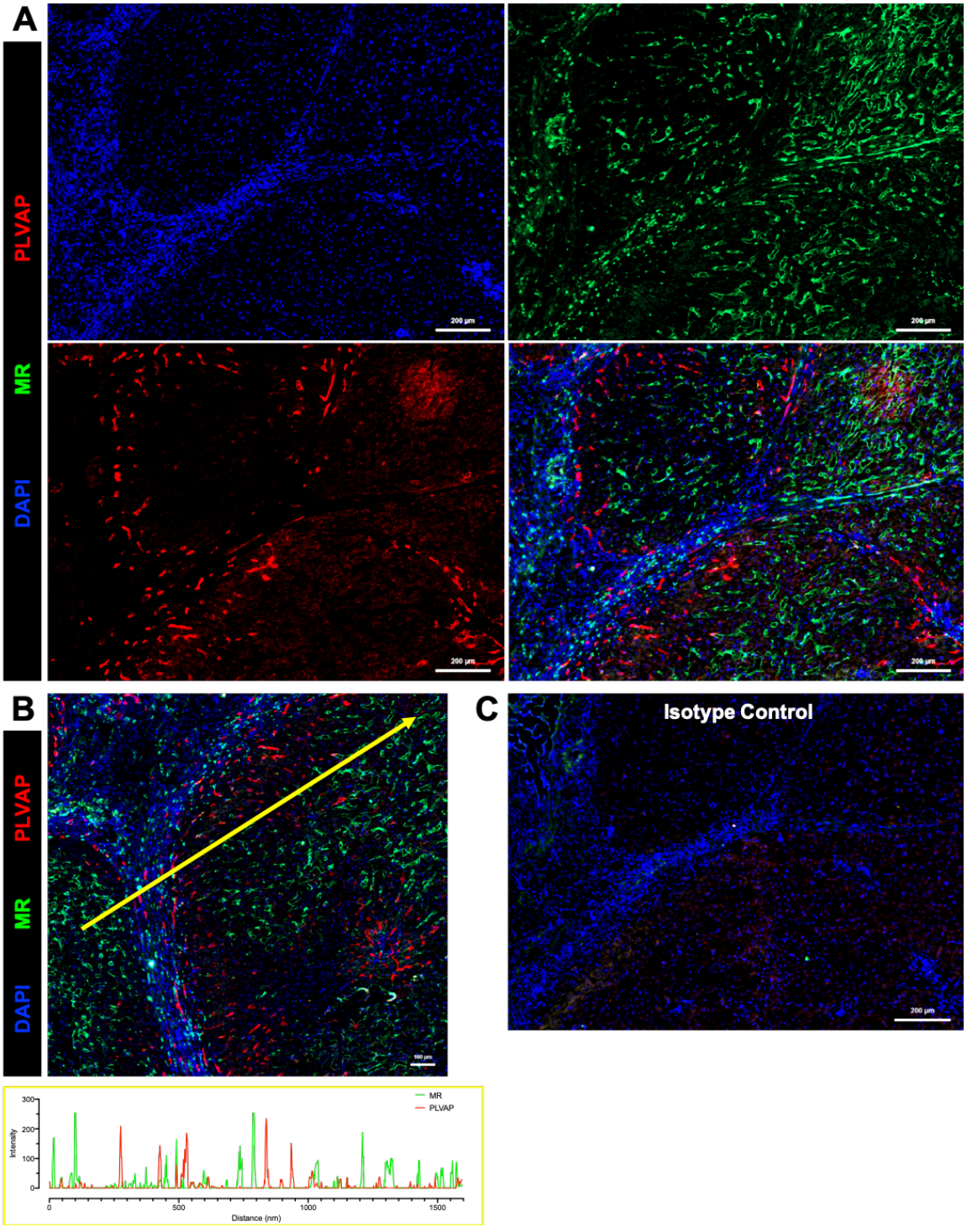

Figure 3.15: Mannose receptor (MR) and plasmalemma vesicle-associated protein (PLVAP) displayed a mutually exclusive expression pattern in human liver.

(A, B) Dual immunofluorescent staining for MR (*green*) and PLVAP (*red*) was performed in cirrhotic liver tissue sections. Field of view shown in **(A)** is the same as that shown in **Figure 3.3** and **Figure 3.9** (NASH, non-alcoholic steatohepatitis). Yellow line in **(B)** depicts the site of intensity measurements. **(C)** Isotype control samples were negative. 4′,6-diamidino-2-phenylindole (DAPI, *blue*) was used as a nuclear counterstain. Fields of view were selected in Zen Blue software (Zeiss) post-acquisition of entire tissue sections using a Zeiss Axio Scan.Z1 and a 20x objective. Scale bars represent **(A, C)** 200 µm or **(B)** 100 µm. Images shown are representative of 6 patient samples.

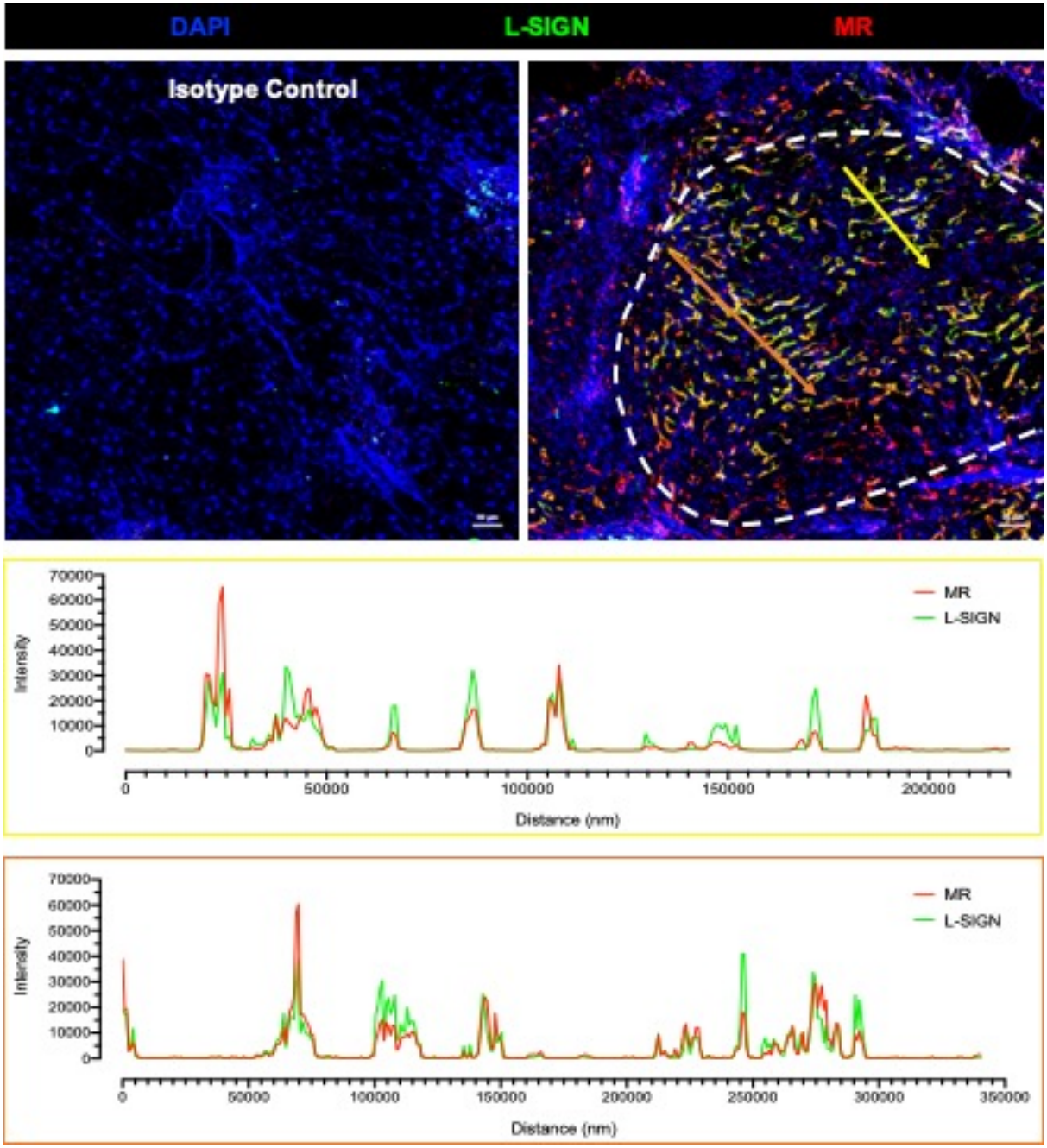

Figure 3.16: Mannose receptor (MR) co-localised with liver-specific intercellular adhesion molecule 3-grabbing non-integrin (L-SIGN) within regenerative liver nodules.

Dual immunofluorescent staining for L-SIGN (*green*) and MR (*red*) was performed in cirrhotic liver tissue sections. Yellow and orange lines depict site of corresponding intensity profiles (*lower*). Isotype controls were negative. 4′,6-diamidino-2-phenylindole (DAPI, *blue*) was used as a nuclear counterstain. Samples were imaged using a Zeiss LSM880 confocal microscope and a 10x objective. Images shown are from a non-alcoholic steatohepatitis patient and are representative of four visual fields. Analysis was performed in Zen blue software (Zeiss). Scale bars represent 50 μm.

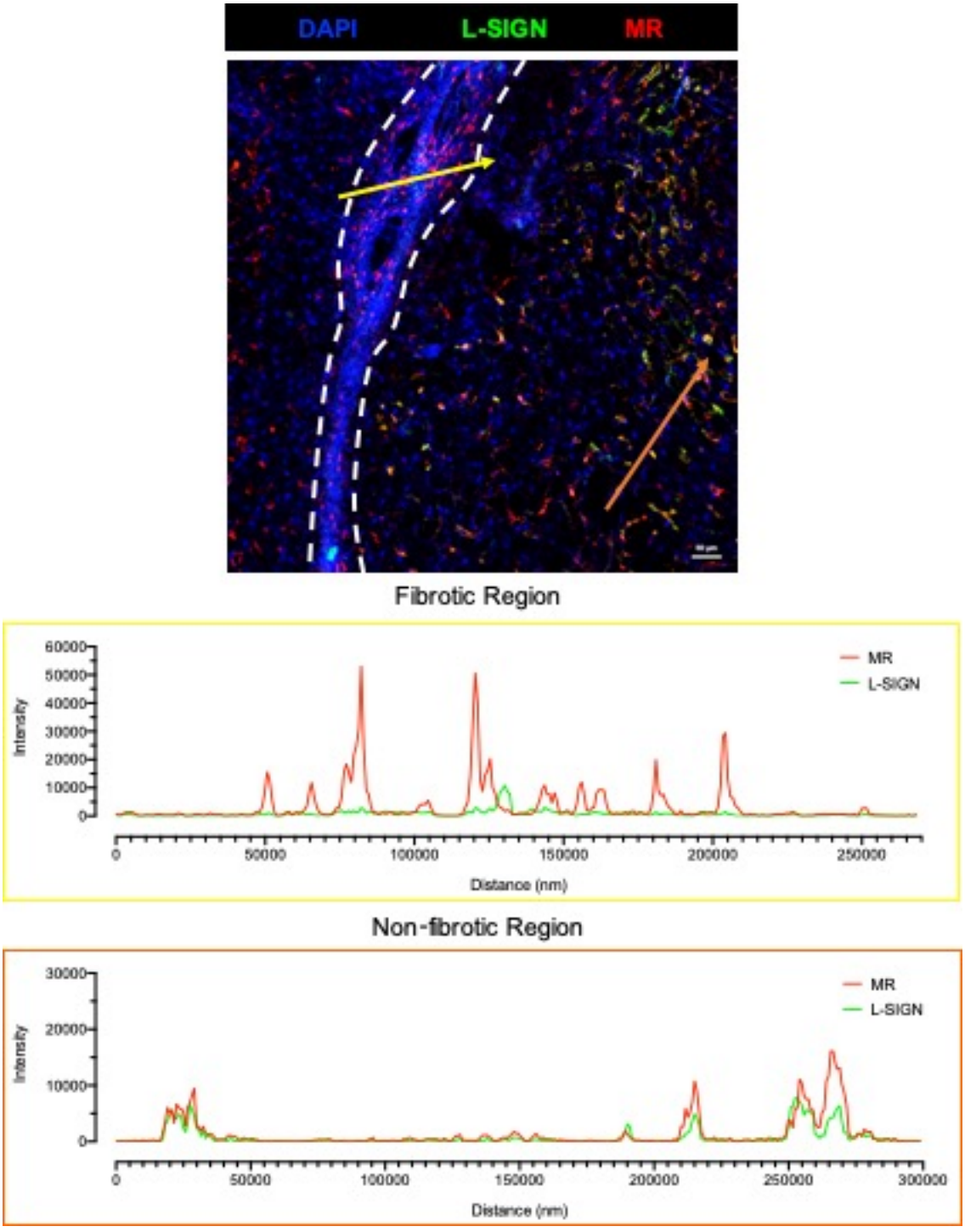

Figure 3.17: Mannose receptor (MR) did not co-localise with liver-specific intercellular adhesion molecule 3-grabbing non-integrin (L-SIGN) within fibrotic septa.

Dual immunofluorescent staining for L-SIGN (*green*) and MR (*red*) was performed in cirrhotic liver tissue sections. Yellow and orange lines depict site of corresponding intensity profiles (*lower*). 4′,6-diamidino-2-phenylindole (DAPI, *blue*) was used as a nuclear counterstain. Samples were imaged using a Zeiss LSM880 confocal microscope and a 10x objective. Images shown are from a non-alcoholic steatohepatitis patient and are representative of four visual fields. Analysis was performed in Zen blue software (Zeiss). Scale bar represents 50 μm.

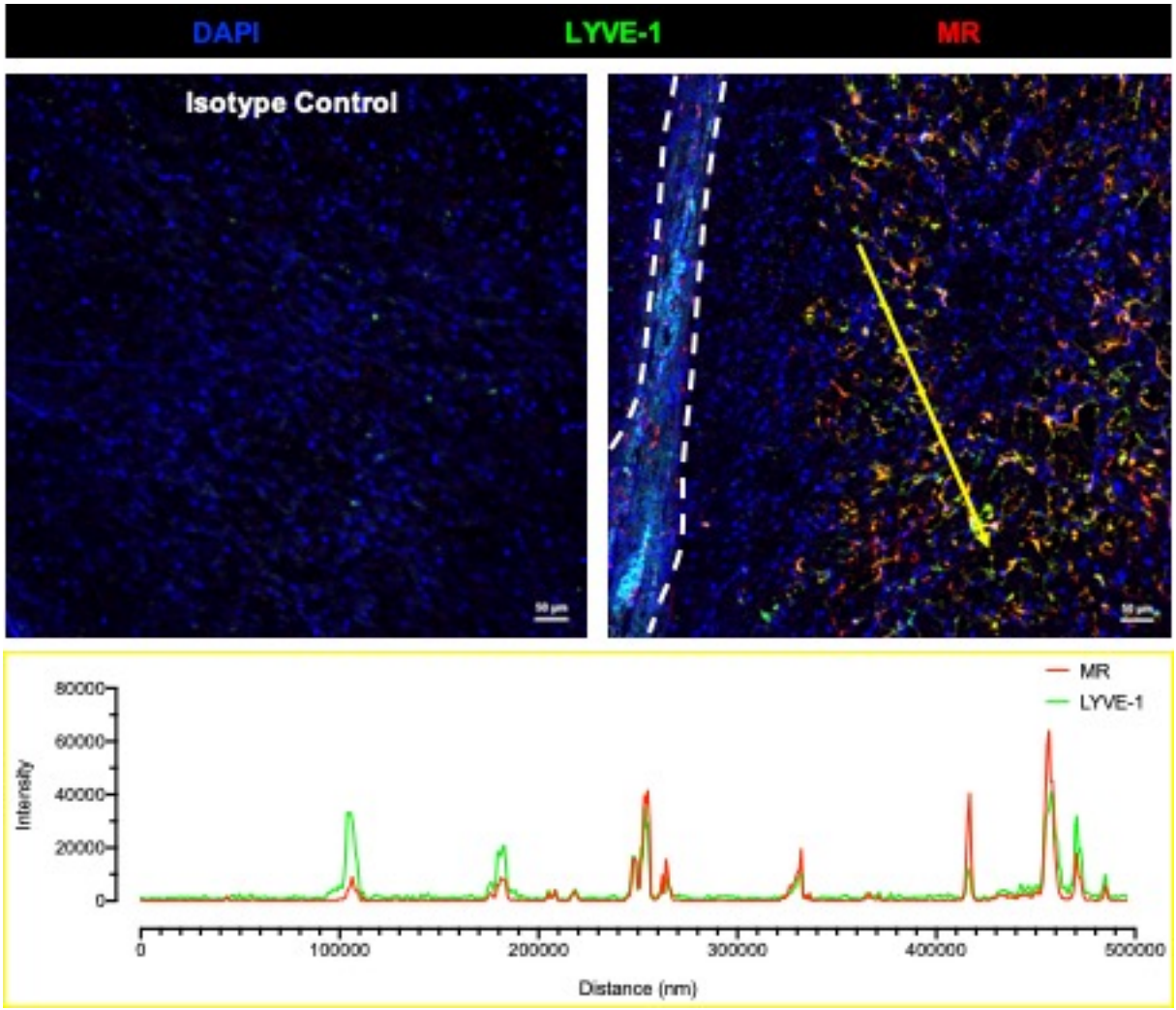

Figure 3.18: Mannose receptor (MR) co-localised with lymphatic vessel endothelial hyaluronan receptor 1 (LYVE-1) within sinusoidal regions.

Dual immunofluorescent staining for LYVE-1 (*green*) and MR (*red*) was performed in cirrhotic liver tissue sections. Yellow line depicts site of intensity profile (*lower*). Isotype controls were negative. 4′,6-diamidino-2-phenylindole (DAPI, *blue*) was used as a nuclear counterstain. Samples were imaged using a Zeiss LSM880 confocal microscope and a 10x objective. Images shown are from an alcoholic liver disease patient and are representative of four visual fields. Analysis was performed in Zen blue software (Zeiss). Scale bars represent 50 μm.

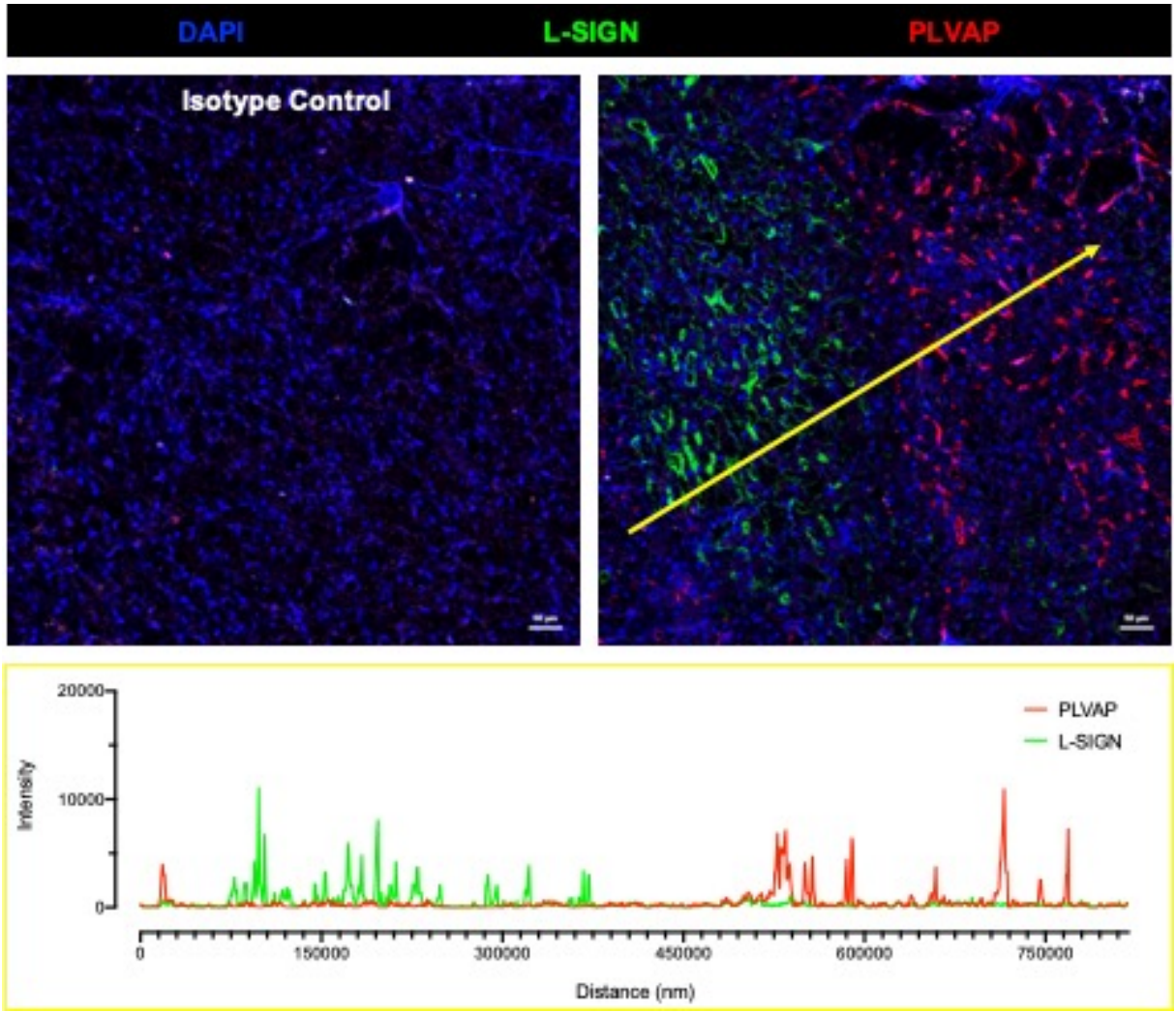

Figure 3.19: Plasmalemma vesicle-associated protein (PLVAP) did not co-localise with liver-specific intercellular adhesion molecule 3-grabbing non-integrin (L-SIGN).

Dual immunofluorescent staining for L-SIGN (*green*) and PLVAP (*red*) was performed in cirrhotic liver tissue sections. Yellow line depicts site of intensity profile (*lower*). Isotype controls were negative. 4′,6-diamidino-2-phenylindole (DAPI, *blue*) was used as a nuclear counterstain. Samples were imaged using a Zeiss LSM880 confocal microscope and a 10x objective. Images shown are from a non-alcoholic steatohepatitis patient and are representative of five visual fields. Analysis was performed in Zen blue software (Zeiss). Scale bars represent 50 µm.

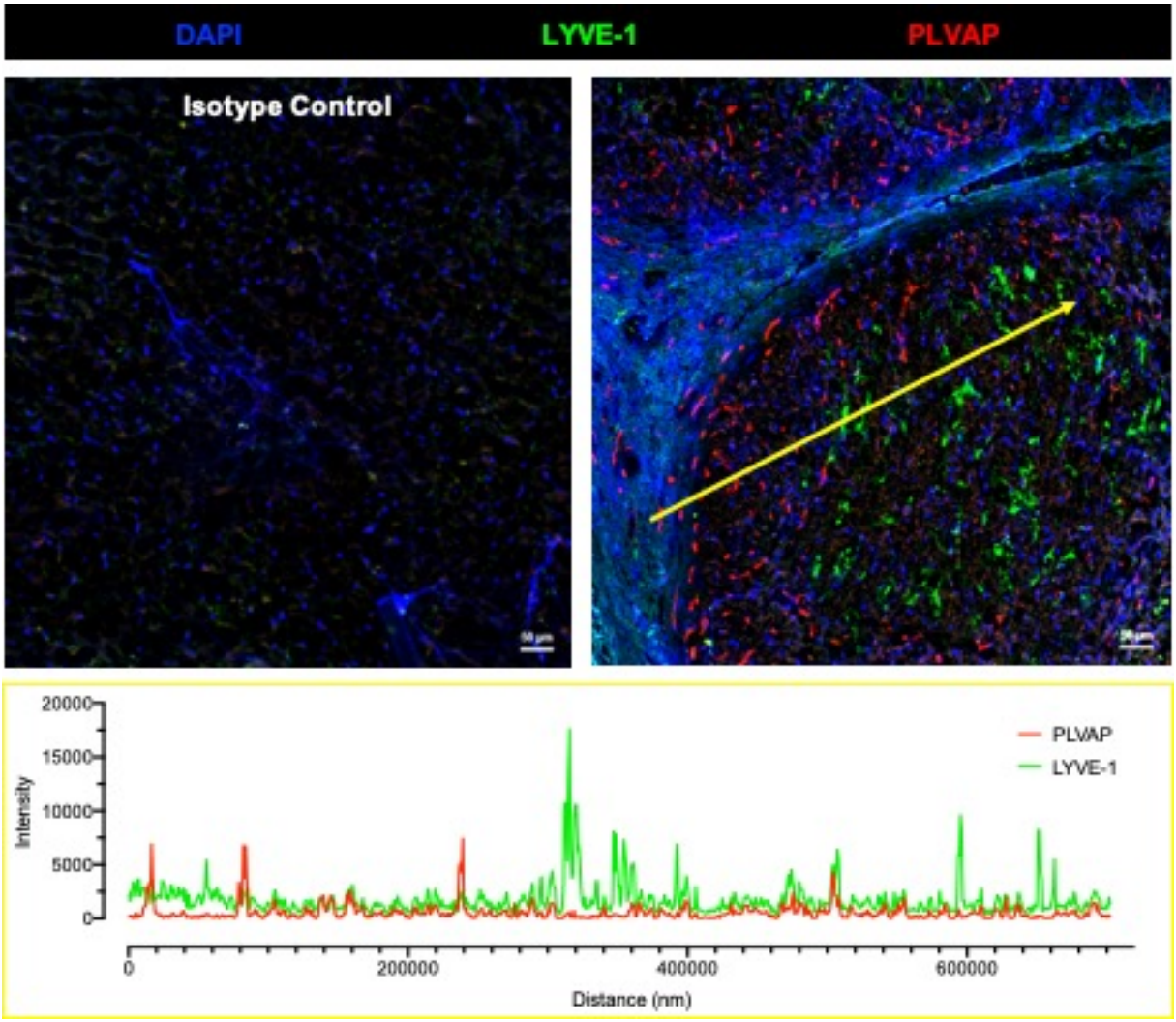

Figure 3.20: Plasmalemma vesicle-associated protein (PLVAP) did not co-localise with lymphatic vessel endothelial hyaluronan receptor 1 (LYVE-1).

Dual immunofluorescent staining for LYVE-1 (*green*) and PLVAP (*red*) was performed in cirrhotic liver tissue sections. Yellow line depicts site of intensity profile (*lower*). Isotype controls were negative. 4′,6-diamidino-2-phenylindole (DAPI, *blue*) was used as a nuclear counterstain. Samples were imaged using a Zeiss LSM880 confocal microscope and a 10x objective. Images shown are from an alcoholic liver disease patient and are representative of four visual fields. Analysis was performed in Zen blue software (Zeiss). Scale bars represent 50 μm.

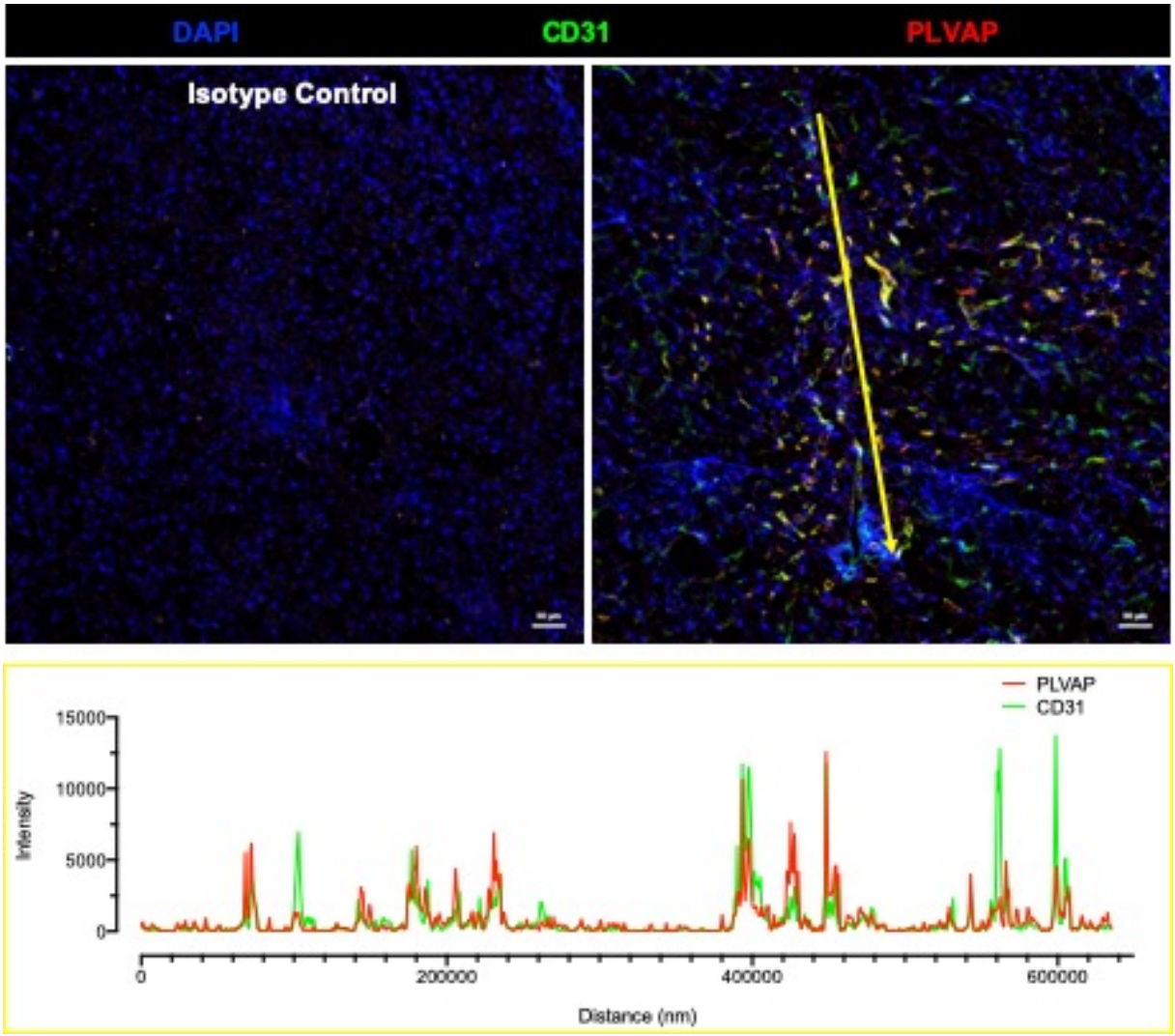

Figure 3.21: Plasmalemma vesicle-associated protein (PLVAP) co-localised with CD31 in cirrhotic liver.

Dual immunofluorescent staining for CD31 (*green*) and PLVAP (*red*) was performed in cirrhotic liver tissue sections. Yellow line depicts site of intensity profile (*lower*). Isotype controls were negative. 4′,6-diamidino-2-phenylindole (DAPI, *blue*) was used as a nuclear counterstain. Samples were imaged using a Zeiss LSM880 confocal microscope and a 10x objective. Images shown are from a non-alcoholic steatohepatitis patient and are representative of eight visual fields. Analysis was performed in Zen blue software (Zeiss). Scale bars represent 50 μm.

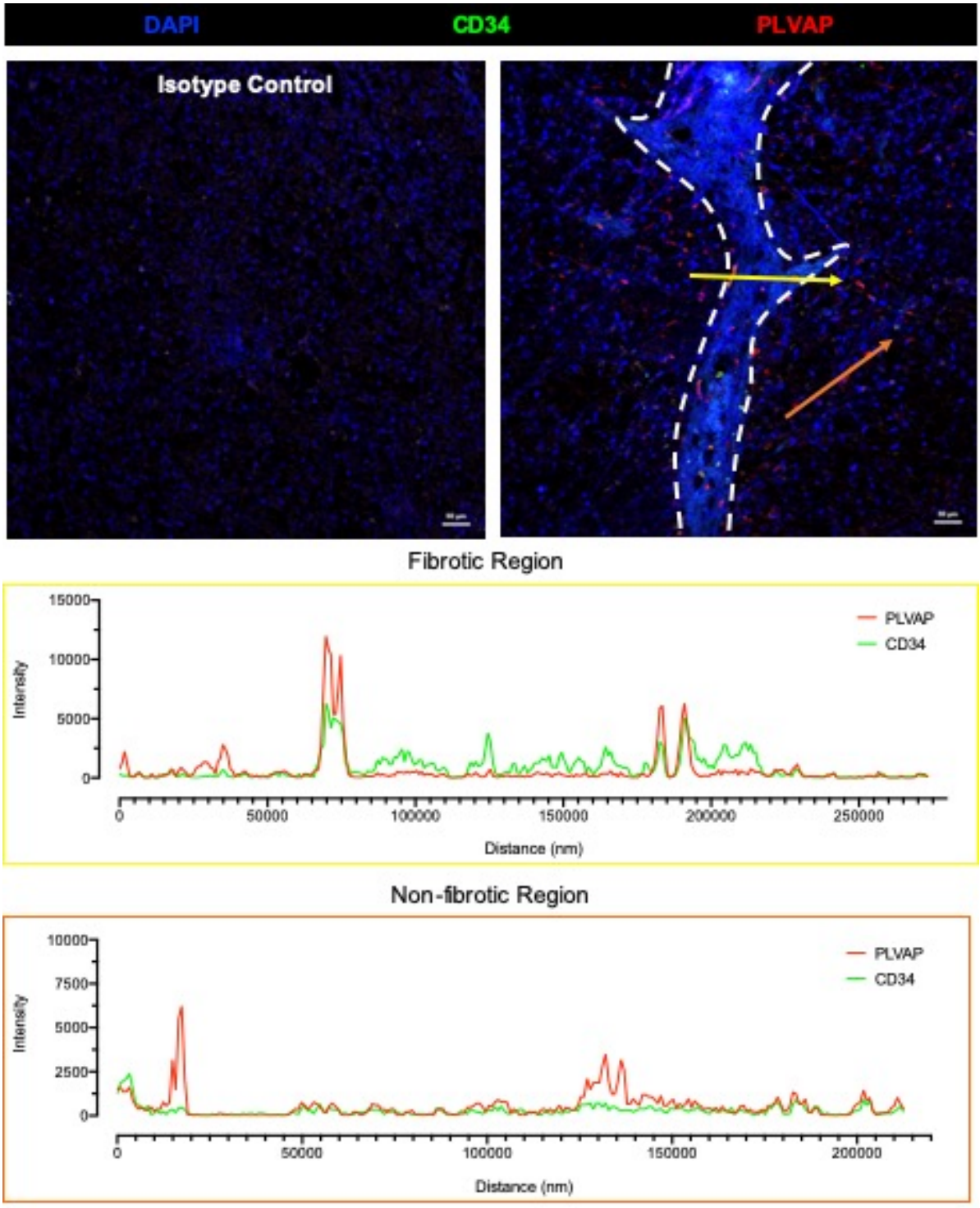

Figure 3.22: Plasmalemma vesicle-associated protein (PLVAP) partially co-localised with CD34 in cirrhotic liver.

Dual immunofluorescent staining for CD34 (*green*) and PLVAP (*red*) was performed in cirrhotic liver tissue sections. Yellow and orange line depict sites of corresponding intensity profile (*lower*). Isotype controls were negative. 4′,6-diamidino-2-phenylindole (DAPI, *blue*) was used as a nuclear counterstain. Samples were imaged using a Zeiss LSM880 confocal microscope and a 10x objective. Images shown are from a non-alcoholic steatohepatitis patient and are representative of three visual fields. Analysis was performed in Zen blue software (Zeiss). Scale bars represent 50 μm.

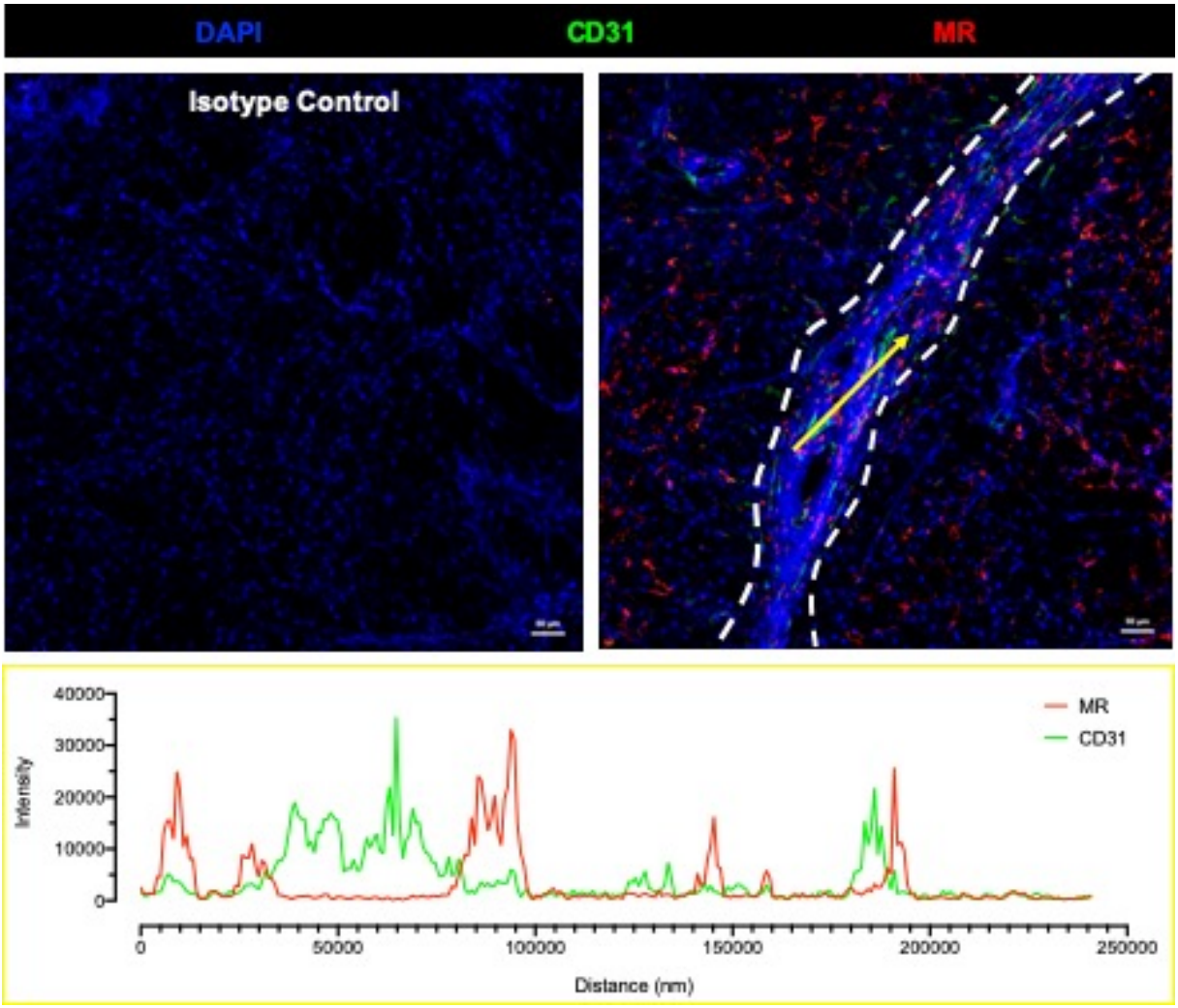

Figure 3.23: Mannose receptor (MR) did not co-localise with CD31 within fibrotic regions of cirrhotic liver.

Dual immunofluorescent staining for CD31 (*green*) and MR (*red*) was performed in cirrhotic liver tissue sections. Yellow line depicts site of intensity profile (*lower*). Isotype controls were negative. 4′,6-diamidino-2-phenylindole (DAPI, *blue*) was used as a nuclear counterstain. Samples were imaged using a Zeiss LSM880 confocal microscope and a 10x objective. Images shown are from a non-alcoholic steatohepatitis patient and are representative of seven visual fields. Analysis was performed in Zen blue software (Zeiss). Scale bars represent 50 μm.

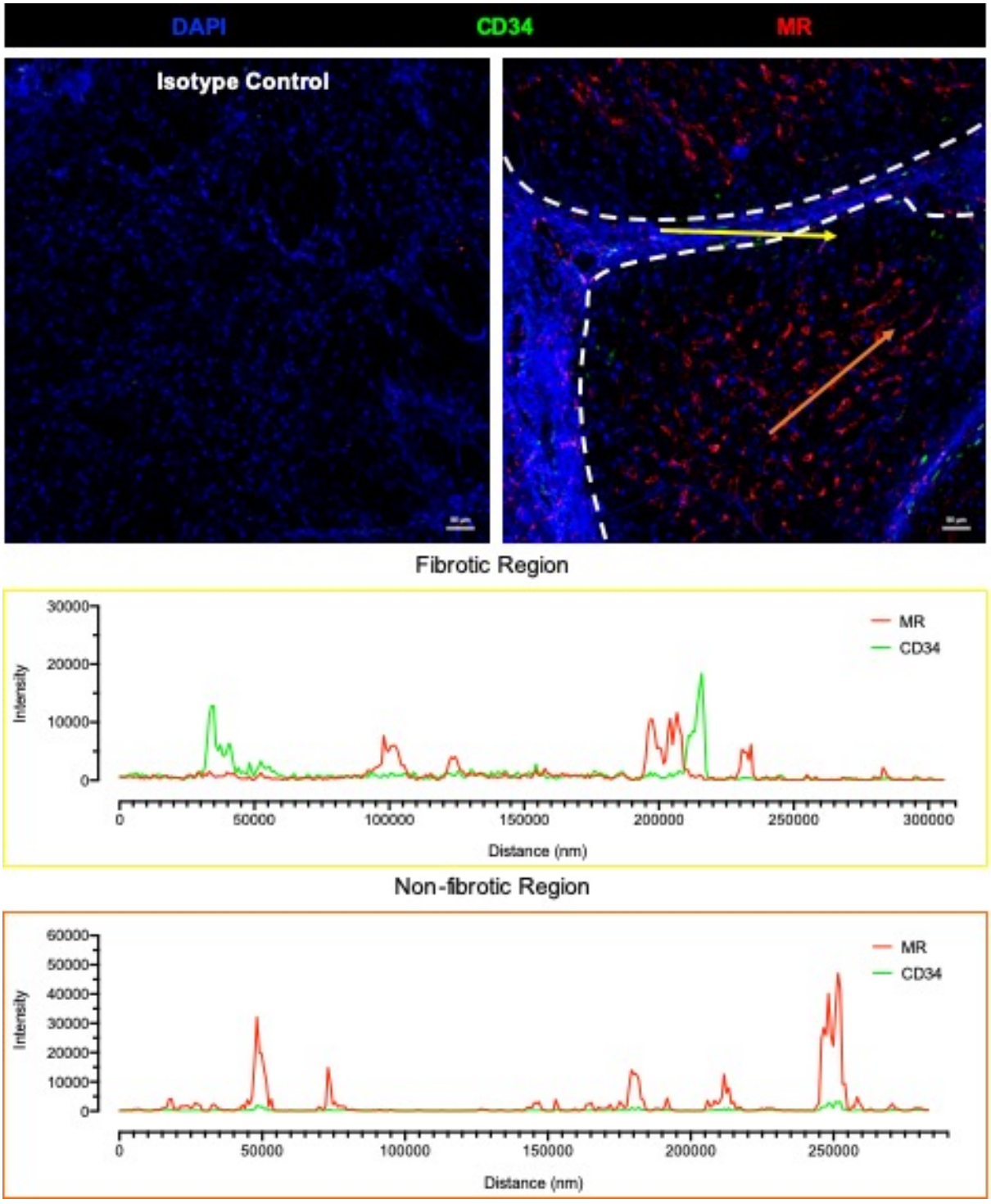

Figure 3.24: Mannose receptor (MR) did not co-localise with CD34 within fibrotic regions of cirrhotic liver.

Dual immunofluorescent staining for CD34 (*green*) and MR (*red*) was performed in cirrhotic liver tissue sections. Yellow and orange lines depict site of corresponding intensity profiles (*lower*). Isotype controls were negative. 4′,6-diamidino-2-phenylindole (DAPI, *blue*) was used as a nuclear counterstain. Samples were imaged using a Zeiss LSM880 confocal microscope and a 10x objective. Images shown are from a non-alcoholic steatohepatitis patient and are representative of four visual fields. Analysis was performed in Zen blue software (Zeiss). Scale bars represent 50 μm.

3.1.7 MR was also expressed in Kupffer cells

Mannose receptor is known to be highly expressed in cells of myeloid lineage, including macrophages and dendritic cells, in addition to the sinusoidal endothelium[397, 400, 470]. Dual immunofluorescent staining of MR with macrophage marker CD68 showed the presence of MR^+ Kupffer cells residing within the MR-expressing hepatic sinusoids (**Figure 3.25**). Within fibrotic septa, however, there was a distinct MR^+ population of cells which were CD68-negative (**Figure 3.26**).

Endo180 is the fourth member of the macrophage mannose receptor family of C-type lectins, which is known to be expressed by fibroblasts, in addition to endothelial cells and macrophages[471]. To investigate whether scar-associated MR^+ cells could be fibroblasts, dual immunofluorescence was performed with mesenchymal marker, vimentin (**Figure 3.27**). Partial co-localisation of MR and vimentin was observed in non-fibrotic sinusoidal regions, that likely highlights the close proximity of HSEC and HSCs, which are known to express vimentin[397]. In contrast, there was little co-localisation between MR and vimentin in fibrotic septa, suggesting MR^+ cells are not scar-associated fibroblasts.

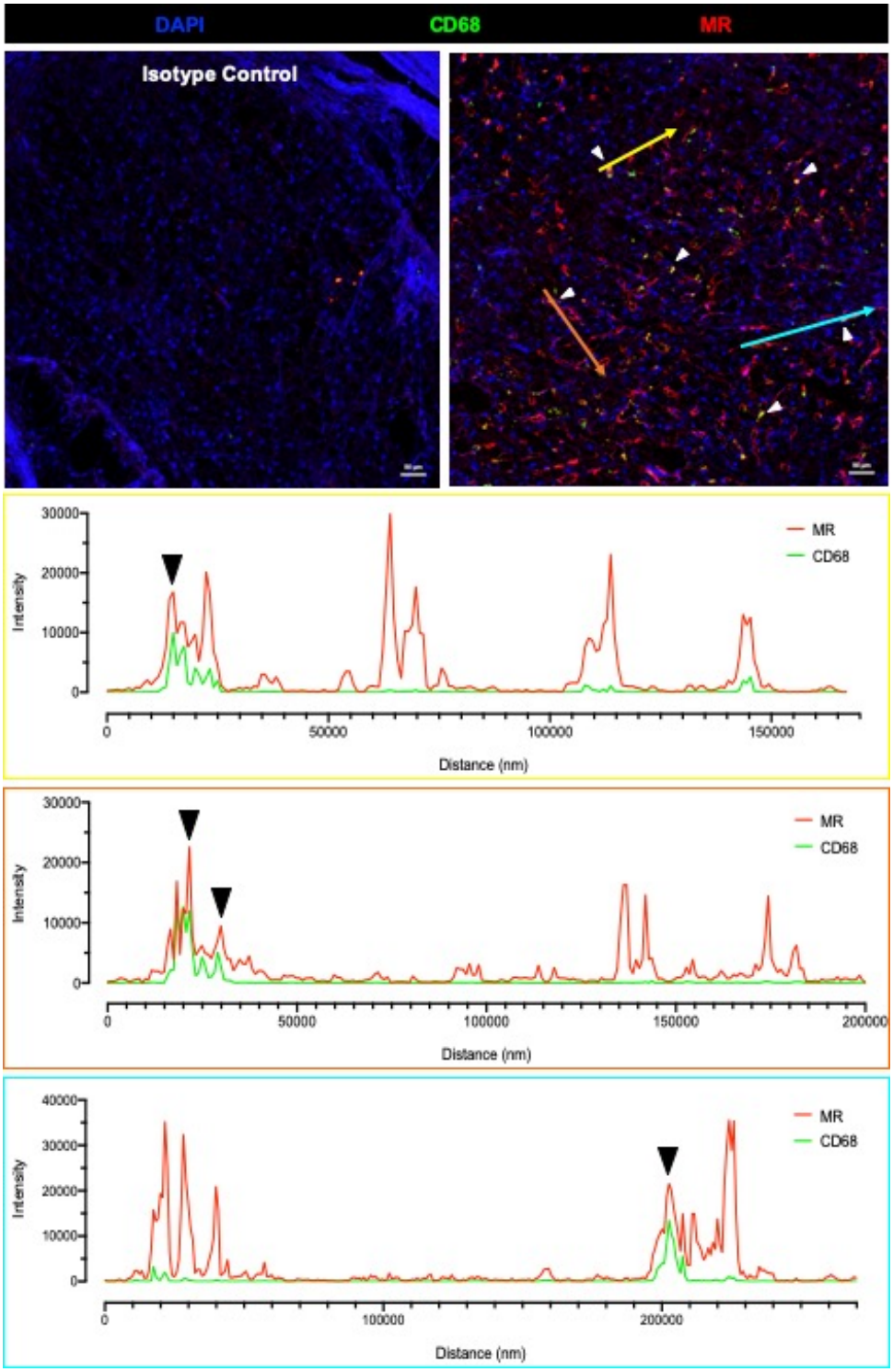

Figure 3.25: Mannose receptor (MR) partially co-localised with CD68-positive Kupffer cells (KCs) within the hepatic sinusoids.

Dual immunofluorescent staining for CD68 (*green*) and MR (*red*) was performed in cirrhotic liver tissue sections. Yellow, orange and blue lines depict site of corresponding intensity profiles (*lower*). White and black arrowheads indicate MR/CD68 overlap (KCs). Isotype controls were negative. 4′,6-diamidino-2-phenylindole (DAPI, *blue*) was used as a nuclear counterstain. Samples were imaged using a Zeiss LSM880 confocal microscope and a 10x objective. Images shown are from a non-alcoholic steatohepatitis patient and are representative of four visual fields. Analysis was performed in Zen blue software (Zeiss). Scale bars represent 50 μm.

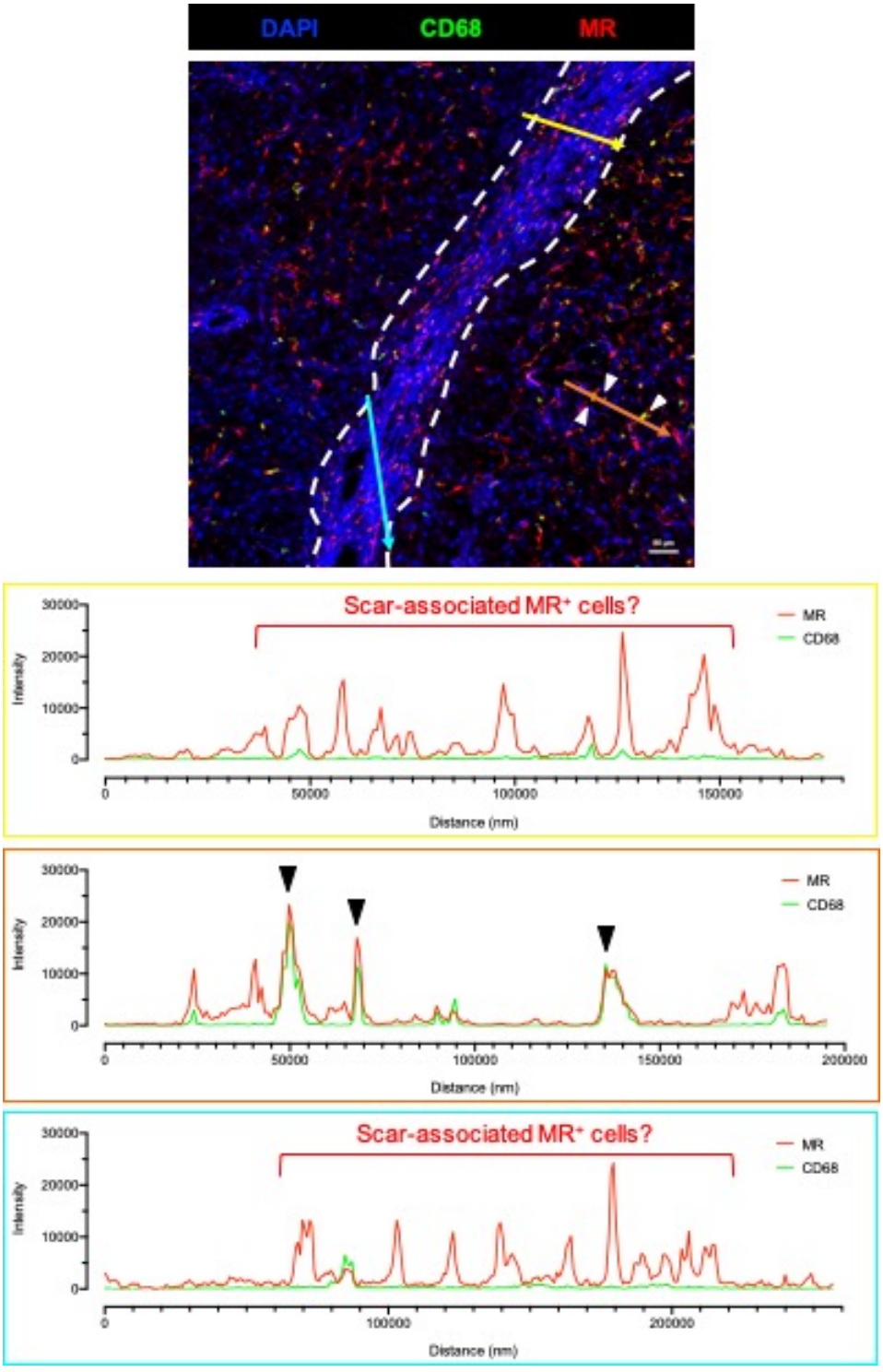

Figure 3.26: Mannose receptor (MR) defined a distinct CD68-negative scar-associated cell population within fibrous septa.

Dual immunofluorescent staining for CD68 (*green*) and MR (*red*) was performed in cirrhotic liver tissue sections. Yellow, orange and blue lines depict site of corresponding intensity profiles (*lower*). White and black arrowheads indicate MR/CD68 overlap (KCs) in sinusoidal regions. Isotype controls were negative. 4′,6-diamidino-2-phenylindole (DAPI, *blue*) was used as a nuclear counterstain. Samples were imaged using a Zeiss LSM880 confocal microscope and a 10x objective. Images shown are from a non-alcoholic steatohepatitis patient and are representative of four visual fields. Analysis was performed in Zen blue software (Zeiss). Scale bar represents 50 µm.

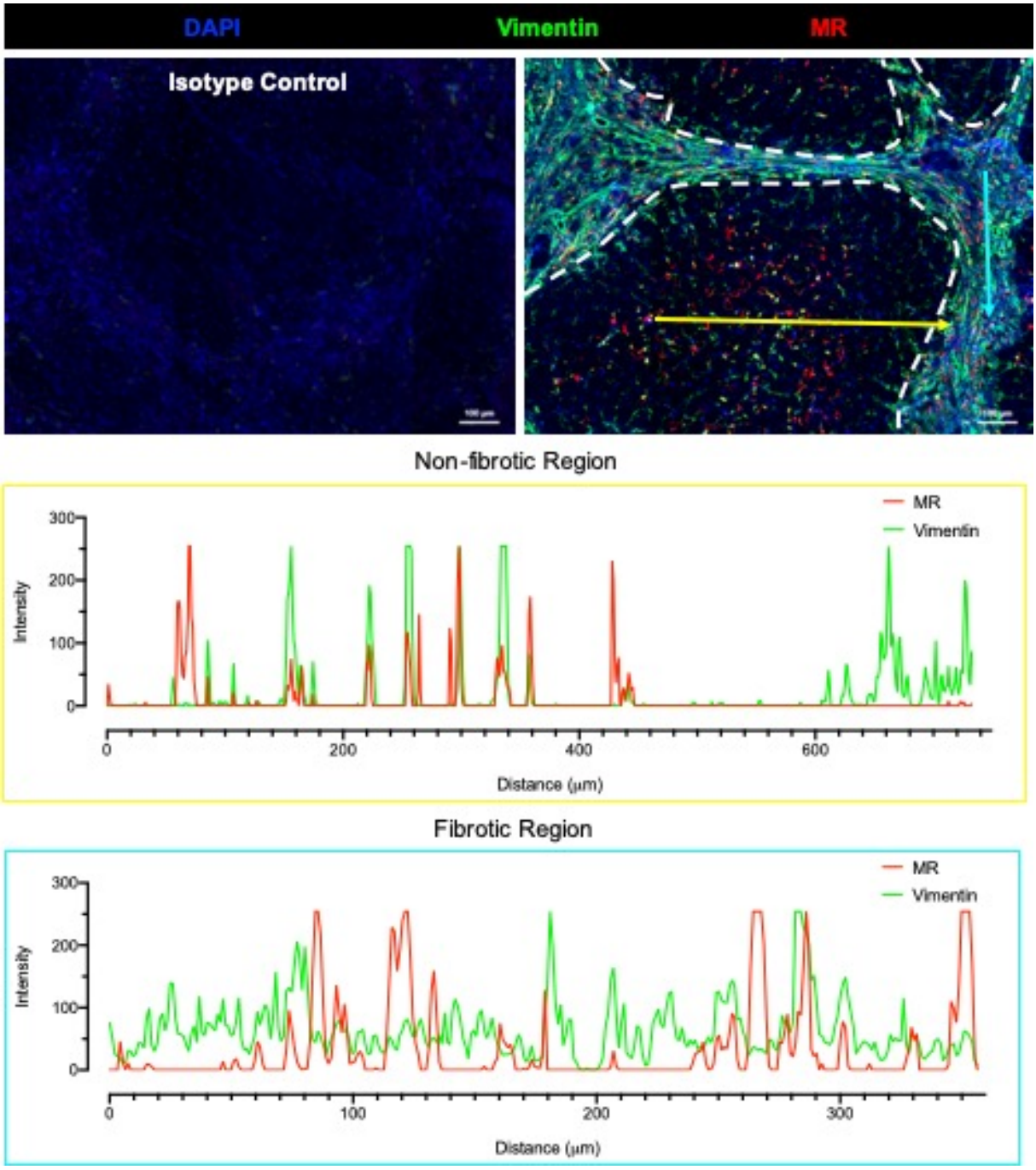

Figure 3.27: Scar-associated mannose receptor (MR)-positive cells did not co-localise with vimentin within fibrotic septa.

Dual immunofluorescent staining for vimentin (*green*) and MR (*red*) was performed in cirrhotic liver tissue sections. Yellow and blue lines depict site of corresponding intensity profiles (*lower*). Isotype controls were negative. 4′,6-diamidino-2-phenylindole (DAPI, *blue*) was used as a nuclear counterstain. Images shown are from an alcoholic liver disease patient. Fields of view were selected in Zen Blue software (Zeiss) post-acquisition of entire tissue sections using a Zeiss Axio Scan.Z1 and a 20x objective. Scale bars represent 100 µm.

3.1.8 PLVAP-expressing cells displayed both endothelial and mesenchymal characteristics

The endothelial specificity of PLVAP has long been documented, and is supported by recent single-cell RNA sequencing studies of normal and cirrhotic human liver[397]. As shown in **Figure 3.21** and **Figure 3.22**, $PLVAP^+$ cells seemed to express classic vascular endothelial marker, CD31, and neovessel marker, CD34, rather than sinusoidal markers L-SIGN and LYVE-1 (**Figure 3.19, Figure 3.20**). This cell population was also associated with caveolin-1 (**Figure 3.28**), another marker highly enriched within all types of liver endothelial cells[397].

Recent work has highlighted a phenomenon known as endothelial-to-mesenchymal transition (EndMT) whereby endothelial cells adopt a more "mesenchymal-like" phenotype, and have been suggested as drivers of fibrosis[472-474]. Given the scar-associated nature of $PLVAP^+$ endothelial cells, dual staining was performed with mesenchymal markers to investigate this further. Whilst there did not seem to be any obvious association between myofibroblast marker αSMA (**Figure 3.29**), there was substantial overlap between PLVAP and vimentin (**Figure 3.30**) and PLVAP and collagen III (**Figure 3.31**). These data suggest that the $PLVAP^+$ population of cells express both endothelial and mesenchymal markers, displaying characteristics of both cell types in fibrotic human liver.

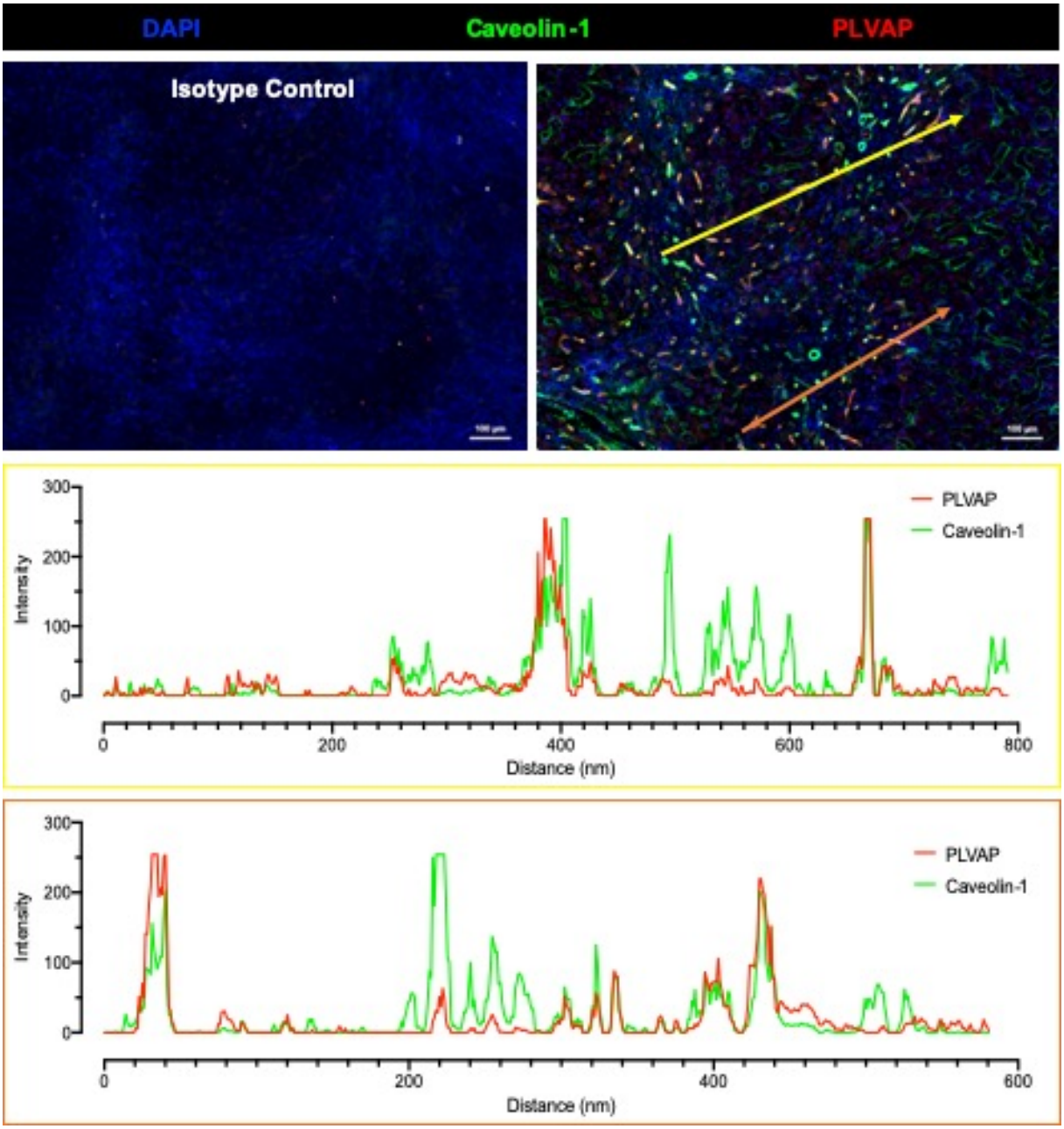

Figure 3.28: Plasmalemma vesicle-associated protein (PLVAP)-positive cells localised with caveolin-1.

Dual immunofluorescent staining for caveolin-1 (*green*) and PLVAP (*red*) was performed in cirrhotic liver tissue sections. Yellow and orange lines depict site of corresponding intensity profiles (*lower*). Isotype controls were negative. 4′,6-diamidino-2-phenylindole (DAPI, *blue*) was used as a nuclear counterstain. Images shown are from primary biliary cholangitis patient. Fields of view were selected in Zen Blue software (Zeiss) post-acquisition of entire tissue sections using a Zeiss Axio Scan.Z1 and a 20x objective. Scale bars represent 100 μm.

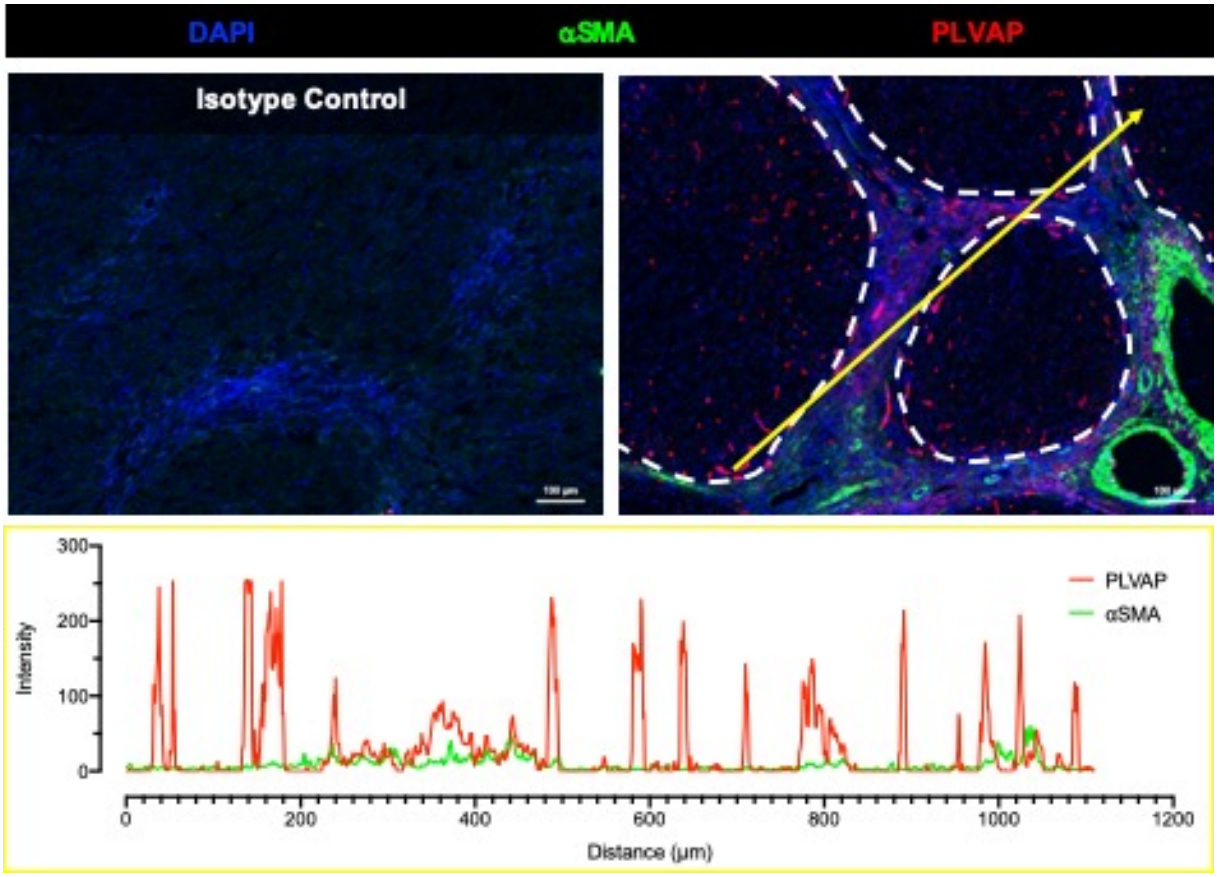

Figure 3.29: Plasmalemma vesicle-associated protein (PLVAP) did not co-localise with alpha smooth muscle actin (αSMA) within fibrotic septa.

Dual immunofluorescent staining for αSMA (*green*) and PLVAP (*red*) was performed in cirrhotic liver tissue sections. Yellow line depicts site of intensity profile (*lower*). Isotype controls were negative. 4′,6-diamidino-2-phenylindole (DAPI, *blue*) was used as a nuclear counterstain. Images shown are from non-alcoholic steatohepatitis patient. Fields of view were selected in Zen Blue software (Zeiss) post-acquisition of entire tissue sections using a Zeiss Axio Scan.Z1 and a 20x objective. Scale bars represent 100 µm.

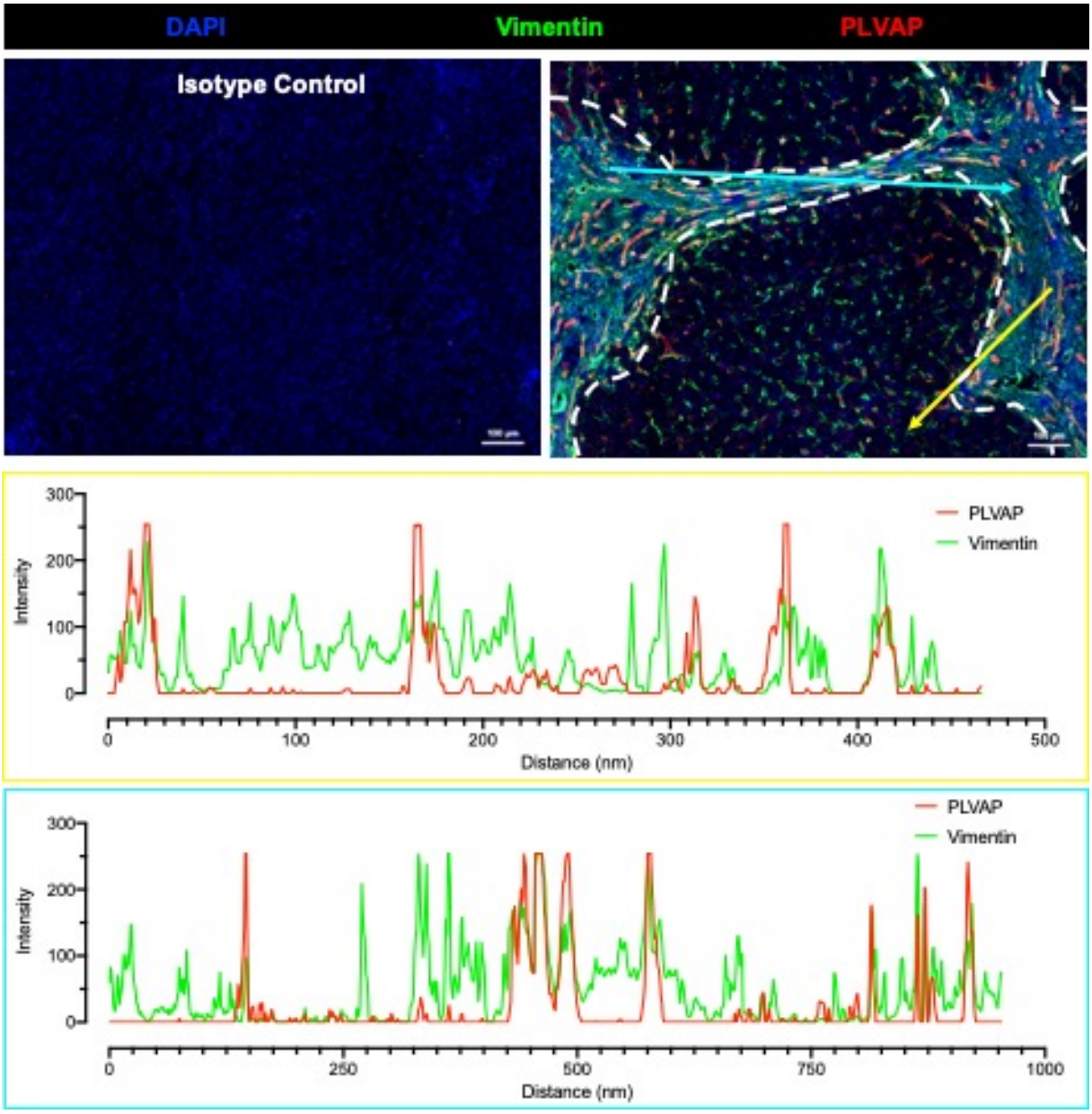

Figure 3.30: Plasmalemma vesicle-associated protein (PLVAP) co-localised with vimentin within fibrotic septa of cirrhotic livers.

Dual immunofluorescent staining for vimentin (*green*) and PLVAP (*red*) was performed in cirrhotic liver tissue sections. Yellow and blue lines depict site of corresponding intensity profiles (*lower*). Isotype controls were negative. 4′,6-diamidino-2-phenylindole (DAPI, *blue*) was used as a nuclear counterstain. Images shown are from an alcoholic liver disease patient. Fields of view were selected in Zen Blue software (Zeiss) post-acquisition of entire tissue sections using a Zeiss Axio Scan.Z1 and a 20x objective. Scale bars represent 100 µm.

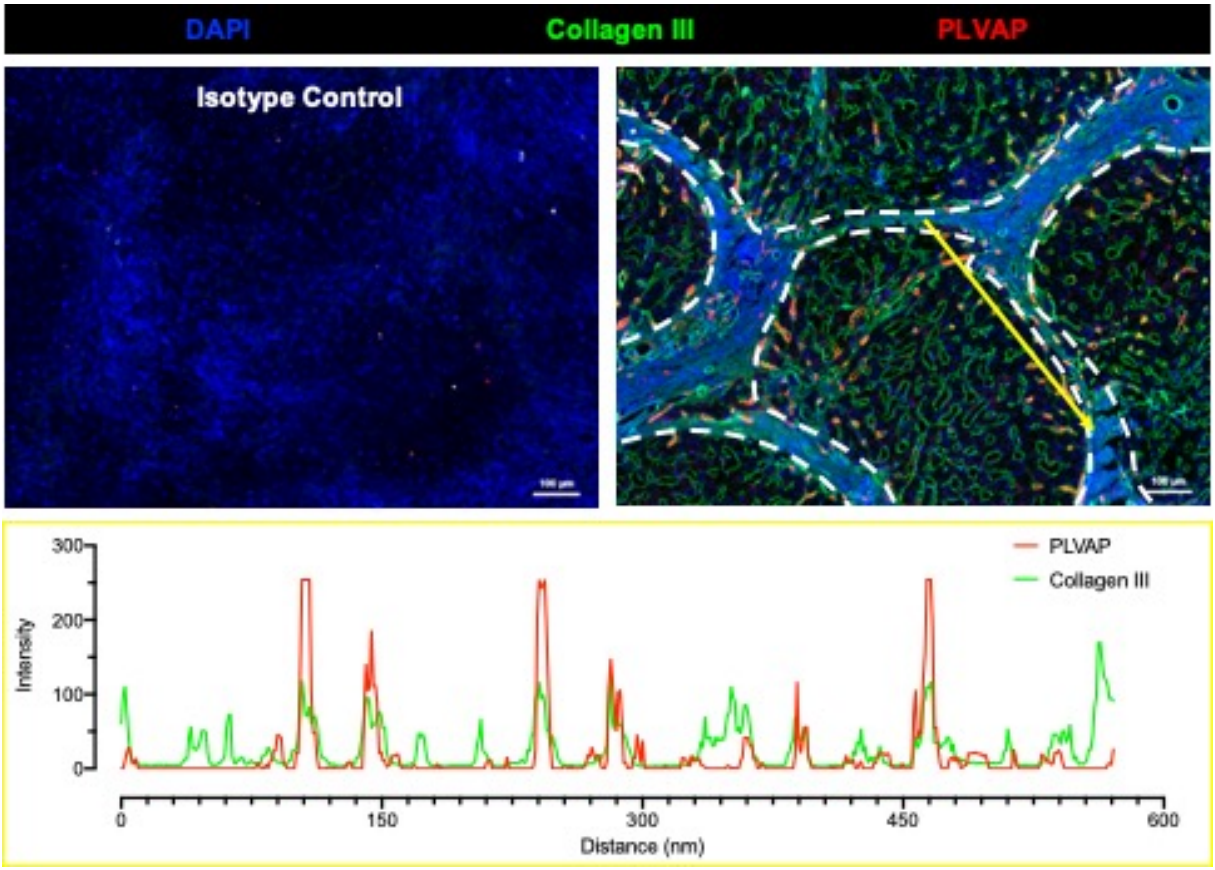

Figure 3.31: Plasmalemma vesicle-associated protein (PLVAP) co-localised with collagen III within fibrotic septa of cirrhotic livers.

Dual immunofluorescent staining for collagen III (*green*) and PLVAP (*red*) was performed in cirrhotic liver tissue sections. Yellow line depicts site of intensity profile. Isotype controls were negative. 4′,6-diamidino-2-phenylindole (DAPI, *blue*) was used as a nuclear counterstain. Images shown are from a non-alcoholic steatohepatitis patient. Fields of view were selected in Zen Blue software (Zeiss) post-acquisition of entire tissue sections using a Zeiss Axio Scan.Z1 and a 20x objective. Scale bars represent 100 µm.

3.1.9 Summary

- MR was highly expressed in the sinusoidal endothelium of normal human liver and its expression was downregulated in CLD and HCC tumours
- PLVAP was expressed at low levels in normal human liver but was significantly upregulated in CLD and HCC tumours
- PLVAP correlated with the extent of fibrosis in CLD localising within and proximal to fibrotic septa
- *PLVAP* gene expression was inversely associated with cancer stage and tumour grade and displayed higher expression in well-differentiated tumours
- *PLVAP* gene expression negatively correlated with markers of tumour aggression and was predictive of improved overall and disease-free survival in HCC patients
- MR and PLVAP displayed a reciprocal and mutually exclusive expression pattern in human liver
- MR^+ endothelial cells displayed a sinusoidal phenotype whilst $PLVAP^+$ endothelial cells exhibited a scar-associated inflammatory phenotype

4 REGULATION OF MR AND PLVAP IN PRIMARY HSEC

4.1 Introduction

In the previous chapter, results highlighted the distinct expression patterns of MR and PLVAP in normal liver, CLD and HCC, suggesting these proteins are also likely to be differentially regulated. The regulation mechanisms of MR and PLVAP have been studied in various cell types and several modulators of expression have been identified. These are summarised in **Table 4.1** and **Table 4.2**. However, very few studies have been performed in HSEC, and those that have solely focus on murine HSEC, leaving the regulation mechanisms of MR and PLVAP expression in human HSEC entirely unknown. This is pertinent given the known differences in expression between mice and humans, particularly for PLVAP. Identification of MR and PLVAP regulators in primary HSEC would allow manipulation of their expression *in vitro* and use in subsequent functional studies. This would also offer insight into how these molecules are regulated *in vivo*, since components of the tissue microenvironment in various disease contexts, either solely or in combination, are almost certainly key in maintaining (MR) or stimulating (PLVAP) their expression through autocrine and paracrine signalling.

Table 4.1: Summary of previously reported mannose receptor (MR) regulators.

Treatment	Effect	Cell Type	Pathway	Reference
15d-PGJ2	Upregulation (↑ Man-BSA binding)	Peritoneal mMφ	PPARγ	[475]
ATRA	Downregulation (↓ mRNA)	THP-1	pSTAT6, CLCA1	[476]
Aspirin	Upregulation (↑ surface expression)	RAW264.7	PPARγ	[477]
Ciglitazone	Upregulation (↑ Man-BSA binding)	Peritoneal mMφ	PPARγ	[475]
CX_3CL1	Upregulation (↑ protein)	THP-1	Src	[478]
Cytochalasin D	Downregulation (↓ expression/sMR shedding)	Peritoneal mMφ	Actin polymerisation	[403]
Dexamethasone	↑ MR activity (^{125}I-Mannose degradation)	Peritoneal mMφ	-	[479, 480]
Dimethyl Fumarate	Upregulation (↑ mRNA)	THP-1	Nrf2	[481]
Dynorphin	Upregulation (↑ surface expression)	BV-2 microglia	TLR4, NFκB	[482]

Ginsenoside Rg1	Upregulation (↑ surface expression)	RAW264.7	PPARγ	483
Ginsenoside Rg3	Upregulation (↑ surface expression)	RAW264.7, THP-1	PPARγ	484
Hep B core antigen	Downregulation (↓ mRNA/surface expression)	Chronic HBV M_2 hMφs	-	485
IFNγ	↓ MR activity (^{125}I-Mannose degradation) Downregulation (↓ transcription)	Peritoneal mMφ, J774E	-	480, 486
IL-10	Upregulation (↑ sMR) Downregulation (↓ mRNA)	mMφ, Rat astrocytes	-	487, 488
IL-13	Upregulation (↑ expression/activity)	Peritoneal mMφ	PPARγ, pA2	475, 489
IL-1β	Upregulation (↑ ^{125}I-Mannose uptake)	mHSEC	IL-1Ra	490
IL-4	Upregulation (↑ sMR) ↑ MR activity (^{125}I-Mannose binding/degradation) Upregulation (↑ mRNA)	Peritoneal mMφ, THP-1, Rat astrocytes	-	476, 480, 487 488
Latrunculin A	Downregulation (↓ expression/sMR shedding)	Peritoneal mMφ	Actin polymerisation	403
LPS	Upregulation (↑ 125I-Mannose uptake) Upregulation (↑ surface expression) Downregulation (↓ mRNA) Downregulation (↓ surface expression/activity)	mHSEC, BV-2 microglia, Rat astrocytes, hMDDCs	IL-1Ra TLR4, NFκB	482, 490 433, 488
LPA	Upregulation (↑ surface expression)	Murine microglia	LPAR, JNK/p38/ERK1/2 MAPKs	491
Mannose	Upregulation (↑ mRNA/protein)	Rat lung tissue	-	483
Pam3CSK4	Upregulation (↑ MR^+ M_2 Mφs)	Peritoneal mMφ	-	492
PGE1/2	Upregulation (~4-6-fold ↑expression) (↑ 125I-Mannose binding)	mBMDMφ	-	493
Rapamycin	Downregulation (↓ mannose RME)	mBMDDCs	mTOR	494
Rosiglitazone	Upregulation (↑ Man-BSA binding, ↑ surface expression)	Peritoneal mMφ mKCs	PPARγ	475, 495
Silvestrol	Downregulation (↓ surface expression)	hMDMφ	-	496
Substance P	Upregulation (↑ protein expression)	rBMDMs	PI3K/Akt/mTOR/S6K	497
Sulforaphane	Upregulation (↑ mRNA)	THP-1	Nrf2	481

TGFβ	Downregulation (↓ mRNA)	Murine microglia	TGFβR1	[498]
TNFα	Downregulation (↓ surface expression/activity)	hMDDCs	-	[433]
Wogonin	Upregulation (↑ mRNA)	THP-1	Nrf2	[481]

15dPGJ$_2$, 15-Deoxy-Delta-12,14-prostaglandin J2; **Man-BSA**, mannosylated-bovine serum albumin; **PPAR**, peroxisome proliferator-activated receptor; **mMφ**, murine macrophage; **ATRA**, all-trans retinoic acid; **pSTAT6**, phospho-signal transducer and activator of transcription 6; **CLCA1**, chloride channel accessory 1; **CX$_3$CL1**, fractalkine; **sMR**, soluble mannose receptor; **TLR4**, toll-like receptor 4; **NFκB**, nuclear factor kappa-light-chain-enhancer of activated B cells; **hMφ**, human macrophage; **IFNγ**, interferon γ; **IL**, interleukin; **pA2**, phospholipase A2; **LPS**, lipopolysaccharide; **hMDDC**, human monocyte-derived dendritic cell; **LPA**, lysophosphatidic acid; **MAPK**, mitogen-activated protein kinases; **PGE1/2**, prostaglandin E1/2; **mBMDMφ**, murine bone marrow-derived macrophage; **RME**, receptor-mediated endocytosis; **mBMDDC**, murine bone marrow-derived dendritic cell; **mTOR**, mammalian target of rapamycin; **mKC**, murine Kupffer cell; **hMDMφ**, human monocyte-derived macrophage; **rBMDM**, rat bone marrow-derived macrophage; **PI3K**, phosphoinositide 3-kinase; **TGFβ**, transforming growth factor β; **TNFα**, tumour necrosis factor α.

Table 4.2: Summary of previously reported plasmalemma vesicle-associated protein (PLVAP) regulators.

Treatment	Effect	Cell Type	Pathway	Reference
Angiopoietin I (KO)	Downregulation	Murine UUO kidney	Tie2	[499]
Angiotensin II	Upregulation (↑ permeability/caveolae)	HUVEC	AT1, p38 MAPK	[500]
β-catenin (GOF)	Downregulation (↓ fenestrations)	Murine subfornical organ	Norrin/Wnt/β-catenin	[501]
β-catenin (KO)	Upregulation	CNS mECs	Wnt/β-catenin	[502]
BMP-9	Upregulation (prevents fenestration loss in culture)	mHSEC	ALK1	[503]
Cancer cell CM (U87MG, U251MG)	Upregulation	HMVEC	-	[456]
Caveolin-1 (KO)	Downregulation (Internalisation/degradation)	Lung mECs	-	[504]
Dexamethasone	Downregulation (↓ permeability)	Zebrafish larvae	-	[505]
Fibrinogen	Upregulation (↑ caveolin-1)	Brain mECs	MMP9	[506]
FZD4 (KO)	Upregulation	CNS mECs	Norrin/Wnt	[507]
FZD4 (Ab)	Upregulation	Retinal mECs	Norrin/Wnt3a/β-catenin	[508]
HGF	Upregulation	HMVEC	-	[456]
LiCl	Downregulation	Brain mECs	GSK3/Norrin/Wnt/β-catenin	[509]
LPS	Downregulation	CNS mECs	-	[510]
PMA	Upregulation	HUVEC, HDMVEC, HMVEC	VEGF, VEGFR2, MEK1, ERK1/2 MAPK	[367, 456, 511]

S1P	Upregulation	MS-1 (mEC cell line)	S1PR1	[512]
SB431542	Downregulation (FISH)	Zebrafish larvae	TGFβR, ALK5	[505]
Shear Stress	Upregulation	HUVEC	-	[463]
TGFβ	Upregulation	HUVEC	-	[463]
Thrombin	↑ permeability/monocyte adhesion (↑ PLVAP?)	HUVEC	Angiopoietin-2, Gab1/SHP2/p38 MAPK	[513]
TNFα	Downregulation Redistribution towards cell periphery	HUVEC	-	[459, 463]
Tspan12 (KO)	Upregulation (phenocopies FRD4/LRP5/Norrin mutants)	Retinal mECs	Norrin/β-catenin	[514]
VEGF	Upregulation (↑ mRNA, ↑ caveolin-1, ↑ permeability/caveolae, fenestration loss)	HUVEC, HMVEC, HDMVEC, glomerular mECs, choroidal hECs	VEGFR2, PI3K, p38 MAPK	[456, 500, 515-518]
Wnt3a	Downregulation	Brain mECs	Norrin/Wnt/β-catenin	[509]

KO, knockout; **UUO**, unilateral ureteral obstruction; **HUVEC**, human umbilical vein endothelial cells; **AT1**, angiotensin II type 1 receptor; **MAPK**, mitogen-activated protein kinase; **GOF**, gain-of-function; **CNS**, central nervous system; **mEC**, murine endothelial cell; **BMP-9**, bone morphogenic protein 9; **mHSEC**, murine hepatic sinusoidal endothelial cell; **ALK**, activin receptor-like kinase; **CM**, conditioned medium; **HMVEC**, human microvascular endothelial cells; **MMP9**, matrix metalloproteinase 9; **FZD4**, frizzled class receptor 4; **HGF**, hepatocyte growth factor; **LiCl**, lithium chloride; **GSK3**, glycogen synthase kinase 3; **LPS**, lipopolysaccharide; **PMA**, phorbol 12-myristate 13-acetate; **HDMVEC**, human dermal microvascular endothelial cells; **VEGF**, vascular endothelial growth factor; **S1P**, sphinosine-1-phosphate; **TGFβ**, transforming growth factor β; **TNFα**, tumour necrosis factor α; **Tspan12**, tetraspanin 12; **LRP5**, LDL receptor-related protein 5; **hEC**, human endothelial cells.

4.2 Regulation Studies

Regulation studies were performed with primary human HSEC isolated from fresh liver tissue by immunomagnetic selection, using a well-established protocol[376] (**Figure 4.1**). Briefly, slices of liver tissue were mechanically and enzymatically digested before separation of the non-parenchymal cell fraction by density centrifugation. Biliary epithelial cells and immune cells were removed by positive immunomagnetic selection for epithelial cell adhesion molecule (EpCAM) and CD45, respectively. Endothelial cells were then isolated by immunomagnetic selection for $CD31^+$ cells and placed in culture in the presence of VEGF and HGF up to a maximum passage of 6 (p6). The HSEC phenotype was

confirmed by immunofluorescent staining for several markers which characterise HSEC in culture[469], including endothelial markers CD31 and LYVE-1, as well as CD32b and scavenger receptors CD36, stabilin-1 and stabilin-2 (**Figure 4.2**). Another characteristic of HSEC is their rapid endocytic capacity[76]. *In vitro*, HSEC maintained their ability to endocytose fluorescein isothiocyanate (FITC)-conjugated dextran (40 kDa) within 15 minutes of exposure, which peaked at 30 minutes and began to drop off after 60 minutes (**Figure 4.3A**). Hepatic sinusoidal endothelial cells also represent key scavengers in the liver, and similar to their endocytic capacity, the ability to rapidly scavenge acetylated low-density lipoproteins (LDLs) was conserved *in vitro*[469, 519] (**Figure 4.3B**). Thus, primary human HSEC isolated by this method represent a valid model for investigating the regulation and function of MR and PLVAP, since they are able to recapitulate HSEC phenotype and function under cultured conditions. The expression of *MRC1* and *PLVAP* mRNA was determined in freshly isolated and passaged HSEC by performing qRT-PCR analysis of cell lysates. The expression and localisation of MR and PLVAP protein within primary HSEC was determined by immunocytochemistry followed by confocal microscopy and high-content imaging.

4.2.1 MR was expressed in freshly isolated and passaged primary human HSEC from all aetiologies

To investigate MR expression at the mRNA level, qRT-PCR analysis was performed using whole cell lysates from freshly isolated patient-matched $CD31^+$ HSEC and $CD45^+$ immune cells, as well as HSEC isolated from various aetiologies and passaged *in vitro* (up to a maximum of p6) (**Figure 4.4A, B**). *MRC1* was expressed in $CD31^+$ HSEC and $CD45^+$ immune cells to a comparable extent, with a median relative expression (and interquartile range) of 0.017 (0.007, 0.089) vs. 0.024 (0.004, 0.123), respectively. These studies also showed that MR expression was maintained in HSEC following *in vitro* culture and passage, although there were significantly higher *MRC1* levels in cells of a later passage (p6) compared to p3 (3.15-fold), p4 (2.82-fold) and p5 (1.92-fold) HSEC, independently of aetiology (**Figure 4.4B**). Furthermore, *MRC1* was expressed at similar levels in HSEC isolated from donor and chronically diseased liver samples (0.028 (0.017, 0.037) vs. 0.024 (0.016, 0.037)) (**Figure 4.4B**). At the protein level, MR was expressed in practically all HSEC in culture and was located intracellularly often

within perinuclear stores, as determined by immunofluorescence and confocal microscopy (**Figure 4.4C, D**).

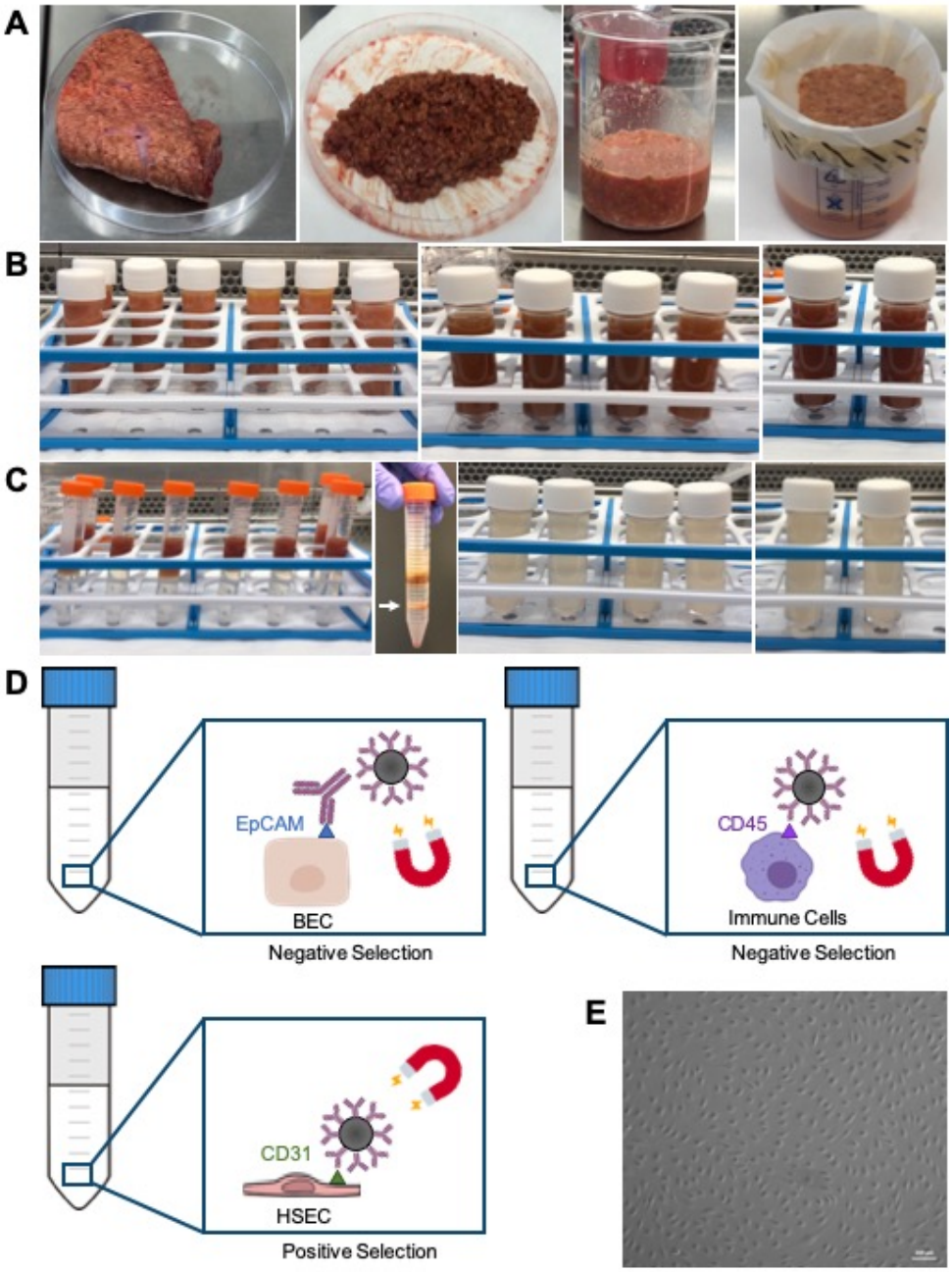

Figure 4.1: Isolation of primary hepatic sinusoidal endothelial cells (HSEC) from fresh human liver tissue.

(A) Liver slices from donor or diseased explants were mechanically and enzymatically digested and strained through a fine mesh. **(B, C)** The digest was concentrated through a series of centrifugation steps and the non-parenchymal cell fraction (*white arrow*) was isolated by density centrifugation using a 33:77% Percoll™ gradient. Non-parenchymal cells were washed with phosphate buffered saline and concentrated into one tube by centrifugation. **(D)** Biliary epithelial cells (BEC) and immune cells were removed by immunomagnetic selection against epithelial cell adhesion molecule (EpCAM) and CD45, respectively. HSEC were then isolated by immunomagnetic selection for CD31. **(E)** Cells were placed in culture in the presence of vascular endothelial growth factor and hepatocyte growth factor and passaged up to a maximum of six passages (p6). Scale bar represents 200 µm.

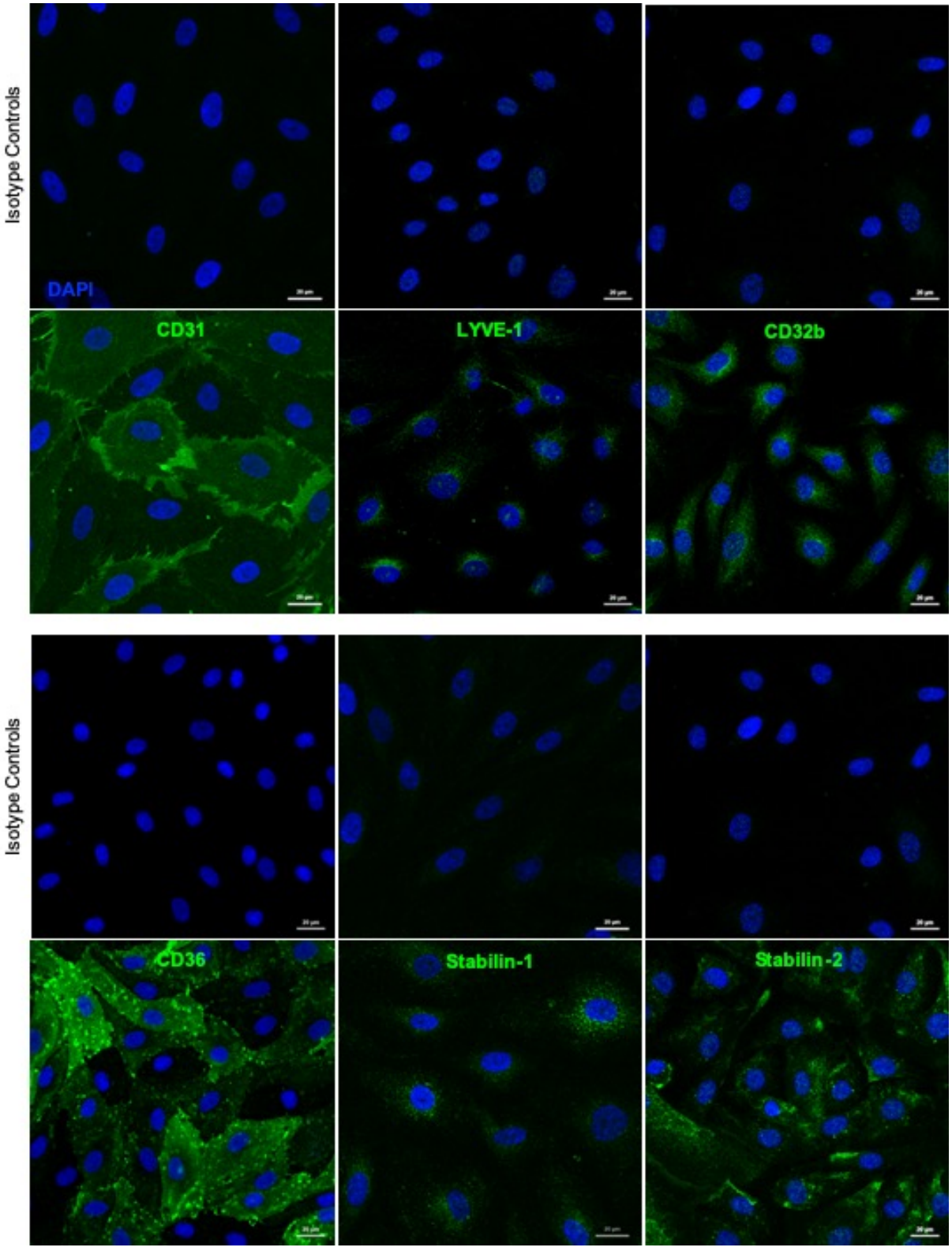

Figure 4.2: Hepatic sinusoidal endothelial cells (HSEC) are characterised by expression of several phenotypic markers in culture.

These include CD31, lymphatic vessel endothelial hyaluronan receptor 1 (LYVE-1), and CD32b, as well as scavenger receptors CD36, stabilin-1, and stabilin-2. Scale bars represent 20 μm.

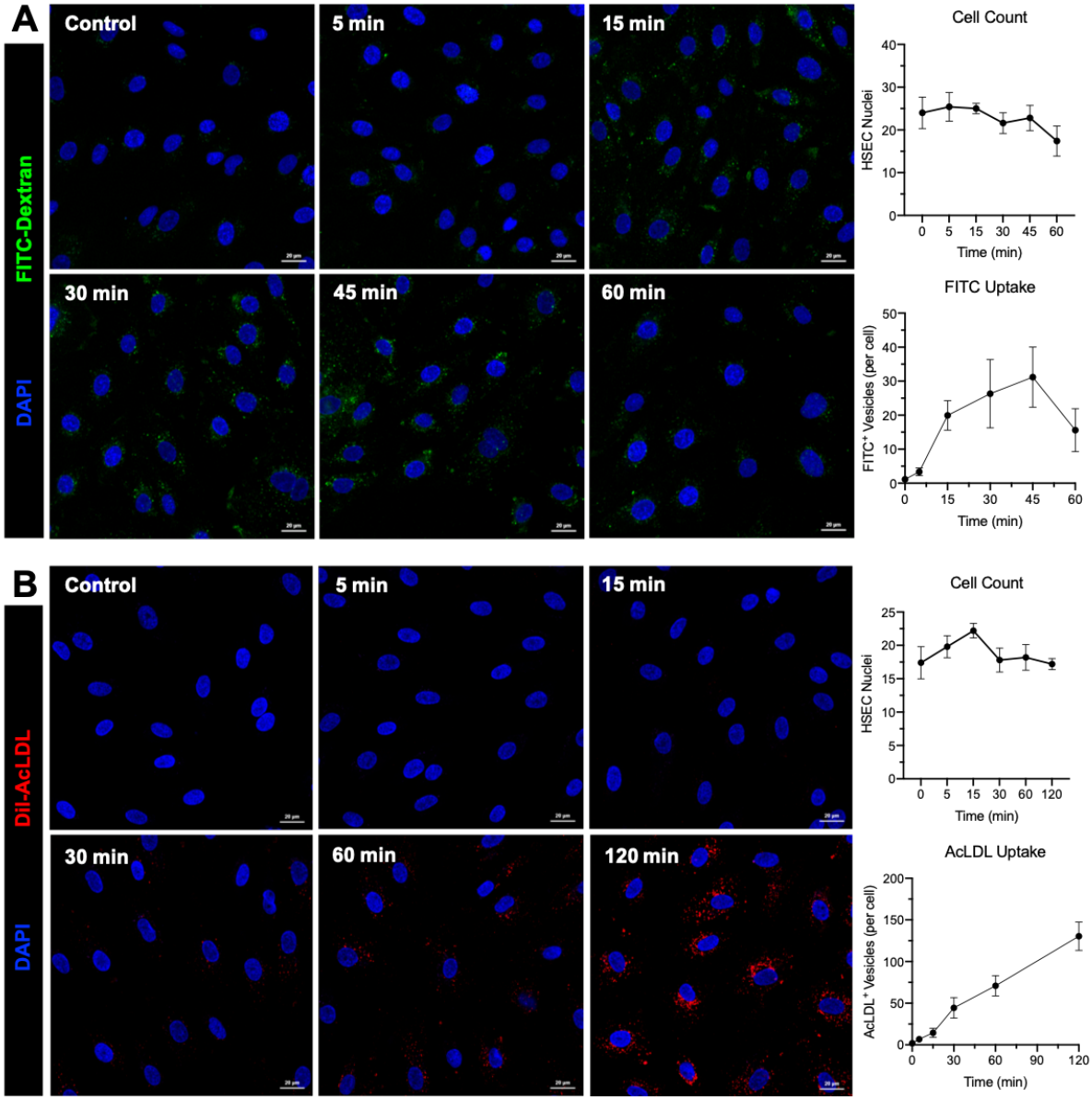

Figure 4.3: Hepatic sinusoidal endothelial cells (HSEC) maintained their rapid endocytic and scavenging capacity *in vitro*.

(A) Fluorescein isothiocyanate (FITC)-conjugated dextran (40 kDa) (1 mg/mL) (*green*) or **(B)** Dil-conjugated acetylated low-density lipoproteins (Dil-AcLDLs) (10 μg/mL) (*red*) were incubated with HSEC for times indicated before cells were fixed and imaged using an LSM880 confocal microscope and a 40x objective. Endocytosis was quantified using the "Analyse Particles" function in ImageJ and is shown as mean ± standard deviation of $FITC^+$ or $AcLDL^+$ vesicles per cell from five visual fields. Cell counts (mean ± standard deviation per visual field) are shown for each time point. 4′,6-diamidino-2-phenylindole (DAPI, *blue*) was used as a nuclear counterstain. Images and data shown are representative of two independent experiments. Scale bars represent 20 μm.

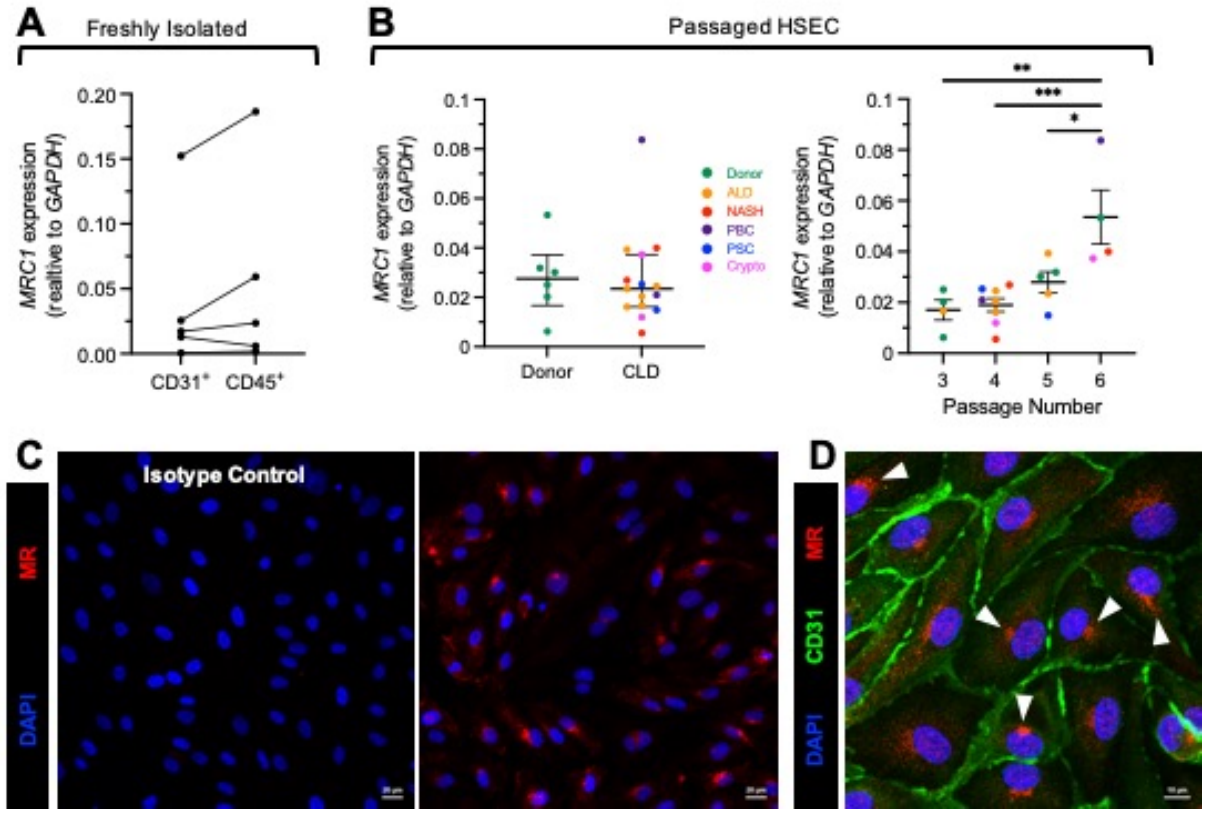

Figure 4.4: Mannose receptor (MR) was expressed at the mRNA and protein level in freshly isolated and passaged hepatic sinusoidal endothelial cells (HSEC).

(A, B) *MRC1* mRNA was quantified in freshly isolated CD31$^+$ and CD45$^+$ cell fractions (n=5), as well as in passaged donor- (n=6) and chronic liver disease (CLD) patient-derived (n=15) HSEC. *MRC1* expression was also studied relative to HSEC passage number (*p<0.05, **p<0.01, ***p<0.001, one-way ANOVA, followed by Tukey's multiple comparisons test). Data shown are *MRC1* expression (Donor vs. CLD – median ± interquartile range, passage number – mean ± SEM) relative to *GAPDH*, where each data point represents a biological replicate. **(C, D)** MR protein expression (*red*) in HSEC was determined by immunocytochemistry followed by confocal microscopy using a **(C)** 25x or **(D)** 63x objective. 4′,6-diamidino-2-phenylindole (DAPI, *blue*) was used as a nuclear counterstain and CD31 (*green*) was used as a plasma membrane counterstain. White arrowheads in **(D)** indicate perinuclear MR localisation. Isotype control samples were negative. Scale bars represent **(C)** 20 µm and **(D)** 10 µm.

4.2.2 PLVAP was enriched in HSEC over other liver cell types and heterogeneity was maintained in vitro

PLVAP gene expression was studied in both freshly isolated CD31$^+$ and CD45$^+$ cell fractions (**Figure 4.5A**), as well as in passaged HSEC, activated liver myofibroblasts (aLMF), HSC and BEC (**Figure 4.5B**). These data showed significant enrichment of *PLVAP* mRNA in HSEC compared to other liver cell types. Levels of *PLVAP* mRNA were 19.57-fold higher in the CD31$^+$ cell fraction (1.067 ± 0.46) compared to the CD45$^+$ immune cell fraction (0.055 ± 0.02) from matched patient samples (**Figure**

4.5A). Further, HSEC displayed a significantly higher expression of *PLVAP* compared to other cell types isolated and cultured from the human liver, including aLMF (~2058-fold), BEC (~4682-fold), and HSC (~7359-fold) (**Figure 4.5B**). In passaged HSEC isolated from donor and chronically diseased liver samples, there was no significant difference in *PLVAP* expression (**Figure 4.5C**). However, there was a positive correlation between the number of passages and the amount of *PLVAP* expressed, with HSEC at p5 or higher expressing significantly more *PLVAP* compared to lower passages (p3 and p4), irrespective of the livers from which they were derived (**Figure 4.5C**). At the protein level, only a subset of HSEC seemed to express PLVAP in primary cell culture (**Figure 4.5D**), recapitulating heterogeneity observed *in situ* in human liver samples (**Chapter 3**). In addition, PLVAP seemed to localise throughout the cell cytoplasm and within aggregates towards the cell periphery (**Figure 4.5D**).

4.2.3 MR predominantly resided intracellularly within the Golgi apparatus, early endosomes and recycling endosomes

As depicted in **Figure 4.4**, MR was predominantly located within intracellular stores as opposed to being associated with the plasma membrane. To investigate which intracellular compartments MR resided in, immunocytochemistry was performed with Golgi apparatus marker, GM130, early endosome-associated protein (early endosomal antigen 1, EEA-1), recycling endosomal marker, Rab11a, and late endosomal/lysosomal marker, vesicle-associated membrane protein 7 (VAMP7). As shown in **Figure 4.6**, within cells that displayed prominent perinuclear MR staining, MR co-localised with GM130, suggesting these intracellular stores reside within the Golgi apparatus (**Figure 4.6A**). In cells that showed a vesicular staining pattern, MR co-localised incompletely with endosomal markers EEA-1 and Rab11a, which is consistent with the idea that MR undergoes constant trafficking through the endosomal system (**Figure 4.6B, C**). Under steady-state conditions, MR did not reside within late endosomes/lysosomes since there was little colocalisation observed between MR and VAMP7 (**Figure 4.6D**).

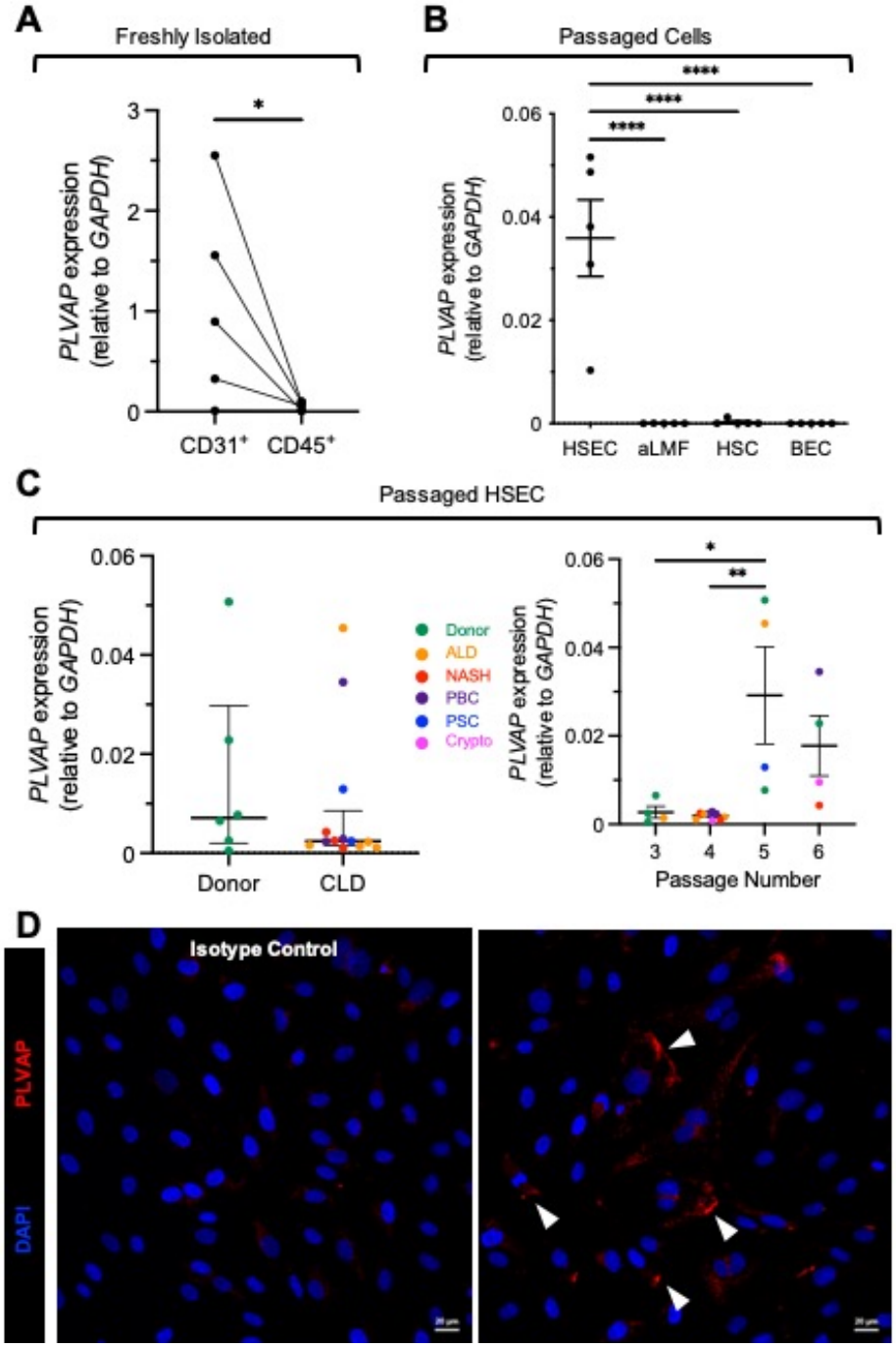

Figure 4.5: Plasmalemma vesicle-associated protein (PLVAP) was expressed at the mRNA and protein level in freshly isolated and passaged hepatic sinusoidal endothelial cells (HSEC).

(A-C) *PLVAP* mRNA was quantified in freshly isolated CD31$^+$ and CD45$^+$ cell fractions (n=5) (*p<0.05, student's paired *t*-test), as well as in passaged HSEC, activated liver myofibroblasts (aLMF), hepatic stellate cells (HSC) and biliary epithelial cells (BEC) (n=4-5) (****p<0.0001, one-way ANOVA, followed by Holm-Šídák's multiple comparison test). **(C)** *PLVAP* expression was also compared in donor- (n=6) and chronic liver disease (CLD) patient-derived (n=15) HSEC, and in HSEC of different passage numbers (*p<0.05, **p<0.01, one-way ANOVA, followed by Tukey's multiple comparisons test). Data shown are *PLVAP* expression (mean ± SEM, except Donor vs. CLD – median ± interquartile range) relative to *GAPDH*, where each data point represents a biological replicate. **(D)** PLVAP protein expression in HSEC was determined by immunocytochemistry followed by confocal microscopy using a 25x objective. 4′,6-diamidino-2-phenylindole (DAPI, *blue*) was used as a nuclear counterstain. White arrowheads in **(D)** indicate peripheral PLVAP localisation. Isotype control samples were negative. Scale bars represent 20 µm.

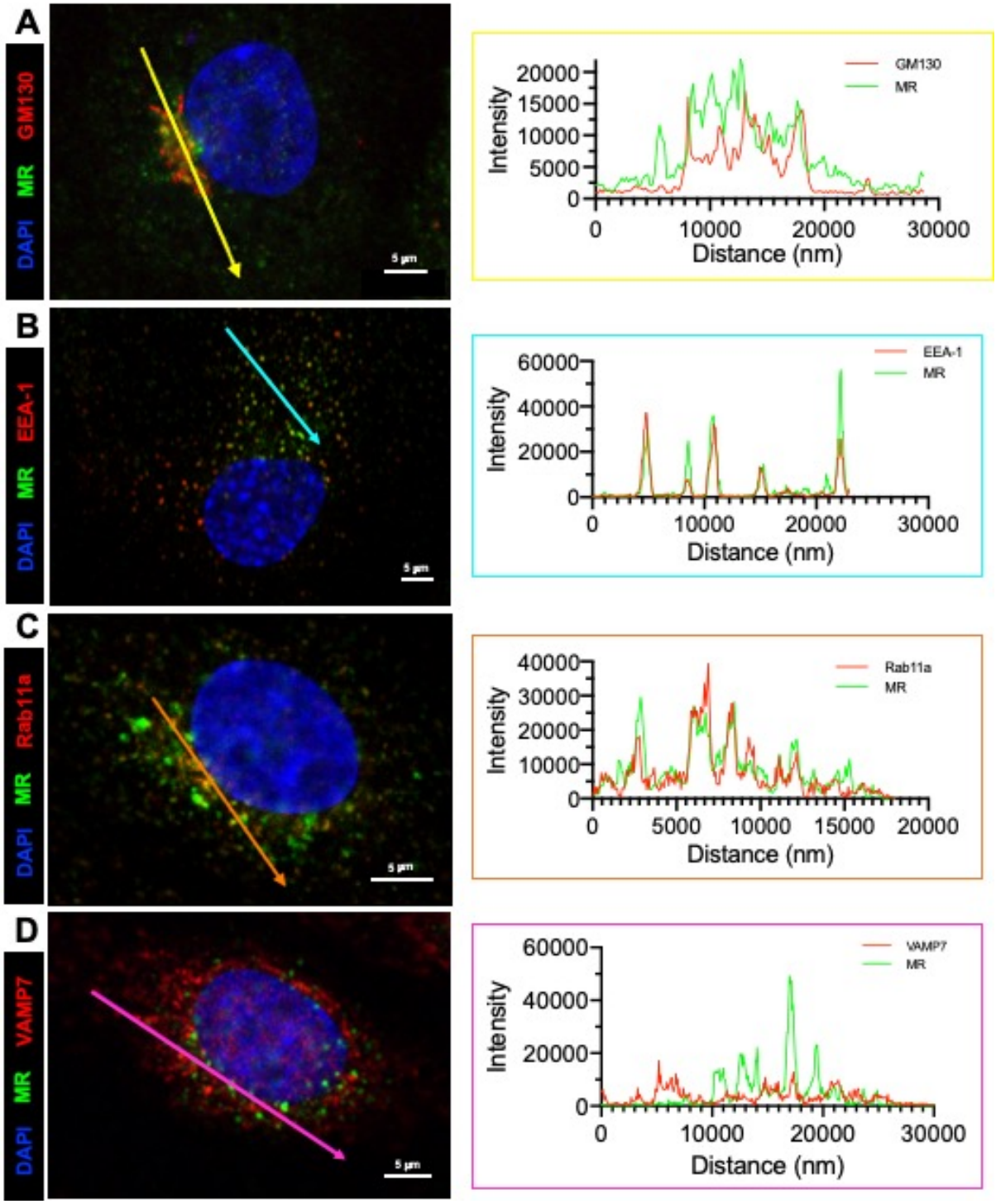

Figure 4.6: Mannose receptor (MR) predominantly resided within the Golgi apparatus and endosomal network in primary HSEC.

Immunocytochemistry and confocal microscopy allowed visualisation of MR (*green*) with **(A)** Golgi marker, GM130 (*red*), **(B)** early endosome marker, EEA-1 (early endosomal antigen 1) (*red*), **(C)** recycling endosome marker, Rab11a (*red*), and **(D)** late endosome/lysosomal marker, VAMP-7 (vesicle-associated membrane protein 7) (*red*). Coloured lines depict site of corresponding intensity profiles. Images were acquired using an LSM880 confocal microscope and a 63x objective. 4′,6-diamidino-2-phenylindole (DAPI, *blue*) was used as a nuclear counterstain. Isotype control samples were negative (see **Appendix 7.3**). Scale bars represent 5 µm.

4.2.4 MR underwent constant endosomal trafficking and recycling which was inhibited by bafilomycin

To investigate whether MR undergoes endosomal trafficking within HSEC as has been previously described in other cell types, HSEC were treated with bafilomycin A1, an inhibitor of vacuolar type H^+-ATPase which is known to perturb endocytic transport as well as lysosomal acidification[461, 462]. Following bafilomycin A1 treatment, the cytoplasmic pool was altered in that MR appeared to aggregate within larger intracellular vesicles (**Figure 4.7**). When these vesicles were characterised, it seemed that the localisation of MR within recycling endosomes was lost, since MR no longer co-localised with Rab11a in bafilomycin-treated HSEC (**Figure 4.7C**). Instead, the majority of the intracellular MR pool seemed to reside within the Golgi and $GM130^+$ vesicular structures (**Figure 4.7B**). These data suggest that, under steady state conditions, MR undergoes continuous endosomal trafficking and recycling.

4.2.5 MR was rapidly internalised into early endosomes following antibody ligation

To investigate the effects of receptor ligation on the localisation of MR, HSEC were treated with a mouse anti-human MR antibody for various time points, fixed and then stained with a fluorescently-conjugated anti-mouse secondary antibody to visualise receptor localisation in response to treatment (**Figure 4.8A**). Antibody treatment induced rapid MR internalisation within 15 minutes which peaked at 30 minutes and was maintained at 60 minutes post-receptor ligation. This was demonstrated by analysis of the number of MR^+ vesicles per number of HSEC. These data are consistent with the function of MR as an endocytic receptor. Following treatment, cells were fixed and co-stained with a rabbit polyclonal MR antibody, confirming the MR^+ identity of the internalised vesicles and also the specificity of both antibodies (**Figure 4.8B**). These vesicles were identified as early endosomes since there was substantial colocalisation with early endosomal marker, EEA-1 (**Figure 4.8C**).

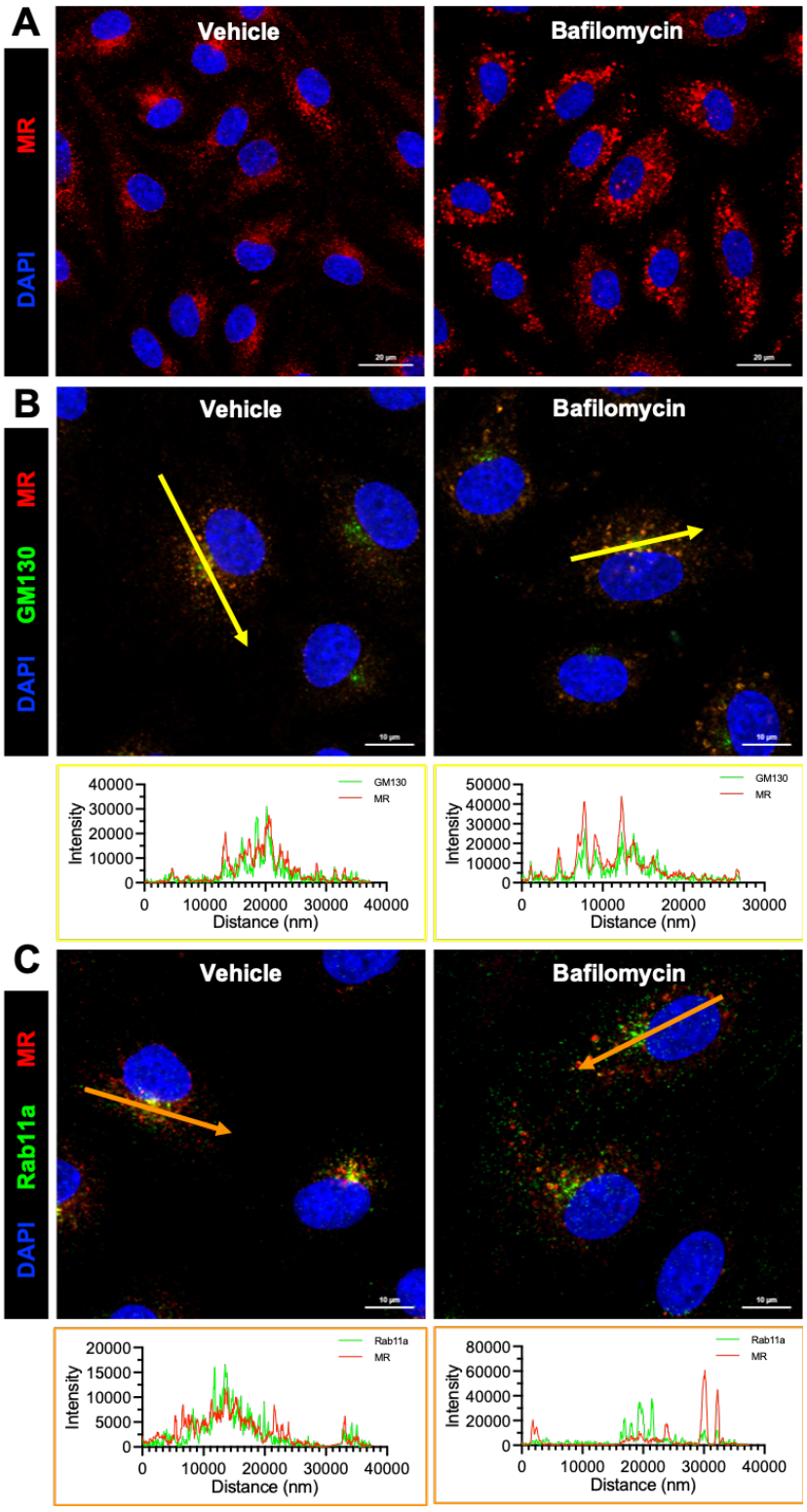

Figure 4.7: Mannose receptor (MR) underwent constant endosomal trafficking and recycling which was inhibited by bafilomycin A1.

Hepatic sinusoidal endothelial cells were treated with 10 nM bafilomycin (or DMSO) for 24 h, before being fixed and stained for **(A-C)** MR (*red*), **(B)** GM130 (*green*) and **(C)** Rab11a (*green*). Coloured lines depict site of corresponding intensity profiles. Images were acquired using an LSM880 confocal microscope and a 63x objective. 4′,6-diamidino-2-phenylindole (DAPI, *blue*) was used as a nuclear counterstain. Scale bars represent **(A)** 20µm or **(B, C)** 10 µm.

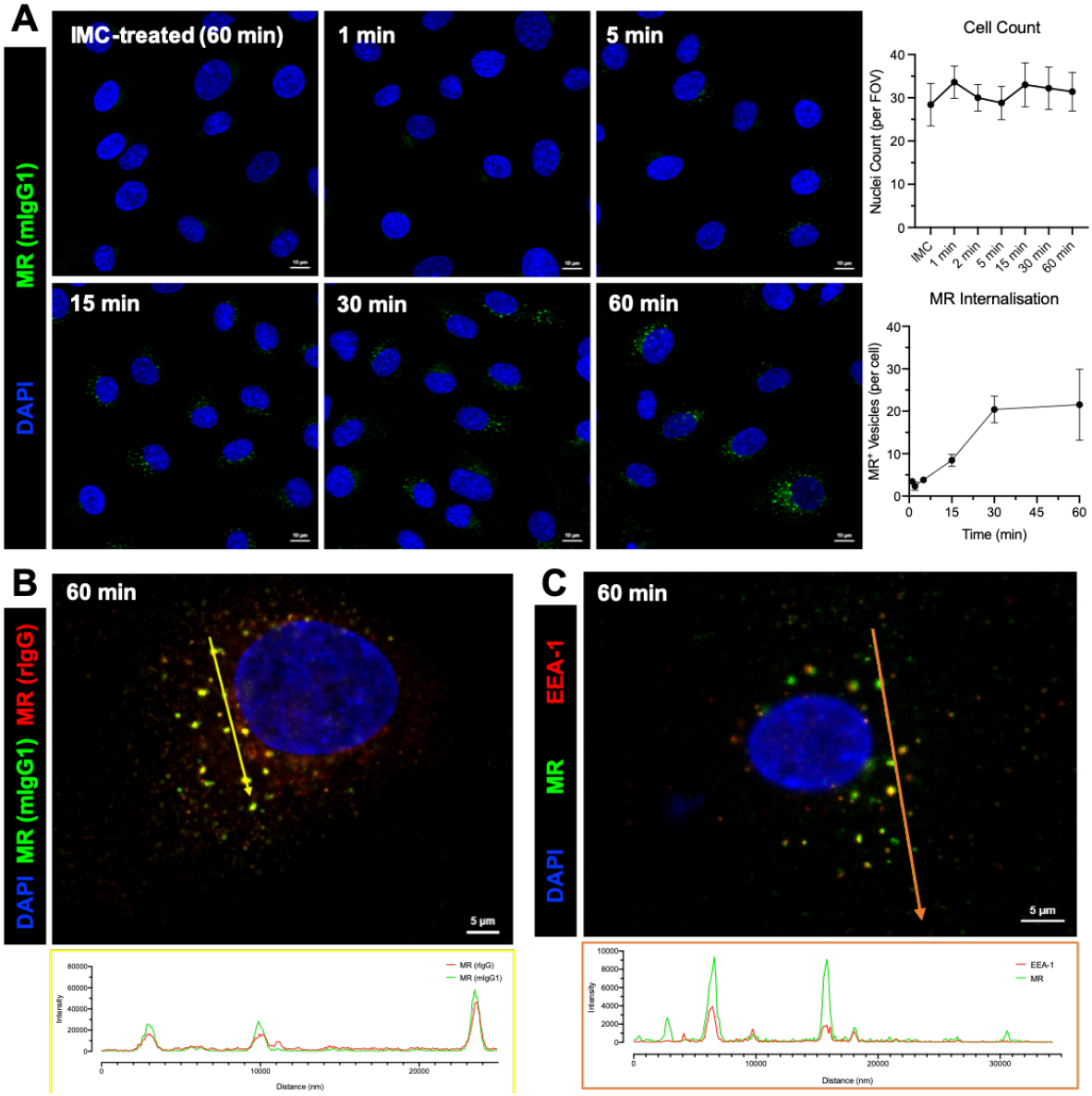

Figure 4.8: Mannose receptor (MR) underwent rapid internalisation into early endosomes following antibody ligation.

(A) Hepatic sinusoidal endothelial cells (HSEC) were treated with an anti-MR antibody (mIgG1) for time points indicated, before being fixed, permeabilised and stained with an anti-mIgG1 antibody (*green*). The number of MR^+ vesicles per cell for each time point was quantified using the "Analyse Particles" function in ImageJ, as were the cell counts for each condition via quantification of HSEC nuclei. Data shown are mean ± SD of five visual fields per time point and are representative of two independent experiments. **(B)** The localisation of MR within internalised vesicles was confirmed by co-staining with a rabbit polyclonal anti-MR antibody (*red*) post-fixation. **(C)** MR^+ vesicles co-localised with early endosomal antigen 1 (EEA-1, *red*). Yellow and orange lines in **(B)** and **(C)** depict the site of intensity profiles. Images were acquired using an LSM880 confocal microscope and a 63x objective. 4′,6-diamidino-2-phenylindole (DAPI, *blue*) was used as a nuclear counterstain. Scale bars represent **(A)** 10 µm or **(B, C)** 5 µm.

4.2.6 PLVAP was excluded from cell-cell junctions, localised mostly intracellularly, and was insensitive to bafilomycin treatment

In contrast to MR, which often resided within perinuclear stores, PLVAP was located throughout the cytoplasm and towards the cell periphery (**Figure 4.5D**). Previous work has suggested that PLVAP is almost completely excluded from cell-cell junctions of lymphatic endothelial cells[366]. Immunocytochemistry was performed to visualise PLVAP and junctional protein vascular endothelial-cadherin (VE-cadherin) by confocal microscopy (**Figure 4.9**). As has been previously described, PLVAP was excluded from VE-cadherin$^+$ junctions between primary HSEC. Given the enrichment of PLVAP at the cell periphery, immunocytochemistry was performed in non-permeabilised HSEC to investigate the proportion of PLVAP which resided within the cell membrane (**Figure 4.10A**). The % staining area was approximately 5-fold higher in permeabilised HSEC, with only 18.16 ± 4.71% of PLVAP residing at the cell surface. However, the localisation of PLVAP was unchanged in response to bafilomycin A1 treatment, suggesting that PLVAP does not undergo endosomal trafficking in primary HSEC (**Figure 4.10B**).

4.2.7 PLVAP co-localised with caveolin-1 and underwent trafficking to the cell periphery in response to TNFα

Given the well-established relationship between PLVAP and caveolae, immunofluorescent staining was performed to investigate PLVAP's localisation relative to caveolin-1. Whilst all HSEC were positive for caveolin-1, only a subset expressed PLVAP, which recapitulated observations in human liver sections (**Chapter 3**). Interestingly, in PLVAP$^+$ cells, there was evident colocalisation with caveolin-1, which could suggest these molecules lie in close proximity to one another, perhaps within the same structures (**Figure 4.11**). These data also confirmed observations in characterisation studies, which showed complete colocalisation between PLVAP and caveolin-1 in liver samples, but also highlighted evident caveolin-1$^+$ regions which were PLVAP-negative (**Figure 3.24**). In response to TNFα, both caveolin-1 and PLVAP underwent trafficking towards the cell periphery where they continued to co-

localise in PLVAP^{+} cells (**Figure 4.11**). Since these studies were performed in permeabilised cells, whether PLVAP or caveolin-1 are trafficked to the cell membrane in response to TNFα is not known.

4.2.8 Antibodies targeted towards PLVAP rapidly bound to HSEC

To understand whether treatment with an anti-PLVAP antibody could lead to altered PLVAP localisation, as was observed with MR, time-course experiments were performed with primary HSEC. As shown in **Figure 4.12**, PLVAP antibodies were able to rapidly bind to the HSEC surface within five minutes, which increased in a time-dependent manner up to the final time point of 60 minutes. Notably, the level of antibody binding was significantly higher (~5-fold) at 60 minutes compared to the fixed untreated control, where PLVAP was often observed to aggregate following 30-60 minutes of treatment. This could suggest either that antibody binding to PLVAP is more efficient in live cells, possibly due to epitope changes following fixation, or that antibody treatment led to PLVAP redistribution and aggregation which was not observed in untreated cells.

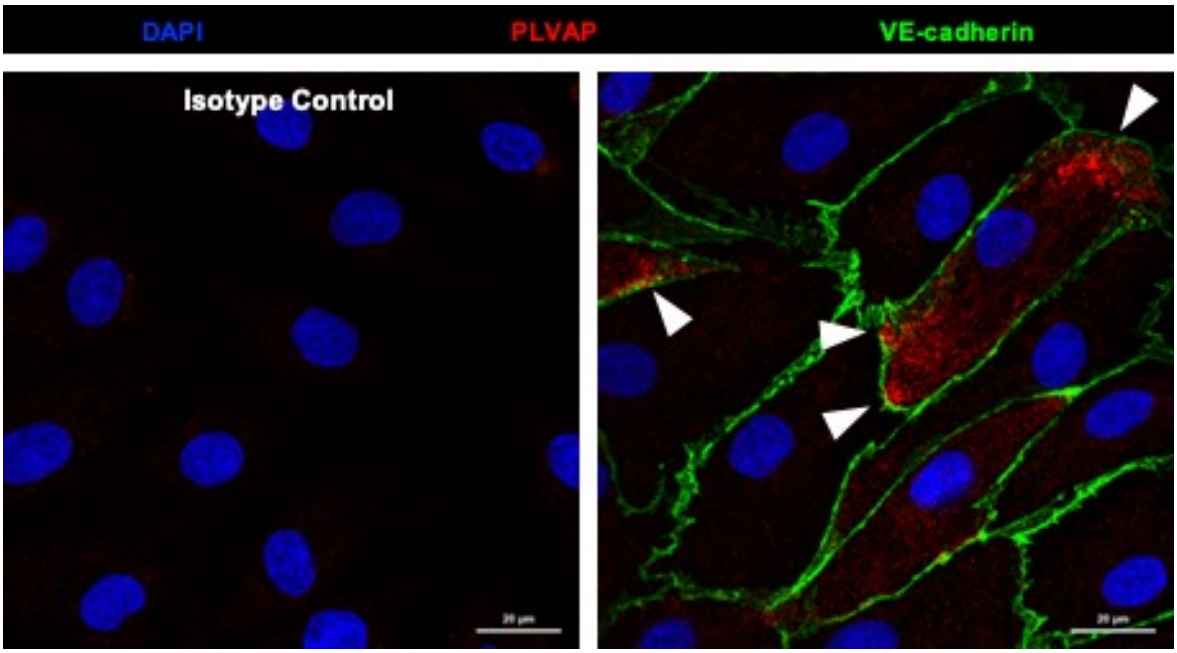

Figure 4.9: Plasmalemma vesicle-associated protein (PLVAP) was excluded from cell-cell junctions and often localised at the cell periphery.

PLVAP (*red*) was visualised with junctional marker vascular endothelial cadherin (VE-cadherin, *green*) by immunocytochemistry and confocal microscopy. White arrowheads indicate PLVAP localisation proximal to, but not within, intercellular junctions. Images were acquired using an LSM880 confocal microscope and a 40x objective. 4′,6-diamidino-2-phenylindole (DAPI, *blue*) was used as a nuclear counterstain. Isotype control samples were negative. Scale bars represent 20 μm.

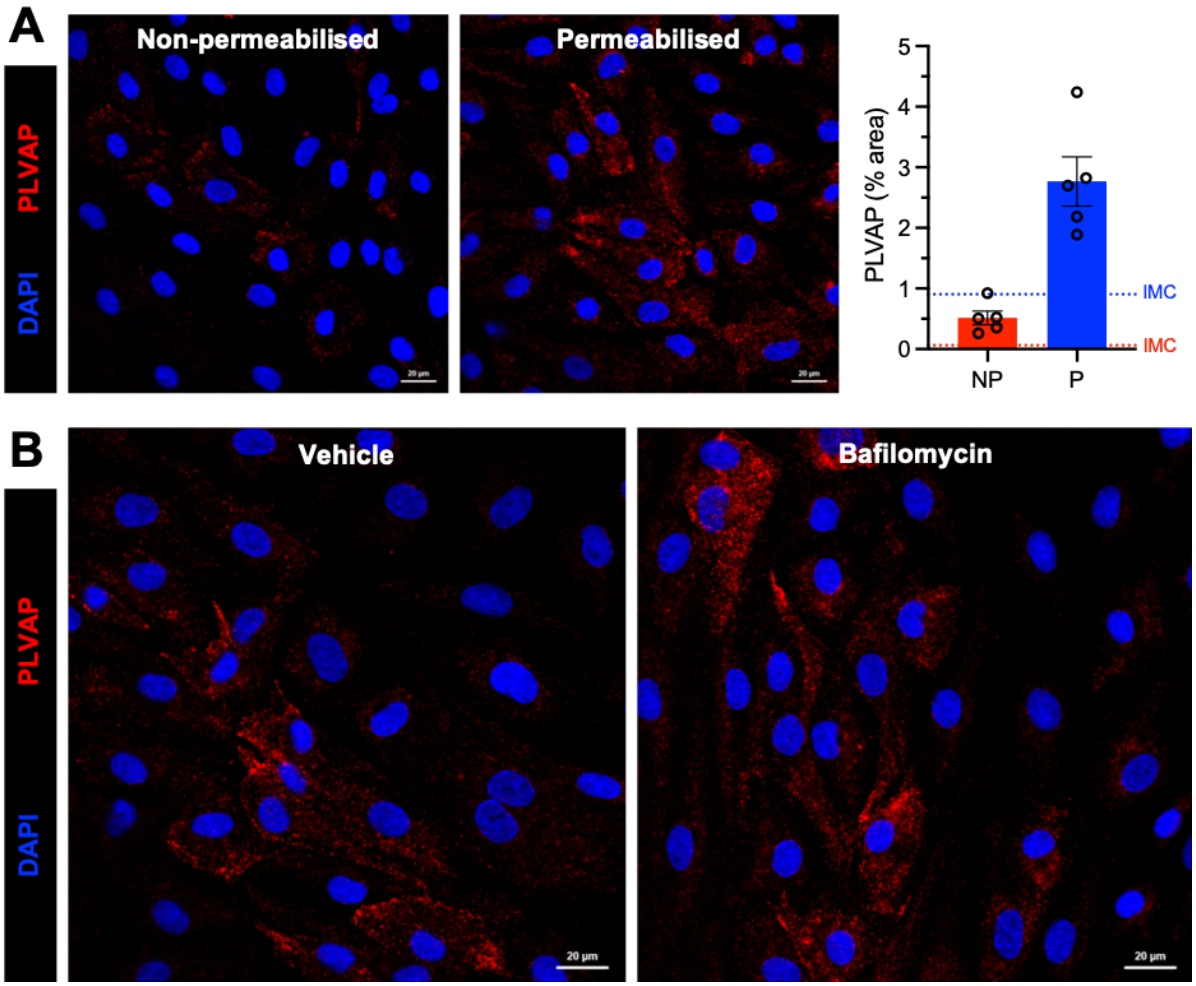

Figure 4.10: Plasmalemma vesicle-associated protein (PLVAP) was predominantly localised intracellularly and was insensitive to bafilomycin treatment.

(A, B) PLVAP (*red*) localisation in non-permeabilised (NP) and permeabilised (P) (0.3% Triton™-X 100) cells was assessed via immunocytochemistry and confocal microscopy. **(A)** PLVAP staining area (%) was quantified for five visual fields using ImageJ. Isotype-matched control (IMC) levels for each permeabilisation protocol are indicated by the corresponding gridlines. **(B)** Hepatic sinusoidal endothelial cells were treated for 24 h with bafilomycin A1 (10 nM) or vehicle (DMSO) control before analysis of PLVAP in permeabilised cells. 4′,6-diamidino-2-phenylindole, (DAPI; *blue*) was used as a nuclear counterstain. Data shown are mean ± SD from one independent experiment. Scale bars represent 20 µm.

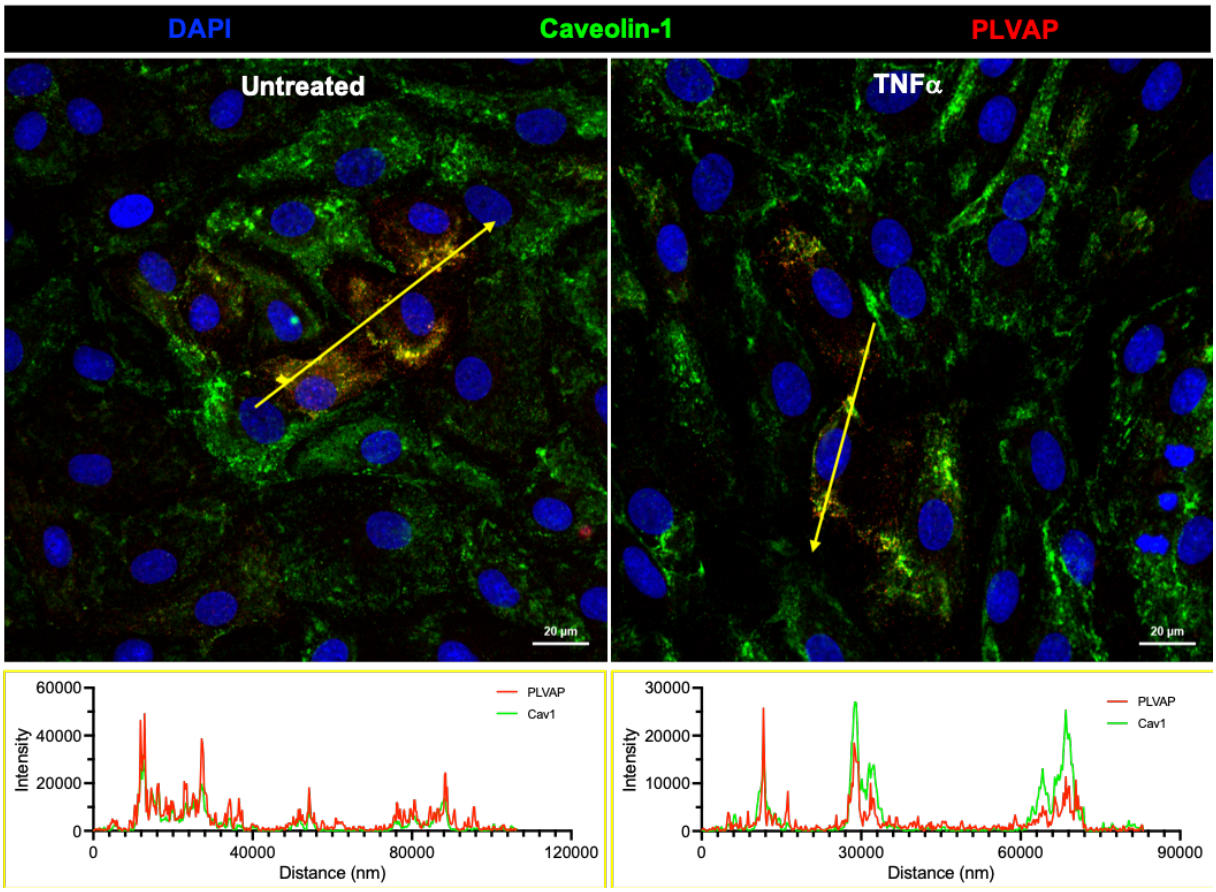

Figure 4.11: Plasmalemma vesicle-associated protein (PLVAP) co-localised with caveolin-1 in untreated and tumour necrosis factor α (TNFα)-stimulated hepatic sinusoidal endothelial cells (HSEC).

PLVAP (*red*) and caveolin-1 (*green*) were visualised by immunocytochemistry and confocal microscopy. TNFα treatment redistributed caveolin-1 and PLVAP to the cell periphery. Yellow lines depict sites of intensity profiles. Images were acquired using an LSM880 confocal microscope and a 40x objective. 4′,6-diamidino-2-phenylindole (DAPI, *blue*) was used as a nuclear counterstain. Scale bars represent 20 µm.

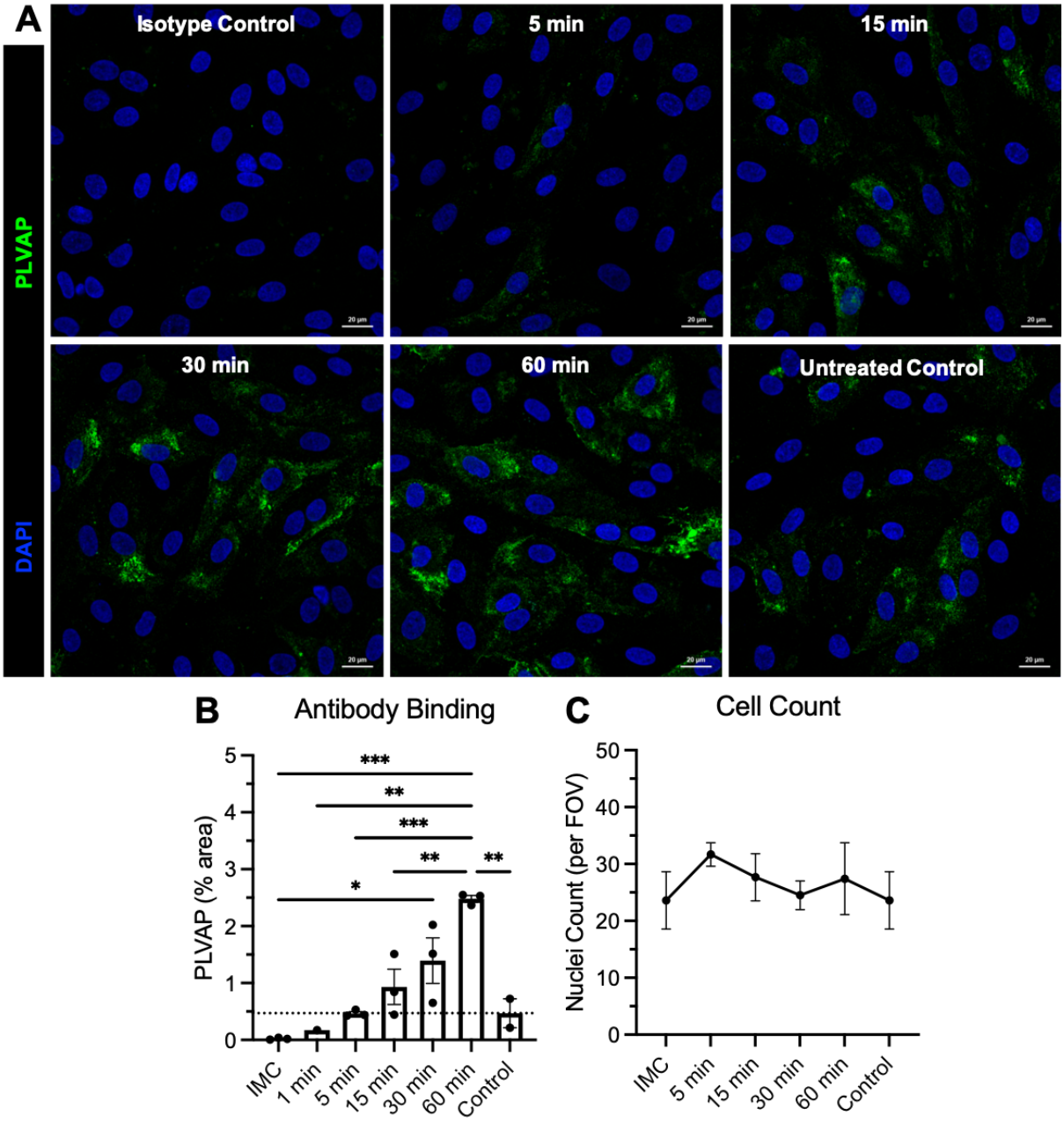

Figure 4.12: Antibodies targeted to plasmalemma vesicle-associated protein (PLVAP) rapidly bound to hepatic sinusoidal endothelial cells (HSEC).

(A-C) HSEC were treated with an anti-PLVAP antibody for time points indicated, before being fixed, permeabilised and stained with an anti-mIgG1 antibody (*green*). The staining area (%) for each time point was measured in ImageJ, as were the cell counts for each condition via quantification of HSEC nuclei (DAPI, *blue*). Data shown are **(B)** mean ± SEM (where each data point represents an independent HSEC isolate) (*p<0.05, **p<0.01, ***p<0.001, one-way ANOVA followed by Tukey's multiple comparison test) or **(C)** mean ± SD (3-5 visual fields per time point) and are representative of three independent experiments. Scale bars represent 20 µm.

4.2.9 MR and PLVAP were not transcriptionally regulated by high shear stress

Endothelial cells are known to alter their transcriptional profiles in response to biomechanical stimuli such as shear stress[463], which is thought to be important for maintaining the flow-adapted endothelial phenotype *in vivo.* To investigate whether shear stress could alter MR and PLVAP mRNA levels, qRT-PCR was performed following exposure of HSEC to arterial shear stress (~10 dyn/cm^2), by culturing cells on an orbital shaker for 72 hours. There were no significant differences in *MRC1* and *PLVAP* gene expression when cells were cultured under static or fluid shear conditions (**Figure 4.13A, B**). Interestingly, cells subject to flow conditions seemed to elongate and align with the direction of flow, as can be seen in representative brightfield images (**Figure 4.13C**).

4.2.10 MR and PLVAP were not transcriptionally regulated by hypoxia

Most *in vitro* studies are carried out with cells subject to atmospheric O_2 levels (~150 mmHg or ~20%)[520]. However, within the liver sinusoids, normoxia is thought to range from 60-65 mmHg in periportal regions to 30-35 mmHg in pericentral areas (~4-9% O_2)[521]. Further, hypoxic conditions within the tumour microenvironment are thought to range from 0.5 – 2% O_2[522, 523]. To investigate whether the expression of *MRC1* and *PLVAP* was altered in response to hypoxic conditions, HSEC were cultured in either 20% or 2% O_2 for 24 hours before being lysed and prepared for qRT-PCR analysis. As shown in **Figure 4.14A**, although there was an increasing trend in *MRC1* expression (~1.5-fold) following hypoxic exposure (4/5 HSEC isolates), there were no significant differences observed between the two groups. In contrast, trends in *PLVAP* expression in response to hypoxia were variable (two HSEC donors showed an increase whilst two showed a decrease), and so no significant differences were identified (**Figure 4.14B**). The viability of HSEC following 24-hour culture in 2% O_2 was confirmed via brightfield microscopy (**Figure 4.14C**).

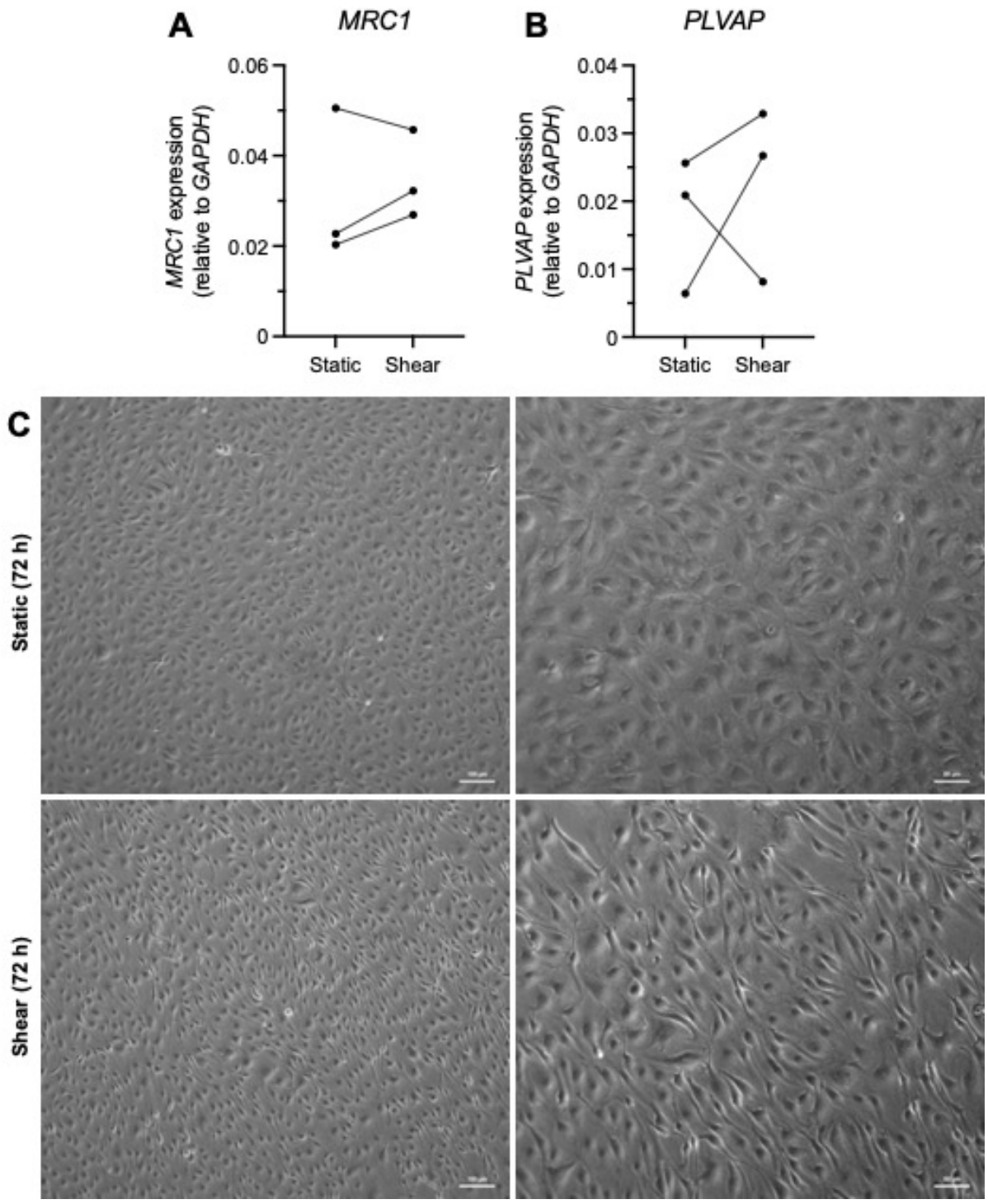

Figure 4.13: Mannose receptor (*MRC1*) and plasmalemma vesicle-associated protein (*PLVAP*) were not transcriptionally regulated by high shear stress.

(A-C) Hepatic sinusoidal endothelial cells (HSEC) were cultured either under static conditions or in a humidified temperature-controlled orbital shaker to induce fluid shear stress (~10 dyn/cm^2) for 72 hours (n=3). Cells were then lysed and analysed for **(A)** *MRC1* and **(B)** *PLVAP* gene expression by qRT-PCR. Data shown are gene expression values relative to *GAPDH*, from three independent HSEC isolates. Groups were compared using a student's paired *t*-test and no significant differences were found. Representative brightfield images are shown in **(C)** and were acquired on a Zeiss inverted microscope. Scale bars represent 100 µm (*left*) or 50 µm (*right*).

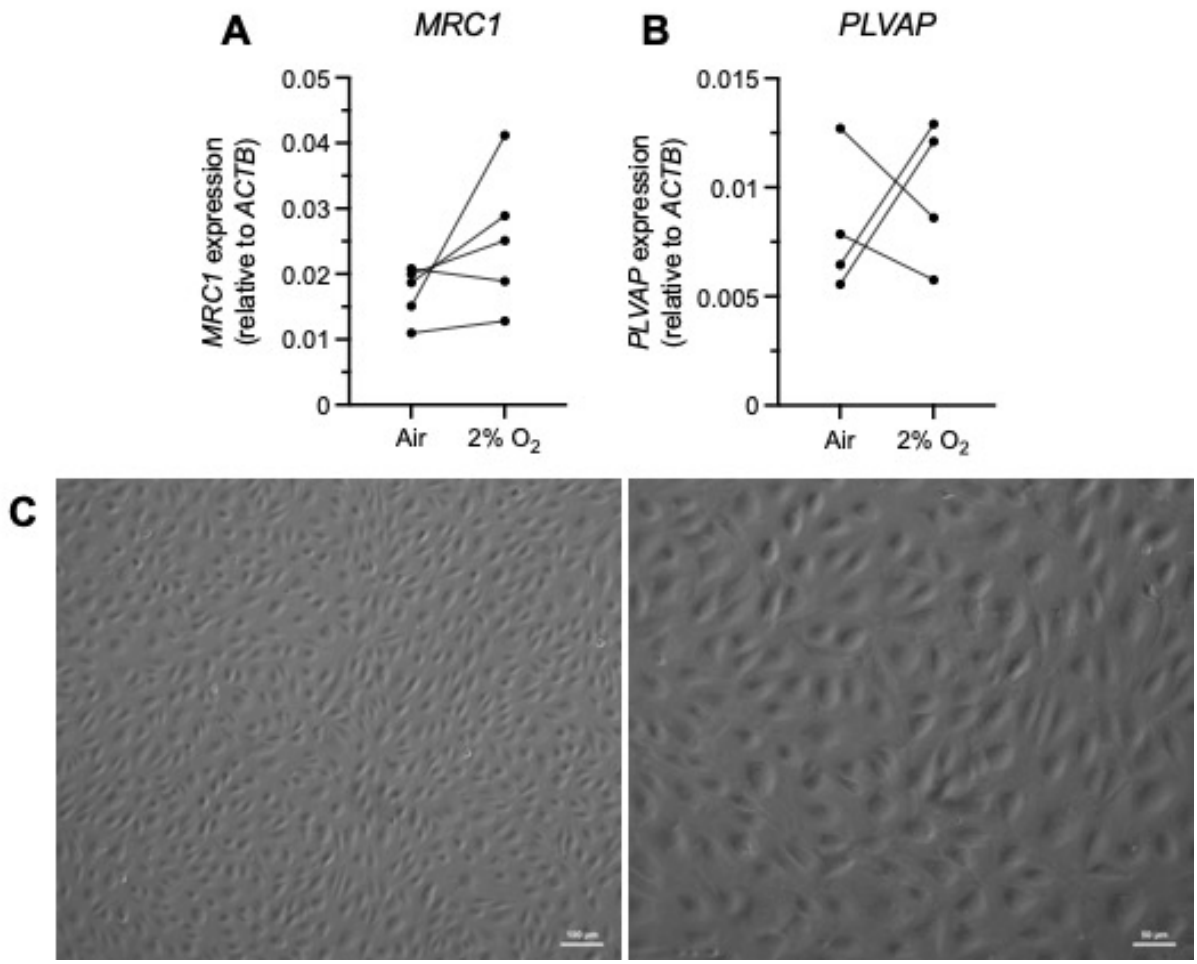

Figure 4.14: Mannose receptor (*MRC1*) and plasmalemma vesicle-associated protein (*PLVAP*) were not transcriptionally regulated by hypoxia.

(A-C) Hepatic sinusoidal endothelial cells (HSEC) were cultured either in 95% air:5% CO_2 (hyperoxia) or 2% O_2:5% CO_2 (hypoxia) for 24 hours (n=4-5). Cells were then lysed and analysed for **(A)** *MRC1* and **(B)** *PLVAP* gene expression by qRT-PCR. Data shown are gene expression values relative to *ACTB*, from four independent HSEC isolates. Groups were compared using a student's paired *t*-test and no significant differences were found. Representative brightfield images are shown in **(C)** and were acquired on a Zeiss inverted microscope. Scale bars represent 100 µm (*left*) or 50 µm (*right*).

4.2.11 MR and PLVAP were differentially regulated in primary HSEC in vitro

Several regulators of MR expression have been identified previously in macrophages (**Table 4.1**), although only a handful have been studied in murine HSEC, with limited studies in humans. Similarly, a number of PLVAP regulators have been reported in various endothelial cell types, with the most well-studied being VEGF (**Table 4.2**). To identify regulators of MR and PLVAP expression in primary human HSEC, a high-content imaging (HCI) assay was designed to allow high-throughput detection of

immunofluorescent changes in a randomised and automated manner (**Figure 4.15**). This was validated by treating HSEC with increasing concentrations of TNFα, which is known to cause a dose-dependent upregulation of ICAM-1[376]. A spot detection algorithm was developed and Object.SpotTotalArea.Ch2 and Object.SpotTotalInten.Ch2 were deemed valid parameters based on their ability to differentiate between variable ICAM-1 levels in response to TNFα.

The HCI assay was applied to study the effects of 24-hour treatment with pro-inflammatory stimuli. These included TNFα, IL-1β and LPS, along with master regulator of endothelial function VEGF, all of which have been studied previously in HSEC with respect to MR and/or PLVAP expression. When HSEC were treated with increasing concentrations of TNFα MR fluorescence area and intensity did not change (**Figure 4.16A**). In contrast, although there were no significant changes as responses were variable, PLVAP area (1.78-fold ± 0.50) and intensity (1.65-fold ± 0.70) seemed to increase following treatment with 10 ng/mL TNFα (**Figure 4.16B**). Notably, the fold-change difference between the IMC and the control group was considerably larger for MR than PLVAP, reflecting the higher basal expression of MR by HSEC compared to PLVAP. As shown during optimisation of the high-content imaging assay (**Figure 4.15**), TNFα induced a robust concentration-dependent increase in ICAM-1, with 10 ng/mL driving a significant upregulation in fluorescence area (230-fold ± 96.6) and intensity (95.7-fold ± 37.9) compared to the untreated control (**Figure 4.16C**). This upregulation was mirrored by a significant 35.7-fold increase in *ICAM1* gene expression following 10 ng/mL TNFα treatment (**Figure 4.16F**). Interestingly, the effects of 24-hour TNFα treatment (10 ng/mL) on MR and PLVAP were not recapitulated at the mRNA level, since a decrease in *MRC1* (1.38-fold) and *PLVAP* (3.06-fold) gene expression was observed compared to the control, although this was not statistically significant (**Figure 4.16D, E**).

At the protein level, IL-1β induced a modest increase in MR area (1.18-fold ± 0.02) and intensity (1.25-fold ± 0.08), although the latter was not statistically significant (**Figure 4.17A, C**). As with TNFα, the effects of treatment with IL-1β on MR and PLVAP protein expression did not seem to correlate with

mRNA levels at the 24-hour time point, since *MRC1* and *PLVAP* gene expression were reduced by 1.56-fold and 3.06-fold, respectively (**Figure 4.17D, E**). In contrast to IL-1β, LPS had no effect on MR area or intensity, whereas there was a slight increase in MR intensity in response to VEGF (1.21-fold ± 0.09), although this was not significant. Similarly, LPS treatment did not seem to influence PLVAP area or intensity, whilst a slight increase was observed in response to IL-1β, but this did not reach statistical significance (**Figure 4.17B**). The lack of effect of LPS on MR and PLVAP was also recapitulated at the mRNA level (**Figure 4.17D, E**). As has been shown previously in multiple endothelial cell types, VEGF significantly upregulated PLVAP area (1.89-fold ± 0.22) and intensity (1.96-fold ± 0.18), whilst having minimal impact on MR expression (**Figure 4.17A-C**). Again, the effects of VEGF on PLVAP were not mimicked at the mRNA level, at least not at the 24-hour time point (**Figure 4.17E**). This could be due to a transient increase in gene expression that is not evident at 24 hours, or due to differences in post-translational modifications, which may influence protein stability and/or rate of degradation, and therefore not be reflected at the mRNA level. In summary, these data not only validated the use of the high-content imaging assay as an appropriate screening tool for identifying MR and PLVAP regulators, they also suggest that MR and PLVAP are differentially regulated *in vitro* in primary human HSEC.

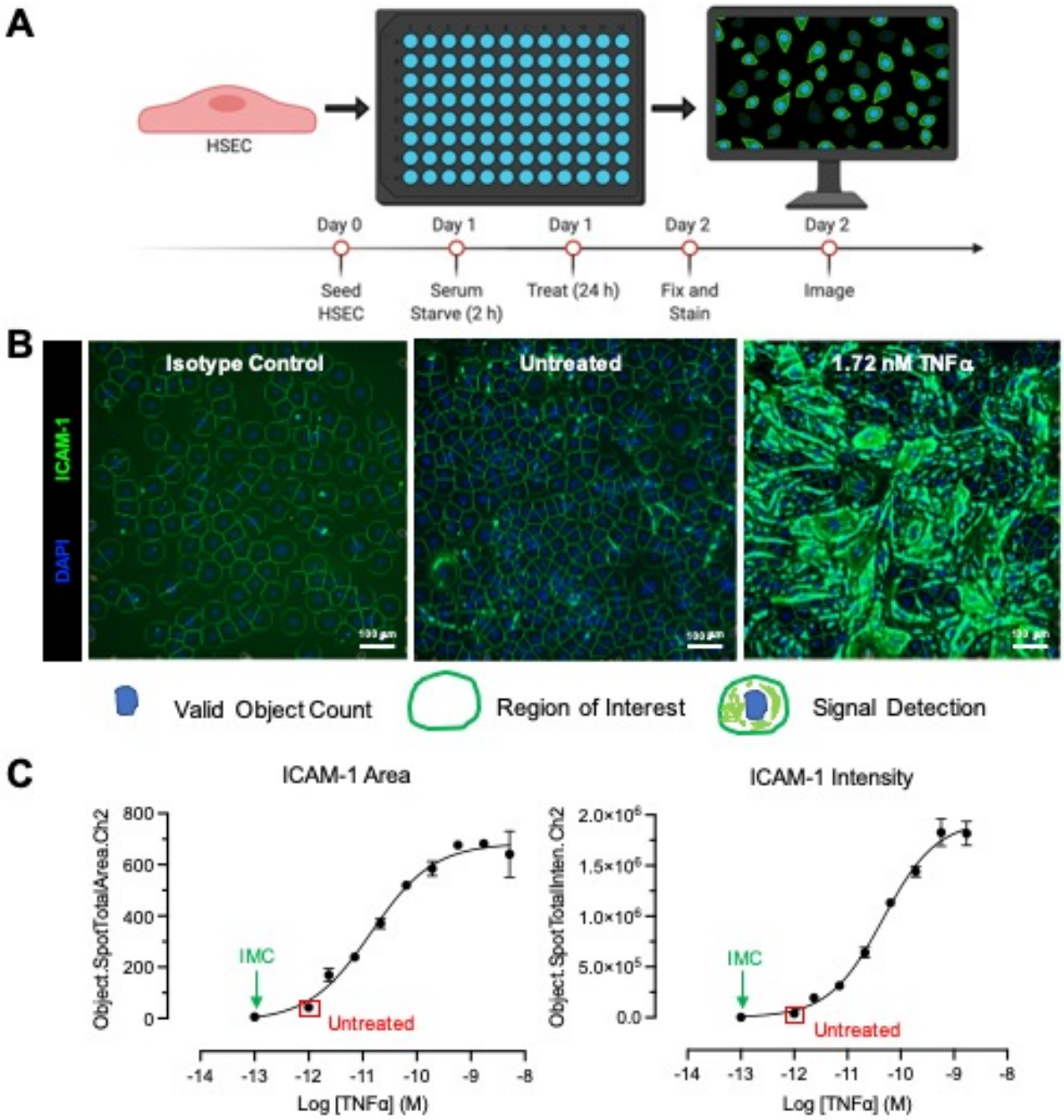

Figure 4.15: High-content imaging assay optimisation.

(A) Hepatic sinusoidal endothelial cells (HSEC) were seeded in collagen-coated black 96-well imaging plates and left to adhere overnight. The following day cells were serum- and growth factor-starved for two hours before addition of treatments and incubation for 24 hours. Cells were then fixed in 4% paraformaldehyde, permeabilised with 0.3% Triton™ X-100 and stained by immunocytochemistry. Imaging was performed using a CellInsight CX5 High-content Imaging Platform (ThermoFisher) and analysis was performed in HSC Studio software. **(B, C)** The assay was optimised and validated by treatment of HSEC with increasing concentrations of tumour necrosis factor α (TNFα) which is known to upregulate expression of intercellular adhesion molecule 1 (ICAM-1). **(B)** Signal detection (*green*) was performed via a user-defined threshold and fluorescence area and intensity were quantified within a defined region of interest relative to HSEC nuclei (4′,6-diamidino-2-phenylindole, DAPI; *blue*). Images shown are representative of nine visual fields per well with each condition performed in at least duplicate. **(C)** There was a dose-dependent increase in ICAM-1 area (*left*) and intensity (*right*) in response to 24-hour treatment with TNFα. Data shown are mean ± SD of duplicate wells. Scale bars represent 100 µm.

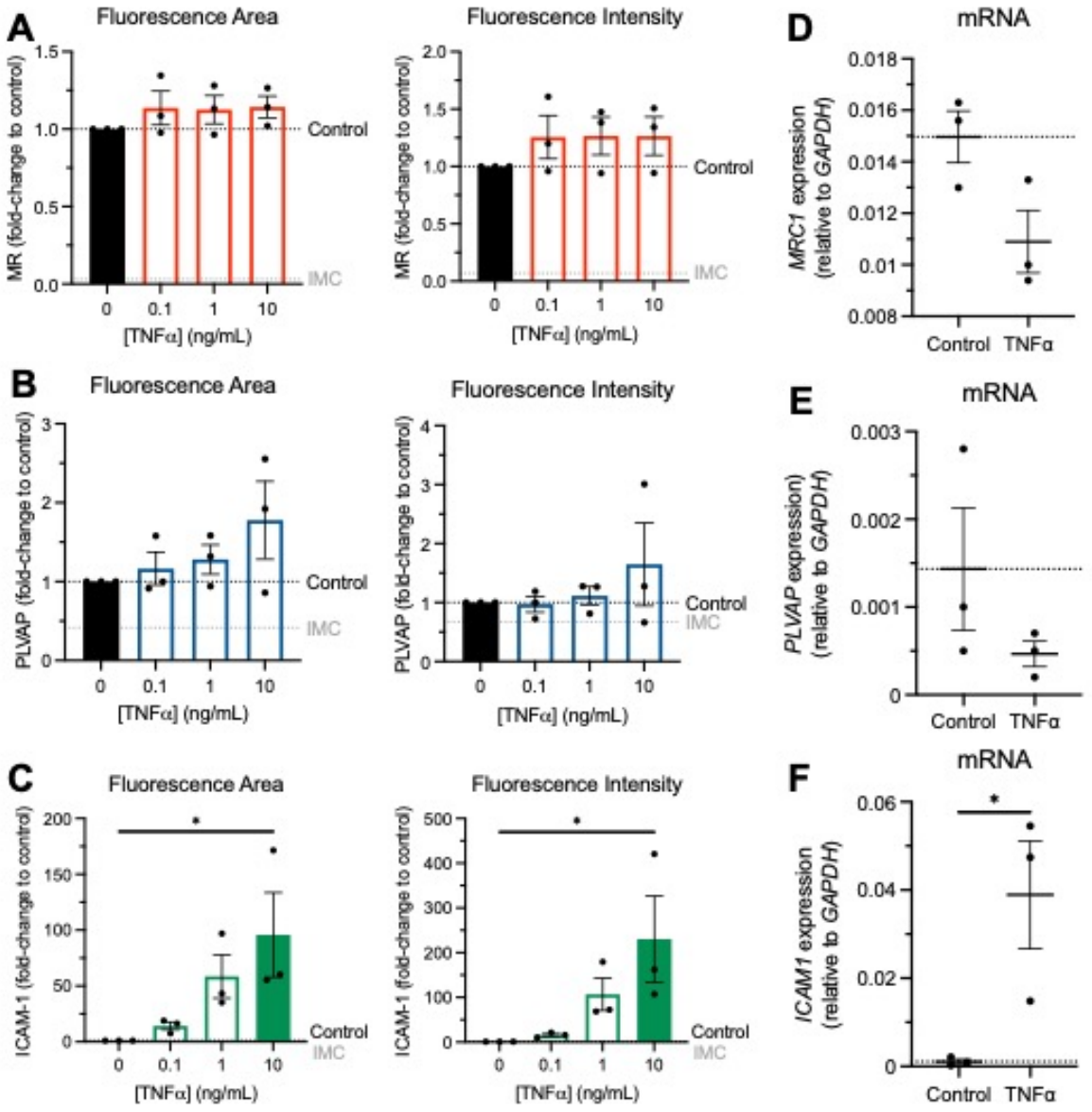

Figure 4.16: The effects tumour necrosis factor α (TNFα) on the expression of mannose receptor (MR) and plasmalemma vesicle-associated protein (PLVAP).

(A-C) Protein expression in response to 24-hour treatment with TNFα was determined via high-content imaging and was quantified for nine visual fields per well with each condition performed in at least duplicate (**p*<0.05, one-way ANOVA followed by Dunnett's multiple comparison test). Isotype control levels are indicated by the grey gridlines. **(D-F)** The effects of TNFα (10 ng/mL, 24 h) on gene expression was determined by qRT-PCR (**p*<0.05, student's unpaired *t*-test). Gene expression data are relative to *GAPDH*. Data shown are mean ± SEM from three independent experiments.

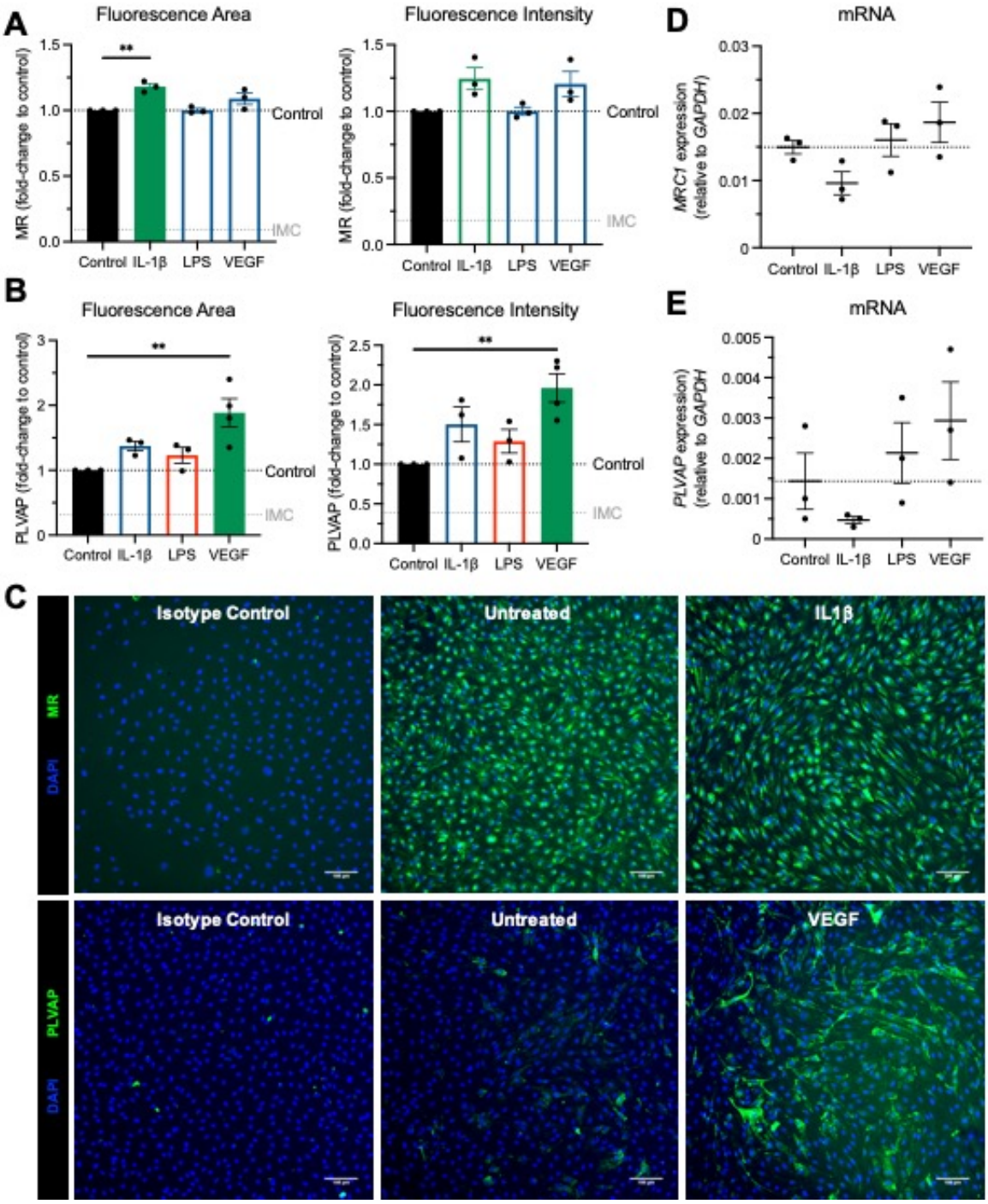

Figure 4.17: The effects of pro-inflammatory stimuli and vascular endothelial growth factor (VEGF) on mannose receptor (MR) and plasmalemma vesicle-associated protein (PLVAP) expression.

(A-E) Hepatic sinusoidal endothelial cells were treated for 24 hours with interleukin 1β (IL-1β, 10 ng/mL), lipopolysaccharide (LPS, 1 μg/mL), or vascular endothelial growth factor (VEGF) (100 ng/mL). **(A-C)** Protein expression was determined via high-content imaging and was quantified for nine visual fields per well with each condition performed in at least duplicate (**p<0.01, one-way ANOVA followed by Dunnett's multiple comparison test). **(D, E)** Gene expression relative to *GAPDH* was determined by qRT-PCR. Data shown are **(A, B)** mean fold-change to control ± SEM or **(D, E)** mean gene expression ± SEM from 3-4 independent experiments. Representative images are shown in (**C**). Scale bars represent 100 μm.

4.2.12 MR expression remained stable following HSEC stimulation with various cytokines, growth factors and small molecule compounds

A high-content screen was performed to test the effects of several putative MR regulators on its protein expression in primary human HSEC (**Figure 4.15**). These regulators consisted of several cytokines, chemokines, and pharmacological agents. Fluorescence area and intensity were quantified in response to 24-hour treatment and a summary of results are shown in the table in **Figure 4.18A**. No significant changes were observed in MR immunofluorescence area, although a small decrease was observed in response to ATRA (0.93-fold ± 0.03) and latrunculin (0.84-fold ± 0.08), and a small increase occurred in response to cytochalasin D (1.37-fold ± 0.16). Similar changes were found in MR immunofluorescence intensity in response to ATRA (0.85-fold ± 0.05) and cytochalasin D (1.64-fold ± 0.19), yet an increase in intensity was observed following latrunculin A treatment (1.30-fold ± 0.22). There was also a small increase in fluorescence intensity in response to IFNγ (1.20-fold ± 0.11) which did not reach significance, whereas a small but significant decrease in fluorescence intensity was noted in response to PGE1 (0.93-fold ± 0.03). Representative images for PGE1 and ATRA along with their respective controls are shown in **Figure 4.18B**. Cell counts were also quantified for each condition to ensure there was no cell toxicity (**Figure 4.18C**). Although the most profound changes appeared to occur in response to cytochalasin D and latrunculin A, the considerable reduction in cell numbers in response to these treatments, and also the HSEC morphology, indicated that these apparent changes in MR expression were in fact due to cellular toxicity. Overall, these data suggest that MR expression is resistant to stimulation in human HSEC, and also highlight distinct MR regulation mechanisms in endothelial cells compared to the better studied macrophage.

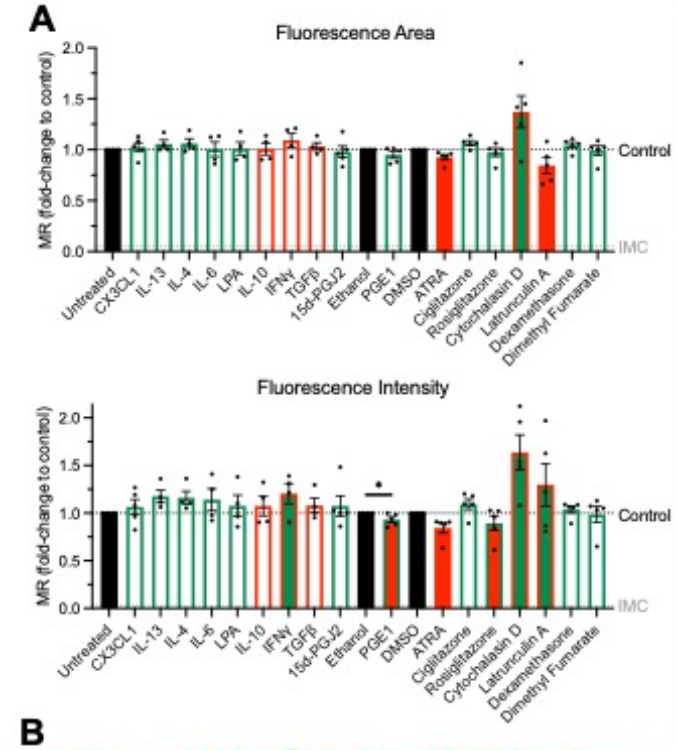

	Area	Intensity
Fractalkine (CX_3CL1)	1.02 ± 0.04	1.07 ±0.08
Interleukin 13 (IL-13)	1.06 ± 0.04	1.18 ±0.07
Interleukin 4 (IL-4)	1.06 ± 0.05	1.16 ±0.07
Interleukin 6 (IL-6)	1.00 ± 0.07	1.14 ±0.11
Lysophosphatidic Acid (LPA)	1.01 ± 0.06	1.08 ±0.11
Interleukin 10 (IL-10)	1.01 ± 0.06	1.07 ±0.10
Interferon γ (IFNγ)	1.09 ± 0.07	1.20 ±0.11
Transforming Growth Factor β (TGFβ)	1.03 ± 0.04	1.08 ±0.08
15-deoxy-Δ12, 14-prostaglandin J2 (15d-PGJ2)	0.98 ± 0.06	1.08 ±0.11
Prostaglandin E1 (PGE1)	0.95 ± 0.03	**0.93 ±0.03 (*)**
All Trans Retinoic Acid (ATRA)	0.93 ± 0.03	0.85 ±0.05
Ciglitazone	1.07 ± 0.02	1.09 ±0.05
Rosiglitazone	0.97 ± 0.04	0.89 ±0.08
Cytochalasin D	1.37 ± 0.16	1.64 ±0.19
Latrunculin A	0.84 ± 0.08	1.30 ±0.22
Dexamethasone	1.04 ± 0.03	1.04 ±0.04
Dimethyl Fumarate	0.99 ± 0.05	0.99 ±0.09

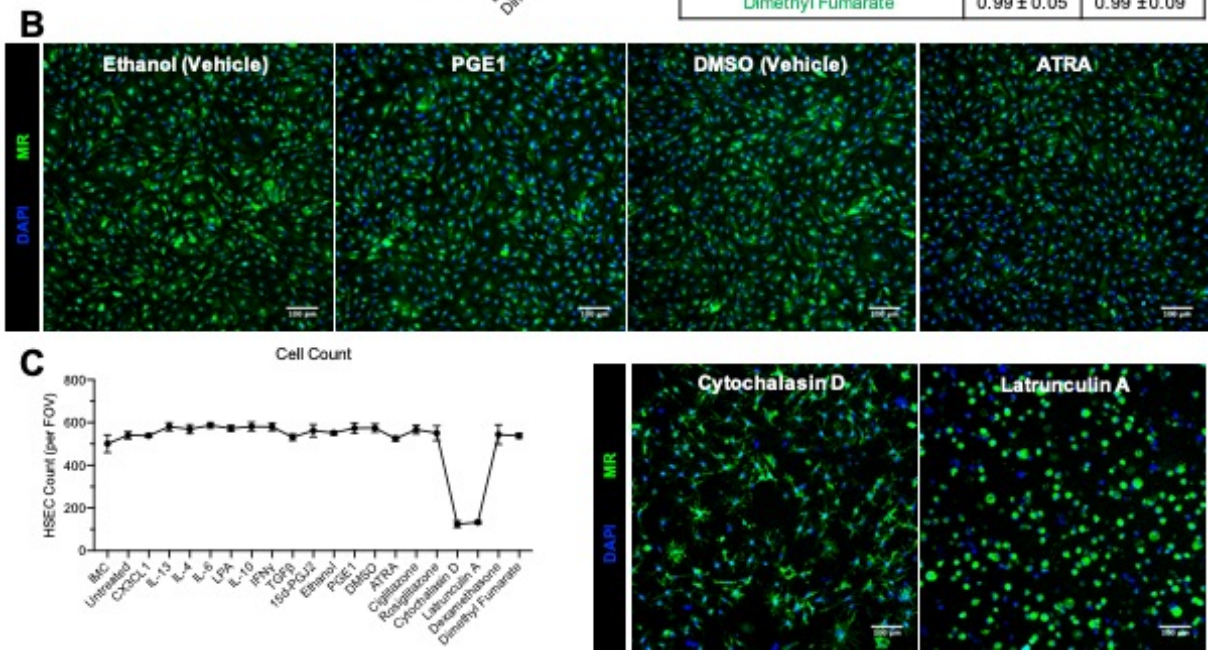

Figure 4.18: Mannose receptor (MR) expression remained stable following stimulation with various cytokines and small-molecule compounds.

(A-C) Hepatic sinusoidal endothelial cells (HSEC) were stimulated for 24 h with the treatments indicated before analysis of MR expression via high-content imaging. **(A)** Putative MR enhancers are colour-coded in green (bar outlines and in table) whilst inhibitors are shown in red (bar outlines and in table). In graphs, vehicle controls are indicated by black filled bars, and green and red filled bars indicate observed enhancement or inhibition of MR, respectively. In table, values in green/red depict observed increase/decrease (*** indicates a significant fold-change** – $p<0.05$, student's unpaired *t*-test). Data shown are mean fold-change to respective control ± SEM of five independent experiments. Data and images shown in (**B**) and (**C**) are representative of nine visual fields per well, with each condition performed in triplicate, from five independent HSEC isolates. Scale bars represent 100 µm.

4.2.13 PLVAP was upregulated by pro-inflammatory stimuli and factors which influence endothelial function

In the high-content screen, several hits were identified to significantly upregulate both PLVAP immunofluorescence area and intensity (**Figure 4.19A, B**), including PMA (Area: 2.32-fold ± 0.26; Intensity: 2.79-fold ± 0.37), VEGF (Area: 1.81-fold ± 0.20; Intensity: 1.71-fold ± 0.30), fibrinogen (Area: 1.60-fold ± 0.09; Intensity: 1.75-fold ± 0.18), and BMP-9 (Area: 1.53-fold ± 0.09; Intensity: 1.41-fold ± 0.09). As shown in **Figure 4.19B**, these treatments increased both the amount of PLVAP per cell and the proportion of $PLVAP^{+}$ HSEC per field of view, although the heterogeneity observed in unstimulated cells seemed to be maintained following treatment. TNFα significantly increased immunofluorescence area by 1.45-fold ± 0.22, but did not impact intensity values. Cell counts remained fairly stable across treatment conditions suggesting no cytotoxicity was observed, although there was a small decrease in cell number in response to TNFα treatment (**Figure 4.19C**). Since PMA had the most profound impact on total PLVAP expression, the effects of PMA on PLVAP surface expression was assessed in non-permeabilised cells (**Figure 4.20**). Under steady state PLVAP (~80%) was mostly located intracellularly. Total PLVAP expression was increased by 3.16-fold ± 1.18, whilst surface PLVAP expression displayed an 8.13-fold ± 3.64 upregulation, in response to PMA treatment. This suggests that PMA stimulates both PLVAP synthesis and trafficking of PLVAP to the cell surface. Collectively, these data highlight several novel regulators of PLVAP expression in human HSEC, including pro-inflammatory stimuli and factors which are known to influence endothelial phenotype and function.

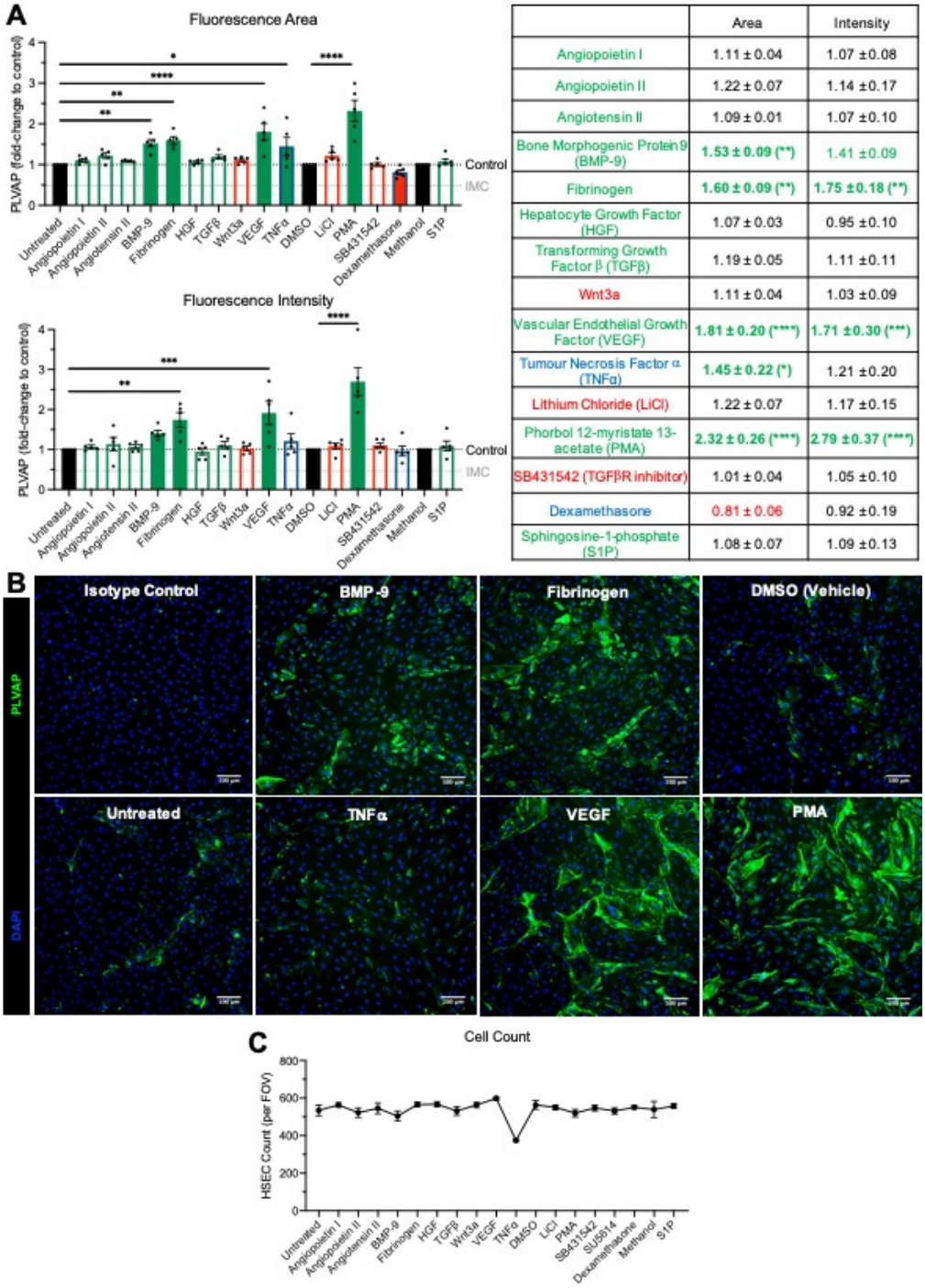

	Area	Intensity
Angiopoietin I	1.11 ± 0.04	1.07 ± 0.08
Angiopoietin II	1.22 ± 0.07	1.14 ± 0.17
Angiotensin II	1.09 ± 0.01	1.07 ± 0.10
Bone Morphogenic Protein 9 (BMP-9)	**1.53 ± 0.09 (**)**	1.41 ± 0.09
Fibrinogen	**1.60 ± 0.09 (**)**	**1.75 ± 0.18 (**)**
Hepatocyte Growth Factor (HGF)	1.07 ± 0.03	0.95 ± 0.10
Transforming Growth Factor β (TGFβ)	1.19 ± 0.05	1.11 ± 0.11
Wnt3a	1.11 ± 0.04	1.03 ± 0.09
Vascular Endothelial Growth Factor (VEGF)	**1.81 ± 0.20 (****)**	**1.71 ± 0.30 (***)**
Tumour Necrosis Factor α (TNFα)	**1.45 ± 0.22 (*)**	1.21 ± 0.20
Lithium Chloride (LiCl)	1.22 ± 0.07	1.17 ± 0.15
Phorbol 12-myristate 13-acetate (PMA)	**2.32 ± 0.26 (****)**	**2.79 ± 0.37 (****)**
SB431542 (TGFβR inhibitor)	1.01 ± 0.04	1.05 ± 0.10
Dexamethasone	0.81 ± 0.06	0.92 ± 0.19
Sphingosine-1-phosphate (S1P)	1.08 ± 0.07	1.09 ± 0.13

Figure 4.19: Plasmalemma vesicle-associated protein (PLVAP) expression was upregulated by several soluble factors *in vitro*.

(A-C) Hepatic sinusoidal endothelial cells (HSEC) were stimulated for 24 h with the treatments indicated before analysis of PLVAP expression via high-content imaging. **(A)** Putative PLVAP enhancers are colour-coded in green (bar outlines and in table) whilst inhibitors are shown in red (bar outlines and in table). In graphs, vehicle controls are indicated by black filled bars, and green and red filled bars indicate observed enhancement or inhibition of PLVAP, respectively (*p<0.05, **p<0.01, ***p<0.001, ****p<0.0001, one-way ANOVA and Dunnett's multiple comparisons test). In table, values in green/red depict observed increase/decrease (*** indicates a significant fold-change**). Data shown are mean fold-change to respective control ± SEM of five independent experiments. Data and images shown in (**B**) and (**C**) are representative of nine visual fields per well, with each condition performed in triplicate, from five independent HSEC isolates. Scale bars represent 100 µm.

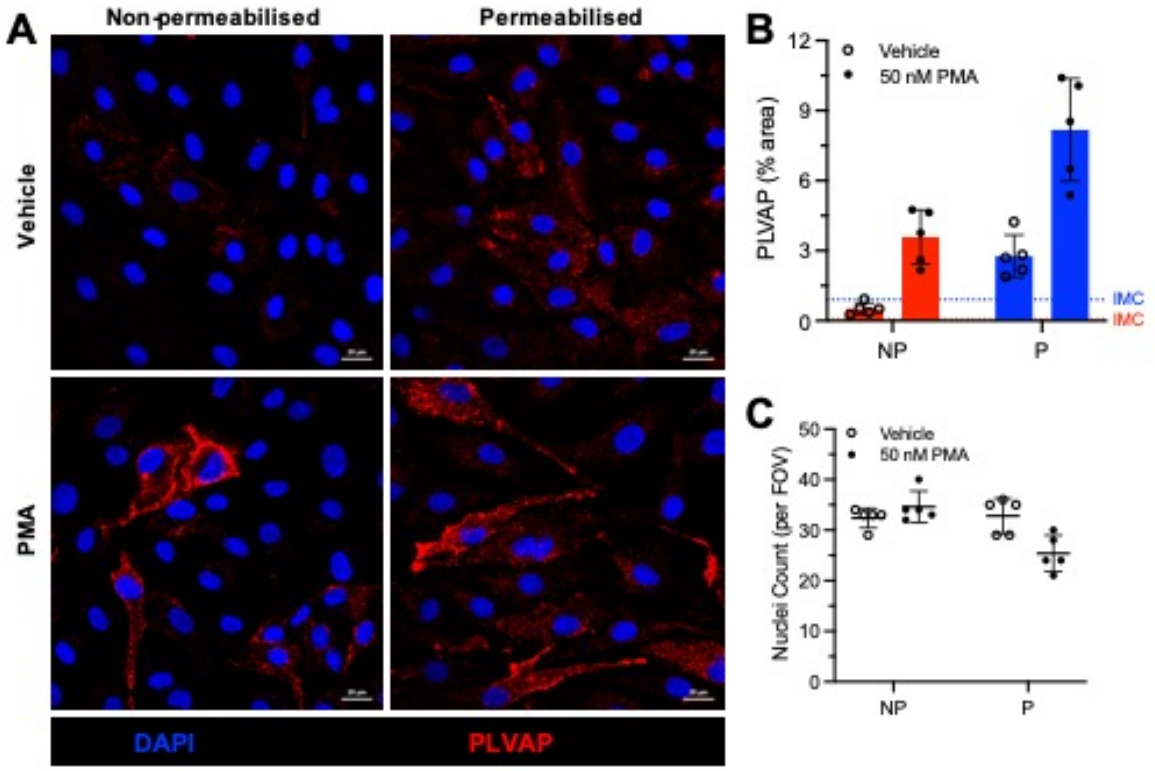

Figure 4.20: Phorbol 12-myristate 13-acetate (PMA) upregulated both surface and total plasmalemma vesicle-associated protein (PLVAP) expression.

(A) Hepatic sinusoidal endothelial cells (HSEC) were treated for 24 h with PMA (50 nM) or vehicle (DMSO) control before analysis of PLVAP (*red*) in non-permeabilised (NP) and permeabilised (P) (0.3% Triton™-X 100) cells via immunocytochemistry and confocal microscopy. **(B)** PLVAP staining area (%) was quantified for five visual fields using ImageJ. Isotype-matched control (IMC) levels for each permeabilisation protocol are indicated by the corresponding gridlines. **(C)** HSEC nuclei were counted using the "Analyse Particles" function in ImageJ (4′,6-diamidino-2-phenylindole, DAPI; *blue*). **(A, B)** Images and data shown for vehicle-treated controls are the same as those shown in **Figure 4.10**. Data shown in **(B)** and **(C)** are mean ± SD from one independent experiment. Scale bars represent 20 µm.

4.2.14 PLVAP was regulated by factors found within the tumour microenvironment

Given the upregulation of PLVAP within tumours of HCC patients (**Chapter 3**), the high-content imaging assay was applied to study the effects of conditioned medium from HCC cell lines on PLVAP expression in primary HSEC. Although there was an increase in immunofluorescence area (1.31-fold ± 0.23) and intensity (1.41-fold ± 0.18) following 24-hour treatment with conditioned medium from Huh-7 cells (Huh-7-CM), this did not reach statistical significance (**Figure 4.21A**). Similarly, PLVAP area (1.46-fold ± 0.09) and intensity (1.36-fold ± 0.28) were upregulated following treatment with HepG2-CM, with the former being significantly different to the vehicle DMEM control (**Figure 4.21B**). As can be seen from the representative images shown in **Figure 4.21C**, the impact on PLVAP expression was more pronounced with HepG2-CM treatment. These data suggest that PLVAP expression is regulated by factors secreted by HCC tumour cells.

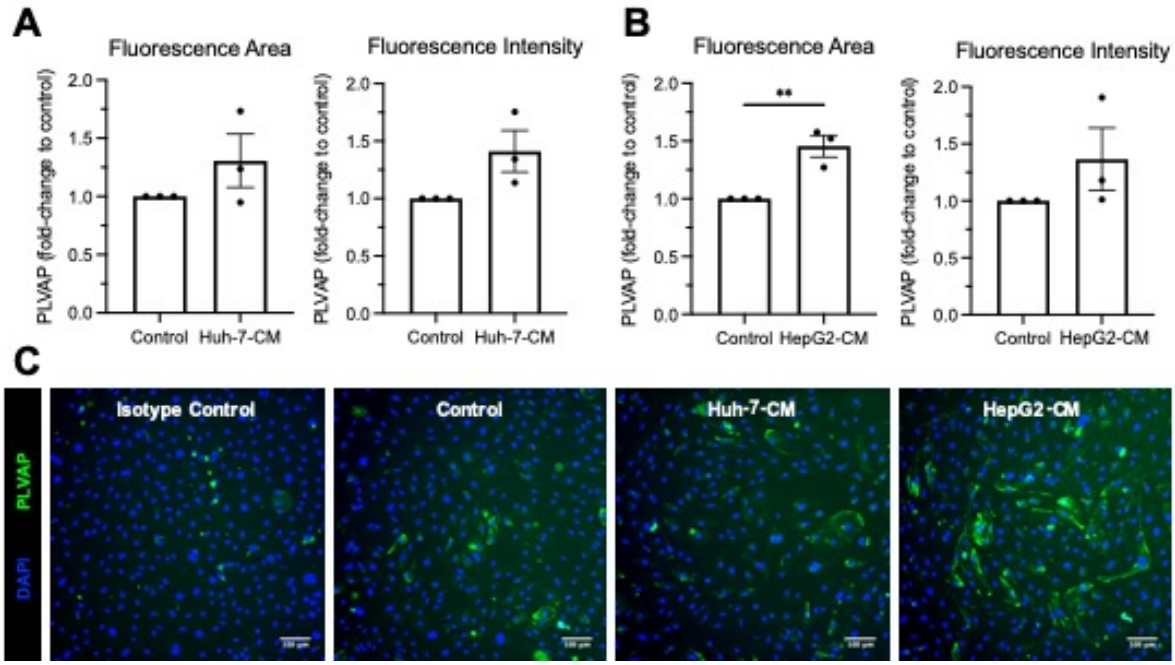

Figure 4.21: Plasmalemma vesicle-associated protein (PLVAP) expression was upregulated by factors found within the tumour microenvironment.

PLVAP expression in hepatic sinusoidal endothelial cells was quantified by high-content imaging following 24-hour treatment with conditioned medium from **(A)** Huh-7 and **(B)** HepG2 hepatocellular carcinoma cell lines. Data shown are mean fold-change to DMEM control ± SEM of three independent experiments (**p<0.01, student's unpaired t-test). Images shown in (**C**) are representative of nine visual fields per well with each condition performed in triplicate wells. Scale bars represent 100 µm.

4.2.15 Summary

- Primary human HSEC isolated by immunomagnetic selection for CD31 displayed a sinusoidal phenotype *in vitro*, including expression of sinusoidal endothelial markers and rapid scavenging function
- Expression of MR and PLVAP was maintained *in vitro* and the level of mRNA expression was comparable in donor- and CLD patient-derived HSEC
- *MRC1* and *PLVAP* expression were increased with HSEC passage number
- MR underwent constant endosomal trafficking, residing predominantly within early endosomes, recycling endosomes and the Golgi apparatus
- MR was rapidly internalised into early endosomes following antibody ligation
- Under resting conditions, PLVAP mostly resided intracellularly within vesicles often located at the cell periphery, and its localisation was insensitive to bafilomycin treatment
- PLVAP co-localised with caveolae marker, caveolin-1, in both untreated and TNFα-stimulated HSEC
- MR and PLVAP were not significantly regulated by high shear stress or hypoxia at the transcript level
- MR expression was resistant to regulation by multiple cytokines, chemokines and small molecule compounds
- PLVAP was upregulated by several soluble factors including VEGF, PMA, BMP-9 and fibrinogen, as well as by conditioned medium from HCC cell lines

5 SENESCENT CELL-ENDOTHELIAL CROSSTALK IN CLD AND HCC

5.1 Introduction

5.1.1 Senescence

Cellular senescence is defined as an irreversible state of cell cycle arrest in which cells cease to proliferate but remain metabolically active[252]. The mechanisms of senescence can be broadly stratified into two distinct pathways: (1) replicative senescence, during which a cell senses endogenous DNA damage as a result of successive rounds of cellular replication and subsequent telomere shortening; (2) stress-induced senescence, whereby injurious stimuli including traumatic injury, oxidative stress, radiation or chemotherapy induce rapid DNA damage. Although senescence is a widely studied phenomenon, its pleiotropic effects are largely context-dependent, with outcomes influenced heavily by the nature of the trigger, duration of stimulus and cell type(s) involved. This heterogeneity has led to a lack of consensus on a unanimous senescence biomarker which has mandated the identification of multiple traits in order to ascertain a cell's senescent status. These characteristics include cell cycle arrest, macromolecular damage, dysregulated metabolism and an altered secretome, and are summarised in **Figure 1.1**[524, 525].

Cell cycle arrest is maintained by two families of cyclin-dependent kinase (CDK) inhibitors – the INK4 family ($p16^{INK4A}$ [*CDKN2A*], $p15^{INK4B}$, $p18^{INK4C}$, and $p19ARF^{INK4D}$) and the Cip/Kip family ($p27^{Kip1}$, $p57^{Kip2}$, and $p21^{WAF1/Cip1}$ [*CDKN1A*]). Irreversible proliferative arrest is also accompanied by BCL-2 family-mediated apoptosis inhibition[526]. DNA damage response (DDR) is characterised by accumulation of double-strand break sensor proteins γH2A.X, 53BP1, CHK2 and MDC1 and lack of DNA repair proteins RPA and RAD51. Senescence-associated heterochromatin foci (SAHF) can also be visualised as DAPI-dense areas within the nucleus. Cells that have undergone senescence form aggregates of lipofuscin due to increased lysosomal content, which can be distinguished using SA-β-Gal, DDAOG, Sudan Black B (SBB) or GL13 staining. Furthermore, senescence is accompanied by

morphological changes including increased cell size, vacuolised appearance of the cytoplasm and nucleus, and plasma membrane alterations, likely due to lipid damage which can be detected via perilipin. Senescent cells also display an abnormal metabolic profile due to aberrant mitochondrial activity, dysregulated ATP production and excess ROS production.

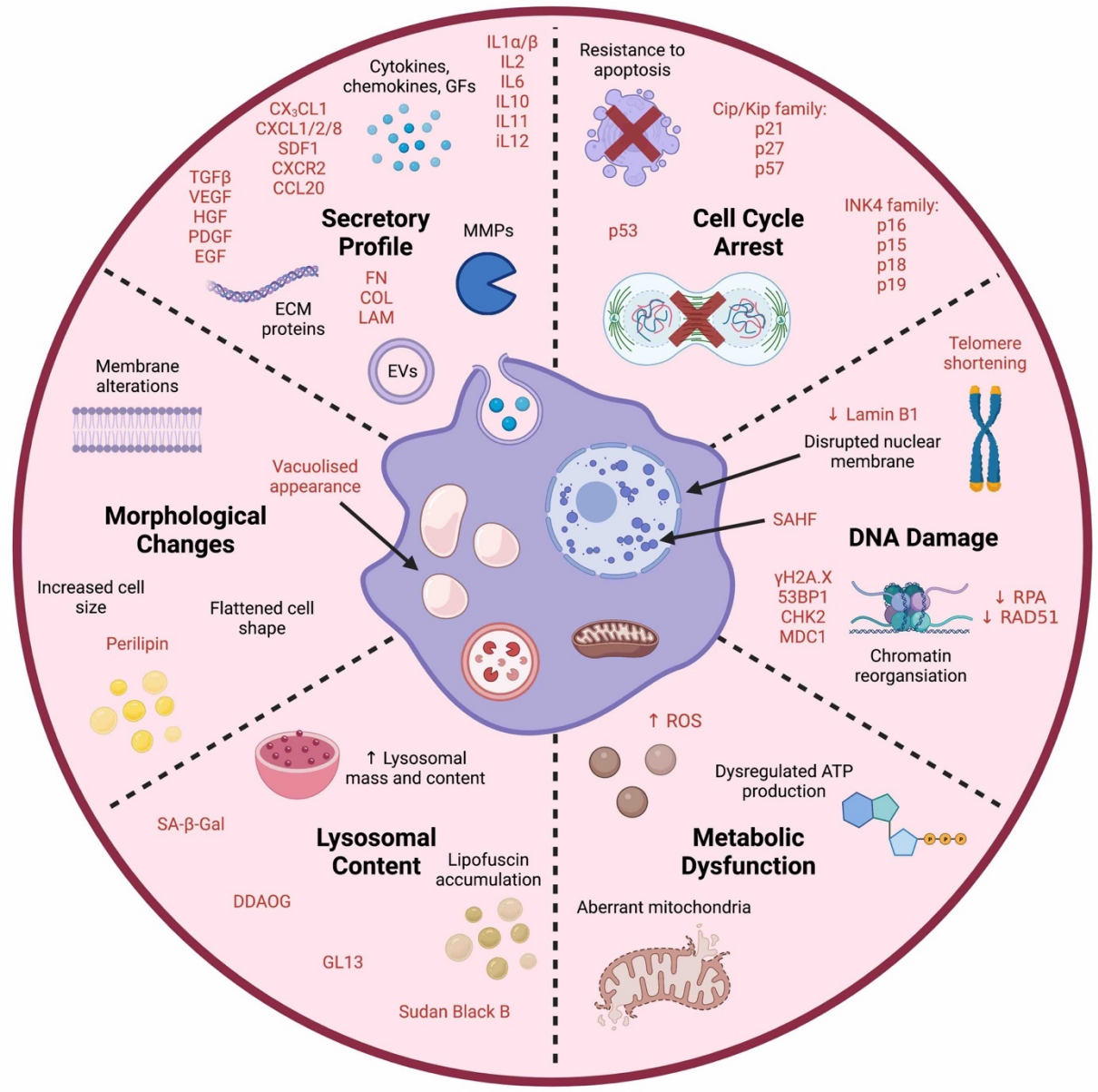

Figure 5.1: The hallmarks of senescence.

These include cell cycle arrest, DNA damage response, lipofuscin accumulation, morphological and metabolic changes and production of senescence-associated secretory phenotype (SASP). Markers of senescence cells are shown in red.

5.1.2 Senescence-associated secretory phenotype

Following induction of senescence, cells secrete a combination of factors that act in an autocrine and paracrine manner to reinforce senescence ("bystander effect"), alert and sensitise neighbouring cells to the stressful stimulus, and activate immune surveillance mechanisms to promote their clearance. This is known as the senescence-associated secretory phenotype (SASP) and is comprised of numerous cytokines, chemokines, growth factors, ECM proteins and extracellular vesicles, all of which facilitate multi-cellular crosstalk within the senescent microenvironment (**Figure 1.1**).

Release of the SASP is thought to enable recruitment of immune cells which stimulates tissue repair and regeneration. However, chronic senescence leads to sustained SASP release which has been shown to aggravate multiple age-related diseases including atherosclerosis, diabetes, osteoarthritis, obesity and neurodegeneration[524, 525]. In the liver, the SASP has been shown to exacerbate disease progression, contributing to fibrosis, promoting monocyte recruitment and differentiation into macrophages, and driving paracrine senescence in the surrounding parenchyma[266]. Furthermore, despite being comprised of numerous pro-inflammatory cytokines and chemokines, the SASP has been shown to contribute to a pro-tumourigenic microenvironment, through CCL2-mediated immature myeloid cell recruitment and exposure to HCC-derived secretory factors which drive their immunosuppressive phenotype[527]. Moreover, stromal-derived SASP has been shown to drive tumour invasiveness and metastasis, an effect thought to be mediated by induction of epithelial-to-mesenchymal transition and increased recruitment of myeloid-derived suppressor cells[528, 529]. Thus, the SASP can elicit pleiotropic effects depending on the biological context.

5.1.3 Models to study senescence

There are several *in vitro* and *in vivo* models that have been developed to study senescence which have been extensively reviewed[525, 530]. Mechanisms of senescence induction are based on the multiple triggers of senescence *in vivo*, including DNA damage, oxidative stress, and CDK inhibitor or oncogene

activation. Progeroid murine models developed to recapitulate human syndromes of premature ageing are also characterised by accelerated senescence[530].

Oncogene-induced senescence (OIS) is a fail-safe anti-tumourigenic mechanism which prevents transformation and propagation of pre-malignant cells. Kang *et al.* (2011) describe a murine model of OIS, in which transposable elements expressing the oncogene *Nras* (*Nras*^{G12V}) are stably delivered to hepatocytes via hydrodynamic tail vein injection[531]. Control animals were administered with transposable elements encoding a non-signalling mutant (*Nras*$^{G12V/D38A}$) for comparison. Authors confirmed induction of senescence by staining of mouse livers for p21, p16, and SA-β-Gal, and observed similar findings following intra-hepatic Cre-recombinase-mediated oncogenic *Kras* activation (*Kras*^{G12D}). It was shown that the secretory program of *Nras*^{G12V}-expressing hepatocytes facilitated immune-mediated senescent cell clearance, which was dependent on intact $CD4^+$ T cell-mediated adaptive immunity and the presence of monocytes/macrophages. Impaired immune surveillance of senescent cells led to development of HCC in *Nras*^{G12V} severe combined immunodeficient (SCID) mice.

Senescence can also be induced by oncogene activation *in vitro*. A gold-standard *in vitro* OIS model is the overexpression of *HRAS*^{G12V} in IMR90 fibroblasts[532]. This is achieved through stable transduction with a tamoxifen-inducible ER:RAS construct; upon addition of tamoxifen to the cell culture medium, IMR90 cells become growth arrested, displaying several senescence hallmarks including chromatin changes, increased cell size, positivity for SA-β-Gal, p21 and p16, and production of SASP. This model has proven invaluable for the study of senescence mechanisms *in vitro* and the effects of the SASP in numerous contexts.

Another murine model of senescence involves the hepatocyte-specific deletion of the *Mdm2* gene (Δ*Mdm2*^{Hep})[259]. Murine double minute 2 (MDM2) is a negative regulator of p53; since the p53/p21 axis is central to senescence induction, hepatocyte specific deletion of *Mdm2* drives p21-dependent senescence by p53 upregulation. *Mdm2*$^{-/-}$ mice display multiple hallmarks of senescence and impaired regeneration in response to paracetamol-induced liver damage, an observation that was dependent on

induction of paracrine senescence by macrophage-derived TGFβ1. Similar observations were made in a mouse model of biliary senescence, in which conditional *Mdm2* deletion in the bile ducts (via a Krt19 promoter) exacerbates biliary injury and impairs regeneration following partial hepatectomy[266].

5.2 Senescence Studies

5.2.1 Senescence was a key feature of CLD and HCC

Senescence is thought to be a key component of the tissue microenvironment during injury, chronic inflammation and cancer. There are several markers which can be used to identify senescent cells, two of which are CDK inhibitors p21 (*CDKN1A*) and p16 (*CDKN2A*) that maintain cell cycle arrest, a key hallmark of senescence. The expression of p21 and p16 in CLD patient samples was assessed at the gene level by qRT-PCR and compared to donor liver controls. Whilst there was no significant difference between *CDKN1A* gene expression in diseased and donor livers, *CDKN2A* expression displayed a significant 9.95-fold upregulation in CLD compared to donor controls (**Figure 5.2A**).

Analysis of publicly-available TCGA datasets demonstrated a modest, yet significant, increase in *CDKN1A* expression within non-tumour tissue from HCC patients compared to both normal liver (~1.52-fold) and tumour (~1.23-fold) tissue (**Figure 5.2B**). In contrast, *CDKN2A* mRNA levels were significantly higher in HCC tumours compared to both non-tumour (~20.82-fold) and normal liver (~34.3-fold) tissue. Although there was a 1.65-fold increase in *CDKN2A* expression in non-tumour compared to normal liver this was not statistically significant (**Figure 5.2B**).

Given the upregulation of p16 in HCC tumours, TCGA datasets were analysed to correlate *CDKN2A* expression with clinical parameters. Despite no association between *CDKN2A* expression and tumour grade, its expression was significantly upregulated in cancers of a higher stage (**Figure 5.3A**). Furthermore, higher *CDKN2A* expression was indicative of poorer clinical outcomes, since $CDKN2A^{high}$ patients had worse overall and disease-free survival (**Figure 5.3B**).

The expression and localisation of p21 and p16 protein was next assessed by immunohistochemistry in donor and cirrhotic liver specimens. The frequency of $p21^{+}$ hepatocytes was significantly increased from

11.5 ± 5.74 in donor liver to 41.6 ± 9.70 in CLD (**Figure 5.4A**). Expression of p16 appeared to be more widespread in hepatocytes of both donor and CLD livers, yet in CLD, the presence of other $p16^{+}$ cell types was also apparent. However, staining area was variable across the patient cohort and so no significant differences in p16 were observed between normal and cirrhotic liver (**Figure 5.4B**). Collectively, these data suggest that senescence is a key feature of liver disease, and that p16 expression could be a valuable prognostic marker in HCC patients.

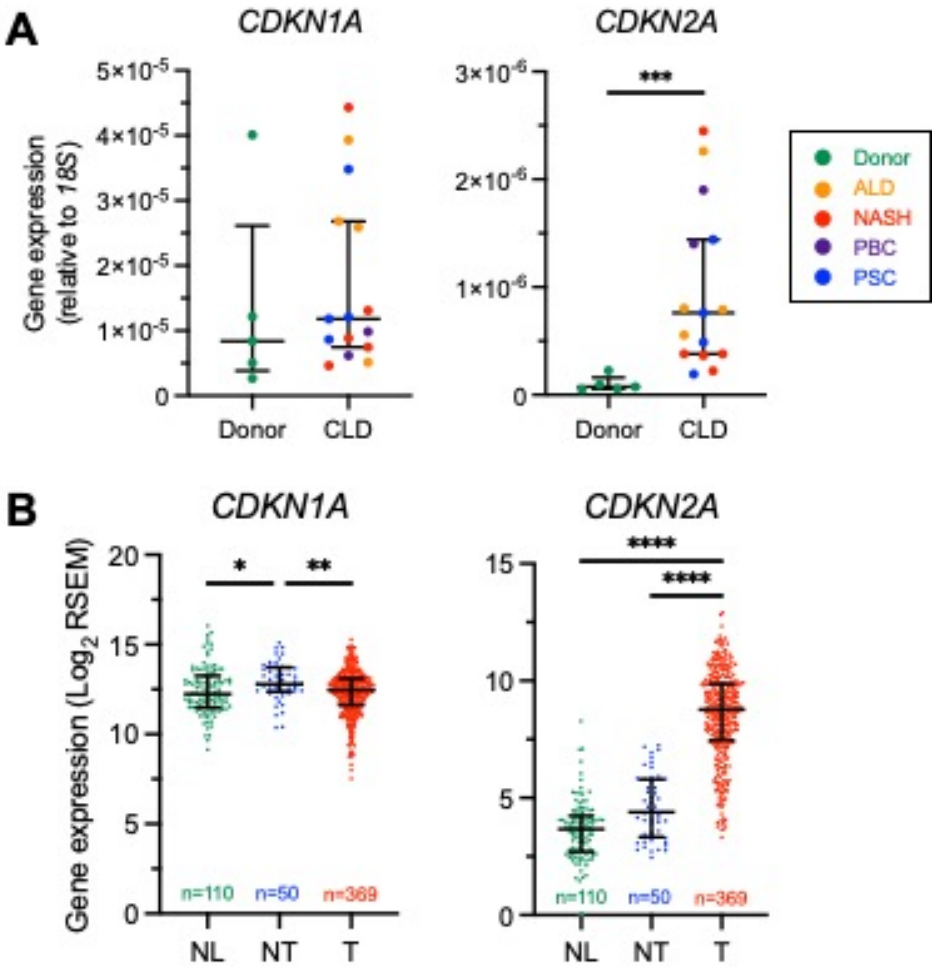

Figure 5.2: Expression of senescence markers, p21 (*CDKN1A*) and p16 (*CDKN2A*), in chronic liver disease (CLD) and hepatocellular carcinoma (HCC).

(A) *CDKN1A* and *CDKN2A* expression was quantified in whole tissue lysates from donor (n=5) and cirrhotic (n=15) livers by qRT-PCR (***p<0.001, Mann-Whitney test). Gene expression data are shown relative to *18S*, where each data point represents an independent patient sample. **(B)** The Cancer Genome Atlas (TCGA) datasets were analysed for *CDKN1A* and *CDKN2A* expression in normal liver (NL) (n=110), non-tumour (NT) (n=50) and tumour (T) (n=369) samples from HCC patients (*p<0.05, **p<0.01, ****p<0.0001, Kruskal-Wallis test followed by Dunn's multiple comparison test). Data shown are median ± interquartile range.

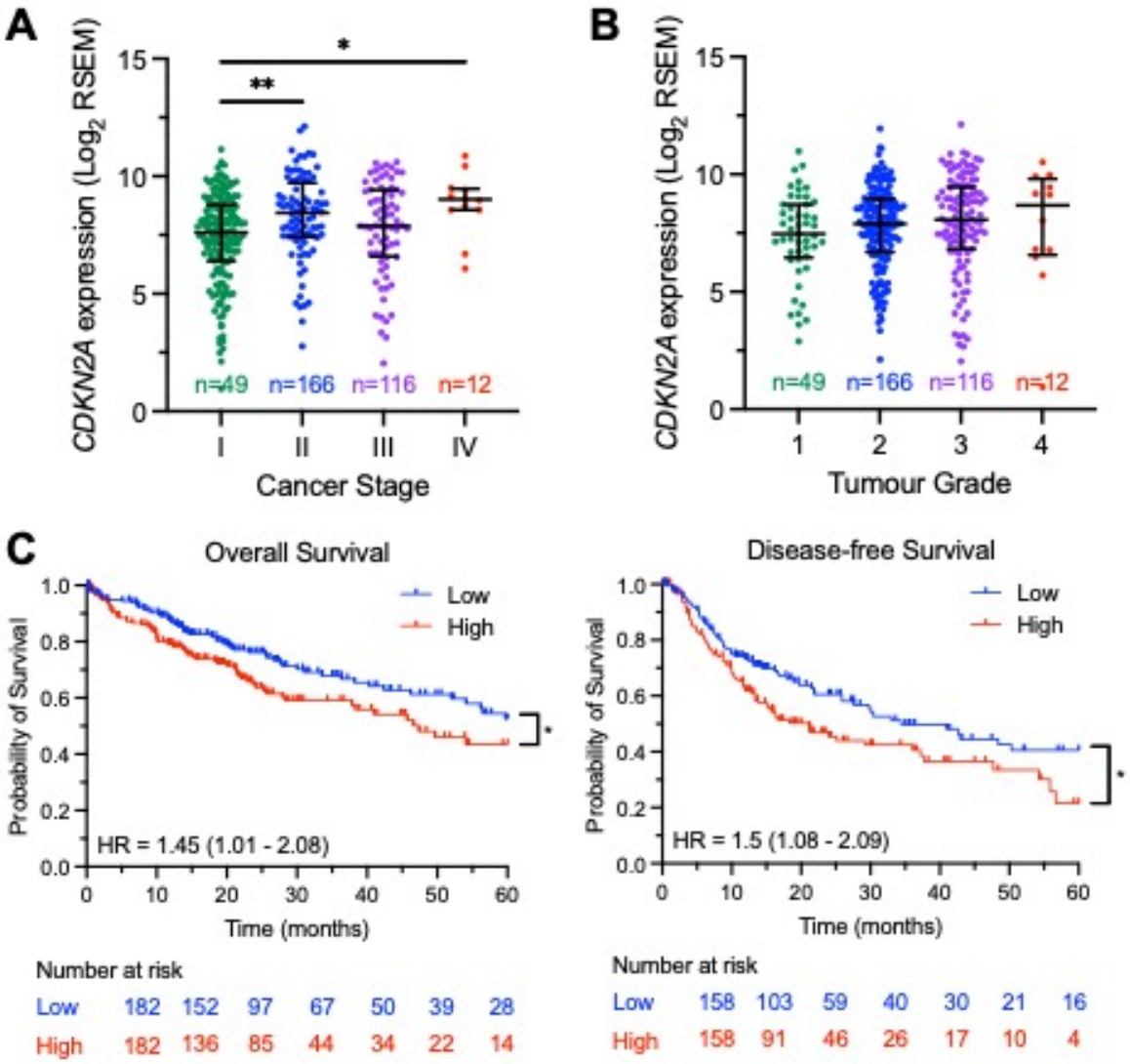

Figure 5.3: *CDKN2A* expression correlated with cancer stage and was a predicter of worse overall and disease-free survival in hepatocellular carcinoma (HCC) patients.

(A, B) The Cancer Genome Atlas (TCGA) datasets were analysed for *CDKN2A* gene expression in HCC tumours and stratified according to **(A)** cancer stage (**p*<0.05, ***p*<0.01, Kruskal-Wallis test followed by Dunn's multiple comparison test) or (**B**) tumour grade. **(C)** Kaplan-Meier plots depicting overall and disease-free survival data for *CDKN2A*^{high} and *CDKN2A*^{low} HCC patients (**p*<0.05, Log-rank test) (HR, hazard ratio). High and low expressing groups were stratified based on the median *CDKN2A* expression. Survival data is accessible via https://kmplot.com/analysis/.

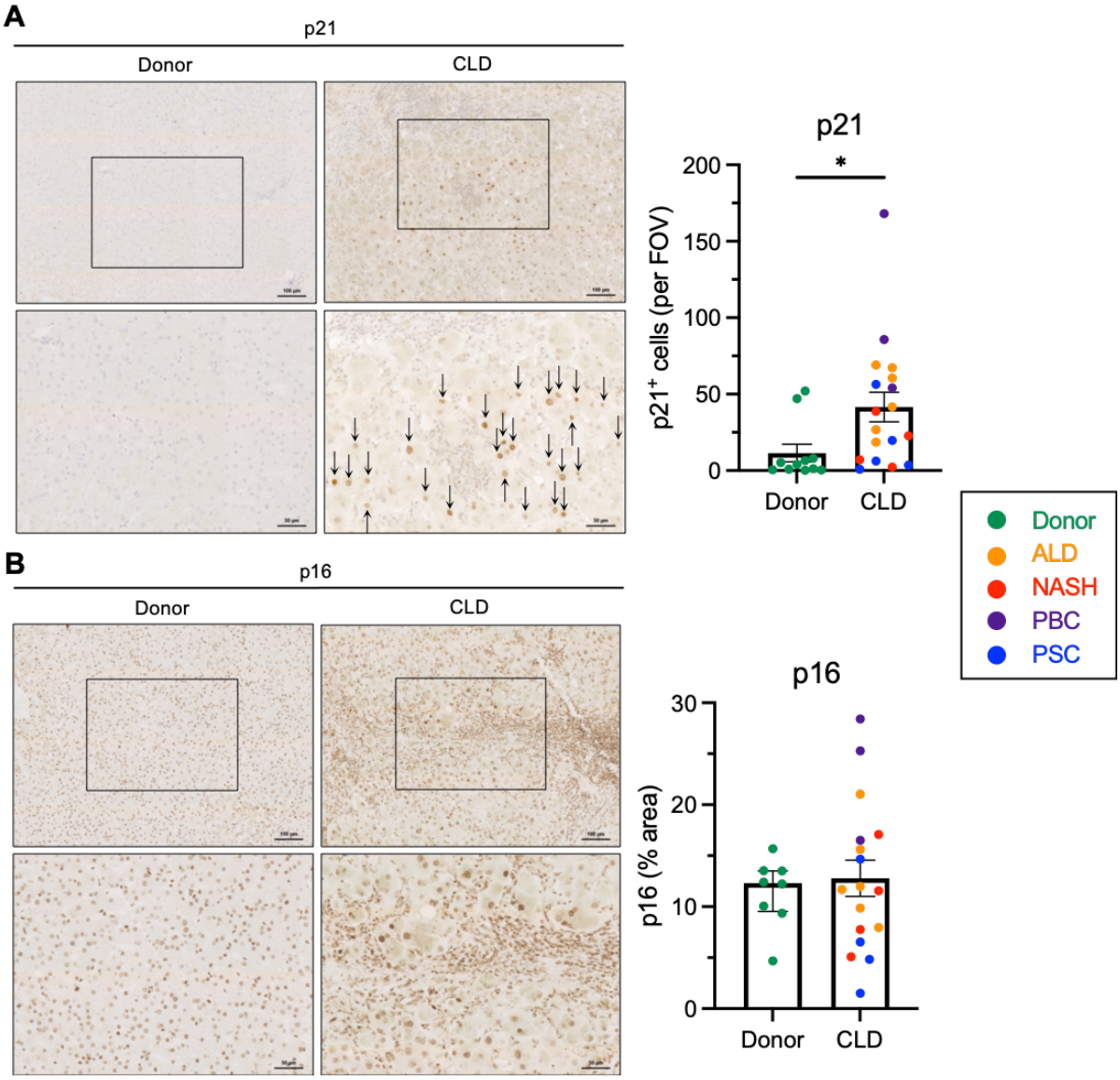

Figure 5.4: Immunohistochemical staining of senescence markers, p21 and p16, in donor and cirrhotic human liver tissue.

Representative images showing localisation of **(A)** p21 (*black arrows*) and **(B)** p16 in donor (*left panels*) and chronic liver disease (CLD) (*right panels*) patient specimens. Insets are shown below. Quantification of p21 (positive cells per field of view) and p16 staining (% area) is shown (*right*). Data shown are mean ± SEM (*p<0.05, student's unpaired *t*-test). Scale bars represent 100 μm (*upper*) or 50 μm (*lower*).

5.2.2 The senescent secretome influenced HSEC phenotype and function

Senescent cells release a secretome known as SASP, comprising numerous cytokines, chemokines and growth factors. These factors contribute to the biological milieu during tissue homeostasis and inflammation, instigating autocrine and paracrine signalling in neighbouring cells. It was hypothesised that components within the SASP, either solely or in combination, could drive phenotypic and functional alterations in HSEC, perhaps to facilitate leukocyte migration across the sinusoidal endothelium and subsequent clearance of senescent cells. The impact of the SASP on HSEC phenotype and function was characterised by stimulating isolated primary human HSEC for 24 hours with either conditioned medium from IMR90 fibroblasts undergoing RAS-mediated oncogene-induced senescence (Ras-CM), or the growing IMR90 control (Grow-CM) (**Figure 5.5**). The effect of SASP stimulation was then assessed by investigating gene expression by qRT-PCR, visualising morphological changes by brightfield and confocal microscopy, and quantifying alterations in protein expression by immunofluorescence.

Brightfield microscopy highlighted distinct morphological changes in Ras-CM-treated HSEC compared to the Grow-CM-treated controls, with these cells appearing more elongated and with an aligned orientation (**Figure 5.6A**). These morphological alterations were confirmed by visualising the perimeter of each cell, via immunocytochemistry for junctional marker VE-cadherin, followed by confocal microscopy (**Figure 5.6B**). Following measurement of cell length and width, the ratio between these parameters was calculated to give an elongation factor (length/width) per cell (**Figure 5.6C**). Ras-CM treatment significantly increased cell length from 61.7 ± 1.48 μm to 71.7 ± 0.92 μm, reduced cell width from 36.8 ± 1.55 μm to 30.9 ± 2.07 μm, and consequently, the cell elongation factor was significantly increased (1.48-fold) following Ras-CM treatment. Treatment with Ras-CM also drove profound changes in the HSEC actin cytoskeleton, which were visualised by phalloidin staining of F-actin followed by confocal microscopy (**Figure 5.7A**). Ras-CM treatment induced a significant and dose-dependent increase in F-actin staining area, from 11.5 ± 2.29% (Grow-CM) to 22.9 ± 0.67% (Ras-CM, 1 in 4) and 33.8 ± 1.17 (Ras-CM, 1 in 2) (**Figure 5.7B**). There was also a small but significant step-wise increase in F-actin intensity (mean grey value) with increasing concentrations of Ras-CM (1 in 4 – 1.06-

fold; 1 in 2 – 1.15-fold) compared to the Grow-CM control (**Figure 5.7C**). These increases were accompanied by the formation of stress fibres in Ras-CM-treated HSEC which is consistent with the morphological changes observed in **Figure 5.6**.

The expression of endothelial activation markers was also studied following Ras-CM treatment of HSEC. At the mRNA level, HSEC increased their expression of pro-inflammatory genes including *ICAM1* (11-fold), *CCL2* (6.27-fold), *IL6* (112-fold), *IL1B* (26.2-fold) and *CXCL8* (67.4-fold) in response to SASP stimulation (**Figure 5.8A**). The upregulation of *CCL2* and *CXCL8* was shown to be statistically significant. Given their well-established role in lymphocyte and monocyte recruitment, respectively, ICAM-1 and CCL2 were studied at the protein level by immunocytochemistry and confocal microscopy. ICAM-1 displayed a significant and dose-dependent increase following Ras-CM treatment, from 0.02 ± 0.01% (Grow-CM) to 6.34 ± 1.03% (Ras-CM, 1 in 4) and 19.8 ± 4.13% (Ras-CM, 1 in 2) (**Figure 5.8B**). Although following quantification of CCL2 % staining area there was no significant difference after Ras-CM treatment, there was in fact a re-distribution of CCL2 in SASP-stimulated HSEC (**Figure 5.8C**). CCL2 appeared to localise within the nucleus of both Grow-CM and Ras-CM-treated HSEC, however following SASP stimulation, there were a subset of HSEC with prominent perinuclear localisation of CCL2. Since CCL2 co-localised with GM130 in Ras-CM-treated HSEC, this suggests increased trafficking to the Golgi apparatus, and perhaps also enhanced synthesis and/or secretion of CCL2 (**Figure 5.8D**). In summary, these data suggest that exposure of HSEC to the senescent secretome results in phenotypic changes, such as elongation and cellular activation, which likely influence HSEC function.

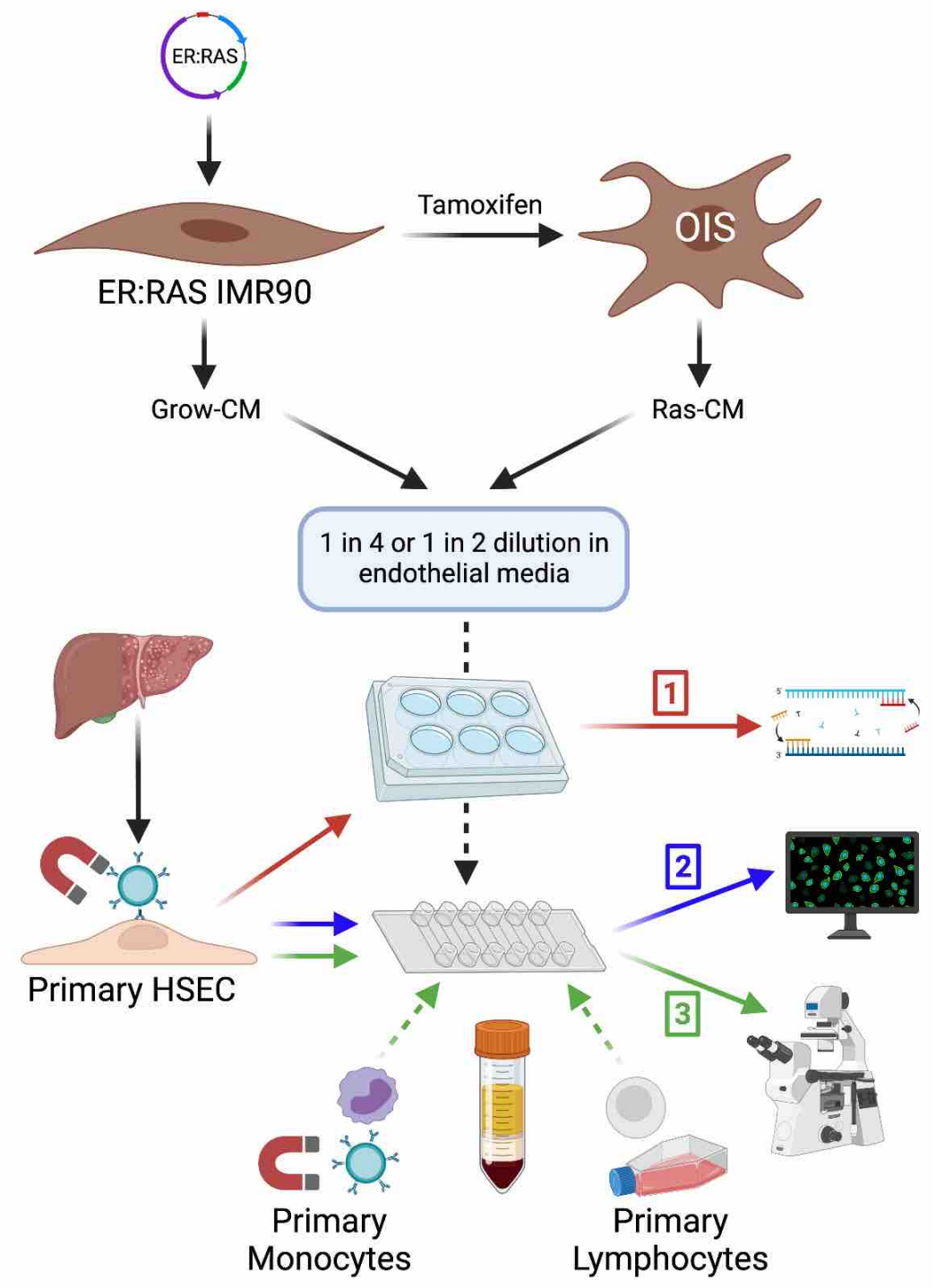

Figure 5.5: Summary of *in vitro* studies using the senescence-associated secretory phenotype (SASP).

The SASP was derived from the conditioned medium of IMR90 fibroblasts undergoing oncogene-induced senescence (OIS). IMR90 fibroblasts were stably transduced with a plasmid encoding the RAS oncogene under a tamoxifen-inducible promoter (ER:RAS IMR90). Following addition of tamoxifen to the cell culture medium IMR90 cells overexpress RAS and undergo OIS. These cells produce SASP (termed Ras-CM) which can then be compared to the conditioned medium from the untreated growing IMR90 cells (Grow-CM). Primary hepatic sinusoidal endothelial cells (HSEC) were then treated for 24 hours with Grow-CM or Ras-CM: (1) in 6-well plates and lysed for analysis of gene expression by qRT-PCR; (2) in 6-channel ibidi® slides, fixed and subject to immunocytochemistry and confocal microscopy; (3) in 6-channel ibidi® slides for use in flow adhesion assays with peripheral blood monocytes or lymphocytes isolated from healthy volunteers.

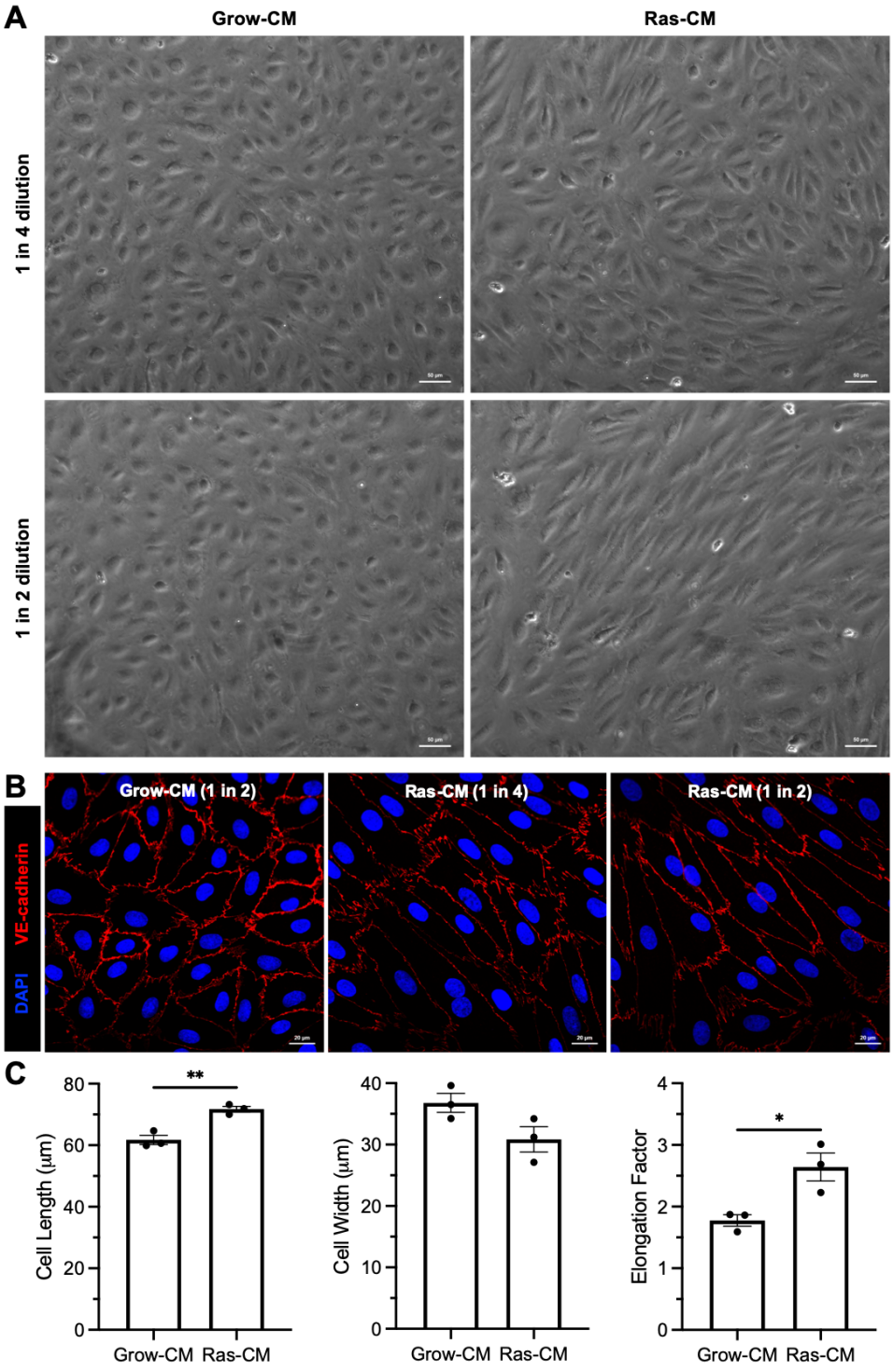

Figure 5.6: The senescent secretome induced morphological changes in hepatic sinusoidal endothelial cells (HSEC).

(A-C) HSEC were treated for 24 hours with either Grow-CM or Ras-CM (1 in 4 or 1 in 2 dilution) and then **(A)** imaged by brightfield microscopy or **(B)** fixed, stained for VE-cadherin (*red*), and imaged by confocal microscopy. 4′,6-diamidino-2-phenylindole (DAPI, *blue*) was used as a nuclear counterstain. **(C)** Cell length and width (μm) were measured using Zen blue software and the elongation factor was calculated by dividing the cell length by the cell width (*p<0.05, **p<0.01, student's unpaired t-test). Data shown are mean ± SEM from three independent HSEC isolates, from a total of 71-93 cells across five visual fields per experimental condition. Scale bars represent **(A)** 50 μm or **(B)** 20 μm.

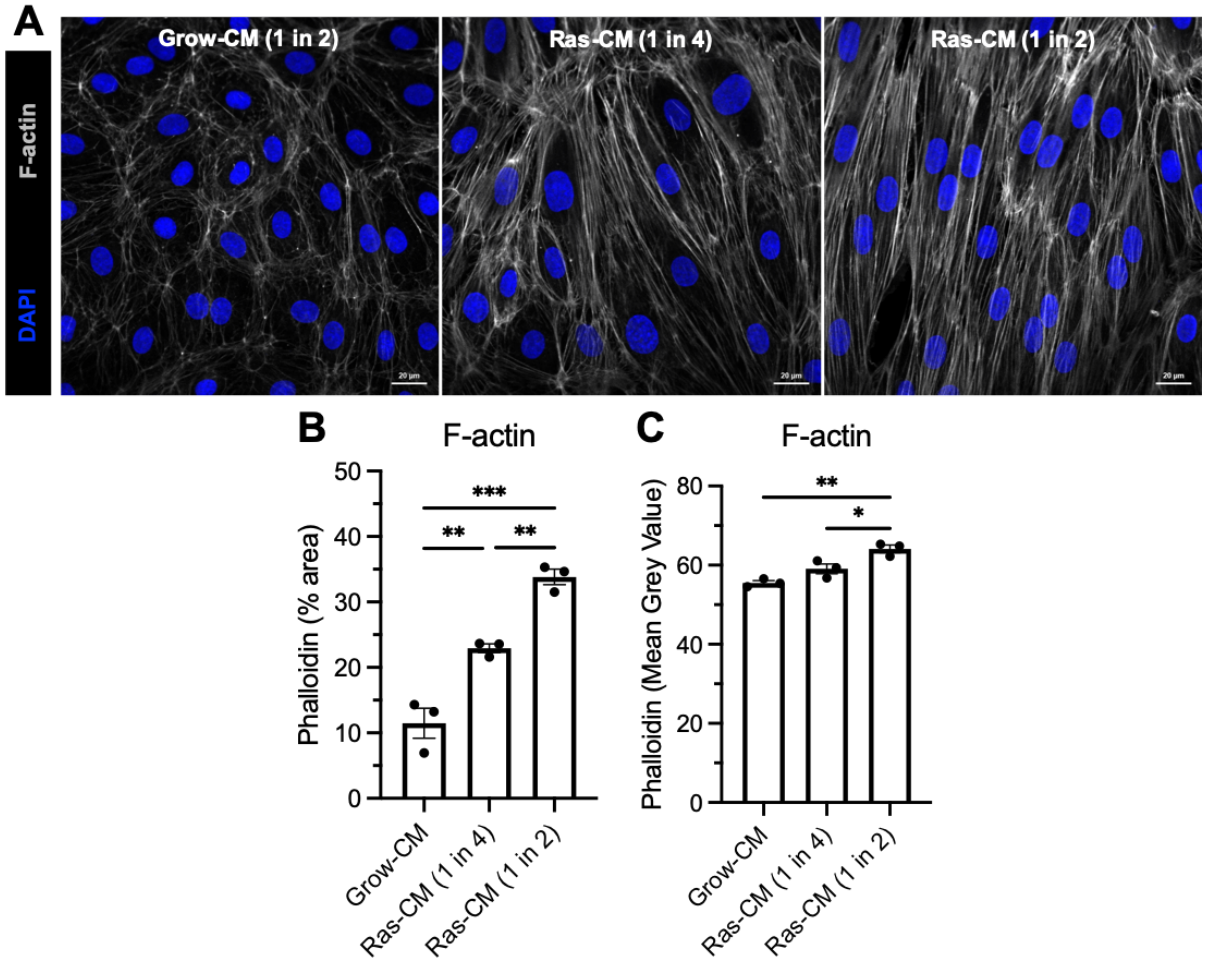

Figure 5.7: The senescent secretome drove cytoskeletal changes in hepatic sinusoidal endothelial cells (HSEC).

(A) HSEC were treated for 24 hours with either Grow-CM or Ras-CM (1 in 4 or 1 in 2 dilution) and then fixed, stained with phalloidin (*grey*), and imaged by confocal microscopy. 4′,6-diamidino-2-phenylindole (DAPI, *blue*) was used as a nuclear counterstain. **(B)** F-actin area (%) and (**C**) intensity (mean grey value) was quantified for a minimum of five visual fields (*p<0.05, **p<0.01, ***p<0.001, one-way ANOVA followed by Tukey's multiple comparison test). Data shown are mean ± SEM from three independent HSEC isolates. Scale bars represent 20 μm.

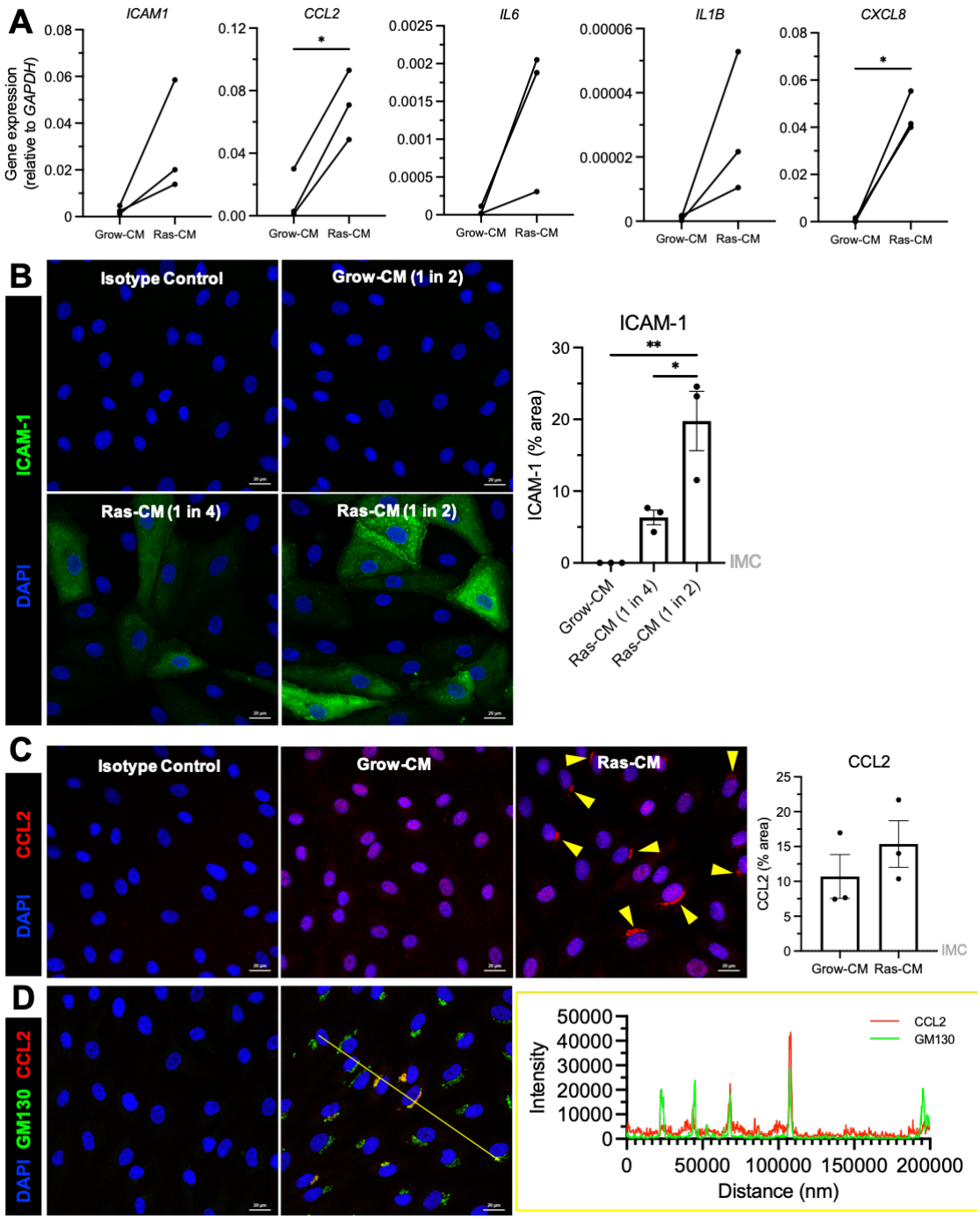

Figure 5.8: The senescent secretome increased expression of adhesion molecules, cytokines and chemokines in hepatic sinusoidal endothelial cells (HSEC).

HSEC were treated for 24 hours with either Grow-CM or Ras-CM (1 in 4 or 1 in 2 dilution) and then either **(A)** lysed and analysed for gene expression via qRT-PCR (*p<0.05, student's paired t-test) or **(B-D)** fixed and subject to immunocytochemistry and confocal microscopy (*p<0.05, **p<0.01, one-way ANOVA followed by Tukey's multiple comparison test). **(A)** Gene expression is shown relative to *GAPDH*, where each data point represents a biological replicate. **(B)** Intercellular adhesion molecule 1 (ICAM-1, *green*) and **(C)** CCL2 (*red*) staining area (%) was quantified for a minimum of five visual fields per condition using ImageJ. Data shown are mean ± SEM from three independent HSEC isolates. Perinuclear CCL2 localisation in Ras-CM-treated HSEC is indicated by the yellow arrowheads. **(D)** CCL2 (*red*) co-localised with Golgi apparatus marker, GM130 (*green*). The yellow line depicts the site of intensity profile. 4′,6-diamidino-2-phenylindole (DAPI, *blue*) was used as a nuclear counterstain. Scale bars represent 20 µm.

5.2.3 PLVAP was upregulated in HSEC by the senescent secretome in vitro

Given the ability of the SASP to stimulate transcription and protein synthesis of multiple endothelial activation markers, the effects of Ras-CM treatment on PLVAP expression were assessed by qRT-PCR and immunocytochemistry followed by high-content imaging or confocal microscopy. Ras-CM treatment for 24 hours significantly increased *PLVAP* gene expression by 3.02-fold (**Figure 5.9A**). This was recapitulated at the protein level, since SASP treatment significantly increased PLVAP immunofluorescence area (2.09-fold ± 0.19) and intensity (2.04-fold ± 0.34) (**Figure 5.9B, C**).

Since PLVAP has been shown in the previous chapter to localise at the cell periphery, paired with the profound effects of SASP treatment on cytoskeletal organisation, the localisation of PLVAP and F-actin was studied by Airyscan confocal microscopy. As shown in **Figure 5.10**, PLVAP appeared to localise within F-actin-rich regions at the cell periphery, proximal to but not within the intercellular junctions. PLVAP was also often observed to localise at polar ends of elongated HSEC (**Figure 5.10**). Since the perinuclear localisation of CCL2 was observed only in a subset of HSEC following SASP treatment, much like the expression pattern of PLVAP *in vitro*, both of these proteins were studied simultaneously by dual immunofluorescence. As shown in **Figure 5.11**, there was no clear association between CCL2 localisation and PLVAP positivity. In fact, when the proportions of single- and double-positive cells were quantified, the incidence was approximately equal for $PLVAP^+$ (30.6%), $CCL2^+$ (37.6%) and $PLVAP^+CCL2^+$ (31.8%) populations.

5.2.4 SASP stimulation altered the HSEC secretome which was relatively unchanged by PLVAP knockdown

To study the impact of PLVAP on the HSEC secretome in response to SASP treatment, cell supernatants from genetically manipulated, SASP-stimulated cells were analysed with cytokine arrays. As shown in **Figure 5.8**, exposure of HSEC to the senescent secretome led to cellular activation, including upregulation of pro-inflammatory cytokines and chemokines. To investigate the effects of Ras-CM treatment on the HSEC secretome in the presence and absence of PLVAP, cell supernatants obtained

from genetically manipulated Grow-CM- or Ras-CM-stimulated HSEC were analysed using commercially-available cytokine arrays (**Figure 5.12**). When comparing Grow-CM and Ras-CM treatment in the control arm (siControl), secretion of several factors was shown to be upregulated in response to SASP treatment, including G-CSF (146-fold), IL-6 (11.5-fold), GM-CSF (5-fold), IL-21 (3.62-fold), CXCL1 (1.32-fold), CXCL12 (1.29-fold), C5a (1.19-fold) and IL-8 (1.14-fold). In contrast, secretion of PAI-1 (0.84-fold) and MIF (0.86-fold) were downregulated in response to Ras-CM (in the presence of PLVAP). Secretion of ICAM-1, CCL2 and CCL5 did not seem to change following SASP treatment. When the effects of Grow-CM and Ras-CM treatment were studied following knockdown of PLVAP, results were variable depending on each cytokine/chemokine. The absence of PLVAP did not seem to influence the SASP-mediated effects on GM-CSF, IL-6 and PAI-1 production. In contrast, the absence of PLVAP reduced the baseline (Grow-CM) secretion of several factors including MIF, CXCL12 and CCL2, yet this effect seemed to be reversed following Ras-CM treatment in the absence of PLVAP. Notably, several factors which had comparable baseline (Grow-CM) secretion in the absence of PLVAP, yet were upregulated to a slightly lesser extent following Ras-CM treatment (siControl + Ras vs. siPLVAP + Ras in **Figure 5.12**). These included IL-21 (0.13-fold), C5a (0.87-fold), G-CSF (0.88-fold), IL-8 (0.91-fold) and CXCL1 (0.94-fold). These data suggest that SASP treatment stimulates secretion of multiple soluble factors capable of promoting leukocyte recruitment, yet the role of PLVAP in shaping this secretory profile appears to be minimal.

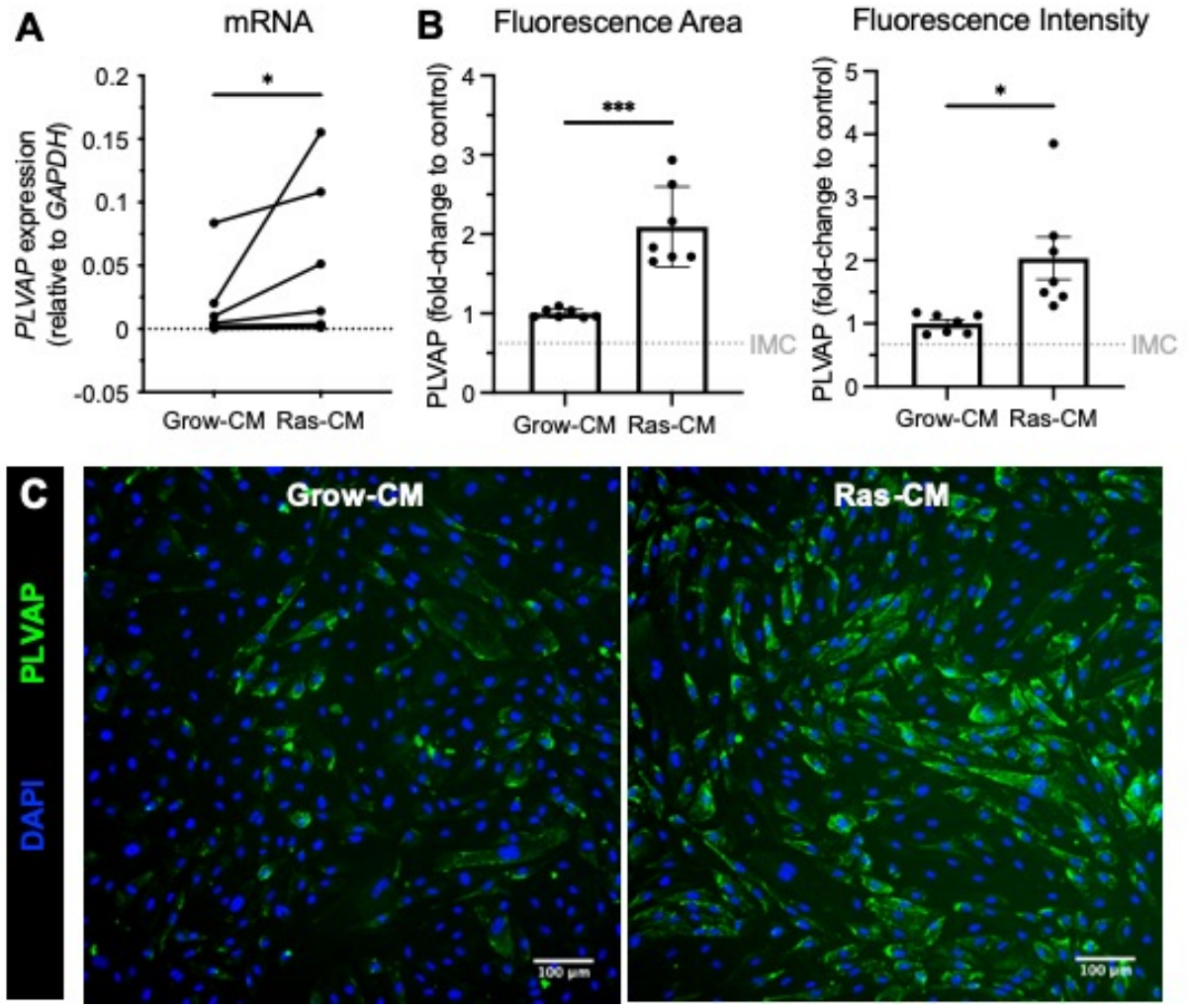

Figure 5.9: The senescent secretome upregulated plasmalemma vesicle-associated protein (PLVAP) expression in hepatic sinusoidal endothelial cells (HSEC).

(A-C) HSEC were treated for 24 hours with either Grow-CM or Ras-CM (1 in 4 dilution) and then either **(A)** lysed and analysed for *PLVAP* gene expression via qRT-PCR (**p*<0.05, Wilcoxon test) or **(B)** fixed and subject to immunocytochemistry and high-content imaging (****p*<0.001, Mann-Whitney test, **p*<0.001, student's unpaired *t*-test). **(A)** Gene expression is shown relative to *GAPDH*, where each data point represents a biological replicate. Data shown in **(B)** are mean fold-change to Grow-CM control ± SEM of three HSEC isolates with each condition performed in at least duplicate. Representative images of PLVAP (*green*) are shown in (**C**). 4′,6-diamidino-2-phenylindole (DAPI, *blue*) was used as a nuclear counterstain. Scale bars represent 100 µm.

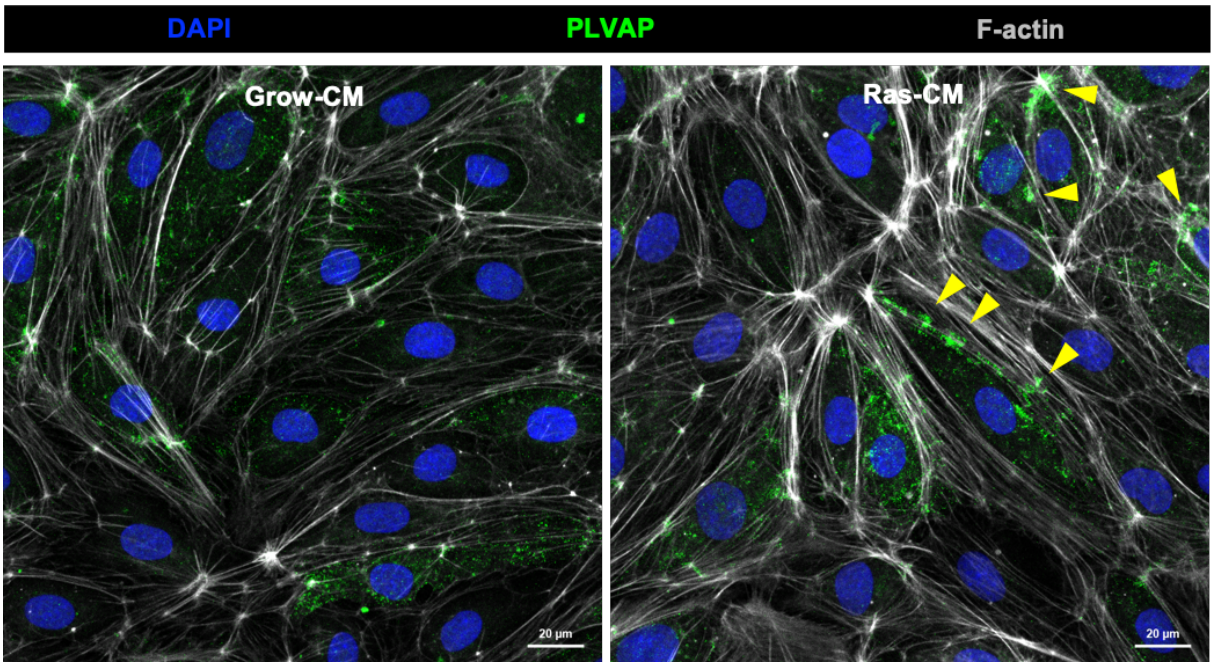

Figure 5.10: Plasmalemma vesicle-associated protein (PLVAP) localised with F-actin-rich areas proximal to the cellular junctions in response to the senescent secretome.

Hepatic sinusoidal endothelial cells (HSEC) were treated with Grow-CM (*left*) or Ras-CM (*right*) (1 in 2 dilution) for 24 hours before fixation, immunocytochemistry to visualise PLVAP (*green*) and F-actin (*grey*), followed by confocal microscopy. PLVAP and F-actin enrichment is indicated by the yellow arrowheads. 4′,6-diamidino-2-phenylindole (DAPI, *blue*) was used as a nuclear counterstain. Scale bars represent 20 µm.

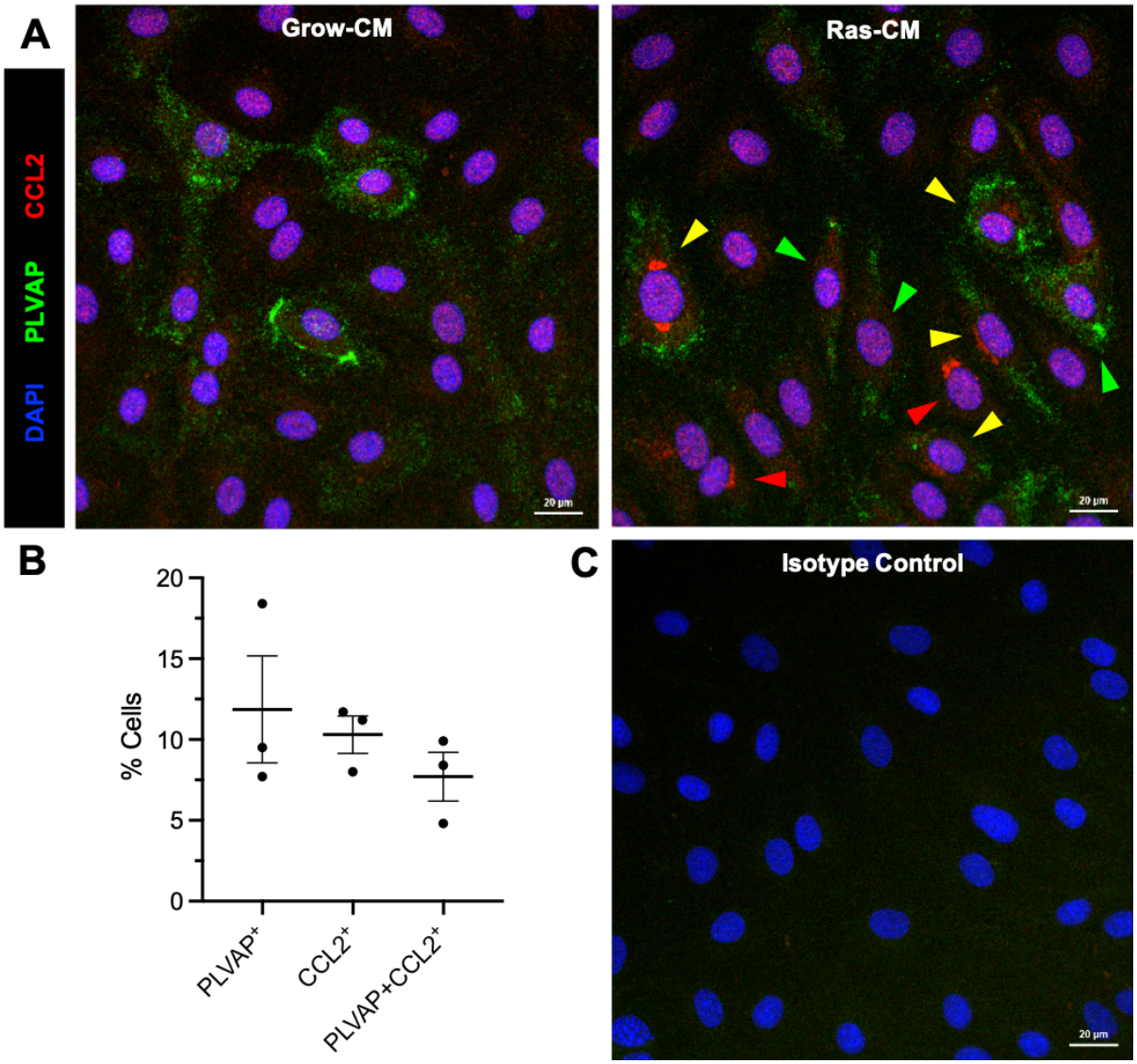

Figure 5.11: The subset-specific expression of plasmalemma vesicle-associated protein (PLVAP) did not correlate with perinuclear CCL2 localisation following exposure to the senescent secretome.

(A-C) Hepatic sinusoidal endothelial cells (HSEC) were treated with Grow-CM or Ras-CM (1 in 4 dilution) for 24 hours before fixation, immunocytochemistry to visualise PLVAP (*green*) and CCL2 (*red*), followed by confocal microscopy. 4′,6-diamidino-2-phenylindole (DAPI, *blue*) was used as a nuclear counterstain. (**A**) Perinuclear CCL2 localisation in $PLVAP^{+}$ (*yellow arrowheads*) and $PLVAP^{-}$ (*red arrowheads*) HSEC was observed, as was PLVAP expression in the absence of perinuclear CCL2 localisation (*green arrowheads*). **(B)** The frequency of these events was quantified for ten visual fields from three independent HSEC isolates. Isotype control samples were negative (**C**). Scale bars represent 20 µm.

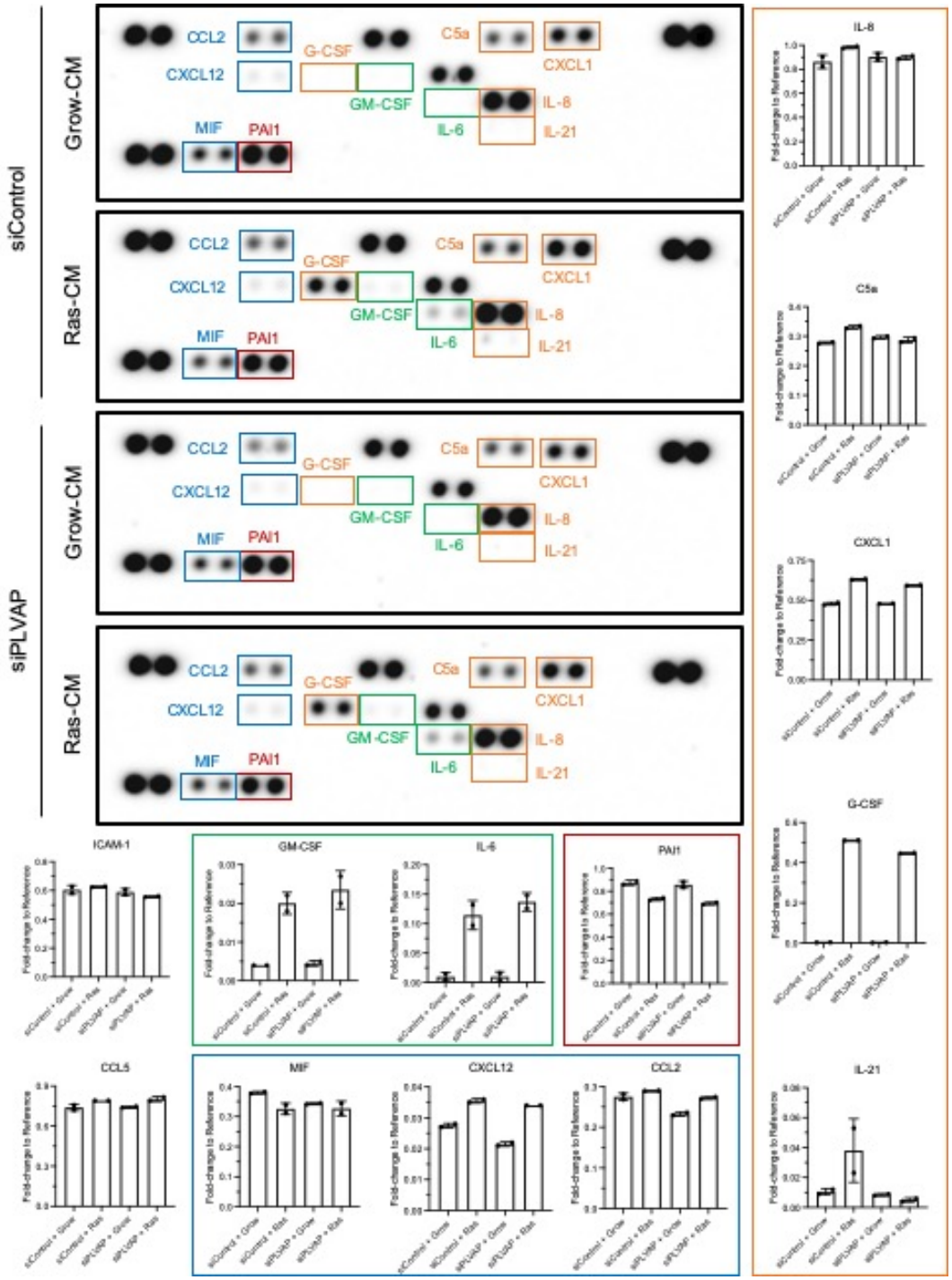

Figure 5.12: The senescent secretome altered the secretory profile of hepatic sinusoidal endothelial cells (HSEC) which was largely unaffected by plasmalemma vesicle-associated protein (PLVAP) knockdown.

HSEC were treated with siRNA targeted against PLVAP (siPLVAP) or a negative control (siControl) and then stimulated with either Grow-CM or Ras-CM (1 in 2 dilution) 24 hours post-knockdown. Cells were then thoroughly washed with phosphate buffered saline before addition of basal endothelial medium for 24 hours. Cells were then lysed for validation of successful genetic knockdown (KD) (data not shown) and supernatants were collected and analysed using a Proteome Profiler Human Cytokine Array Kit (R&D). Data shown are mean fold-change to reference spots per nitrocellulose membrane from one individual experiment. Colour coding is as follows: *None*, no change in response to Ras-CM ± KD; *green*, increase with Ras-CM ± PLVAP KD; *red*, decrease with Ras-CM ± PLVAP KD; *blue*, decrease in baseline (Grow-CM) following PLVAP KD; *orange*, less upregulation in response to Ras-CM following PLVAP KD.

5.2.5 The senescent secretome facilitated lymphocyte and monocyte recruitment via distinct routes

Previous work, by our group and others, has shown that the senescent tissue microenvironment and soluble factors within it are able to facilitate hepatic recruitment of lymphocytes under physiological shear stress[464, 531]. To test the hypothesis that the senescent secretome also promotes monocyte recruitment, flow adhesion assays were performed with SASP-stimulated donor- and CLD patient-derived HSEC and healthy volunteer peripheral blood monocytes. Phase-contrast videos were then manually scored to assess the numbers of adhered, shape-changed and transmigrated leukocytes (**Figure 5.13**). Indeed, Ras-CM treatment of HSEC facilitated the recruitment of monocytes under flow conditions, significantly increasing monocyte adhesion from 80 ± 22.3 to 262 ± 40 (3.28-fold), shape-change from 42.3 ± 12.7 to 130 ± 23.9 (3.07-fold) and transmigration from 11.2 ± 2.25 to 85.7 ± 15 (7.65-fold) (monocytes/mm^2/million cells perfused) (**Figure 5.13B**). The percentage of adhered monocytes which underwent transmigration was also significantly increased from 20.7 ± 5.52% to 35 ± 3.53%, but the proportion of adhered cells which underwent a shape-change was not significantly different (**Figure 5.13B**).

Transendothelial migration can occur via the paracellular pathway, through the intercellular junctions of adjacent endothelial cells, or via the transcellular route, where leukocytes extravasate through pores which traverse the endothelial cell body. To characterise the route of leukocyte transmigration in response to the senescent secretome, flow adhesion assays were performed with fluorescently-labelled (CellTracker Green and SiR-actin) Ras-CM-treated HSEC and peripheral blood monocytes or lymphocytes (**Figure 5.14**). Transmigration events were first identified by the presence of a leukocyte (visualised with DAPI and distinguished from HSEC nuclei based on size), along with disruption of the HSEC cytoplasm (CellTracker Green), which allowed differentiation between leukocytes adhered to the HSEC monolayer and those protruding through the HSEC cell body (**Figure 5.14A, B**). The route of transmigration was determined by the location of diapedesis (at the cellular junction or not) and also the integrity of the VE-cadherin cell junctions; that is, disruption of VE-cadherin indicated a paracellular transmigratory event. Visualisation of the HSEC cytoskeleton was also possible by pre-labelling with

live cell actin probe, SiR-actin. Strikingly, almost all monocytes transmigrated via the paracellular route (92.6 ± 2.86%) in response to SASP treatment (**Figure 5.14C**). In contrast, the majority of lymphocytes transmigrated via the transcellular route (62.4 ± 1.12%). There were also notable differences observed in the localisation of F-actin with adhered and transmigrating leukocytes; whilst lymphocytes were most frequently (>80%) surrounded by F-actin regardless of their transmigratory pathway, the same F-actin enrichment was not commonly observed for monocytes (<20%) (**Figure 5.14D**). Instead, monocyte transmigration was associated with disrupted F-actin at the cellular junctions and a pore devoid of F-actin through which the monocytes extravasate (**Figure 5.14A, B**).

To study the molecular mechanisms involved in SASP-mediated monocyte and lymphocyte recruitment, flow adhesion assays were performed with Ras-CM-stimulated HSEC following treatment with antibodies targeted against known adhesion molecules, ICAM-1 and CD31. There were no significant differences in the number of adhered, shaped-changed or transmigrated monocytes following ICAM-1 blockade, nor were there any changes in the percentage of adhered monocytes that underwent shape-change or transmigration, despite successful binding of the ICAM-1 antibody following treatment (**Figure 5.15A-C**). Furthermore, although monocytes frequently transmigrated through ICAM-1^+ cells, there was no obvious localisation of ICAM-1 with monocytes undergoing extravasation (**Figure 5.15D**). In contrast, SASP-mediated lymphocyte adhesion and transmigration were sensitive to ICAM-1 inhibition, with a significant reduction of 0.69-fold ± 0.08 and 0.54 ± 0.05, respectively, following antibody treatment compared to the IMC (**Figure 5.16**). In support of its role in SASP-mediated lymphocyte recruitment, ICAM-1 localised with transmigrating lymphocytes in association with F-actin-rich pores through the endothelial cell body (**Figure 5.16C**).

Following antibody-mediated CD31 blockade (**Figure 5.17A, B**), SASP-mediated monocyte transmigration was significantly inhibited (0.66-fold ± 0.05) whilst the number of adhered monocytes remained comparable. The number shape-changed monocytes displayed a concomitant significant increase (1.38-fold ± 0.15) with CD31 inhibition. These observations were mirrored by a significant increase in the percentage of adhered monocytes which appeared shape-changed (from 44.2 ± 1.91% to

59.6 ± 1.91%), and a significant decrease in the fraction of adhered monocytes which underwent transmigration (from 32.6 ± 3.66% to 19.8 ± 1.33%), in response to CD31 inhibition compared to the IMC. Fixation, permeabilisation and staining with an anti-mIgG1 AF488 secondary antibody post-treatment, followed by quantification of % staining area, highlighted successful binding of the CD31 antibody (**Figure 5.17C**). During both monocyte adhesion and transmigration, Airyscan confocal microscopy highlighted a prominent enrichment of CD31, with HSEC appearing to extend F-actin-containing CD31-rich protrusions from the membrane which enveloped monocytes during recruitment (**Figure 5.17D**). Interestingly, a slight decrease in SASP-mediated lymphocyte transmigration was observed, both in absolute numbers (0.82-fold ± 0.10) and in the percentage of adhered cells (from 39.4 ± 2.95% to 32.0 ± 3.34%), although this did not reach statistical significance (**Figure 5.18A, B**). Similar to observations with monocytes, the proportion of adhered lymphocytes which underwent a shape-change was significantly increased from 36.1 ± 1.93% to 44.7 ± 1.03% following CD31 blockade compared to the IMC. The binding of the CD31 antibody was also confirmed for lymphocyte flow assays (**Figure 5.18C**). Despite no significant inhibitory effect on lymphocyte transmigration, there was clear localisation of CD31 during both paracellular and transcellular transmigration events, as shown by Airyscan confocal microscopy (**Figure 5.19**). Although there was colocalisation between CD31 and F-actin during both of these events, the associated membrane protrusions were considerably less prominent than those observed during monocyte adhesion and transmigration (**Figure 5.17D**).

These data highlight that the senescent secretome is capable of driving hepatic recruitment of both lymphocytes and monocytes under physiologically low shear conditions, yet these processes occur via discrete endothelial routes and involve distinct molecular pathways.

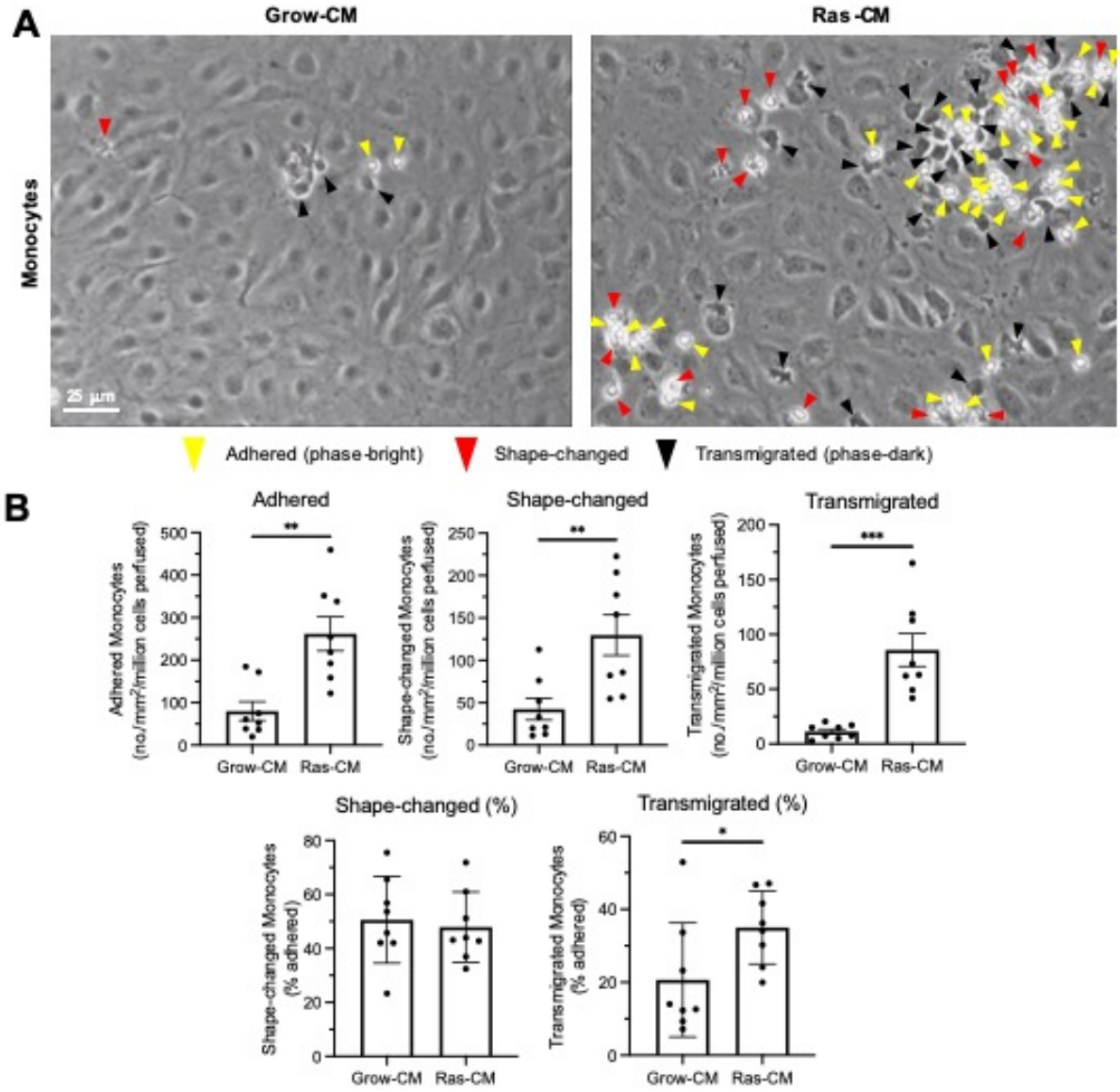

Figure 5.13: The senescent secretome facilitated monocyte recruitment across hepatic sinusoidal endothelial cells (HSEC) under physiological shear stress.

(A, B) Flow adhesion assays were performed with Grow-CM or Ras-CM stimulated HSEC and monocytes isolated from healthy volunteer peripheral blood. Representative phase-contrast images are shown in **(A)**. **(B)** The number of adhered (*yellow arrowheads*), shape-changed (*red arrowheads*) and transmigrated (*black arrowheads*) monocytes were quantified in ten visual fields per lane. Data shown are mean ± SEM from six independent experiments (*p<0.05, **p<0.01, ***p<0.001, Mann-Whitney test (adhered and % transmigrated) or student's unpaired t-test). Scale bar represents 25 µm.

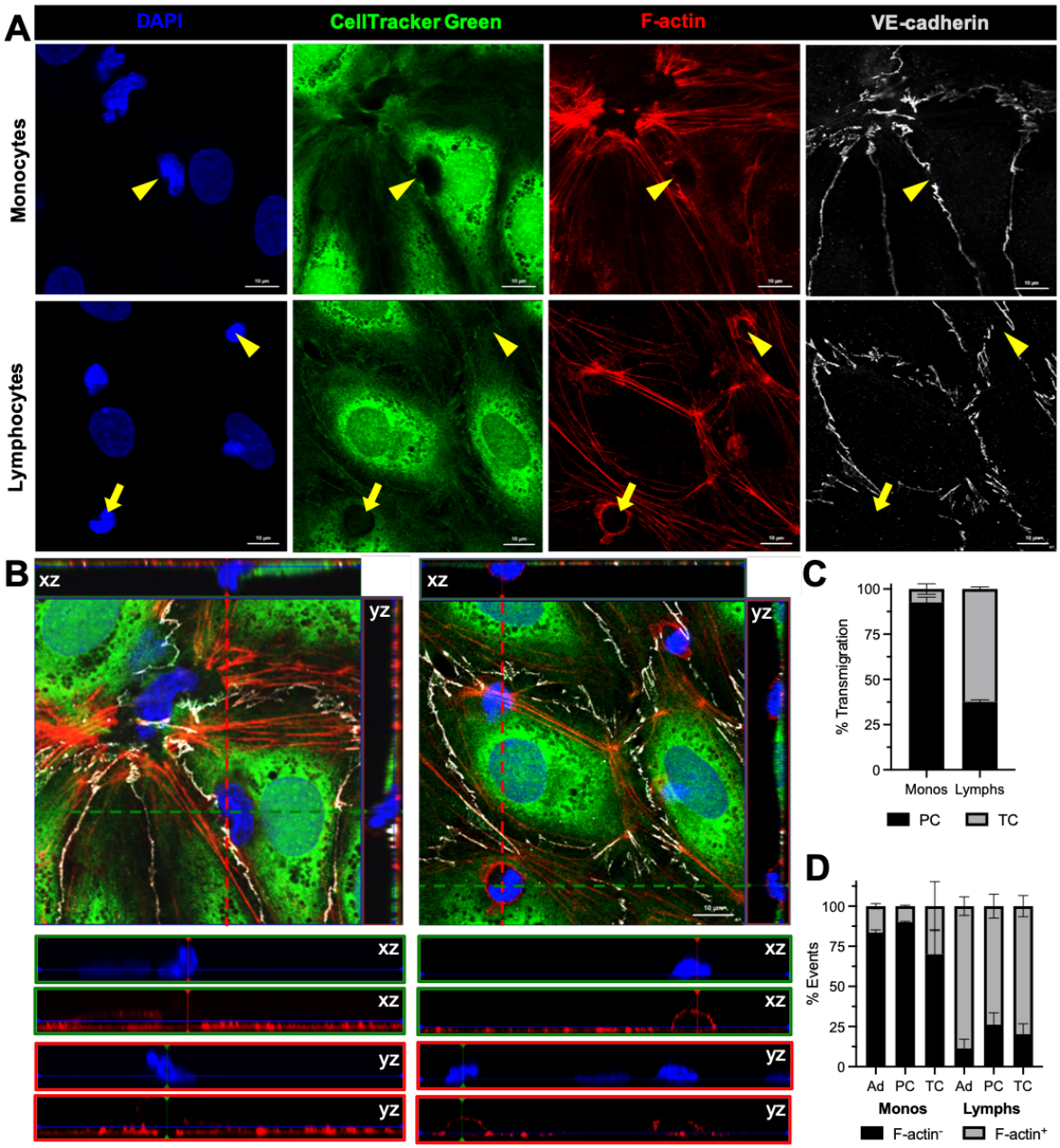

Figure 5.14: Monocyte and lymphocyte recruitment across hepatic sinusoidal endothelial cells (HSEC) in response to the senescent secretome occurred by distinct routes.

(A-C) Flow adhesion assays were performed with Ras-CM stimulated HSEC and monocytes or lymphocytes isolated from healthy volunteer peripheral blood. HSEC were pre-labelled with CellTracker Green (*green*) and SiR-actin (*red*), and following the flow assay, cells were fixed and stained for junctional marker vascular endothelial-cadherin (VE-cadherin, *grey*). Orthogonal merged images are shown in **(B)** from the visual fields in **(A)**. **(C)** The route of transmigration was determined based on whether the VE-cadherin^{+} junctions were disrupted (PC, paracellular, *yellow arrowheads*) or not (TC, transcellular, *yellow arrows*). This was quantified for transmigration events from at least 15 visual fields for three HSEC isolates (159 total lymphocyte events and 327 total monocyte events). **(D)** The association of F-actin with adhered (Ad) and transmigrating (PC or TC) monocytes and lymphocytes was quantified (n=3). Data shown are mean ± SEM. Scale bars represent 10 μm.

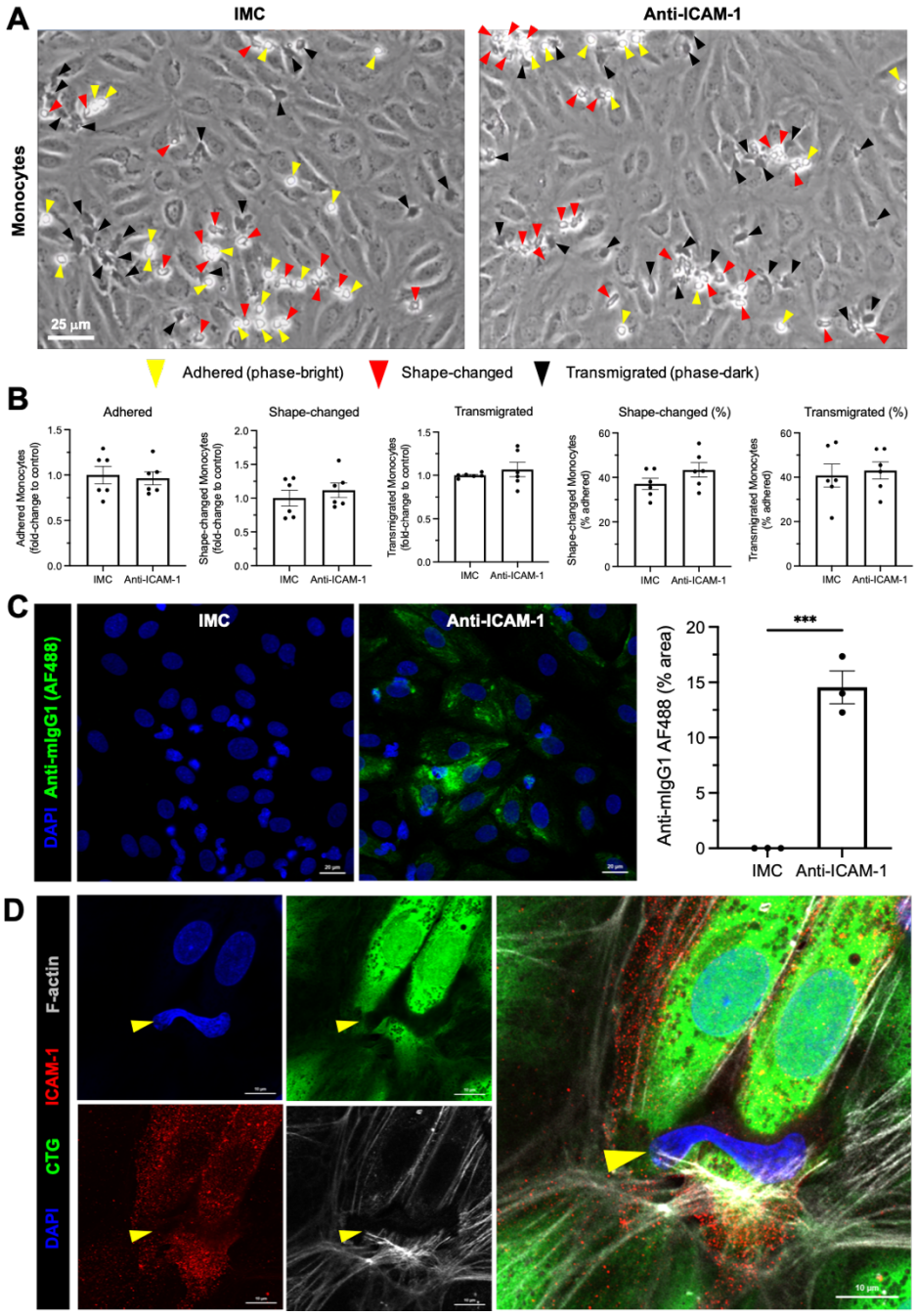

Figure 5.15: Monocyte recruitment across hepatic sinusoidal endothelial cells (HSEC) in response to the senescent secretome occurred independently of intercellular adhesion molecule 1 (ICAM-1).

(A-D) Flow adhesion assays were performed with Ras-CM stimulated HSEC and monocytes isolated from healthy volunteer peripheral blood following antibody-mediated ICAM-1 blockade (or isotype-matched control, IMC). Representative phase-contrast images are shown in **(A)**. **(B)** The number of adhered (*yellow arrowheads*), shape-changed (*red arrowheads*) and transmigrated (*black arrowheads*) monocytes were quantified in ten visual fields per lane with each condition performed in duplicate. Data shown are mean ± SEM from three independent experiments. **(C)** Following the flow assay, cells were fixed, permeabilised, and stained with an anti-mIgG1 AF488 secondary antibody (*green*). Staining area (%) was quantified for a minimum of three visual fields per condition using ImageJ (***p<0.001, student's unpaired t-test). 4′,6-diamidino-2-phenylindole (DAPI, *blue*) was used as a nuclear counterstain. **(D)** HSEC were also pre-labelled with CellTracker Green (CTG, *green*) and SiR-actin (*grey*), and following the flow assay, cells were fixed and stained for ICAM-1 (*red*). There was no association of ICAM-1 with transmigrating monocytes (*yellow arrowhead*). Scale bars represent **(A)** 25 µm, **(C)** 20µm or **(D)** 10 µm.

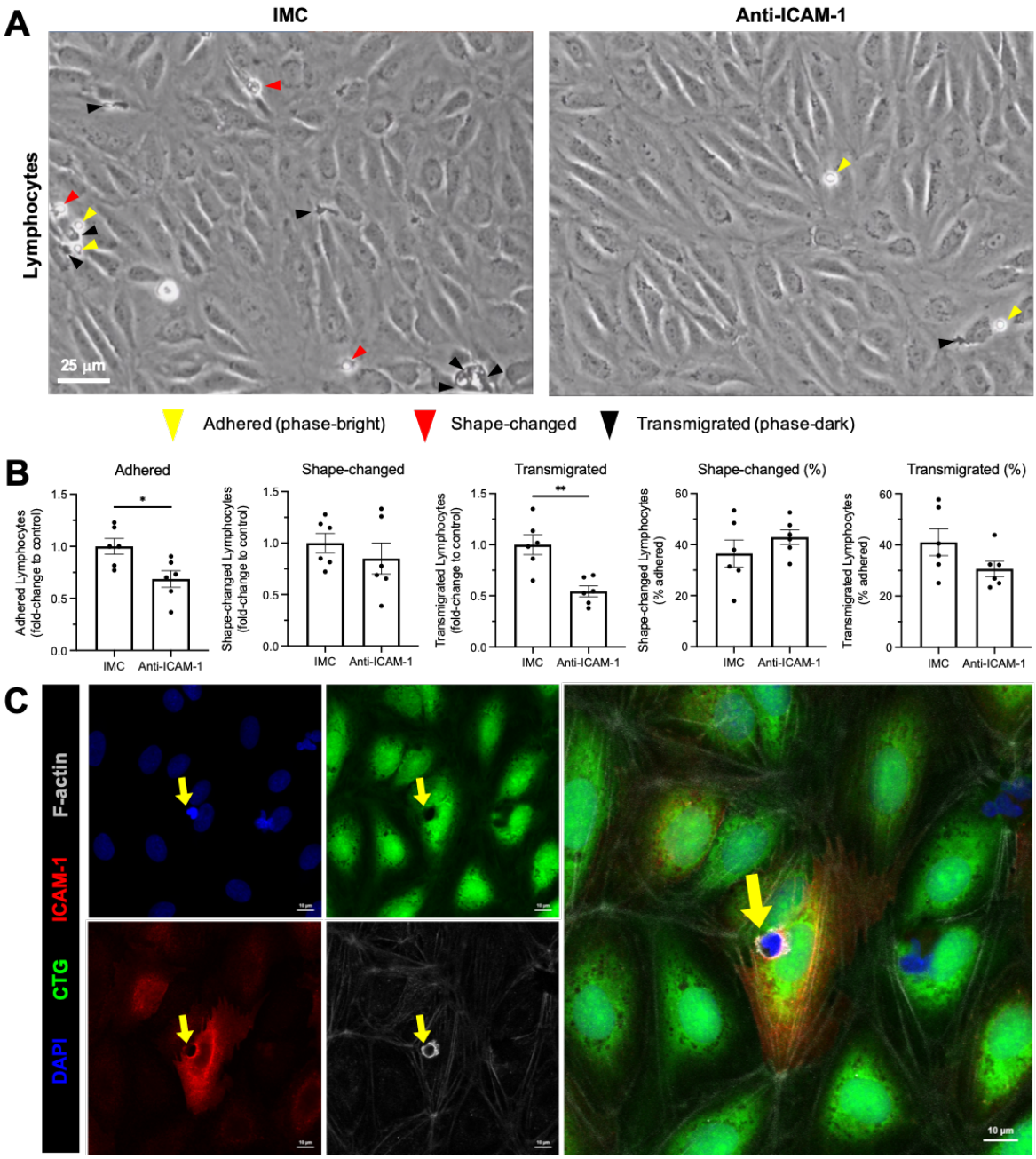

Figure 5.16: Lymphocyte recruitment across hepatic sinusoidal endothelial cells (HSEC) in response to the senescent secretome was mediated by intercellular adhesion molecule 1 (ICAM-1).

(A-C) Flow adhesion assays were performed with Ras-CM stimulated HSEC and lymphocytes isolated from healthy volunteer peripheral blood following antibody-mediated ICAM-1 blockade (or isotype-matched control, IMC). Representative phase-contrast images are shown in **(A)**. **(B)** The number of adhered (*yellow arrowheads*), shape-changed (*red arrowheads*) and transmigrated (*black arrowheads*) lymphocytes were quantified in ten visual fields per lane with each condition performed in duplicate. Data shown are mean ± SEM from three independent experiments (*p<0.05, **p<0.01, student's unpaired t-test). **(C)** HSEC were pre-labelled with CellTracker Green (CTG, *green*) and SiR-actin (*grey*), and following the flow assay, cells were fixed and stained for ICAM-1 (*red*). ICAM-1 localised with transmigrating lymphocytes (*yellow arrow*). Scale bars represent **(A)** 25 µm or **(C)** 10 µm.

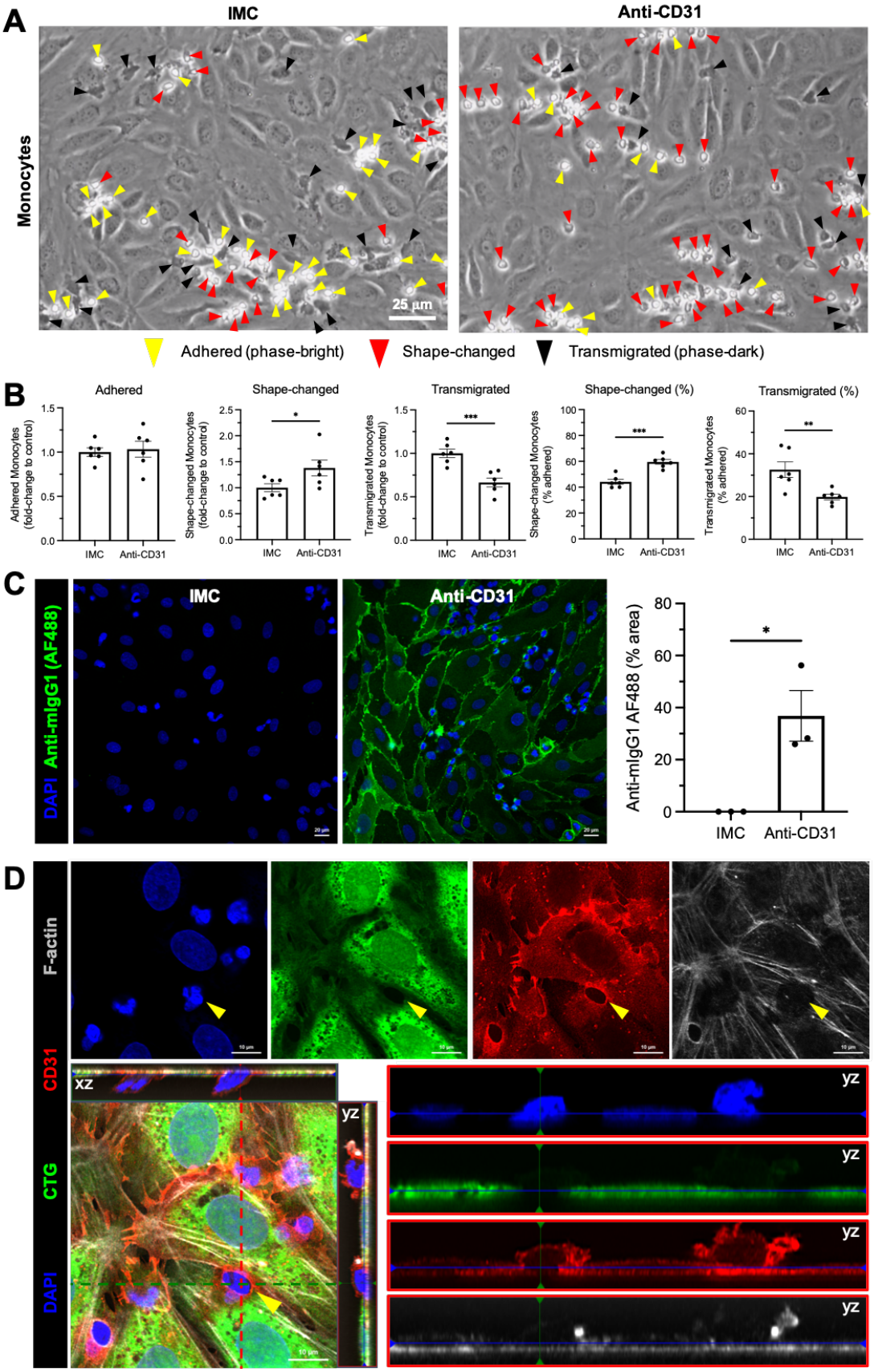

Figure legend on next page.

Figure 5.17: Monocyte transmigration across hepatic sinusoidal endothelial cells (HSEC) in response to the senescent secretome was mediated by CD31.

(A-D) Flow adhesion assays were performed with Ras-CM stimulated HSEC and monocytes isolated from healthy volunteer peripheral blood following antibody-mediated CD31 blockade (or isotype-matched control, IMC). Representative phase-contrast images are shown in **(A)**. **(B)** The number of adhered (*yellow arrowheads*), shape-changed (*red arrowheads*) and transmigrated (*black arrowheads*) monocytes were quantified in ten visual fields per lane with each condition performed in duplicate. Data shown are mean ± SEM from three independent experiments (*p<0.05, **p<0.01, ***p<0.001, student's unpaired *t*-test). **(C)** Following the flow assay, cells were fixed, permeabilised, and stained with an anti-mIgG1 AF488 secondary antibody (*green*). Staining area (%) was quantified for a minimum of six visual fields per condition using ImageJ (*p<0.05, student's unpaired *t*-test). 4′,6-diamidino-2-phenylindole (DAPI, *blue*) was used as a nuclear counterstain. **(D)** HSEC were pre-labelled with CellTracker Green (*green*) and SiR-actin (*grey*), and following the flow assay, cells were fixed and stained for CD31 (*red*). CD31 localises with adhered and transmigrating monocytes (*yellow arrowhead and cross hairs*). Scale bars represent **(A)** 25 µm, **(C)** 20µm or **(D)** 10 µm.

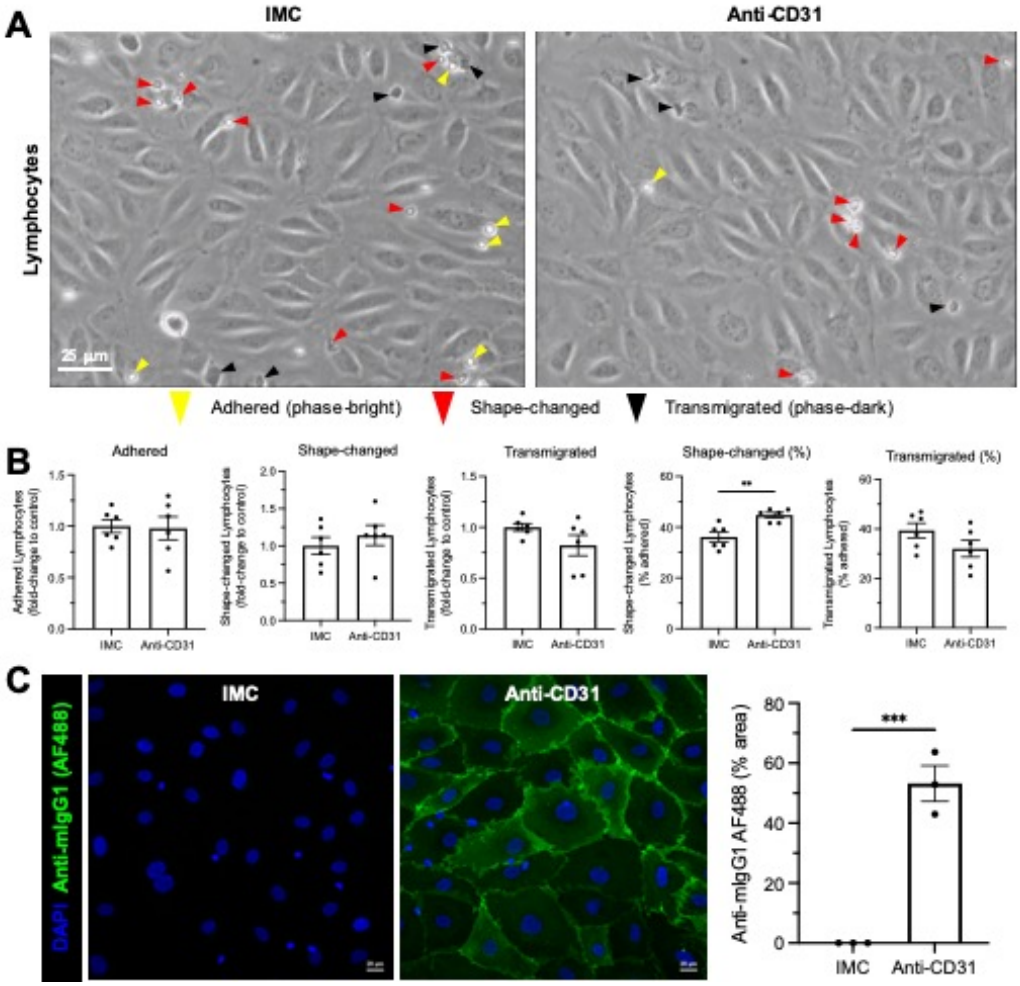

Figure 5.18: Lymphocyte recruitment in response to the senescent secretome was partially dependent on CD31.

(A-C) Flow adhesion assays were performed with Ras-CM stimulated HSEC and lymphocytes isolated from healthy volunteer peripheral blood following antibody-mediated CD31 blockade (or isotype-matched control, IMC). Representative phase-contrast images are shown in **(A)**. **(B)** The number of adhered (*yellow arrowheads*), shape-changed (*red arrowheads*) and transmigrated (*black arrowheads*) lymphocytes were quantified in ten visual fields per lane with each condition performed in duplicate. Data shown are mean ± SEM from three independent experiments (**p<0.01, Mann-Whitney test). **(C)** Following the flow assay, cells were fixed, permeabilised, and stained with an anti-mIgG1 AF488 secondary antibody (*green*). Staining area (%) was quantified for a minimum of six visual fields per condition using ImageJ (***p<0.001, student's unpaired *t*-test). 4′,6-diamidino-2-phenylindole (DAPI, *blue*) was used as a nuclear counterstain. Scale bars represent **(A)** 25 µm or **(C)** 20µm.

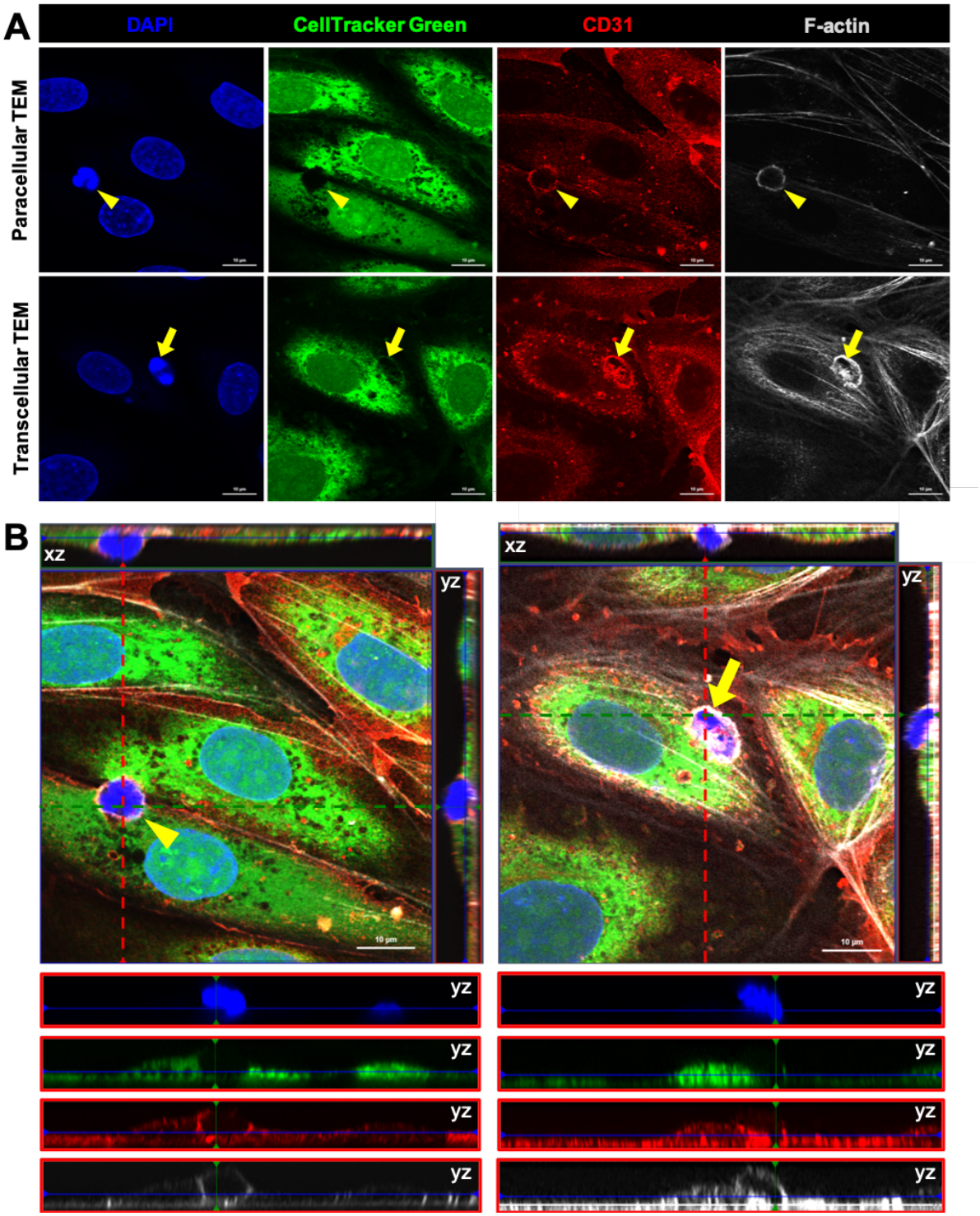

Figure 5.19: CD31 localised with lymphocytes during transendothelial migration (TEM) across hepatic sinusoidal endothelial cells (HSEC) in response to the senescent secretome.

(A, B) Flow adhesion assays were performed with Ras-CM stimulated HSEC and lymphocytes isolated from healthy volunteer peripheral blood. HSEC were pre-labelled with CellTracker Green (*green*) and SiR-actin (*grey*), and following the flow assay, cells were fixed and stained for CD31 (*red*). 4′,6-diamidino-2-phenylindole (DAPI, *blue*) was used as a nuclear counterstain. **(A)** CD31 localised with lymphocytes transmigrating by both the paracellular (*yellow arrowhead*) and transcellular (*yellow arrow*) route. Orthogonal merged images are shown in **(B)** from the visual fields in **(A)**, where transmigrating lymphocytes are indicated by the cross hairs. Scale bars represent 10 µm.

5.2.6 *PLVAP expression correlated with senescence markers and immune cell infiltrate in CLD and HCC*

To understand whether there is a link between PLVAP and senescence in CLD and HCC, gene expression data were obtained from matched patient samples via qRT-PCR or from TCGA databases, respectively. In CLD, expression of *CDKN1A* and *CDKN2A* showed a significant positive correlation with *PLVAP* expression (**Figure 5.20A**). Similarly, *CDKN2A* and *PLVAP* were also strongly correlated in HCC tumours, although there was no association observed between *CDKN1A* and *PLVAP* (**Figure 5.20B**). Notably, normal, non-tumour and tumour tissues seemed to cluster together, with normal tissues having the lowest *PLVAP/CDKN2A* levels and tumour tissues displaying the highest expression of *PLVAP/CDKN2A*.

To visualise the spatial localisation of senescent cells relative to fibrotic septa and PLVAP expression, immunohistochemistry for PLVAP and senescent markers, p21 and p16, along with Sirius red staining, were performed on serial liver sections from donor and CLD patients (**Figure 5.21**). Cells positive for p21 and p16 were spatially enriched within peri-fibrotic regions which coincided with PLVAP localisation (**Figure 5.21A**). Furthermore, quantification of staining highlighted a significant positive correlation between PLVAP and p21/p16 across a range of liver aetiologies (**Figure 5.21B**).

Given the limited accessibility of matched non-tumour and tumour tissue from HCC patients, the TCGA datasets were analysed to explore a potential link between *PLVAP* expression and immune infiltrate, using the ESTIMATE and TIMER online resources (**Figure 5.22**)[533]. *PLVAP* showed a weak positive correlation with the immune score and partially correlated with infiltration levels of $CD4^+$ and $CD8^+$ T cells, dendritic cells and neutrophils. To investigate whether immune infiltrate correlated with PLVAP in CLD, immunohistochemistry was performed in serial sections from CLD patients to visualise several leukocyte markers (**Figure 5.23**). MAC387 is an antibody (recognising S100A9 which forms calprotectin heterodimer with S100A8) that has previously been used as a marker of newly infiltrating monocytes[534, 535]. Whilst $MAC387^+$ cells were evenly distributed within normal liver, they showed an increased localisation and enrichment in the fibrotic regions of cirrhotic liver, positively correlating with

PLVAP expression. A similar spatial enrichment with PLVAP was also observed for $CD3^+$ and $CD20^+$ lymphocytes, although to a much lesser extent than MAC387. The incidence of $CD20^+$ B cells was low in most cases, except in liver sections from PBC patients in which B cell aggregates were frequently observed (**Appendix 7.7**). Whilst $CD3^+$ T cells (% area) positively correlated with PLVAP expression, no correlation was observed with $CD20^+$ B cells. Neutrophil elastase$^+$ (NE^+) neutrophils were not readily detected in neither normal nor cirrhotic liver sections. Collectively, these data suggest a link between PLVAP expression, senescence and infiltration of monocytes and lymphocytes during chronic liver inflammation.

5.2.7 PLVAP was upregulated in vivo in a murine model of senescence

There are several murine models of hepatic senescence which have been extremely valuable in allowing the study of senescence pathways and their biological impact *in vivo*. Mdm2 is a negative regulator of p53, and its deletion in hepatocytes ($\Delta Mdm2^{Hep}$) leads to p53 overexpression and induction of p21-mediated senescence. This model has previously been characterised to drive several hallmarks of senescence, including cell-cycle arrest (p21 expression), DNA damage (γH2A.X), lipofuscin accumulation (SA-β-Gal) and SASP production (IL1α), as well as considerable acute liver injury[259]. Given the upregulation of PLVAP expression during human chronic liver inflammation and cancer, and the associated senescent tissue microenvironment, immunohistochemistry was performed on murine liver sections from the $\Delta Mdm2^{Hep}$ senescence model. The widespread expression of PLVAP (MECA-32) in control mice was striking (**Figure 5.24**), which greatly contrasted that observed in normal human liver (**Figure 3.9**). Following induction of senescence via hepatocyte-specific deletion of *Mdm2* ($\Delta Mdm2^{Hep}$), there was a significant upregulation of PLVAP expression, with a staining area % increase from 9.29 ± 1.23% to 22.8 ± 3.32% (**Figure 5.24**). These data suggest that, *in vivo*, PLVAP is upregulated within a senescent tissue microenvironment in mouse liver, further supporting a link between hepatic senescence and PLVAP expression, and validating this murine model for future studies.

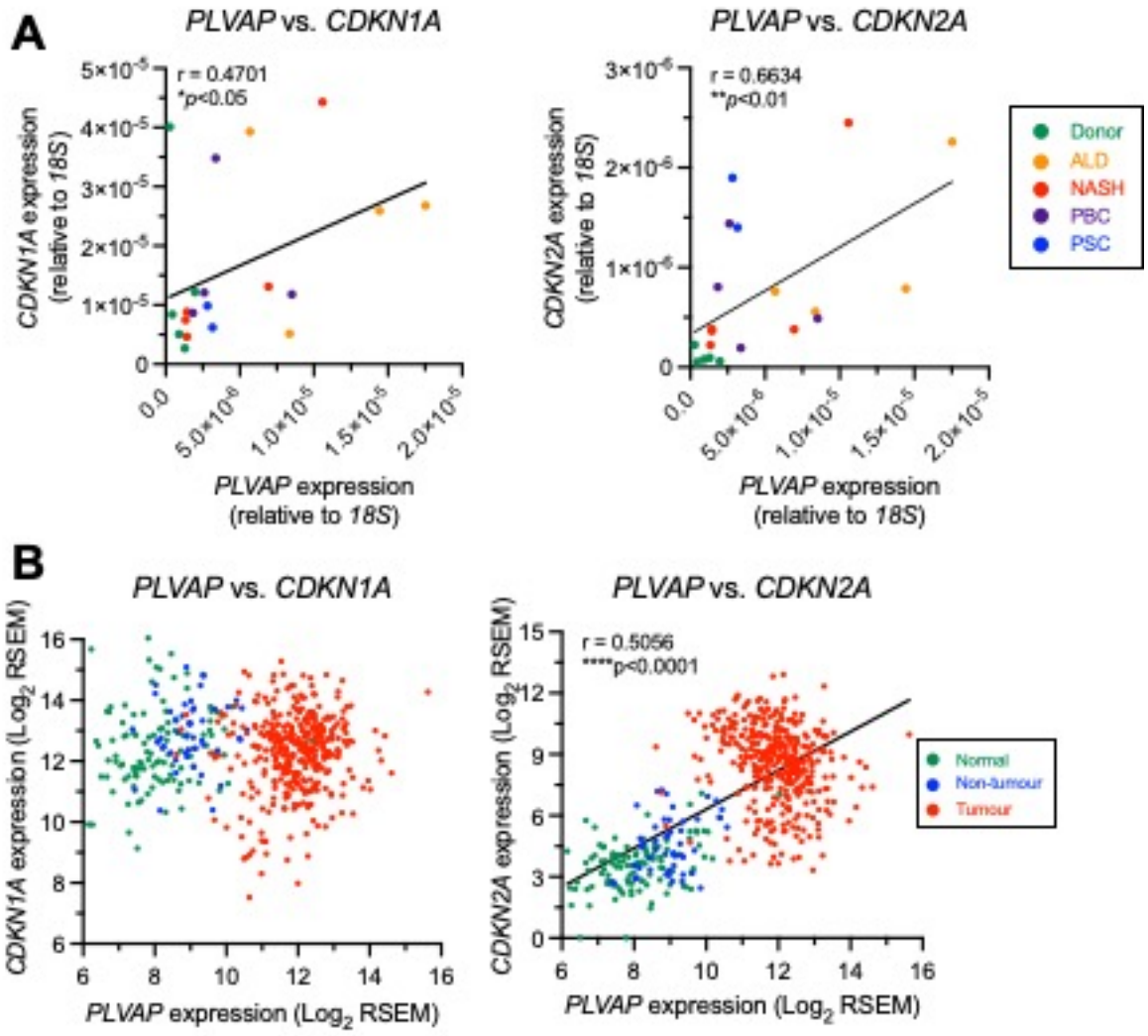

Figure 5.20: Expression of senescence markers, p21 (*CDKN1A*) and p16 (*CDKN2A*), correlated with *PLVAP* expression in chronic liver disease (CLD) and hepatocellular carcinoma (HCC).

(A) *CDKN1A*, *CDKN2A* and *PLVAP* expression was determined in whole liver lysates from donor and cirrhotic patients by qRT-PCR. Gene expression is shown relative to *18S* where each data point represents an independent patient sample (n=20). *PLVAP* showed a significant positive correlation with *CDKN1A* and *CDKN2A* expression in CLD (**p*<0.05, ***p*<0.01, Spearman's correlation test). **(B)** The Cancer Genome Atlas (TCGA) datasets were analysed for *CDKN1A* and *CDKN2A* gene expression in normal liver and matched non-tumour (NT) and tumour (T) tissues from HCC patients (n=529). *CDKN1A* and *CDKN2A* gene expression was then correlated with *PLVAP* expression (*****p*<0.0001, Spearman's correlation test).

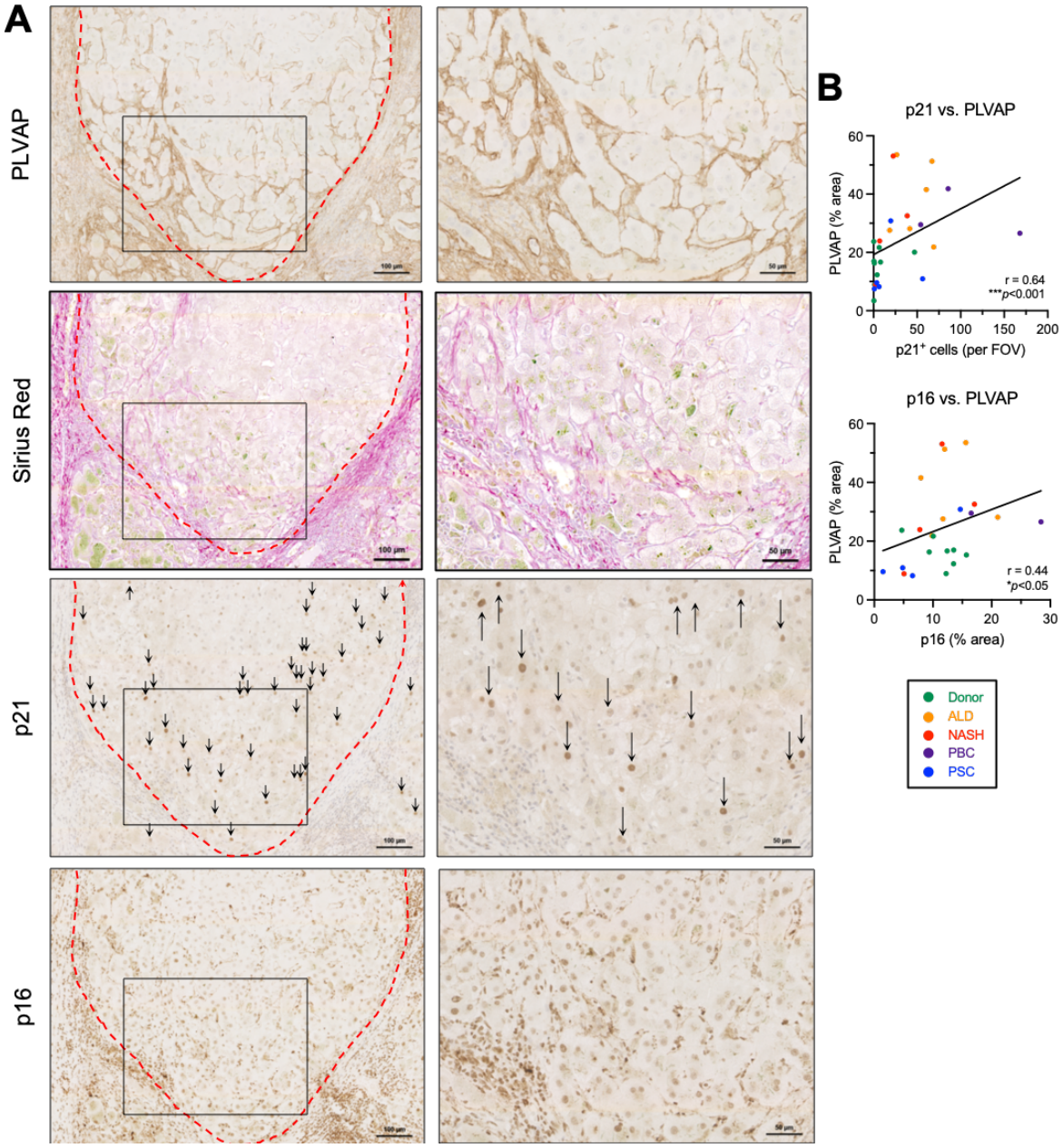

Figure 5.21: PLVAP correlated with senescence markers, p21 and p16, in cirrhotic human liver tissue.

(A) Representative images showing PLVAP, p21 (*black arrows*) and p16 relative to fibrotic septa (Sirius Red, *red dashed lines*) in serial liver sections from cirrhotic patients. Insets are shown (*right panels*). **(B)** Quantification of p21 (positive cells per field of view) (*upper*) and p16 staining (% area) (*lower*) against PLVAP (% area) in matched liver samples (*p<0.05, **p<0.01, Spearman's correlation test). Scale bars represent 100 µm (*left*) or 50 µm (*right*).

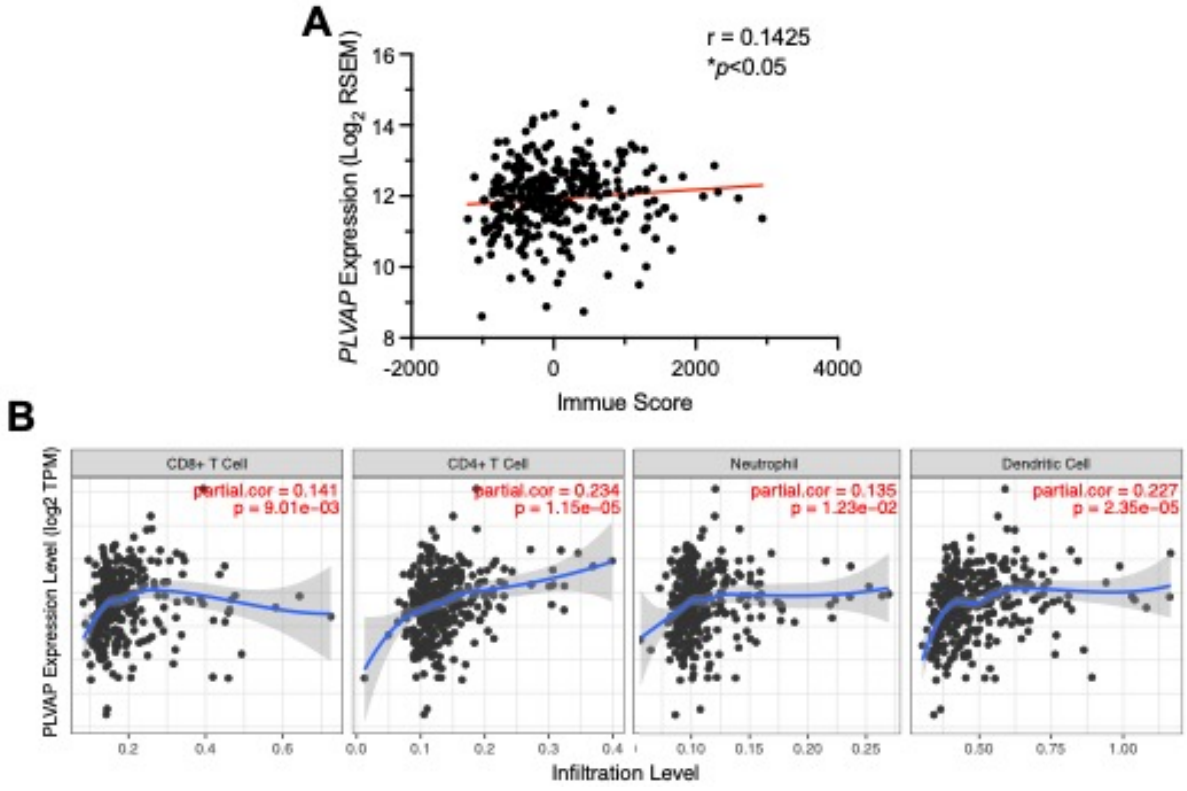

Figure 5.22: *PLVAP* expression positively correlated with immune score and infiltration level in hepatocellular carcinoma (HCC) tumours.

(A) *PLVAP* expression was plotted against immune score (**p*<0.05, Spearman's correlation) determined for each TCGA (The Cancer Genome Atlas) sample (n=319) using ESTIMATE (Estimation of STromal and Immune cells in MAlignant Tumor tissues using Expression data) https://bioinformatics.mdanderson.org/estimate/. Data shown are $\log_2$(RNAseq by Expectation-Maximum). **(B)** *PLVAP* expression showed partial positive correlation with infiltration level of $CD8^+$ T cells, $CD4^+$ T cells, neutrophils and dendritic cells, determined using TIMER (Tumour Immune Estimation Resource) which is available at https://cistrome.shinyapps.io/timer/.

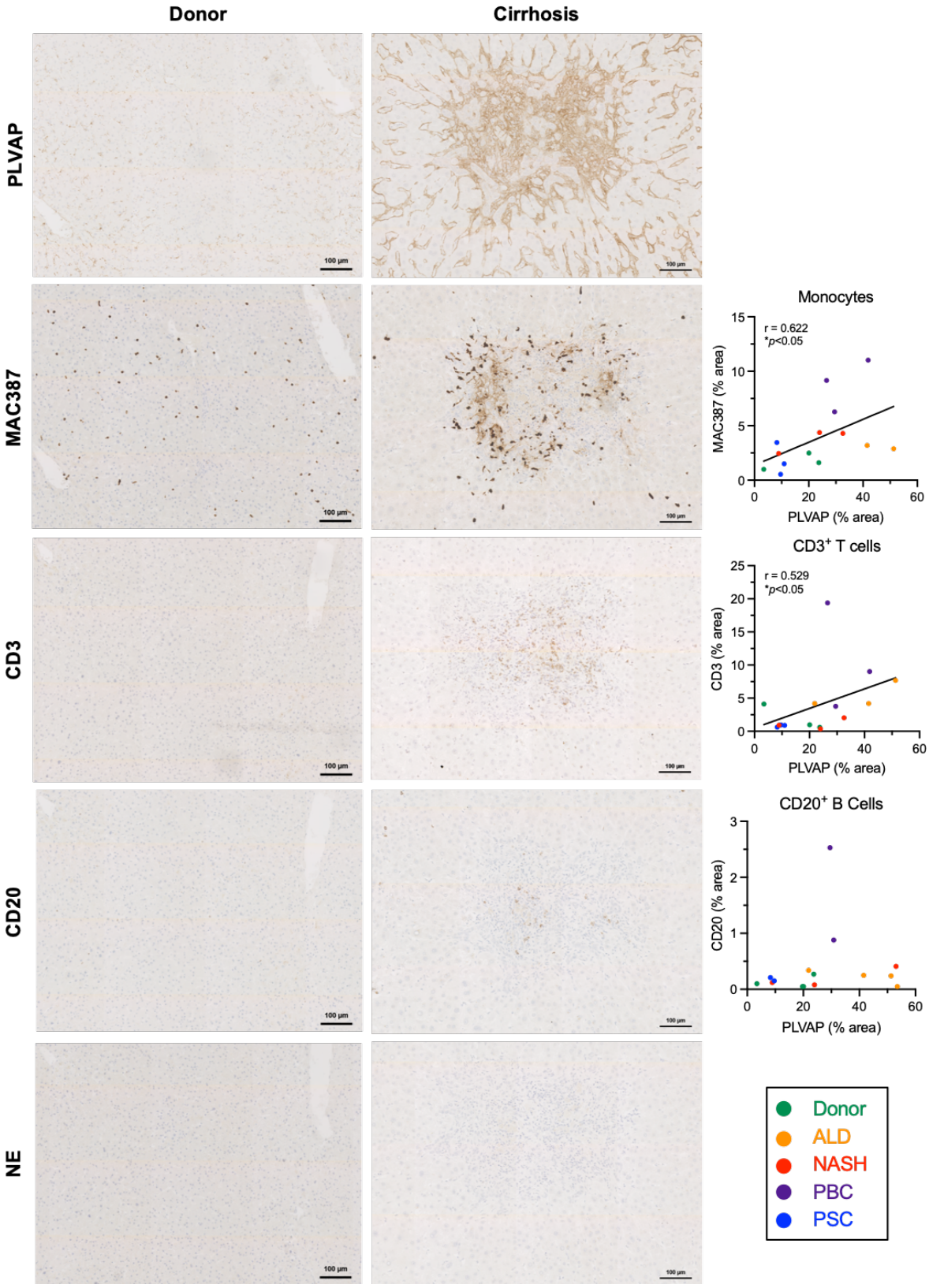

Figure 5.23: Plasmalemma vesicle-associated protein (PLVAP) correlated with immune cell infiltrate in chronic liver disease (CLD).

Figure legend continued on next page.

Immunohistochemistry for PLVAP, S100A9 (MAC387), CD3, CD20 and neutrophil elastase (NE) was undertaken in donor and cirrhotic liver serial sections from alcoholic liver disease (ALD), non-alcoholic steatohepatitis (NASH), primary biliary cholangitis (PBC) and primary sclerosing cholangitis (PSC) patients. Images shown are matched visual fields and are representative of normal (*left*) and cirrhotic (ALD) (*right*) samples. Graphs display correlation analysis of staining area (%), where each data point represents a matched independent patient sample (*p<0.05, Spearman's correlation test). Isotype control samples were negative and are shown in **Appendix 7.7**. Scale bars represent 100 µm.

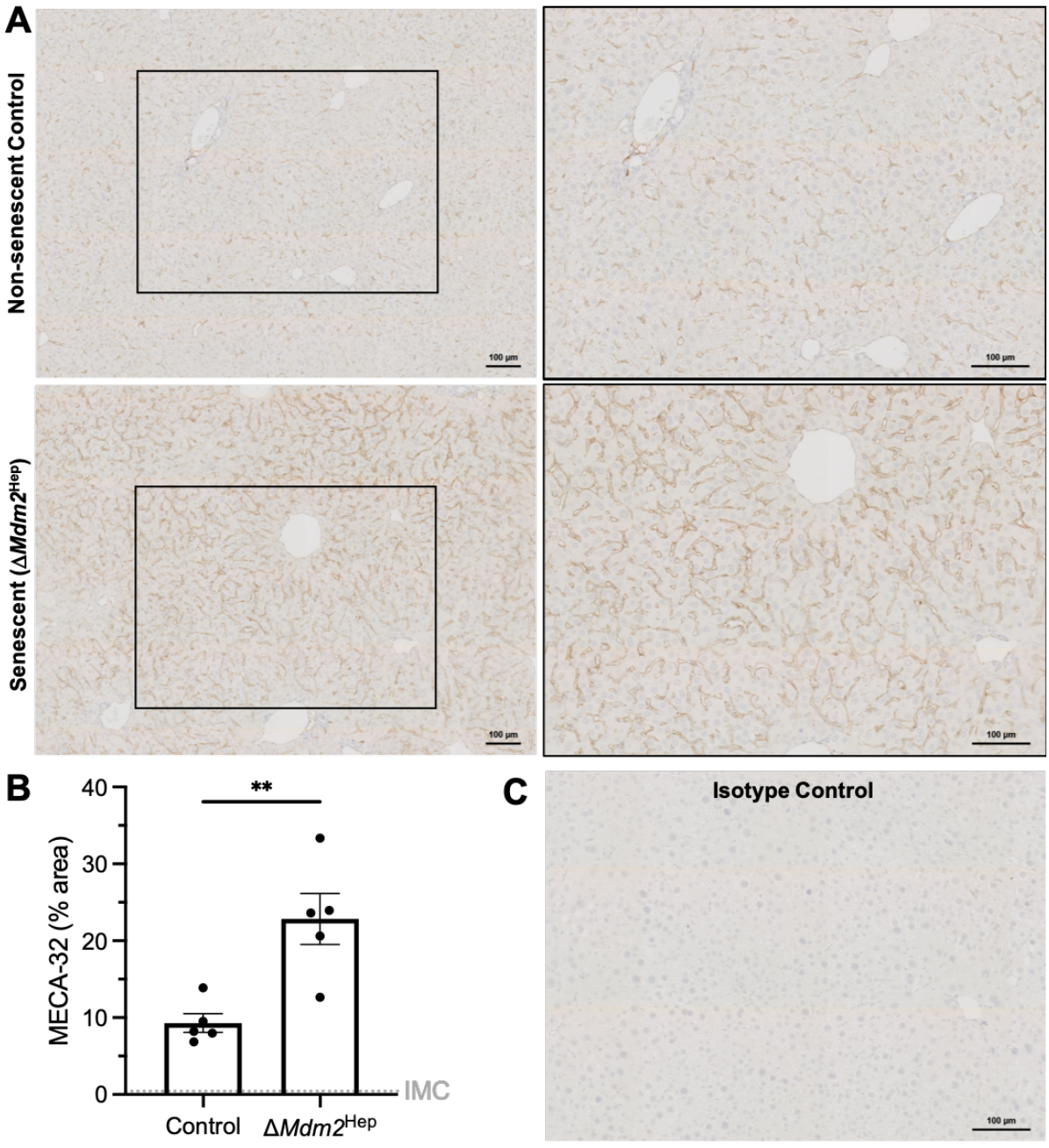

Figure 5.24: Expression of plasmalemma vesicle-associated protein (MECA-32) was upregulated following hepatocyte-specific deletion of p53 negative regulator, *Mdm2*.

(A-C) Immunohistochemistry was performed to stain for mouse PLVAP (MECA-32, *brown*) in the livers of senescent ($\Delta Mdm2^{Hep}$, n=5) and control (n=5) mice. **(B)** Staining area (%) was quantified for five visual fields per sample using ImageJ and data shown are mean ± SEM (**p<0.01, student's unpaired t-test). **(C)** Isotype control samples were negative. Scale bars represent 100 µm.

5.2.8 Monocyte, but not lymphocyte, transmigration across diseased HSEC was impaired following PLVAP inhibition

Since the senescent secretome drives both leukocyte recruitment and PLVAP expression in the sinusoidal endothelium, the contribution of PLVAP to SASP-mediated monocyte and lymphocyte recruitment was assessed by genetic manipulation or antibody-mediated blockade of PLVAP in primary HSEC. The successful knockdown of PLVAP following siRNA transfection was confirmed at the mRNA and protein level, by qRT-PCR and immunofluorescence, respectively (**Figure 5.25**). Following PLVAP genetic knockdown (siPLVAP) in CLD patient-derived HSEC (**Figure 5.26**), there was a small reduction in the number of transmigrated monocytes (0.73-fold ± 0.12) compared to the negative control (siControl), whilst monocyte adhesion and shape-changed numbers were unaffected. Moreover, the percentage of adhered monocytes which underwent shape-change was increased from 46 ± 3.06% to 55.5 ± 3.20%, and the fraction of adhered monocytes which transmigrated was significantly inhibited from 37.6 ± 1.88% to 26.1 ± 2.05%. Similarly, the number of transmigrated monocytes was significantly decreased in response to treatment with an anti-PLVAP antibody (0.60-fold ± 0.08), whilst there was also a slight decrease in the number of adhered monocytes (0.85-fold ± 0.046) (**Figure 5.27**). In addition, the percentage of adhered monocytes which had undergone transmigration was significantly inhibited from 31.1 ± 2.17% to 21.5 ± 2.77% following PLVAP blockade, whereas the % shape-change was significantly enhanced from 45.4 ± 3.21 to 57.2 ± 3.69%. Following the flow assay cells were then fixed and stained for PLVAP and junctional marker VE-cadherin (**Figure 5.28**). Although monocytes frequently transmigrated through the junctions of $PLVAP^{+}$ HSEC, there did not seem to be any PLVAP enrichment around transmigrating monocytes, as was observed with CD31. Therefore, PLVAP inhibition impairs SASP-mediated monocyte recruitment in diseased HSEC, but does not seem to localise with transmigrating monocytes.

Similar experiments were next performed with HSEC derived from donor livers, and interestingly, PLVAP genetic knockdown did not affect SASP-mediated monocyte adhesion, shape-change or transmigration compared to the negative control, despite successful *PLVAP* mRNA knockdown

efficiency (**Figure 5.29**). Likewise, there were no significant differences in monocyte adhesion, shape-change or transmigration following antibody-mediated PLVAP inhibition in donor HSEC, although there was a decreasing trend in the percentage transmigration compared to the IMC from 32.1 ± 2.51% to 26.8 ± 1.45% (**Figure 5.30A, B**). The successful binding of the PLVAP antibody was confirmed by quantification of the % staining area following fixation, permeabilisation and staining of treated cells with an anti-mIgG1 AF488 secondary antibody (**Figure 5.30C**). Thus, the extent of inhibition, if any, on SASP-mediated monocyte transmigration across donor HSEC following PLVAP blockade was considerably less than that observed in patient-derived HSEC.

To understand whether the impact of PLVAP inhibition on SASP-mediated transmigration was a monocyte-specific effect, flow assays were also performed with peripheral blood lymphocytes following PLVAP knockdown or antibody treatment. Notably, the number of adhesion events per visual field were substantially less than those for monocytes, even in the presence of double the SASP concentration (**Figure 5.31A**). Nevertheless, in response to siPLVAP transfection, there were no differences observed in the numbers of adhered or shape-changed lymphocytes, nor were there any changes in the proportion of adhered cells which underwent shape-change or transmigration (**Figure 5.31B**). There was a slight reduction in absolute numbers of lymphocyte transmigration events by 0.9-fold (± 0.06) but this did not reach statistical significance. Following treatment with an anti-PLVAP antibody, lymphocyte adhesion was unaffected, whilst lymphocyte shape-change and transmigration were slightly decreased (0.9-fold ± 0.10) and increased (1.12-fold ± 0.11), respectively, although these changes were not statistically significant (**Figure 5.32**). There was also a reduction in the % shape-changed lymphocytes from 32.8 ± 2.54% to 26.9 ± 3.14% and a significant increase in the % transmigration from 37.3 ± 1.89% to 44.1 ± 2.34%. Therefore, these data suggest that PLVAP is specifically involved in SASP-mediated monocyte recruitment whilst having minimal contribution to lymphocyte recruitment in response to the senescent secretome.

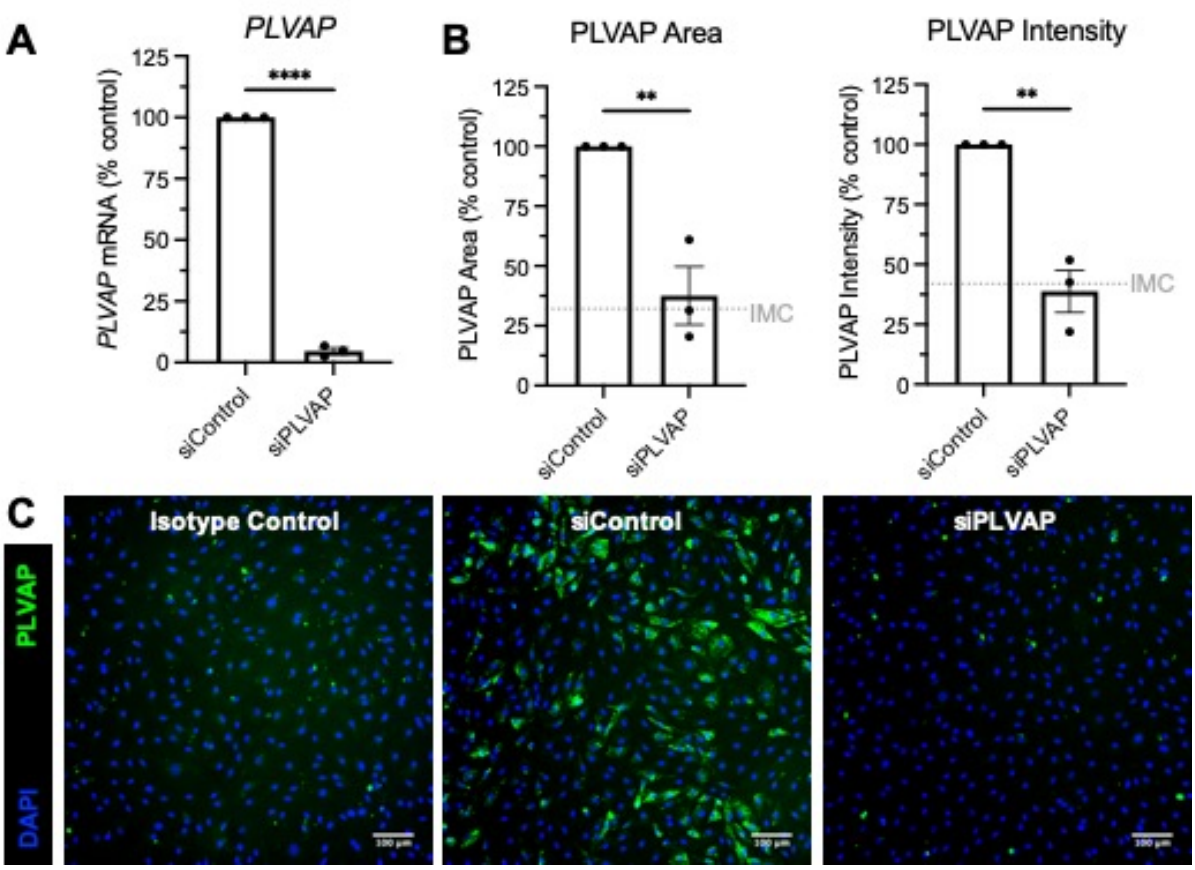

Figure 5.25: Genetic knockdown of plasmalemma vesicle-associated protein (PLVAP) via short-interfering RNA (siRNA) transfection was successful at the gene and protein level.

(A-C) Hepatic sinusoidal endothelial cells were treated for four hours with siRNA (3.125 nM) targeted against *PLVAP* (siPLVAP) or a negative control (siControl) and then cultured in antibiotic- and growth factor-free medium for 48 hours before assessment of knockdown. **(A)** *PLVAP* mRNA was measured by qRT-PCR and gene expression, relative to *GAPDH*, was normalised to a % of the control (****p<0.0001, student's unpaired t-test). **(B)** PLVAP protein expression was determined by immunocytochemistry followed by high-content imaging (**p<0.01, student's unpaired t-test). Fluorescence area and intensity were normalised to a % of the control. Representative images are shown in **(C)**. 4′,6-diamidino-2-phenylindole (DAPI, *blue*) was used as a nuclear counterstain. Fluorescence levels in siPLVAP-treated HSEC were comparable to isotype controls. Data shown are mean ± SEM for three independent HSEC isolates. Scale bars represent 100 μm.

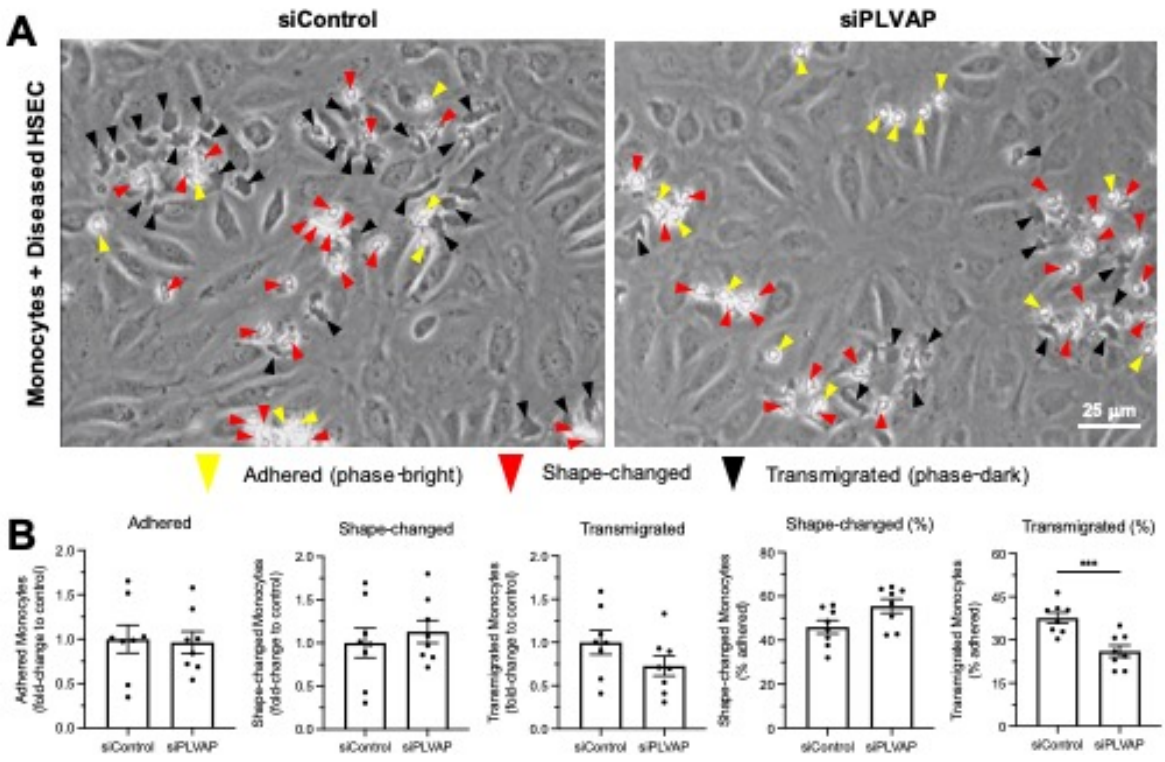

Figure 5.26: Genetic knockdown of plasmalemma vesicle-associated protein (PLVAP) impaired monocyte transmigration across diseased hepatic sinusoidal endothelial cells (HSEC) in response to the senescent secretome.

(A, B) Flow adhesion assays were performed with Ras-CM stimulated HSEC and monocytes isolated from healthy volunteer peripheral blood following siRNA transfection (siPLVAP) or transfection with a negative control (siControl). Representative phase-contrast images are shown in **(A)**. **(B)** The number of adhered (*yellow arrowheads*), shape-changed (*red arrowheads*) and transmigrated (*black arrowheads*) monocytes were quantified in ten visual fields per lane with each condition performed in duplicate. Data shown are mean ± SEM from four independent experiments (***p<0.001, student's unpaired t-test). Scale bar represents 25 µm.

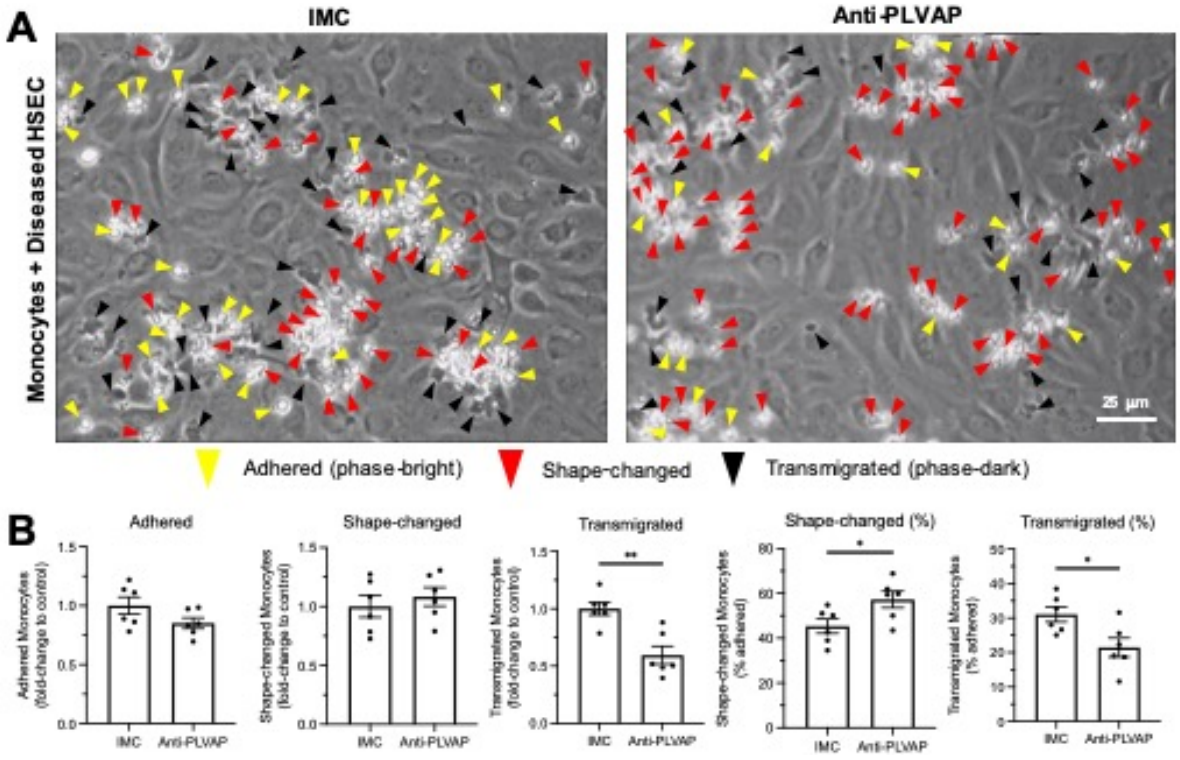

Figure 5.27: Antibody-mediated blockade of plasmalemma vesicle-associated protein (PLVAP) impaired monocyte transmigration across diseased hepatic sinusoidal endothelial cells (HSEC) in response to the senescent secretome.

(A, B) Flow adhesion assays were performed with Ras-CM stimulated HSEC and monocytes isolated from healthy volunteer peripheral blood following treatment with an anti-PLVAP antibody (or isotype-matched control, IMC). Representative phase-contrast images are shown in **(A)**. **(B)** The number of adhered (*yellow arrowheads*), shape-changed (*red arrowheads*) and transmigrated (*black arrowheads*) monocytes were quantified in ten visual fields per lane with each condition performed in duplicate. Data shown are mean ± SEM from three independent experiments (*p<0.05, **p<0.01, student's unpaired t-test). Scale bar represents 25 µm.

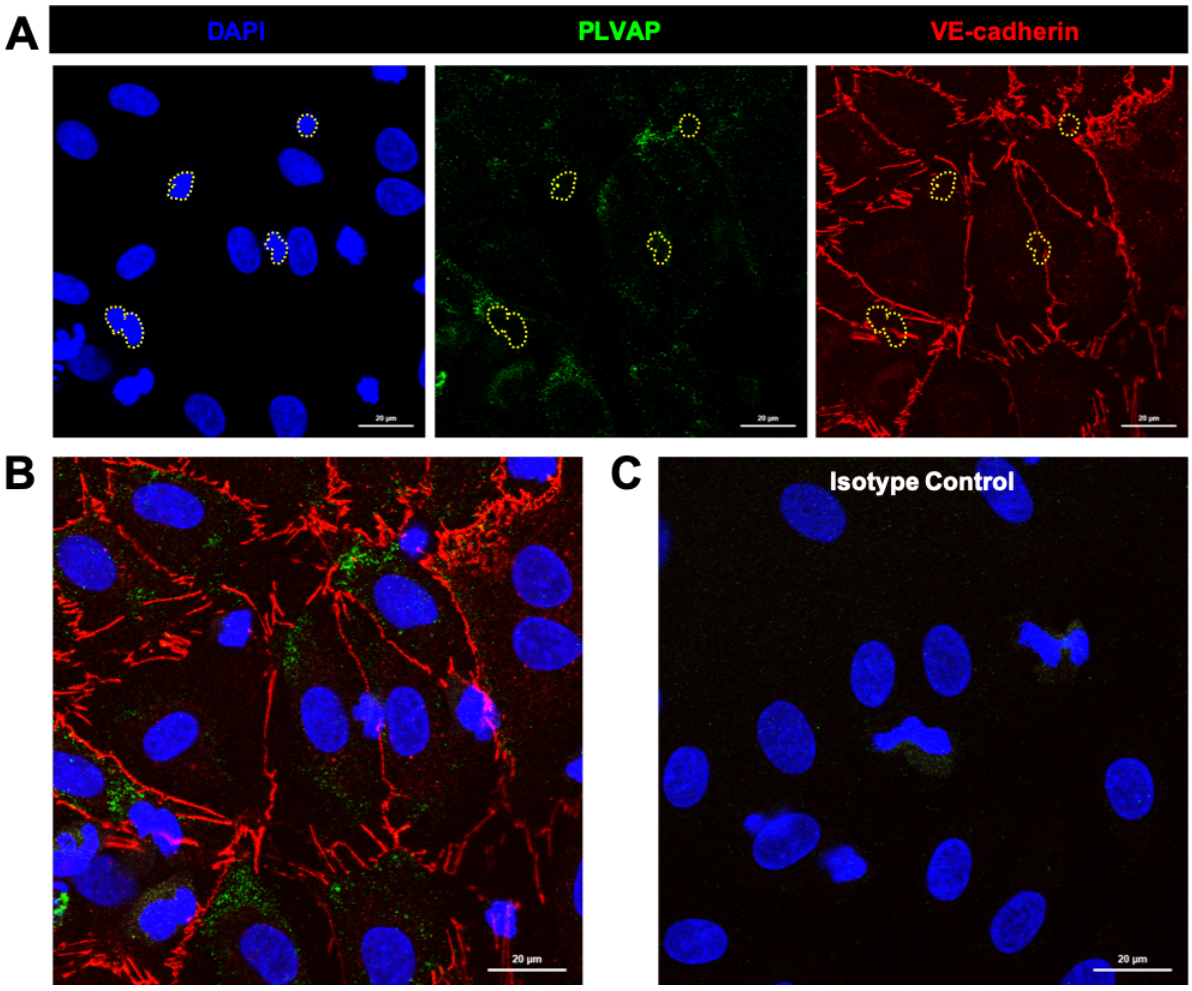

Figure 5.28: Monocytes often transmigrated through plasmalemma vesicle-associated protein$^+$ (PLVAP) hepatic sinusoidal endothelial cells (HSEC) but there did not seem to be any specific PLVAP localisation during this process.

(A, B) Flow adhesion assays were performed with Ras-CM stimulated HSEC and monocytes isolated from healthy volunteer peripheral blood. Cells were then fixed and stained for PLVAP (*green*) and vascular endothelial (VE)-cadherin (*red*). 4′,6-diamidino-2-phenylindole (DAPI, *blue*) was used as a nuclear counterstain. Transmigrating monocytes are indicated by the yellow dashed lines and a merged image for the visual fields in **(A)** is shown in **(B)**. **(C)** Isotype control samples were negative. Scale bars represent 20 µm.

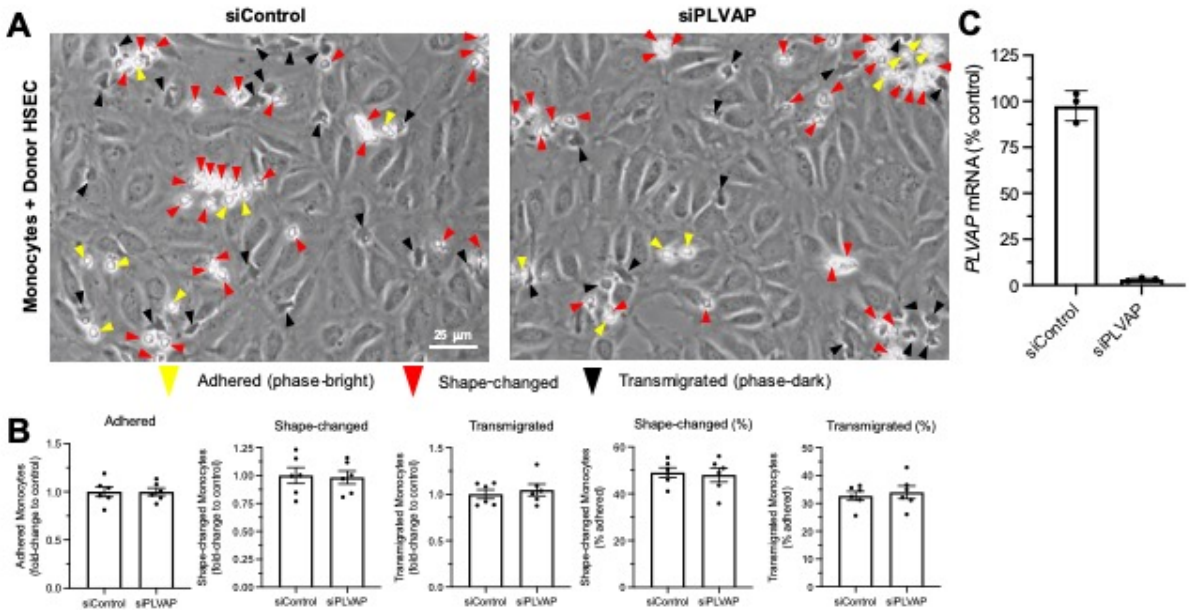

Figure 5.29: Genetic knockdown of plasmalemma vesicle-associated protein (PLVAP) in donor hepatic sinusoidal endothelial cells (HSEC) did not affect monocyte recruitment in response to the senescent secretome.

(A, B) Flow adhesion assays were performed with Ras-CM stimulated HSEC and monocytes isolated from healthy volunteer peripheral blood following siRNA transfection (siPLVAP) or transfection with a negative control (siControl). Representative phase-contrast images are shown in **(A)**. **(B)** The number of adhered (*yellow arrowheads*), shape-changed (*red arrowheads*) and transmigrated (*black arrowheads*) monocytes were quantified in ten visual fields per lane with each condition performed in duplicate. Data shown are mean ± SEM from three independent experiments. **(C)** Where possible, genetic knockdown of PLVAP was confirmed at the mRNA level by qRT-PCR. Scale bar represents 25 µm.

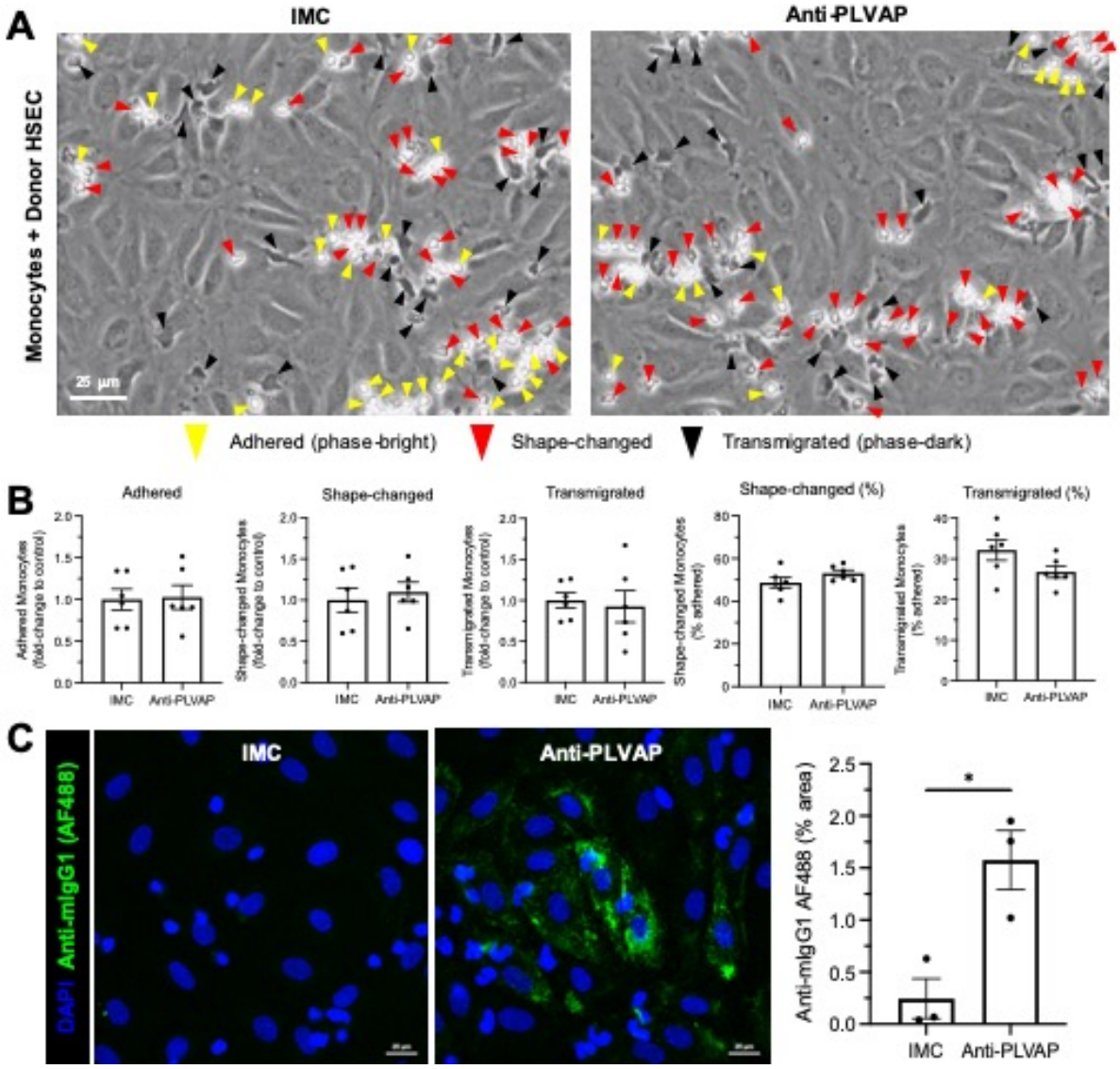

Figure 5.30: Antibody-mediated blockade of plasmalemma vesicle-associated protein (PLVAP) slightly reduced monocyte transmigration across donor hepatic sinusoidal endothelial cells (HSEC) in response to the senescent secretome.

(A, B) Flow adhesion assays were performed with Ras-CM stimulated HSEC and monocytes isolated from healthy volunteer peripheral blood following treatment with an anti-PLVAP antibody (or isotype-matched control, IMC). Representative phase-contrast images are shown in **(A)**. **(B)** The number of adhered (*yellow arrowheads*), shape-changed (*red arrowheads*) and transmigrated (*black arrowheads*) monocytes were quantified in ten visual fields per lane with each condition performed in duplicate. Data shown are mean ± SEM from three independent experiments. Scale bars represent **(A)** 25 µm or **(C)** 20 µm.

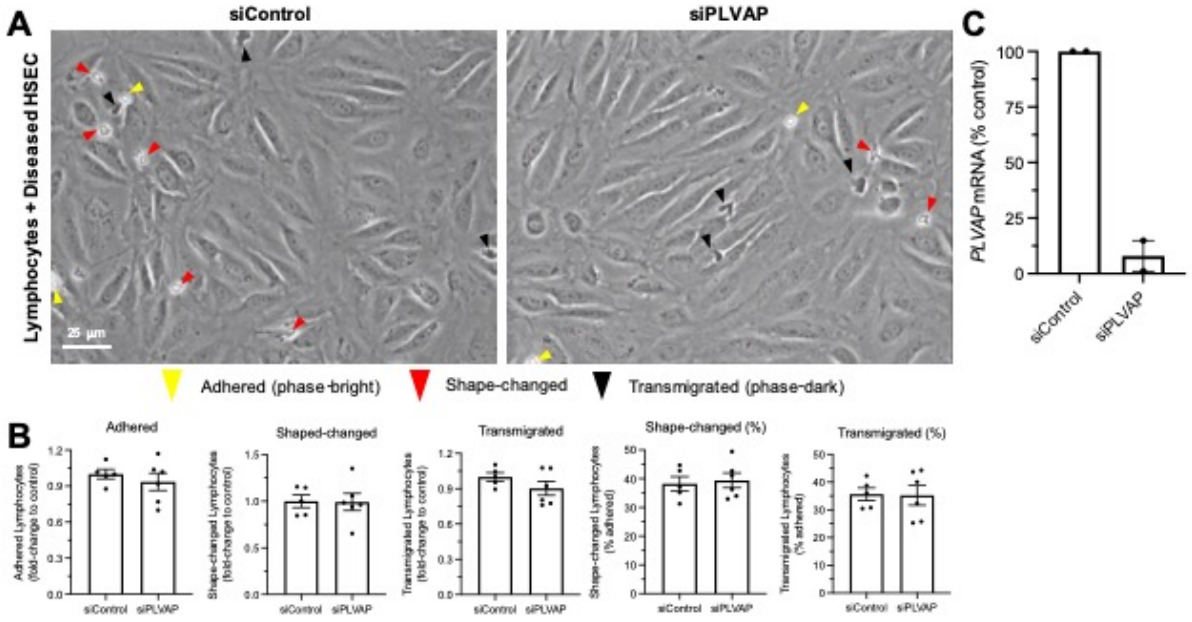

Figure 5.31: Lymphocyte recruitment across diseased hepatic sinusoidal endothelial cells (HSEC) in response to the senescent secretome was unaffected by plasmalemma vesicle-associated protein (PLVAP) genetic knockdown.

(A, B) Flow adhesion assays were performed with Ras-CM stimulated HSEC and lymphocytes isolated from healthy volunteer peripheral blood following siRNA transfection (siPLVAP) or transfection with a negative control (siControl). Representative phase-contrast images are shown in **(A)**. **(B)** The number of adhered (*yellow arrowheads*), shape-changed (*red arrowheads*) and transmigrated (*black arrowheads*) lymphocytes were quantified in ten visual fields per lane with each condition performed in duplicate. Data shown are mean ± SEM from three independent experiments. **(C)** Where possible, genetic knockdown of PLVAP was confirmed at the mRNA level by qRT-PCR. Scale bar represents 25 µm.

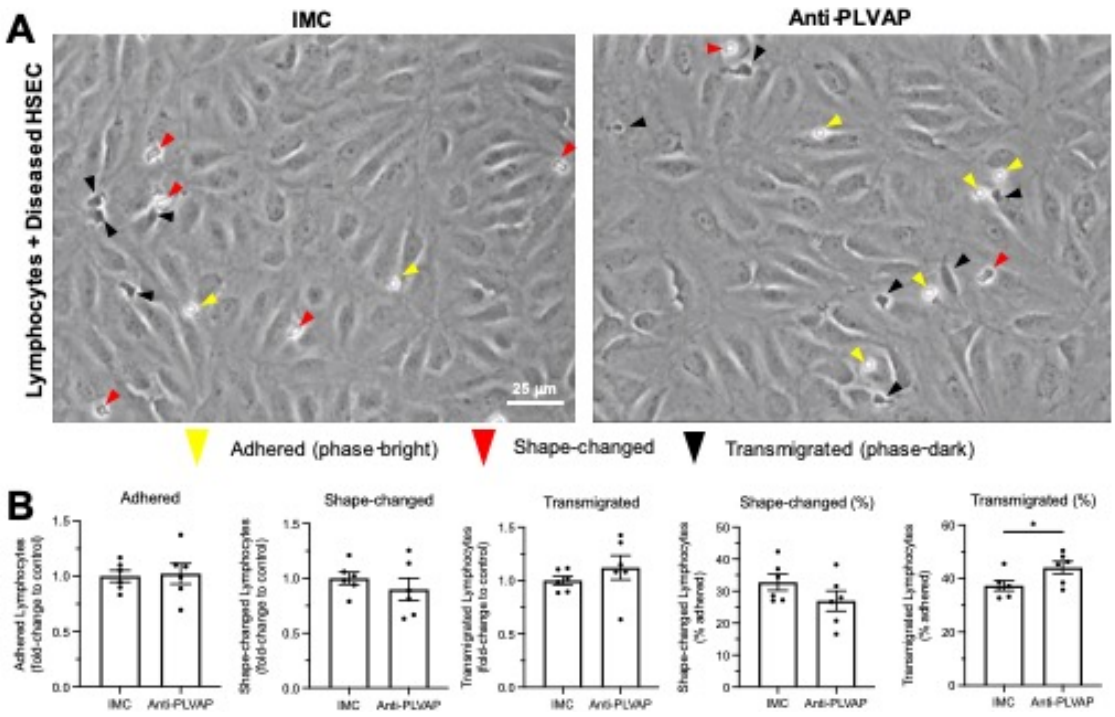

Figure 5.32: Antibody-mediated blockade of plasmalemma vesicle-associated protein (PLVAP) did not impair lymphocyte transmigration across diseased hepatic sinusoidal endothelial cells (HSEC) in response to the senescent secretome.

(A, B) Flow adhesion assays were performed with Ras-CM stimulated HSEC and lymphocytes isolated from healthy volunteer peripheral blood following treatment with an anti-PLVAP antibody (or isotype-matched control, IMC). Representative phase-contrast images are shown in **(A)**. **(B)** The number of adhered (*yellow arrowheads*), shape-changed (*red arrowheads*) and transmigrated (*black arrowheads*) lymphocytes were quantified in ten visual fields per lane with each condition performed in duplicate. Data shown are mean ± SEM from three independent experiments (**p*<0.05, student's unpaired *t*-test). Scale bar represents 25 µm.

5.2.9 Summary

- Senescence was observed as a key feature of CLD and HCC, correlating with PLVAP expression and immune infiltrate in human patient samples
- The senescent cell secretome influenced HSEC phenotype and function, driving recruitment of monocytes and lymphocytes via distinct molecular mechanisms
- Senescent cell-endothelial crosstalk drove expression of PLVAP, in human primary HSEC *in vitro*, and in a Δ*Mdm2*^{Hep} mouse model of senescence *in vivo*
- PLVAP was identified to play a specific role in SASP-mediated monocyte transmigration, whilst its contribution to lymphocyte recruitment was minimal, further highlighting the molecular distinction of these two processes

6 DISCUSSION

6.1 Expression of MR and PLVAP in human liver tissue

6.1.1 The expression of MR and PLVAP in non-diseased human liver

In **Chapter 3**, the expression of MR and PLVAP in normal and diseased human liver tissue was characterised, using immunohistochemical and molecular approaches. Within normal liver, MR was highly expressed in the hepatic sinusoids, present within both Kupffer cells and the sinusoidal endothelium. This is consistent with recently published single-cell RNA sequencing data which demonstrated *MRC1* gene expression in mononuclear phagocyte and endothelial cell fractions of the human liver[397]. In this study, of the mononuclear phagocyte populations, KCs demonstrated the highest *MRC1* expression, whilst expression in tissue monocytes was negligible. *MRC1* expression was also highlighted in some conventional DC populations, although to a much lesser extent than KCs. Moreover, *MRC1*-expressing endothelial cells were characterised as having a liver sinusoidal phenotype, co-expressing *CLEC4M* (L-SIGN), *LYVE-1*, *CLEC4G*, *STAB2* and *CD14* whilst definitively lacking in *CD34*. Another recent single-cell study confirmed this sinusoidal genetic signature and identified additional endothelial genes including *FLT1, PECAM1*, and *VWF*[67]. These gene expression data are corroborated by findings from dual immunofluorescence studies detailed within **Chapter 3**, which show co-localisation of MR and L-SIGN/LYVE-1, and lack of CD34, in the hepatic sinusoidal endothelium.

In contrast to MR, PLVAP was expressed only at very low levels in normal human liver. This expression appeared to be restricted to larger vessels (perhaps branches of the portal and central veins) and peri-portal sinusoids, a finding which is in keeping with previous reports[438, 536]. It is interesting to consider the lack of PLVAP within peri-central sinusoids in the context of liver zonation and Wnt signalling. Indeed, research surrounding the role of PLVAP in the BBB and BRB have implicated β-catenin/Wnt canonical signalling in the negative regulation of PLVAP[452]. Generally, in PLVAP-expressing non-barrier endothelium, the absence of Wnt and Norrin ligands means that the canonical β-catenin signalling pathway is inactive due to phosphorylation of the β-catenin destruction complex. In the case

of barrier endothelium, the presence of Wnt and Norrin ligands and subsequent β-catenin signalling inhibits PLVAP expression and is integral for maturation of the BBB/BRB. As such, the presence of PLVAP in barrier tissues is indicative of vascular leakage, characterising multiple pathologies including diabetic retinopathy, brain ischaemia and brain tumours[455]. This is supported by *in vitro* studies which demonstrate that *PLVAP* gene expression is downregulated by Wnt/Norrin ligands, such as Wnt3a and LiCl (glycogen synthase kinase 3 inhibitor), and upregulated by inhibitor of β-catenin activity, ICRT-3[509]. Furthermore, studies in mice have shown that PLVAP is upregulated in CNS-associated endothelial cells following knockout or antibody-mediated blockade of Frizzled4 and β-catenin, whilst a gain of function mutation in β-catenin led to reduced PLVAP[501, 502, 507, 537]. With this in mind, it is possible that PLVAP expression in normal human liver is inhibited within peri-central sinusoids due to increased Wnt signalling. Alternatively, others have suggested that the presence of PLVAP in normal liver is not due to sinusoidal expression, but rather expression within a distinct subset of capillaries which form a network to supply the hepatic artery and surrounding bile ducts[536]. This network is known as the peribiliary capillary plexus which has been shown to express vasoactive proteins, such as eNOS and ET-1, as well as CD34[538]. Future work to incorporate these additional markers, including biliary markers, into immunohistochemistry studies would investigate this further.

Immunohistochemistry, detailed in **Chapter 5** and by others, in murine tissues highlighted a drastic distinction between species with regard to PLVAP expression. This divergence in PLVAP expression between normal human and mouse liver is striking. As shown in control mice from senescence models, PLVAP (also known as MECA-32) was present throughout the hepatic sinusoids. This is consistent with previous work which indicates PLVAP is highly expressed in the portal and central veins, as well as within peri-portal, mid-lobular and peri-central sinusoids, albeit to a lesser extent[444]. Notably, peri-central sinusoids were found to have the lowest PLVAP expression, although this was not significantly different from that observed in the other sinusoidal zones. Another noteworthy observation is the phenotypic distinction between $PLVAP^{+}$ liver endothelial cells in mice and humans; that is, co-localisation of PLVAP and LYVE-1 in murine liver sinusoids which was not observed in humans[444]. In

mice, the role of PLVAP in the formation of fenestral and stomatal diaphragms has been extensively studied, and in the liver, these structures are prominent during foetal development[444, 445]. After birth, fenestral diaphragms are lost, yet PLVAP expression on the HSEC surface was maintained throughout adulthood. Furthermore, the formation of fenestrations was unaltered, and the contribution of stomatal diaphragms to the presence of PLVAP was considered minimal since PLVAP expression was comparable in caveolin-1-deficient mice which lack all caveolae[444]. Whether this is the case in the human foetal liver is yet to be confirmed, and will remain a challenge due to the ethical and logistical constraints surrounding the use of human foetal tissue in scientific research. Nevertheless, one recent study has utilised scRNA-seq to investigate the genetic landscape of the human foetal liver, in particular the enrichment of $PLVAP^{+}$ endothelial cells which are absent in normal adult liver[398]. These data not only validate observations made in this thesis in humans, it also highlights clear species differences which must be considered when interpreting *in vivo* data regarding PLVAP.

In summary, whilst single-cell sequencing studies have documented MR and PLVAP expression in human liver at the gene level, and other groups have characterised their presence in alternative tissues and cell types, to our knowledge this is the first extensive characterisation of MR and PLVAP in human hepatic endothelium.

6.1.2 The expression of MR and PLVAP in cirrhotic human liver

The expression of MR and PLVAP in cirrhotic liver tissue was investigated in samples obtained from ALD, NASH, PBC and PSC patients and compared with normal tissue from donor livers. Whereas MR was abundantly expressed in normal liver tissue, in CLD MR was significantly downregulated, particularly in areas proximal to fibrotic septa. This occurred independently of the patient aetiology, which is suggestive of a common regulatory pathway in liver pathology (such as fibrosis), as opposed to a disease-specific mechanism. Given the co-localisation of MR with sinusoidal markers L-SIGN and LYVE-1, this could suggest a universal disruption in the sinusoidal phenotype during chronic inflammation and fibrosis, a phenomenon known as sinusoidal capillarisation. During capillarisation, HSEC undergo substantial phenotypic alterations, including loss of fenestrations, basement membrane

synthesis, loss of sinusoidal markers and upregulation of vascular endothelial markers such as CD31 and CD34[76]. Consistent with this, expression of L-SIGN and LYVE-1 was also reduced in these areas. These findings are supported by human scRNA-seq studies which report a significant reduction in the fraction of endothelial cells which display a sinusoidal phenotype (*CLEC4M*$^+$*CLEC4G*$^+$*LYVE1*$^+$*CD14*$^+$*STAB2*$^+$*MRC1*$^+$) in liver cirrhosis[397]. Disrupted MR expression in CLD could therefore represent one of the many phenotypic changes during HSEC capillarisation.

MR was also shown to localise within fibrotic septa. These MR$^+$ cells were distinct from sinusoidal endothelium in that they did not co-localise with L-SIGN and LYVE-1, and were also found to be CD68-negative unlike the CD68$^+$ KCs residing within the hepatic sinusoids. Staining with additional markers also showed this population was negative for CD31, CD34 and vimentin. These data suggest that cells belonging to this MR$^+$ scar-associated population are not endothelial cells or CD68$^+$ macrophages, but their identity remains an area for future research. For instance, there are certain subsets of monocytes and monocyte-derived macrophages that do not express CD68. Instead, they express an array of markers depending on their origin and activation status, including CD14, CD16, CCR2, CD163, MERTK and CX_3CR1[539]. Single-cell sequencing technology has also identified novel scar-associated macrophage markers including *TREM2* and *CD9*[397]. Future work would incorporate a selection of these myeloid markers in order to identify and characterise hepatic scar-associated MR$^+$ cell populations.

Once again in contrast to MR, PLVAP expression was significantly upregulated in CLD-patient derived samples, both at the gene and the protein level, independently of aetiology. Furthermore, PLVAP localised within and proximal to fibrotic septa, displaying a significant positive correlation with the extent of collagen deposition and fibrosis in matched patient samples. These observations are consistent with a recent study of hepatitis-C-positive cirrhotic patients, which demonstrated a proportional upregulation of PLVAP expression with more advanced disease (Child-Pugh Grade A – bridging fibrosis vs. Child-Pugh Grade C – decompensated cirrhosis)[536]. As with MR, the consistency of these observations across multiple aetiologies suggest a generic pathway of PLVAP upregulation during chronic inflammation and/or fibrosis. The expansion of two distinct *PLVAP*$^+$ scar-associated endothelial

cell populations within the fibrotic niche of human cirrhosis has been described recently[397]. As was also shown in **Chapter 3**, these cells were positive for *CD34*, a factor which distinguished this population from sinusoidal endothelial cells. Additional staining confirmed the non-sinusoidal phenotype of these cells, including lack of L-SIGN and LYVE-1 expression and co-localisation with CD31 and vimentin, along with CD34. Immunohistochemical staining highlighted a clear localisation of PLVAP to neovessels within fibrous septa which co-express CD34. Consistent with this, previous reports have identified a circulating population of $CD34^{+}VEGFR2^{+}$ endothelial precursors that also express haematopoietic stem cell marker AC133, which migrate in response to SDF-1 and VEGF via CXCR4[540]. These cells are therefore thought to play a role in neo-vascularisation and angiogenesis. Interestingly, PLVAP has also been implicated in angiogenesis, both in the developing foetal liver and during pathologies such as diabetic retinopathy and cancer[444, 454, 457]. Despite being eluded to in previous studies[457, 536], a definitive functional role for PLVAP in angiogenesis during CLD remains to be confirmed.

As discussed above, HSEC undergo capillarisation during CLD which is thought to precede inflammation and fibrosis. PLVAP may therefore act as a biomarker of capillarisation as has been suggested previously[536]. It has also been proposed that PLVAP is closely associated with caveolae of capillarised liver endothelial cells, perhaps localised within these structures, as indicated by immunoelectron microscopy[536]. This is supportive of the fluorescent immunohistochemical data presented in **Chapter 3**, which showed partial co-localisation of caveolin-1 and PLVAP in cirrhotic liver tissue. Yet, caveolin-$1^{+}PLVAP^{-}$ endothelium was also frequently observed, suggesting PLVAP is not generically associated with all caveolae, *per se*. Whether PLVAP acts as a molecular component of stomatal diaphragms associated with caveolae in capillarised HSEC still remains unclear.

The role of activated myofibroblasts in orchestrating liver fibrosis is well-established[541]. In addition to capillarisation, some endothelial cells have also been shown to adopt a more mesenchymal-like phenotype in CLD, a phenomenon referred to as endothelial-to-mesenchymal transition (EndMT). These cells have been shown to co-express CD31, αSMA and collagens and are suggested to represent a source

of mesenchymal cells in fibrotic disease[472-474]. These observations also coincided with increased expression of transcription factors zinc-finger E-box binding homeobox 1 (Zeb1) and Snail1, both of which are implicated in acquisition of a mesenchymal-like phenotype[472]. This process was stimulated by TGFβ treatment *in vitro*, whilst BMP-7 significantly inhibited EndMT both *in vitro* and *in vivo*. In our CLD patient cohort, PLVAP showed partial co-localisation with CD31 and collagen III, but did not seem to co-localise with αSMA, which was prominent in larger vessels and within fibrotic septa. Furthermore, PLVAP also co-localised with vimentin, a protein highly expressed in hepatic mesenchymal and endothelial cells but largely absent from HSEC[397]. These data could suggest that $PLVAP^+$ cells represent an endothelial population which has undergone EndMT since they have both endothelial and mesenchymal characteristics. However, one alternative explanation for the partial colocalisation of PLVAP and collagen III could be due to the presence of collagens within the space of Disse, where HSEC lie within close proximity. This possibility is supported by scRNA-seq data which demonstrates an enrichment of *COL3A1* gene expression in myofibroblasts within cirrhotic liver but minimal expression in endothelia (aside from a handful of scar-associated endothelial cells)[397]. This is contradictive of immunofluorescence shown in **Chapter 3**, which presented an apparent sinusoidal staining pattern of collagen III; this localisation could be due to basement membrane synthesis and collagen deposition by activated stellate cells rather than expression of collagen III by HSEC. Whether PLVAP-expressing cells have undergone EndMT and therefore contribute to fibrogenesis cannot be concluded from the data presented here.

Dual immunofluorescence studies of MR and PLVAP with multiple markers has allowed characterisation of cells which express these proteins in cirrhotic human liver. One limitation of using pixel intensities to measure colocalisation is that tissue sections are five-seven microns thick meaning it is uncertain whether two markers are truly expressed in the same cell type or just residing in close proximity. Furthermore, there is also an element of random colocalisation, in which two markers may overlap by chance, rather than due to a genuine association. Future work should confirm the findings reported here, by performing z-stacks of tissue sections to allow 3-D rendering, and statistical analyses

of receptor colocalisation, such as calculation of the Manders overlap coefficient. Given the suggested differential expression of the key phenotypic markers mentioned above by MR^+ and $PLVAP^+$ cell populations, it is unsurprising that these proteins display a mutually exclusive and reciprocal expression pattern. This suggests the presence of at least two distinct endothelial sub-populations which are differentially regulated in diseased states. Future work would endeavour to resolve this further, by isolation of pure MR^+ and $PLVAP^+$ endothelial cell populations for extensive phenotyping, including RNA sequencing and *in vitro* characterisation. This would allow investigation into the functions of these distinct endothelial subsets and their contribution to liver homeostasis and inflammation.

6.1.3 The expression of MR and PLVAP in HCC tumours

Hepatocellular carcinoma is a frequent consequence of end-stage CLD, arising on a background of liver cirrhosis in 90% of cases[270]. The expression of MR and PLVAP was characterised in matched non-tumour and tumour samples from HCC patients, both at the gene level by analysis of TCGA datasets and in-house qRT-PCR, and at the protein level by immunohistochemistry. Overall, *MRC1* expression was downregulated in HCC tumours whilst MR protein levels were variable across patient samples. The downregulation of MR in tumour tissue is interesting given that MR is already significantly downregulated during chronic inflammation and fibrosis; this could suggest an even further reduction in endothelial MR expression in a neoplastic context. Consistent with this, MR sinusoidal staining was reduced in tumour compared with non-tumour tissues despite being prominent within the tumour stroma. Correlation analysis of *MRC1* co-expression with a selection of tumour-associated cell-specific genes revealed a strong tumour endothelial (*PECAM1, CD34, PLVAP, AQP1, CLEC14A, IGFBP7, SPARC, COL4A2, VIM*) and TAM signature (*SEMA3C, LGALS1, IL21R, CCL2, LSP1, PSMB9*)[67, 466]. It therefore remains challenging to determine the sole contribution of MR downregulation in endothelial cells in shaping the tumour microenvironment. MR is known to be expressed in tumour-associated macrophages (TAMs), often being used as a marker of "M2" alternative activation, and associated with poor patient prognosis[542, 543]. These TAMs promote an immunosuppressive phenotype and can facilitate immune evasion of cancer cells; notably, MR has also been suggested to drive immunosuppression via direct

binding of tumoural mucins and IL-10-mediated T_{reg} induction[544, 545]. Nevertheless, there was no correlation between *MRC1* expression in HCC tumours and clinical parameters such as patient prognosis or survival. The conclusions that can be drawn from these studies are limited by the fact that this is gene expression data only which does not necessarily correlate with protein expression. Future work on the expression of MR at the protein level, within distinct cell subsets, and correlation with clinical parameters would offer further insight into the potential impact of sinusoidal MR downregulation in HCC.

As observed in CLD, PLVAP was upregulated in HCC tumours compared to matched non-tumour controls, at both the gene and protein level. Remarkably, PLVAP showed a further upregulation in HCC tumour tissue compared with the cirrhotic marginal non-tumour tissue, which already has increased PLVAP expression compared to normal liver. These data therefore suggest activity of additional pathological pathways in cancer important for PLVAP regulation. Consistent with this, PLVAP has previously been shown to be upregulated in multiple human cancers, including HCC and cholangiocarcinoma[457, 458]. Further, Sharma *et al*. (2020) used scRNA-seq to delineate the "onco-foetal reprogramming" of the tumour microenvironment in HCC, a process that involves the re-emergence of $PLVAP^{+}VEGFR2^{+}$ foetal-like endothelial cells which were suggested to drive immunosuppressive TAMs[398]. In support of this, *PLVAP*-expressing cell populations displayed a strong endothelial signature in HCC, positively correlating with expression of tumour-associated endothelial markers *PECAM1, CD34, AQP1, CLEC14A, IGFBP7, SPARC, COL4A2,* and *VIM*[67]. Some tumour-associated fibroblast-related genes were also significantly co-expressed, including *ACTA2* and *PDGFRB*, suggesting these cells may also be linked with the stromal tumour compartment[467]. A similar finding was observed in immunohistochemical studies of liver fibrosis, where PLVAP was shown to correlate with collagen deposition and fibrotic septa formation, discussed above.

PLVAP gene expression was also studied relative to clinical parameters, including cancer stage and tumour grade, as well as patient survival. A negative correlation was observed between *PLVAP* expression and cancer stage/tumour grade, and a downregulation of PLVAP in poorly-differentiated

tumours was confirmed by IHC. *PLVAP* also seemed to inversely correlate with markers of tumour aggressiveness, including aneuploidy score and Buffa hypoxia score, whilst higher *PLVAP* expression conferred improved overall and disease-free survival. Upon initial interpretation, these data could suggest that PLVAP is a favourable prognostic marker in HCC. This contrasts with a recent study in cholangiocarcinoma patients, where high PLVAP expression was indicative of poorer clinical outcomes (i.e. higher TNM (tumour, node and metastasis) stage and reduced survival)[457]. The same study also demonstrated a significant positive correlation between PLVAP levels and the microvascular density, as determined by CD31 IHC in patient samples. Not only does this support the notion that PLVAP is linked with neovascularisation, as discussed above, these data also suggest that HCC survival data could be confounded by the differentiation status of the tumour. That is, well-differentiated tumours, which are often associated with better patient outcomes, have a higher proportion of endothelial cells and therefore increased PLVAP expression by default. In keeping with this hypothesis, several studies have highlighted that antibody-mediated PLVAP inhibition reduces tumour growth in murine xenograft models of HCC and cholangiocarcinoma[457, 458]. Future work should attempt to mitigate potential confounding factors by correcting for the presence of endothelial cells, such as co-staining for CD31 or VE-cadherin, within tumour tissue to allow the percentage of $PLVAP^+$ endothelium to be quantified. Given the variable expression across HCC patient cohorts, it may be necessary to stratify patients on the basis of PLVAP and/or microvascular density, in order to identify those which could respond best to future anti-PLVAP therapies. Nevertheless, the data presented here are generally in keeping with recent advancements and could suggest that PLVAP is a valid novel therapeutic target in the context of CLD and HCC.

6.2 Regulation of MR and PLVAP in primary HSEC

6.2.1 Use of primary HSEC as a model to study MR and PLVAP regulation and function

Both human and murine HSEC are highly specialised cell types characterised by their fenestrated morphology, superior endocytic capacity and expression of various sinusoidal markers and scavenger receptors. However, aside from the presence of diaphragm-less fenestrae arranged in sieve plates, there

is no single HSEC-specific marker, meaning a combination of markers are required to identify them[23, 233]. The use of fresh primary HSEC is limited by low cell yields following isolation, making their application challenging without cell passage. Notably, when cultured *in vitro* primary HSEC de-differentiate and undergo capillarisation; that is, fenestration loss, basement membrane synthesis and altered expression of sinusoidal markers[469]. Despite this, early passage primary HSEC can be characterised based on their expression of several phenotypic markers, including endothelial markers CD31 and LYVE-1, as well as CD32b and scavenger receptors CD36, stabilin-1 and stabilin-2[469]. Expression of these markers paired with demonstration of their rapid endocytic and scavenging functions *in vitro* confirmed the sinusoidal phenotype of endothelial cells isolated by the method described in this thesis, validating their use in further studies.

The maintenance of MR and PLVAP expression in primary human HSEC *in vitro* offered the opportunity to further investigate their regulation and functional properties in these cells. Unsurprisingly, *MRC1* expression was comparable in freshly isolated $CD31^+$ and $CD45^+$ hepatic cell populations, which is consistent with the expression of MR in both sinusoidal endothelial cells and immune cells. In contrast, *PLVAP* expression was enriched in freshly isolated $CD31^+$ cells compared with $CD45^+$ cells, and also showed significantly higher expression in passaged HSEC compared with other hepatic cell types. These data are consistent with PLVAP being an endothelial-specific protein, as has been reported consistently for almost 40 years[438]. Despite their differential expression in normal and chronically-diseased liver tissue, expression of *MRC1* and *PLVAP* were comparable in HSEC derived from donors and CLD patients. This suggests that HSEC revert to a common phenotype once they are placed in culture, possibly because they are no longer receiving cues from the hepatic microenvironment.

Intriguingly, immunocytochemistry revealed that whilst MR was expressed in practically all HSEC, PLVAP maintained the subset-specific expression in distinct HSEC clusters, similar to that observed *in situ* in human liver. This could suggest a certain level of heterogeneity in cultured HSEC which has not been reported previously. There are several possible explanations for this selective PLVAP expression: (1) the population of $CD31^+$ cells which are isolated is heterogeneous to begin with, containing some

PLVAP$^+$ cells which proliferate *in vitro*; (2) PLVAP expression is associated with a transient cell state (e.g. a particular stage of the cell cycle) which appears as a heterogeneous population at any given time; (3) PLVAP is regulated in spatially discrete clusters by release of soluble factors which act in a paracrine manner to drive PLVAP expression in neighbouring cells. The former hypothesis is interesting to consider in the context of the zonal PLVAP expression observed in normal liver; PLVAP$^+$ cells in culture could represent the *in situ* periportal HSEC population, although this is based on the unlikely assumption that signalling which controls hepatic zonation is maintained *in vitro*. This also assumes an element of rigidity regarding PLVAP expression i.e. cells are either PLVAP-positive or PLVAP-negative. Yet, stimulation of PLVAP expression (discussed in more detail below) increased not only the amount of PLVAP present but also the proportion of PLVAP$^+$ cells, suggesting most HSEC are capable of PLVAP expression if exposed to the appropriate stimulus. Alternatively, PLVAP may be an indication of cells undergoing capillarisation in culture, as has been suggested *in vivo*[536]. In keeping with this idea, *PLVAP* expression was higher in cells of a later passage, suggesting a possible link with de-differentiation or cellular senescence. The factors controlling the subset-specific expression of PLVAP *in vitro*, however, remain undefined. Similarly, *MRC1* expression was also increased in higher passage cells, which could also be due to secretion of soluble factors by "capillarised" or senescent HSEC. The localisation and regulation mechanisms of MR and PLVAP *in vitro* are discussed in more detail below.

6.2.2 Trafficking of MR in primary HSEC

Many proteins undergo post-translational modification within the Golgi apparatus following their synthesis, a process which involves sorting within intracellular vesicles. Membranous proteins also often undergo trafficking through the endosomal system, frequently recycling between the cell surface and intracellular stores. At steady state, MR was found to reside predominantly intracellularly, within the Golgi apparatus as well as early and recycling endosomes. This is in keeping with the role of MR as an endocytic receptor and is consistent with previous reports which state that, under basal conditions, around 10-30% of MR is found at the cell surface and 70-90% is located intracellularly[399]. Futhermore, this trafficking was susceptible to inhibition by bafilomycin, a vacuolar type H$^+$-ATPase inhibitor that

is known to perturb both endosomal trafficking and lysosomal acidification[461, 462]. The accumulation of MR in large vesicles following bafilomycin treatment also suggests a rapid protein turnover (synthesis and degradation). Following receptor ligation with a specific monoclonal antibody, MR underwent rapid internalisation into early endosomes which peaked at 60 minutes. Understanding the fate of MR post-ligation, whether it be sorted for lysosomal degradation or dissociated from its ligand and returned to the cell surface, would be interesting to investigate in future studies.

6.2.3 The intracellular localisation of PLVAP in primary HSEC

PLVAP has been well-characterised as the only known molecular component of diaphragms which span the openings of fenestrae and caveolae[367, 440]. As such, PLVAP has frequently been found to localise to the luminal endothelial surface, both in HSEC and vascular endothelial cells[444, 536]. Immunocytochemistry studies indicated that PLVAP was present throughout the HSEC cytoplasm within punctate, vesicular-like structures, as well as being localised at the cell periphery. Additional staining revealed that PLVAP was located proximal to, but excluded from, the intercellular junctions. This is in keeping with previous studies in HUVEC and human/mouse lymphatic endothelial cells[366, 459].

Although PLVAP was often enriched at polar ends of the cell, immunocytochemistry studies in non-permeabilised cells indicated that PLVAP was predominantly located intracellularly, with only around 18% residing at the cell surface in resting cells. This intracellular pool was seemingly insensitive to bafilomycin treatment, unlike MR, suggesting $PLVAP^+$ vesicles do not undergo basal trafficking through the endosomal system. Yet, following treatment with PMA, which was highlighted to upregulate total PLVAP expression (discussed in more detail below), surface expression was also increased suggesting PLVAP redistribution can occur in response to stimulation. Similarly, PLVAP was also shown to traffic towards the cell periphery in response to TNFα stimulation, although these studies were only performed in permeabilised HSEC which could not distinguish between the membranous and intracellular PLVAP pools. Whether this trafficking in response to pro-inflammatory stimuli is sensitive to bafilomycin treatment remains unknown.

Interestingly, in the small subset of untreated and TNFα-stimulated cells which were PLVAP-positive, colocalisation with caveolin-1 was observed. A similar observation was made by Keuschnigg *et al.* in HUVEC[459]. This could suggest that PLVAP can undergo trafficking in response to stimulation via the caveolar system. Yet, in contrast to PLVAP, caveolin-1 was present in practically all HSEC *in vitro*, a finding which is consistent with those made in immunohistochemistry studies in **Chapter 3**. Collectively, these data support the idea that, whilst PLVAP may closely associate with caveolae in some cells, it is not universally associated with all caveolar structures. However, one way to definitively conclude this would be to knockdown caveolin-1, preventing caveolae formation, and then assess the expression and localisation of PLVAP as has been done previously *in vivo*[444].

The effects of antibody ligation on PLVAP localisation was assessed for various time points up to 60 minutes, indicating that antibody binding began to occur as early as five minutes and increased in a time-dependent manner. These data suggest that a large proportion of PLVAP is readily accessible from the extracellular space, and yet, only a small proportion of PLVAP was localised to cell membrane in fixed, non-permeabilised cells. This could suggest that antibody could gain access to the intracellular PLVAP pool following its uptake via caveolin-mediated endocytosis. This notion could also partly explain why PLVAP appears to form aggregates in antibody-treated HSEC. Interestingly, immunofluorescence levels were significantly higher following 60-minute antibody treatment compared with the fixed untreated control. It is highly unlikely that these observations are due to upregulated PLVAP protein synthesis given the short time frame. Instead, it is probably more feasible that: (1) antibody binding is more efficient in live cells due to alterations in the recognised epitope following fixation; (2) antibody treatment leads to PLVAP redistribution and concentration within specific intracellular compartments. Which of these possibilities is the case here is unknown, however, the former hypothesis could suggest immunocytochemistry studies in fixed HSEC may actually underestimate their PLVAP expression.

6.2.4 The regulation of MR in primary HSEC

Previous work has extensively characterised the regulation mechanisms of MR in myeloid cells including macrophages and DCs, with its expression often being driven by factors which promote "M2"

alternative activation. However, very few studies have investigated MR regulation in HSEC, and the handful that have solely focus on murine HSEC, leaving the regulatory pathways in primary human HSEC entirely unknown. In **Chapter 4**, the regulation of MR and PLVAP in HSEC was studied at the gene and protein level, by qRT-PCR and immunocytochemistry/HCI, respectively. Treatment with classic pro-inflammatory cytokine, TNFα, showed no significant effect on MR mRNA or protein expression, despite a significant upregulation of ICAM-1 being detected. This contradicts previous studies in human monocyte-derived DCs which showed a downregulation of MR surface expression and activity in response to TNFα[433].

Previous studies in murine HSEC have shown that IL-1β treatment upregulated MR activity[490], a finding also supported here by the small but significant increase in MR immunofluorescence area. In contrast, responses to LPS treatment regarding MR expression have proven conflicting, with some studies demonstrating increased uptake activity in murine HSEC[490], and others suggesting downregulation of MR mRNA and membranous protein expression in rat astrocytes and human monocyte-derived DCs, respectively[433, 488]. Data presented in **Chapter 4** demonstrated that LPS had no effect on the levels of MR mRNA or protein in primary human HSEC. This could be due to the well-characterised hypo-responsiveness of HSEC to LPS, given that they are continuously exposed to gut-derived LPS *in vivo*[106, 164].

A high-content screen of multiple putative MR regulators was performed, highlighting a general resistance of MR to regulation by multiple cytokines, chemokines, growth factors and small molecules previously reported to modulate its expression. Aside from inhibitors of actin polymerisation, which induced cellular toxicity, there were only two viable hits – ATRA and PGE1. In THP-1 cells, ATRA was shown to downregulate MR mRNA levels, whilst PGE1 upregulated MR expression and binding activity in murine bone marrow-derived macrophages[476, 493]. Here, both induced a significant but modest downregulation of MR expression; the minimal fold-change in response to these treatments compared to the control, however, casts doubt on the biological significance of these findings. Overall, these data demonstrate the existence of distinct regulatory mechanisms in primary HSEC, compared to the better

studied macrophage, and even murine HSEC. Furthermore, whilst MR expression appears to be tightly regulated by various stimuli in myeloid cells, the same cannot be said for HSEC which express high basal levels of MR and are resistant to stimulation.

Given the downregulation of MR in HCC tumours, which are frequently hypoxic with oxygen levels of 0.5-2%, the effects of hypoxia on *MRC1* expression were investigated. An increasing trend of MR mRNA following HSEC exposure to 2% oxygen was observed compared to atmospheric oxygen levels, suggesting hypoxic conditions may drive MR expression. The effects of hypoxia have not been studied regarding MR expression in HSEC, but one study found that MR surface expression was upregulated in both M1- and M2-polarised macrophages when exposed to 1% O_2[546]. One limitation of the work presented here is that hypoxic conditions are compared to atmospheric oxygen levels, which do not represent normoxia within the liver sinusoids (4-9% O_2)[521]. Further work in HSEC is therefore required to confirm this at varying O_2 concentrations and at the protein level.

6.2.5 The regulation of PLVAP in primary HSEC

The regulatory mechanisms of PLVAP expression were also studied in primary human HSEC by qRT-PCR and HCI. Several groups have presented compelling evidence that PLVAP expression is driven by master regulator of endothelial function, VEGF[456, 500, 515-518]. Specifically, VEGF-mediated stimulation of PLVAP expression occurs downstream of VEGFR2, via activation of PI3K and p38 MAPK signalling pathways[500, 515]. Contradictory to this, one study reported that PLVAP expression is negatively regulated by VEGF in caveolin-1, but not caveolin-2, knockout mice[547]. VEGFR2 is known to localise within caveolae which are lacking in caveolin-1 knockout mice. These paradoxical findings could therefore be explained by altered VEGF-mediated PLVAP expression in the absence of caveolae due to changes in VEGFR2 availability. Interestingly, PLVAP interacts with VEGFR2 co-receptor neuropilin 1 (NRP1)[444, 548]; this presents the possibility of a positive feedback loop in which VEGF-mediated PLVAP expression stabilises VEGFR2-NRP1 signalling complexes, leading to further PLVAP upregulation. In HSEC, VEGF treatment led to a robust and significant upregulation of PLVAP although this was not recapitulated at the mRNA level, at least at the 24-hour time point. Given the increased angiocrine

factors such as VEGF within the tumour microenvironment, this could explain, at least in part, the upregulation of PLVAP within HCC tumours described in **Chapter 3**.

PLVAP has also previously been shown to be regulated by pro-inflammatory stimuli in various cell types, including TNFα, PMA and fibrinogen; here, these factors were also shown to upregulate PLVAP in primary human HSEC. Published data on the effects of TNFα treatment in HUVEC are conflicting, with one study suggesting that *PLVAP* expression is downregulated by 24-hour TNFα treatment, whereas another demonstrated PLVAP redistribution to the cell periphery and increased colocalisation with caveolin-1[459, 463]. These data are therefore consistent with the findings reported here, where at 24 hours TNFα treatment downregulated *PLVAP* mRNA whilst an increase in fluorescent area, but not intensity, was observed which could indicate PLVAP redistribution within the cell. PMA was identified as the biggest hit in the HCS increasing PLVAP expression in HSEC by ~2-3-fold. PMA has previously been shown to induce PLVAP expression and *de novo* diaphragm formation in HUVEC, HMVEC and HDMVEC in a VEGFR2- and ERK1/2 MAPK-dependent manner[367, 456, 511]. Furthermore, the effects of PMA were shown to rely on synthesis of soluble factors, including VEGF, which act in an autocrine manner to drive PLVAP expression[511]. PMA could therefore upregulate PLVAP indirectly in HSEC, via VEGF secretion, although further studies which investigate the effects of PMA treatment following VEGF receptor manipulation would be required to confirm this. Fibrinogen is a coagulation factor which is enzymatically converted to fibrin by thrombin, acting as an acute-phase protein that is increased in the circulation during systemic inflammation and tissue injury. In murine cortical brain endothelial cells, fibrinogen was shown to upregulate PLVAP expression, increasing co-localisation with caveolin-1 and caveolae formation, a process found to be dependent on MMP-9[506]. Here, fibrinogen treatment of HSEC also increased PLVAP expression, although whether this was due to increased caveolae formation in these cells cannot be confirmed or refuted. Collectively, the upregulation of PLVAP in response to pro-inflammatory stimuli is consistent with its upregulation in CLD discussed in **Chapter 3**.

BMP-9 is member of the TGFβ superfamily of proteins which is released by HSC and is important for maintenance of vascular quiescence. The relationship between BMP-9 and PLVAP expression is

interesting to consider in the context of capillarisation and fibrosis, although studies to date have only been performed in murine liver. Desroches-Castan *et al.* (2019) depict a protective role for BMP-9 in hepatic fibrosis, where *Bmp9* knockout was associated with HSEC capillarisation, including loss of sinusoidal markers (*Lyve1, Stab1, Stab2, Ehd3, Cd209b, eNos, Maf* and *Plvap*), increased CD34 expression, basal lamina deposition and fenestration loss[503]. Synonymously, culturing HSEC in the presence of recombinant BMP-9 prevented this reduction in fenestrae and maintained expression of *Gata4* and *Plvap*. In contrast, human PLVAP expression is associated with HSEC capillarisation and loss of sinusoidal markers, yet BMP-9 still upregulates PLVAP in primary human HSEC *in vitro*. Given the well-characterised differences in mouse and human PLVAP expression, this seemingly paradoxical relationship is perhaps not that surprising. This could however, suggest a more direct role of BMP-9 and subsequent ALK1 signalling in PLVAP upregulation, rather than this occurring as an indirect consequence of regulating the HSEC phenotype.

Results discussed in **Chapter 3** present compelling evidence for the upregulation of PLVAP in HCC tumours. Because cells residing within the tumour microenvironment are frequently subject to hypoxic conditions, the expression of PLVAP was studied following HSEC exposure to 2% oxygen and compared with atmospheric oxygen levels. The association between PLVAP expression and hypoxia has been proposed, due to the common observation of its upregulation in several cancers, as well as in brain tissues of patients with acute ischaemia[455]. Hypoxia is also an inducer of VEGF secretion, via activation of HIF-1α, which is known to drive PLVAP expression in an autocrine manner. Yet, *PLVAP* expression in HSEC did not appear to be regulated by 24-hour exposure to hypoxic conditions. However, as mentioned above, these studies are limited by a lack of "normoxic" control (4-9% O_2). Cancer cells are known to produce a myriad of soluble factors which shape the tumour microenvironment, driving immune suppression and tumour persistence. Carson-Walter *et al.* provided evidence that conditioned medium from human brain tumour cell lines, U87MG and U251MG, increased PLVAP expression in HMVEC[456]. The effects of HSEC treatment with conditioned medium from HCC cell lines was assessed by HCI, demonstrating a modest upregulation of PLVAP in response to tumour-derived factors. It would

be interesting to characterise the components of this conditioned medium which have the ability to stimulate or suppress PLVAP expression in HSEC; this remains an avenue for future studies.

6.3 The role of MR in leukocyte recruitment across HSEC

The functional role of MR in lymphocyte recruitment was assessed by performing flow assays with TNFα-stimulated HSEC following *MRC1* genetic knockdown (**Appendix 7.4**) or antibody-mediated blockade of MR (**Appendix 7.5**). The localisation of MR during lymphocyte adhesion and transmigration following flow assays was also explored by immunocytochemistry and confocal microscopy (**Appendix 7.6**). Collectively, these data suggested that lymphocyte recruitment is not dependent on MR, since adhesion, shape-change and transmigration were unaltered following MR inhibition. In addition, there was no localisation or redistribution of MR during lymphocyte recruitment, further supporting its likely unnecessary role. These findings are contradictive of previous reports which suggest that MR plays a role in lymphocyte adhesion within the lymphatic system[363-365]. Since HSEC are known to express a vast array of scavenger receptors, which often display substantial redundancy regarding their recognition of carbohydrate and sulphated ligands, it is possible that the lack of MR is compensated for by other C-type lectins. Interestingly, the *MRC1* transcript is known to also encode a microRNA (miR-511-3p) which is predicted to regulate various genes involved in transcription, morphogenesis, metabolism and protein localisation[549]. Thus, it would be informative to perfume bulk RNA sequencing on siMRC1-transfected HSEC to understand the effects of MR genetic knockdown on the HSEC transcriptome. This could elucidate the functional role of MR in HSEC, which is so highly expressed at steady state, and is an avenue for future research. Furthermore, MR has also been implicated in cancer cell adhesion to lymphatic vessels[288]. Given the variable MR expression observed in tumour endothelium of HCC patients described in **Chapter 3**, it would be interesting to understand whether MR can also mediate cancer cell binding to HSEC. This also remains an area for future work.

6.4 Senescent cell-endothelial crosstalk in CLD and HCC

6.4.1 Expression of senescent markers in CLD and HCC

Senescence is a key feature of multiple chronic liver diseases of varying aetiology, including being a hallmark of cancer, yet whether senescence is an inducer of injury or arises as a consequence of tissue damage is unclear. The biological impact of senescence appears to be both cell type- and context-dependent and has been reviewed recently[524, 550]. Several markers can be used to identify senescent cells; in this thesis, gene expression of CDK inhibitors, p21 and p16, were assessed to study senescence in CLD and HCC. Whilst p21 gene expression was fairly comparable in normal, cirrhotic and cancerous liver tissue, p16 gene expression was upregulated in a diseased setting and was associated with unfavourable outcomes in HCC patients. These data are supported by previous studies which show p16 upregulation in almost every aetiology of liver disease[524]. Furthermore, inhibition of p16 ameliorated inflammation and fibrosis in murine models of NASH and PSC[265, 551]. At the protein level, p21-expressing hepatocytes were more frequently observed in CLD, whilst p16 expression was widespread across multiple cell types and highly variable within the CLD patient cohort. In keeping with this finding, p21 expression in hepatocytes is a feature of both acute and chronic liver injury, as well as tumourigenesis in HCC[524]. Furthermore, p16 is expressed in cholangiocytes, hepatocytes, HSC, HSEC and immune cells across a range of aetiologies and disease models[524]. However, the data reported in this thesis are limited since they only focus on two senescence markers, both of which relate to the cell cycle arrest aspect of senescence. Given the disparity observed between transcription and translation of p21 and p16, additional work is required to investigate other markers of senescence, in order to strengthen these findings. Nevertheless, these data highlight that senescence is a key feature of CLD and HCC as is well-described in the literature.

6.4.2 The effects of the senescent secretome on HSEC phenotype

Senescent cells release a secretome (SASP) comprised of numerous soluble factors with the potential to influence the HSEC phenotype. Importantly, the tissue microenvironment during homeostasis,

inflammation and cancer encompasses a complex biological milieu. Thus, investigation into the effects of SASP exposure offers a unique opportunity to study cellular responses in a physiologically relevant context rather than use of discrete factors in isolation. Conditioned medium from IMR90 fibroblasts undergoing Ras-mediated senescence (Ras-CM) was shown to drive pronounced morphological, phenotypic and functional changes in primary HSEC. These included cell elongation and alignment, as well as rearrangement of the actin cytoskeleton, including formation of stress fibres. Endothelial cell elongation is an important physiological component of angiogenesis and is thought to be regulated by several transcriptional regulators (Mef2, Foxo1) and signal transduction cascades (VEGF-mediated pathways such as PI3K-Akt, mTOR and Notch)[552]. For instance, mTORC2 is known to drive vascular endothelial cell elongation and stress fibre formation through reorganisation of the actin cytoskeleton via Rho-ROCK signalling, whereas mTORC1 and PI3K-Akt negatively regulate this actin remodelling[553]. Moreover, VEGF-induced expression of Notch1 and its ligand, Dll4, activates Notch signalling which converges on mTOR and PI3K-Akt signalling pathways[554]. HSEC elongation could therefore be induced by the components of the SASP which influence these pathways, including VEGF and Notch ligands, but also activation of other receptors which involve downstream mTOR/PI3K-Akt signalling.

Several groups have characterised the composition of the SASP derived from senescent IMR90 cells, with as many as 7748 significant differentially expressed proteins compared to the growing IMR90 control, as determined by SILAC proteomics[464, 555]. Many of these are pro-inflammatory stimuli such as interleukins and chemokines which are known to drive endothelial cell activation. It is therefore unsurprising that treatment of HSEC with the conditioned medium from these senescent cells led to upregulation of activation genes *ICAM1, CCL2, IL6, IL1B* and *CXCL8*, protein expression of ICAM-1 and CCL2, and secretion of soluble cytokines and chemokines. Identifying which particular SASP components are responsible for driving these changes would require vast high-throughput screening with genetically-manipulated (or otherwise inhibited) HSEC, to determine which receptors and/or signalling pathways are critical for said alterations to occur. Given the low yields of primary HSEC

following isolation and their finite lifespan in culture, this would be an unrealistic task. Furthermore, it is almost certain that these phenotypic changes are driven by exposure to a combination of factors working synergistically, as opposed to a single agent. Nevertheless, increased expression of endothelial adhesion molecules and chemotactic factors supports the hypothesis that SASP exposure may drive functional changes in HSEC, perhaps facilitating leukocyte recruitment.

6.4.3 The association between PLVAP, senescence and immune infiltrate in human and mouse liver

Given the upregulation of PLVAP and senescence markers in CLD and HCC, which are conditions characterised by leukocyte recruitment, associations between PLVAP expression, senescence and immune infiltrate composition were assessed. Amongst driving several interesting phenotypic changes in HSEC, the SASP also stimulated expression of PLVAP mRNA and protein levels *in vitro*, suggesting that senescent cell-endothelial crosstalk may drive expression of PLVAP *in vivo*. This is perhaps not surprising since the SASP is known to contain several known enhancers of PLVAP, including VEGF, HGF, TGFβ, angiopoietins and Notch ligands[555]. The presence of putative inhibitors of PLVAP expression within the SASP, such as Wnt/Frizzled ligands, could also suggest that the impact on PLVAP may be dependent on the SASP composition. The SASP is known to comprise a complex array of factors which act in a paracrine manner on neighbouring cells to reinforce senescence[464, 555]. This is interesting if we consider the upregulation of *PLVAP* expression with HSEC passage discussed in **Chapter 4**; perhaps late passage cells begin to undergo senescence, secrete their own SASP, which drives both paracrine senescence and PLVAP expression. Nevertheless, these data suggest that PLVAP is upregulated by factors, either solely or in combination, found within a senescent tissue microenvironment. To explore this further in human liver, gene expression data for PLVAP and p21/p16 were obtained in CLD and HCC patients. In both CLD and HCC tissues, *PLVAP* gene expression was directly proportional to *CDKN2A* expression, whilst a positive correlation with *CDKN1A* was only observed in CLD. Quantification of immunohistochemical staining revealed that the correlation between PLVAP and senescence was also maintained at the protein level. These data further support a link between PLVAP and senescence in human liver disease.

The SASP released from senescent cells is thought to act as a driver of leukocyte recruitment in order to facilitate senescent cell clearance[531]. Furthermore, PLVAP is readily expressed in periportal sinusoids and $CD34^+$ neovessels within fibrotic septa, which are likely sites of leukocyte recruitment during chronic inflammation. Paired with the notion that PLVAP may be implicated in leukocyte trafficking[366, 459, 460], this could suggest an association between senescence, PLVAP expression and immune infiltrate in CLD and HCC. To explore this further, the immune infiltrate in the context of PLVAP expression was characterised in HCC and CLD patients. TCGA datasets and widely-available online resources (ESTIMATE and TIMER) were used to assess immune score and composition of the inflammatory infiltrate in HCC tumours[533]. There was a conservative yet significant positive correlation between *PLVAP* gene expression and immune score, where partial correlations with infiltration levels of $CD4^+$ and $CD8^+$ T cells, dendritic cells and neutrophils were observed. Whilst these findings are gene expression data only, this could suggest a possible link (either directly or indirectly) between PLVAP and the immune microenvironment of HCC. Future work to investigate this *in situ* will be required to consolidate this finding.

Immunohistochemistry for PLVAP and several leukocyte-specific markers was performed in serial liver sections from cirrhotic patients. MAC387 is a mouse monoclonal antibody which recognises calcium binding protein, S100A9, also known as migration inhibitory factor-related protein 14 (MRP14) or calgranulin B[556]. S100A9 associates with S100A8 to form calprotectin heterodimers which are enriched in the cytosol of monocytes and granulocytes. MAC387 has therefore previously been used to visualise infiltrating monocytes and neutrophils in human tissue[534, 535]. In this case, the level of hepatic neutrophil infiltration was minimal even in the acute setting, as shown by immunohistochemistry in seronegative hepatitis patients which were characterised by substantial $MAC387^+$ cell infiltration (**Appendix 7.8**). This suggests the contribution of neutrophils to the $MAC387^+$ immunoreactivity in CLD was minimal, and was confirmed by neutrophil elastase staining in matched tissue sections. MAC387 has also been shown previously to stain tissue-resident macrophages including KCs[557]. Yet, KCs were inconsistently positive for MAC387, and those that were had considerably lower staining intensities. Thus, monocytic

cells were clearly distinguishable from KCs based on shape and intensity, which was supported by clear immunolabelling of KCs with CD45 but not MAC387 in normal liver (**Appendix 7.9**). This suggests that the majority of $MAC387^+$ cells are infiltrating monocytes or recently differentiated monocyte-derived macrophages. Following quantification of immunohistochemical staining, PLVAP was observed to correlate both spatially and quantitatively with the infiltration of $MAC387^+$ and $CD3^+$ cells, suggesting PLVAP may be involved in the recruitment of monocytes and lymphocytes. Whether this is also the case in HCC remains an area for future research.

The expression of PLVAP was also studied in an *in vivo* murine model of senescence, displaying a robust and significant upregulation in response to hepatocyte-specific deletion of *Mdm2* ($\Delta Mdm2^{Hep}$). Mdm2 is a key negative regulator of the tumour suppressor p53 and the p53/p21 axis is central to senescence induction. Thus, $\Delta Mdm2^{Hep}$ leads to p53 overexpression and induces acute p21-dependent hepatocellular senescence characterised by increased expression of multiple senescence markers, including p21 itself, but also γH2A.X, IL1α and SA-β-Gal[259]. This finding is further supportive of the correlation between a senescent microenvironment and PLVAP expression, validating the observations made in human liver tissue and cultured primary HSEC. It would be interesting to also characterise the immune infiltrate in murine liver following senescence induction allowing parallels to be drawn between mice and humans. Despite the widespread PLVAP expression in mice in contrast to humans, this robust upregulation in the $\Delta Mdm2^{Hep}$ mice validates this model for future studies, which will aim to understand the effects of PLVAP inhibition on hepatic leukocyte recruitment *in vivo*.

Collectively, these data suggest an intriguing and previously unreported link between PLVAP and senescence in chronic liver injury, which could have pivotal implications for leukocyte recruitment during chronic inflammation.

6.4.4 Mechanisms of SASP-mediated leukocyte recruitment

One physiological function of SASP release is the capacity to drive leukocyte recruitment which is thought to facilitate senescent cell clearance[531]. In the liver, this senescence surveillance is thought to

prevent cancer development, by reducing the likelihood of accumulation and persistence of pre-malignant hepatocytes[531]. This surveillance was shown to be mediated by cytokine and chemokine release and was dependent on monocyte/macrophage and $CD4^+$ T cell compartments[531]. Similarly, HSEC also increase their expression and/or secretion of cytokines, chemokines and adhesion molecules in response to SASP exposure, as demonstrated here by qRT-PCR, immunocytochemistry and cytokine array of cell supernatants. This suggests that SASP-stimulated HSEC may be capable of supporting hepatic leukocyte recruitment. In favour of this concept, previous work in our lab has shown that lymphocytes are recruited across HSEC, under physiological shear stress, in response to SASP treatment[464].

In this thesis, the hypothesis that SASP stimulation can also promote monocyte recruitment was investigated by undertaking flow adhesion assays with HSEC and peripheral blood monocytes. Indeed, Ras-CM treatment robustly increased the number of adhered, shape-changed and transmigrated monocytes in both donor- and patient-derived HSEC. Furthermore, this was shown to occur much more readily in monocytes than lymphocytes, even at twice the SASP concentration. This could suggest a more predominant role for monocytes in senescence surveillance, or could perhaps reflect variation in the kinetic profiles of monocyte vs. lymphocyte recruitment. Additional time-lapse experiments which allow the study of these processes in real-time would be required to confirm this theory.

Lymphocytes and monocytes were shown to transmigrate via morphologically distinct routes through the endothelial monolayer, with almost all monocytes migrating paracellularly, and lymphocytes preferring to extravasate through the transcellular pathway (~60%). To our knowledge, this is the first report which compares the route of transmigration for monocytes and lymphocytes in primary HSEC. In support of these findings, previous studies in HUVEC have documented a similar observation with monocytes in response to TNFα[338], whilst 62% of lymphocytes were observed to transmigrate transcellularly across HSEC in response to TNFα/IFNγ[381]. This suggests similarity between recruitment mechanisms in response to the SASP and classic pro-inflammatory stimuli, although additional studies would be required to explicitly confirm this.

When attempting to compare and contrast the molecular mechanisms of monocyte and lymphocyte recruitment, it is important to first consider the stages of adhesion and diapedesis for each transmigratory route. Generally, and irrespective of the route of transmigration, integrin-mediated adhesion of leukocytes is associated with clustering of VCAM-1 and ICAM-1, as well as tetraspanins (e.g. CD9, CD151), leading to recruitment of adaptor proteins which link these clustered proteins to the actin cytoskeleton[337, 558]. Simultaneously, endothelial RhoGTPases activate downstream signalling pathways which reduce cell-cell adhesion, favouring paracellular migration[558].

Paracellular migration, in which leukocytes squeeze between adjacent endothelial cells, is initiated by two key stages: (1) membrane influx from the lateral border recycling compartment (LBRC)[559]; (2) VE-cadherin mobilisation away from the transmigration site[560]. The LBRC is a complex invagination of the plasma membrane, harbouring several adhesion molecules which are important for paracellular transmigration, including CD31, CD99, JAM-A and PVR[352, 559, 561]. It has been suggested that this acts as a reservoir of both the adhesion molecules, and the addition junctional membrane, necessary for transmigration to occur. Transcellular migration, during which a leukocyte extravasates through the endothelial cell body, is considerably less well-studied than paracellular migration. Yet, many of the molecules necessary for junctional leukocyte transmigration have also been implicated in transcellular migration, including ICAM-1, CD31, CD99 and JAM-A[337, 352]. Importantly, in the liver, transcellular migration has been shown to act as the key pathway for lymphocyte recruitment, in response to both cytokine and SASP stimulation[381].

Experiments performed with antibody-treated HSEC identified CD31 and ICAM1 as key adhesion molecules involved in SASP-mediated monocyte and lymphocyte recruitment, respectively, confirming that these processes occur by molecularly distinct mechanisms. Neither monocyte adhesion nor transmigration were affected following ICAM-1 inhibition, despite successful binding of the ICAM-1 antibody under these conditions. Furthermore, there was no localisation of ICAM-1 with transmigrating monocytes in response to the SASP. It is possible, therefore, that ICAM-1 is not required for paracellular migration across HSEC. This notion is contradicted by previous work in TNFα-treated HUVEC,

suggesting that ICAM-1 localises within apical protrusions associated with transmigratory pores, and is required for neutrophil paracellular transmigration[338]. Yet, previous work in TNFα-stimulated HSEC showed that adhesion of $CD16^+$ monocytes was significantly impaired by dual VCAM-1/ICAM-1 blockade, whilst monocyte transmigration was unaffected[390]. In the context of data presented here, this could suggest that monocyte adhesion to HSEC is mediated primarily by VCAM-1. In favour of this, HUVEC transduced with an adenoviral vector encoding VCAM-1 were able to support adhesion of peripheral blood monocytes at $\leq$1.5 dyne/cm^2 shear stress in the absence of stimulation[562]. Additional flow experiments following VCAM-1 and VCAM-1/ICAM-1 inhibition with SASP-stimulated HSEC would provide further mechanistic insight into monocyte adhesion and transmigration.

In contrast to monocytes, SASP-mediated lymphocyte adhesion and transmigration were significantly impaired following ICAM-1 inhibition. These experiments were limited however by the low numbers of adhesion events observed with lymphocytes following SASP-stimulation, despite doubling the SASP concentration in attempt to mitigate this potentially confounding variable. Nevertheless, previous work in TNFα-activated HSEC have provided convincing evidence for the role of ICAM-1 in lymphocyte recruitment[27, 376, 381]. Moreover, the enrichment of ICAM-1 around transmigrating lymphocytes in close association with F-actin was frequently observed in response to the SASP, further supporting its adhesive role. This is consistent with previous reports, demonstrating ICAM-1 translocation to caveolin-rich membrane domains in association with F-actin-rich transcellular pores, through which lymphocytes extravasate[563].

Lymphocyte adhesion was unaffected by CD31 inhibition, whilst a partial reduction in transmigration was observed, although this did not reach statistical significance. The percentage of adhered lymphocytes which underwent shape-change was significantly increased, perhaps indicating that transmigration of arrested lymphocytes was delayed. Given that 60% of lymphocytes extravasate via the transcellular route, this could suggest that CD31 is only important for paracellular migration, and therefore only a fraction of the lymphocyte transmigratory events are affected by CD31 inhibition. Yet, CD31, along with other LBRC components, has also been implicated in transcellular migration, albeit

of monocytes and neutrophils[352]. Furthermore, CD31 was seen to form rings around transmigrating lymphocytes regardless of their transmigration route, which is consistent with findings reported previously[338, 352]. Since leukocytes are considered to take the path of least resistance in order to cross the endothelial barrier, it is conceivable that CD31 plays a more predominant role in paracellular migration, and so its inhibition may push lymphocytes towards migration via the transcellular route. The factors which determine the route of transmigration, however, are poorly understood and further work would be required to investigate whether this is the case here.

Following CD31 inhibition, SASP-mediated monocyte transmigration was perturbed, whilst monocyte shape-change increased and adhesion was unaffected. This is consistent with a role for CD31 in SASP-mediated monocyte transmigration, since cells were able to adhere and locomote the apical endothelial surface but not complete diapedesis. As mentioned above, CD31 is a key component of the LBRC (~30%), and is therefore integral for paracellular transmigration[564]. During transmigration, targeted recycling occurs, whereby the LBRC moves along microtubules in order to interact with extravasating leukocytes. As such, inhibition of CD31-CD31 homophilic interactions ablates both transmigration and targeted recycling[564, 565]. Here, enrichment of CD31 around transmigrating monocytes was consistently detected, which is in keeping with previous studies[352]. Although CD31 is known to be present on both monocytes and endothelial cells, it is likely that the majority of this CD31 is endothelial-derived, since there was colocalisation with F-actin which was visualised by SiR-actin treatment of HSEC only. Furthermore, endothelial cells were observed to extend CD31- and F-actin-rich protrusions which appeared to envelop transmigrating monocytes; these membrane ruffles were not observed during lymphocyte transmigration irrespective of the route taken. Similar observations have been made during neutrophil transmigration, where junctional membrane protrusions enriched in CD31 and F-actin serve as hotspots for leukocyte migration[566].

Another distinction between monocyte and lymphocyte transmigration was the association of F-actin. As mentioned above, monocyte transmigration was associated with extension of F-actin-rich membrane ruffles, whilst observations of F-actin enriched pores at the cell junctions were rare. In fact, almost a

complete void of F-actin was more commonly observed, despite the formation of CD31-rich transmigratory channels. In contrast, transmigrating lymphocytes were predominantly surrounded by F-actin when migrating either para- and transcellularly. These findings highlight possible differences in actin cytoskeletal rearrangement may occur during SASP-mediated monocyte vs. lymphocyte transmigration which is not necessarily dictated by the migratory route. These data contradict previous studies of neutrophils and monocytes, in which transmigratory events were actually defined by the presence of F-actin-rich pores due to their high incidence[338]. Authors proposed that this actin cytoskeletal integrity, mediated by ICAM-1 and RhoA activation, was critical in maintaining endothelial cell barrier function. Interestingly, apical F-actin protrusions similar to those documented here were also observed, although these were found to be insensitive to RhoA inhibition. It would therefore be interesting to explore a possible functional role for RhoA in mediating HSEC vascular permeability during monocyte transmigration, particularly given the seemingly redundant role of ICAM-1.

There are two key differences between the study mentioned above and the results reported here, which could explain the conflicting observations regarding F-actin pore formation. Firstly, Heemskerk *et al.* study neutrophil and monocyte recruitment in response to classic pro-inflammatory stimulus, TNFα[338]. In contrast, the SASP comprises a myriad of factors, possibly eliciting varying effects on expression of endothelial adhesion molecules that are then available to interact with monocytes. Since leukocytes are known to interact with multiple molecules within the LBRC, increased monocyte binding avidity at the endothelial junction may limit additional mechanisms required to maintain endothelial barrier integrity[567]. Investigation into expression of other LBRC adhesion molecules, alongside CD31, in response to the SASP would elucidate this further. Secondly, Heemskerk *et al.* use HUVEC to understand these processes, which are known to differ drastically from HSEC in terms of their transcriptional profiles, metabolic activity and response to stimulation[470]. For instance, previous work by our group has shown reduced expression of junctional molecules (VE-cadherin, JAM-A, occludin) in HSEC compared to HUVEC, which was thought to underpin intracellular crawling of lymphocytes between adjacent HSEC specifically[470]. These findings provide evidence that variations in the

endothelial phenotype can translate into differences in lymphocyte behaviour. This poses the question of whether this could also be the case for cytoskeletal rearrangements during monocyte transmigration across HSEC. Live cell imaging of actin dynamics during SASP-mediated monocyte and lymphocyte recruitment would offer further insight into this phenomenon and is an area of ongoing research.

Collectively, these data suggest the SASP-mediated monocyte and lymphocyte recruitment occurs by morphologically and molecularly distinct routes through the hepatic endothelium.

6.4.5 The role of PLVAP in SASP-mediated monocyte transmigration

Results in **Chapter 5** have identified a previously unreported link between PLVAP expression, senescence and immune cell infiltrate in CLD and HCC patients. Furthermore, the stimulatory effects of the senescent secretome on PLVAP expression proposes a mechanism by which senescent cells may communicate with the hepatic endothelium, altering its immunomodulatory phenotype and perhaps facilitating recruitment. Given that PLVAP has previously been implicated the trafficking of both monocytes and lymphocytes[366, 460], we sought to investigate a functional role for PLVAP in SASP-mediated leukocyte recruitment. Genetic knockdown or antibody-mediated blockade was used to inhibit PLVAP and flow assays were undertaken to compare monocyte and lymphocyte recruitment across SASP-treated HSEC under physiological shear stress. Whilst PLVAP did not seem to be involved in the adhesion stage of either monocyte or lymphocyte recruitment, monocyte transmigration was selectively impaired following PLVAP inhibition. Furthermore, this finding was only consistently observed in CLD patient-derived HSEC, as results in donor HSEC were variable. This could suggest a mechanistic pathway which is selectively upregulated in a diseased setting, which is consistent with the upregulation of PLVAP during chronic inflammation. Although *PLVAP* gene expression was comparable in donor and diseased HSEC, we cannot confirm at this stage whether there are differences in protein expression at baseline, and responses to stimulation may also vary across different aetiologies. Additional work is required in order to further understand these functional differences.

There are several possible explanations for the differential results obtained for SASP-mediated monocyte and lymphocyte recruitment following PLVAP blockade: (1) its role is indirect, having consequences for downstream effectors specifically involved in monocyte transmigration, such as by altering transcriptional or secretory profiles; (2) PLVAP is specifically involved in paracellular transmigration, leaving lymphocyte transmigration intact since they predominantly migrate transcellularly; (3) PLVAP interacts with a specific monocyte-derived ligand that is not found on lymphocytes. Each of these theories, including evidence for and against them, is outlined in more detail below.

It is possible that genetic knockdown of PLVAP could drive changes in the HSEC transcriptome that may influence expression of genes, and therefore production of proteins, important for monocyte transmigration. It would be interesting to characterise any alterations in HSEC transcription by performing bulk RNA sequencing following PLVAP genetic knockdown. Analysis of the HSEC secretome in response to PLVAP knockdown did not reveal any obvious impairments, with only minor reductions in CXCL12, CCL2, IL-8, CXCL1, IL-21, G-CSF and complement C5a, some of which were restored following SASP stimulation. Furthermore, the consistent effects observed with the anti-PLVAP antibody are suggestive of a direct effect on monocyte transmigration, although a potential impact on the trafficking or interactions of other adhesion molecules necessary for monocyte transmigration cannot be ruled out.

It is conceivable that PLVAP plays a specific role in paracellular transmigration since over 90% of monocytes extravasated via this route. However, the evidence against this idea is two-fold. Firstly, around 40% of lymphocytes transmigrated paracellularly, and so if PLVAP plays a generic role in paracellular migration, we would anticipate at least a partial reduction in lymphocyte transmigration (similar to that observed following CD31 blockade). Instead, genetic knockdown had no effect on lymphocyte transmigration, and if anything was increased in response to the anti-PLVAP antibody. It remains plausible however, that inhibition of PLVAP does in fact impair paracellular lymphocyte migration, forcing them to take the path of least resistance (i.e. the transcellular route) and therefore

masking any effects. Additional studies into the route of transmigration following PLVAP inhibition would be required to confirm this. Secondly, there is evidence to suggest PLVAP may also be important for transcellular migration of lymphocytes, where it has been shown to localise to transmigratory pores observed in TNFα-treated HUVEC[459]. However, these experiments were limited since they were performed under static conditions. Flow assays following HUVEC treatment with an anti-PLVAP antibody showed a similar partial transmigratory defect, but these experiments were undertaken using peripheral blood mononuclear cells (PBMCs), making it difficult to delineate the specific effects on lymphocytes and monocytes[459]. Similar observations were made in HSEC following PLVAP genetic knockdown, and whilst transmigration was not significantly inhibited, again these experiments used PBMCs which could potentially conceal any monocyte-specific observations[397].

Our data suggest that PLVAP does not play a role in SASP-mediated lymphocyte recruitment across HSEC. In addition, although data here suggests that PLVAP plays an undeniable role in SASP-mediated paracellular monocyte transmigration, that is not to say it may not also play a role in transcellular migration of monocytes (or other immune cells for that matter), in settings where this is a more frequent occurrence. One way to investigate whether PLVAP has a role in paracellular migration generally, or is involved in monocyte transmigration specifically, would be to repeat PLVAP inhibition experiments with neutrophils since they are known to predominantly migrate paracellularly. Interestingly, in the context of spinal cord injury, PLVAP-expressing microvessels appear to be spatially correlated with neutrophil extravasation[568]. Moreover, PLVAP inhibition was shown to impair migration of neutrophils, as well as lymphocytes and macrophages, in a murine model of peritonitis[459]. This remains an area for future research.

Given the points discussed above, it is reasonable to predict that PLVAP may interact with a monocyte-enriched ligand to facilitate transmigration. Aside from the homodimeric interactions which occur between PLVAP molecules within fenestral and stomatal diaphragms[443], relatively little is known about its other prospective ligands. Molecular approaches have identified several of PLVAP's binding partners, including NRP1, vimentin, LYVE-1, VEGF, VEGFR2 and heparin, yet how these interactions

relate to its biological functions is still unclear[444, 459, 460, 548]. Rantakari *et al.* proposed that monocytes interact with foetal HSEC-derived PLVAP indirectly, through binding of NRP1 and VEGFR1 via a heparin bridge[460]. However, whether similar interactions occur during SASP-mediated monocyte recruitment across HSEC remain to be explored. Alternatively, PLVAP may interact with, or influence trafficking of, other adhesion molecules important for monocyte transmigration, as mentioned above. Although PLVAP did not seem to be enriched around transmigrating monocytes as observed with CD31, it is known to localise within caveolae, and caveolar structures (including vesiculo-vacuolar organelles) have been implicated in transcellular migration due to their role in vesicular trafficking. Previous work in HUVEC has demonstrated an enrichment of caveolin-1 around lymphocytes undergoing transcellular diapedesis[333, 459], suggesting that caveolar structures could be a source of additional membrane and adhesion molecules required for leukocyte extravasation. Moreover, inhibition of caveolin-1, via RNA interference, reduced transcellular migration of T lymphoblasts across HUVEC[348]. This could also be the case for paracellular transmigration although a definitive role for caveolar structures in this process remains controversial. Future work should aim to elucidate the contribution of caveolae to PLVAP-mediated monocyte transmigration.

Given the frequent localisation of PLVAP towards the cellular junctions, in close association with F-actin, it is possible that PLVAP is a component of the LBRC which is known to contain several other molecules important for transmigration. Interestingly, PLVAP has been shown to bind vimentin which has been identified within the LBRC, and is excluded from the VE-cadherin junctions. The definitive lack of VE-cadherin within the LBRC could provide evidence in favour of PLVAP's residence within this structure. Whether PLVAP permanently resides within this compartment, or whether it is trafficked there specifically in SASP-treated or otherwise stimulated HSEC, also remains a key question. Answering these enquires would require application of super-resolution microscopy techniques in order to understand the dynamics of these complex subcellular structures.

6.5 Clinical implications and future prospects

The hepatic sinusoidal endothelium forms a specialised barrier which supports leukocyte recruitment in response to injury and/or infection as well as during chronic inflammation. The composition of the hepatic immune infiltrate during CLD and cancer has critical implications for disease outcome, since the complex interplay between liver cell types underpins both resolution of inflammation and fibrosis. The liver sinusoids represent a unique environment in which leukocyte recruitment occurs, due to low shear forces, distinct cellular junctions, and expression of atypical adhesion molecules. As such, several receptors have been reported to mediate hepatic leukocyte recruitment specifically, whilst their contribution to recruitment across classic vascular endothelium is thought to be minimal. Furthermore, these molecules seem to selectively recruit distinct immune cell subsets rather than acting as generic recruitment signals. This offers the potential to therapeutically target cell- and liver-specific recruitment whilst preserving leukocyte trafficking at distal sites.

The molecules involved in hepatic leukocyte recruitment are discussed in detail in **Chapter 1**; the majority of these have been identified to play a role in the adhesion stage of the leukocyte adhesion cascade, whilst the mechanisms of transmigration across HSEC remain considerably more elusive. Stabilin-1 has been implicated in the transmigration of $CD4^+$ T and B lymphocytes where it collaborates with ICAM-1 and VAP-1[381]. However, the knowledge surrounding the molecular mechanisms of hepatic monocyte transmigration is limited. Here, PLVAP was identified as a novel regulator of monocyte transmigration, alongside CD31. Whether these two molecules act in synergy during the same stage of transmigration, or whether their roles are sequential, remains to be explored. Additional mechanistic experiments combining antibodies targeted against multiple receptors would delineate this process further. The contribution of other adhesion molecules suggested to be involved in paracellular migration, such as JAM-A, CD99, CD155, endothelial cell-selective adhesion molecule (ESAM), and VAP-1, is also unknown and remains an area for future research.

The process of leukocyte recruitment is complex and dynamic, and mechanistic understanding would be expanded by application of "organ-on-a-chip" approaches, which would incorporate multiple cell types to more accurately recapitulate the sinusoidal microenvironment[569]. In this regard, reconstitution of endothelial, epithelial and stromal cell types within microfluidic chambers, followed by introduction of leukocytes under flow conditions, would allow multi-cellular crosstalk to be modelled *in vitro*. Indeed, Gröger *et al.* (2016) co-cultured HUVEC, primary monocyte-derived macrophages, LX-2 stellate cells and HepaRG cells within multi-organ-tissue-flow (MOTiF) biochips to study monocyte adhesion and transmigration under shear stress[570]. Similar experiments using HSEC instead of HUVEC would offer greater mechanistic insight in the context of hepatic recruitment, but also allow broader assessment of the biological impact of leukocyte migration on liver functionality. Furthermore, use of patient-derived primary cells in chip-based platforms offers the opportunity to model human disease, enhancing discovery of novel targets and drug screening against known targets.

Additionally, live cell imaging of flow assays would allow the study of leukocyte behaviour during recruitment in real-time. Interestingly, reverse transmigration of monocytes has been observed across HSEC under static conditions, which were predominantly found to belong to the $CD16^+$ subset[571]. Whether this occurs under physiological shear stress could also be investigated by live cell imaging of flow assays. This notion also introduces the idea of monocyte subset-specific behaviours; given the subset-specificity of multiple non-classical adhesion molecules, it is conceivable that PLVAP may also mediate selective transmigration of a particular monocyte subpopulation. This could also underpin the partial inhibitory effect of PLVAP blockade observed when using a mixed population of peripheral blood monocytes. The properties of classical, intermediate and non-classical monocytes have been well-characterised, and in the context of the liver, these are known to be functionally distinct[571, 572]. Selective PLVAP-mediated transmigration of a particular subset could therefore have important implications during liver disease. For instance, recruitment of intermediate pro-fibrogenic monocytes across $PLVAP^+$ inflamed sinusoids could be detrimental for the resolution phase of inflammation[572], whilst recruitment of myeloid-derived suppressor cells across $PLVAP^+$ tumour endothelium may support immune evasion

of cancer cells[573]. Additional flow assays with different subsets of monocytes are needed to elucidate this further.

Flow adhesion assays using primary human HSEC and leukocytes have allowed the in-depth mechanistic study of SASP-mediated leukocyte recruitment. However, this does not fully recapitulate recruitment as it occurs *in vivo.* It would therefore be valuable to test the effects of PLVAP inhibition on monocyte recruitment and senescent cell clearance *in vivo*, which would also offer insight into the biological implications in a disease setting. The Δ*Mdm2*^{Hep} model would be a reasonable starting point given that it is associated with senescence, liver injury and PLVAP upregulation, however there would also be scope to test this in various other acute/chronic liver injury and cancer models to understand the implications in several disease contexts. These studies could however be limited by the species-dependent expression of PLVAP, which is considerably more prominent in normal mouse liver than humans, and could therefore present translatability issues. Nevertheless, promising *in vivo* data would further support the pursuit of PLVAP as a potential therapeutic target in CLD and HCC. One possible concern of targeting PLVAP is its widespread expression in vascular endothelium throughout the body, which could lead to unwanted off-target effects following systemic administration of potential therapies. It may therefore be desirable to administer anti-PLVAP pharmacological or biological agents to the liver directly, which can be achieved through intrahepatic delivery via the hepatic artery or hepatic portal vein.

On a more general note, the work presented in this thesis has identified two distinct endothelial cell populations which are differentially regulated in human liver and can be defined based on their expression of MR and PLVAP. Future work should endeavour to characterise these populations in more depth, through RNA sequencing and *in vitro* phenotyping, which would offer insight into their functional contribution to liver homeostasis and inflammation. Overall, the findings presented in this study offer valuable insight into the expression and regulation of MR and PLVAP in the hepatic sinusoids and address the hypothesis of their predicted involvement in hepatic leukocyte recruitment. However, given the limited availability of human samples many of these experiments, particularly flow assays, are likely

underpowered. As a result, in some instances, data trends have been mentioned but are not considered informative without further validation. As such, future work should perform relevant power calculations using existing datasets to ensure the statistical robustness of these results.

6.6 Conclusions

This thesis provides a detailed investigation into the expression and regulation of MR and PLVAP in human liver tissue and primary HSEC. Whilst MR is highly expressed in normal sinusoidal endothelium and likely plays a homeostatic role due to its resistance to regulation, PLVAP is upregulated in CLD and HCC. This is consistent with the upregulation of PLVAP *in vitro* by pro-inflammatory stimuli and the senescent cell secretome, both of which are key components of the tissue microenvironment in chronic liver injury and cancer. Whilst MR does not appear to play a role in lymphocyte recruitment across HSEC, data presented here implicate PLVAP as a leukocyte trafficking molecule in the liver. This work highlights a previously unreported link between PLVAP and senescence, in which senescent cell-endothelial crosstalk drives expression of PLVAP and shapes the immune landscape in CLD and HCC. Specifically, PLVAP was shown to play a selective functional role in SASP-mediated monocyte transmigration which could facilitate senescent cell clearance *in vivo*. PLVAP could therefore be a novel therapeutic target allowing perturbation of aberrant monocyte recruitment during liver inflammation. These data support the further study of PLVAP in pre-clinical models to explore its clinical potential as a therapeutic target for CLD and HCC patients.

7 APPENDICES

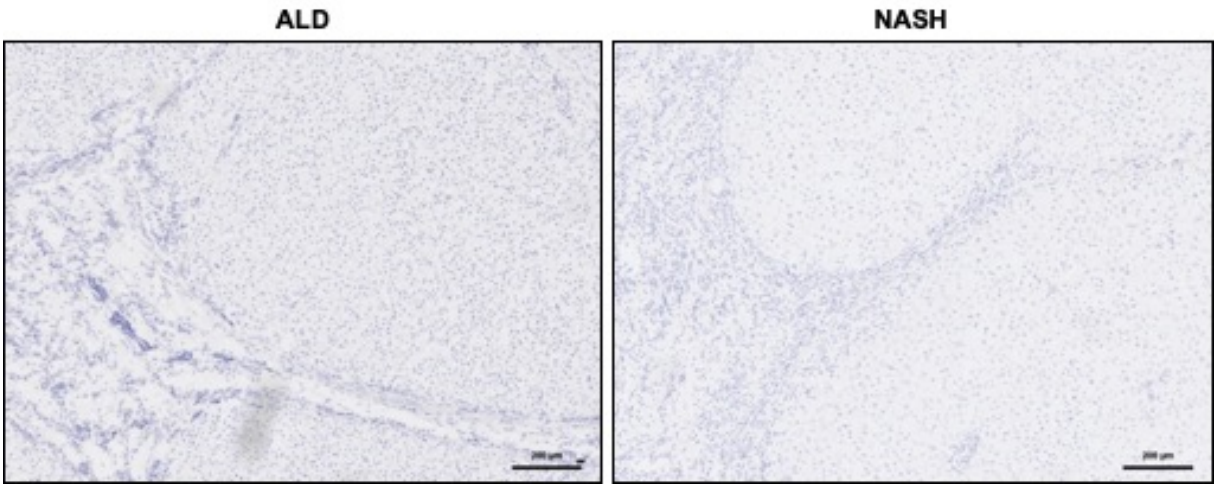

Appendix 7.1: Isotype controls for mannose receptor immunohistochemical staining shown in Figure 3.3. Immunohistochemistry for isotype controls was performed on tissue sections from matched patient samples where possible. Scale bars represent 200 μm.

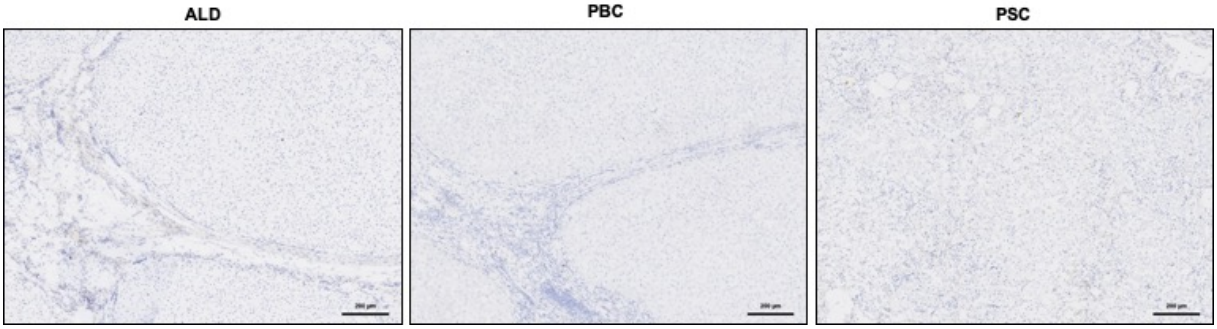

Appendix 7.2: Isotype controls for plasmalemma vesicle-associated protein immunohistochemical staining shown in Figure 3.9. Immunohistochemistry for isotype controls was performed on tissue sections from matched patient samples where possible. Scale bars represent 200 μm.

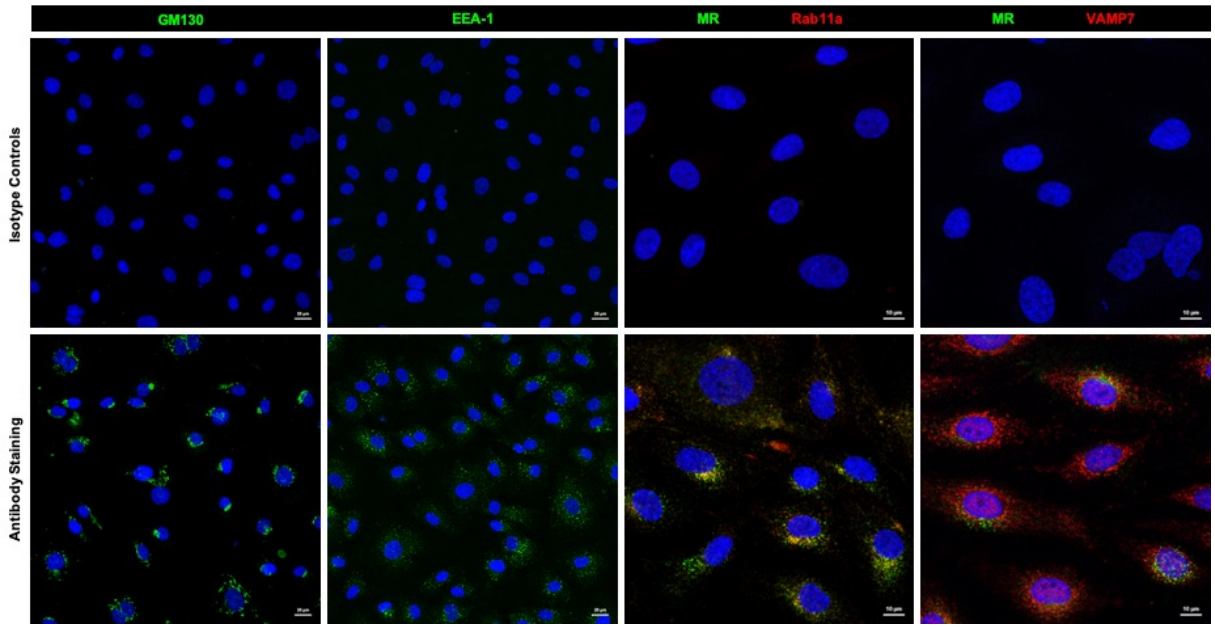

Appendix 7.3: Isotype controls for immunocytochemical staining shown in Figure 4.6. Images were acquired using an LSM880 confocal microscope and a 40x or 63x objective. 4′,6-diamidino-2-phenylindole (DAPI, *blue*) was used as a nuclear counterstain. Scale bars represent 20 µm (GM130, EEA-1) or 10 µm (Rab11a, VAMP7).

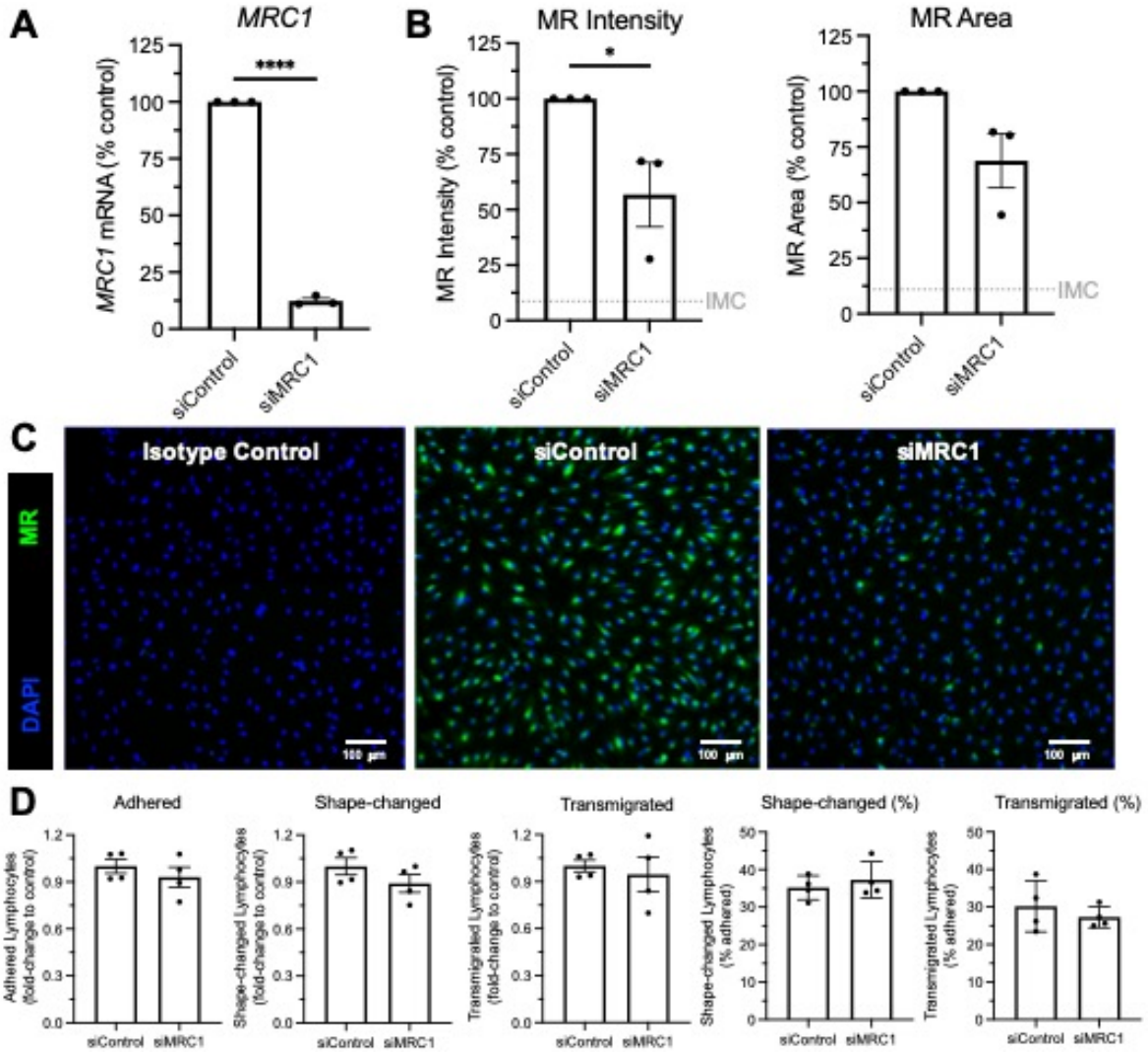

Appendix 7.4: Lymphocyte recruitment was unaffected following mannose receptor (*MRC1*) knockdown. Flow adhesion assays were performed with tumour necrosis factor α (TNFα)-stimulated HSEC following *MRC1* knockdown (or negative control) and lymphocytes isolated from healthy volunteer peripheral blood. (**A-C)** Genetic knockdown was confirmed at the **(A)** mRNA and **(B, C)** protein level by qRT-PCR and immunofluorescence, respectively (**p*<0.05, *****p*<0.0001, student's unpaired *t*-test). Gene expression was measured relative to *GAPDH* and normalised to a % of the negative control. **(D)** The number of adhered, shape-changed and transmigrated lymphocytes were quantified in ten visual fields per lane with each condition performed in duplicate (*p*>0.05, student's unpaired *t*-test or Mann-Whitney test). Data shown are mean ± SEM from 2-3 independent experiments. Scale bars represent 100 µm.

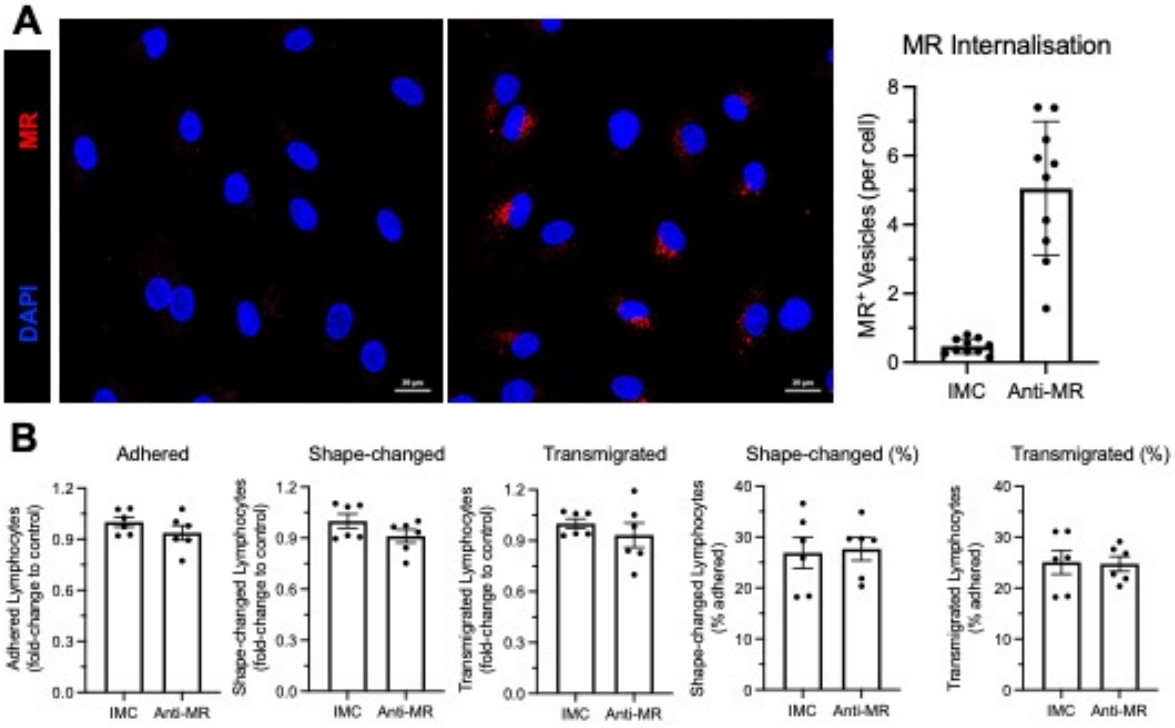

Appendix 7.5: Lymphocyte recruitment was unaffected following antibody-mediated mannose receptor (MR) blockade. Flow adhesion assays were performed with tumour necrosis factor α (TNFα)-stimulated HSEC following treatment with an anti-MR antibody or an isotype-matched control (IMC) and lymphocytes isolated from healthy volunteer peripheral blood. (**A)** MR internalisation was confirmed by immunofluorescence and confocal microscopy. The number of MR^+ vesicles per cell was quantified using the "Analyse Particles" function in ImageJ. Data shown are representative of three independent experiments. **(B)** The number of adhered, shape-changed and transmigrated lymphocytes were quantified in ten visual fields per lane with each condition performed in duplicate (p>0.05, student's unpaired t-test or Mann-Whitney test). Data shown are mean ± SEM from three independent experiments. Scale bars represent 20 μm.

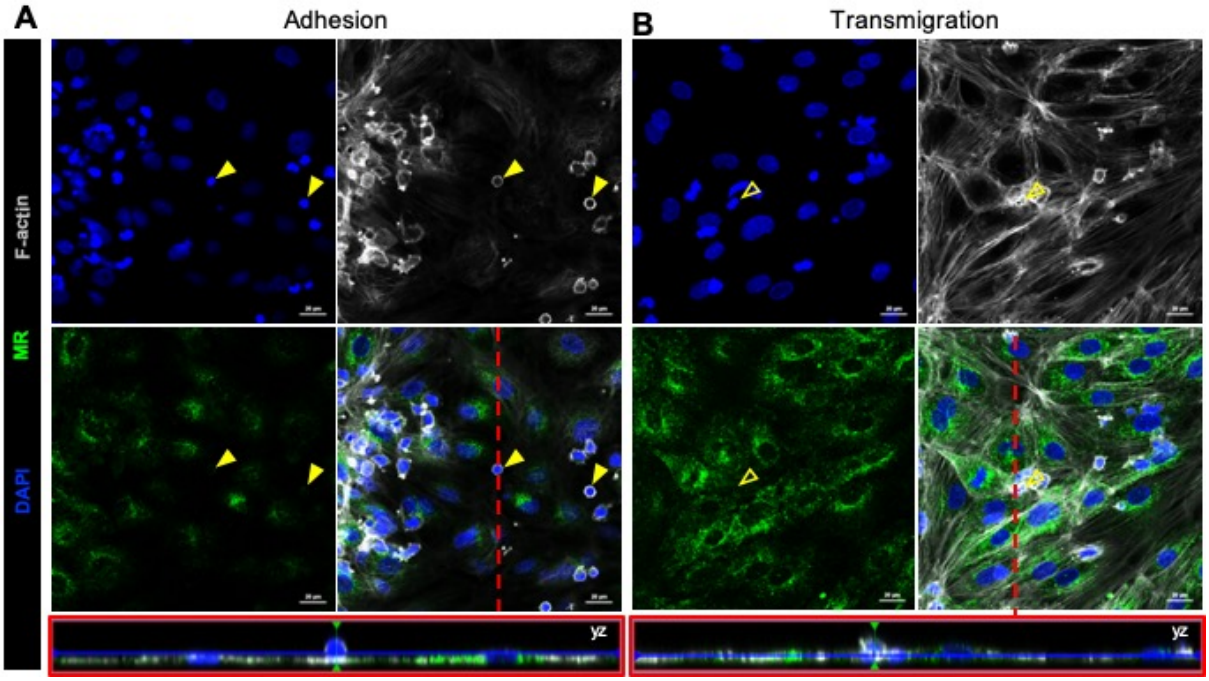

Appendix 7.6: Mannose receptor (MR) did not localise with adhered or transmigrating lymphocytes. Flow adhesion assays were performed with tumour necrosis factor α (TNFα)-stimulated HSEC and lymphocytes isolated from healthy volunteer peripheral blood. Cells were fixed and stained for MR (*green*) and F-actin (phalloidin, *grey*) and **i**mages of **(A)** adhered and **(B)** transmigrating lymphocytes were acquired using an LSM880 confocal microscope. 4′,6-diamidino-2-phenylindole (DAPI, *blue*) was used as a nuclear counterstain. Scale bars represent 20 µm.

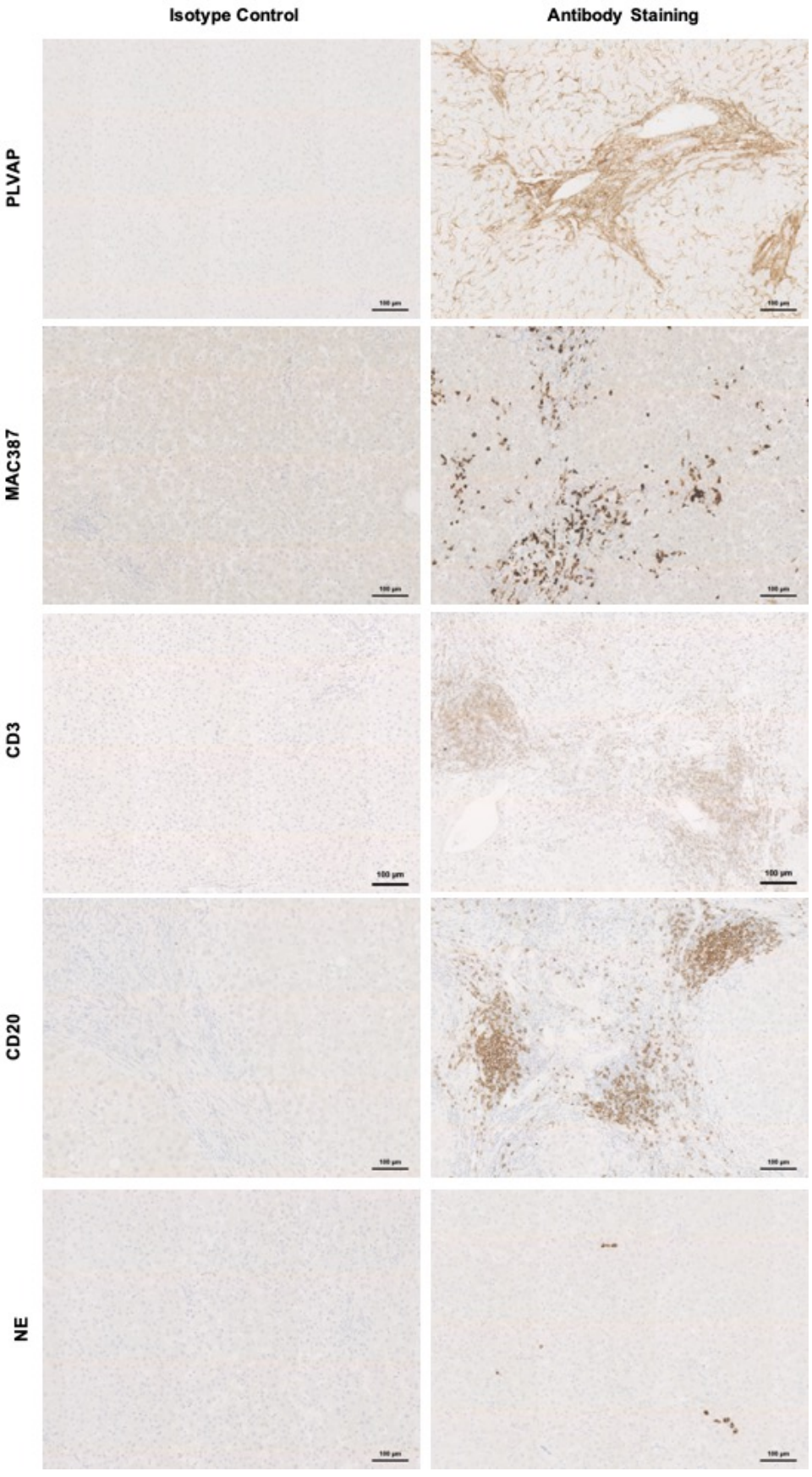

Figure legend on next page.

Appendix 7.7: Isotype controls for immunohistochemical staining shown in Figure 5.21. Isotype controls were performed for each batch of staining. Scale bars represent 100 µm.

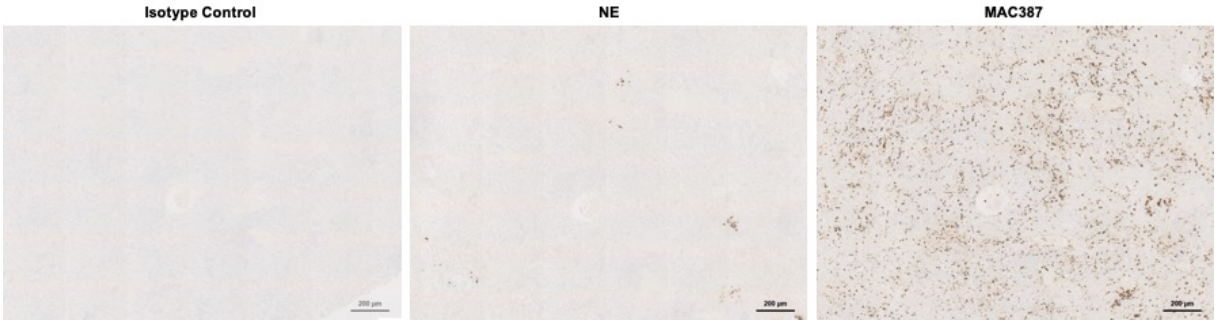

Appendix 7.8: Immunohistochemical staining for neutrophil elastase (NE) and MAC387 highlighted that the contribution of neutrophils to MAC387 immunoreactivity was minimal. Immunohistochemistry was performed on serial tissue sections from matched seronegative hepatitis patient samples (n=4). Isotype control for NE staining (*left*) is shown. Scale bars represent 200 µm.

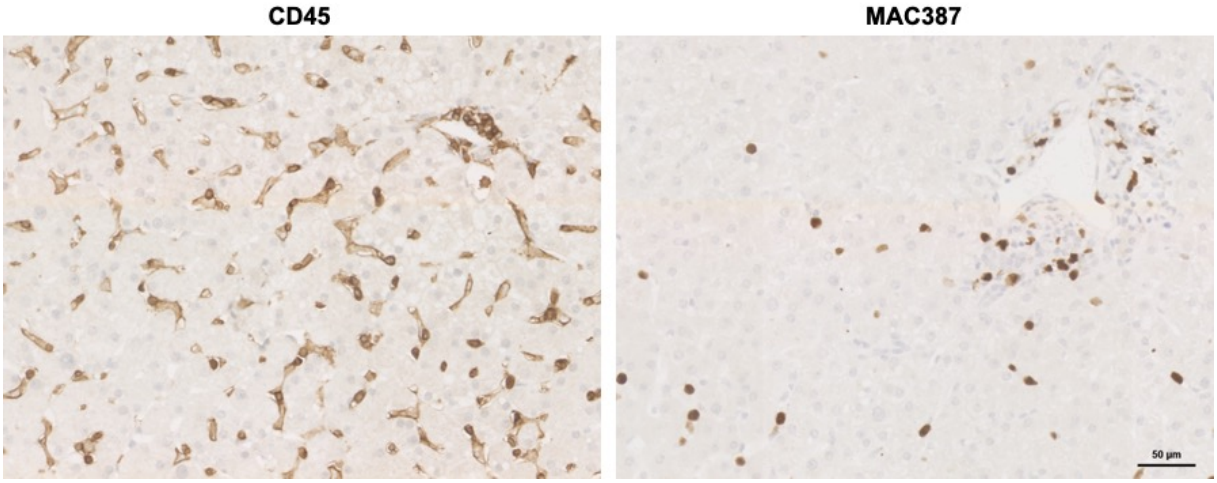

Appendix 7.9: Immunohistochemical staining for CD45 and MAC387 highlighted Kupffer cells (KCs) are generally MAC387-negative. Immunohistochemistry was performed on tissue sections from donor liver. CD45 (*left*) allowed visualisation of immune cell populations showing prominent KC staining, whilst MAC387^{+} cells (*right*) were circular and often localised to the portal tracts. Images shown are matched fields of view from the same patient. Scale bar represents 50 µm.

8 BIBLIOGRAPHY

1. Asrani SK, Devarbhavi H, Eaton J, Kamath PS. Burden of liver diseases in the world. Journal of Hepatology. 2019;70(1):151-71.

2. Geneva world health organisation 2020 [Available from: https://www.who.int/data/gho/data/themes/mortality-and-global-health-estimates/ghe-leading-causes-of-death.

3. British liver trust [Disease Report]. 2019 [updated June 2019. 2019:[Available from: https://britishlivertrust.org.uk/wp-content/uploads/The-alarming-impact-of-liver-disease-FINAL-June-2019.pdf.

4. Abarca-Gómez L, Abdeen ZA, Hamid ZA, Abu-Rmeileh NM, Acosta-Cazares B, Acuin C, et al. Worldwide trends in body-mass index, underweight, overweight, and obesity from 1975 to 2016: A pooled analysis of 2416 population-based measurement studies in 128· 9 million children, adolescents, and adults. The Lancet. 2017;390(10113):2627-42.

5. Younossi ZM, Koenig AB, Abdelatif D, Fazel Y, Henry L, Wymer M. Global epidemiology of nonalcoholic fatty liver disease—meta-analytic assessment of prevalence, incidence, and outcomes. Hepatology. 2016;64(1):73-84.

6. Chuncharunee L, Yamashiki N, Thakkinstian A, Sobhonslidsuk A. Alcohol relapse and its predictors after liver transplantation for alcoholic liver disease: A systematic review and meta-analysis. BMC Gastroenterol. 2019;19(1):150.

7. Neuberger J. Liver transplantation for alcoholic liver disease: What is the risk and consequence of relapse? Dig Dis Sci. 2020.

8. Kok B, Dong V, Karvellas CJ. Graft dysfunction and management in liver transplantation. Crit Care Clin. 2019;35(1):117-33.

9. Jadlowiec CC, Taner T. Liver transplantation: Current status and challenges. World J Gastroenterol. 2016;22(18):4438-45.

10. Moini M, Schilsky ML, Tichy EM. Review on immunosuppression in liver transplantation. World J Hepatol. 2015;7(10):1355-68.

11. Abdel-Misih SRZ, Bloomston M. Liver anatomy. Surgical Clinics of North America. 2010;90(4):643-53.

12. Martini F, Nath JL, Bartholomew EF, Ober WC, Ober CE, Welch K, et al. Fundamentals of anatomy & physiology: Pearson Benjamin Cummings San Francisco, CA; 2012. 890-5 p.

13. Sakamoto Y, Kokudo N, Kawaguchi Y, Akita K. Clinical anatomy of the liver: Review of the 19th meeting of the japanese research society of clinical anatomy. Liver Cancer. 2017;6(2):146-60.

14. Ishizawa T, Gumbs AA, Kokudo N, Gayet B. Laparoscopic segmentectomy of the liver: From segment i to viii. Annals of surgery. 2012;256(6):959-64.

15. Calise F, Giuliani A, Sodano L, Crolla E, Bianco P, Rocca A, et al. Segmentectomy: Is minimally invasive surgery going to change a liver dogma? Updates Surg. 2015;67(2):111-5.

16. Bogdanos DP, Gao B, Gershwin ME. Liver immunology. Compr Physiol. 2013;3(2):567-98.

17. Si-Tayeb K, Lemaigre FP, Duncan SA. Organogenesis and development of the liver. Dev Cell. 2010;18(2):175-89.

18. Mathew RP, Venkatesh SK. Liver vascular anatomy: A refresher. Abdom Radiol (NY). 2018;43(8):1886-95.

19. Naish J, Revest P. Medical sciences: Elsevier Health Sciences; 2009.

20. Corless JK, Middleton HM, 3rd. Normal liver function. A basis for understanding hepatic disease. Arch Intern Med. 1983;143(12):2291-4.

21. Blouin A, Bolender RP, Weibel ER. Distribution of organelles and membranes between hepatocytes and nonhepatocytes in the rat liver parenchyma. A stereological study. J Cell Biol. 1977;72(2):441-55.

22. Braet F, Kalle WH, De Zanger RB, De Grooth BG, Raap AK, Tanke HJ, et al. Comparative atomic force and scanning electron microscopy: An investigation on fenestrated endothelial cells in vitro. J Microsc. 1996;181(Pt 1):10-7.

23. Elvevold K, Smedsrod B, Martinez I. The liver sinusoidal endothelial cell: A cell type of controversial and confusing identity. Am J Physiol Gastrointest Liver Physiol. 2008;294(2):G391-400.

24. Braet F, Wisse E. Structural and functional aspects of liver sinusoidal endothelial cell fenestrae: A review. Comp Hepatol. 2002;1(1):1.

25. Warren A, Le Couteur DG, Fraser R, Bowen DG, McCaughan GW, Bertolino P. T lymphocytes interact with hepatocytes through fenestrations in murine liver sinusoidal endothelial cells. Hepatology. 2006;44(5):1182-90.

26. Guidotti LG, Inverso D, Sironi L, Di Lucia P, Fioravanti J, Ganzer L, et al. Immunosurveillance of the liver by intravascular effector cd8(+) t cells. Cell. 2015;161(3):486-500.

27. Edwards S, Lalor PF, Nash GB, Rainger GE, Adams DH. Lymphocyte traffic through sinusoidal endothelial cells is regulated by hepatocytes. Hepatology. 2005;41(3):451-9.

28. Pineiro-Carrero VM, Pineiro EO. Liver. Pediatrics. 2004;113(4 Suppl):1097-106.

29. Zanger UM, Schwab M. Cytochrome p450 enzymes in drug metabolism: Regulation of gene expression, enzyme activities, and impact of genetic variation. Pharmacol Ther. 2013;138(1):103-41.

30. Smith HS. Opioid metabolism. Mayo Clin Proc. 2009;84(7):613-24.

31. Takahashi T, Lasker JM, Rosman AS, Lieber CS. Induction of cytochrome p-4502e1 in the human liver by ethanol is caused by a corresponding increase in encoding messenger rna. Hepatology. 1993;17(2):236-45.

32. Oneta CM, Lieber CS, Li J, Ruttimann S, Schmid B, Lattmann J, et al. Dynamics of cytochrome p4502e1 activity in man: Induction by ethanol and disappearance during withdrawal phase. J Hepatol. 2002;36(1):47-52.

33. Cederbaum AI. Alcohol metabolism. Clin Liver Dis. 2012;16(4):667-85.

34. Seitz HK, Bataller R, Cortez-Pinto H, Gao B, Gual A, Lackner C, et al. Alcoholic liver disease. Nat Rev Dis Primers. 2018;4(1):16.

35. Leung TM, Nieto N. Cyp2e1 and oxidant stress in alcoholic and non-alcoholic fatty liver disease. J Hepatol. 2013;58(2):395-8.

36. Schattenberg JM, Czaja MJ. Regulation of the effects of cyp2e1-induced oxidative stress by jnk signaling. Redox Biol. 2014;3:7-15.

37. Kensler TW, Roebuck BD, Wogan GN, Groopman JD. Aflatoxin: A 50-year odyssey of mechanistic and translational toxicology. Toxicol Sci. 2011;120 Suppl 1:S28-48.

38. Gu X, Manautou JE. Molecular mechanisms underlying chemical liver injury. Expert Rev Mol Med. 2012;14:e4.

39. Gunawan B, Kaplowitz N. Clinical perspectives on xenobiotic-induced hepatotoxicity. Drug Metab Rev. 2004;36(2):301-12.

40. Shull HJ, Wilkinson GR, Johnson R, Schenker S. Normal disposition of oxazepam in acute viral hepatitis and cirrhosis. Ann Intern Med. 1976;84(4):420-5.

41. Kraus J, Desmond P, Marshall J, Johnson R, Schenker S, Wilkinson G. Effects of aging and liver disease on disposition of lorazepam. Clinical Pharmacology & Therapeutics. 1978;24(4):411-9.

42. Mitchell JR, Thorgeirsson SS, Potter WZ, Jollow DJ, Keiser H. Acetaminophen-induced hepatic injury: Protective role of glutathione in man and rationale for therapy. Clin Pharmacol Ther. 1974;16(4):676-84.

43. Yan M, Huo Y, Yin S, Hu H. Mechanisms of acetaminophen-induced liver injury and its implications for therapeutic interventions. Redox Biol. 2018;17:274-83.

44. Nyblom H, Berggren U, Balldin J, Olsson R. High ast/alt ratio may indicate advanced alcoholic liver disease rather than heavy drinking. Alcohol Alcohol. 2004;39(4):336-9.

45. Gopal DV, Rosen HR. Abnormal findings on liver function tests. Interpreting results to narrow the diagnosis and establish a prognosis. Postgrad Med. 2000;107(2):100-2, 5-9, 13-4.

46. Cahill GF, Jr. Starvation in man. N Engl J Med. 1970;282(12):668-75.

47. Frayn KN, Arner P, Yki-Järvinen H. Fatty acid metabolism in adipose tissue, muscle and liver in health and disease. Essays Biochem. 2006;42:89-103.

48. Tall AR, Small DM. Plasma high-density lipoproteins. New England Journal of Medicine. 1978;299(22):1232-6.

49. Rothschild MA, Oratz M, Schreiber SS. Albumin synthesis. 1. N Engl J Med. 1972;286(14):748-57.

50. Palta S, Saroa R, Palta A. Overview of the coagulation system. Indian J Anaesth. 2014;58(5):515-23.

51. Jelkmann W. The role of the liver in the production of thrombopoietin compared with erythropoietin. Eur J Gastroenterol Hepatol. 2001;13(7):791-801.

52. Matsusaka T, Niimura F, Shimizu A, Pastan I, Saito A, Kobori H, et al. Liver angiotensinogen is the primary source of renal angiotensin ii. J Am Soc Nephrol. 2012;23(7):1181-9.

53. Capdevila J, Chacos N, Werringloer J, Prough RA, Estabrook RW. Liver microsomal cytochrome p-450 and the oxidative metabolism of arachidonic acid. Proceedings of the National Academy of Sciences. 1981;78(9):5362.

54. Bozza PT, Bakker-Abreu I, Navarro-Xavier RA, Bandeira-Melo C. Lipid body function in eicosanoid synthesis: An update. Prostaglandins, Leukotrienes and Essential Fatty Acids. 2011;85(5):205-13.

55. Franco RS. Measurement of red cell lifespan and aging. Transfus Med Hemother. 2012;39(5):302-7.

56. Williams R, Schalm SW, O'Grady JG. Acute liver failure: Redefining the syndromes. The Lancet. 1993;342(8866):273-5.

57. Stanger BZ. Cellular homeostasis and repair in the mammalian liver. Annu Rev Physiol. 2015;77:179-200.

58. Kietzmann T. Metabolic zonation of the liver: The oxygen gradient revisited. Redox Biol. 2017;11:622-30.

59. Birchmeier W. Orchestrating wnt signalling for metabolic liver zonation. Nature Cell Biology. 2016;18(5):463-5.

60. Gebhardt R. Metabolic zonation of the liver: Regulation and implications for liver function. Pharmacol Ther. 1992;53(3):275-354.

61. Jungermann K, Kietzmann T. Zonation of parenchymal and nonparenchymal metabolism in liver. Annu Rev Nutr. 1996;16:179-203.

62. Yang J, Mowry LE, Nejak-Bowen KN, Okabe H, Diegel CR, Lang RA, et al. Beta-catenin signaling in murine liver zonation and regeneration: A wnt-wnt situation! Hepatology. 2014;60(3):964-76.

63. Preziosi M, Okabe H, Poddar M, Singh S, Monga SP. Endothelial wnts regulate beta-catenin signaling in murine liver zonation and regeneration: A sequel to the wnt-wnt situation. Hepatol Commun. 2018;2(7):845-60.

64. Dobie R, Wilson-Kanamori JR, Henderson BEP, Smith JR, Matchett KP, Portman JR, et al. Single-cell transcriptomics uncovers zonation of function in the mesenchyme during liver fibrosis. Cell Rep. 2019;29(7):1832-47.e8.

65. Halpern KB, Shenhav R, Massalha H, Toth B, Egozi A, Massasa EE, et al. Paired-cell sequencing enables spatial gene expression mapping of liver endothelial cells. Nat Biotechnol. 2018;36(10):962-70.

66. Su T, Yang Y, Lai S, Jeong J, Jung Y, McConnell M, et al. Single-cell transcriptomics reveals zone-specific alterations of liver sinusoidal endothelial cells in cirrhosis. Cellular and Molecular Gastroenterology and Hepatology. 2021;11(4):1139-61.

67. Aizarani N, Saviano A, Sagar, Mailly L, Durand S, Herman JS, et al. A human liver cell atlas reveals heterogeneity and epithelial progenitors. Nature. 2019;572(7768):199-204.

68. Gola A, Dorrington MG, Speranza E, Sala C, Shih RM, Radtke AJ, et al. Commensal-driven immune zonation of the liver promotes host defence. Nature. 2021;589(7840):131-6.

69. Ding C, Li Y, Guo F, Jiang Y, Ying W, Li D, et al. A cell-type-resolved liver proteome. Mol Cell Proteomics. 2016;15(10):3190-202.

70. Marrone G, Shah VH, Gracia-Sancho J. Sinusoidal communication in liver fibrosis and regeneration. J Hepatol. 2016;65(3):608-17.

71. Washabau RJ. Liver. In: Washabau RJ, Day MJ, editors. Canine and feline gastroenterology. Saint Louis: W.B. Saunders; 2013. p. 849-957.

72. Celton-Morizur S, Merlen G, Couton D, Desdouets C. Polyploidy and liver proliferation: Central role of insulin signaling. Cell Cycle. 2010;9(3):460-6.

73. MacDonald RA. Lifespan of liver cells: Autoradiographic study using tritiated thymidine in normal, cirrhotic, and partially hepatectomized rats. Archives of internal medicine. 1961;107(3):335-43.

74. Berasain C, Avila MA. Regulation of hepatocyte identity and quiescence. Cell Mol Life Sci. 2015;72(20):3831-51.

75. Patten DA, Shetty S. More than just a removal service: Scavenger receptors in leukocyte trafficking. Front Immunol. 2018;9:2904.

76. Wilkinson AL, Qurashi M, Shetty S. The role of sinusoidal endothelial cells in the axis of inflammation and cancer within the liver. Frontiers in Physiology. 2020;11.

77. Shetty S, Lalor PF, Adams DH. Liver sinusoidal endothelial cells - gatekeepers of hepatic immunity. Nat Rev Gastroenterol Hepatol. 2018;15(9):555-67.

78. Geerts A. History, heterogeneity, developmental biology, and functions of quiescent hepatic stellate cells. Semin Liver Dis. 2001;21(3):311-35.

79. Hendriks HFJ, Verhoofstad WAMM, Brouwer A, De Leeuw AM, Knook DL. Perisinusoidal fat-storing cells are the main vitamin a storage sites in rat liver. Experimental Cell Research. 1985;160(1):138-49.

80. McCuskey RS. Morphological mechanisms for regulating blood flow through hepatic sinusoids. Liver. 2000;20(1):3-7.

81. Rockey D. The cellular pathogenesis of portal hypertension: Stellate cell contractility, endothelin, and nitric oxide. Hepatology. 1997;25(1):2-5.

82. Pellicoro A, Ramachandran P, Iredale JP, Fallowfield JA. Liver fibrosis and repair: Immune regulation of wound healing in a solid organ. Nat Rev Immunol. 2014;14(3):181-94.

83. Patten DA, Shepherd EL, Weston CJ, Shetty S. Novel targets in the immune microenvironment of the hepatic sinusoids for treating liver diseases. Semin Liver Dis. 2019;39(2):111-23.

84. Wang Y, Zhang C. The roles of liver-resident lymphocytes in liver diseases. Frontiers in Immunology. 2019;10(1582).

85. Doherty DG, Norris S, Madrigal-Estebas L, McEntee G, Traynor O, Hegarty JE, et al. The human liver contains multiple populations of nk cells, t cells, and cd3+cd56+ natural t cells with distinct cytotoxic activities and th1, th2, and th0 cytokine secretion patterns. The Journal of Immunology. 1999;163(4):2314.

86. Skon CN, Lee J-Y, Anderson KG, Masopust D, Hogquist KA, Jameson SC. Transcriptional downregulation of s1pr1 is required for the establishment of resident memory cd8+ t cells. Nature immunology. 2013;14(12):1285.

87. Shiow LR, Rosen DB, Brdičková N, Xu Y, An J, Lanier LL, et al. Cd69 acts downstream of interferon-α/β to inhibit s1p 1 and lymphocyte egress from lymphoid organs. Nature. 2006;440(7083):540-4.

88. Geissmann F, Cameron TO, Sidobre S, Manlongat N, Kronenberg M, Briskin MJ, et al. Intravascular immune surveillance by cxcr6+ nkt cells patrolling liver sinusoids. PLoS biology. 2005;3(4).

89. Peng H, Sun R. Liver-resident nk cells and their potential functions. Cellular & molecular immunology. 2017;14(11):890-4.

90. Mori L, Lepore M, De Libero G. The immunology of cd1- and mr1-restricted t cells. Annual Review of Immunology. 2016;34(1):479-510.

91. Yin C, Evason KJ, Asahina K, Stainier DY. Hepatic stellate cells in liver development, regeneration, and cancer. J Clin Invest. 2013;123(5):1902-10.

92. Kmieć Z. Cooperation of liver cells in health and disease. Adv Anat Embryol Cell Biol. 2001;161:Iii-xiii, 1-151.

93. Gracia-Sancho J, Russo L, Garcia-Caldero H, Garcia-Pagan JC, Garcia-Cardena G, Bosch J. Endothelial expression of transcription factor kruppel-like factor 2 and its vasoprotective target genes in the normal and cirrhotic rat liver. Gut. 2011;60(4):517-24.

94. Shah V, Haddad FG, Garcia-Cardena G, Frangos JA, Mennone A, Groszmann RJ, et al. Liver sinusoidal endothelial cells are responsible for nitric oxide modulation of resistance in the hepatic sinusoids. J Clin Invest. 1997;100(11):2923-30.

95. Parmar KM, Larman HB, Dai G, Zhang Y, Wang ET, Moorthy SN, et al. Integration of flow-dependent endothelial phenotypes by kruppel-like factor 2. J Clin Invest. 2006;116(1):49-58.

96. Kawada N, Tran-Thi TA, Klein H, Decker K. The contraction of hepatic stellate (ito) cells stimulated with vasoactive substances. Possible involvement of endothelin 1 and nitric oxide in the regulation of the sinusoidal tonus. Eur J Biochem. 1993;213(2):815-23.

97. Deleve LD, Wang X, Guo Y. Sinusoidal endothelial cells prevent rat stellate cell activation and promote reversion to quiescence. Hepatology. 2008;48(3):920-30.

98. DeLeve LD, Wang X, Hu L, McCuskey MK, McCuskey RS. Rat liver sinusoidal endothelial cell phenotype is maintained by paracrine and autocrine regulation. American Journal of Physiology-Gastrointestinal and Liver Physiology. 2004;287(4):G757-G63.

99. Kubes P, Jenne C. Immune responses in the liver. Annu Rev Immunol. 2018;36:247-77.

100. Jenne CN, Kubes P. Immune surveillance by the liver. Nat Immunol. 2013;14(10):996-1006.

101. Bode JG, Albrecht U, Häussinger D, Heinrich PC, Schaper F. Hepatic acute phase proteins--regulation by il-6- and il-1-type cytokines involving stat3 and its crosstalk with nf-κb-dependent signaling. Eur J Cell Biol. 2012;91(6-7):496-505.

102. Mehrfeld C, Zenner S, Kornek M, Lukacs-Kornek V. The contribution of non-professional antigen-presenting cells to immunity and tolerance in the liver. Front Immunol. 2018;9:635.

103. You Q, Cheng L, Kedl RM, Ju C. Mechanism of t cell tolerance induction by murine hepatic kupffer cells. Hepatology. 2008;48(3):978-90.

104. Katz SC, Pillarisetty VG, Bleier JI, Shah AB, DeMatteo RP. Liver sinusoidal endothelial cells are insufficient to activate t cells. J Immunol. 2004;173(1):230-5.

105. Knolle P, Schlaak J, Uhrig A, Kempf P, Meyer zum Büschenfelde KH, Gerken G. Human kupffer cells secrete il-10 in response to lipopolysaccharide (lps) challenge. J Hepatol. 1995;22(2):226-9.

106. Knolle PA, Germann T, Treichel U, Uhrig A, Schmitt E, Hegenbarth S, et al. Endotoxin down-regulates t cell activation by antigen-presenting liver sinusoidal endothelial cells. The Journal of Immunology. 1999;162(3):1401-7.

107. Knolle P, Uhrig A, Hegenbarth S, Löser E, Schmitt E, Gerken G, et al. Il-10 down-regulates t cell activation by antigen-presenting liver sinusoidal endothelial cells through decreased antigen uptake via the mannose receptor and lowered surface expression of accessory molecules. Clinical and experimental immunology. 1998;114(3):427.

108. Knolle PA, Schmitt E, Jin S, Germann T, Duchmann R, Hegenbarth S, et al. Induction of cytokine production in naive cd4(+) t cells by antigen-presenting murine liver sinusoidal endothelial cells but failure to induce differentiation toward th1 cells. Gastroenterology. 1999;116(6):1428-40.

109. Diehl L, Schurich A, Grochtmann R, Hegenbarth S, Chen L, Knolle PA. Tolerogenic maturation of liver sinusoidal endothelial cells promotes b7-homolog 1-dependent cd8+ t cell tolerance. Hepatology. 2008;47(1):296-305.

110. Limmer A, Ohl J, Kurts C, Ljunggren HG, Reiss Y, Groettrup M, et al. Efficient presentation of exogenous antigen by liver endothelial cells to cd8+ t cells results in antigen-specific t-cell tolerance. Nat Med. 2000;6(12):1348-54.

111. Limmer A, Ohl J, Wingender G, Berg M, Jüngerkes F, Schumak B, et al. Cross-presentation of oral antigens by liver sinusoidal endothelial cells leads to cd8 t cell tolerance. European journal of immunology. 2005;35(10):2970-81.

112. Rubinstein D, Roska AK, Lipsky PE. Liver sinusoidal lining cells express class ii major histocompatibility antigens but are poor stimulators of fresh allogeneic t lymphocytes. J Immunol. 1986;137(6):1803-10.

113. Lohse AW, Knolle PA, Bilo K, Uhrig A, Waldmann C, Ibe M, et al. Antigen-presenting function and b7 expression of murine sinusoidal endothelial cells and kupffer cells. Gastroenterology. 1996;110(4):1175-81.

114. Berg M, Wingender G, Djandji D, Hegenbarth S, Momburg F, Hämmerling G, et al. Cross-presentation of antigens from apoptotic tumor cells by liver sinusoidal endothelial cells leads to tumor-specific cd8+ t cell tolerance. European journal of immunology. 2006;36(11):2960-70.

115. Schurich A, Böttcher JP, Burgdorf S, Penzler P, Hegenbarth S, Kern M, et al. Distinct kinetics and dynamics of cross-presentation in liver sinusoidal endothelial cells compared to dendritic cells. Hepatology. 2009;50(3):909-19.

116. Böttcher Jan P, Schanz O, Wohlleber D, Abdullah Z, Debey-Pascher S, Staratschek-Jox A, et al. Liver-primed memory t cells generated under noninflammatory conditions provide anti-infectious immunity. Cell Reports. 2013;3(3):779-95.

117. Carambia A, Freund B, Schwinge D, Heine M, Laschtowitz A, Huber S, et al. Tgf-β-dependent induction of cd4+ cd25+ foxp3+ tregs by liver sinusoidal endothelial cells. Journal of hepatology. 2014;61(3):594-9.

118. Kruse N, Neumann K, Schrage A, Derkow K, Schott E, Erben U, et al. Priming of cd4+ t cells by liver sinusoidal endothelial cells induces cd25low forkhead box protein 3− regulatory t cells suppressing autoimmune hepatitis. Hepatology. 2009;50(6):1904-13.

119. Tang L, Yang J, Liu W, Tang X, Chen J, Zhao D, et al. Liver sinusoidal endothelial cell lectin, lsectin, negatively regulates hepatic t-cell immune response. Gastroenterology. 2009;137(4):1498-508.e5.

120. Schildberg FA, Hegenbarth SI, Schumak B, Limmer A, Knolle PA. Liver sinusoidal endothelial cells veto cd8 t cell activation by antigen-presenting dendritic cells. European journal of immunology. 2008;38(4):957-67.

121. Pillarisetty VG, Shah AB, Miller G, Bleier JI, DeMatteo RP. Liver dendritic cells are less immunogenic than spleen dendritic cells because of differences in subtype composition. J Immunol. 2004;172(2):1009-17.

122. Goddard S, Youster J, Morgan E, Adams DH. Interleukin-10 secretion differentiates dendritic cells from human liver and skin. Am J Pathol. 2004;164(2):511-9.

123. Tokita D, Sumpter TL, Raimondi G, Zahorchak AF, Wang Z, Nakao A, et al. Poor allostimulatory function of liver plasmacytoid dc is associated with pro-apoptotic activity, dependent on regulatory t cells. Journal of hepatology. 2008;49(6):1008-18.

124. Bamboat ZM, Stableford JA, Plitas G, Burt BM, Nguyen HM, Welles AP, et al. Human liver dendritic cells promote t cell hyporesponsiveness. J Immunol. 2009;182(4):1901-11.

125. Pillarisetty VG, Katz SC, Bleier JI, Shah AB, Dematteo RP. Natural killer dendritic cells have both antigen presenting and lytic function and in response to cpg produce ifn-gamma via autocrine il-12. J Immunol. 2005;174(5):2612-8.

126. Chen L, Calomeni E, Wen J, Ozato K, Shen R, Gao JX. Natural killer dendritic cells are an intermediate of developing dendritic cells. J Leukoc Biol. 2007;81(6):1422-33.

127. Bertolino P, Trescol-Biémont MC, Rabourdin-Combe C. Hepatocytes induce functional activation of naive cd8+ t lymphocytes but fail to promote survival. Eur J Immunol. 1998;28(1):221-36.

128. Wahl C, Bochtler P, Chen L, Schirmbeck R, Reimann J. B7-h1 on hepatocytes facilitates priming of specific cd8 t cells but limits the specific recall of primed responses. Gastroenterology. 2008;135(3):980-8.

129. Holz LE, Benseler V, Bowen DG, Bouillet P, Strasser A, O'Reilly L, et al. Intrahepatic murine cd8 t-cell activation associates with a distinct phenotype leading to bim-dependent death. Gastroenterology. 2008;135(3):989-97.

130. Herkel J, Jagemann B, Wiegard C, Lazaro JFG, Lueth S, Kanzler S, et al. Mhc class ii-expressing hepatocytes function as antigen-presenting cells and activate specific cd4 t lymphocyutes. Hepatology. 2003;37(5):1079-85.

131. Sumpter TL, Dangi A, Matta BM, Huang C, Stolz DB, Vodovotz Y, et al. Hepatic stellate cells undermine the allostimulatory function of liver myeloid dendritic cells via stat3-dependent induction of ido. The Journal of Immunology. 2012;189(8):3848.

132. Höchst B, Schildberg FA, Sauerborn P, Gäbel YA, Gevensleben H, Goltz D, et al. Activated human hepatic stellate cells induce myeloid derived suppressor cells from peripheral blood monocytes in a cd44-dependent fashion. Journal of Hepatology. 2013;59(3):528-35.

133. Yu MC, Chen CH, Liang X, Wang L, Gandhi CR, Fung JJ, et al. Inhibition of t-cell responses by hepatic stellate cells via b7-h1-mediated t-cell apoptosis in mice. Hepatology. 2004;40(6):1312-21.

134. Dunham RM, Thapa M, Velazquez VM, Elrod EJ, Denning TL, Pulendran B, et al. Hepatic stellate cells preferentially induce foxp3+ regulatory t cells by production of retinoic acid. The Journal of Immunology. 2013;190(5):2009.

135. Schildberg FA, Wojtalla A, Siegmund SV, Endl E, Diehl L, Abdullah Z, et al. Murine hepatic stellate cells veto cd8 t cell activation by a cd54-dependent mechanism. Hepatology. 2011;54(1):262-72.

136. Ebe Y, Hasegawa G, Takatsuka H, Umezu H, Mitsuyama M, Arakawa M, et al. The role of kupffer cells and regulation of neutrophil migration into the liver by macrophage inflammatory protein-2 in primary listeriosis in mice. Pathol Int. 1999;49(6):519-32.

137. Lee WY, Moriarty TJ, Wong CH, Zhou H, Strieter RM, van Rooijen N, et al. An intravascular immune response to borrelia burgdorferi involves kupffer cells and inkt cells. Nat Immunol. 2010;11(4):295-302.

138. Helmy KY, Katschke KJ, Jr., Gorgani NN, Kljavin NM, Elliott JM, Diehl L, et al. Crig: A macrophage complement receptor required for phagocytosis of circulating pathogens. Cell. 2006;124(5):915-27.

139. Notas G, Kisseleva T, Brenner D. Nk and nkt cells in liver injury and fibrosis. Clin Immunol. 2009;130(1):16-26.

140. Sun JC, Madera S, Bezman NA, Beilke JN, Kaplan MH, Lanier LL. Proinflammatory cytokine signaling required for the generation of natural killer cell memory. J Exp Med. 2012;209(5):947-54.

141. Sun JC, Beilke JN, Lanier LL. Adaptive immune features of natural killer cells. Nature. 2009;457(7229):557-61.

142. Geissmann F, Cameron TO, Sidobre S, Manlongat N, Kronenberg M, Briskin MJ, et al. Intravascular immune surveillance by cxcr6+ nkt cells patrolling liver sinusoids. PLOS Biology. 2005;3(4):e113.

143. Bendelac A, Rivera MN, Park SH, Roark JH. Mouse cd1-specific nk1 t cells: Development, specificity, and function. Annu Rev Immunol. 1997;15:535-62.

144. Dashtsoodol N, Shigeura T, Aihara M, Ozawa R, Kojo S, Harada M, et al. Alternative pathway for the development of v(α)14(+) nkt cells directly from cd4(-)cd8(-) thymocytes that bypasses the cd4(+)cd8(+) stage. Nat Immunol. 2017;18(3):274-82.

145. Brossay L, Chioda M, Burdin N, Koezuka Y, Casorati G, Dellabona P, et al. Cd1d-mediated recognition of an alpha-galactosylceramide by natural killer t cells is highly conserved through mammalian evolution. J Exp Med. 1998;188(8):1521-8.

146. Gumperz JE, Miyake S, Yamamura T, Brenner MB. Functionally distinct subsets of cd1d-restricted natural killer t cells revealed by cd1d tetramer staining. J Exp Med. 2002;195(5):625-36.

147. Kawano T, Cui J, Koezuka Y, Toura I, Kaneko Y, Sato H, et al. Natural killer-like nonspecific tumor cell lysis mediated by specific ligand-activated vα14 nkt cells. Proceedings of the National Academy of Sciences. 1998;95(10):5690.

148. Stetson DB, Mohrs M, Reinhardt RL, Baron JL, Wang Z-E, Gapin L, et al. Constitutive cytokine mrnas mark natural killer (nk) and nk t cells poised for rapid effector function. The Journal of experimental medicine. 2003;198(7):1069-76.

149. Wong CH, Jenne CN, Lee WY, Léger C, Kubes P. Functional innervation of hepatic inkt cells is immunosuppressive following stroke. Science. 2011;334(6052):101-5.

150. Liew PX, Lee WY, Kubes P. Inkt cells orchestrate a switch from inflammation to resolution of sterile liver injury. Immunity. 2017;47(4):752-65.e5.

151. Winau F, Hegasy G, Weiskirchen R, Weber S, Cassan C, Sieling PA, et al. Ito cells are liver-resident antigen-presenting cells for activating t cell responses. Immunity. 2007;26(1):117-29.

152. Zeissig S, Peuker K, Iyer S, Gensollen T, Dougan SK, Olszak T, et al. Cd1d-restricted pathways in hepatocytes control local natural killer t cell homeostasis and hepatic inflammation. Proceedings of the National Academy of Sciences. 2017;114(39):10449.

153. Trobonjaca Z, Leithäuser F, Möller P, Schirmbeck R, Reimann J. Activating immunity in the liver. I. Liver dendritic cells (but not hepatocytes) are potent activators of ifn-γ release by liver nkt cells. The Journal of Immunology. 2001;167(3):1413.

154. Zeissig S, Murata K, Sweet L, Publicover J, Hu Z, Kaser A, et al. Hepatitis b virus–induced lipid alterations contribute to natural killer t cell–dependent protective immunity. Nature Medicine. 2012;18(7):1060-8.

155. Wohlleber D, Kashkar H, Gärtner K, Frings Marianne K, Odenthal M, Hegenbarth S, et al. Tnf-induced target cell killing by ctl activated through cross-presentation. Cell Reports. 2012;2(3):478-87.

156. Lumsden AB, Henderson JM, Kutner MH. Endotoxin levels measured by a chromogenic assay in portal, hepatic and peripheral venous blood in patients with cirrhosis. Hepatology. 1988;8(2):232-6.

157. Berg RD. Bacterial translocation from the gastrointestinal tract. Trends Microbiol. 1995;3(4):149-54.

158. Paulos CM, Wrzesinski C, Kaiser A, Hinrichs CS, Chieppa M, Cassard L, et al. Microbial translocation augments the function of adoptively transferred self/tumor-specific cd8+ t cells via tlr4 signaling. J Clin Invest. 2007;117(8):2197-204.

159. Gorgani NN, He JQ, Katschke KJ, Jr., Helmy KY, Xi H, Steffek M, et al. Complement receptor of the ig superfamily enhances complement-mediated phagocytosis in a subpopulation of tissue resident macrophages. J Immunol. 2008;181(11):7902-8.

160. He JQ, Katschke KJ, Jr., Gribling P, Suto E, Lee WP, Diehl L, et al. Crig mediates early kupffer cell responses to adenovirus. J Leukoc Biol. 2013;93(2):301-6.

161. Zeng Z, Surewaard BG, Wong CH, Geoghegan JA, Jenne CN, Kubes P. Crig functions as a macrophage pattern recognition receptor to directly bind and capture blood-borne gram-positive bacteria. Cell Host Microbe. 2016;20(1):99-106.

162. Wu J, Meng Z, Jiang M, Zhang E, Trippler M, Broering R, et al. Toll-like receptor-induced innate immune responses in non-parenchymal liver cells are cell type-specific. Immunology. 2010;129(3):363-74.

163. Sørensen KK, McCourt P, Berg T, Crossley C, Le Couteur D, Wake K, et al. The scavenger endothelial cell: A new player in homeostasis and immunity. Am J Physiol Regul Integr Comp Physiol. 2012;303(12):R1217-30.

164. Uhrig A, Banafsche R, Kremer M, Hegenbarth S, Hamann A, Neurath M, et al. Development and functional consequences of lps tolerance in sinusoidal endothelial cells of the liver. Journal of leukocyte biology. 2005;77(5):626-33.

165. Schurich A, Berg M, Stabenow D, Böttcher J, Kern M, Schild H-J, et al. Dynamic regulation of cd8 t cell tolerance induction by liver sinusoidal endothelial cells. The Journal of Immunology. 2010;184(8):4107.

166. Huang LR, Wohlleber D, Reisinger F, Jenne CN, Cheng RL, Abdullah Z, et al. Intrahepatic myeloid-cell aggregates enable local proliferation of cd8(+) t cells and successful immunotherapy against chronic viral liver infection. Nat Immunol. 2013;14(6):574-83.

167. Brinkmann V, Reichard U, Goosmann C, Fauler B, Uhlemann Y, Weiss DS, et al. Neutrophil extracellular traps kill bacteria. Science. 2004;303(5663):1532-5.

168. Jenne CN, Wong CH, Zemp FJ, McDonald B, Rahman MM, Forsyth PA, et al. Neutrophils recruited to sites of infection protect from virus challenge by releasing neutrophil extracellular traps. Cell Host Microbe. 2013;13(2):169-80.

169. McDonald B, Urrutia R, Yipp BG, Jenne CN, Kubes P. Intravascular neutrophil extracellular traps capture bacteria from the bloodstream during sepsis. Cell Host Microbe. 2012;12(3):324-33.

170. Jenne CN, Wong CH, Petri B, Kubes P. The use of spinning-disk confocal microscopy for the intravital analysis of platelet dynamics in response to systemic and local inflammation. PLoS One. 2011;6(9):e25109.

171. Davies SP, Terry LV, Wilkinson AL, Stamataki Z. Cell-in-cell structures in the liver: A tale of four e's. Frontiers in Immunology. 2020;11:650.

172. Shi J, Fujieda H, Kokubo Y, Wake K. Apoptosis of neutrophils and their elimination by kupffer cells in rat liver. Hepatology. 1996;24(5):1256-63.

173. Canbay A, Taimr P, Torok N, Higuchi H, Friedman S, Gores GJ. Apoptotic body engulfment by a human stellate cell line is profibrogenic. Laboratory investigation. 2003;83(5):655-63.

174. Rong GH, Yang GX, Ando Y, Zhang W, He XS, Leung PS, et al. Human intrahepatic biliary epithelial cells engulf blebs from their apoptotic peers. Clinical & Experimental Immunology. 2013;172(1):95-103.

175. Davies SP, Reynolds GM, Stamataki Z. Clearance of apoptotic cells by tissue epithelia: A putative role for hepatocytes in liver efferocytosis. Frontiers in immunology. 2018;9:44.

176. Shi J, Gilbert GE, Kokubo Y, Ohashi T. Role of the liver in regulating numbers of circulating neutrophils. Blood. 2001;98(4):1226-30.

177. Grozovsky R, Hoffmeister KM, Falet H. Novel clearance mechanisms of platelets. Curr Opin Hematol. 2010;17(6):585-9.

178. Ganesan LP, Kim J, Wu Y, Mohanty S, Phillips GS, Birmingham DJ, et al. Fcγriib on liver sinusoidal endothelium clears small immune complexes. J Immunol. 2012;189(10):4981-8.

179. Kosugi I, Muro H, Shirasawa H, Ito I. Endocytosis of soluble igg immune complex and its transport to lysosomes in hepatic sinusoidal endothelial cells. J Hepatol. 1992;16(1-2):106-14.

180. Johansson AG, Sundqvist T, Skogh T. Igg immune complex binding to and activation of liver cells. An in vitro study with igg immune complexes, kupffer cells, sinusoidal endothelial cells and hepatocytes. Int Arch Allergy Immunol. 2000;121(4):329-36.

181. Skogh T, Blomhoff R, Eskild W, Berg T. Hepatic uptake of circulating igg immune complexes. Immunology. 1985;55(4):585-94.

182. Steffan AM, Gendrault JL, McCuskey RS, McCuskey PA, Kirn A. Phagocytosis, an unrecognized property of murine endothelial liver cells. Hepatology. 1986;6(5):830-6.

183. Crispe IN. Liver antigen-presenting cells. J Hepatol. 2011;54(2):357-65.

184. Cargill T, Culver EL. The role of b cells and b cell therapies in immune-mediated liver diseases. Frontiers in Immunology. 2021;12.

185. Takahashi T, Miura T, Nakamura J, Yamada S, Miura T, Yanagi M, et al. Plasma cells and the chronic nonsuppurative destructive cholangitis of primary biliary cirrhosis. Hepatology. 2012;55(3):846-55.

186. Tucci FA, Broering R, Lutterbeck M, Schlaak JF, Küppers R. Intrahepatic b-cell follicles of chronically hepatitis c virus-infected individuals lack signs of an ectopic germinal center reaction. Eur J Immunol. 2014;44(6):1842-50.

187. Chung BK, Guevel BT, Reynolds GM, Gupta Udatha DB, Henriksen EK, Stamataki Z, et al. Phenotyping and auto-antibody production by liver-infiltrating b cells in primary sclerosing cholangitis and primary biliary cholangitis. J Autoimmun. 2017;77:45-54.

188. Zhang X, Meng Z, Qiu S, Xu Y, Yang D, Schlaak JF, et al. Lipopolysaccharide-induced innate immune responses in primary hepatocytes downregulates woodchuck hepatitis virus replication via interferon-independent pathways. Cell Microbiol. 2009;11(11):1624-37.

189. Franco A, Barnaba V, Natali P, Balsano C, Musca A, Balsano F. Expression of class i and class ii major histocompatibility complex antigens on human hepatocytes. Hepatology. 1988;8(3):449-54.

190. Gitlin L, Barchet W, Gilfillan S, Cella M, Beutler B, Flavell RA, et al. Essential role of mda-5 in type i ifn responses to polyriboinosinic:Polyribocytidylic acid and encephalomyocarditis picornavirus. Proceedings of the National Academy of Sciences. 2006;103(22):8459.

191. Yoneyama M, Kikuchi M, Natsukawa T, Shinobu N, Imaizumi T, Miyagishi M, et al. The rna helicase rig-i has an essential function in double-stranded rna-induced innate antiviral responses. Nat Immunol. 2004;5(7):730-7.

192. Eksioglu EA, Zhu H, Bayouth L, Bess J, Liu HY, Nelson DR, et al. Characterization of hcv interactions with toll-like receptors and rig-i in liver cells. PLoS One. 2011;6(6):e21186.

193. Scott MJ, Chen C, Sun Q, Billiar TR. Hepatocytes express functional nod1 and nod2 receptors: A role for nod1 in hepatocyte cc and cxc chemokine production. J Hepatol. 2010;53(4):693-701.

194. Huang S, Wu J, Gao X, Zou S, Chen L, Yang X, et al. Lsecs express functional nod1 receptors: A role for nod1 in lsec maturation-induced t cell immunity in vitro. Mol Immunol. 2018;101:167-75.

195. Balam S, Romero JF, Bongfen SE, Guillaume P, Corradin G. Csp--a model for in vivo presentation of plasmodium berghei sporozoite antigens by hepatocytes. PLoS One. 2012;7(12):e51875.

196. Qian S, Wang Z, Lee Y, Chiang Y, Bonham C, Fung J, et al. Hepatocyte-induced apoptosis of activated t cells, a mechanism of liver transplant tolerance, is related to the expression of icam-1 and hepatic lectin. Transplant Proc. 2001;33(1-2):226.

197. Bertolino P, Bowen DG, McCaughan GW, Fazekas de St Groth B. Antigen-specific primary activation of cd8+ t cells within the liver. J Immunol. 2001;166(9):5430-8.

198. Bertolino P, McCaughan GW, Bowen DG. Role of primary intrahepatic t-cell activation in the 'liver tolerance effect'. Immunol Cell Biol. 2002;80(1):84-92.

199. Pannen BH, Robotham JL. The acute-phase response. New Horiz. 1995;3(2):183-97.

200. Sarma JV, Ward PA. The complement system. Cell Tissue Res. 2011;343(1):227-35.

201. Inatsu A, Kinoshita M, Nakashima H, Shimizu J, Saitoh D, Tamai S, et al. Novel mechanism of c-reactive protein for enhancing mouse liver innate immunity. Hepatology. 2009;49(6):2044-54.

202. Bilzer M, Roggel F, Gerbes AL. Role of kupffer cells in host defense and liver disease. Liver Int. 2006;26(10):1175-86.

203. Selzner N, Selzner M, Odermatt B, Tian Y, Van Rooijen N, Clavien PA. Icam-1 triggers liver regeneration through leukocyte recruitment and kupffer cell-dependent release of tnf-alpha/il-6 in mice. Gastroenterology. 2003;124(3):692-700.

204. Cressman DE, Greenbaum LE, DeAngelis RA, Ciliberto G, Furth EE, Poli V, et al. Liver failure and defective hepatocyte regeneration in interleukin-6-deficient mice. Science. 1996;274(5291):1379-83.

205. Akerman P, Cote P, Yang SQ, McClain C, Nelson S, Bagby GJ, et al. Antibodies to tumor necrosis factor-alpha inhibit liver regeneration after partial hepatectomy. Am J Physiol. 1992;263(4 Pt 1):G579-85.

206. DeLeve LD, Wang X, Wang L. Vegf-sdf1 recruitment of cxcr7+ bone marrow progenitors of liver sinusoidal endothelial cells promotes rat liver regeneration. Am J Physiol Gastrointest Liver Physiol. 2016;310(9):G739-46.

207. Ding BS, Nolan DJ, Butler JM, James D, Babazadeh AO, Rosenwaks Z, et al. Inductive angiocrine signals from sinusoidal endothelium are required for liver regeneration. Nature. 2010;468(7321):310-5.

208. Meijer C, Wiezer MJ, Diehl AM, Schouten HJ, Schouten HJ, Meijer S, et al. Kupffer cell depletion by ci2mdp-liposomes alters hepatic cytokine expression and delays liver regeneration after partial hepatectomy. Liver. 2000;20(1):66-77.

209. Duffield JS, Forbes SJ, Constandinou CM, Clay S, Partolina M, Vuthoori S, et al. Selective depletion of macrophages reveals distinct, opposing roles during liver injury and repair. J Clin Invest. 2005;115(1):56-65.

210. Rantakari P, Patten DA, Valtonen J, Karikoski M, Gerke H, Dawes H, et al. Stabilin-1 expression defines a subset of macrophages that mediate tissue homeostasis and prevent fibrosis in chronic liver injury. Proceedings of the National Academy of Sciences. 2016;113(33):9298.

211. Fallowfield JA, Mizuno M, Kendall TJ, Constandinou CM, Benyon RC, Duffield JS, et al. Scar-associated macrophages are a major source of hepatic matrix metalloproteinase-13 and facilitate the resolution of murine hepatic fibrosis. J Immunol. 2007;178(8):5288-95.

212. Ramachandran P, Pellicoro A, Vernon MA, Boulter L, Aucott RL, Ali A, et al. Differential ly-6c expression identifies the recruited macrophage phenotype, which orchestrates the regression of murine liver fibrosis. Proceedings of the National Academy of Sciences. 2012;109(46):E3186.

213. Dal-Secco D, Wang J, Zeng Z, Kolaczkowska E, Wong CH, Petri B, et al. A dynamic spectrum of monocytes arising from the in situ reprogramming of ccr2+ monocytes at a site of sterile injury. J Exp Med. 2015;212(4):447-56.

214. Miyaoka Y, Ebato K, Kato H, Arakawa S, Shimizu S, Miyajima A. Hypertrophy and unconventional cell division of hepatocytes underlie liver regeneration. Curr Biol. 2012;22(13):1166-75.

215. Malato Y, Naqvi S, Schürmann N, Ng R, Wang B, Zape J, et al. Fate tracing of mature hepatocytes in mouse liver homeostasis and regeneration. J Clin Invest. 2011;121(12):4850-60.

216. Farber E. Similarities in the sequence of early histological changes induced in the liver of the rat by ethionine, 2-acetylamino-fluorene, and 3′-methyl-4dimethylaminoazobenzene. Cancer research. 1956;16(2):142.

217. Roskams TA, Libbrecht L, Desmet VJ. Progenitor cells in diseased human liver. Semin Liver Dis. 2003;23(4):385-96.

218. Lee JS, Heo J, Libbrecht L, Chu IS, Kaposi-Novak P, Calvisi DF, et al. A novel prognostic subtype of human hepatocellular carcinoma derived from hepatic progenitor cells. Nat Med. 2006;12(4):410-6.

219. Preisegger KH, Factor VM, Fuchsbichler A, Stumptner C, Denk H, Thorgeirsson SS. Atypical ductular proliferation and its inhibition by transforming growth factor beta1 in the 3,5-diethoxycarbonyl-1,4-dihydrocollidine mouse model for chronic alcoholic liver disease. Lab Invest. 1999;79(2):103-9.

220. Grisham JW, Porta EA. Origin and fate of proliferated hepatic ductal cells in the rat: Electron microscopic and autoradiographic studies. Experimental and Molecular Pathology. 1964;3(3):242-61.

221. Evarts RP, Nagy P, Nakatsukasa H, Marsden E, Thorgeirsson SS. In vivo differentiation of rat liver oval cells into hepatocytes. Cancer Res. 1989;49(6):1541-7.

222. Zhou H, Rogler LE, Teperman L, Morgan G, Rogler CE. Identification of hepatocytic and bile ductular cell lineages and candidate stem cells in bipolar ductular reactions in cirrhotic human liver. Hepatology. 2007;45(3):716-24.

223. Yanger K, Zong Y, Maggs LR, Shapira SN, Maddipati R, Aiello NM, et al. Robust cellular reprogramming occurs spontaneously during liver regeneration. Genes Dev. 2013;27(7):719-24.

224. Sekiya S, Suzuki A. Hepatocytes, rather than cholangiocytes, can be the major source of primitive ductules in the chronically injured mouse liver. Am J Pathol. 2014;184(5):1468-78.

225. Michalopoulos GK, Barua L, Bowen WC. Transdifferentiation of rat hepatocytes into biliary cells after bile duct ligation and toxic biliary injury. Hepatology. 2005;41(3):535-44.

226. Tanimizu N, Nishikawa Y, Ichinohe N, Akiyama H, Mitaka T. Sry hmg box protein 9-positive (sox9+) epithelial cell adhesion molecule-negative (epcam-) biphenotypic cells derived from hepatocytes are involved in mouse liver regeneration. The Journal of biological chemistry. 2014;289(11):7589-98.

227. Limaye PB, Bowen WC, Orr AV, Luo J, Tseng GC, Michalopoulos GK. Mechanisms of hepatocyte growth factor-mediated and epidermal growth factor-mediated signaling in transdifferentiation of rat hepatocytes to biliary epithelium. Hepatology. 2008;47(5):1702-13.

228. Zhao B, Tumaneng K, Guan KL. The hippo pathway in organ size control, tissue regeneration and stem cell self-renewal. Nat Cell Biol. 2011;13(8):877-83.

229. Camargo FD, Gokhale S, Johnnidis JB, Fu D, Bell GW, Jaenisch R, et al. Yap1 increases organ size and expands undifferentiated progenitor cells. Curr Biol. 2007;17(23):2054-60.

230. Avruch J, Zhou D, Fitamant J, Bardeesy N. Mst1/2 signalling to yap: Gatekeeper for liver size and tumour development. Br J Cancer. 2011;104(1):24-32.

231. Raven A, Lu WY, Man TY, Ferreira-Gonzalez S, O'Duibhir E, Dwyer BJ, et al. Cholangiocytes act as facultative liver stem cells during impaired hepatocyte regeneration. Nature. 2017;547(7663):350-4.

232. Amin A, Mookerjee RP. Acute-on-chronic liver failure: Definition, prognosis and management. Frontline Gastroenterology. 2020;11(6):458.

233. Poisson J, Lemoinne S, Boulanger C, Durand F, Moreau R, Valla D, et al. Liver sinusoidal endothelial cells: Physiology and role in liver diseases. J Hepatol. 2017;66(1):212-27.

234. Pasarín M, La Mura V, Gracia-Sancho J, García-Calderó H, Rodríguez-Vilarrupla A, García-Pagán JC, et al. Sinusoidal endothelial dysfunction precedes inflammation and fibrosis in a model of nafld. PLOS ONE. 2012;7(4):e32785.

235. Xu B, Broome U, Uzunel M, Nava S, Ge X, Kumagai-Braesch M, et al. Capillarization of hepatic sinusoid by liver endothelial cell-reactive autoantibodies in patients with cirrhosis and chronic hepatitis. Am J Pathol. 2003;163(4):1275-89.

236. Xie G, Wang X, Wang L, Wang L, Atkinson RD, Kanel GC, et al. Role of differentiation of liver sinusoidal endothelial cells in progression and regression of hepatic fibrosis in rats. Gastroenterology. 2012;142(4):918-27.e6.

237. Rockey DC, Chung JJ. Reduced nitric oxide production by endothelial cells in cirrhotic rat liver: Endothelial dysfunction in portal hypertension. Gastroenterology. 1998;114(2):344-51.

238. Francque S, Laleman W, Verbeke L, Van Steenkiste C, Casteleyn C, Kwanten W, et al. Increased intrahepatic resistance in severe steatosis: Endothelial dysfunction, vasoconstrictor overproduction and altered microvascular architecture. Laboratory Investigation. 2012;92(10):1428-39.

239. Marrone G, Russo L, Rosado E, Hide D, Garcia-Cardena G, Garcia-Pagan JC, et al. The transcription factor klf2 mediates hepatic endothelial protection and paracrine endothelial-stellate cell deactivation induced by statins. J Hepatol. 2013;58(1):98-103.

240. Marrone G, Maeso-Díaz R, García-Cardena G, Abraldes JG, García-Pagán JC, Bosch J, et al. Klf2 exerts antifibrotic and vasoprotective effects in cirrhotic rat livers: Behind the molecular mechanisms of statins. Gut. 2015;64(9):1434-43.

241. Wang W, Zhao C, Zhou J, Zhen Z, Wang Y, Shen C. Simvastatin ameliorates liver fibrosis via mediating nitric oxide synthase in rats with non-alcoholic steatohepatitis-related liver fibrosis. PLOS ONE. 2013;8(10):e76538.

242. Tateya S, Rizzo NO, Handa P, Cheng AM, Morgan-Stevenson V, Daum G, et al. Endothelial no/cgmp/vasp signaling attenuates kupffer cell activation and hepatic insulin resistance induced by high-fat feeding. Diabetes. 2011;60(11):2792.

243. Ford AJ, Jain G, Rajagopalan P. Designing a fibrotic microenvironment to investigate changes in human liver sinusoidal endothelial cell function. Acta Biomaterialia $V 24. 2015:220-7.

244. Soydemir S, Comella O, Abdelmottaleb D, Pritchett J. Does mechanocrine signaling by liver sinusoidal endothelial cells offer new opportunities for the development of anti-fibrotics? Front Med (Lausanne). 2019;6:312.

245. Georges PC, Hui J-J, Gombos Z, McCormick ME, Wang AY, Uemura M, et al. Increased stiffness of the rat liver precedes matrix deposition: Implications for fibrosis. American Journal of Physiology-Gastrointestinal and Liver Physiology. 2007;293(6):G1147-G54.

246. Sakata R, Ueno T, Nakamura T, Ueno H, Sata M. Mechanical stretch induces tgf-β synthesis in hepatic stellate cells. European journal of clinical investigation. 2004;34(2):129-36.

247. Hilscher MB, Sehrawat T, Arab JP, Zeng Z, Gao J, Liu M, et al. Mechanical stretch increases expression of cxcl1 in liver sinusoidal endothelial cells to recruit neutrophils, generate sinusoidal microthombi, and promote portal hypertension. Gastroenterology. 2019;157(1):193-209.e9.

248. Geraud C, Koch PS, Zierow J, Klapproth K, Busch K, Olsavszky V, et al. Gata4-dependent organ-specific endothelial differentiation controls liver development and embryonic hematopoiesis. J Clin Invest. 2017;127(3):1099-114.

249. Winkler M, Staniczek T, Kürschner SW, Schmid CD, Schönhaber H, Cordero J, et al. Endothelial gata4 controls liver fibrosis and regeneration by preventing a pathogenic switch in angiocrine signaling. J Hepatol. 2021;74(2):380-93.

250. Syn WK, Agboola KM, Swiderska M, Michelotti GA, Liaskou E, Pang H, et al. Nkt-associated hedgehog and osteopontin drive fibrogenesis in non-alcoholic fatty liver disease. Gut. 2012;61(9):1323-9.

251. Zhao N, Hao J, Ni Y, Luo W, Liang R, Cao G, et al. Vγ4 γδ t cell-derived il-17a negatively regulates nkt cell function in con a-induced fulminant hepatitis. J Immunol. 2011;187(10):5007-14.

252. Hayflick L, Moorhead PS. The serial cultivation of human diploid cell strains. Experimental Cell Research. 1961;25(3):585-621.

253. Besancenot R, Chaligné R, Tonetti C, Pasquier F, Marty C, Lécluse Y, et al. A senescence-like cell-cycle arrest occurs during megakaryocytic maturation: Implications for physiological and pathological megakaryocytic proliferation. PLOS Biology. 2010;8(9):e1000476.

254. Rajagopalan S, Long EO. Cellular senescence induced by cd158d reprograms natural killer cells to promote vascular remodeling. Proceedings of the National Academy of Sciences. 2012;109(50):20596.

255. Muñoz-Espín D, Cañamero M, Maraver A, Gómez-López G, Contreras J, Murillo-Cuesta S, et al. Programmed cell senescence during mammalian embryonic development. Cell. 2013;155(5):1104-18.

256. Donehower LA, Harvey M, Slagle BL, McArthur MJ, Montgomery CA, Jr., Butel JS, et al. Mice deficient for p53 are developmentally normal but susceptible to spontaneous tumours. Nature. 1992;356(6366):215-21.

257. Martín-Caballero J, Flores JM, García-Palencia P, Serrano M. Tumor susceptibility of p21(waf1/cip1)-deficient mice. Cancer Res. 2001;61(16):6234-8.

258. Sharpless NE, Bardeesy N, Lee KH, Carrasco D, Castrillon DH, Aguirre AJ, et al. Loss of p16ink4a with retention of p19arf predisposes mice to tumorigenesis. Nature. 2001;413(6851):86-91.

259. Bird Thomas G, Müller M, Boulter L, Vincent David F, Ridgway Rachel A, Lopez-Guadamillas E, et al. Tgfβ inhibition restores a regenerative response in acute liver injury by suppressing paracrine senescence. Science Translational Medicine. 2018;10(454):eaan1230.

260. Rudolph KL, Chang S, Millard M, Schreiber-Agus N, DePinho RA. Inhibition of experimental liver cirrhosis in mice by telomerase gene delivery. Science. 2000;287(5456):1253-8.

261. Yosef R, Pilpel N, Papismadov N, Gal H, Ovadya Y, Vadai E, et al. P21 maintains senescent cell viability under persistent DNA damage response by restraining jnk and caspase signaling. The EMBO Journal. 2017;36(15):2280-95.

262. Krizhanovsky V, Yon M, Dickins RA, Hearn S, Simon J, Miething C, et al. Senescence of activated stellate cells limits liver fibrosis. Cell. 2008;134(4):657-67.

263. Kim K-H, Chen C-C, Monzon RI, Lau LF. Matricellular protein ccn1 promotes regression of liver fibrosis through induction of cellular senescence in hepatic myofibroblasts. Mol Cell Biol. 2013;33(10):2078-90.

264. Kong X, Feng D, Wang H, Hong F, Bertola A, Wang FS, et al. Interleukin-22 induces hepatic stellate cell senescence and restricts liver fibrosis in mice. Hepatology. 2012;56(3):1150-9.

265. Omori S, Wang T-W, Johmura Y, Kanai T, Nakano Y, Kido T, et al. Generation of a p16 reporter mouse and its use to characterize and target p16^{high} cells in vivo. Cell Metabolism. 2020;32(5):814-28.e6.

266. Ferreira-Gonzalez S, Lu W-Y, Raven A, Dwyer B, Man TY, O'Duibhir E, et al. Paracrine cellular senescence exacerbates biliary injury and impairs regeneration. Nature Communications. 2018;9(1):1020.

267. Sasaki M, Miyakoshi M, Sato Y, Nakanuma Y. Modulation of the microenvironment by senescent biliary epithelial cells may be involved in the pathogenesis of primary biliary cirrhosis. J Hepatol. 2010;53(2):318-25.

268. Gutierrez-Reyes G, Garcia de Leon MdC, Varela-Fascinetto G, Valencia P, Pérez Tamayo R, Rosado CG, et al. Cellular senescence in livers from children with end stage liver disease. PLOS ONE. 2010;5(4):e10231.

269. International agency for research on cancer GLOBOCAN 2018 [Available from: https://gco.iarc.fr/today/online-analysis-map?v=2020&mode=population&mode_population=continents&population=900&populations=900&key=asr&sex=0&cancer=11&type=0&statistic=5&prevalence=0&population_group=0&ages_group%5B%5D=0&ages_group%5B%5D=17&nb_items=10&group_cancer=1&include_nmsc=1&include_nmsc_other=1&projection=natural-earth&color_palette=default&map_scale=quantile&map_nb_colors=5&continent=0&show_ranking=0&rotate=%255B10%252C0%255D.

270. O'Rourke JM, Sagar VM, Shah T, Shetty S. Carcinogenesis on the background of liver fibrosis: Implications for the management of hepatocellular cancer. World J Gastroenterol. 2018;24(39):4436-47.

271. Wang J, Chenivesse X, Henglein B, Bréchot C. Hepatitis b virus integration in a cyclin a gene in a hepatocellular carcinoma. Nature. 1990;343(6258):555-7.

272. Schulze K, Imbeaud S, Letouzé E, Alexandrov LB, Calderaro J, Rebouissou S, et al. Exome sequencing of hepatocellular carcinomas identifies new mutational signatures and potential therapeutic targets. Nat Genet. 2015;47(5):505-11.

273. Wang B, Huang G, Wang D, Li A, Xu Z, Dong R, et al. Null genotypes of gstm1 and gstt1 contribute to hepatocellular carcinoma risk: Evidence from an updated meta-analysis. J Hepatol. 2010;53(3):508-18.

274. Buch S, Stickel F, Trépo E, Way M, Herrmann A, Nischalke HD, et al. A genome-wide association study confirms pnpla3 and identifies tm6sf2 and mboat7 as risk loci for alcohol-related cirrhosis. Nat Genet. 2015;47(12):1443-8.

275. Ringelhan M, Pfister D, O'Connor T, Pikarsky E, Heikenwalder M. The immunology of hepatocellular carcinoma. Nat Immunol. 2018;19(3):222-32.

276. Llovet JM, Kelley RK, Villanueva A, Singal AG, Pikarsky E, Roayaie S, et al. Hepatocellular carcinoma. Nature Reviews Disease Primers. 2021;7(1):6.

277. Kuang D-M, Zhao Q, Peng C, Xu J, Zhang J-P, Wu C, et al. Activated monocytes in peritumoral stroma of hepatocellular carcinoma foster immune privilege and disease progression through pd-l1. Journal of Experimental Medicine. 2009;206(6):1327-37.

278. Biswas SK, Gangi L, Paul S, Schioppa T, Saccani A, Sironi M, et al. A distinct and unique transcriptional program expressed by tumor-associated macrophages (defective nf-κb and enhanced irf-3/stat1 activation). Blood. 2006;107(5):2112-22.

279. Ihling C, Naughton B, Zhang Y, Rolfe PA, Frick-Krieger E, Terracciano LM, et al. Observational study of pd-l1, tgf-beta, and immune cell infiltrates in hepatocellular carcinoma. Front Med (Lausanne). 2019;6:15.

280. Langhans B, Nischalke HD, Krämer B, Dold L, Lutz P, Mohr R, et al. Role of regulatory t cells and checkpoint inhibition in hepatocellular carcinoma. Cancer Immunol Immunother. 2019;68(12):2055-66.

281. Karikoski M, Marttila-Ichihara F, Elima K, Rantakari P, Hollmén M, Kelkka T, et al. Clever-1/stabilin-1 controls cancer growth and metastasis. Clin Cancer Res. 2014;20(24):6452-64.

282. Shetty S, Weston CJ, Oo YH, Westerlund N, Stamataki Z, Youster J, et al. Common lymphatic endothelial and vascular endothelial receptor-1 mediates the transmigration of regulatory t cells across human hepatic sinusoidal endothelium. The Journal of Immunology. 2011;186(7):4147-55.

283. Virtakoivu R, Rannikko J, Viitala M, Vaura F, Takeda A, Lonnberg T, et al. Systemic blockade of clever-1 elicits lymphocyte activation alongside checkpoint molecule downregulation in patients with solid tumors. medRxiv. 2020.

284. Patten DA, Wilkinson AL, O'Rourke JM, Shetty S. Prognostic value and potential immunoregulatory role of scarf1 in hepatocellular carcinoma. Frontiers in Oncology. 2020;10:1947.

285. Budczies J, von Winterfeld M, Klauschen F, Bockmayr M, Lennerz JK, Denkert C, et al. The landscape of metastatic progression patterns across major human cancers. Oncotarget. 2015;6(1):570-83.

286. Mielgo A, Schmid MC. Liver tropism in cancer: The hepatic metastatic niche. Cold Spring Harb Perspect Med. 2020;10(3).

287. Shetty S, Bruns T, Weston CJ, Stamataki Z, Oo YH, Long HM, et al. Recruitment mechanisms of primary and malignant b cells to the human liver. Hepatology. 2012;56(4):1521-31.

288. Irjala H, Alanen K, Grénman R, Heikkilä P, Joensuu H, Jalkanen S. Mannose receptor (mr) and common lymphatic endothelial and vascular endothelial receptor (clever)-1 direct the binding of cancer cells to the lymph vessel endothelium. Cancer Research. 2003;63(15):4671.

289. Benedicto A, Romayor I, Arteta B. Role of liver icam-1 in metastasis. Oncology letters. 2017;14(4):3883-92.

290. Benedicto A, Herrero A, Romayor I, Marquez J, Smedsrod B, Olaso E, et al. Liver sinusoidal endothelial cell icam-1 mediated tumor/endothelial crosstalk drives the development of liver metastasis by initiating inflammatory and angiogenic responses. Sci Rep. 2019;9(1):13111.

291. Aychek T, Miller K, Sagi-Assif O, Levy-Nissenbaum O, Israeli-Amit M, Pasmanik-Chor M, et al. E-selectin regulates gene expression in metastatic colorectal carcinoma cells and enhances hmgb1 release. Int J Cancer. 2008;123(8):1741-50.

292. Tremblay PL, Huot J, Auger FA. Mechanisms by which e-selectin regulates diapedesis of colon cancer cells under flow conditions. Cancer Res. 2008;68(13):5167-76.

293. Ye C, Kiriyama K, Mistuoka C, Kannagi R, Ito K, Watanabe T, et al. Expression of e-selectin on endothelial cells of small veins in human colorectal cancer. International journal of cancer. 1995;61(4):455-60.

294. Ou J, Peng Y, Deng J, Miao H, Zhou J, Zha L, et al. Endothelial cell-derived fibronectin extra domain a promotes colorectal cancer metastasis via inducing epithelial–mesenchymal transition. Carcinogenesis. 2014;35(7):1661-70.

295. Brodt P. Role of the microenvironment in liver metastasis: From pre-to prometastatic niches. Clinical Cancer Research. 2016;22(24):5971-82.

296. Gabrilovich DI. Myeloid-derived suppressor cells. Cancer immunology research. 2017;5(1):3-8.

297. Millrud CR, Bergenfelz C, Leandersson K. On the origin of myeloid-derived suppressor cells. Oncotarget. 2017;8(2):3649.

298. Shetty S, Lalor PF, Adams DH. Lymphocyte recruitment to the liver: Molecular insights into the pathogenesis of liver injury and hepatitis. Toxicology. 2008;254(3):136-46.

299. Springer TA. Traffic signals on endothelium for lymphocyte recirculation and leukocyte emigration. Annu Rev Physiol. 1995;57:827-72.

300. Ley K, Laudanna C, Cybulsky MI, Nourshargh S. Getting to the site of inflammation: The leukocyte adhesion cascade updated. Nature Reviews Immunology. 2007;7(9):678-89.

301. Jones DA, Abbassi O, McIntire LV, McEver RP, Smith CW. P-selectin mediates neutrophil rolling on histamine-stimulated endothelial cells. Biophysical journal. 1993;65(4):1560-9.

302. Sugama Y, Tiruppathi C, offakidevi K, Andersen TT, Fenton JW, 2nd, Malik AB. Thrombin-induced expression of endothelial p-selectin and intercellular adhesion molecule-1: A mechanism for stabilizing neutrophil adhesion. J Cell Biol. 1992;119(4):935-44.

303. Pober JS, Gimbrone MA, Jr., Lapierre LA, Mendrick DL, Fiers W, Rothlein R, et al. Overlapping patterns of activation of human endothelial cells by interleukin 1, tumor necrosis factor, and immune interferon. J Immunol. 1986;137(6):1893-6.

304. Pugin J, Schürer-Maly CC, Leturcq D, Moriarty A, Ulevitch RJ, Tobias PS. Lipopolysaccharide activation of human endothelial and epithelial cells is mediated by lipopolysaccharide-binding protein and soluble cd14. Proceedings of the National Academy of Sciences. 1993;90(7):2744.

305. Zeuke S, Ulmer AJ, Kusumoto S, Katus HA, Heine H. Tlr4-mediated inflammatory activation of human coronary artery endothelial cells by lps. Cardiovascular Research. 2002;56(1):126-34.

306. Amberger A, Maczek C, Jürgens G, Michaelis D, Schett G, Trieb K, et al. Co-expression of icam-1, vcam-1, elam-1 and hsp60 in human arterial and venous endothelial cells in response to cytokines and oxidized low-density lipoproteins. Cell Stress Chaperones. 1997;2(2):94-103.

307. Cominacini L, Garbin U, Pasini AF, Davoli A, Campagnola M, Contessi GB, et al. Antioxidants inhibit the expression of intercellular cell adhesion molecule-1 and vascular cell adhesion molecule-1 induced by oxidized ldl on human umbilical vein endothelial cells. Free Radical Biology and Medicine. 1997;22(1):117-27.

308. Leeuwenberg JF, Smeets EF, Neefjes JJ, Shaffer MA, Cinek T, Jeunhomme TM, et al. E-selectin and intercellular adhesion molecule-1 are released by activated human endothelial cells in vitro. Immunology. 1992;77(4):543-9.

309. Yang L, Froio RM, Sciuto TE, Dvorak AM, Alon R, Luscinskas FW. Icam-1 regulates neutrophil adhesion and transcellular migration of tnf-α-activated vascular endothelium under flow. Blood. 2005;106(2):584-92.

310. Fries JW, Williams AJ, Atkins RC, Newman W, Lipscomb MF, Collins T. Expression of vcam-1 and e-selectin in an in vivo model of endothelial activation. Am J Pathol. 1993;143(3):725-37.

311. Pigott R, Dillon LP, Hemingway IH, Gearing AJH. Soluble forms of e-selectin, icam-1 and vcam-1 are present in the supernatants of cytokine activated cultured endothelial cells. Biochemical and Biophysical Research Communications. 1992;187(2):584-9.

312. Sugimoto MA, Sousa LP, Pinho V, Perretti M, Teixeira MM. Resolution of inflammation: What controls its onset? Frontiers in Immunology. 2016;7(160).

313. McEver RP. Selectins: Initiators of leucocyte adhesion and signalling at the vascular wall. Cardiovascular Research. 2015;107(3):331-9.

314. Marshall BT, Long M, Piper JW, Yago T, McEver RP, Zhu C. Direct observation of catch bonds involving cell-adhesion molecules. Nature. 2003;423(6936):190-3.

315. Yago T, Zarnitsyna VI, Klopocki AG, McEver RP, Zhu C. Transport governs flow-enhanced cell tethering through l-selectin at threshold shear. Biophysical journal. 2007;92(1):330-42.

316. Sundd P, Gutierrez E, Koltsova EK, Kuwano Y, Fukuda S, Pospieszalska MK, et al. 'Slings' enable neutrophil rolling at high shear. Nature. 2012;488(7411):399-403.

317. Marki A, Buscher K, Mikulski Z, Pries A, Ley K. Rolling neutrophils form tethers and slings under physiologic conditions in vivo. Journal of Leukocyte Biology. 2018;103(1):67-70.

318. Abadier M, Pramod AB, McArdle S, Marki A, Fan Z, Gutierrez E, et al. Effector and regulatory t cells roll at high shear stress by inducible tether and sling formation. Cell Reports. 2017;21(13):3885-99.

319. Alon R, Kassner PD, Carr MW, Finger EB, Hemler ME, Springer TA. The integrin vla-4 supports tethering and rolling in flow on vcam-1. J Cell Biol. 1995;128(6):1243-53.

320. Berlin C, Bargatze RF, Campbell JJ, von Andrian UH, Szabo MC, Hasslen SR, et al. Alpha 4 integrins mediate lymphocyte attachment and rolling under physiologic flow. Cell. 1995;80(3):413-22.

321. Lalor PF, Clements JM, Pigott R, Humphries MJ, Spragg JH, Nash GB. Association between receptor density, cellular activation, and transformation of adhesive behavior of flowing lymphocytes binding to vcam-1. Eur J Immunol. 1997;27(6):1422-6.

322. Wadkin JCR, Patten DA, Kamarajah SK, Shepherd EL, Novitskaya V, Berditchevski F, et al. Cd151 supports vcam-1-mediated lymphocyte adhesion to liver endothelium and is upregulated in chronic liver disease and hepatocellular carcinoma. Am J Physiol Gastrointest Liver Physiol. 2017;313(2):G138-g49.

323. Olson TS, Ley K. Chemokines and chemokine receptors in leukocyte trafficking. American Journal of Physiology-Regulatory, Integrative and Comparative Physiology. 2002;283(1):R7-R28.

324. Oo YH, Shetty S, Adams DH. The role of chemokines in the recruitment of lymphocytes to the liver. Digestive Diseases. 2010;28(1):31-44.

325. Campbell JJ, Hedrick J, Zlotnik A, Siani MA, Thompson DA, Butcher EC. Chemokines and the arrest of lymphocytes rolling under flow conditions. Science. 1998;279(5349):381-4.

326. Tanaka Y, Adams DH, Hubscher S, Hirano H, Siebenlist U, Shaw S. T-cell adhesion induced by proteoglycan-immobilized cytokine mip-1 beta. Nature. 1993;361(6407):79-82.

327. Alon R, Shulman Z. Chemokine triggered integrin activation and actin remodeling events guiding lymphocyte migration across vascular barriers. Experimental Cell Research. 2011;317(5):632-41.

328. Campbell JJ, Qin S, Bacon KB, Mackay CR, Butcher EC. Biology of chemokine and classical chemoattractant receptors: Differential requirements for adhesion-triggering versus chemotactic responses in lymphoid cells. J Cell Biol. 1996;134(1):255-66.

329. Auffray C, Fogg D, Garfa M, Elain G, Join-Lambert O, Kayal S, et al. Monitoring of blood vessels and tissues by a population of monocytes with patrolling behavior. Science. 2007;317(5838):666.

330. Phillipson M, Heit B, Colarusso P, Liu L, Ballantyne CM, Kubes P. Intraluminal crawling of neutrophils to emigration sites: A molecularly distinct process from adhesion in the recruitment cascade. Journal of Experimental Medicine. 2006;203(12):2569-75.

331. Schenkel AR, Mamdouh Z, Muller WA. Locomotion of monocytes on endothelium is a critical step during extravasation. Nat Immunol. 2004;5(4):393-400.

332. Barreiro O, Yanez-Mo M, Serrador JM, Montoya MC, Vicente-Manzanares M, Tejedor R, et al. Dynamic interaction of vcam-1 and icam-1 with moesin and ezrin in a novel endothelial docking structure for adherent leukocytes. J Cell Biol. 2002;157(7):1233-45.

333. Carman CV, Springer TA. A transmigratory cup in leukocyte diapedesis both through individual vascular endothelial cells and between them. J Cell Biol. 2004;167(2):377-88.

334. Lee J, Song KH, Kim T, Doh J. Endothelial cell focal adhesion regulates transendothelial migration and subendothelial crawling of t cells. Frontiers in Immunology. 2018;9(48).

335. Song KH, Lee J, Park H, Kim HM, Park J, Kwon KW, et al. Roles of endothelial a-type lamins in migration of t cells on and under endothelial layers. Scientific Reports. 2016;6(1):23412.

336. Proebstl D, Voisin M-B, Woodfin A, Whiteford J, D'Acquisto F, Jones GE, et al. Pericytes support neutrophil subendothelial cell crawling and breaching of venular walls in vivo. Journal of Experimental Medicine. 2012;209(6):1219-34.

337. Muller WA. Transendothelial migration: Unifying principles from the endothelial perspective. Immunological Reviews. 2016;273(1):61-75.

338. Heemskerk N, Schimmel L, Oort C, van Rijssel J, Yin T, Ma B, et al. F-actin-rich contractile endothelial pores prevent vascular leakage during leukocyte diapedesis through local rhoa signalling. Nature Communications. 2016;7(1):10493.

339. Huang AJ, Manning JE, Bandak TM, Ratau MC, Hanser KR, Silverstein SC. Endothelial cell cytosolic free calcium regulates neutrophil migration across monolayers of endothelial cells. Journal of Cell Biology. 1993;120(6):1371-80.

340. Millán J, Ridley AJ. Rho gtpases and leucocyte-induced endothelial remodelling. Biochem J. 2005;385(Pt 2):329-37.

341. Sullivan DP, Watson RL, Muller WA. 4d intravital microscopy uncovers critical strain differences for the roles of pecam and cd99 in leukocyte diapedesis. American Journal of Physiology-Heart and Circulatory Physiology. 2016;311(3):H621-H32.

342. Nourshargh S, Krombach F, Dejana E. The role of jam-a and pecam-1 in modulating leukocyte infiltration in inflamed and ischemic tissues. Journal of Leukocyte Biology. 2006;80(4):714-8.

343. Ostermann G, Weber KSC, Zernecke A, Schröder A, Weber C. Jam-1 is a ligand of the β2 integrin lfa-1 involved in transendothelial migration of leukocytes. Nature Immunology. 2002;3(2):151-8.

344. Schenkel AR, Mamdouh Z, Chen X, Liebman RM, Muller WA. Cd99 plays a major role in the migration of monocytes through endothelial junctions. Nature Immunology. 2002;3(2):143-50.

345. Schulte D, Küppers V, Dartsch N, Broermann A, Li H, Zarbock A, et al. Stabilizing the ve-cadherin–catenin complex blocks leukocyte extravasation and vascular permeability. The EMBO Journal. 2011;30(20):4157-70.

346. Shaw SK, Bamba PS, Perkins BN, Luscinskas FW. Real-time imaging of vascular endothelial-cadherin during leukocyte transmigration across endothelium. The Journal of Immunology. 2001;167(4):2323.

347. Alon R, van Buul JD. Leukocyte breaching of endothelial barriers: The actin link. Trends in Immunology. 2017;38(8):606-15.

348. Millán J, Hewlett L, Glyn M, Toomre D, Clark P, Ridley AJ. Lymphocyte transcellular migration occurs through recruitment of endothelial icam-1 to caveola- and f-actin-rich domains. Nature Cell Biology. 2006;8(2):113-23.

349. van Buul JD, Allingham MJ, Samson T, Meller J, Boulter E, García-Mata R, et al. Rhog regulates endothelial apical cup assembly downstream from icam1 engagement and is involved in leukocyte trans-endothelial migration. Journal of Cell Biology. 2007;178(7):1279-93.

350. Cinamon G, Shinder V, Shamri R, Alon R. Chemoattractant signals and beta 2 integrin occupancy at apical endothelial contacts combine with shear stress signals to promote transendothelial neutrophil migration. J Immunol. 2004;173(12):7282-91.

351. Carman CV, Sage PT, Sciuto TE, de la Fuente MA, Geha RS, Ochs Hans D, et al. Transcellular diapedesis is initiated by invasive podosomes. Immunity. 2007;26(6):784-97.

352. Mamdouh Z, Mikhailov A, Muller WA. Transcellular migration of leukocytes is mediated by the endothelial lateral border recycling compartment. Journal of Experimental Medicine. 2009;206(12):2795-808.

353. Stark K, Eckart A, Haidari S, Tirniceriu A, Lorenz M, von Brühl M-L, et al. Capillary and arteriolar pericytes attract innate leukocytes exiting through venules and 'instruct' them with pattern-recognition and motility programs. Nature Immunology. 2013;14(1):41-51.

354. Carman CV, Martinelli R. T lymphocyte–endothelial interactions: Emerging understanding of trafficking and antigen-specific immunity. Frontiers in Immunology. 2015;6(603).

355. Girard J-P, Moussion C, Förster R. Hevs, lymphatics and homeostatic immune cell trafficking in lymph nodes. Nature Reviews Immunology. 2012;12(11):762-73.

356. Guermonprez P, Valladeau J, Zitvogel L, Théry C, Amigorena S. Antigen presentation and t cell stimulation by dendritic cells. Annual Review of Immunology. 2002;20(1):621-67.

357. Iftakhar-E-Khuda I, Fair-Mäkelä R, Kukkonen-Macchi A, Elima K, Karikoski M, Rantakari P, et al. Gene-expression profiling of different arms of lymphatic vasculature identifies candidates for manipulation of cell traffic. Proceedings of the National Academy of Sciences. 2016;113(38):10643.

358. Geng YJ, Hansson GK. High endothelial cells of postcapillary venules express the scavenger receptor in human peripheral lymph nodes. Scandinavian Journal of Immunology. 1995;42(3):289-96.

359. Irjala H, Elima K, Johansson E-L, Merinen M, Kontula K, Alanen K, et al. The same endothelial receptor controls lymphocyte traffic both in vascular and lymphatic vessels. European Journal of Immunology. 2003;33(3):815-24.

360. Salmi M, Koskinen K, Henttinen T, Elima K, Jalkanen S. Clever-1 mediates lymphocyte transmigration through vascular and lymphatic endothelium. Blood. 2004;104(13):3849-57.

361. Karikoski M, Irjala H, Maksimow M, Miiluniemi M, Granfors K, Hernesniemi S, et al. Clever-1/stabilin-1 regulates lymphocyte migration within lymphatics and leukocyte entrance to sites of inflammation. European Journal of Immunology. 2009;39(12):3477-87.

362. Karikoski M, Marttila-Ichihara F, Elima K, Rantakari P, Hollmén M, Kelkka T, et al. Clever-1/stabilin-1 controls cancer growth and metastasis. Clinical Cancer Research. 2014;20(24):6452.

363. Irjala H, Johansson E-L, Grenman R, Alanen K, Salmi M, Jalkanen S. Mannose receptor is a novel ligand for l-selectin and mediates lymphocyte binding to lymphatic endothelium. Journal of Experimental Medicine. 2001;194(8):1033-42.

364. Marttila-Ichihara F, Turja R, Miiluniemi M, Karikoski M, Maksimow M, Niemelä J, et al. Macrophage mannose receptor on lymphatics controls cell trafficking. Blood. 2008;112(1):64-72.

365. Salmi M, Karikoski M, Elima K, Rantakari P, Jalkanen S. Cd44 binds to macrophage mannose receptor on lymphatic endothelium and supports lymphocyte migration via afferent lymphatics. Circulation Research. 2013;112(12):1577-82.

366. Rantakari P, Auvinen K, Jappinen N, Kapraali M, Valtonen J, Karikoski M, et al. The endothelial protein plvap in lymphatics controls the entry of lymphocytes and antigens into lymph nodes. Nat Immunol. 2015;16(4):386-96.

367. Stan RV, Tkachenko E, Niesman IR. Pv1 is a key structural component for the formation of the stomatal and fenestral diaphragms. Mol Biol Cell. 2004;15(8):3615-30.

368. Wong J, Johnston B, Lee SS, Bullard DC, Smith CW, Beaudet AL, et al. A minimal role for selectins in the recruitment of leukocytes into the inflamed liver microvasculature. The Journal of clinical investigation. 1997;99(11):2782-90.

369. Volpes R, van den Oord JJ, Desmet VJ. Vascular adhesion molecules in acute and chronic liver inflammation. Hepatology. 1992;15(2):269-75.

370. Johnson Z, Proudfoot AE, Handel TM. Interaction of chemokines and glycosaminoglycans: A new twist in the regulation of chemokine function with opportunities for therapeutic intervention. Cytokine & Growth Factor Reviews. 2005;16(6):625-36.

371. Middleton J, Patterson AM, Gardner L, Schmutz C, Ashton BA. Leukocyte extravasation: Chemokine transport and presentation by the endothelium. Blood, The Journal of the American Society of Hematology. 2002;100(12):3853-60.

372. Neumann K, Erben U, Kruse N, Wechsung K, Schumann M, Klugewitz K, et al. Chemokine transfer by liver sinusoidal endothelial cells contributes to the recruitment of cd4+ t cells into the murine liver. PLoS One. 2015;10(6):e0123867.

373. Schrage A, Wechsung K, Neumann K, Schumann M, Schulzke JD, Engelhardt B, et al. Enhanced t cell transmigration across the murine liver sinusoidal endothelium is mediated by transcytosis and surface presentation of chemokines. Hepatology. 2008;48(4):1262-72.

374. Adams DH, Hubscher SG, Fisher NC, Williams A, Robinson M. Expression of e-selectin and e-selectin ligands in human liver inflammation. Hepatology. 1996;24(3):533-8.

375. Miyachi Y, Tsuchiya K, Komiya C, Shiba K, Shimazu N, Yamaguchi S, et al. Roles for cell-cell adhesion and contact in obesity-induced hepatic myeloid cell accumulation and glucose intolerance. Cell Rep. 2017;18(11):2766-79.

376. Lalor PF, Edwards S, McNab G, Salmi M, Jalkanen S, Adams DH. Vascular adhesion protein-1 mediates adhesion and transmigration of lymphocytes on human hepatic endothelial cells. The Journal of Immunology. 2002;169(2):983-92.

377. Patten DA, Kamarajah SK, Rose JM, Tickle J, Shepherd EL, Adams DH, et al. Scarf-1 promotes adhesion of cd4+ t cells to human hepatic sinusoidal endothelium under conditions of shear stress. Scientific reports. 2017;7(1):1-15.

378. Lalor PF, Sun PJ, Weston CJ, Martin-Santos A, Wakelam MJ, Adams DH. Activation of vascular adhesion protein-1 on liver endothelium results in an nf-κb–dependent increase in lymphocyte adhesion. Hepatology. 2007;45(2):465-74.

379. Liaskou E, Karikoski M, Reynolds GM, Lalor PF, Weston CJ, Pullen N, et al. Regulation of mucosal addressin cell adhesion molecule 1 expression in human and mice by vascular adhesion protein 1 amine oxidase activity. Hepatology. 2011;53(2):661-72.

380. Bonder CS, Norman MU, Swain MG, Zbytnuik LD, Yamanouchi J, Santamaria P, et al. Rules of recruitment for th1 and th2 lymphocytes in inflamed liver: A role for alpha-4 integrin and vascular adhesion protein-1. Immunity. 2005;23(2):153-63.

381. Shetty S, Weston CJ, Oo YH, Westerlund N, Stamataki Z, Youster J, et al. Common lymphatic endothelial and vascular endothelial receptor-1 mediates the transmigration of regulatory t cells across human hepatic sinusoidal endothelium. J Immunol. 2011;186(7):4147-55.

382. Jung M-Y, Park S-Y, Kim I-S. Stabilin-2 is involved in lymphocyte adhesion to the hepatic sinusoidal endothelium via the interaction with alphambeta2 integrin. Journal of leukocyte biology. 2007;82(5):1156-65.

383. DeGrendele HC, Estess P, Siegelman MH. Requirement for cd44 in activated t cell extravasation into an inflammatory site. Science. 1997;278(5338):672-5.

384. McDonald B, McAvoy EF, Lam F, Gill V, de la Motte C, Savani RC, et al. Interaction of cd44 and hyaluronan is the dominant mechanism for neutrophil sequestration in inflamed liver sinusoids. J Exp Med. 2008;205(4):915-27.

385. Briskin M, Winsor-Hines D, Shyjan A, Cochran N, Bloom S, Wilson J, et al. Human mucosal addressin cell adhesion molecule-1 is preferentially expressed in intestinal tract and associated lymphoid tissue. The American journal of pathology. 1997;151(1):97-110.

386. Curbishley SM, Eksteen B, Gladue RP, Lalor P, Adams DH. Cxcr3 activation promotes lymphocyte transendothelial migration across human hepatic endothelium under fluid flow. The American journal of pathology. 2005;167(3):887-99.

387. Ajuebor MN, Hogaboam CM, Le T, Proudfoot AE, Swain MG. Ccl3/mip-1α is pro-inflammatory in murine t cell-mediated hepatitis by recruiting ccr1-expressing cd4+ t cells to the liver. European journal of immunology. 2004;34(10):2907-18.

388. Shields PL, Morland CM, Salmon M, Qin S, Hubscher SG, Adams DH. Chemokine and chemokine receptor interactions provide a mechanism for selective t cell recruitment to specific liver compartments within hepatitis c-infected liver. The Journal of Immunology. 1999;163(11):6236-43.

389. Hokeness KL, Deweerd ES, Munks MW, Lewis CA, Gladue RP, Salazar-Mather TP. Cxcr3-dependent recruitment of antigen-specific t lymphocytes to the liver during murine cytomegalovirus infection. Journal of virology. 2007;81(3):1241-50.

390. Aspinall AI, Curbishley SM, Lalor PF, Weston CJ, Blahova M, Liaskou E, et al. Cx3cr1 and vascular adhesion protein-1-dependent recruitment of cd16+ monocytes across human liver sinusoidal endothelium. Hepatology. 2010;51(6):2030-9.

391. Hudspeth K, Donadon M, Cimino M, Pontarini E, Tentorio P, Preti M, et al. Human liver-resident cd56bright/cd16neg nk cells are retained within hepatic sinusoids via the engagement of ccr5 and cxcr6 pathways. Journal of autoimmunity. 2016;66:40-50.

392. Stegmann KA, Robertson F, Hansi N, Gill U, Pallant C, Christophides T, et al. Cxcr6 marks a novel subset of t-bet lo eomes hi natural killer cells residing in human liver. Scientific reports. 2016;6(1):1-10.

393. Heydtmann M, Lalor PF, Eksteen JA, Hübscher SG, Briskin M, Adams DH. Cxc chemokine ligand 16 promotes integrin-mediated adhesion of liver-infiltrating lymphocytes to cholangiocytes and hepatocytes within the inflamed human liver. The Journal of Immunology. 2005;174(2):1055-62.

394. Sato T, Thorlacius H, Johnston B, Staton TL, Xiang W, Littman DR, et al. Role for cxcr6 in recruitment of activated cd8+ lymphocytes to inflamed liver. The Journal of Immunology. 2005;174(1):277-83.

395. Karlmark KR, Weiskirchen R, Zimmermann HW, Gassler N, Ginhoux F, Weber C, et al. Hepatic recruitment of the inflammatory gr1+ monocyte subset upon liver injury promotes hepatic fibrosis. Hepatology. 2009;50(1):261-74.

396. Krenkel O, Puengel T, Govaere O, Abdallah AT, Mossanen JC, Kohlhepp M, et al. Therapeutic inhibition of inflammatory monocyte recruitment reduces steatohepatitis and liver fibrosis. Hepatology. 2018;67(4):1270-83.

397. Ramachandran P, Dobie R, Wilson-Kanamori JR, Dora EF, Henderson BEP, Luu NT, et al. Resolving the fibrotic niche of human liver cirrhosis at single-cell level. Nature. 2019;575(7783):512-8.

398. Sharma A, Seow JJW, Dutertre C-A, Pai R, Blériot C, Mishra A, et al. Onco-fetal reprogramming of endothelial cells drives immunosuppressive macrophages in hepatocellular carcinoma. Cell. 2020;183(2):377-94.e21.

399. East L, Isacke CM. The mannose receptor family. Biochim Biophys Acta. 2002;1572(2-3):364-86.

400. Martinez-Pomares L. The mannose receptor. Journal of Leukocyte Biology. 2012;92(6):1177-86.

401. Martínez-Pomares L, Mahoney JA, Káposzta R, Linehan SA, Stahl PD, Gordon S. A functional soluble form of the murine mannose receptor is produced by macrophages in vitro and is present in mouse serum. Journal of biological chemistry. 1998;273(36):23376-80.

402. Jordens R, Thompson A, Amons R, Koning F. Human dendritic cells shed a functional, soluble form of the mannose receptor. International immunology. 1999;11(11):1775-80.

403. Gazi U, Rosas M, Singh S, Heinsbroek S, Haq I, Johnson S, et al. Fungal recognition enhances mannose receptor shedding through dectin-1 engagement. Journal of Biological Chemistry. 2011;286(10):7822-9.

404. Leteux C, Chai W, Loveless RW, Yuen C-T, Uhlin-Hansen L, Combarnous Y, et al. The cysteine-rich domain of the macrophage mannose receptor is a multispecific lectin that recognizes chondroitin sulfates a and b and sulfated oligosaccharides of blood group lewisa and lewisx types in addition to the sulfated n-glycans of lutropin. Journal of Experimental Medicine. 2000;191(7):1117-26.

405. Liu Y, Chirino AJ, Misulovin Z, Leteux C, Feizi T, Nussenzweig MC, et al. Crystal structure of the cysteine-rich domain of mannose receptor complexed with a sulfated carbohydrate ligand. Journal of Experimental Medicine. 2000;191(7):1105-16.

406. Martinez-Pomares L, Wienke D, Stillion R, McKenzie EJ, Arnold JN, Harris J, et al. Carbohydrate-independent recognition of collagens by the macrophage mannose receptor. European journal of immunology. 2006;36(5):1074-82.

407. Madsen DH, Ingvarsen S, Jürgensen HJ, Melander MC, Kjøller L, Moyer A, et al. The non-phagocytic route of collagen uptake a distinct degradation pathway. Journal of Biological Chemistry. 2011;286(30):26996-7010.

408. Taylor PR, Gordon S, Martinez-Pomares L. The mannose receptor: Linking homeostasis and immunity through sugar recognition. Trends in immunology. 2005;26(2):104-10.

409. Taylor ME, Bezouska K, Drickamer K. Contribution to ligand binding by multiple carbohydrate-recognition domains in the macrophage mannose receptor. Journal of Biological Chemistry. 1992;267(3):1719-26.

410. Taylor ME, Drickamer K. Structural requirements for high affinity binding of complex ligands by the macrophage mannose receptor. Journal of Biological Chemistry. 1993;268(1):399-404.

411. Boskovic J, Arnold JN, Stilion R, Gordon S, Sim RB, Rivera-Calzada A, et al. Structural model for the mannose receptor family uncovered by electron microscopy of endo180 and the mannose receptor. Journal of Biological Chemistry. 2006;281(13):8780-7.

412. Su Y, Bakker T, Harris J, Tsang C, Brown GD, Wormald MR, et al. Glycosylation influences the lectin activities of the macrophage mannose receptor. Journal of Biological Chemistry. 2005;280(38):32811-20.

413. Wileman TE, Lennartz MR, Stahl PD. Identification of the macrophage mannose receptor as a 175-kda membrane protein. Proc Natl Acad Sci U S A. 1986;83(8):2501-5.

414. Smeekens SP, van de Veerdonk FL, Joosten LA, Jacobs L, Jansen T, Williams DL, et al. The classical cd14++ cd16− monocytes, but not the patrolling cd14+ cd16+ monocytes, promote th17 responses to candida albicans. European journal of immunology. 2011;41(10):2915-24.

415. Allavena P, Chieppa M, Bianchi G, Solinas G, Fabbri M, Laskarin G, et al. Engagement of the mannose receptor by tumoral mucins activates an immune suppressive phenotype in human tumor-associated macrophages. Clinical and Developmental Immunology. 2010;2010:547179.

416. Martinez-Pomares L, Hanitsch LG, Stillion R, Keshav S, Gordon S. Expression of mannose receptor and ligands for its cysteine-rich domain in venous sinuses of human spleen. Laboratory investigation. 2005;85(10):1238-49.

417. Linehan SA, Martínez-Pomares L, Stahl PD, Gordon S. Mannose receptor and its putative ligands in normal murine lymphoid and nonlymphoid organs: In situ expression of mannose receptor by selected macrophages, endothelial cells, perivascular microglia, and mesangial cells, but not dendritic cells. The Journal of experimental medicine. 1999;189(12):1961-72.

418. Smedsrød B, Melkko J, Risteli L, Risteli J. Circulating c-terminal propeptide of type i procollagen is cleared mainly via the mannose receptor in liver endothelial cells. Biochem J. 1990;271(2):345-50.

419. Malovic I, Sørensen KK, Elvevold KH, Nedredal GI, Paulsen S, Erofeev AV, et al. The mannose receptor on murine liver sinusoidal endothelial cells is the main denatured collagen clearance receptor. Hepatology. 2007;45(6):1454-61.

420. Jürgensen HJ, Madsen DH, Ingvarsen S, Melander MC, Gårdsvoll H, Patthy L, et al. A novel functional role of collagen glycosylation interaction with the endocytic collagen receptor uparap/endo180. Journal of Biological Chemistry. 2011;286(37):32736-48.

421. Elvevold K, Simon-Santamaria J, Hasvold H, McCourt P, Smedsrod B, Sorensen KK. Liver sinusoidal endothelial cells depend on mannose receptor-mediated recruitment of lysosomal enzymes for normal degradation capacity. Hepatology. 2008;48(6):2007-15.

422. Lee SJ, Evers S, Roeder D, Parlow AF, Risteli J, Risteli L, et al. Mannose receptor-mediated regulation of serum glycoprotein homeostasis. Science. 2002;295(5561):1898-901.

423. Gazi U, Martinez-Pomares L. Influence of the mannose receptor in host immune responses. Immunobiology. 2009;214(7):554-61.

424. Ezekowitz R, Sastry K, Bailly P, Warner A. Molecular characterization of the human macrophage mannose receptor: Demonstration of multiple carbohydrate recognition-like domains and phagocytosis of yeasts in cos-1 cells. The Journal of experimental medicine. 1990;172(6):1785-94.

425. Ezekowitz R, Williams D, Koziel H, Armstrong M, Warner A, Richards F, et al. Uptake of pneumocystis carinii mediated by the macrophage mannose receptor. Nature. 1991;351(6322):155-8.

426. Schlesinger L. Macrophage phagocytosis of virulent but not attenuated strains of mycobacterium tuberculosis is mediated by mannose receptors in addition to complement receptors. The Journal of Immunology. 1993;150(7):2920-30.

427. Athamna A, Ofek I, Keisari Y, Markowitz S, Dutton G, Sharon N. Lectinophagocytosis of encapsulated klebsiella pneumoniae mediated by surface lectins of guinea pig alveolar macrophages and human monocyte-derived macrophages. Infection and immunity. 1991;59(5):1673-82.

428. Heinsbroek SE, Taylor PR, Martinez FO, Martinez-Pomares L, Brown GD, Gordon S. Stage-specific sampling by pattern recognition receptors during candida albicans phagocytosis. PLoS Pathog. 2008;4(11):e1000218.

429. Lee SJ, Zheng N-Y, Clavijo M, Nussenzweig MC. Normal host defense during systemic candidiasis in mannose receptor-deficient mice. Infection and immunity. 2003;71(1):437-45.

430. Swain SD, Lee SJ, Nussenzweig MC, Harmsen AG. Absence of the macrophage mannose receptor in mice does not increase susceptibility to pneumocystis carinii infection in vivo. Infection and immunity. 2003;71(11):6213-21.

431. Engering AJ, Cella M, Fluitsma D, Brockhaus M, Hoefsmit EC, Lanzavecchia A, et al. The mannose receptor functions as a high capacity and broad specificity antigen receptor in human dendritic cells. European journal of immunology. 1997;27(9):2417-25.

432. Prigozy TI, Sieling PA, Clemens D, Stewart PL, Behar SM, Porcelli SA, et al. The mannose receptor delivers lipoglycan antigens to endosomes for presentation to t cells by cd1b molecules. Immunity. 1997;6(2):187-97.

433. Sallusto F, Cella M, Danieli C, Lanzavecchia A. Dendritic cells use macropinocytosis and the mannose receptor to concentrate macromolecules in the major histocompatibility complex class ii compartment: Downregulation by cytokines and bacterial products. The Journal of experimental medicine. 1995;182(2):389-400.

434. Dan JM, Kelly RM, Lee CK, Levitz SM. Role of the mannose receptor in a murine model of cryptococcus neoformans infection. Infection and immunity. 2008;76(6):2362-7.

435. Burgdorf S, Kautz A, Bohnert V, Knolle PA, Kurts C. Distinct pathways of antigen uptake and intracellular routing in cd4 and cd8 t cell activation. Science. 2007;316(5824):612-6.

436. Burgdorf S, Lukacs-Kornek V, Kurts C. The mannose receptor mediates uptake of soluble but not of cell-associated antigen for cross-presentation. The Journal of Immunology. 2006;176(11):6770.

437. Niemelä H, Elima K, Henttinen T, Irjala H, Salmi M, Jalkanen S. Molecular identification of pal-e, a widely used endothelial-cell marker. Blood. 2005;106(10):3405-9.

438. Schlingemann RO, Dingjan GM, Emeis JJ, Blok J, Warnaar SO, Ruiter DJ. Monoclonal antibody pal-e specific for endothelium. Lab Invest. 1985;52(1):71-6.

439. Terkelsen MK, Bendixen SM, Hansen D, Scott EAH, Moeller AF, Nielsen R, et al. Transcriptional dynamics of hepatic sinusoid-associated cells after liver injury. Hepatology. 2020.

440. Stan RV, Ghitescu L, Jacobson BS, Palade GE. Isolation, cloning, and localization of rat pv-1, a novel endothelial caveolar protein. J Cell Biol. 1999;145(6):1189-98.

441. Stan RV, Arden KC, Palade GE. Cdna and protein sequence, genomic organization, and analysis of cis regulatory elements of mouse and human plvap genes. Genomics. 2001;72(3):304-13.

442. Stan R-V, Kubitza M, Palade GE. Pv-1 is a component of the fenestral and stomatal diaphragms in fenestrated endothelia. Proceedings of the National Academy of Sciences. 1999;96(23):13203.

443. Stan RV. Multiple pv1 dimers reside in the same stomatal or fenestral diaphragm. Am J Physiol Heart Circ Physiol. 2004;286(4):H1347-53.

444. Auvinen K, Lokka E, Mokkala E, Jappinen N, Tyystjarvi S, Saine H, et al. Fenestral diaphragms and plvap associations in liver sinusoidal endothelial cells are developmentally regulated. Sci Rep. 2019;9(1):15698.

445. Stan RV, Tse D, Deharvengt SJ, Smits NC, Xu Y, Luciano MR, et al. The diaphragms of fenestrated endothelia: Gatekeepers of vascular permeability and blood composition. Dev Cell. 2012;23(6):1203-18.

446. Herrnberger L, Seitz R, Kuespert S, Bosl MR, Fuchshofer R, Tamm ER. Lack of endothelial diaphragms in fenestrae and caveolae of mutant plvap-deficient mice. Histochem Cell Biol. 2012;138(5):709-24.

447. Herrnberger L, Hennig R, Kremer W, Hellerbrand C, Goepferich A, Kalbitzer HR, et al. Formation of fenestrae in murine liver sinusoids depends on plasmalemma vesicle-associated protein and is required for lipoprotein passage. PLoS One. 2014;9(12):e115005.

448. Elkadri A, Thoeni C, Deharvengt SJ, Murchie R, Guo C, Stavropoulos JD, et al. Mutations in plasmalemma vesicle associated protein result in sieving protein-losing enteropathy characterized by hypoproteinemia, hypoalbuminemia, and hypertriglyceridemia. Cellular and molecular gastroenterology and hepatology. 2015;1(4):381-94. e7.

449. Broekaert IJ, Becker K, Gottschalk I, Körber F, Dötsch J, Thiele H, et al. Mutations in plasmalemma vesicle-associated protein cause severe syndromic protein-losing enteropathy. Journal of medical genetics. 2018;55(9):637-40.

450. Gorukmez O, Gorukmez O, Demiroren K. Novel plvap mutation in protein losing enteropathy. Fetal Pediatr Pathol. 2019;38(6):534-7.

451. Umans RA, Henson HE, Mu F, Parupalli C, Ju B, Peters JL, et al. Cns angiogenesis and barriergenesis occur simultaneously. Developmental Biology. 2017;425(2):101-8.

452. Bosma EK, van Noorden CJF, Schlingemann RO, Klaassen I. The role of plasmalemma vesicle-associated protein in pathological breakdown of blood-brain and blood-retinal barriers: Potential novel therapeutic target for cerebral edema and diabetic macular edema. Fluids Barriers CNS. 2018;15(1):24.

453. Tempel D, Dessel Lv, Burgisser P, Cheng C, Pasterkamp G, Schulte-Merker S, et al. Abstract 17550: Plasmalemma vesicle-associated protein promotes angiogenesis by stimulation of the endothelial production of pro-angiogenic sphingosine 1-phosphate. Circulation. 2013;128(suppl_22):A17550-A.

454. Wisniewska-Kruk J, Klaassen I, Vogels IM, Van Noorden CJ, Schlingemann RO, Group OA. Plvap modulates angiogenesis by tuning vegf signaling in endothelial cells. Investigative Ophthalmology & Visual Science. 2014;55(13):2241-.

455. Guo L, Zhang H, Hou Y, Wei T, Liu J. Plasmalemma vesicle-associated protein: A crucial component of vascular homeostasis. Exp Ther Med. 2016;12(3):1639-44.

456. Carson-Walter EB, Hampton J, Shue E, Geynisman DM, Pillai PK, Sathanoori R, et al. Plasmalemmal vesicle associated protein-1 is a novel marker implicated in brain tumor angiogenesis. Clin Cancer Res. 2005;11(21):7643-50.

457. Wang Y, Yu H, Xie X, Deng T, Ye L, Wu L, et al. Plasmalemma vesicle-associated protein promotes angiogenesis in cholangiocarcinoma via the dkk1/ckap4/pi3k signaling pathway. Oncogene. 2021;40(25):4324-37.

458. Wang YH, Cheng TY, Chen TY, Chang KM, Chuang VP, Kao KJ. Plasmalemmal vesicle associated protein (plvap) as a therapeutic target for treatment of hepatocellular carcinoma. BMC Cancer. 2014;14:815.

459. Keuschnigg J, Henttinen T, Auvinen K, Karikoski M, Salmi M, Jalkanen S. The prototype endothelial marker pal-e is a leukocyte trafficking molecule. Blood. 2009;114(2):478-84.

460. Rantakari P, Jappinen N, Lokka E, Mokkala E, Gerke H, Peuhu E, et al. Fetal liver endothelium regulates the seeding of tissue-resident macrophages. Nature. 2016;538(7625):392-6.

461. Yoshimori T, Yamamoto A, Moriyama Y, Futai M, Tashiro Y. Bafilomycin a1, a specific inhibitor of vacuolar-type h(+)-atpase, inhibits acidification and protein degradation in lysosomes of cultured cells. J Biol Chem. 1991;266(26):17707-12.

462. Bayer N, Schober D, Prchla E, Murphy RF, Blaas D, Fuchs R. Effect of bafilomycin a1 and nocodazole on endocytic transport in hela cells: Implications for viral uncoating and infection. J Virol. 1998;72(12):9645-55.

463. Wasserman SM, Mehraban F, Komuves LG, Yang R-B, Tomlinson JE, Zhang Y, et al. Gene expression profile of human endothelial cells exposed to sustained fluid shear stress. Physiological Genomics. 2002;12(1):13-23.

464. Hoare M, Ito Y, Kang T-W, Weekes MP, Matheson NJ, Patten DA, et al. Notch1 mediates a switch between two distinct secretomes during senescence. Nature Cell Biology. 2016;18(9):979-92.

465. Shetty S, Weston CJ, Adams DH, Lalor PF. A flow adhesion assay to study leucocyte recruitment to human hepatic sinusoidal endothelium under conditions of shear stress. JoVE (Journal of Visualized Experiments). 2014(85):e51330.

466. Cassetta L, Fragkogianni S, Sims AH, Swierczak A, Forrester LM, Zhang H, et al. Human tumor-associated macrophage and monocyte transcriptional landscapes reveal cancer-specific reprogramming, biomarkers, and therapeutic targets. Cancer Cell. 2019;35(4):588-602.e10.

467. Costa A, Kieffer Y, Scholer-Dahirel A, Pelon F, Bourachot B, Cardon M, et al. Fibroblast heterogeneity and immunosuppressive environment in human breast cancer. Cancer Cell. 2018;33(3):463-79.e10.

468. Hubert M, Gobbini E, Bendriss-Vermare N, Caux C, Valladeau-Guilemond J. Human tumor-infiltrating dendritic cells: From in situ visualization to high-dimensional analyses. Cancers (Basel). 2019;11(8).

469. Lalor PF, Lai WK, Curbishley SM, Shetty S, Adams DH. Human hepatic sinusoidal endothelial cells can be distinguished by expression of phenotypic markers related to their specialised functions in vivo. World J Gastroenterol. 2006;12(34):5429-39.

470. Patten DA, Wilson GK, Bailey D, Shaw RK, Jalkanen S, Salmi M, et al. Human liver sinusoidal endothelial cells promote intracellular crawling of lymphocytes during recruitment: A new step in migration. Hepatology. 2017;65(1):294-309.

471. Sheikh H, Yarwood H, Ashworth A, Isacke CM. Endo180, an endocytic recycling glycoprotein related to the macrophage mannose receptor is expressed on fibroblasts, endothelial cells and macrophages and functions as a lectin receptor. J Cell Sci. 2000;113 (Pt 6):1021-32.

472. Ribera J, Pauta M, Melgar-Lesmes P, Córdoba B, Bosch A, Calvo M, et al. A small population of liver endothelial cells undergoes endothelial-to-mesenchymal transition in response to chronic liver injury. American Journal of Physiology-Gastrointestinal and Liver Physiology. 2017;313(5):G492-G504.

473. Dufton NP, Peghaire CR, Osuna-Almagro L, Raimondi C, Kalna V, Chuahan A, et al. Dynamic regulation of canonical tgfβ signalling by endothelial transcription factor erg protects from liver fibrogenesis. Nature communications. 2017;8(1):1-14.

474. Li Z, Chen B, Dong W, Kong M, Fan Z, Yu L, et al. Mkl1 promotes endothelial-to-mesenchymal transition and liver fibrosis by activating twist1 transcription. Cell Death Dis. 2019;10(12):899.

475. Coste A, Dubourdeau M, Linas MD, Cassaing S, Lepert J-C, Balard P, et al. Pparγ promotes mannose receptor gene expression in murine macrophages and contributes to the induction of this receptor by il-13. Immunity. 2003;19(3):329-39.

476. Chen C, Smith AD, Cheung L, Pham Q, Urban JF, Jr., Dawson HD. Potentiation of il-4 signaling by retinoic acid in intestinal epithelial cells and macrophages-mechanisms and targets. Frontiers in immunology. 2020;11:605-.

477. Han YM, Lee YJ, Jang YN, Kim HM, Seo HS, Jung TW, et al. Aspirin improves nonalcoholic fatty liver disease and atherosclerosis through regulation of the pparδ-ampk-pgc-1α pathway in dyslipidemic conditions. Biomed Res Int. 2020;2020:7806860.

478. Sun C, Hu A, Wang S, Tian B, Jiang L, Liang Y, et al. Adam17-regulated cx3cl1 expression produced by bone marrow endothelial cells promotes spinal metastasis from hepatocellular carcinoma. Int J Oncol. 2020;57(1):249-63.

479. Shepherd VL, Konish MG, Stahl P. Dexamethasone increases expression of mannose receptors and decreases extracellular lysosomal enzyme accumulation in macrophages. J Biol Chem. 1985;260(1):160-4.

480. Stein M, Keshav S, Harris N, Gordon S. Interleukin 4 potently enhances murine macrophage mannose receptor activity: A marker of alternative immunologic macrophage activation. J Exp Med. 1992;176(1):287-92.

481. Ali M, Bonay M, Vanhee V, Vinit S, Deramaudt TB. Comparative effectiveness of 4 natural and chemical activators of nrf2 on inflammation, oxidative stress, macrophage polarization, and bactericidal activity in an in vitro macrophage infection model. PloS one. 2020;15(6):e0234484-e.

482. Liu L, Xu Y, Dai H, Tan S, Mao X, Chen Z. Dynorphin activation of kappa opioid receptor promotes microglial polarization toward m2 phenotype via tlr4/nf-κb pathway. Cell Biosci. 2020;10:42-
.

483. Zhang X, Liu M-H, Qiao L, Zhang X-Y, Liu X-L, Dong M, et al. Ginsenoside rb1 enhances atherosclerotic plaque stability by skewing macrophages to the m2 phenotype. Journal of cellular and molecular medicine. 2018;22(1):409-16.

484. Guo M, Xiao J, Sheng X, Zhang X, Tie Y, Wang L, et al. Ginsenoside rg3 mitigates atherosclerosis progression in diabetic apoe–/– mice by skewing macrophages to the m2 phenotype. Frontiers in Pharmacology. 2018;9(464).

485. Yi H, Zhang Y, Yang X, Li M, Hu H, Xiong J, et al. Hepatitis b core antigen impairs the polarization while promoting the production of inflammatory cytokines of m2 macrophages via the tlr2 pathway. Frontiers in immunology. 2020;11:535-.

486. Harris N, Super M, Rits M, Chang G, Ezekowitz RA. Characterization of the murine macrophage mannose receptor: Demonstration that the downregulation of receptor expression mediated by interferon-gamma occurs at the level of transcription. Blood. 1992;80(9):2363-73.

487. Martinez-Pomares L, Reid DM, Brown GD, Taylor PR, Stillion RJ, Linehan SA, et al. Analysis of mannose receptor regulation by il-4, il-10, and proteolytic processing using novel monoclonal antibodies. J Leukoc Biol. 2003;73(5):604-13.

488. Chistyakov DV, Gavrish GE, Goriainov SV, Chistyakov VV, Astakhova AA, Azbukina NV, et al. Oxylipin profiles as functional characteristics of acute inflammatory responses in astrocytes pre-treated with il-4, il-10, or lps. Int J Mol Sci. 2020;21(5):1780.

489. Doyle AG, Herbein G, Montaner LJ, Minty AJ, Caput D, Ferrara P, et al. Interleukin-13 alters the activation state of murine macrophages in vitro: Comparison with interleukin-4 and interferon-gamma. Eur J Immunol. 1994;24(6):1441-5.

490. Asumendi A, Alvarez A, Martinez I, Smedsrød B, Vidal-Vanaclocha F. Hepatic sinusoidal endothelium heterogeneity with respect to mannose receptor activity is interleukin-1 dependent. Hepatology. 1996;23(6):1521-9.

491. Plastira I, Bernhart E, Joshi L, Koyani CN, Strohmaier H, Reicher H, et al. Mapk signaling determines lysophosphatidic acid (lpa)-induced inflammation in microglia. Journal of neuroinflammation. 2020;17:1-17.

492. Horuluoglu B, Bayik D, Kayraklioglu N, Goguet E, Kaplan MJ, Klinman DM. Pam3 supports the generation of m2-like macrophages from lupus patient monocytes and improves disease outcome in murine lupus. Journal of autoimmunity. 2019;99:24-32.

493. Schreiber S, Blum JS, Chappel JC, Stenson WF, Stahl PD, Teitelbaum SL, et al. Prostaglandin e specifically upregulates the expression of the mannose-receptor on mouse bone marrow-derived macrophages. Cell regulation. 1990;1(5):403-13.

494. Hackstein H, Taner T, Logar AJ, Thomson AW. Rapamycin inhibits macropinocytosis and mannose receptor–mediated endocytosis by bone marrow–derived dendritic cells. Blood. 2002;100(3):1084-7.

495. Linares I, Farrokhi K, Echeverri J, Kaths JM, Kollmann D, Hamar M, et al. Ppar-gamma activation is associated with reduced liver ischemia-reperfusion injury and altered tissue-resident macrophages polarization in a mouse model. PLoS One. 2018;13(4):e0195212.

496. Blum L, Geisslinger G, Parnham MJ, Grünweller A, Schiffmann S. Natural antiviral compound silvestrol modulates human monocyte-derived macrophages and dendritic cells. J Cell Mol Med. 2020;24(12):6988-99.

497. Lim JE, Chung E, Son Y. A neuropeptide, substance-p, directly induces tissue-repairing m2 like macrophages by activating the pi3k/akt/mtor pathway even in the presence of ifnγ. Scientific reports. 2017;7(1):9417-.

498. von Ehr A, Attaai A, Neidert N, Potru PS, Ruß T, Zöller T, et al. Inhibition of microglial tgfβ signaling increases expression of mrc1. Front Cell Neurosci. 2020;14:66-.

499. Loganathan K, Salem Said E, Winterrowd E, Orebrand M, He L, Vanlandewijck M, et al. Angiopoietin-1 deficiency increases renal capillary rarefaction and tubulointerstitial fibrosis in mice. PloS one. 2018;13(1):e0189433.

500. Bodor C, Nagy JP, Végh B, Németh A, Jenei A, MirzaHosseini S, et al. Angiotensin ii increases the permeability and pv-1 expression of endothelial cells. American Journal of Physiology-Cell Physiology. 2012;302(1):C267-C76.

501. Benz F, Wichitnaowarat V, Lehmann M, Germano RF, Mihova D, Macas J, et al. Low wnt/β-catenin signaling determines leaky vessels in the subfornical organ and affects water homeostasis in mice. Elife. 2019;8.

502. Liebner S, Corada M, Bangsow T, Babbage J, Taddei A, Czupalla CJ, et al. Wnt/β-catenin signaling controls development of the blood–brain barrier. The Journal of cell biology. 2008;183(3):409-17.

503. Desroches-Castan A, Tillet E, Ricard N, Ouarne M, Mallet C, Belmudes L, et al. Bone morphogenetic protein 9 is a paracrine factor controlling liver sinusoidal endothelial cell fenestration and protecting against hepatic fibrosis. Hepatology. 2019;70(4):1392-408.

504. Tkachenko E, Tse D, Sideleva O, Deharvengt SJ, Luciano MR, Xu Y, et al. Caveolae, fenestrae and transendothelial channels retain pv1 on the surface of endothelial cells. PLOS ONE. 2012;7(3):e32655.

505. Anbalagan S, Gordon L, Blechman J, Matsuoka RL, Rajamannar P, Wircer E, et al. Pituicyte cues regulate the development of permeable neuro-vascular interfaces. Dev Cell. 2018;47(6):711-26.e5.

506. Muradashvili N, Benton RL, Tyagi R, Tyagi SC, Lominadze D. Elevated level of fibrinogen increases caveolae formation; role of matrix metalloproteinase-9. Cell biochemistry and biophysics. 2014;69(2):283-94.

507. Wang Y, Rattner A, Zhou Y, Williams J, Smallwood Philip M, Nathans J. Norrin/frizzled4 signaling in retinal vascular development and blood brain barrier plasticity. Cell. 2012;151(6):1332-44.

508. Stenman J, Rajagopal J, Carroll T, Ishibashi M, McMahon J, McMahon A. Stenman jm, rajagopal j, carroll tj, ishibashi m, mcmahon j, mcmahon apcanonical wnt signaling regulates organ-specific assembly and differentiation of cns vasculature. Science 322:1247-1250. Science (New York, NY). 2008;322:1247-50.

509. Laksitorini MD, Yathindranath V, Xiong W, Hombach-Klonisch S, Miller DW. Modulation of wnt/beta-catenin signaling promotes blood-brain barrier phenotype in cultured brain endothelial cells. Sci Rep. 2019;9(1):19718.

510. Morita-Takemura S, Nakahara K, Tatsumi K, Okuda H, Tanaka T, Isonishi A, et al. Changes in endothelial cell proliferation and vascular permeability after systemic lipopolysaccharide administration in the subfornical organ. Journal of neuroimmunology. 2016;298:132-7.

511. Hamilton BJ, Tse D, Stan RV. Phorbol esters induce plvap expression via vegf and additional secreted molecules in mek 1-dependent and p38, jnk and pi 3k/akt-independent manner. Journal of cellular and molecular medicine. 2019;23(2):920-33.

512. Shi X, Wang W, Li J, Wang T, Lin Y, Huang S, et al. Sphingosine 1-phosphate receptor 1 regulates cell-surface localization of membrane proteins in endothelial cells. Biochim Biophys Acta Gen Subj. 2019;1863(6):1079-87.

513. Rathnakumar K, Savant S, Giri H, Ghosh A, Fisslthaler B, Fleming I, et al. Angiopoietin-2 mediates thrombin-induced monocyte adhesion and endothelial permeability. J Thromb Haemost. 2016;14(8):1655-67.

514. Junge HJ, Yang S, Burton JB, Paes K, Shu X, French DM, et al. Tspan12 regulates retinal vascular development by promoting norrin- but not wnt-induced fzd4/beta-catenin signaling. Cell. 2009;139(2):299-311.

515. Strickland LA, Jubb AM, Hongo JA, Zhong F, Burwick J, Fu L, et al. Plasmalemmal vesicle-associated protein (plvap) is expressed by tumour endothelium and is upregulated by vascular endothelial growth factor-a (vegf). The Journal of Pathology: A Journal of the Pathological Society of Great Britain and Ireland. 2005;206(4):466-75.

516. Suyama M, Miyazaki Y, Matsusaka T, Sugano N, Ueda H, Kawamura T, et al. Forced expression of vascular endothelial growth factor-a in podocytes decreases mesangial cell numbers and attenuates endothelial cell differentiation in the mouse glomerulus. Clin Exp Nephrol. 2018;22(2):266-74.

517. Kim SA, Kim SJ, Choi YA, Yoon H-J, Kim A, Lee J. Retinal vegfa maintains the ultrastructure and function of choriocapillaris by preserving the endothelial plvap. Biochemical and Biophysical Research Communications. 2020;522(1):240-6.

518. Nakagami Y, Hatano E, Chayama Y, Inoue T. An anti-plvap antibody suppresses laser-induced choroidal neovascularization in monkeys. European Journal of Pharmacology. 2019;854:240-6.

519. Patten DA, Wilkinson AL, O'Keeffe A, Shetty S. Scavenger receptors: Novel roles in the pathogenesis of liver inflammation and cancer. Semin Liver Dis. 2021.

520. Sullivan M, Galea P, Latif S. What is the appropriate oxygen tension for in vitro culture? Molecular Human Reproduction. 2006;12(11):653-.

521. Kietzmann T. Liver zonation in health and disease: Hypoxia and hypoxia-inducible transcription factors as concert masters. Int J Mol Sci. 2019;20(9):2347.

522. Muz B, de la Puente P, Azab F, Azab AK. The role of hypoxia in cancer progression, angiogenesis, metastasis, and resistance to therapy. Hypoxia (Auckl). 2015;3:83-92.

523. McKeown SR. Defining normoxia, physoxia and hypoxia in tumours-implications for treatment response. Br J Radiol. 2014;87(1035):20130676-.

524. Ferreira-Gonzalez S, Rodrigo-Torres D, Gadd VL, Forbes SJ. Cellular senescence in liver disease and regeneration. Semin Liver Dis. 2021;41(1):50-66.

525. Beck J, Horikawa I, Harris C. Cellular senescence: Mechanisms, morphology, and mouse models. Veterinary Pathology. 2020;57(6):747-57.

526. Yosef R, Pilpel N, Tokarsky-Amiel R, Biran A, Ovadya Y, Cohen S, et al. Directed elimination of senescent cells by inhibition of bcl-w and bcl-xl. Nature Communications. 2016;7(1):11190.

527. Eggert T, Wolter K, Ji J, Ma C, Yevsa T, Klotz S, et al. Distinct functions of senescence-associated immune responses in liver tumor surveillance and tumor progression. Cancer Cell. 2016;30(4):533-47.

528. Parrinello S, Coppe JP, Krtolica A, Campisi J. Stromal-epithelial interactions in aging and cancer: Senescent fibroblasts alter epithelial cell differentiation. J Cell Sci. 2005;118(Pt 3):485-96.

529. Ruhland MK, Loza AJ, Capietto A-H, Luo X, Knolhoff BL, Flanagan KC, et al. Stromal senescence establishes an immunosuppressive microenvironment that drives tumorigenesis. Nature Communications. 2016;7(1):11762.

530. Yousefzadeh MJ, Melos KI, Angelini L, Burd CE, Robbins PD, Niedernhofer LJ. Mouse models of accelerated cellular senescence. Methods Mol Biol. 2019;1896:203-30.

531. Kang T-W, Yevsa T, Woller N, Hoenicke L, Wuestefeld T, Dauch D, et al. Senescence surveillance of pre-malignant hepatocytes limits liver cancer development. Nature. 2011;479(7374):547-51.

532. Innes AJ, Gil J. Imr90 er:Ras: A cell model of oncogene-induced senescence. Methods Mol Biol. 2019;1896:83-92.

533. Yoshihara K, Shahmoradgoli M, Martínez E, Vegesna R, Kim H, Torres-Garcia W, et al. Inferring tumour purity and stromal and immune cell admixture from expression data. Nature Communications. 2013;4(1):2612.

534. McGuinness PH, Painter D, Davies S, McCaughan GW. Increases in intrahepatic cd68 positive cells, mac387 positive cells, and proinflammatory cytokines (particularly interleukin 18) in chronic hepatitis c infection. Gut. 2000;46(2):260.

535. Soulas C, Conerly C, Kim W-K, Burdo TH, Alvarez X, Lackner AA, et al. Recently infiltrating mac387(+) monocytes/macrophages a third macrophage population involved in siv and hiv encephalitic lesion formation. The American journal of pathology. 2011;178(5):2121-35.

536. Yokomori H, Ando W, Oda M. Plasmalemmal vesicle-associated protein is associated with endothelial cells sprouting from the peribiliary capillary plexus in human cirrhotic liver. Journal of Vascular Research. 2021;58(6):361-9.

537. Paes KT, Wang E, Henze K, Vogel P, Read R, Suwanichkul A, et al. Frizzled 4 is required for retinal angiogenesis and maintenance of the blood-retina barrier. Investigative Ophthalmology & Visual Science. 2011;52(9):6452-61.

538. Koda W, Harada K, Tsuneyama K, Kono N, Sasaki M, Matsui O, et al. Evidence of the participation of peribiliary mast cells in regulation of the peribiliary vascular plexus along the intrahepatic biliary tree. Laboratory Investigation. 2000;80(7):1007-17.

539. Weston CJ, Zimmermann HW, Adams DH. The role of myeloid-derived cells in the progression of liver disease. Frontiers in Immunology. 2019;10.

540. Peichev M, Naiyer AJ, Pereira D, Zhu Z, Lane WJ, Williams M, et al. Expression of vegfr-2 and ac133 by circulating human cd34+ cells identifies a population of functional endothelial precursors. Blood. 2000;95(3):952-8.

541. Cai X, Wang J, Wang J, Zhou Q, Yang B, He Q, et al. Intercellular crosstalk of hepatic stellate cells in liver fibrosis: New insights into therapy. Pharmacol Res. 2020;155:104720.

542. Dong P, Ma L, Liu L, Zhao G, Zhang S, Dong L, et al. Cd86+/cd206+, diametrically polarized tumor-associated macrophages, predict hepatocellular carcinoma patient prognosis. Int J Mol Sci. 2016;17(3):320.

543. Ren C-X, Leng R-X, Fan Y-G, Pan H-F, Li B-Z, Wu C-H, et al. Intratumoral and peritumoral expression of cd68 and cd206 in hepatocellular carcinoma and their prognostic value. Oncology reports. 2017;38(2):886-98.

544. Monti P, Leone BE, Zerbi A, Balzano G, Cainarca S, Sordi V, et al. Tumor-derived muc1 mucins interact with differentiating monocytes and induce il-10highil-12low regulatory dendritic cell. The Journal of Immunology. 2004;172(12):7341-9.

545. Sica A, Saccani A, Bottazzi B, Polentarutti N, Vecchi A, Damme JV, et al. Autocrine production of il-10 mediates defective il-12 production and nf-κb activation in tumor-associated macrophages. The Journal of Immunology. 2000;164(2):762.

546. Raggi F, Pelassa S, Pierobon D, Penco F, Gattorno M, Novelli F, et al. Regulation of human macrophage m1-m2 polarization balance by hypoxia and the triggering receptor expressed on myeloid cells-1. Front Immunol. 2017;8:1097.

547. Hnasko R, Carter JM, Medina F, Frank PG, Lisanti MP. Pv-1 labels trans-cellular openings in mouse endothelial cells and is negatively regulated by vegf. Cell Cycle. 2006;5(17):2021-8.

548. Keuschnigg J, Tvorogov D, Elima K, Salmi M, Alitalo K, Salminen T, et al. Pv-1 is recognized by the pal-e antibody and forms complexes with nrp-1. Blood. 2012;120(1):232-5.

549. Squadrito ML, Pucci F, Magri L, Moi D, Gilfillan GD, Ranghetti A, et al. Mir-511-3p modulates genetic programs of tumor-associated macrophages. Cell Rep. 2012;1(2):141-54.

550. Hoare M, Narita M. The power behind the throne: Senescence and the hallmarks of cancer. Annual Review of Cancer Biology. 2018;2(1):175-94.

551. Kyritsi K, Francis H, Zhou T, Ceci L, Wu N, Yang Z, et al. Downregulation of p16 decreases biliary damage and liver fibrosis in the mdr2(/) mouse model of primary sclerosing cholangitis. Gene Expr. 2020;20(2):89-103.

552. Tsuji-Tamura K, Ogawa M. Morphology regulation in vascular endothelial cells. Inflammation and Regeneration. 2018;38(1):25.

553. Tsuji-Tamura K, Ogawa M. Inhibition of the pi3k-akt and mtorc1 signaling pathways promotes the elongation of vascular endothelial cells. J Cell Sci. 2016;129(6):1165-78.

554. Liu ZJ, Shirakawa T, Li Y, Soma A, Oka M, Dotto GP, et al. Regulation of notch1 and dll4 by vascular endothelial growth factor in arterial endothelial cells: Implications for modulating arteriogenesis and angiogenesis. Mol Cell Biol. 2003;23(1):14-25.

555. Acosta JC, Banito A, Wuestefeld T, Georgilis A, Janich P, Morton JP, et al. A complex secretory program orchestrated by the inflammasome controls paracrine senescence. Nature Cell Biology. 2013;15(8):978-90.

556. Goebeler M, Roth J, Teigelkamp S, Sorg C. The monoclonal antibody mac387 detects an epitope on the calcium-binding protein mrp14. J Leukoc Biol. 1994;55(2):259-61.

557. Flavell DJ, Jones DB, Wright DH. Identification of tissue histiocytes on paraffin sections by a new monoclonal antibody. Journal of Histochemistry & Cytochemistry. 1987;35(11):1217-26.

558. Nourshargh S, Hordijk PL, Sixt M. Breaching multiple barriers: Leukocyte motility through venular walls and the interstitium. Nature Reviews Molecular Cell Biology. 2010;11(5):366-78.

559. Mamdouh Z, Mikhailov A, Muller WA. Transcellular migration of leukocytes is mediated by the endothelial lateral border recycling compartment. J Exp Med. 2009;206(12):2795-808.

560. Allport JR, Muller WA, Luscinskas FW. Monocytes induce reversible focal changes in vascular endothelial cadherin complex during transendothelial migration under flow. The Journal of cell biology. 2000;148(1):203-16.

561. Sullivan DP, Seidman MA, Muller WA. Poliovirus receptor (cd155) regulates a step in transendothelial migration between pecam and cd99. Am J Pathol. 2013;182(3):1031-42.

562. Gerszten RE, Lim Y-C, Ding HT, Snapp K, Kansas G, Dichek DA, et al. Adhesion of monocytes to vascular cell adhesion molecule-1–transduced human endothelial cells. Circulation Research. 1998;82(8):871-8.

563. Millán J, Hewlett L, Glyn M, Toomre D, Clark P, Ridley AJ. Lymphocyte transcellular migration occurs through recruitment of endothelial icam-1 to caveola- and f-actin-rich domains. Nat Cell Biol. 2006;8(2):113-23.

564. Mamdouh Z, Chen X, Pierini LM, Maxfield FR, Muller WA. Targeted recycling of pecam from endothelial surface-connected compartments during diapedesis. Nature. 2003;421(6924):748-53.

565. Muller WA, Weigl SA, Deng X, Phillips DM. Pecam-1 is required for transendothelial migration of leukocytes. J Exp Med. 1993;178(2):449-60.

566. Arts JJ, Mahlandt EK, Grönloh ML, Schimmel L, Noordstra I, Gordon E, et al. Endothelial junctional membrane protrusions serve as hotspots for neutrophil transmigration. eLife. 2021;10:e66074.

567. Sullivan DP, Muller WA. Neutrophil and monocyte recruitment by pecam, cd99, and other molecules via the lbrc. Seminars in Immunopathology. 2014;36(2):193-209.

568. Mozer AB, Whittemore SR, Benton RL. Spinal microvascular expression of pv-1 is associated with inflammation, perivascular astrocyte loss, and diminished ec glucose transport potential in acute sci. Curr Neurovasc Res. 2010;7(3):238-50.

569. Rennert K, Steinborn S, Gröger M, Ungerböck B, Jank A-M, Ehgartner J, et al. A microfluidically perfused three dimensional human liver model. Biomaterials. 2015;71:119-31.

570. Gröger M, Rennert K, Giszas B, Weiß E, Dinger J, Funke H, et al. Monocyte-induced recovery of inflammation-associated hepatocellular dysfunction in a biochip-based human liver model. Scientific reports. 2016;6(1):1-16.

571. Zimmermann HW, Bruns T, Weston CJ, Curbishley SM, Liaskou E, Li K-K, et al. Bidirectional transendothelial migration of monocytes across hepatic sinusoidal endothelium shapes monocyte differentiation and regulates the balance between immunity and tolerance in liver. Hepatology (Baltimore, Md). 2016;63(1):233-46.

572. Liaskou E, Zimmermann HW, Li K-K, Oo YH, Suresh S, Stamataki Z, et al. Monocyte subsets in human liver disease show distinct phenotypic and functional characteristics. Hepatology. 2013;57(1):385-98.

573. Resheq YJ, Menzner AK, Bosch J, Tickle J, Li KK, Wilhelm A, et al. Impaired transmigration of myeloid-derived suppressor cells across human sinusoidal endothelium is associated with decreased expression of cd13. J Immunol. 2017;199(5):1672-81.